# THE EARLY
# OBSERVABLE UNIVERSE
# FROM DIFFUSE BACKGROUNDS

XXVIth Rencontre de Moriond
XIth Moriond Astrophysics Meetings
Les Arcs, Savoie, France - March 10-17, 1991

**THE EARLY OBSERVABLE UNIVERSE FROM DIFFUSE BACKGROUNDS**
Series : Moriond Astrophysics Meetings

ISBN 2-86332-107-2


**EDITIONS FRONTIERES**
B. P. 33
91192 Gif-sur-Yvette Cedex - France

Printed in Singapore by Fong & Sons Printers Pte Ltd

Proceedings of the XXVIth RENCONTRE DE MORIOND
XIth Moriond Astrophysics Meetings
Les Arcs, Savoie, France March 10-17, 1991

# THE EARLY OBSERVABLE UNIVERSE FROM DIFFUSE BACKGROUNDS

edited by

**Rocca-Volmerange B.**
**Deharveng J. M.**
**Trân Thanh Vân J.**



EDITIONS
FRONTIERES

**The Astrophysics Session of the XXVIth Rencontre de Moriond**

# The Early Observable Universe from Diffuse Backgrounds

*was organized by :*


Rocca-Volmerange B. *(Paris and Orsay)*
Deharveng J. M. *(Marseille)*
Trân Thanh Vân J. *(Orsay)*


Cover : COBE DIRBE full sky maps in galactic coordinates. 1A. Combined 1.2, 2.2, and 3.4 micron map in respective blue, green, and red colors. The image shows both the thin disk and central bulge of the galaxy. 1B. Combined 25, 60, and 100 micron map in respective blue, green, and red colors. Both maps are preliminary results of a full sky scan by the DIRBE instrument. The discontinuities apparent are due primarily to the change in zodiacal light as the spacecraft and earth move around in the zodiacal dust but may in part be due to not having final instrument calibration.

## AVANT-PROPOS

Le choix du fond diffus cosmologique comme thème des Rencontres de Moriond en Astrophysique a été motivé par un certain nombre d'évènements remarquables: la confirmation de la nature isotrope et thermique de ce rayonnement diffus dans le domaine des ondes millimétriques et centimétriques par le satellite COBE, les contraintes sévères qui en résultent sur les inhomogénéités primordiales, les contraintes nouvelles sur le milieu intergalactique chaud, les premiers résultats de ROSAT, la comparaison de plus en plus fertile entre les comptages profonds de sources discrètes et les mesures de fond diffus dans la plupart des domaines spectraux.

Ce colloque a rassemblé dans une merveilleuse atmosphère de soleil et de neige environ 50 participants provenant de laboratoires français et étrangers qui ont mis en commun leur démarche scientifique et leurs résultats dans chaque domaine de longueur d'onde, des plus énergétiques (X, $\gamma$, UV) aux plus froids (visible et infrarouge). Les émissions des différents objets (cirrus, gaz, étoiles, galaxies et amas) sont successivement apparues comme un jeu de puzzle auquel on ajoute des morceaux bien ajustés mais qui ne sera complet qu'avec les perspectives des futurs instruments dans l'UV, l'infrarouge avec ISO et le submillimétrique.

Les conférences invitées et les contributions d'excellent niveau ont été rassemblées dans ce livre qui constitue le onzième de la série des Rencontres de Moriond en Astrophysique. Nous remercions B. Sadoulet d'avoir accepté de présenter sa revue sur la matière noire en introduction. Le colloque a été marqué par des sessions jointes avec des physiciens des particules, au cours desquelles nous avons eu le plaisir d'entendre plusieurs conférences sur l'historique de dix ans de cosmologie à Moriond par J. Audouze, les résultats du satellite COBE par G. Smoot, les problèmes des neutrinos solaires et l'énigme du neutrino à 17 keV par de nombreux orateurs dont D. Morrisson.

Nous remercions particulièrement J. Tran Thanh Van et son équipe pour l'accueil chaleureux et l'organisation remarquable, qui restent des constantes de ces Rencontres de Moriond. Nos remerciements s'adressent également à Lucienne Norry, Colette Douillet, Valérie Demailly, Aïda Ramos qui avec beaucoup de compétence et de patience ont rendu ce séjour très agréable et ont permis l'édition de ce livre.

Ces Rencontres de Moriond n'auraient pas eu lieu sans l'aide financière du CNRS, du CNES, du CEA, de l'Institut d'Astrophysique de Paris et du Laboratoire d'Astronomie Spatiale.

## PREFACE

Cosmological Diffuse Backgrounds have been chosen as topics of the Rencontres de Moriond, Astrophysics because of several outstanding events: the confirmation of a thermal and isotropic diffuse microwave background by the COBE satellite, the resulting severe constraints on primeval inhomogeneities, new constraints on the hot intergalactic medium, the first results from ROSAT, and a more and more exciting comparison of discrete–source deep counts with diffuse background measurements in most spectral ranges.

This meeting gathered in a wonderful sun and snow atmosphere about fifty participants from french and foreign laboratories, who were allowed to share their scientific approaches and results from the highest energetic domains (X, $\gamma$, UV) to the coldest ones (visible and infrared). Emissions from various sources (cirrus, gas, stars, galaxies and clusters) are pieces of a deep puzzle which will be complete only with the perspectives of the future UV, infrared (ISO) and submillimetric projects.

This book which summarizes excellent invited papers and reviews is the eleventh of the Rencontres de Moriond Series, Astrophysics. We thank B. Sadoulet for his introduction on Dark Matter. The meeting participants had the pleasure to attend some joined sessions with particle physicists marked by several conferences: the results of the COBE satellite by G. Smoot, ten years of Cosmology at Moriond by J. Audouze, and some news on solar neutrinos by D. Morrisson as well as the riddle of the 17 keV neutrino.

We gratefully acknowledge J. Tran Thanh Van and his collaborators for their warm welcome and remarkable organisation which are constants of the Rencontres de Moriond. We also thank Lucienne Norry, Colette Douillet, Valérie Demailly and Aïda Ramos who make this stay so pleasant, and the edition of this book possible.

This meeting could not be organised without the financial help of the Centre National de la Recherche Scientifique, the Centre National d'Etudes Spatiales, the Commissariat à l'Energie Atomique, the Institut d'Astrophysique de Paris and the Laboratoire d'Astronomie Spatiale.

# *Contents*

## IV. FAINT GALAXY COUNTS



## V. FAR-IR AND SUBMILLIMETER BACKGROUND RADIATION



## VI. INTERGALACTIC MEDIUM, GALAXY EVOLUTION, GALAXY FORMATION MODELS

# INTRODUCTION

# DARK MATTER

Bernard Sadoulet
Center for Particle Astrophysics
and Physics Department, University of California, Berkeley

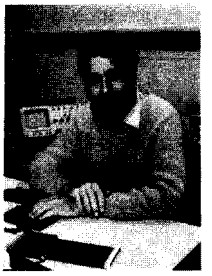

## ABSTRACT

More than 90% of the stuff in the universe does not emit any light and constitutes the elusive dark matter. There is a growing consensus that such dark matter exists, but its exact amount and its nature remain unknown. This dark matter puzzle is probably one the most fundamental problems of science today, and its solution may have to combine tools from cosmology, astrophysics and particle physics. This paper presents a short review of the current situation of the problem, emphasizing recent results and the perspectives for progress in the near future.

There is mounting evidence that at least 90% of the mass in the universe is "dark." By dark we mean that it is does not emit nor absorb any kind of electromagnetic radiation and is only seen by its gravitational effect on visible objects. We do not yet know the exact amount, nor the nature, of this obviously major component of the physical universe. This fundamental puzzle constitutes the "dark matter problem" which dates back to Zwicky[1], and has been often reviewed in the past[2]. Its solution touches central issues in cosmology and astrophysics, and probably also involves particle physics. At the 25th anniversary of the Moriond workshops, which have focused on current fundamental scientific problems in particle physics and in astrophysics and have attempted to establish bridges between these two fields, dark matter seemed a very suitable and symbolic subject for a review addressed both to particle physicists and astrophysicists. The competence of the particular reviewer chosen, however, will tilt this presentation towards particle physicists, attempting to summarize for them therecent progress on the astrophysics side.

## 1 EVIDENCE FOR DARK MATTER

Although Zwicky's initial suggestion of the presence of dark matter stayed controversial for a long time, there is a growing consensus in the astronomy community that dark matter indeed exists. Four types of evidence have been found.

### *1.1 Rotation curves*

In individual spiral galaxies, the measured velocities of objects (typically isolated stars, gas clouds or globular clusters) that are apparently bound to the galaxies, allow us to estimate the centripetal gravitational force which has to balance the centrifugal force:

$$\frac{GM(r)}{r^2} = \frac{v^2}{r}$$

Figure 1 shows the famous measurements made by V. Rubin and collaborators[3]. The needed centripetal force is much larger than the gravitational force generated by the stars we can see in the galaxies, and as the velocity appears constant at high radii, the mass M(r) enclosed in the orbit has to increase as r, in a region where practically no stars are seen.

Similar evidence based on the velocity dispersion of stars in elliptical galaxies (which do not exhibit overall rotation) indicates that dark matter is also present in these objects.

### *1.2 Velocity Dispersion in Cluster of Galaxies*

In a cluster of galaxies, each galaxy has a finite "peculiar" velocity, swinging back and forth in the potential well created by the galaxy concentration. As these systems are believed to be bound and stationary, the dispersion of these velocities can be related to the depth of the potential well through the virial theorem

<kinetic energy>= -1/2 <potential energy>.

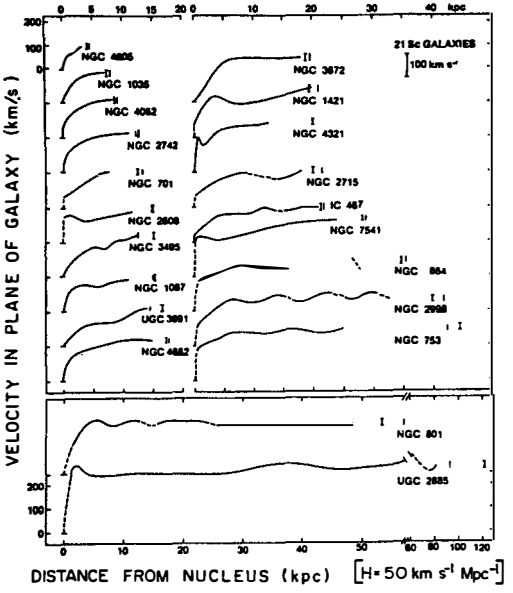


Figure 1
Rotation curves for many spiral galaxies obtained from optical measurement. (From V.C. Rubin *et al*,. 1980.)

Figure 2 shows the observations for the Coma cluster. The large observed dispersion velocities of some 1000km/s to 1500 km/s implies a mass to light ratio of 400h times that of the sun, where h is the Hubble expansion parameter measured in the usual units of 100 km/s/Mpc (experimentally $1/2 \leq h \leq 1$).

*1.4 X-ray Emission by Galaxy Clusters*

Similar velocity dispersions can be inferred from the temperature of the x rays emitted by the intergalactic gas which appears[4] to be present in clusters of galaxies (Figure 3). If the gas has the same spatial distribution as the galaxies, we expect that

$$\frac{3}{2}kT_{gas} = \frac{1}{2}m\sigma^2$$

where $\sigma$ is the dispersion velocity of gas molecules. A typical 5 keV x-ray temperature corresponds to $\sigma \approx 1200$km/s, a value analogous to that of galaxies. A detailed analysis is impeded

by the lack of precise measurement of the temperature profile[5], but the results are in general agreement with those derived from the galaxy velocity dispersion.

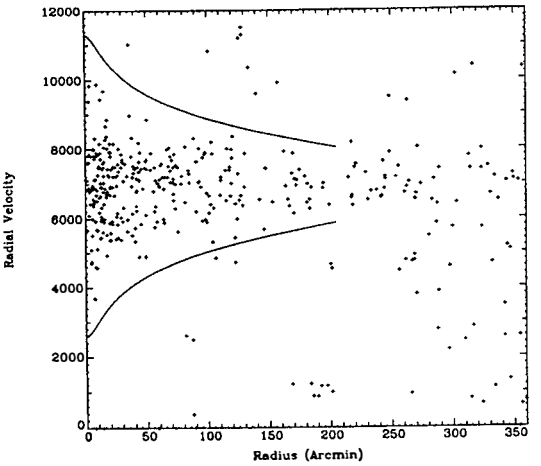


Figure 2
Line-of-sight velocities of galaxies in the Coma cluster (in $kms^{-1}$) as a function of distance from the cluster center in minutes of arc. The curves mark the authors' estimate of the boundary between cluster members and interlopers. At the distance of Coma 1 arcmin = $20h^{-1}$ kpc. (From Kent and Gunn, 1982.)

### *1.5 Gravitational Lensing by Galaxy Clusters*

New independent evidence on the depth of potential wells in clusters of galaxies has been obtained by Tyson and coworkers[6] who have studied the gravitational lensing of distant galaxies by foreground clusters. A round object located far behind the cluster will appear elliptical after lensing, with its major axis tangential to the mass distribution contours. In extreme cases, arcs and arclets should be seen. This indeed is what is observed. In Figure 4, most of the galaxies of the foreground cluster Abell 1689, which is roughly in the center and provides the gravitational lens, have been subtracted (using their reddish color) and a definite trend towards tangential structures is evidenced. From these many lensed objects it is possible to reconstruct the mass distribution of dark matter (Figure 5) and we can "see" the accumulation of stuff in the center of the cluster, in a way similar to the distribution of gas. A high velocity dispersion of some 1200 km/s is also inferred, confirming the independent analysis of velocity dispersion and x-rays. This method promises to allow a detailed mapping of dark matter in large structures.

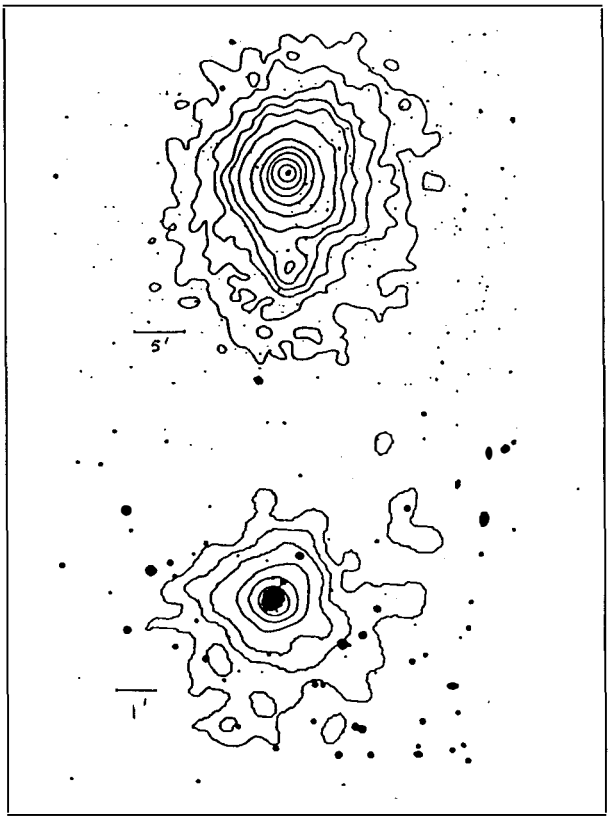


Figure 3
X-ray isodensity contours for cluster Abell 85, at two different resolutions (top with the Einstein Satellite IPC, bottom with the HRS). (From Forman and Jones, 1982.)

*1.5 Potential Loopholes*

Many authors have outlined the potential loopholes in the above arguments. In particular, our kinematic arguments have implicitly assumed spherical symmetry, and it is indeed possible to explain individual rotation curves by peculiar, highly non-spherical, matter distributions without introducing dark matter. However, for each type of observation and at each scale, an *ad hoc* argument has to be devised. In such an approach, the compatibility observed in clusters between results of the virial theorem, the x-ray temperature and gravitational lensing would

appear accidental. In spite of its far-reaching consequences, the dark matter explanation is much more natural.

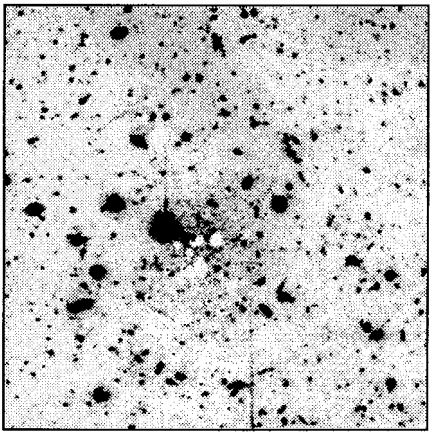

Figure 4
Image of background galaxies (in the blue) lensed by cluster A 1689. The cluster light has been eliminated by subtraction of a scaled red image. Several nearby arcs and systematic distortion along circles about the lens center can be seen.

Figure 5
Distribution of dark matter in cluster A 1689 as inferred from Fig. 4.

It has also been proposed that Newtonian gravity could be modified[7] on scales larger than the solar system or the binary pulsar, where General Relativity has been extensively tested. So far, it appears difficult to construct such alternative gravity models in a way consistent with General Relativity at smaller scales, they fail to explain the magnitude of the gravitational lensing effects[8], and they may be incompatible with the compact dark halo observed around dwarf galaxies[9].

## 2 THE VALUE OF Ω

Arguments are therefore strong for dark matter to exist. However, its amount is still uncertain by about a factor 5. As it dominates the mass density in the universe, measuring the amount of dark matter is essentially equivalent to the determination of Ω, the average density in units of the critical density

$$\Omega = \frac{\rho}{\rho_c}$$

$$\rho_c = \frac{3H^2}{8\pi G}$$

where H is the Hubble expansion parameter. As is well known, Ω is related to the curvature of space and to the ultimate fate of the universe[10]. $\Omega>1$ corresponds to a closed (i.e. spherical) universe which will eventually recollapse, while $\Omega<1$ corresponds to an open (i.e. hyperbolic) universe which expands forever. For $\Omega=1$, space is flat, and the expansion will stall at infinite time. An important point in the debate is that in General Relativity, the spatial curvature of a non-flat universe evolves extremely rapidly, and it is difficult to understand why our universe is so close to being flat ($\Omega\approx 0.1$-1) without being exactly flat. This flatness problem is much discussed, and is one of the reasons why inflation scenarios[11] are favored by many cosmologists (usually originating from particle physics), as it naturally predicts $\Omega=1$. Inflation also explains why the cosmic microwave background can have basically the same temperature at points which naively appear causally disconnected. Another crisis seems to arise from the apparent incompatibility between an $\Omega=1$ universe, the most recent determinations of the Hubble parameters ($H\approx 90$km/s/Mpc) and the age of the universe. If this discrepancy persists, we may have to accept the presence of a vacuum energy in the form of a cosmological constant Λ. Defining

$$\Omega_\Lambda = \frac{\Lambda}{3H^2}$$

spatial flatness requires then that

$$\Omega + \Omega_\Lambda = 1$$

We examine in turn the three types of methods which astrophysicists attempt to use to determine the universe curvature and a potential cosmological constant.

*2.1 Direct Summation*

We may first attempt to sum the mass observed with the virial theorem in various systems. Usually it is done with the mass to light ratio M/L, which allows us to compute the mass density from the luminosity distribution of the considered objects.

$$\rho_m = \int \left(\frac{M}{L}\right) L \left(\frac{d^2N}{dV dL}\right) dL$$

where L is the absolute luminosity of the objects. Typical values obtained in this method are given in Table 1, and they are significantly smaller than 1. We would need a M/L of 1600h (where h is the Hubble parameter in usual units of 100km/s/Mpc), in orderto have $\Omega$=1. None of the known objects have such high mass to light ratio. However, it should be noted that the virial theorem is only sensitive to *inhomogeneities* of the mass distribution, and that such methods can only give a lower limit of $\Omega$. Another problem is that it is difficult to know where the system stops. We are running out of objects for measuring rotation curves at large distances and galaxies for the cluster core fade in the field!

Table 1
Cosmological Density Estimates

| | Scale | $\Omega$ |
|---|---|---|
| Visible parts of galaxies | ~$20h^{-1}$kpc | 0.01 |
| Halos of galaxies and groups of galaxies | ~$0.1h^{-1}$Mpc | 0.02-0.2 |
| Cosmic virial theorem | ~$3h^{-1}$Mpc | ~0.2 |
| Virgo infall | ~$10h^{-1}$Mpc | ~0.2 |
| Large scale infall | ~$30h^{-1}$Mpc | ~0.2-1 |
| Cosmological tests | $3000h^{-1}$Mpc | 0.1-2 |
| Cosmic inflation | | 1 |

*2.3 Dynamical Methods*

Attempts to apply the virial theorem on even larger scale structure are prevented by the fact that the systems are not stationary, with structure still clearly forming. Not only do we observe on the large scale a complex distribution of galaxies[12] (Figure 6) with voids, filaments, bubbles and the like, not typical of a virialised system, but large scale velocity coherent flows can be deduced from the comparison of the distance and redshift of (relatively close-by) galaxies[13], or reconstructed[14] from the density of galaxies detected in the infrared by the IRAS satellite

(Figure 7).

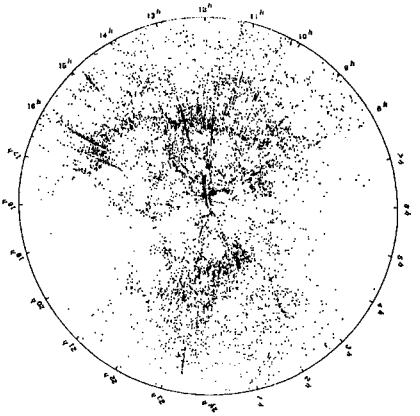

Figure 6
Distribution of galaxies as a function of redshift. We are at the center. Each galaxy is plotted at a radius proportional to its recession velocity and an azymuth equal to its right ascension. This is a slice in declination between 10° and 40°. The magnitude limit of the sample is 14.5. (From Huchra and Geller, 1989.)

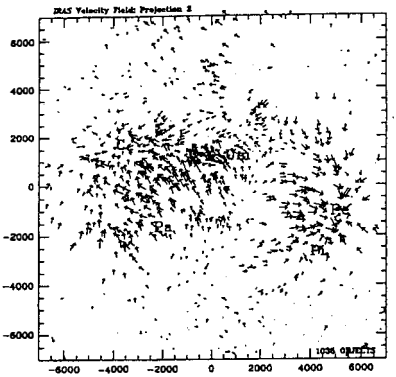


Figure 7
Velocity flows reconstructed from a redshift survey of galaxies selected with the IRAS catalog. The Great Attractor is seen on the left and the Perseus Pisces cluster is identifiable at the right. (From Strauss and Davis, 1987.)

As the time that structure takes to form is sensitive to the underlying averaged density,

one can attempt to use the large scale distribution of galaxies and the associated velocity flows to estimate $\Omega$. Basically, one writes the equations

observed velocities=acceleration (due to density inhomogeneities) x time of formation

or

observed inhomogeneities=rate of variation (due to peculiar velocities) x time.

In the linear regime[15], these equations become

$$\bar{v} = G\rho_b \bar{\nabla} \int d^3x' \frac{\frac{\delta\rho}{\rho_b}}{[x-x']} \cdot \frac{2}{3}\frac{f}{H\Omega}$$

$$= \frac{Hf}{4\pi} \bar{\nabla} \int d^3x' \frac{\frac{\delta\rho}{\rho_b}}{[x-x']}$$

$$\frac{\delta\rho}{\rho_b} = -\bar{\nabla}.\bar{v}\frac{1}{Hf}$$

$$f \approx \Omega^{0.6}$$

We can either compare the measured value of our peculiar velocity with respect to the cosmic microwave background to that obtained from summing the acceleration due to observed density inhomogeneities, or compare the observed density fluctuations to those predicted by the divergence of the observed velocity field. The second method is very recent, and became possible through the realization[16] that the three dimensional velocity field can be deduced from the radial components which are the only measured quantities, through the natural assumption of zero vorticity ($\nabla$ x v=0). Any initial vorticity would be erased by the Hubble expansion. This procedure, which is called "POTENT," is demonstrated in Figure 8, which compares the density contrast observed in the IRAS catalog[14] to that reconstructed through POTENT from measured peculiar velocities[13]. The density enhancement in the region of the Great Attractor (left) is seen in the two plots, while there are obvious discrepancies in the Perseus-Pisces region (right), where direct measurement of velocity fields are still in disagreement with density measurements. In spite of these observational disagreements, the method appears to be very promising.

However, there is a fundamental difficulty in applying these methods, as we cannot measure directly the background density contrast $\delta\rho/\rho_b$, but only the density contrast $\delta n/n$ in the number of galaxies, and we have numerous indications that light does not trace mass. It is usually assumed that the two densities are related by

$$\frac{\delta n}{n} = b\frac{\delta\rho}{\rho_b}$$

where b is the "biasing parameter" which is usually taken as constant (but does not need to be!). The POTENT method can then only give the value of $\Omega^{0.6}/b$. From Figure 8 it can be deduced that

$$\frac{\Omega^{0.6}}{b} \approx 0.8$$

As b is believed not to be much smaller than 1, this result points to a large value of $\Omega$. Taking into account non-linear effects, it may be possible to extract $\Omega$ and the biasing parameter b separately, and one obtains[17]

$$\Omega \approx 0.8$$
$$b \approx 0.66$$

with large error bars. In any case, both quantities appear to be greater that 0.5.

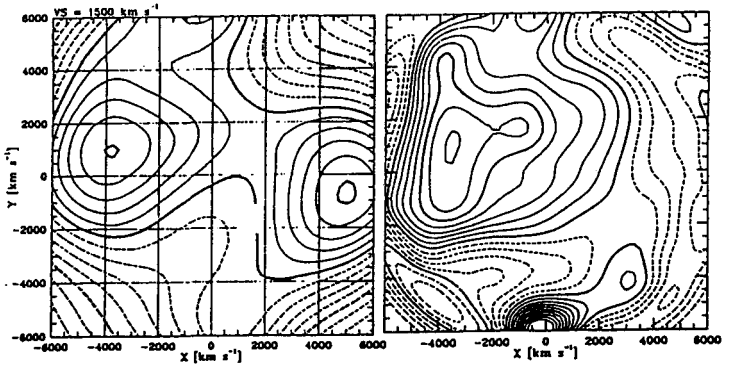


Figure 8
*Left:* IRAS galaxy density contrast. *Right:* The underlying mass-density contrast reconstructed by POTENT from the ESm peculiar velocities. The effective smoothing in both cases is 1500 kms-1. Spacing between contours is 0.1. (From Bertshinger *et al.*, 1990.)

This method is clearly very promising, but in order to be put on firmer ground it requires the measurement of the peculiar velocities of a much larger sample of galaxies. This would certainly be one of the exciting products of the Million Galaxy Redshift Survey that Chicago, Princeton and Fermilab are starting.

*3.3 Geometry Measurements*

A potentially powerful set of methods is to attempt to measure directly the geometry of the universe by measuring quantities sensitive to this geometry. For instance, the variation of the apparent luminosity of a "standard candle" (i.e. constant absolute luminosity) as a function of redshift would tell us about potential deviation from the $1/r^2$ law which is only valid in a flat space, or the change with redshift of the volume element traced by the density of galaxies would be a

direct indication of spatial curvature. These cosmological tests directly address the question of the value of $\Omega$ (and $\Lambda$), but they require that one be able to differentiate between the variation due to cosmology and the evolution of the objects.

This problem has so far plagued the first type of measurement. For instance, in the classical test of Sandage and coworkers[18] using the brightest galaxy in a cluster as a standard candle, the luminosity evolution dominated cosmological effect. In recent years, a new idea has been developed[19]: Type Ia supernovae appear to be reasonable standard candles "locally", they can be seen at intermediate redshifts (0.3)[20] and they are probably the best hope to perform this luminosity test. The main problem appears to be the need for a very large amount of 4 meter class telescope time.

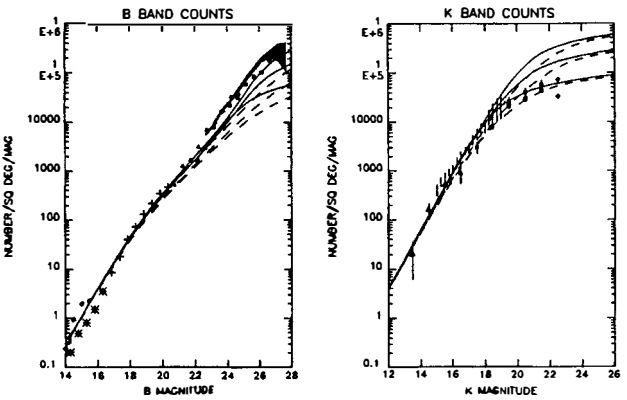


Figure 9
Comparison of blue and infrared counts with model predictions. Two classes of model are shown. The dashed lines show models in which galaxies do not change at all in luminosity or type. The bottom curve has $\Omega$ =1, the middle $\Omega$=0.04, and the top a zero curvature model with $\Omega$=0.1 and $\Omega_\Lambda$=0.9. The three solid lines show models with the same three geometries as above but in which the galaxies evolve with z following the prescription of Yoshii and Takahara (1988). The galaxies are assumed to form at z=3. (From Cowie, 1990.)

The volume variation test was first attempted on radio-galaxies, counting their number as a function of luminosity, but they evolve too rapidly with redshift. More recently, with the advent of very sensitive CCDs, several groups had been counting the number of galaxies as a function of their visible magnitude (luminosity). Figure 9a shows the results obtained in the blue, which presented a major puzzle as the number of galaxies at the faint end (large magnitudes), appeared to increase too fast, not only for an $\Omega$=1 universe, but even for $\Omega$=0.04 or $\Omega$=0.1, $\Omega_\Lambda$=0.9 universes where the volume is dramatically larger at high redshift. In the last year, the nature of the problem has been partially unravelled by the infrared survey of Cowie and collaborators[21]

who used new pixel devices ( a Rockwell 256x256 Hg Cd T e array) sensitive at 2.2μ (K band). In this survey the number appears to behave much more normally, even flattening up in a way compatible with Ω=1. A clearer picture emerges. On one hand, the blue survey is dominated by a population of small galaxies with intense star burst activity which seem to appear and disappear at a not very high redshift (z≈0.4). The blue counts, therefore, are probably useless for the cosmological test. The K band, on the other hand, probes the old star component of galaxies, which have lifetimes of the same order as that of the universe. It is therefore much more promising as a cosmological test, and its seems to indicate a large value of Ω!

The real way to do the volume test would to directly measure the counts as a function of redshift, and not rely on luminosity which is not simply related to redshift. This approach was pioneered by Loh and Spillar[22]. Using a 6-band photometry, they estimated the redshift of their objects, and concluded that Ω=1 with errors of about 0.5. Unfortunately, this result has been criticized on a number of counts, and has remained extremely controversial. Their redshift measurement is at best imprecise; the statistical method used may be partially responsible forthe high value, as Caditz and Petrosian[23] obtain a low Ω ≈0.2 with the same data. Mergers and luminosity evolution could be responsible for an uncertainty of ±1[24]. Gravitational lensing may also not be negligible[25]. With the operation of the Keck 10m telescope, it will soon be possible to do this measurement in a much more convincing way with a suitable multi-slit spectrograph. In particular, not only the color and redshift of the object could be measured, but also its mass through the measurement of the internal velocity dispersion. This would be a powerful method to detect merging, gravitational lensing and luminosity evolution, and should provide a much more reliable determination of the geometry. The Center for Particle Astrophysics in Berkeley is proposing to the NSF to embark on such a program.

## 3 THE NATURE OF DARK MATTER

Even more that its existence and its abundance, the nature of dark matter is a central scientific question, especially if it turns out that it is not made of ordinary baryons. Figure 10 sketches the range of possibilities. One of the main current goals of experimental cosmology is to narrow down the choice. In this fundamental quest, we can obtain information both from classical astrophysical observations and from new attempts to directly observe dark matter, often using particle and nuclear physics methods. We analyze in this section what we can say today and what we may be able to find out in the near future from indirect astrophysical methods and direct searches, considering in turn baryonic and non-baryonic dark matter.

### *3.1 Baryonic Dark Matter*

#### 3.1.1 Indirect astrophysical evidence

What can we learn about baryons from astrophysics? The main information comes from the measurements of primordial abundances of light elements (helium 4, deuterium, helium 3 and lithium 7). They depend both on the expansion rate of the universe (related to the number of

neutrinos) and on the number of baryons some three minutes after the Big Bang. The conventional nucleosynthesis scenario in a uniform universe agrees amazingly well with observations[26] (Figure 11). If the number of light neutrinos is imposed to be three, as shown by LEP, the average density of baryons in units of the critical density is inferred to be

$$\Omega_b=\rho_b/\rho_c= (1.6 \pm 0.2 )\ 10^{-2}/h^2$$

where h is as usual the Hubble expansion rate in units of 100km/s/Mpc ($1/2 \leq h \leq 1$). A possible quark hadron transition can only slightly change this result[27]. This result seriously limits the range of $\Omega_b$, making it difficult to reconcile the baryon density with the amount of dark matter observed by some astronomical methods ($\Omega_{\nu_e} < 10^{-2}$). Confirmation of a large value of $\Omega$ would definitely require the existence of non-baryonic dark matter.

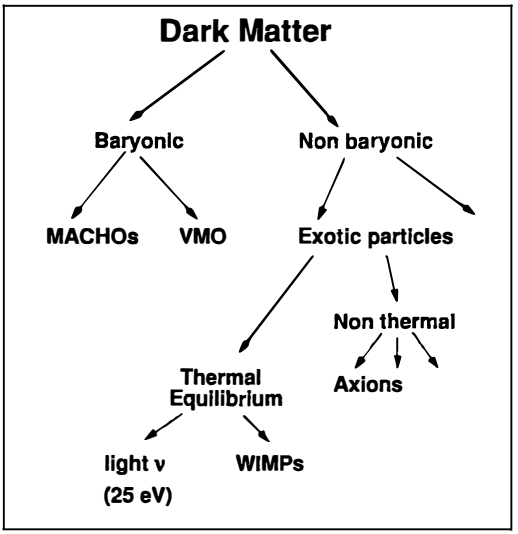


Figure 10
Nature of dark matter.

Note, however, that the same results argues for the existence *in any case* of baryonic dark matter, especially if h is small, as with stars and cluster gas it is difficult to go beyond a value $\Omega_{\nu_e} \approx 10^{-2}$.

3.1.2 Direct searches

What can it be? From the absence of a Gunn-Peterson absorption trough in the spectrum of quasars, we know that in cannot be in the form of cold gas[28], and too much hot gas will either impose Compton distortions on the cosmic microwave background, if it is diffuse, or emit too many x-rays, if it is clumped. The COBE results[29] put severe limits on the first possibility, while

the second problem, related to the puzzle of the diffuse hard x-ray background[30], is still very much debated. Instead of being in the form of gas, dark matter could be made of condensed objects, somehow formed in the very early universe. However, the possibilities are severely limited, and presently the only ones compatible with observations[31] are Very Massive Objects (VMOs) of at least 100 $M_{sun}$ or Massive Compact Halo Objects (MACHOs, also called Brown Dwarfs). Because of their high mass, the VMOs very quickly underwent supernova explosions and formed black holes sufficiently massive to absorb all the material around them, therefore preventing contamination of the interstellar medium by high Z elements produced in the explosions. These objects can in principle be observed directly through the far infrared relic radiation they should have produced, and the DIRBE experiment aboard the COBE satellite is actively searching for such a signature.

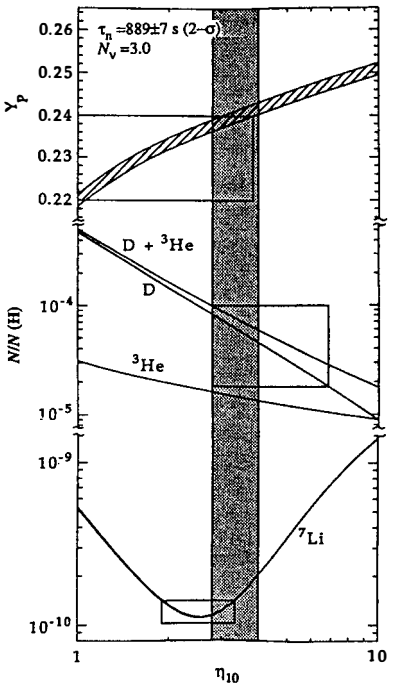


Figure 11
The mass fraction of $^4$He, Yp, and the abundances by number of D, $^3$He, D + $^3$He, and $^7$Li as a function of the ratio of photons to baryons $\eta 10 = \eta \times 10^{10}$. The vertical band delimits the range for h consistent with the observations. (From K. A. Olive, 1991.)

The second class of dark baryonic objects is formed by small jupiter-like objects that are not massive enough to bum hydrogen and are therefore not shining. These MACHOs can, however, be observed by gravitational lensing[32]. If one of them passes in front of a star located, say, in the Large Magellanic Cloud, a small galaxy at the periphery of our halo, its gravitational field is sufficient to focus the star light and produce a temporary increase of the stellar intensity. As the MACHO is moving at some 200km/s, this increase will only last for a short time, which can be estimated to be

$$\Delta t = 3 \text{ days} \sqrt{\frac{M}{.001 M_{sun}}}$$

The intensity increase can be rather substantial (30% or more) but the probability is small, typically $10^{-6}$ at a given time independently of the mass of the object. For 0.001 $M_{sun}$ to 0.1 $M_{sun}$ objects, this requires the observation of $10^6$ objects every night for a year or more to have a few candidates. This leads to rather unconventional types of astronomy observations which are currently attempted by two groups: the Livermore/Berkeley/ Australia group focuses on observations with a large field-of-view and two color CCD camera, while the French group is mostly using photographic plates for the same purpose. The French group is actively pursuing CCD also. The amount of data processing and the problem of finding a feeble signal in a large background requires methods very similar to particle physics, and it is not an accident that in both cases the collaborations involve particle physicists and astronomers. Results are expected within the next two years.

*3.2 Non-Baryonic Dark Matter*

If $\Omega$ observed by gravitational method is indeed larger than 0.2, we are obliged within the current picture of primordial nucleosynthesis to postulate the existence of non-baryonic dark matter. We refer again to Figure 10 to give an overall perspective.

3.2.1 Indirect astrophysical evidence

In our attempt to narrow down the possible choices, we may be usefully guided by the distribution of mass and large scale structure that we observe in the universe. The formation of structure is certainly due, at least in part, to gravitational collapse of density fluctuations, and since dark matter is gravitationally dominant, its nature may imprint characteristic features on the observed universe[33].

In fact, the mere fact that the 2.7K cosmic microwave background is so smooth and the large scale structure is so clumpy is difficult to understand without the presence of non-baryonic dark matter. If the background photons tell us about the baryonic density fluctuations at time of recombination, without dark matter, there is simply not enough time to grow the large fluctuations observed today. With non-baryonic dark matter, this is much easier. Before protons and electrons recombine into hydrogen, they are prevented from growing density fluctuations by their coupling to photons, which diffuse easily through the medium. Dark matter density

fluctuations, on the contrary, can grow since they are uncoupled to photons. After recombination, the baryons fall into the potential wells prepared by dark matter, and there is enough time then to form the structure observed today. There are ways to circumvent the difficulty (e.g. the so-called "non-adiabatic" scenarios[34]) but they are less natural.

The characteristics of the structure can also tell us whether dark matter was or was not relativistic at the time of galaxy formation. Technically, cosmologists speak of "hot" or "cold" dark matter. Cold dark matter includes, in addition to condensed baryonic objects, weakly interacting massive particles, axions (which are in most models created cold, in spite of their light mass), primordial black holes, etc. The prototype of hot dark matter is a light neutrino of, say, 25eV, which would close the universe.

Recently, the newspapers were full of articles announcing the demise of the "cold dark matter model." It should be realized that in no way this implies that dark matter is not made of cold particles. The "cold dark matter model" has many ingredients: it includes in addition to cold dark matter, the assumption of a particular spectrum of initial density fluctuations (Harrison-Zel'dovich spectrum), which are also assumed to be gaussian and uncorrelated on different scales. With a few parameters (overall amplitude, and biasing parameter), the resulting model[35] gives an amazingly good first approximation of the observed structure at small and intermediate scales. But recent observations show that it has serious difficulties at large scale: it barely can explain the large scale clumpiness of the distribution of galaxies (Figure 6) with large voids and a large concentration of galaxies extending over 100Mpc (the so-called Great Wall), and the observed large scale velocity flows (Figure 7). It fails to fit the recently measured galaxy correlation function[36] (Figure 12). It would have even greater difficulties to explain the very large scale structures recently suggested by redshift surveys of galaxies at very large distances[37] (Figure 13). The claim by the authors that the structure has a period of $128h^{-1}$Mpc is presently the subject of intense controversy. In any case, apart from the quasi-periodicity, which is likely to be at best coincidental, all these effects can be traced to a lack of power at large scales in the spectrum of initial density fluctuations. It is therefore clear that the cold dark matter model, which has been sometimes presented as the "Standard Model" of cosmology, has at least to be enlarged, and the present difficulties may the sign of some new exciting physics (such as late phase transitions and/or topological defects). In any case, the cold dark matter candidates are still very much alive!

With the indications by the Soviet-American Gallium Experiment[38] that the pp solar neutrinos are also depressed, a fact which would be explained most likely by finite neutrino masses and the MSW effect, hot dark matter in the form of light neutrinos returns to the front scene. Three astrophysical arguments had previously disfavored this hypothesis. If neutrinos were the only constituents of dark matter and no additional seeds for structure growth were present, it would be difficult to explain galaxy formation[35] as primordial density fluctuations are erased by neutrino streaming below a scale of 40 $h^{-1}$ Mpc. The larger structures would have

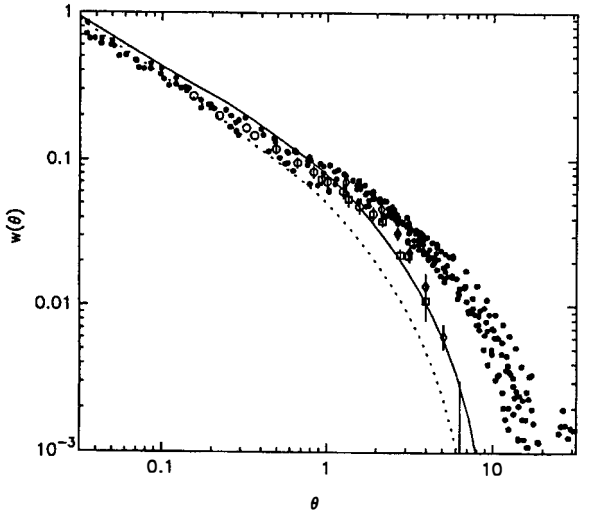


Figure 12
Comparison of the angular correlation function w(θ) obtained by the APM survey with the previous results from the Lick Survey (open symbols) and the usual cold dark matter models. They fail to describe the data at large angular separation. (From Maddox *et al.*, 1990.)

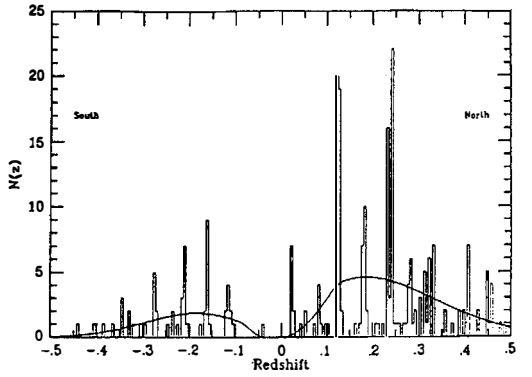


Figure 13
Distribution of galaxies as a function of redshift along several deep pencil beams. (From Broadhurst *et al.*, 1990.)

formed first with the galaxies originating from instabilities inside large pancakes. In addition, the velocity of cosmological neutrinos of 25 eV mass and 2 K temperature would be larger than the escape velocities of most galaxies, and they could not congregate into galactic halos. Moreover, for smaller galaxies (dwarf spheroïdals), the halos appear too compact to be compatible with the observed velocity dispersion and the maximum phase space density expected for initially non-degenerate Fermi-Dirac particles[39]. These arguments can be circumvented by assuming at least one additional element: a two component dark matter (e.g hot+cold, or hot+baryonic) or topological singularities seeding galaxy formation[40].

The picture arising from the astrophysical study of large scale structure is therefore still uncertain. Tension between the simplest models and the observations is increasing, and we may soon witness some major rearrangement of paradigms. In any case, it is clear that we need more data, in the form of more precise velocity flow measurement on a large number of galaxies, and larger redshift surveys, in particular at high redshift when the structure is forming. The planned Million Galaxy Redshift Survey and the proposed pencil beam studies at the Keck promise to provide such crucial information.

3.2.2 Direct searches for non-baryonic dark matter

A very complementary approach is to attempt to directly detect non-baryonic dark matter in the form of particles. Three such candidates are well motivated within the framework of particle physics: massive light neutrinos, axions and weakly interacting massive particles.

Unfortunately no experimentally viable method has yet been proposed[41] so far for the direct detection of cosmological *light neutrinos* of mass of about 25 eV. We will require laboratory measurements of the neutrino mass for the *three* neutrino generations to fully test this hypothesis. The detection of a large number of neutrinos from distant supernovae could eventually provide interesting direct mass limits (>100 eV). A 17 keV neutrino, recently suggested by a number of experiments, cannot directly form dark matter as it has to be unstable not to overclose the universe. If its existence is confirmed, however, it may modify considerably the theoretical framework in which the dark matter problem (and the solar neutrino puzzle) have to be solved.

*The axion*, a very light (mass of about $10^{-3}$ eV to $10^{-6}$ eV) pseudoscalar particle, still represents the best solution to the strong CP problem of QCD. A combination of laboratory experiments and astrophysics measurements, such as the lifetime of red giant stars and the energy observed in neutrinos from the supernova 1987A, have considerably restricted the range of parameter space. It still covers, however, the region in which axions can constitute dark matter. The weakness of the axion interactions make them extremely difficult to detect. Figure 14 gives the current limits obtained by the Brookhaven-Fermilab-Rochester group[42] and by the University of Florida team[43]. They can only exclude couplings which are a few hundred times larger than commonly predicted[44]. Two ideas are being proposed to get the needed sensitivity gain: using the large magnets of the MBF at Livermore[45] or trying to use the large coupling of axions to

electrons through some kind of collective phenomena (e.g. magnetic waves in the medium[46]).

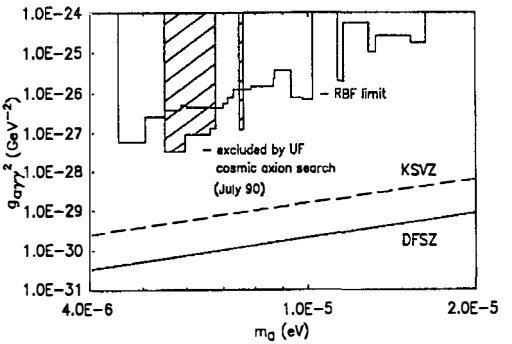


Figure 14
Experimental limit on the electromagnetic coupling $g_{a\gamma\gamma}$ of the axion. Also shown is the limit obtained by the Brookhaven-Fermilab-Rochestester collaboration. The solid and dashed straight lines are the theoretical values of $g_{a\gamma\gamma}$ for the DFSZ axion and the KSVZ axion ($E/N = 0$).

The *Weakly Interacting Massive Particles* (WIMPs) are a general form of dark matter. If a species of dark matter particles had been once in thermal equilibrium with the rest of matter, its density today is proportional to the inverse of its annihilation rate at the time it dropped out of equilibrium[47]. In order to obtain a density close to the critical density, the interaction comes out to be of the order expected for Weak Interactions, as if the physics at the scale of the W and the Z vector bosons was also responsible for dark matter. It may be a numerical coincidence (it presumably is!), or it may be a deep hint that something like supersymmetry may be responsible for dark matter. In any case, we have to check! We should, however, emphasize that this weak interaction strength is a general property independent of the particular model, hence the name given to these hypothetical particles. Within a specific model, it is possible to relate the interaction rates responsible for the thermal equilibrium in the early universe to the elastic scattering rate of this dark matter contained in the halo of our galaxy with a suitable target in the laboratory. These rates are quite low, ranging from a few hundred interactions per kilogram per day for heavy Dirac neutrinos on a germanium target of the order of 0.1 events per kilogram per day on silicon 29 for a neutralino of some 20 GeV[48]. The energy deposition distribution is completely fixed by the fact that the scattering is in the s-wave, and is unfortunately at best a few keV. The detection of the WIMPs represents therefore a formidable experimental challenge. The experimental teams involved have been employing a dual strategy. At the same time, these groups have been converting existing double beta decay experiments to push down their threshold and look at the low end of their energy spectrum for the roughly exponential

contribution expected from WIMPs, and they are developing new technologies based on the novel "cryogenic detectors" using phonons or broken Cooper pairs in materials at very low temperature. All three collaborations involved[49] in the first effort agree that Dirac neutrino of a mass greater 10 GeV/$c^2$ and smaller than some 6 TeV/$c^2$ cannot be the *sole* dark matter of the halo of our galaxy. If this is combined with the LEP results which exclude any Dirac neutrino between 35 MeV/$c^2$ (the upper bound for the $\nu_\tau$ mass) and ≈45 GeV/$c^2$, heavy Dirac neutrinos basically cannot form the bulk of the dark matter in the halo. By using small silicon detectors, the Berkeley-Santa Barbara group[50] also put severe limits on Cosmions[51], those particles suggested to explain, in addition to dark matter, the deficit of $^8$B solar neutrinos!

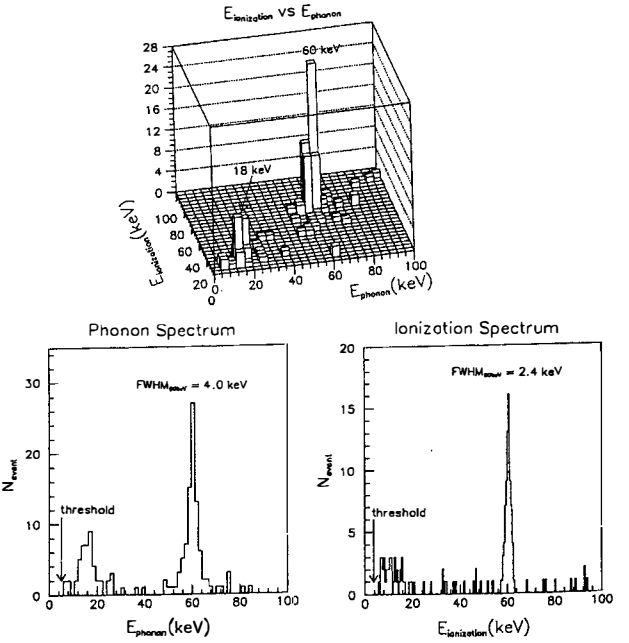


Figure 15
Simultaneous measurement of ionization charge and phonons for 60 keV and 18 keV photons in a 60 gram germanium crystal at 30mk [Berkeley]. The events off the diagonal are due to pile-up in our still primitive electronics.

On the development front of cryogenic detectors, great strides have been made recently with several groups now experimenting with detectors of a few tens of grams[52], and the technology advances fairly quickly. As an example of this progress, Figure 15 displays the

present results obtained at Berkeley in a 60 g detector operated at 30 mK[53]. This represents the first demonstration in a large crystal of the possibility of simultaneously detecting ionization charge and phonons. Such a method opens the possibility of simultaneously measuring the ionization yield and the total energy released in the interaction, and therefore differentiating between electron recoils, which represent our main background and our signal, nuclear recoils, which should have a much lower ionization yield. The current resolution at 60 keV is 2.4 keV and 4 keV FWHM (total energy) in the ionization and phonon channels respectively. The resolution per unit mass obtained in the phonon channel is the best one achieved so far by any group working on massive low temperature calorimeters (Figure 16), although Coron and collaborators are not far behind. Although these results are still rather crude, they represent an existence proof that cryogenic detectors have nearly reached (within a factor of three) the performance necessary for a successful dark matter search.

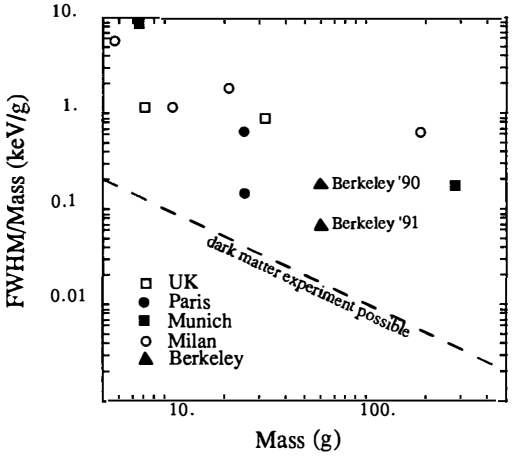


Figure 16
Resolution per unit mass obtained by all the groups working on massive calorimeters. This is the relevant figure of merit when the sensor sensitivity is the limiting factor.

Meanwhile, accelerator experiments have not been idle, and have constrained the properties of these potential weakly interacting massive particles[54]. In particular, no direct evidence has yet been obtained for supersymmetry, which remains the most attractive model. This pushes the supersymmetry scale somewhat higherthan previously thought, and although the lower limits on the mass of the lightest supersymmetric particles are model dependent[55], higher masses are favored. For those higher values, the energy deposition is then relatively large, but

as the mass increases, the expected rates decrease. This modifies slightly the experimental strategy which has to focus more on a low rate capability and background rejection rather than very low thresholds. However, this does not decrease in any way the high scientific priority of searches for WIMPs. A small extrapolation of the current technology, developed with cryogenic detectors, may allow us to reach sensitivity gains which will allow us to probe in the coming years an interesting region of the neutralino parameter space.

## 4 CONCLUSION

Dark matter is an example of the fascinating connections between the infinitely large and infinitely small. Beautiful pages have been written on the subject by Blaise Pascal[56] in the 17th century. They were, however, speculations mostly based on intuition. Modern cosmology and particle astrophysics are beginning to probe experimentally these connections, and the coming years will be particularly exciting, with qualitatively new data being gathered by detailed studies of large scale structure and the direct searches for dark matter, including the MACHOs and the WIMPs. These data are likely to increase even more the tension growing between the observations and our models, and this is likely to lead us to substantial changes in our paradigms. It may even lead, if dark matter can indeed be shown to be non-baryonic, to the ultimate Copernican revolution[57]: not only we are not at the center of the universe, but we may not even made of the same stuff as most of the universe!

### Acknowledgments

This review draws very much from many conversations with my colleagues, especially those of the Center for Particle Astrophysics. It is through constant interactions with them that I learned the astrophysics aspects of the problem, and developed a picture of the field. However, I bear the responsibility for errors and inaccuracies of this text.

This work was supported by the Center for Particle Astrophysics, a National Science and Technology Center operated by the University of California under Cooperative Agreement no. ADT-8809616.

### References

1] Zwicky, F., *Helv. Phys. Acta,* **6**, 110, (1933).

2] Faber, S.M., and Gallagher, J.S., *Ann. Rev. Astron. Ap.,* **17**, 135, (1979); Trimble, V., "Existence and Nature of Dark Matter in the Universe," *Ann. Rev. Astron. Ap.,* **25**, 245, (1987).

3] Rubin, V.C. *et al., Ap. J.,* **238**, 471, (1980).

4] Forman, W., and Jones, C., *Ann. Rev. Astron. Ap,* **20**, 547, (1982).

5] See e.g. Cowie, L.L., Henriksen, M., Mushotzky, R., "Are the Virial Masses of Clusters Smaller Than We Think?," *Ap. J.*, **317**, 593, (1987).

6] Tyson, J.A., Valdes, F.,Wenk, R.A., "Detection of Systematic Gravitational Lens Galaxy Image Alignments: Mapping Dark Matter in Galaxy Clusters," *Ap. J. Lett.,* **349**, L1, (1990).

7] Milgrom, M., and Bekenstein, J., in *Dark Matter in the Universe,* Kormendy, J.; Knapp, G.R., Edits, 1986, -Reidel, Dordrecht-, 319, (1986); Milgrom, M., *Ap. J.,* **270**, 365, (1983); Sanders, R.H., *Astron. Ap Lett.,* **136**, L21, (1984); Sanders, R.H., *Astron. Ap.,* **154**, 135, (1985).

8] Dar, A., Preprint 1991.

9] Spergel, D. Princeton University preprint 1991.

10] Weinberg, S., "Gravitation and Cosmology," (1972); Kolb, E.W., Turner, M.S., *The Early Universe,* Addison-Wesley, Redwood City, California, (1990).

11] Guth, A., *Phys. Rev.,* **D23**, 347, (1981); Linde, A. D., "Chaotic Inflation", *Phys. Lett.,* **129B**, 177, (1983); Albrecht, A., and Steinhardt, P.J., "Cosmology for Grand Unified Theories with Radiatively-Induced Symmetry Breaking", *Phys. Rev. Lett.,* **48**, 1220, (1982).

12] Huchra, J., and Geller, M., *Science,* **246**, 891, (1989).

13] Dresler, A., Faber, S.M., Burstein, D., Davies, R.L., Lynden-Bell, D., Tervelich, R.J., and Wegner, G., "Spectroscopy and Photometry of Elliptical Galaxies: A Large Streaming Motion in the Local Universe," *Ap. J. Lett.,* **313**, L37, (1987); Dressler, A., Lynden-Bell, D., and Burstein, D. *et al., Ap. J.,* **313**, 42, (1987).

14] Strauss, M.A., and Davis, M., "A Redshift Survey of IRAS Galaxies," in *Proceedings of IAU Symposium No. 130, Large Scale Structure of the Universe,* Balaton, Hungary, June, 1987; Davis, M., Strauss, M.A., Yahil, A., "A Redshift Survey of Iras Galaxies: III Reconstruction of the Velocity and Density Fields," *UCB/SUNY/Cal Tech,* (July, 1990); Saunders, W. *et al.,* "The Density Field of the Local Universe," *Nature,* **349**, 32, (1991).

15] Peebles, P.J.E., "The Large Scale Structure of the Universe" Princeton University Press, (1980), section 14.

16] Bertschinger, E., and Dekel, A., *Ap. J. Lett.,* **336**, 15, (1990); Dekel, A., Berstchinger, E., and Faber, S.M., *Ap. J.,* **364**, (1990); Bertschinger, E., Dekel, A., Faber, S.M., Dressler, A., and Burstein, D., *Ap. J.,* **364**, (1990).

17] Yahil, Talk at the 14th Texas Symposium, Brighton, (1990).

18] Sandage, A., *Physics Today,* **34**, (1970).

19] Pennypacker, C. *et al.,* in preparation, (1991).

20] Norgaard-Nielsen, H.U. *et al., Nature,* **339**, 523, (1989).

21] Cowie, L.L., "Galaxy Formation and Evolution," to appear in *Physica Scripta,* (1990) and Gardner, J.P. "Visible and Near Infrared Galaxy counts," in these proceedings. The evolution calculations have been made following the prescription of Yoshii, Y., and Takahara, F., *Ap. J.,* **326**, 1, (1988).

22] Loh, E. and Spillar, *Ap. J.,* **303**, 154, (1986), *Ap. J. Lett.,* **307**, L1, (1988); Loh, E., *Ap. J.,* **329**, 24, (1988).

23] Caditz and Petrosian, *Ap. J. Lett.,* **337**, L65, (1989).

24] Bahcall and Tremaine, *Ap. J. Lett.,* **326**, L1, (1988).

25] Omote and Yoshida, *Ap. J.,* **361**, 27, (1990).

26] Yang, J. *et al.,* "Primordial Nucleosynthesis: A Critical Comparison of Theory and Observation," *Ap. J.,* **281**, 493, (1984). See the recent reviews by Olive, K.A., Schramm, D.N., Steigman, G., and Walker, T., *Phys. Lett.,* **B426**, (1990), Denegri, D., Sadoulet, B., and Spiro, M., "The Number of Neutrinos Species," *Rev. of Modern Physics,* **62**, 1, (1990), and Olive, K.A., "The Quark Hadron Transition in Cosmology and Astrophysics," *Science,* **251**, 1194, (1991).

27] Surki-Suonio, H., Matzner, R.A., Olive, K.A., and Schramm, D.N., *Ap. J.,* **353**, 406, (1990).

28] Gunn, J.E., and Peterson, B.A., *Ap. J.,* **142**, 1633, (1965).

29] Mather, J.C. *et al., Ap. J. Lett.,* **354**, L37, (1990).

30] See e.g. De Zotti,"The x-ray background spectrum" in these proceedings
31] Carr, B., and Primack, J.R., *Nature,* **345**, 478, (1990).
32] Pazcinski, B., "Gravitational Microlensing by the Galactic Halo," *Ap. J.*, **304**, 1, (1986); Griest, K., "Galactic Microlensing as a Method of Detecting Massive Compact Halo Objects," *Ap. J.*, **366**, 412, (1991).
33] see, for instance, Primack, J.R., "Dark Matter, Galaxies, and Large Scale Structure in the Universe," *Lectures Presented at the International School of Physics" Enrico Fermi" Varenna, Italy, June 26-July 6, 1984,* SLAC-PUB-3387, (1984).
34] Peebles, P.J.E., *Nature,* **327**, 210, (1987).
35] White, S.D.M., Frenk, C.S., Davis, M., and Efstathiou, G., *Ap. J.,* **313**, 505, (1987); Frenk, C.S., White, S.D.M., Efstathiou, G., and Davis, M., *Ap. J.,* **351**, 10, (1990).
36] Maddox, S.J. *et al.*, "Galaxy Correlations on Large Scales," *Nature,* (1990).
37] Broadhurst, T.J., Ellis, R.S., Koo, D.C., and Szalay, A.S., *Nature,* **343,** 726-728, (1990).
38] Gavrin, V., in *Proceedings of the Geneva Conference on Neutrinos,* 1990, and Wilkerson, J., private communication.
39] Tremaine, S.D., and Gunn, J.E., *Phys. Rev. Lett.,* **42**, 407, (1979); Spergel, D.N., Weinberg, D.H., and Gott III, J.R., "Can Neutrinos be the Galactic Missing Mass?," Princeton Univ. Observatory preprint, (1988).
40] See e.g. Vilenkin, A., "Cosmic Strings and Domain Walls," *Phys. Rep.,* **121**, 263, (1985); Turok, N., *Phys. Rev. Lett.,* **63**, 2625, (1989); Turok, N., and Spergel, D.N., *Phys. Rev. Lett.,* **64**, 2736, (1990).
41] Smith, P.F., and Lewin, J.D., *Physics Reports*, **187**, 203, (1990).
42] DePanfilis, S. *et al.*, "Limits on the Abundance and Coupling of Cosmic Axions at 4.5<ma<5.0meV," *Phys. Rev. Lett.,* **59**, 839, (1987); DePanfilis, S. *et al., Phys. Rev.,* **D40**, 3153, (1989).
43] Hagmann, C.A., "A Search for Cosmic Axions," University of Florida/thesis, (1990).
44] KSVZ (Hadronic): Kim, J.E., *Phys. Rev. Lett.,* **43**, 103, (1979); Shifman, M.A., Vainshtein, A.I., and Zakharov, V.I., *Nucl. Phys.,* **B166**, 493, (1980); DFFSZ: Dine, M., Fischler, W., and Srednicki, M., *Phys. Lett.,* **104B**, 199, (1981); Zhitniskii, A.P., *Sov. J. Nucl. Phys.,* **31**, 260, (1980).
45] Sikivie, P. *et al.*, "Experimental Search for Dark Matter Axions in the 0.6-16μeV Mass Range," Proposal to DOE, (1990).
46] See e.g. Caspers, F., Semertzidis, Y., "Ferri-Magnetics Resonance, Magnetostatic Waves and Open Resonators for Axion Detection;" Vorobjev, P.V., Kolokolov, I.V., and Fogel, V.F., "The Ferromagnetic Detector of (Pseudo) Goldstone Bosons," *Preprint Novosibirsk,* **89-87**, (1989).
47] See e.g. Lee, B.W., and Weinberg, S., "Cosmological Lower Bound on Heavy-Neutrino Masses," *Phys. Rev. Lett.,* **39**, 165, (1977). For a discussion of the generality of the argument see: Griest, K., and Sadoulet, B., "Model Independence of Constraints on Particle Dark Matter," in *Proceedings of the Second Particle Astrophysics School on Dark Matter,* Schramm, D. and Galeotti, P., Edit., Erice (Italy), March 1988, in press -Fermilab Preprint FERMILAB-Conf-89/57A-, (1989).
48] Primack, J.R., Seckel, D., and Sadoulet, B., "Detection of Cosmic Dark Matter," *Ann. Rev. Nucl. Part. Sci.,* **38**, 751, (1988); and Smith, P.F. and Lewin, J.D., refer. 39.
49] Ahlen, S.P. *et al.*, "Limits on Cold Dark Matter Candidates from an Ultralow Background Germanium Detector," *Phys. Lett. B,* **195**, 603, (1987), and Avignone, F. and Morales, A. private communication; Caldwell, D.O., Eisberg, R.M., and Grumm, D.M. *et al.*, "Laboratory

Limits on Galactic Cold Dark Matter," *Phys. Rev. Lett.*, **61**, 510, (1988) and private communication; Reusser, D. *et al.*, "Limits on Cold Dark Matter from the Gotthard Germanium Experiment," *Phys. Lett.*, **B235**, 143, (1991).

50] Caldwell, D.O. *et al.*, "Searching for the Cosmion by Scattering in Si Detectors," *Phys. Rev. Lett.*, **65**, 1305, (1990).

51] Gilliland, R.L., Faulkner, J., Press, W.H., and Spergel, D.N., "Solar Models with Energy Transport by Weakly Interacting Particles," *Ap.J.*, **306**, 703, (1986) and references therein.

52] Seidel, G. *et al.*, in *Proceedings of the Third European Workshop on Low Temperature Detectors for Neutrinos and Dark Matter*, Gran Sasso, Sept. 89, in press, (1989); Alessandrello, A., Camin, D.V., Fiorini, E., and Giuliani, A., "Construction of a massive germanium thermal detector for experiments on rare decays," *Phys. Lett. B*, **202**, 611, (1988); Coron, N. *et al.*, "Thermal Spectrometry of Particles and γ-rays with Cooled Composite Bolometers of Mass up to 25 Grams," in *Proceedings of the Conference on Superconducting and Low Temperature Particle Detectors*, Waysand, G.; Chardin, G., Strasbourg, 1988, Elsevier Sc., Amsterdam, (1989); Cummings, A., Wang, N., Shutt, T., Barnes, P., Emes, J., Giraud-Heraud, Y., Haller, E.E., Lange, A.E., Rich, J., Ross, R.R., Sadoulet, B., Smith, G., and Stubbs, C., "Performance of a 60 gram Cryogenic Germanium Detector," accepted for publication in *IEEE Trans. in Nucl. Sci.*, (1991).

53] Shutt, T. *et al.*, in preparation.

54] See, for instance, Ellis, J. *et al.*, *Phys. Rev. B*, **245**, 251 (1989).

55] Griest, K., 1991, CfPA-TH-91-001, to appear in *Proceedings of UCLA Conference on Trends in Astroparticle Physics, Dec. 1990.*

56] Pascal, B., "Les Pensées," #347, 348, 352 in *Oeuvres Complètes*, Bibliothèque de la Pléiade, NRF, Paris 1954.

57] Courtesy of J. Primack.

# X-RAY AND γ-RAY EXTRAGALACTIC BACKGROUND RADIATION

# THE X-RAY BACKGROUND

G. De Zotti[1], J.M. Martín-Mirones[1,2], A. Franceschini[1], and L. Danese[3]

[1]Osservatorio Astronomico, Padova, Italy

[2]Departamento de Física Moderna, Universidad de Cantabria, Santander, Spain

[3]Dipartimento di Astronomia, Padova, Italy

## ABSTRACT

COBE measurements of the microwave background spectrum have ruled out a truly diffuse origin of the X-ray background (XRB). Several independent lines of argument converge in indicating that cosmological evolution is definitely required to account for the XRB; the contribution of local, non-evolving sources is $< 50\%$ and probably $\simeq 20$–$30\%$. Stellar nucleosynthesis is unlikely to be the primary energy source: due to the relative inefficiency in producing high energy photons, there are severe problems with the energy budget as well as with the observational limits on the intensity of the extragalactic background at IR to mm wavelengths. Activity of galactic nuclei remains the strongest candidate, although "canonical" AGN's have a too soft X-ray spectrum; a most interesting possibility are nuclei characterized by strong photoelectric absorption, putting out the bulk of their X-ray emission above $\approx 10$ keV. A reliable estimate of the contribution to the XRB of "canonical" AGN's is made difficult by our poor knowledge of their evolution properties as well as by the complexity and diversity of their X-ray spectra. On the other hand, measurements of the XRB and counts in different X-ray bands provide valuable constraints on the evolution properties of these sources. Anisotropies of the XRB carry information on the large scale structure of the universe. Analyses of HEAO-1 A2 and *Ginga* data yield bounds on clustering of rich clusters of galaxies and of AGN's consistent with optical data. Recent upper limits on the autocorrelation of intensity fluctuations at arcmin scale in the *Einstein Observatory* IPC band suggest that the clustering length of sources of the XRB may be smaller than that of normal galaxies.

## 1. Introduction

Almost 30 years after its discovery[1], the extragalactic X-ray background (XRB) continues to be a fascinating topic to work on. Its origin is still a challenging problem and very interesting links are emerging with a variety of astrophysical and cosmological problems. On one hand, recent measurements[2] of the far-IR and sub-mm background have ruled out the possibility that the XRB is originated by a hot, dense intergalactic medium (see § 3) and have set interesting constraints on the possible contribution to the XRB from active star forming galaxies (see § 5).

On the other hand, the isotropy of the XRB has significant implications for the space distribution of the main classes of extragalactic X-ray sources (§ 7) and, in particular, of active galactic nuclei (AGN). Also, measurements of the XRB are providing valuable pieces of information on the AGN evolution. It seems likely that a new class of AGN's (or a different evolutionary stage of conventional AGN's), possibly highly obscured by surrounding cold material is required to account for the XRB spectrum (§ 6).

## 2. Observed properties

### *2.1 Spectrum*

As is well known, the spectrum of the extragalactic X-ray background (XRB) has been accurately measured by the A2 experiment on HEAO-1 in the energy range 3–50 keV[3]. It was found to be very smooth and remarkably close to a "thermal" spectrum[4]:

$$dI/dE \simeq 5.6[E/(3\,\mathrm{keV})]^{-0.29} \exp(-E/W)\ \mathrm{keV\,keV^{-1}\,cm^{-2}\,s^{-1}\,sr^{-1}}, \qquad (1)$$

where $W = 40\,\mathrm{keV}$.

At higher energies, up to at least 500 keV, the data are described by a power law of energy index 1.8[5]. The local energy density of the 3–500 keV background is $\epsilon_{XRB} \simeq 5.2 \times 10^{-5}\,\mathrm{eV\,cm^{-3}} \simeq 8.4 \times 10^{-17}\,\mathrm{erg\,cm^{-3}}$, almost four orders of magnitude below the energy density of the microwave background ($\epsilon_{MWB} \simeq 0.26\,\mathrm{eV\,cm^{-3}}$).

In this review, we will concentrate, as usual, primarily on the 3–50 keV band, where the XRB spectrum is best known and most (about 71%) of the energy resides.

Below 3 keV the extragalactic flux becomes increasingly uncertain. In the 1–3 keV range the total observed intensity might be about 30% higher than an extrapolation of the 3–10 keV spectrum[6,7]; the excess, if real, may be of either galactic or extragalactic origin. Constraints on the intensity in this range provide interesting limits on the contribution to the XRB from active galactic nuclei whose X-ray spectra are softer than the background[8]. At still lower energies, the extragalactic contribution is essentially unknown; the poorly determined galactic emission could well be dominant also at high galactic latitudes[6].

### *2.2 Isotropy*

Albeit its intensity is small ($\simeq$ 2% of the 2–50 keV XRB at high galactic latitudes[9]) the galactic emission is responsible for most of the observed large scale anisotropies. However, after having

excluded the regions close to the galactic equator, a residual dipole anisotropy, repeating for the independent surveys carried out with HEAO-1, shows up[4),10),11)]. Within the (relatively large) uncertainties, the amplitude and the direction of the dipole are consistent with the velocity vector inferred from microwave measurements. The spectrum of the XRB dipole is also consistent with that expected from a Compton-Getting effect, and is inconsistent with an interpretation in terms of anisotropies of the unresolved galactic emission[4)].

The small scale fluctuations measured by the A2 experiment on HEAO-1 on scales of 9–25 square degrees ($\simeq$ 6% on a scale of 9 square degrees[12)]) are consistent with those expected from discrete sources below the detection limit; a 90% confidence upper limit of 2.3% for an effective solid angle of 25 square degrees was set on any additional contributions[10),11)]. Weak ($\simeq 3\sigma$) evidence for excess fluctuations on an effective scale of 2 square degrees was recenly reported[13)].

Analyses[79),80),81)] of fluctuations on arcmin scales for several deep *Einstein Observatory* IPC fields have allowed to constrain the counts of unresolved X-ray sources. The recent study by Soltan[81)], carefully accounting for instrumental effects, does not confirm the earlier conclusions[79),80)] that the $\log N$–$\log S$ curve must flatten just below the deep survey limit; a flattening of the counts is, however, observed in deep ROSAT images[95)].

More direct information on clustering of X-ray sources may be obtained from the *autocorrelation function* of intensity fluctuations. No unambiguous signal has been reported so far. Upper limits of $\simeq 10^{-2}$ on

$$\Gamma(\theta) = |W(\theta)|^{1/2}, \quad \text{where} \quad W(\theta) = \frac{\langle \delta I \times \delta I' \rangle_\theta}{\langle I_{XRB} \rangle^2}, \tag{2}$$

for angular separations $\theta \simeq 2$–$3^\circ$ have been derived from both A2 data[13)] and from *Ginga* data[14)]. Upper limits on larger angular scales (up to 27°) are higher by factors of 2–3[15),16)]. Carrera et al.[14),16)] report some indications of a negative $W(\theta)$ at angles between 3° and 6° and between 7° and 14°. A weak ($2\sigma$) indication of a negative $W(3^\circ)$ is also seen in A2 data[13)].

Analyses of deep IPC fields[96),81)] have yielded tight constraints on the autocorrelation function at arcmin scales. Soltan[81)] finds $W(\theta) < 2.9 \times 10^{-3}$ for scales of 2′–5′.

### 3. Hot intergalactic medium and the XRB

As already mentioned, the recent COBE measurements[2)] (see also[17)]) have ruled out a truly diffuse origin of the XRB. In fact, a *homogeneous* hot intergalactic medium (IGM) capable of accounting for the XRB would have produced a substantial sub-mm excess in the spectrum of the microwave background[18),19),20),21),22)], in strong contradiction with COBE data. In the case of non-relativistic electrons of temperature $T_e$, the distorted microwave background spectrum is characterized by a value of the comptonization parameter $y \simeq (kT_e/m_ec^2)\tau_e \approx 10^{-2}$ ($\tau_e$ being the optical depth of the IGM for Thomson scattering), while COBE data imply $y < 10^{-3}$ ($3\sigma$ limit[2)]). It follows that the contribution of a homogeneous IGM to the XRB cannot exceed a few percent ($y \propto n_e$, IGM emissivity $\propto n_e^2$). Similar constraints are obtained if electrons are relativistic.

Strong clumping of the IGM may decrease $y$ below the COBE limit, but the high values of $T_e$ required to account for the XRB spectrum unavoidably entail[23),24),25)]:

- excessive microwave fluctuations due to comptonization in the clumps [Sunyaev-Zeldovich effect; the most stringent upper limits on scales ranging from $\simeq 1'$ to several degrees are (see e.g.[26)]) at a level $\Delta T/T \lesssim 3 \times 10^{-5}$], and/or
- excessive X-ray fluctuations, and/or
- too many optically unidentified X-ray sources, and/or
- too many deep potential wells causing gravitational lensing of quasars, and/or
- serious confinement problems.

Nevertheless, an important contribution to the soft ( $\lesssim 10$ keV) XRB might come from high density transient clumps heated by large-scale shocks during non linear pancake formation[27)]. Conversely, observations of the soft XRB constrain large scale dissipative processes as well as the baryon density involved in dissipational structure formation[25),28)].

Well known clumps of gas, associated to clusters of galaxies, have typical temperatures $<$ 10 keV; their estimated contribution to the 2–10 keV XRB, without evolution, is $\simeq 5\%$[29)]. X-ray counts of these sources are flat[30)], suggesting negative evolution[31),32)].

No clear evidence has been found of a significant contribution from intra-supercluster gas[33)], although preliminary results of *Ginga* suggest the presence of extended, low-surface-brightness halos in some peripheral supercluster regions[34)].

### 4. XRB from non-evolving sources

If the power-law representation of the X-ray local luminosity function (XLLF) of AGN's[29)] is extrapolated by a factor $\simeq 10$ downward in luminosity, these sources would saturate the XRB intensity without evolution. However, a detailed analysis of the HEAO-1 A2 database[35)] led to the conclusion that the contributions to the XLLF of sources associated to galaxies is well below such extrapolation. Sources with $L_X(2\text{–}10\,\mathrm{keV}) < 10^{42}\,\mathrm{erg\,s^{-1}}$ cannot produce more than 10–15% of the XRB, without evolution.

A similar conclusion follows from constraints on the autocorrelation function of XRB intensity fluctuations[36)]. The contribution of non evolving X-ray sources to $\Gamma(\theta)$ [eq. (2)] is proportional to their volume emissivity [see eq. (6)]. The observational constraints on $\Gamma(\theta)$ imply that local sources clustered like galaxies cannot account for more than $\simeq 50\%$ of the XRB.

Miyaji and Boldt[37)] showed that X-ray emission is a strong tracer of mass. Then, the observed dipole moment and the observed peculiar velocity of the local group allow to set a tight constraint on the global X-ray volume emissivity of local sources (basically, once the mass/X-ray luminosity ratio has been determined, the limit on the mass density following from dynamical arguments translates into a constraint on the global X-ray luminosity density). Boldt[38)] finds that all possible

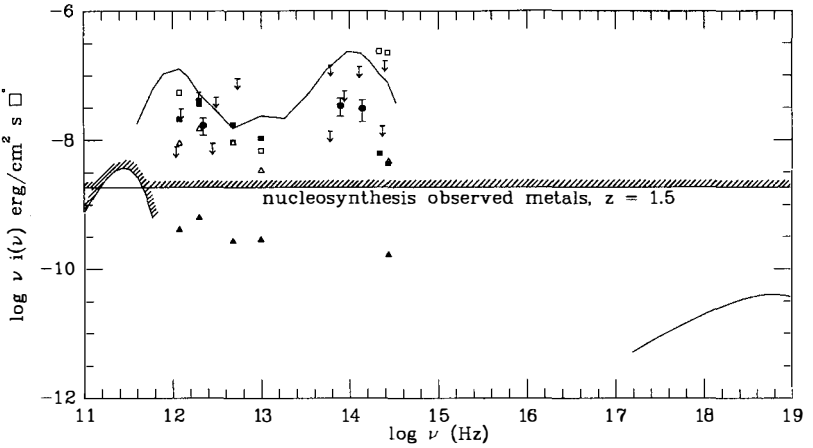


**Figure 1.** Constraints on the broadband spectra of sources of the XRB from data on the extragalactic background at IR to mm wavelengths. The horizontal line shows the upper limit on the light expected from stellar nucleosynthesis[40], assumed to occur at an effective redshift of 1.5. The dots with error bars and the arrows show the current estimates or upper limits on the extragalactic near- and far-IR background as summarized by Hauser et al.[41]. The DIRBE upper limits correspond to the total observed sky brightness in a dark direction plus the $1\sigma$ error; no attempt has been done to subtract the, probably dominant, foreground light. The shaded line on the left hand side shows the upper limit following from the absence of observable distortions in the microwave background spectrum (the internal uncertainty of COBE/FIRAS measurements was taken to be 10 mK). The curve on the lower right hand corner represents the spectrum of the XRB. The upper solid curve shows the broadband spectrum of the Milky Way[42], redshifted to $z = 1.5$ and normalized to the observed XRB intensity at $2/(1+z)$ keV. Data on four additional galaxies, redshifted and normalized in the same way are also shown: NGC 7714 (open triangles), NGC 5408 (filled triangles), M 82 (filled squares) and the LMC (open squares). X-ray data on the Milky Way and the LMC are from [56], on M 82 from [55]; multifrequency data on NGC 5408 and NGC 7714 are from [44] and [57], respectively.

populations not represented in the Piccinotti survey cannot make up more than 20% of the 2–10 keV XRB, without evolution.

A tighter limit has been most recently obtained by Jahoda et al.[39]. They have cross-correlated the 2–10 keV XRB fluctuations with the surface density of nearby galaxies; a significant correlation was found and an estimate of the X-ray emissivity of the local universe was derived, implying that unevolving X-ray sources correlated with nearby galaxies contribute $18 \pm 5\%$ of the XRB.

## 5. Can stellar nucleosynthesis be the primary energy source?

As illustrated by Fig. 1, energetics, per se, is not a problem. The present average density of metals in observed galaxies is estimated to be[40]: $3 \times 10^{-34} \lesssim \rho_z(\mathrm{g\,cm^{-3}}; H_0 = 50) < 10^{-33}$. If the bulk of stellar nucleosynthesis occurred at a redshift $z$, it would have produced a radiation energy density $2 \times 10^{-15}/(1+z) \lesssim \rho_z(\mathrm{erg cm^{-3}}) < 6 \times 10^{-15}/(1+z)$, more than one order of magnitude above

the energy density of the XRB if $z \approx 1$.

The main difficulty is the relatively low efficiency in producing high energy photons. It is clear from Fig. 1 that objects with far-IR/X-ray or optical/X-ray luminosity ratios similar to those observed for our own galaxy cannot make up more than a few percent of the XRB to be consistent with the nucleosynthesis constraint. Recent measurements of the diffuse near- and far-IR background directly constrain the contribution to the XRB of galaxies like our own to be $\lesssim 10\%$.

On the other hand, galaxies with intense star formation have enhanced X-ray emission (compared to normal galaxies), powered by supernovae and by X-ray binaries[43),44),45),46),47)]. Also, deep IRAS counts[48),49)] and VLA surveys at sub-mJy levels[50),51)] suggest substantial cosmological evolution of these sources[52),53)]. Firm estimates of the contribution of active star forming galaxies to the XRB are difficult because of their uncertain evolution properties. Extrapolations to X-rays of models accounting for both IRAS and sub-mJy counts suggest a contribution at 2 keV of $\lesssim$ 5–10%, and anyway not exceeding 30%[53),54)].

Still, the observed far-IR/X-ray or optical/X-ray luminosity ratios for starburst galaxies for which such comprehensive data are available are generally at least a factor of several too high to allow accounting for the bulk of the XRB without violating the nucleosynthesis constraint as well as upper limits on the IR background intensity (far-IR data on objects in Fig. 1 or quoted in the following are from [58),59),60)]). This is illustrated in Fig. 1 for the well known nearby starburst galaxy M 82 (the other nearby starburster, NGC 253, is a significantly less efficient X-ray emitter[55)]), as well as for the prototype starburst nucleus NGC 7714. The global spectral shape of the other well observed starburst nuclei, NGC 2782[61)] and the X-ray selected source MS0834.0+6517[62)] [so far, the only certain starburst galaxy in the Extended Medium Sensitivity Survey[30)] (EMSS)], is similar to that of NGC 7714 (note that, based on the quoted count rate, the flux at 2 keV of NGC 2782 given in Table I of Kinney et al.[61)] seems to be overestimated).

To our knowledge, the only exception is the small irregular galaxy NGC 5408, undergoing a violent burst of star formation, which has X-ray/optical and X-ray/far-IR luminosity ratios[44)] at least 20 to 30 times higher than any other starburst galaxy (see above and Fabbiano et al.[45)]). If a large fraction of the light from nucleosynthesis is emitted by objects of this kind, the XRB intensity could indeed be accounted for. On the other hand, galaxies with $L_X/L_{opt}$ as high as NGC 5408 must be rare, at least locally. The Piccinotti survey would have detected such sources down to $B \approx 12$ and the Deep Survey[63)] [covering $\approx$ 2.3 square degrees with a typical limiting sensitivity $S_X(0.8\text{–}3.5\,\mathrm{keV}) \simeq 5 \times 10^{-14}\,\mathrm{erg\,cm^{-2}\,s^{-1}}$] down to $B \approx 18.4$; the expected surface density of galaxies brighter than the quoted limits in the surveyed areas are $\simeq$ 70 and $\simeq$ 100; no galaxy like NGC 5408 was found. Such objects may correspond to a short lived stage in the galaxy evolution, characterized by a very low metallicity[44)] (the metallicity of NGC 5408 is $Z_\odot/14$). The Magellanic Clouds, having a metallicity higher than NGC 5408, but substantially lower than our own galaxy, have $L_X/L_{opt}$ not much different from the latter (X-ray data from Fabbiano[56)]; see Fig. 1).

Furthermore, spectral observations[55),64)] of the nearby starburst galaxies NGC 253, M 82 and M 83 suggest that the X-radiation from this population is significantly softer than the XRB.

## 6. Active galactic nuclei

### *6.1 Some puzzles*

The situation is rather confusing, with apparently contradictory observational information. On one hand AGN's dominate X-ray counts down to the faintest observed levels[30),63)] and thus certainly account for a substantial fraction of the XRB (at least 30–40% at 2 keV[65)]).

On the other hand, they have a "wrong" spectrum: in the 2–50 keV range Seyfert nuclei have an average spectral index $\alpha \simeq 0.7$ significantly steeper than that of the XRB[66),67)], and IPC data indicate even softer spectra for radio quiet quasars[68),69),101)].

HEAO-1[10)] and *Ginga*[70)] fluctuation analyses indicate a normalization of the source counts in the 2–10 keV or 4–11 keV bands a factor $\simeq 3$ above that derived from the *Einstein Observatory* EMSS (0.3–3.5 keV), *if* AGN's have a "canonical" X-ray spectrum ($\alpha = 0.7$ and negligible absorption). Strong photoelectric absorption ($N_H \sim 10^{22}$ cm$^{-3}$) may explain this result, and is consistent with the spectrum of XRB fluctuations observed by *Ginga*[70)].

EMSS AGN's, however, appear to have rather a *steeper* than canonical spectrum ($\alpha \simeq 1$[69)]). Soft X-ray excesses (above the canonical spectrum) are found to be a common feature of bright AGN's[67),68),71)].

Furthermore there seems to be an excess of a factor of $\approx 2$ between the quasar and Seyfert 1 nuclei predicted on the basis of the optical source counts and of the X-ray to optical luminosity ratios, and the number actually found in the *Einstein Observatory* MSS[72)]. A strong incompleteness of MSS counts seems excluded[73)]. Possible explanations have been discussed by Franceschini et al.[74)]; the problem, however, is still to be definitively settled.

### *6.2 Hard vs. soft X-ray emission of AGN's*

The above discussion suggests that strong selection effects are at work, probably due to the complexity and diversity of X-ray spectra of AGN's. In an attempt to quantify these effects, Martìn-Mirones et al.[75)] have carried out a statistical analysis of the distribution of the ratio $F_H/F_S = S(2\text{–}10\,\text{keV})/S(0.5\text{–}4.5\,\text{keV})$ for different AGN samples: the hard X-ray selected sample by Piccinotti et al.[29)], the EMSS AGN's brighter than $S(0.3\text{–}3.5\,\text{keV}) = 2 \times 10^{12}$ erg cm$^{-2}$ s$^{-1}$, the optically selected Seyfert sample defined by Cheng et al.[76)], the optically selected PG quasar sample[77)]. For a "canonical" AGN spectrum we expect $F_H/F_S \simeq 1$.

Except for the Piccinotti sample, 2–10 keV fluxes are available for only a few sources. Still, an estimate of the sample average $\langle F_H/F_S \rangle$ can be derived from the distribution of A2 count rates in the directions of the sources under study, using the method described by Persic et al.[35)].

AGN's from the EMSS were found to have $\langle F_H/F_S \rangle \simeq 0.6$, i.e. spectra substantially softer than the "canonical" spectrum, consistent with the results of the spectral analysis, within the IPC

band, by Maccacaro et al.[69]. Soft excesses are somewhat less frequent and/or somewhat weaker for PG quasars for which $\langle F_H/F_S\rangle \simeq 0.75$. For the optically selected Seyfert sample $\langle F_H/F_S\rangle \simeq 1.0$: soft excesses are still present, but many objects show strong photoelectric absorption (consistent with the findings of Reichert et al.[78]). The average $\langle F_H/F_S\rangle$ for the Piccinotti sample is $\simeq 1.85$. High absorbing columns ($N_H \sim 10^{22}\,\mathrm{cm}^{-2}$) are common; only a small fraction of Piccinotti sources show values of $F_H/F_S$ as small as those found for EMSS AGN's.

It follows that estimates of AGN contributions to the 3–50 keV XRB based on soft X-ray data must be treated cautiously. In particular, constraints derived from fluctuation analyses of deep IPC fields[79),80),81)] do not necessarily apply to sources of the hard (> 3 keV) XRB.

*6.3 XRB and AGN evolution*

An assessment of the total contribution of AGN's to the XRB is difficult because their evolution properties are still poorly understood. Nevertheless, important constraints follow from general arguments. On one side, we have a *mass constraint*[83]: pure luminosity evolution of AGN's accounting for the XRB entails, if $L_X/L_{bol} \simeq$ const, $(L_{bol}/L_{Edd})_{z=0} < 10^{-3}$, while the best current estimates[82),83),84)] yield $(L_{bol}/L_{Edd})_{z=0} \simeq 3\text{–}5 \times 10^{-2}$. A strong increase of $L_X/L_{bol}$ for higher $z$/higher $L$ AGN's seems hardly compatible with the available data; the observed decrease of the ratio $L_X/L_{opt}$ for higher $L$/higher $z$ quasars[100] rather points to the opposite direction.

There is also an *energy constraint*:[54] precursor AGN's[85], at an effective redshift $z_*$, making up a fraction $C_X$ of the XRB, should have a mean 2–10 keV luminosity

$$L_{2-10\,\mathrm{keV}}(z_*) \simeq 2.2\cdot 10^{45}\,\frac{C_X}{0.5}\,\frac{1+z_*}{4}\left(\frac{L_{bol}}{L_X}\right)_{z_*}\left(\frac{L_{bol}}{L_{Edd}}\right)_{z_*}\left(\frac{0.1}{\eta}\right)\left(\frac{4\cdot 10^{-4}}{n_0}\right)\ \mathrm{ergs}^{-1}. \qquad (3)$$

where $L_X$ is the total X-ray luminosity and the AGN spectrum has been taken to be similar to that of the XRB. Even if $(L_X/L_{bol})_{z_*} \simeq 1$ (for local AGN's $L_X/L_{bol} \simeq 0.12$[82)]), in the presence of a luminosity function not much narrower than the local one, we expect that a large number of precursor AGN's (characterized by an average $z \simeq z_*$) show up in the EMSS, unless they are strongly self-absorbed, and possibly even in the Piccinotti survey. Thus, the assumption of a strict continuity between "precursor" and local AGN's faces difficulties.

If the XRB is due to a burst of nuclear activity involving essentially all bright galaxies, they should host a currently inactive nucleus of average mass:

$$\frac{M_{nucl}}{M_\odot} \simeq 2\times 10^7\,\frac{C_X}{0.5}\,\frac{1+z_*}{4}\left(\frac{L_{bol}}{L_X}\right)_{z_*}\left(\frac{\eta}{0.1}\right)^{-1}\left(\frac{n_0}{10^{-3}}\right)^{-1}. \qquad (4)$$

Note that the mass and the energy constraints, taken together, favour a relatively low value of $z_*$.

*6.4 Strongly self-absorbed AGN's*

In previous sections several classes of X-ray sources have been discussed, which could, and possibly do, produce a significant, or even large, contribution to the XRB at 2 keV. They have a variety of

X-ray spectra, all of which, however, are *softer* than the XRB. The residual XRB spectrum, after subtraction of their contributions, must be very flat or turn down below $\approx 10$ keV. As pointed out by several authors [86),87),88)], such spectral shape may be accounted for by AGN's characterized by strong photoelectric absorption (column densities $N_H \approx 10^{24}$–$10^{25}$ cm$^{-2}$).

In the model proposed by Fabian et al.[87] the primary, power-law, AGN spectrum is reprocessed by dense and 'cold' ($T < 10^6$ K) gas surrounding the nuclei. X-rays below 10 keV are predominantly absorbed while Compton scattering steepens the spectral index above $\approx 120$ keV by about one. This leads to a "reflection hump" peaking at 30–50 keV with a break at $\approx 120$ keV, i.e. to a spectrum suitable for explaining the residual XRB, if the effective redshift of sources is $\approx 1.5$. A characteristic fluorescent iron emission line at 6.4 keV is predicted. Both the high energy hump and the iron line have indeed been found in *Ginga* spectra of several bright AGN's[89),90),91)]. Very interesting hints that the average broadband AGN spectrum flattens in the interval 12–40 keV and then steepens again in the range 40–166 keV were obtained from recent investigations of rms fluctuations observed by the HEAO 1 A-4 experiment in different energy bands[92)].

On the other hand, to fit the XRB spectrum, about 90% of the emitted flux must be reprocessed[87),93)]. Such large fraction puts significant constraints on the distribution of cold gas. The fraction of reprocessed flux inferred from *Ginga* spectra of AGN's is substantially lower ($\simeq$ 30–60%[94)]).

### 7. Constraints on large scale structures from XRB anisotropies

Jahoda and Mushotzky[99)] demonstrated that accurate measurements of the surface brightness distribution of the XRB on scales $\gtrsim 1000$ squares degrees can provide important information on nearby large mass concentrations such as the "Great Attractor".

In general, a large scale distribution pattern of extragalactic X-ray sources yields small scale anisotropies in excess of Poisson fluctuations and, of course, translates into power in the autocorrelation function of the extragalactic background brightness.

Assuming the usual parametrization of the two point spatial correlation function, $\xi(r) = (r/r_0)^{-\gamma}$ with $\gamma \simeq 1.8$, the contributions to the rms fluctuations, $\Gamma(0)$, and to autocorrelations on the angular scale $\theta$, $\Gamma(\theta)$, due to clustering of a given class of non-evolving sources are approximately given by[13)]:

$$\Gamma(0) \simeq 0.5 \times 10^{-2} \left(\frac{\omega_{eff}}{1.8 \text{ sq. deg}}\right)^{-0.2} \left(\frac{r_0}{50 \text{ Mpc}}\right)^{0.9} \frac{(j_{sources}/j_{XRB})_{z=0}}{0.04}, \quad (5)$$

$$\Gamma(\theta) \simeq 2.8 \times 10^{-3} \left(\frac{\theta}{3^\circ}\right)^{-0.4} \left(\frac{r_0}{50 \text{ Mpc}}\right)^{0.9} \frac{(j_{sources}/j_{XRB})_{z=0}}{0.04}. \quad (6)$$

where $\omega_{eff}$ is the effective solid angle of the detector ($\omega_{eff} \simeq 1.8$ sq. deg for the HEAO-1 A2 collimators, small field of view) and $j$ is the volume emissivity.

The above equations provide reasonable estimates (accurate to within a factor $\approx 2$) also in the case of evolving sources, provided that the ratio of volume emissivities is replaced with the global contribution to the XRB. A few points are worth noticing:

*i)* Excess fluctuations due to clustering show a substantially weaker dependence on the solid angle (so long as dilution effects are negligible) than Poisson fluctuations.

*ii)* The HEAO-1 A2 bounds are compatible with Bahcall and Soneira's[97] estimate of the correlation length scale of rich clusters.

*iii)* Much stronger constraints are obtained on the clustering properties of AGN's, which yield a much larger contribution to the XRB. The A2 constraints are consistent with optical estimates[98]. The weak ($\simeq 3\sigma$) evidence for excess fluctuations (i.e. fiuctuations above those expected if the counts keep the euclidean slope indicated by the *Einstein Observatory* surveys well below the limit of the A2 survey), reported by Martín-Mirones *et al.*[13], may imply that AGN's are indeed substantially clustered (the observed signal, however, may also be accounted for assuming slightly steeper counts). On the other hand, the tight upper limit on the amplitude of the correlation function derived by Soltan[81] from an analysis of IPC data implies that the correlation length of sources of the XRB (at least in the IPC band), must be significantly below that for normal galaxies.

*Acknoledgements* J.M.M.-M. acknowledges partial financial support from Comisión Mixta Caja Cantabria-Universidad de Cantabria (Spain); his stay at the Padova Astronomical Observatory was supported by the MEC grant EX90 13.741.993. The italian group acknowledges partial financial support by MURST, CNR (through GNA) and ASI.

## References

1)Giacconi, R., Gursky, H., Paolini, F., Rossi, B. 1962, *Phys. Rev. Lett.*, **9**, 139

2)Mather, J.C., *et al.* 1990, *Ap. J.*, **354**, L37

3)Marshall, F.E., Boldt, E.A., Holt, S.S., Miller, R.B., Mushotzky, R.F., Rose, L.A., Rothschild, R.E., & Serlemitsos P.J., 1980, *Ap. J.*, **235**, 4

4)Boldt, E.A. 1987, *Phys. Rep.*, **146**, 215

5)Gruber, D.E., Rothschild, R.E., Matteson, J.L., Kinzer, R.L. 1984, in *X-ray and UV Emission from Active Galactic Nuclei*, MPE rep. 184, p. 129

6)McCammon, D., Sanders, W.T. 1990, *Ann. Rev. Astr. Ap.*, **28**, 657

7)Wu, X., Hamilton, T., Helfand, D.J., Wang, Q. 1991, *Ap. J.*, in press

8)Fabian, A.C., Canizares, C.R., Barcons, X. 1989, *MNRAS*, **239**, 15P

9)Iwan, D., Marshall, F.E., Boldt, E.A., Mushotzky, R.F., Shafer, R.A., Stottlemyer, A. 1982, *Ap. J.*, **260**, 111

10)Shafer, R.A. 1983, Ph. D. thesis, University of Maryland

11)Shafer, R.A., Fabian, A.C. 1983, in *IAU Symposium 104, "Early Evolution of the Universe and its Present Structure"*, p. 333

12)Boldt, E.A. 1989, in *Large Scale Structure and Motions in the Universe*, Kluwer, p. 291

13)Martín-Mirones, J.M., De Zotti, G., Boldt, E.A., Marshall, F.E., Danese, L., Franceschini, A., Persic, M. 1991, *Ap.J.*, in press

14)Carrera, F.J., Barcons, X., Butcher, J., Fabian, A.C., Stewart, G.C., Warwick, R.S., Hayashida, K., Kii, T. 1991, MNRAS, in press

15)Persic, M., De Zotti, G., Boldt, E.A., Marshall, F.E., Danese, L., Franceschini, A., Palumbo, G.G.C. 1989, *Ap. J.*, **336**, L47

16)Carrera, F.J., Barcons, X., Butcher, J., Stewart, G.C., Warwick, Fabian, A.C. 1991, preprint

17)Gush, H.P., Halpern, M., Wishnow, E.H. 1990, *Phys. Rev. Lett.*, **65**, 537

18)Field, G.B., Perrenod, S.C. 1977, *Ap. J.*, **215**, 717

19)Guilbert, P.W., Fabian, A.C. 1986, *MNRAS*, **220**, 439

20)Taylor, G.B., Wright, E.L. 1989, *Ap. J.*, 339, 619

21)Lahav, O., Loeb, A., McKee, C.F. 1990, *Ap. J.*, **349**, L9

22)De Zotti, G., Danese, L., Toffolatti, L., Franceschini, A. 1990, in *Proc. IAU Symp. 139, "The Galactic and Extragalactic Background Radiation"*, p. 333

23)Barcons, X., Fabian, A.C. 1988, *MNRAS*, **230**, 189

24)Rogers, R.D., Field, G.B. 1991, *Ap. J.*, **366**, 22

25)Barcons, X., Fabian, A.C., Rees, M.J. 1991, *Nature*, **350**, 685

26)Wilkinson, D.T., Peebles, P.J.E. 1990, in *The Cosmic Microwave Background: 25 Years later*, Kluwer, p. 17

27)Loeb, A., Ostriker, J.P. 1991, preprint

28)Thomas, P.A., Fabian, A.C. 1990, *MNRAS*, **246**, 156

29)Piccinotti, G., Mushotzky, R.F., Boldt, E.A., Holt, S.S., Marshall, F.E., Serlemitsos, P.J., Shafer, R.A. 1982, *Ap.J.*, **253**, 485

30)Gioia, I.M., Maccacaro, T., Schild, R.E., Wolter, A., Stocke, J.T., Morris, S.L., Henry, J.P. 1990, *Ap.J.Suppl.*, **72**, 567

31)Cavaliere, A., Colafrancesco, S. 1989, in *Large Scale Structure and Motions in the Universe*, Kluwer, Dordrecht, p. 73

32)Edge, A.C., Stewart, G.C., Fabian, A.C., Arnaud, K. 1990, *MNRAS*, **245**, 559

33)Persic, M., Jahoda, K., Rephaeli, Y., Boldt, E.A., Marshall, F.E., Mushotzky, R.F., Rawley, G. 1990, *Ap. J.*, **364**, 1

34)Hayakawa, S. 1990, in *The Cosmic Microwave Background: 25 Years later*, Kluwer, p. 215

35)Persic, M., De Zotti, G., Danese, L., Palumbo, G.G.C., Franceschini, A., Boldt, E.A., Marshall, F.E. 1989, *Ap. J.*, **344**, 125

36)De Zotti, G., Persic, M., Franceschini, A., Danese, L., Palumbo, G.G.C., Boldt, E.A., and Marshall, F.E. 1990, *Ap.J.*, **351**, 22

37)Miyaji, T., Boldt, E. 1990, *Ap.J.*, **353**, L3

38)Boldt, E.A. 1990, in *Proc. IAU Coll. 123, "Observatories in Earth Orbit and Beyond"*, p. 123

39)Jahoda, K., Lahav, O., Mushotzky, R., Boldt, E.A. 1991, preprint

40)Songaila, A., Cowie, L.L., Lilly, S.J. 1990, *Ap. J.*, **348**, 371

41)Hauser, M.G., Kelsall, T., Moseley, S.H.Jr., Silverberg, R.F., Murdock, T., Toller, G., Spiesman, W., Weiland, J. 1991, *Proc. Workshop "After the First Three Minutes"*

42)Mazzei, P., De Zotti, G., Xu, C. 1991, *Astr. Ap.*, submitted

43)Bookbinder, J., Cowie, L.L., Krolik, J.H., Ostriker, J.P., Rees, M.J. 1980, *Ap. J.*, **237**, 647

44)Stewart, G.C., Fabian, A.C., Terlevich, R.J., Hazard, C. 1982, *MNRAS*, **200**, 61P

45)Fabbiano, G., Feigelson, E., Zamorani, G. 1982, *Ap. J.*, **256**, 397

46)Weedman, D.W. 1987, in *Proc. Conf. "Star Formation in Galaxies"*, NASA Conf. Publ. 2466, p. 321

47)Griffiths, R.E., Padovani, P. 1990, *Ap. J.*, **360**, 483

48)Hacking, P.B., Houck, J.R. 1987, *Ap. J. Suppl.*, **63**, 311

49)Lonsdale, C.J., Hacking, P.B., Conrow, T.P., Rowan-Robinson, M. 1990, *Ap. J.*, **358**, 60

50)Windhorst, R.A., Miley, G.K., Owen, F.N., Kron, R.G., Koo, D.C. 1985, *Ap. J.*, **289**, 494

51)Fomalont, E.B., Windhorst, R.A., Kristian, J.A., Kellermann, K.I. 1991, preprint

52)Hacking, P., Condon, J.J., Houck, J.R. 1987, *Ap. J.*, **316**, L15

53)Danese, L., De Zotti, G., Franceschini, A., Toffolatti, L. 1987, *Ap. J.*, **318**, L15

54)De Zotti, G., Danese, L., Franceschini, A., Persic, M., Toffolatti, L. 1989, in *Proc. 23rd ESLAB Symp. "2. AGN and the X-ray Background"*, ESA SP-296, p. 737

55)Fabbiano, G. 1988, *Ap. J.*, **330**, 672

56)Fabbiano, G. 1990, *Ann. Rev. Astr. Ap.*, **27**, 87

57)Weedman, D.W., Feldman, F.R., Balzano, V.A., Ramsey, L.W., Sramek, R.A., Wu, C.-C. 1981, *Ap. J.*, **248**, 105

58)Soifer, B.T., Boehmer, L., Neugebauer, G., Sanders, D.B. 1989, *A. J.*, **98**, 766

59)Rice, W., Lonsdale, C.J., Soifer, B.T., Neugebauer, G., Kopan, E.L., Lawrence, A.L., de Jong, T., Habing, H.J. 1988, *Ap. J. Suppl.*, **68**, 91

60)Lonsdale, C.J., Helou, G., Good, J.C., Rice, W. 1985, *Cataloged galaxies and quasars observed in the IRAS survey*

61)Kinney, A.L., Bregman, J.N., Huggins, P.J., Glassgold, A.E., Cohen, R.D. 1984, *PASP*, **96**, 398

62)Margon, B., Anderson, S.F., Mateo, M., Fich, M., Massey, P. 1988, *Ap. J.*, **334**, 597

63)Primini, F.A., Murray, S.S., Huchra, J., Schild, R., Burg, R., Giacconi, R. 1991, *Ap. J.*, in press

64)Ohashi, T., Makishima, K., Tsuru, T., Takano, S., Koyama, K., Stewart, G.C. 1990, *Ap. J.*, **365**, 180

65)Maccacaro, T., Della Ceca, R., Gioia, I.M., Morris, S.L., Stocke, J.T., Wolter, A. 1991, *Ap. J.*, in press

66)Mushotzky, R.F. 1984, *Adv. Space Res.*, **3**, 157

67)Turner, T.E., Pounds, K.A. 1989, *MNRAS*, **240**, 833

68)Wilkes, B.J., Masnou, J.-L., and Elvis, M. 1989, in *Proc. 23rd ESLAB Symp. "2. AGN and the X-ray Background"*, ESA SP-296, p. 1081

69)Maccacaro, T., Gioia, I.M., Wolter, A., Zamorani, G., Stocke, J.T. 1988, *Ap. J.*, **326**, 680

70)Warwick, R.S., Stewart, G.C. 1989, in *Proc. 23rd ESLAB Symp. "2. AGN and the X-ray Background"*, ESA SP-296, p. 727

71)Urry, C.M., Arnaud, K., Edelson, R.A., Kruper, J.S., Mushotzky, R.F. 1989, in *Proc. 23rd ESLAB Symp. "2. AGN and the X-ray Background"*, ESA SP-296, p. 789

72)Setti, G. 1987, in *IAU Symp. 124, "Observational Cosmology"*, p. 579

73)Maccacaro, T., Gioia, I.M. 1986, *Ap. J.*, **303**, 614

74)Franceschini, A., Gioia, I.M., Maccacaro, T. 1986, *Ap. J.*, **301**, 124

75)Martín-Mirones, J.M., De Zotti, G., Franceschini, A., Danese, L. 1991, in *Proc. TEXAS/ESO-CERN symposium*, in press

76)Cheng, F.-Z., Danese, L., De Zotti, G., Franceschini, A. 1985, *MNRAS*, **212**, 857

77)Schmidt, M., Green, R.F. 1983, *Ap. J.*, **269**, 352

78)Reichert, G.A., Mushotzky, R.F., Petre, R., Holt, S.S. 1985, *Ap. J.*, **296**, 69

79)Hamilton, T.T., Helfand, D.J. 1987, *Ap. J.*, **318**, 93

80)Barcons, X., Fabian, A.C. 1990, *MNRAS*, **243**, 366

81)Soltan, A.M. 1991, *MNRAS*, in press

82)Padovani, P. 1989, *Astr. Ap.*, **209**, 27

83)Cavaliere, A., Padovani, P. 1989, *Ap. J.*, **340**, L5

84)Koratkar, A.P., Gaskell, C.M. 1991, *Ap. J.*, **370**, L61

85)Boldt, E.A., Leiter, D. 1987, *Ap. J.*, **322**, L1

86)Setti, G., Woltjer, L. 1989, *Ap. J.*, **224**, L21

87)Fabian, A.C., George, I.M., Miyoshi, S., Rees, M.J. 1990, *MNRAS*, **242**, 14P

88)Morisawa, K., Matsuoka, M., Takahara, F., Piro, L. 1990, *Astr. Ap.*, **236**, 299

89)Matsuoka, M., Piro, L., Yamauchi, M., Murakami, T. 1990, *Ap. J.*, **361**, 440

90)Piro, L., Yamauchi, M., Matsuoka, M. 1990, *Ap. J.*, **360**, l35

91)Pounds, K.A., Nandra, K., Stewart, G.C., George, I.M., Fabian, A.C. 1990, *Nature*, **344**, 132

92)Boldt, E.A. 1989, in *Proc. 23rd ESLAB Symp. "2. AGN and the X-ray Background"*, ESA SP-296, p. 797

93)Rogers, R.D., Field, G.B. 1991, *Ap. J.*, **370**, L57

94)Piro, L. 1991, in *Proc. Varenna workshop "Iron Line Diagnostic in X-ray sources"*

95)Schmidt, M., Hasinger, G., Trümper, J. 1991, in *Proc. XIth Moriond Astrophysics Meeting*, in press

96)Barcons, X., Fabian, A.C. 1989, *MNRAS*, **237**, 119

97)Bahcall, N.A., Soneira, R.M. 1983, *Ap. J.*, **270**, 20

98)Iovino, A., *et al.* 1989, in *Large Scale Structure and Motions in the Universe*, Kluwer, p. 369

99)Jahoda, K., Mushotzky, R.F. 1989, *Ap. J.*, **346**, 638

100)Avni, Y., Tananbaum, H. 1986, *Ap. J.*, **305**, 83

101)Canizares, C.R., White, J.L. 1989, *Ap. J.*, **339**, 27

## NEW EXTRAGALACTIC RESULTS FROM SIGMA

Jean BALLET, François LEBRUN, Jacques PAUL, Jacqueline BERGERON*
SAp, CEN Saclay, 91191 Gif/Yvette Cedex, France
*IAP, 98bis bd Arago, 75014 Paris, France (guest investigator)
Elizabeth JOURDAIN, Loredana BASSANI, Laurent BOUCHET,
Pierre MANDROU
CESR, 9 av. du C$^{et}$ Roche, BP 4346, 31029 Toulouse Cedex, France
Rashid SUNYAEV, Yury APALKOV, Eugene CHURAZOV, Igor DEKHANOV,
Marat GILFANOV, Sergey GREBENEV, Igor LAGUNOV, Mikhail PAVLINSKY
IKI, Profsouznaya 84/32, Moscow 117296, USSR

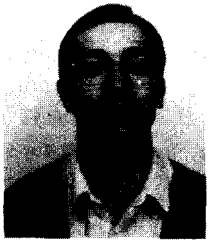

SIGMA is a soft gamma-ray telescope operating from 30 keV to 1 MeV. Active galactic nuclei radiate a large fraction of their luminosity in this range, and their primordial ancestors could be the source of the X-ray background.

We present preliminary results on the three brightest AGNs (Cen A, NGC 4151, 3C 273). Their average fluxes are coherent with previous observations of those sources in their lowest state. NGC 4151 and 3C 273 have been observed several times with no evidence for variations of more than a factor of two.

## I. INTRODUCTION

The origin of the diffuse X-ray background (XRB) between 3 and 300 keV [1] is still not known. Although it looks like a single thermal bremsstrahlung spectrum, there are good reasons [2,3] to believe it is due to a collection of sources. AGNs make up the bulk of the faint sources in the Einstein surveys below 3 keV [3]. They are therefore logical candidates to explain the XRB.

However the spectra of (bright) AGNs differ markedly from the XRB spectrum. In the 2-10 keV range, they are power laws with photon index close to -1.7 [4,5]. A possible reason is that those AGNs are not representative of the faint AGNs that would make up the XRB. On the other hand, their spectra above 20 keV (because of the redshift, this is the part that will contribute to the XRB) are poorly known [1] and it is possible [6] to explain the XRB by assuming flatter spectra for AGNs above 20 keV. The spectrum of AGNs around 100 keV is therefore crucial to validate this kind of hypothesis.

Another motivation for studying AGNs in hard X-rays is that because of their flat spectra they emit a large fraction of their luminosity in this range ( [7] for 3C 273). Because of the photons' energy and the time scale for variations ( [8] for NGC 4151) the hard X-rays are probably emitted close to the central engine, which is another measure of their importance to AGN theory.

Unfortunately, due to the lower sensitivity of hard X-ray experiments (compared to the classical X-ray band), only the three brightest AGNs (Cen A, NGC 4151, 3C 273) can be studied at present. Data have been collected by HEAO 1 A4 [9,10] and HEXE on the MIR space station [11] and also by balloon experiments [12].

## II. CAPACITIES OF SIGMA AND GRANAT

The French SIGMA telescope [13] was launched on December 1, 1989 aboard the Soviet GRANAT space observatory in a highly eccentric orbit (4 days period). It is a coded aperture system (based on a 31x29 URA pattern) designed to provide images of the sky in the 35 keV to 1.3 MeV range with 13 arcmin angular resolution (unprecedented at those energies). The full sensitivity (fully coded) field of view is 4.7° x 4.3°.

The background is dominated by radiation from the telescope matter activated by high-energy particles, rather than the soft γ-ray background. As there is no way to block the cosmic photons, we cannot make a differential measurement either.

SIGMA is best at studying complex regions (usually in the galactic plane) where source confusion was a major problem for previous collimated instruments with angular resolution worse than 1°. Bright AGNs are mostly isolated sources, for which confusion is not much of a problem. Imaging observations may still be more reliable than collimated ones, because the source can be "seen" on the image and the background is measured at the same time and the same pointing direction as the source (and not by rocking the instrument).

The telescope's sensitivity is obtained as the combination of three factors (all depending on energy):

- the effective area of the device (about 300 $cm^2$ at 100 keV). Because of the mask, a source illuminates only half the detector (the other half measures the background).
- the background rate (about 180 cts/s from 40 to 160 keV).
- the imperfect spatial resolution of the detector, that reduces the contrast in the image. The spatial resolution is 5.4 mm HWHM at 100 keV (the mask element is 9.4 mm). The associated loss is about a factor 3.

The result is shown on figure 1. The 3$\sigma$ sensitivity of SIGMA at 100 keV is $10^{-5}$ ph $cm^{-2}$ $s^{-1}$ $keV^{-1}$ for broad band observations in a typical $10^5$ s exposure. This is not very good (some sensitivity was lost to the imaging capacities), and extrapolating X-ray observations of AGNs [5] indicates that only Cen A, NGC 4151 and 3C 273 are expected to be brighter than that.

The GRANAT observatory also features the Soviet ART-P telescope [14], sensitive from 3 to 30 keV. ART-P also uses a coded mask, resulting in a 5 arcmin angular resolution. With ART-P and SIGMA, GRANAT easily spans two decades (3 to more than 300 keV). Although the observations are not exactly simultaneous (ART-P covers typically the first 6 hours of a one-day SIGMA session), the ART-P data firmly anchor the SIGMA results in the classical X-ray range. This is particularly important for variable sources such as AGNs.

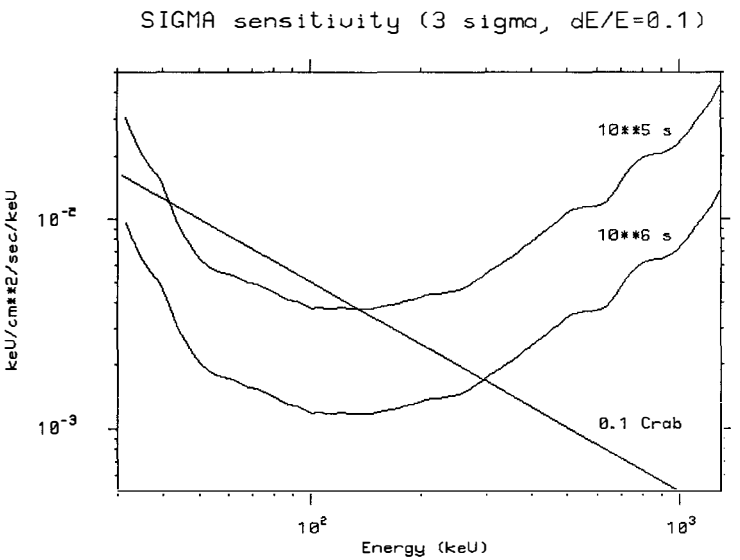


Figure 1: The two curves illustrate the sensitivity of SIGMA in a typical observing time ($10^5$ s) and a very long observing time ($10^6$ s). The approximate Crab spectrum (divided by ten) is shown for comparison. The figure was drawn for spectral observations (bin size $\Delta E/E = 0.1$). For broad band observations ($\Delta E/E = 1$), the $10^5$ s sensitivity is close to that in $10^6$ s for spectral measurements, and the $10^6$ s sensitivity is three times better.

## III. OBSERVATIONS

Three types of data are available in a typical SIGMA observing session:

- Four fine images (248x232 pixels) in four adjacent energy bands (40-80 keV, 80-160 keV, 160-310 keV, over 310 keV). This is the material presented here. Several (up to six poses) sets of 4 images are recorded within a single session, preserving some time information.
- 95 spectral images (124x116 pixels) allowing to build spectra. These have not been fully analyzed yet.
- Counting rates every 4 s in the same energy bands as the four fine images. These are useful only for very strong

sources. Background and statistical variations dominate over ordinary sources.

The data were analyzed as follows:

- For lack of statistics all poses within a single session were co-added.
- The images were then corrected for the background and detector non uniformities, and deconvolved using standard techniques [15]. Sessions up to July 1990 have been corrected with a background reference obtained in January and February 1990, whereas sessions of November 1990 have been corrected with a background reference obtained in January 1991.
- Images have been smoothed with the point spread function of the detector in order to improve the signal to noise ratio.
- Because the background correction was not perfect, source counts have been derived by subtracting the local mean in the image, defined at a distance (2.5 mask elements) at which the source contribution is expected to be negligible.
- Errors quoted are obtained by taking the RMS dispersion in the deconvolved images. These are slightly larger than the statistical errors because of the imperfect background correction.

Table 1: Average fluxes at 60 and 100 keV (in ph $cm^{-2}$ $s^{-1}$ $keV^{-1}$) estimated from the count rates in the first and second band, respectively. A photon spectral index of -1.5 was assumed for the conversion, but it is not critical since each energy is close to the center of the corresponding band. All sessions on a given source have been summed.

| Source | Obs.time | 60 keV flux | 100 keV flux |
|---|---|---|---|
| Cen A | 56200 | $6.3 \pm 1.9 \ 10^{-5}$ | $2.9 \pm 0.8 \ 10^{-5}$ |
| NGC 4151 | 312100 | $6.4 \pm 0.8 \ 10^{-5}$ | $1.7 \pm 0.3 \ 10^{-5}$ |
| 3C 273 | 222500 | $3.2 \pm 1.0 \ 10^{-5}$ | $1.7 \pm 0.4 \ 10^{-5}$ |

Table 2: SIGMA observing log and count rate (40-160 keV) for every individual observation of Cen A, NGC 4151 and 3C 273.

| Date | IF1+IF2 cts/s NGC 4151 |
|---|---|
| 13/07/90 57900 s | 0.14 ± 0.05 |
| 13/07/90 16300 s | 0.28 ± 0.09 |
| 15/11/90 46400 s | 0.21 ± 0.05 |
| 16/11/90 44700 s | 0.19 ± 0.05 |
| 20/11/90 59300 s | 0.14 ± 0.05 |
| 21/11/90 87400 s | 0.10 ± 0.04 |

| Date | IF1+IF2 cts/s 3C 273 |
|---|---|
| 15/06/90 76000 s | 0.14 ± 0.04 |
| 25/07/90 42200 s | 0.24 ± 0.08 |
| 28/11/90 46000 s | 0.09 ± 0.05 |
| 29/11/90 58300 s | 0.10 ± 0.05 |

| Date | IF1+IF2 cts/s Cen A |
|---|---|
| 24/07/90 56200 s | 0.23 ± 0.05 |

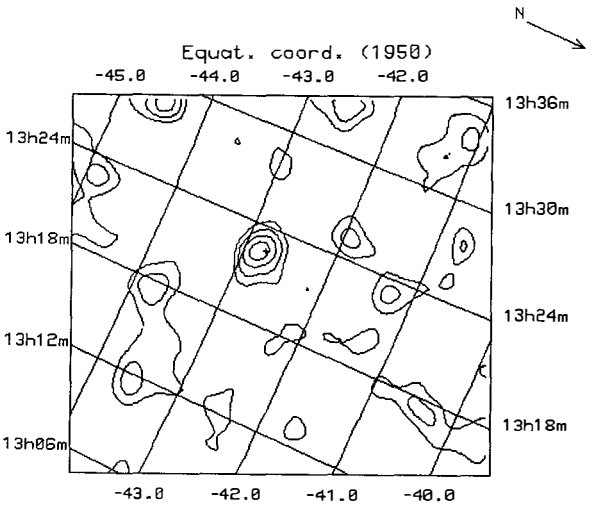


Figure 2: Fully coded field of view around Cen A. The first two bands (40-160 keV) have been summed. The source is apparent at a position compatible with that of the radio nucleus (cross). The contour spacing is 1 σ, starting at 1.

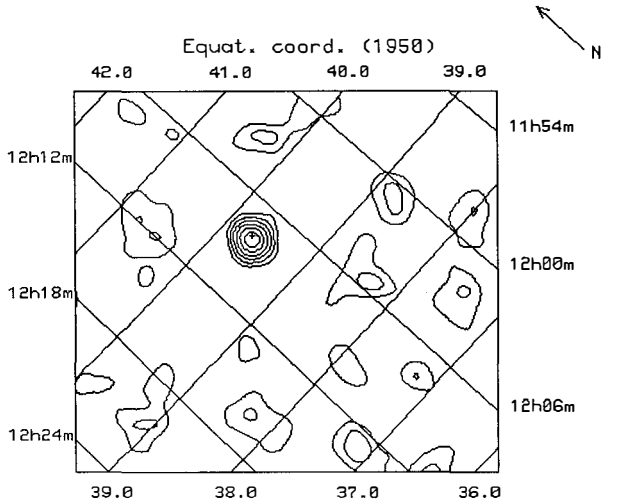


Figure 3: Same as figure 2 for NGC 4151, summed over all sessions. The source is apparent at a position compatible with the optical one (cross).

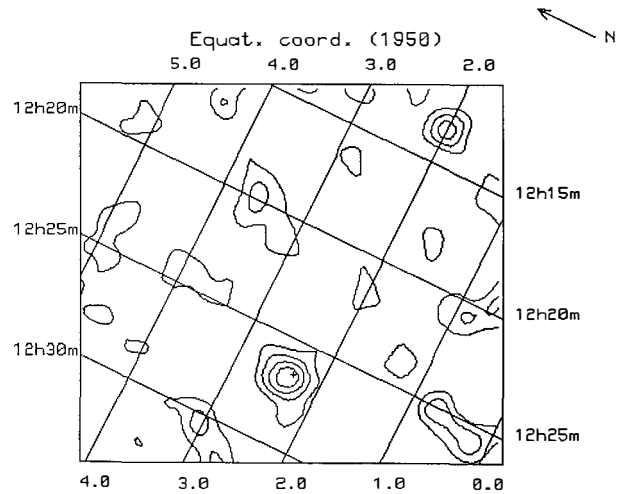


Figure 4: Same as figure 3 for 3C 273. A 3σ feature such as that in the upper right corner can happen in such an image from statistical fluctuations alone and may not be another source.

## IV. DISCUSSION

### A. CEN A

Cen A is the nearest active galaxy, and is intrinsically not very luminous (about 7 $10^{41}$ erg $s^{-1}$ in the 3-10 keV range) [16]. It has been observed to be strongly variable [11] in hard X-rays, extending the well known X-ray variability [16]. Our 100 keV flux of 2.9 $10^{-5}$ ph $cm^{-2}$ $s^{-1}$ $keV^{-1}$ is rather low, midway between that measured by HEXE in 1987 and 1988, but much lower than that observed by HEAO 1 A4 [9]. We have unfortunately observed it successfully only once, and the sensitivity of SIGMA does not allow studies on time scales shorter than one day.

The 10 keV flux observed by ART-P [17] is very low at 6 $10^{-4}$ ph $cm^{-2}$ $s^{-1}$ $keV^{-1}$. The 100/10 keV ratio is indicative of a hard spectrum (average slope -1.3 in photons) associated to this low state.

### B. NGC 4151

NGC 4151 is somewhat more luminous (about 7 $10^{42}$ erg $s^{-1}$ in the 2-10 keV range) and is the best studied AGN. It is also strongly variable in X-rays [8,18,19] and in hard X-rays [10,11]. Our average 100 keV flux of 1.7 $10^{-5}$ ph $cm^{-2}$ $s^{-1}$ $keV^{-1}$ is again low, even lower than that measured by HEXE. However the 60 keV flux (from the first band) is slightly above HEXE's.

The individual observations are mostly coherent around 0.15 cts/s, although the second one (unfortunately very short) may have caught the source in a higher state. We have observed the source often enough to be reasonably confident that the flux we measure is representative of the average NGC 4151 state. This argument is strengthened by the good agreement with the best previous observations of NGC 4151 at 100 keV [10,11].

During the November 1990 observations (that make up the bulk of the data), the 10 keV flux from ART-P was stable at about 1.2 $10^{-3}$ ph $cm^{-2}$ $s^{-1}$ $keV^{-1}$ (slightly higher than the average ART-P flux [17] that includes periods when SIGMA was switched off). NGC 4151 was therefore in a state very similar to that observed by HEAO 1 A4 in June 1978 [10], with a 100/10 keV ratio indicative of a -1.8 (photon index) average slope.

C. 3C 273

3C 273 is intrinsically much brighter (about $10^{46}$ erg $s^{-1}$ in the 2-10 keV range) [20]. Not surprisingly, it is also less variable, and on longer time scales. Most hard X-ray measurements agree on this source [11], and our average 100 keV flux of 1.7 $10^{-5}$ ph $cm^{-2}$ $s^{-1}$ $keV^{-1}$ is compatible with the rest. The 10 keV flux from ART-P [17] is also at a typical value of 5 $10^{-4}$ ph $cm^{-2}$ $s^{-1}$ $keV^{-1}$. The 100/10 keV ratio is indicative of a hard spectrum (average slope -1.5 in photons) also typical of this source.

Table 2 indicates that the source was about two times brighter in our second observation than in the other three. However the background correction is poor for this session (as shown by the large error bar) so that this is barely a 2 $\sigma$ effect.

D. GENERAL

The three bright AGNs that have been discussed here may not be typical: Cen A is very underluminous, and the other two have unusually hard (photon index -1.5 [8,20]) X-ray spectra in the 2-10 keV band. This casts a doubt over any inference over the general behaviour of AGNs from observations of those three. However the SIGMA images confirm that they are sources of 100 keV photons. The fluxes derived are comparable to those obtained by HEAO 1 A4 and HEXE, and lower than most balloon observations. NGC 4151 and 3C 273 were observed several times, with no evidence for flux variations larger than a factor 2.

Such results are not yet specific enough to tell us what is the AGN contribution to the XRB. Spectra of those three sources (that we are currently processing) in the SIGMA range will offer more relevant information, particularly in conjunction with the ART-P X-ray spectra.

Acknowledgements:
We acknowledge the paramount contribution of the SIGMA Project Group of the CNES Toulouse Space Center to the overall success of the SIGMA mission. We thank the staff of the Lavotchin Space Company, of the Babakin Space Center, of the Baikonur Space Center and of the Evpatoria Ground Station for their unfailing support.

References


1) Rothschild,R.E.,Mushotzky,R.F.,Baity,W.A.,Gruber,D.E., Matteson,J.L.,Peterson,L.E. 1983, Ap.J. **269**,423
2) Giacconi,R.,Zamorani,G. 1987, Ap.J. **313**,20
3) de Zotti,G. 1991, this volume
4) Mushotzky,R.F. 1984, Adv.Sp.Res. **3**,10
5) Turner,T.J.,Pounds,K.A. 1989, MNRAS **240**,833
6) Schwartz,D.A.,Tucker,W.H. 1988, Ap.J. **332**,157
7) Courvoisier,T.J.L. et al. 1987, Astr.Ap. **176**,197
8) Yaqoob,T.,Warwick,R.S.,Pounds,K.A. 1989, MNRAS **236**,153
9) Baity,W.A. et al. 1981, Ap.J. **244**,429
10) Baity,W.A.,Mushotzky,R.F.,Worrall,D.M.,Rothschild,R.E., Tennant,A.F.,Primini,F.A. 1984, Ap.J. **279**,555
11) Maisack,M. et al. 1989, Proc.23rd ESLAB Symp.,Bologna, ESA SP-296,975
12) Bassani,L. et al. 1989, Proc.23rd ESLAB Symp.,Bologna, ESA SP-296,897
13) Paul,J. et al. 1991, Proc.18thCOSPAR Symp.(ME.4),The Hague, Adv.Sp.Res., in press
14) Sunyaev,R. et al. 1990, Adv.Sp.Res. **10**,n°2,233
15) Laudet,P.,Roques,J.P. 1988, Nucl.Instr.Meth. **A267**,212
16) Wang,B.,Inoue,H.,Koyama,K.,Tanaka,Y.,Hirano,T.,Nagase,F. 1986, PASJ **38**,685
17) Sunyaev,R. et al. 1991, Sov.Astr.Letters, in press
18) Matsuoka,M.,Ikegami,T.,Inoue,H.,Koyama,K. 1986, PASJ **38**,285
19) Fiore,F.,Perola,G.C.,Romano,M. 1990, MNRAS **243**,522
20) Turner,M.J.L. et al. 1990, MNRAS **244**,310

# EARLY ROSAT RESULTS ON X-RAY SOURCES AND BACKGROUND

M. Schmidt[1,2], G. Hasinger[1], J. Trümper[1]

[1] Max Planck Institut für extraterrestrische Physik, D–8046 Garching bei München, Federal Republic of Germany

[2] California Institute of Technology, Pasadena, CA, U.S.A.

**Abstract**

We report early results on source counts and background based on 8 ROSAT PSPC pointings covering 2.6 $deg^2$. The integral source counts N(>S) flatten below $2 \times 10^{-14} erg\ cm^{-2} s^{-1}$. In the $1 - 2\ keV$ band the fraction of flux in resolved sources is $20 - 30\%$. The spectrum of the resolved sources is similar to that of the remaining background in the $1 - 2\ keV$ range, both with a power law slope of $-1.3$. In the deepest pointing, centered on the North-ecliptic Pole (NEP), we find evidence of structure in the background on a scale of $\sim 20'$. This may be evidence for structure in the universe at redshifts of $\sim 1$.

## 1. Source Counts

We have studied eight pointed PSPC observations with long integration times ($8 - 49\ ksec$) selected from the ROSAT calibration and verification phase (see Hasinger et al., 1991). Observations were generally done in the 'wobble mode', where the spacecraft performs a linear dithering motion with a peak to peak amplitude of $6'$ diagonally to the PSPC support grid to minimize the imprint of the support structure on the sky. We concentrated on the inner part of the PSPC field of view, with a radius of $20'$, with almost uniform sensitivity and telescope resolution of around 25". A circle of radius $2.7'$ around bright targetted X-ray sources was excluded from the analysis. The total surveyed solid angle is $\sim 2.6\ deg^2$. To maximize the sensitivity for source detection, we restricted the analysis to the energy band $0.5 - 1.6\ keV$. A global background map

was constructed from a smoothed image of each field after pixels containing brighter sources had been removed. A source was accepted if its probability of being produced by a background fluctuation was less than $4.54 \times 10^{-5}$ ($likelihood > 10$), corresponding to $1-2$ spurious sources in the surveyed area. The counts in a source were converted to an emitted flux in the $0.1-2.4\ keV$ band assuming a power law spectrum with energy index $-1$ and galactic absorption.

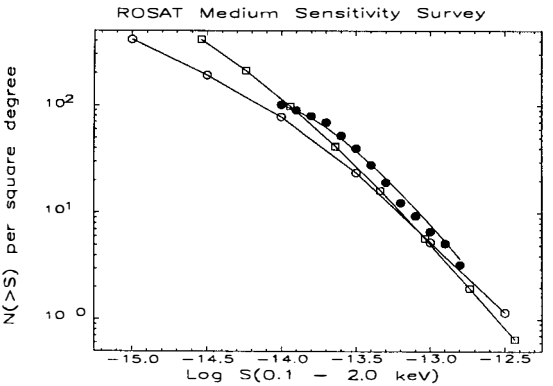


**Figure 1: Integral N(>S) relations. Filled dots give the measurements for the 184 sources, open circles and squares show the prognosis of Schmidt (1989) and Maccacaro (1990), respectively.**

A total of 184 discrete sources were detected in the flux interval $10^{-14} - 2 \times 10^{-13} erg\ cm^{-2} s^{-1}$. Based on the distribution of background counts and hydrogen columns, we constructed a histogram of the surveyed solid angle as a function of limiting sensitivity. Since the faintest sources in our survey are detected from $10-15$ photons, Poisson noise will have a substantial effect on the measured fluxes (cf. Schmitt and Maccacaro 1986). We have taken into account the net gain of the number of sources detected above a given limit as a consequence of the corresponding statistical errors in the measured flux (Eddington 1940). In taking this bias into account, we assumed that the differential N(S) relation can be described by the function

$$N(S) = (A1 \cdot S^{2.4} + A2 \cdot S^{\alpha})^{-1}$$

For a set of trial values of the free parameters, we converted N(S) for each entry in the sensitivity histogram into a differential N(C) of the source photon numbers C. We

redistributed the photon numbers according to Poisson's law and derived the number of sources expected in each flux bin. We finally minimized $\chi^2$ until the expected source distribution agreed with the observed distribution within errors, obtaining the following best-fit parameters: $A1 = 0.0033, A2 = 0.0165, \alpha = 0$ with a $\chi^2_{red}$of 0.96. A fit with a single power law yielded an unacceptable $\chi^2_{red}$ of 2.54 and a slope of $-2.0$. While the fit was made on the differential N(S) distribution, we illustrate in figure 1 the integral N(>S) relation, together with the analytical fit. Also shown is a prognosis of source counts for ROSAT by Schmidt (1989) and a prognosis of AGN source counts by Maccacaro (1990). The observed numbers are somewhat higher than predicted, partly due to the soft spectrum of the ROSAT sources (see below). The integral source count slope changes from $-1.4$ for sources above $5 \times 10^{-14} erg\ cm^{-2} s^{-1}$ to around $-0.9$ at $2 \times 10^{-14} erg\ cm^{-2} s^{-1}$. A similar change in slope in the prognosis by Schmidt (1989) is primarily due to strong flattening of the quasar counts, which is a consequence of their density peak at a redshift around 2.

## 2. Spectrum of Sources and Background

The low PSPC background allows for the first time to compare the average spectrum of the resolved sources and the spectrum of the diffuse background measured with the same instrument.

The average source spectrum was determined for every field by accumulating counts in a ring of radius 48" around every detected source and subtracting the average spectrum from the remaining pixels. This was compared to the total spectrum, integrated across the field (i.e. background plus sources), after the particle background, estimated from the highest energy channels, had been subtracted. Figure 2 compares the count rate spectra of sources and background for the NEP field. As in all other fields the average source spectrum is parallel within the errors to that of the remaining background above $\sim 1\ keV$. The statistical quality of the data and uncertainties in the particle background subtraction prevent a meaningful comparison above $\sim 2\ keV$. Figure 3a (upper curve) shows a power law fit to the NEP average source spectrum, including the galactic absorption through a hydrogen column density of $3.8 \times 10^{20}\ cm^{-2}$. The mean

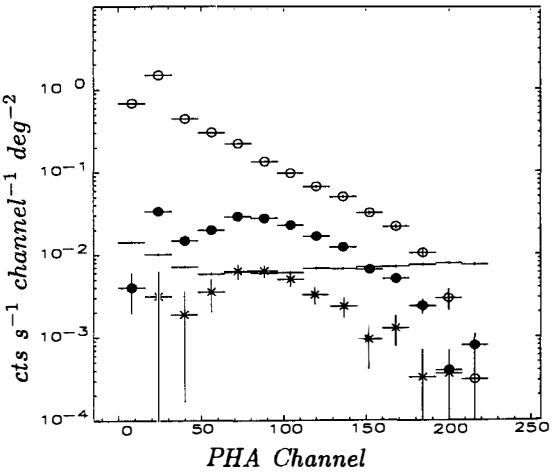


**Figure 2: Raw spectrum of sources (filled circles), total background (open circles), blotch (crosses), and particle background in the NEP field.**

energy index of the average source spectra in the eight different fields is $-1.3 \pm 0.1$ and the derived column densities are consistent with (or slightly higher than) the galactic absorption.

The residual background spectra in all fields (except one in the direction of Loop I) can be fit with a combination of three components: (1) a power law spectrum of slope and absorption similar to the above source spectrum, (2) a very soft component of a temperature on the order of 40 $eV$ (we used a black body, but due to the poor spectral resolution of the PSPC below 0.5 $keV$ we could not distinguish it from other spectral shapes), and (3) a monochromatic line at $0.5 - 0.6$ $keV$. The latter component is the geocoronal oxygen line at $0.53keV$ and only observed during the sunlit phase of the satellite orbit. We compared the day and night background spectra and concluded that the daylight contamination is less than 5% above $0.9keV$. Figure 3b shows the spectral fit to the NEP residual background spectrum and the contribution of the individual components. The mean energy index of the power law components of the background spectra in seven fields is $-1.2 \pm 0.1$.

The fact that the spectrum of the resolved sources is similar to that of the residual background at $0.5-2$ $keV$, suggests that the steepening of the XRB in this energy range

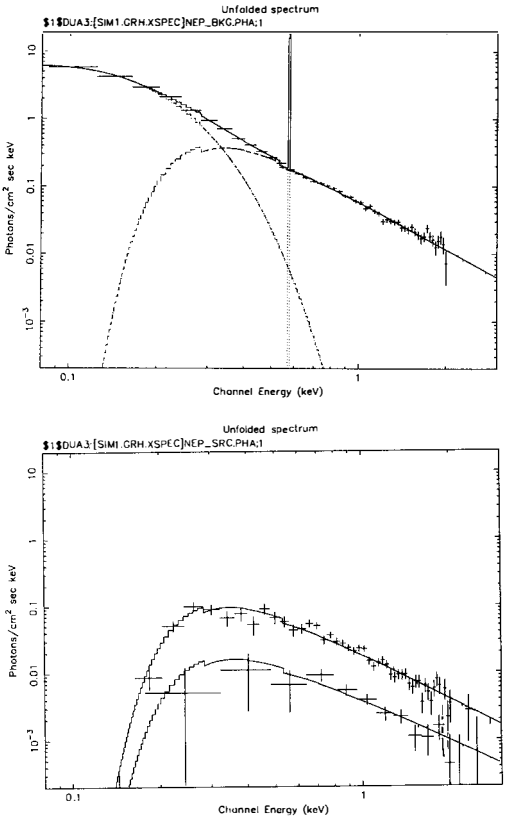


**Figure 3: (a) Photon spectrum of sources (upper curve), and blotch (lower curve) in the NEP field, (b) residual background spectrum and its constituents (see text).**

compared to the extrapolation from higher energies (Marshall et al., 1980; McCammon and Sanders, 1990) is due to extragalactic sources, while the excess diffuse galactic emission starts to dominate only below 0.5 $keV$.

To obtain the fraction $f$ of the total flux resolved into discrete sources in the energy range $1.2 - 2.0$ $keV$, we added the estimated contribution of sources brighter than $2 \times 10^{-13} erg\ cm^{-2} s^{-1}$. The resulting values of $f$ range from $\sim$ 20% for the shallower fields to about 30% for the deeper fields. It should be kept in mind that both the detected sources and the remaining background include an unknown fraction

of galactic foreground - mainly from coronal sources. It is likely, however, that both the fraction of sources that are stars, and the fraction of the background that is galactic above 1.2 $keV$ are small.

### 3. Structure in the Diffuse Background

The field observed near the North ecliptic pole for 49,200 seconds shows some patchiness in the $0.5-1.6$ $keV$ background. Figure 4 shows a contour plot of the background in this field, after the detected sources were replaced by the content of the global background map. In the north-eastern part of the image a 'blotch' of X-ray emission with a diameter of $\sim 20'$ is visible, with a maximum surface brightness of $3.4 \times 10^{-4} cts\ s^{-1} arcmin^{-2}$, a factor of $\sim 1.7$ brighter than the darkest features to the south-west of the map. The crosses in figure 2 show the raw X-ray spectrum of this feature, very similar to the average source spectrum. In particular, the blotch spectrum shows the same effect of galactic absorption as that exhibited by the sources. A power law fit yields an energy index of $-1.2 \pm 0.3$ (see figure 3a).

An angular autocorrelation function (ACF) of the form

$$ACF(r) = \frac{<(I(R)-<I>)\cdot(I(R+r)-<I>)>}{<I>^2}$$

was calculated, where I(R) is the number of photons in each pixel R and the brackets <> denote an average over the whole field (see also Barcons and Fabian, 1989). Figure 5 shows the ACF for the NEP field. It exhibits a significant signal with an e-folding angle of ~300", becomes negative at ~500" and asymptotically approaches zero at ~1300". We analysed the data in two halves of ~25000s exposure and detected the structure in each set separately.

We performed exactly the same analysis on a flat-field image in the same energy band, constructed from a comparable number of photons from the all-sky survey in detector coordinates. The open circles in figure 5 show the flat-field ACF, which, apart from a slight decay due to the vignetting function of the mirror, does not show any significant correlation. We also calculated an ACF for the image in the soft energy band $(0.1 - 0.3\ keV)$ which does not show any correlation. Finally, in order to investi-

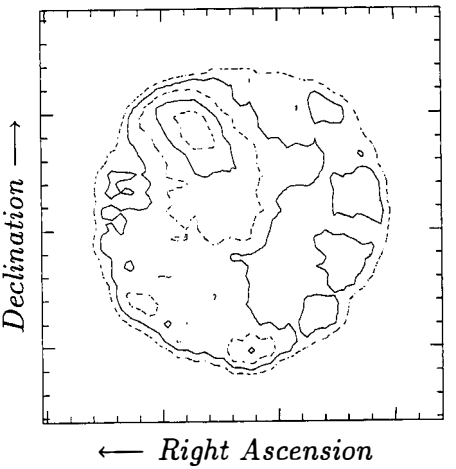


Figure 4: Contour plot of the residual background in the NEP field. Contour levels correspond to 1.79, 2.14, 2.50, 2.86 and 3.22 $\times$ $10^{-4}$ cts $s^{-1}$ arcmin$^{-2}$. The diameter of the image is 40'.

gate whether the NEP signal could be spuriously produced by the Poisson statistic of a small number of unresolved objects below the threshold, we performed as realistic a simulation as possible, drawing randomly distributed sources from approximately the observed N(S) function extrapolated a factor of 100 below the actual sensitivity threshold. The resulting ACF shows some noise, probably due to unresolved sources below the detection threshold, but with a much smaller signal and a completely different angular dependence. These findings are further supported by the fact that in the five other fields suitable for study of the background we could not detect any structure. In one other case, we detected structure reminiscent of the NEP field, however, two relatively bright sources are superposed close to the center of the feature.

We finish with a brief and necessarily speculative discussion of the nature of the 'NEP blotch', using its angular size, surface brightness, integrated flux and spectral signature, as well as a first inspection of the Palomar Sky Atlas. A galactic origin of the 'NEP blotch' is unlikely. If the structure were produced by cold galactic gas, i.e. a variation in the galactic neutral hydrogen absorption along the different lines of sight, the variation in surface brightness of almost a factor of 2 would require relatively

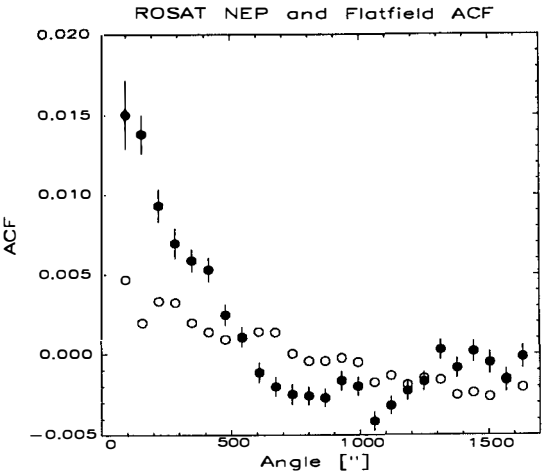


**Figure 5: Angular autocorrelation function of the NEP (solid circles) and the flatfield image (open circles).**

large changes in column density. In this case the difference spectrum between obscured and unobscured areas would be expected to be much softer than the average spectrum, which is not the case. The absorption in the blotch spectrum, yielding a lower limit to the distance of several hundred parsec, as well as the complete absence of this structure in the carbon band makes an origin in the local diffuse galactic background unlikely.

In discussing an extragalactic origin of the NEP blotch, we assume $H_0 = 50\ km\ s^{-1}\ Mpc^{-1}$. If it is a galaxy of size $10 - 40\ kpc$ and say $M = -19$, then its apparent magnitude would be $m = 7 - 10$, but inspection of the Palomar Sky Atlas shows no galaxies brighter than about $m = 16$. If the NEP blotch is a cluster of galaxies with a size of 1 $Mpc$, the typical brightest galaxy of $M = -23$ should show at $m = 14$ which is still brighter than we observe. Also, no cluster of galaxies at such a small redshift is known at this position (from the EXOSAT database); inspection on the Palomar Sky Atlas prints shows no cluster of galaxies.

If the NEP blotch corresponds to a supercluster of diameter in the range $7 - 11\ Mpc$, then the redshift can have any value in the range $z = 0.3 - 3$. For a blotch flux of around $10^{-13} erg\ cm^{-2} s^{-1}$, the X-ray luminosity would be in the range $10^{44} - 10^{46} erg\ s^{-1}$. If most of the extended X-ray flux is contributed by, say a hundred objects,

then depending on the actual redshift these could be star-forming galaxies or AGNs. If this explanation is correct, X-ray observations may yield important information on the nature and evolution of superclusters at large redshifts.

**Acknowledgements**

We would like to thank the principal investigators of ROSAT verification pointings for permission to use their data for our purposes in advance of publication: T. Ayres, K. Beuermann, J. Schmitt and F. Verbunt. We had fruitful discussions with D. McCammon, R. Giacconi, H. Gursky, H. Böhringer, A. Edge and S. Snowden. M.S. acknowledges generous support from the Alexander von Humboldt Stiftung.

**References**

Barcons, X., Fabian, A.C. 1989, MNRAS, 237, 119
Eddington, A.S. 1940, MNRAS, 100, 354
Hasinger, G., Schmidt, M. and Trümper, J. 1991, A&A (in press)
Maccacaro, T. 1990 (priv. comm.)
McCammon, D. and Sanders, W.T. 1990, ARA&A, 28, 657
Marshall, F.E. et al. 1980, ApJ, 235, 4
Schmitt, J.H.M.M. and Maccacaro, T. 1986, ApJ, 310, 334
Schmidt, M. 1989, 23rd ESLAB Symp., ESA SP-296, p. 853

# ACTIVE AND INACTIVE GALACTIC NUCLEI, X-RAY AND GAMMA-RAY BACKGROUND, AND THE INTERGALACTIC MEDIUM

Suzy Collin-Souffrin
DAEC, Observatoire de Paris-Meudon, Meudon, France
Institut d'Astrophysique, Paris, France

## ABSTRACT

The main purpose of this paper is to propose a unifying model for X-ray and gamma-ray backgrounds based on AGN emission

First the link between Active and Inactive Galactic Nuclei is examined in the framework of the accretion model for AGN. According to several recent works, currently inactive galactic nuclei must harbor massive black holes with an average mass of a few $10^7 M_o$. Only a small fraction (1%) of these black holes are in an active phase, in the local Universe as well as at moderate redshifts (z = 2-3). It means that a large fraction of the building up time of black holes is spent in an "unobservable phase" at a high redshift.

Two assumptions are then made, whose reliability is shown to be acceptable: *1. AGN are giving the soft gamma-ray background*; *2. the gamma-ray spectrum of progenitors black holes is the same as that of AGN themselves*. It is then found that black holes can easily account for the observed (hard) X-ray diffuse background, while local AGN can account for the gamma-ray background.

Finally heating of the Intergalactic Medium by gamma-rays emitted at high redshift is discussed. The IGM is heated at a high temperature (about $3\ 10^5$K), even if it contains all baryonic matter of Universe. However the temperature drops at low redshifts (< 5) so it is not sufficient to account for the Gunn-Peterson test, and an additional mechanical or radiative heating mechanism is required.

## I. INTRODUCTION

In spite of its ambitious title, which could be summarized as "AGN, IGN, XRB, GRB, and IGM", this paper does not intend to be an exhaustive review of the hundreds, or even thousands of pages, written on all these subjects. It only aims at giving a few qualitative ideas on a possible link between them, part of these were published in a recent paper (Collin-Souffrin, 1991). The main new idea of the present paper is the suggestion of a connection between X-ray and gamma-ray diffuse backgrounds. Heating of IGM due to the diffuse background is also discussed, and it is shown that the IGM reaches a temperature of a few $10^5$K at high redshifts if $\Omega$(IGM)=0.01, but the temperature decreases at low redshift and is not sufficient to account for the Gunn-Peterson test at $z \sim 4$.

The following section will be devoted to a discussion of the connection between Active and Inactive Galaxies, based on recent works concerning AGN evolution. The conclusion is that a majority of Inactive Galaxies with mass and luminosity comparable to or larger than our own Galaxy must harbor a massive black hole in their nuclei. Since a large fraction of these black holes are not active presently, nor at a moderate redsifts 2-3, they must have grown emitting some radiation at high redshifts and have then been "switched off". In the third section, I will make the hypothesis that they were all radiating down to a redshift of the order 5 a gamma-ray spectrum similar to the observed diffuse gamma-ray background: the observed X-ray background in the range 10-100keV is then well accounted by these black holes, while the gamma-ray background is due mainly to local AGN. Finally the heating of Intergalactic Medium by the high redshift gamma-rays is briefly discussed in the last section. It is not clear that it is always correctly handled by people concerned with thermal equilibrium of IGM.

## II. AGN, IGN AND MASSIVE BLACK HOLES

If quasars and AGN are fueled by accretion onto massive black holes, as it is generally admitted (Rees, 1984), it is possible to determine the total mass accumulated in black holes per covolume unit using the observed quasar counts (Soltan, 1982). This method does not depend on any assumption on $H_o$ and $q_o$, nor on the rate at which black holes are accreting (their "Eddington ratio", i.e. their bolometric to Eddington luminosity ratio, must not be specified). Soltan found a density of about $5\ 10^{13}\ M_o/Gpc^3$, and this value is increased to $2\ 10^{14}\ M_o/Gpc^3$ by more recent determinations (Padovani et al, 1990). The mass is dominated by quasars at an average redshift of about 2. The problem is to find out how this mass is distributed among galaxies in the local Universe and which proportion of time this mass is spending in an "active phase".

The similarity of the luminosity functions of distant quasars and local Seyfert strongly suggests a luminosity evolution (Mathez, 1976, Schmidt and Green, 1983) at least in a statistical sense; i.e. the number of active galaxies stays a small fraction of the number of bright galaxies, but their integrated luminosity decreases by about two orders of magnitude from z = 2 to z = 0. A very natural idea would be that each quasar has dimmed down monotonically, giving rise to a less luminous AGN, namely a Seyfert galaxy. In this case Seyfert galaxies should harbor all black holes required to account for the past quasar luminosity. However this explanation does not hold, both because it would imply extremely large masses in the nuclei of local AGN ($10^{11}M_o$ or more), and because the total mass of local AGN per covolume unit should be equal to the mass of past quasars, which is far from being the case. Let us summarize the discussion given in a series of papers by Cavaliere et al (Cavaliere et al, 1985, 1988, Cavaliere and Padovani,1988, 1989).

The mass of individual black holes can be determined, either by fitting AGN continua in the near UV range with accretion disk emission, or by a dynamical method, amounting to studying the velocities of the broad line region and assuming that it is near gravitational binding. Both methods give about the same result: the mass of low luminosity (and therefore local) AGN, with $L_{bol} \leq 10^{45}$ ergs/s, is about one order of magnitude smaller than the mass of high luminosity ones (therefore high redshift ones), with $L_{bol} \sim 10^{47}$ergs/s. In other words the Eddington ratio $L_{bol}/L_{Edd}$ is smaller in Seyfert than in quasars. Quantitavely one gets from a mixture of both methods $R_{Edd} = L_{bol}/L_{Edd} \sim M_9^{1/2}$, where $M_9$ is in $10^9 M_o$ (Collin-Souffrin and Joly, 1991). It is difficult to disantangle the influence of redshift and luminosity in these studies, although Padovani (1988) favors an absence of correlation between z and the Eddington ratio. At least one does know that the Eddington ratio is a few $10^{-2}$ locally.

The total mass of black holes in AGN per unit volume in the local Universe is then computed (Padovani et al, 1990). This mass is found smaller than the quasars mass by at least two orders of magnitudes. It means that 99% of the mass of past quasars should be archived in nuclei of inactive galaxies.

Another way of reasoning is to consider the different possible activity patterns in relation with the local Eddington ratio or L/M value. Since statistically the luminosity decreases with time, while the mass goes on increasing, "the longer the activity lasts in each nucleus the smaller will be L/M locally, the shorter is the activity, the more numerous will be the generations of AGNs required to reproduce the statistically conserved number of objects" (Cavaliere et al, 1988). On this basis Cavaliere and Padovani (1988, 1989) showed that the local Eddington ratio is compatible only with a short lived activity (cumulated time $\sim 10^8$ years), implying that all galaxies with $L < $ a few $10^{-1}L_*$ have been involved in the activity process and contain a massive black hole. The fact that black holes become "inactive" at low redshifts, except

during short periods of time, is naturally explained if their activity is triggered by mergering, which should take place mainly at high redshifts, especially in a hierarchical scenario.

Several confirmations of this conclusion can be given. First it is well known that a weak Seyfert activity exists in a large fraction of galaxies, the so-called LINERS in particular, and could be due to a massive black hole accreting at a very low rate (cf. for instance Filipenko, 1988). Second, recent dynamical studies have shown the presence of large non-luminous mass concentrations, of $10^7$ - $10^8 M_o$ in the nuclei of otherwise inactive galaxies such as M31 and M32, or even of larger masses ~ $10^9$ $M_o$ as in M104 . The Galactic centre may also harbor a black hole of 3 - 5 $10^6 M_o$.

Therefore a large fraction of the mass of local black holes, representing more than 100 times the mass of local AGN, is built at a high redshift > 3. Adapted from Cavaliere et Padovani (1989) the mass distribution of local black holes in the range $3 10^6$ $M_o$ to $10^9$ $M_o$ is:

$$N(M) = \frac{10^{13}}{M^2} \qquad M_o^{-1}\ Gpc^{-3} \qquad (1)$$

where M is the mass of the hole expressed in solar mass and N(M) the number density of holes per mass interval also expressed in solar mass. The integrated mass is ~ $6\ 10^{13}$ $M_o\ Gpc^{-3}$, and more probably ~ $2\ 10^{14}\ M_o\ Gpc^{-3}$ to take into account the faint and high ends of the mass distribution. The average hole mass $< M >$ is equal to $3\ 10^7 M_o$ (in fact it is slightly larger if one takes into account the bending of mass distribution). It is interesting to note that $< M >$ is equal to the average mass of Seyfert nuclei determined by Padovani et al (1990). This agreement indicates that Seyfert activity is indeed a short lived phenomenon affecting all currently inactive galaxies.

We have now to ask what time it takes for the holes to grow and what is the amount of energy radiated during this growth.

It is difficult to imagine that the holes were not emitting radiation at a high rate during their growth, namely with a mass-energy conversion efficiency $\eta$ ~ 0.1. Even if the black holes are accreting only stars (which is unlikely at high redshifts), these stars are disrupted through the Hills mechanism, and finally it is always expected that the efficiency is determined by high energy plasma processes in the immediate vicinity of the hole, and is constant and close to the canonical value of 0.1 (Rees, 1984). So the energy radiated during the growth should be of the order $0.1Mc^2$, i.e. ~ $2\ 10^{67}$ ergs $Gpc^{-3}$. The energy emitted in the subsequent phase at low redshift is smaller.

The time left for black holes to grow is very short, since it is smaller than the time between the onset of growing and z ~ 3. Turner (1991) estimated that the density required to fuel the holes should be at least $10^{-2}\eta^{-2} M_o/pc^3$. It implies large overdensities relative to the cosmological mean, and large radii of the fuel reservoirs. So the onset

cannot take place before the formation of deep potential wells and it is clear that the holes must be built with large accretion rates.

The largest accretion rate for a radiating object is the critical rate corresponding to the Eddington luminosity. At this rate, the growth of black holes takes place in a time $t_{gr} = \eta\ t_E\ \ln(M_{fin}/M_{in})$, where $M_{in}$ and $M_{fin}$ are respectively the initial and final masses of the black holes, and $t_E$ is the so-called Eddington time, equal to $4\ 10^8$ years. Starting from a few solar masses, the building up time of a massive black hole should therefore be of the order of $5\ 10^8$ years, and is not much smaller than the age of Universe at $z \sim 5$. The growth of black holes should therefore take place during a large range of redshifts. Moreover the onset cannot be instantaneous for all holes, and the initial dispersion should be reflected in the final distribution of masses at a given time.

## III. XRB and GRB

### III. 1: Present status

The present status of the XRB has been summarized in de Zotti's talk at this same meeting. Let us recall a few points.

- In the range 0.5 to 3.5keV the XRB spectrum is consistent with a power law of slope 0.7 with a steep rise at lower energy. The intensity is larger than given by a simple extrapolation from larger energies. This spectrum can be accounted for by a mixture of contributions from AGN, clusters of galaxies, and/or star-forming galaxies.
- In the higher energy range 3 - 100keV the spectrum is well described by the expression $F(E) = 5.6\ (E/3keV)^{\alpha}\ \exp(-E/W)$ keV/(keV cm$^2$ s sr), with $\alpha = -0.29$ and W = 40keV (Marshall et al, 1980). It excludes a dominant contribution both from local AGN whose spectrum is different in this band ($\alpha = -0.7$, Mushotzky, 1984, Rotschild et al, 1983), and from clusters of galaxies whose spectrum corresponds to $\alpha = -0.4$ and W = 7keV. It is the well-known "spectral paradox" displayed by the XRB (Boldt, 1987). The problem is still not solved, in spite of several recent studies giving a better account of the contribution of quasars and galaxy clusters and of other possible sources of radiation such as normal galaxies (Schwartz and Tucker, 1988, Fabbiano, 1989, Fabian, Canizares and Barcons, 1989, Canizares and White, 1989, Persic et al, 1989, Griffitths and Padovani, 1990). The 23rd ESLAB meeting in Bologna (1989) was partly devoted to the study of the contribution of AGN to the XRB, but neither models of an AGN spectrum dominated by a high energy "reflection hump" (Fabian et al, 1990) nor the possibility of a large number of "hidden" quasars with a low energy cut-off (Setti and Woltjer, 1990) seem able to circumvent easily the problem.
- The shape of the residual XRB, once the estimated contribution of all known X-ray sources is subtracted, is controversial. While a majority of authors adopt a fit with an optically thin bremsstrahlung and T = 40keV, (Marshall et al, 1988), Subrahmanian and Cowsik (1989) find a better fit with T = 60keV, significantly hotter than previous estimates. Also,

precise determinations of the contribution of point sources argue for a flatter spectral shape in the 10-30keV range with $-0.2 < \alpha < 0.$ (Leiter and Boldt, 1982, Giacconi and Zamorani, 1987, Boldt, 1987) instead of $\alpha \sim 0.3$. We shall assume here that the background in the range 10-40keV is due to a fraction of radiation from known discrete sources, decreasing from 20% to 0%.

The relatively good agreement of the hard XRB spectrum with an optically thin thermal bremsstrahlung has spurred a great deal of work on the emission of a hot IGM (Cowsik and Kobetich, 1972, Field and Perrenod, 1977, Guilbert and Fabian, 1986, Barcons, 1987, Subrahmanian and Cowsik, 1989, Taylor and Wright, 1989, Lahav, Loeb and McKee, 1990). In order to radiate efficiently, the IGM must be heated to $T \sim 10^9$K at a high redshift $z \sim 4$-6. It then cools mainly by adiabatic expansion.

It is now well known that this model does not satisfy the constraint put by the recent COBE data, which have shown that the distortion of the cosmic background in the 500$\mu$ region is very small, and implies a Compton "y parameter" smaller than 0.001 (Mather et al, 1990), while the value predicted by the hot IGM is y=0.02. Although a clumped IGM can suppress the discrepancy and at the same time can explain the low energy part of the XRB, it cannot account for the 10-100keV spectrum (Loeb and Ostriker, 1991). So one is led to the conclusion that the 10-100keV XRB must be emitted by unknown non local (since otherwise they should be observed) discrete sources.

The origin of the low energy GRB in the range 0.5 - 5MeV, is also not clear. The spectrum is characterized by a conspicuous bump at about 2MeV. Below this value, the distribution is a power law with a spectral index close to 0.5; above 2Mev the spectral index is larger. One attractive model for this background is a dominant contribution from AGN, whose spectrum could have the same characteristics as the GRB - spectral index equal to 0.5, and break at a few MeV (Bignami et al, 1979, Bassani and Dean, 1983, 1984, Yu, 1987, Gao et al, 1990, Mereghetti, 1990). Unfortunately only 2 AGN, possibly 3 (including MCG 8.11.11 whose detection has still not been confirmed by Sigma), were observed so far in this range, so other observations are urgently needed. Also the spectral distribution in $\nu^{-0.5}$ of NGC4151 and 3C273 in the band 100keV - 1MeV has still not been confirmed by SIGMA, owing to its poor sensibility in this band (J.Ballet's talk in this meeting).

III. 2: The proposed model

It was suggested almost a decade ago (Leiter and Boldt, 1982, and later papers, Boldt and Leiter, 1984,1986, Boldt and Leiter, 1987, Boldt, 1987, Zdiarski, 1988) that "precursors" of AGN (PAG) were emitting mainly in the low energy gamma-ray band, and could explain the diffuse X-ray background. When Boldt and Leiter proposed this model, it was not clear that non-active galaxies also harbor massive black holes in

their nuclei, so they relied on the holes existing in local Seyfert galaxies for this. They suggested that the spectral distribution of these PAG was mainly of thermal origin (Comptonized bremsstrahlung).

In the present paper two different hypothesis will be made:

*1. AGN are giving the soft gamma-ray background;*

*2. the gamma-ray spectrum of progenitors black holes is the same as that of AGN.*

The first hypothesis is acceptable, as shown before. It will serve as a guide-line to specify the gamma-ray spectral distribution, since informations on AGN emission are so scarce. The second hypothesis is also quite natural, since the same processes take place in the environment. of the black holes progenitors as of AGN themselves.

The total background intensity radiated in the range 10-100keV can be estimated:

$$I_{10\text{-}100keV} \sim 2\ 10^{-7}\ (1+z)^4 \quad \text{ergs /(s cm}^2\ \text{sr)} \qquad (2)$$

if it is radiated at a redshift z. Note that the spectrum at emission is harder by a factor (1+z). This number has to be compared to the total amount of energy radiated by the black holes, 2 $10^{67}$ ergs $Gpc^{-3}$ (covolume), which corresponds to an intensity:

$$I = \frac{c}{4\pi}\ 1.2\ 10^{-15}\ (1+z)^3 \quad \text{ergs /(s cm}^2\ \text{sr)} \qquad (3)$$

*It is striking that these two intensities compare at z ~ 5-10, the redshift at which the bulk of black holes should have grown and have been switched off.*

AGN models of the GRB are generally based on the AGN luminosity function in the X-ray range extrapolated in the low energy gamma-ray range. Since the purpose of this paper is not to discuss in detail the GRB, *but only to show how it relates to the XRB,* the gamma-ray luminosity function of AGN is not considered in detail: a non-evolving population of emitters is assumed, whose flux level is fitted to that of the gamma-ray background. This assumption is consistent with the fact that the X-ray to optical luminosity ratio decreases with increasing luminosity ($L_X \propto L_{opt}^{0.8}$), so the gamma-ray background, if it is linked to the X-ray, may be dominated by faint, local AGN.

The spectrum emitted by AGN and by progenitor black holes is then parametrized by:

$$I(E) = E^{-\alpha_X} \left[1 + \left(\frac{E}{E_{break}}\right)^{\alpha_\gamma - \alpha_X}\right]^{-1} \qquad (4)$$

where $\alpha_x$ and $\alpha_\gamma$ are the spectral index respectively in the hard X-ray ($h\nu > 10keV$) and in the gamma-ray range, and $E_{break}$ is the energy of the break. $E_{break}$ should be close to the energy of the bump in the

gamma-ray background. Although the average spectral index in the X-ray range is $\alpha_x$ = 0.7, one can safely assume a flatter spectrum in the soft gamma-ray range, since the background should be dominated by the most intense emitters.

To determine the flux level of the black hole emission, we assume that a large fraction of their bolometric luminosity is radiated in the range 10 keV - $E_{break}$ (for the 3 AGN observed so far, this proportion is larger than 50%). The problem is to know how this emission is distributed in time. It is linked with the growth of perturbations and the formation of "seed black holes". To avoid this discussion, which is postponed to a future work, we assume simply that injection of black holes takes place at a uniform rate between $z_{init}$ and $z_{fin}$, and that these black holes are radiating at their Eddington luminosity. So the only constraint is given by the amount of radiative energy available at $z_{fin}$, i.e.1.2 $10^{-15}$ ergs $cm^{-3}$ (covolume).

A satisfactory model is obtained for the following parameters: $\Omega$ = 1, $H_o$ = 75, $\alpha_x$= 0.5, $\alpha_\gamma$= 3, $E_{break}$= 500keV, $z_{init}$ = 24 and $z_{fin}$ = 5: it is clear that other combinations of these parameters could lead also to satisfactory results.

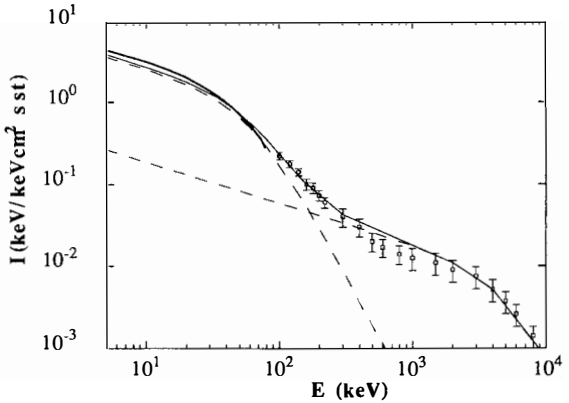


**Figure 1:** Computed and observed X-ray and gamma-ray background for the model whose parameters are given in the text. Dashed lines: separated contributions of black holes and AGN. Full bold line: fit of the observations by Marshall et al. Full thin line: computed spectrum

The computed spectrum in displayed on Figure 1, where the contributions of black holes and of AGN are separated. The observed background is also shown. In the 5-100keV range, Marshall's et al (1983) fit to the observed background is used. In the range 5-40keV a

small contribution is allowed for known discrete sources: it can be reduced, or even suppressed.

This very simple model gives therefore a good agreement with the diffuse background on three decades of magnitudes. An interesting implication of the model is that another important contribution to the diffuse background is expected near 1μ, if the similarity between black hole and AGN spectral distribution extends in other spectral bands, in particular in the UV band (the so-called "UV-bump" of AGN).

To test this model it would be necessary to get some information on the evolution of the X-ray and gamma-ray spectrum of high redshift quasars, in particular at the faint end of the luminosity function, where they will dominate the XRB, and where they are presently completely unobserved. It is also clear that any detection of a kind of "black hole activity" in inactive galaxies, and further determination of the mass setting in galactic nuclei, which could be envisioned with the Space Telescope, would be a major improvement in our understanding of the problem.

## IV. HEATING OF THE INTERGALACTIC MEDIUM

If the diffuse X-ray background is emitted at high redshifts as a gamma-ray background, and independently of the origin of this background (discrete sources, or diffuse radiation), the intergalactic medium will be rapidly heated and ionized by Compton scattering and subsequent thermalisation of high energy electrons (Collin-Souffrin, 1991). The heating process takes place even if the IGM was still cold and neutral before the emission of gamma-rays, and if it contains all baryonic matter of Universe.

In the previous scenario of black hole origin of the X-ray background, the heating takes place immediately after the onset of emission of black holes. So it can play an important role, in particular as a "fit-back" in the formation of galaxies. Another problem is to determine if the heating is sufficient to explain the Gunn-Peterson test at $z \sim 4$, when the quasar population is unable to provide enough photoionisation flux to account for the high level of ionization of IGM. This topic was addressed by P. Shapiro in another talk, but since it was a subject of controversies some comments concerning cooling processes at high redshifts are added here. Moreover the problem seems to have perhaps been misunderstood in previous works.

In the present model, IGM is heated by Compton scatterings of high energy photons on electrons, either free or bound in atoms. This process creates a population of high energy electrons which are rapidly thermalized and heat the medium. In addition to adiabatic cooling, two processes contribute to the cooling: inverse Compton cooling on the CRB, and cooling due to radiation losses, consisting in collisionnally excited bound transitions of He and H, recombinations and free-free transitions.

If the heating is provided by a mechanical process (shock waves, cosmic rays...), or by high energy photons, as it is the case here, the

medium is heated at a temperature which, for a given ionization degree, is higher than in the case of radiative UV heating. In other words the ionization degree is relatively low at high temperature. *It has the important consequence that the medium is optically thick at the Lyman limit and in the soft X-ray range, so that any radiation emitted in this range is reabsorbed "on the spot", and cannot contribute to the cooling.* Resonance line cooling is also inefficient. These lines are indeed reabsorbed on the spot, either if the line optical thickness corresponding to a shift $\Delta z_D = \Delta\nu_D/\nu$ ($\Delta\nu_D$ = the thermal width) is larger than unity, or if these lines have an energy larger than 13.6eV.

Therefore if the medium is optically thick, only recombinations onto excited levels of H and He, and the fraction of free-free transitions with $h\nu < 13.6$eV, lead to a real emission of radiation. However subordinate lines resulting from collisional excitations off the ground level followed by subsequent degradation of photons contribute to the cooling (such as H$\alpha$ which is emitted necessarily after a few diffusions of L$\beta$ or higher Lyman lines, or the transition 10320A occuring after collisional excitations of the ground level of HeI). An error in Collin-Souffrin (1991) was to neglect this last term, which represents less than 10% of the whole collisional cooling, but is however sufficient to act as a strong thermostat (owing to its exponential dependence in T) if the density of IGM is large (however, after having read several papers discussing the thermal equilibrium of IGM at high z, I got the impression that at least some authors make the opposite error, in considering all collisional excitations and recombinations as contributing to the cooling).

To illustrate this discussion, Figures 2a, 2b and 2c display the temperature and the different cooling rates as functions of redshift, for the previous model, with $\Omega$(IGM) = 0.01 and $\Omega$(IGM) = 0.1. The model with $\Omega$(IGM)= 0.01 considers all collisional excitation cooling of H and He, so it underestimates slightly the temperature. Two different computations have been performed for $\Omega$(IGM)= 0.1: one including all collisional excitations (Fig. 2b), and one including only the recombination, free-free, and HI subordinate line coolings (Fig. 2c). The second case is probably closer to reality.

As can be seen on Fig. 2a, for $\Omega$ (IGM) = 0.01 the cooling rate is entirely dominated by inverse Compton at high redshifts, and by adiabatic cooling at low redshifts. The temperature is very high immediately after the onset of heating ($3\ 10^5$K), but decreases rapidly, to reach $2\ 10^4$K at z = 5. Such a temperature cannot account for the Gunn-Peterson effect, which requires $T > 8\ 10^4$K at z = 4 for $\Omega$ (IGM) = 0.01 (Collin-Souffrin, 1991).

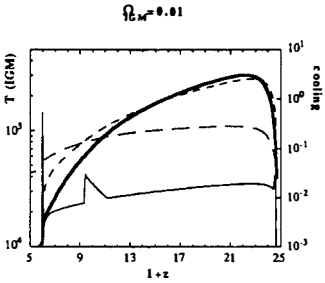


Fig. 2a

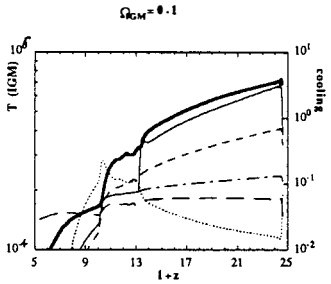


Fig.2b

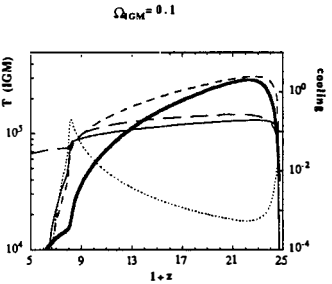


Fig.2c

**Figures 2a to 2c:** Temperature and cooling rates. Full bold line: temperature. Full thin line: total He and H cooling. Dotted-dashed line: recombination and free-free cooling. Large dashed line: adiabatic cooling. Dotted line: subordinate HI cooling. Small dashed line: inverse Compton cooling.

In the dense IGM with $\Omega$ = 0.1, the problem is quite different. Cooling is dominated by radiation if all collisional excitations are taken into account (Fig. 2b), but it is not the case if only recombination, free-free, and subordinate line cooling are taken into account (Fig. 2c). To show that resonance line cooling and a large part of free-free and free-bound cooling are indeed negligible, Figure 3 displays for the same model two important optical thicknesses as functions of z for the $\Omega$(IGM)= 1 case: the optical thickness per redshift unit at the Lyman limit, and the optical thickness at the L$\alpha$ center, corresponding to $\Delta z_D$. Both optical thicknesses are much larger than unity, so all radiative processes can be neglected, except a small proportion of the free-free, bound-free and subordinate line cooling. In this case, the temperature reached by IGM is also of the order of 3 $10^5$K, but again it decreases rapidly with z and the Gunn-Peterson test cannot be satisfied at low redshifts, since it requires T > 2 $10^5$K for $\Omega$ (IGM) = 0.1 at z = 4.

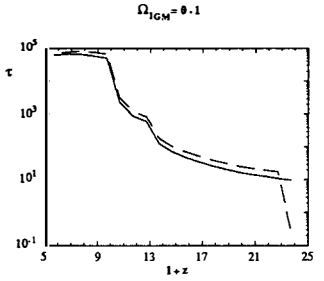


Fig. 3

**Figure 3:** Optical thickness versus redshift. Large dashed line: optical thickness at the Lα center for $\Delta z_D$. Full line: optical thickness at the Lyman limit per redshift unit.

## V. CONCLUSION

Perhaps....

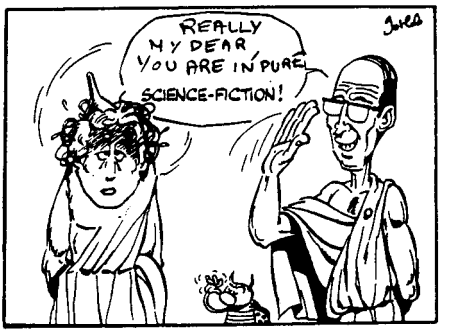


**Aknowledgments**

I thank J. Bergeron, A. Blanchard, E. Boldt, D. Leiter and P.Shapiro for several helpful discussions (oral or by mail).

**Bibliography**

Barcons X., 1987, Ap.J. 313, 547
Bassani L., Dean A.J., 1983, Space Science Review 35, 367
Bassani L., Dean A.J., 1984, Astrophysics and Space Science 100, 457

Boldt E., Leiter D., 1984, Ap.J. 276, 427
Boldt E., Leiter D., 1986, in "Structure and evolution of Active Galactic Nuclei", Ed. Giuricin et al
Boldt E., Leiter D., 1987, Ap.J. 322, L1
Bignami G.F., Fichtel C.E., Hartman R.C., Thomson D.J., 1979, Ap.J. 232,649
Canizares C.R., White J.L., 1989, Ap.J. 339, 27
Cavaliere A., Giallongo E., Vagnetti F., 1985, Ap.J. 296, 402
Cavaliere A., Giallongo E., Padovani P., Vagnetti F., 1988, in "Optical surveys for quasars, Ed. P. Osmer
Cavaliere A., Padovani P., 1988, Ap.J. 333, L33
Cavaliere A., Padovani P., 1989, Ap.J. 340, L5
Collin-Souffrin S., 1991, A & A 243, 5
Collin-Souffrin S., Joly M., 1991, in preparation
Cowsik R., Kobetitch E.J., 1972, Ap.J. 177, 585
Fabian A.C., Canizares C.R., Barcons X., 1989, Mon. Not. R. Astr. Soc. 239,15p
Fabbiano G., 1989, Ann. Rev. Astr. Ap. 27, 87
Field G.B., Perrenod C., 1977, Ap.J. 215, 717
Filippenko A.V., 1988, in "Supermassive Black Holes", Ed. Kafatos
Gao Y-T, Cline D.B., Stecker F.W., 1990, Ap.J. 357, L1
Giacconi R.H., Gursky H., Paolini F., Rossi B., 1962, Phys. Rev. Lett. 9, 439
Giacconi R., Zamorani G., 1987, Ap.J. 313, 20
Griffiths R.E., Padovani P., 1990, Ap.J. 340,, 483
Guilbert P.W., Fabian A.C., 1986, Mon. Not. R. Astr. Soc. 220, 439
Lahav O., Loeb A., McKee C.F., 1990, Ap.J.342, L9
Leiter D., Boldt E., 1982, Ap.J. 260, 1
Loeb A., Ostriker J.P., 1990, preprint
Marshall F.E., Boldt E.A., Holt S.S., Miller R., Mushotzky R.F., Rose L.A., Rotschild R.E., Serlemitsos P.J.,1980, Ap.J. 235, 4
Mather J.C. et al., 1990, Ap.J. 354, L37
Mathez G., 1976, Astron. Astrophys. 53, 15
Mereghetti S., 1990, Ap.J. 354, 58
Mushotzky R.F., 1984, Adv. Space Res. 3 157
Padovani P., 1988, Astron. Astrophys. 192, 9
Padovani P., Burg R., Edelson R.A., 1990, Ap.J. 353, 438
Persic M., De Zotti G., Danese L., Palumbo G.G.C., Franceschini A., Boldt E.A., Marshall F.E., 1989, Ap.J. 344, 125
Rees M.J., 1984, Ann. Rev. Astr. Ap. 22, 471
Rothschild R., Mushotzky R., Baity R., Gruber D., Matteson J., Peterson L., 1983, Ap.J. 269, 423
Schmidt M., Green R.F., 1983, Ap.J. 269, 352
Schwartz D.A., Tucker W.H., 1988, Ap.J. 332, 157
Setti G., Woltjer L., 1990, Astron. Astrophys. L21
Soltan A., 1982, Mon. Not. R. Astr. Soc. 200, 115
Subrahmanyan R., Cowsik R., 1989, Ap.J.347,1
Taylor G.B., Wright E.L., 1989, Ap.J. 339, 619
Turner E.L., 1991, Astron. J. 101, 1
Yu K.N., 1987, Astrophysics and Space Science 136, 1
Zdziarski A.A., 1988, Mon. Not. R. Astr. Soc. 233, 739

# The $\gamma$-ray line signature of the elusive neutrino

Pierre Salati [a] [†] and Pascal Chardonnet [b].

*a) Theory Division, CERN, CH-1211, Geneva 23, Switzerland*
*and*
*b) LAPP, Chemin de Bellevue, BP110, 74941 Annecy-le-Vieux Cedex, France*

**Abstract**

We study the possibility of detecting halo cold dark matter through the annihilation process $\chi\chi \rightarrow \gamma\gamma$. This process produces monoenergetic $\gamma$-rays, and may be a clear signature of particle dark matter. If there is a closure density of photino – so far a favoured candidate – we show that it will be very difficult to observe this annihilation line from a satellite or space station borne experiment. On the contrary, triplet neutrinos which have recently been suggested as a plausible solution to the dark matter conundrum, whilst elusive at accelerators, should produce a clear $\gamma$-ray line signal, well above background.

## 1 - The CDM annihilation $\gamma$-ray line signal.

There is a considerable interest in the possible detection of dark matter [1] through astrophysical observations as well as terrestrial observations [2,3]. If dark matter is made of massive, weakly interacting particles, one of the best indirect signatures would be the detection of annihilation products of these particles [4]. It has been recently suggested [5,6,7] that if particles in the mass range 1 GeV to 100 GeV pervade the halo of our Galaxy and if these species self-annihilate, as most of the potential candidates do, then monoenergetic $\gamma$-rays should be observed when the cold dark matter particles annihilate directly into two photons. The energy of these $\gamma$'s is very nearly equal to the mass of the (non-relativistic : $v/c \sim 10^{-3}$) parent particles. Very narrow $\gamma$ lines in the range 1 GeV

[†] On leave of absence from LAPP, BP110, 74941 Annecy-le-Vieux Cedex, France and from Université de Chambéry, 73000 Chambéry, France.

to 100 GeV would provide a clear signature for dark matter annihilation, if they stand out above the background.

We assume that the dark matter halo of our Galaxy is nearly spherical and nearly isothermal. Then, the dark matter density varies with the distance $r$ to the galactic center as :

$$\rho(r) = \rho_\odot \frac{a^2 + r_\odot^2}{a^2 + r^2} \ , \tag{1}$$

where $\rho_\odot$ is the dark matter density in the solar neighbourhood and $a$ is the core radius. We consider the annihilation process $\chi\chi \rightarrow \gamma\gamma$, the cross-section for which is $\sigma_{2\gamma}$. The mass of the dark matter species $\chi$ ranges from 1 GeV to 100 GeV according to specific models, whereas their mean velocity in the halo is $v \sim 300\,\mathrm{km\,s^{-1}}$. The energy $E_\gamma$ of the outgoing $\gamma$'s is therefore practically equal to the particle mass $m_\chi$. The number of photons received at a detector in the solar system, from pair annihilations taking place at a distance $R$ and in the direction defined by galactic latitude $b$ and longitude $l$ is [8] :

$$F = \frac{\sigma_{2\gamma} v}{4\pi} \int_0^\infty \left[ \frac{\rho(R,b,l)}{m_\chi} \right]^2 dR \ \mathrm{cm^{-2}\,s^{-1}\,sr^{-1}} \tag{2}$$

when summed over the distance $R$. This expression may be evaluated analytically and at high galactic latitudes ($b \sim 90°$) – for which the galactic diffuse background is expected to be the faintest – the flux reduces to :

$$F \sim \frac{\sigma_{2\gamma} v}{16} \left( \frac{\rho_\odot}{m_\chi} \right)^2 a \sqrt{1 + A^2} \ , \tag{3}$$

where $A$ denotes the ratio $r_\odot / a$. Taking $\rho_\odot = 0.4\,\mathrm{GeV cm^{-3}}$ and $a \sim r_\odot \sim 8\,\mathrm{kpc}$, and assuming a typical value of $\sigma_{2\gamma} v \sim 10^{-30}\,\mathrm{cm^3\,s^{-1}}$ for the $\gamma$-ray pair annihilation cross-section, we find that a detector of $1\,\mathrm{m^2\,sr}$ effective area, such as ASTROGAM or HR-GRAF [9], will collect $N_{line}$ photons of energy $E_\gamma = m_\chi$ per year, where :

$$N_{line} \sim 110 \text{ photons} \left( \frac{1\,GeV}{E_\gamma} \right)^2 \ . \tag{4}$$

## 2 - The various $\gamma$ backgrounds.

There is no measurement of $\gamma$-ray fluxes in the GeV-TeV energy range, so we must extrapolate from lower energy data. There are many different sources of background $\gamma$ photons. The $\gamma$'s from the decay of $\pi^0$'s produced by collisions of cosmic ray protons with the interstellar medium are probably the dominant source of galactic background at energies larger than 1 GeV [10]. Bremsstrahlung $\gamma$'s from cosmic ray electrons should be negligible above 1 GeV as well as the inverse Compton emission resulting from the interaction between ultra-relativistic electrons and the electromagnetic field of the galaxy. From the known distribution of cosmic ray protons, one expects a flux [11] :

$$\frac{dN_{galactic}}{dE_\gamma} \sim 8 \times 10^{-7} \,\mathrm{photons\,cm^{-2}\,s^{-1}\,sr^{-1}\,GeV^{-1}} \left( \frac{1\,GeV}{E_\gamma} \right)^{2.7 \pm 0.3} \tag{5}$$

at high galactic latitudes, and a correspondingly larger flux in the galactic plane.

The extra-galactic background is not well known, and different analyses do not agree on the extrapolation of COS-B and SAS-2 measurements to energies larger than 1 GeV [12]. Since it may drop sharply above 1 GeV, we do not consider it any further, but keep in mind the possibility that it could be of the same order of magnitude as the galactic background.

Dark matter provides its own background when it annihilates into fermion-antifermion pairs, which give $\gamma$-rays among their decay and annihilation end-products, but these $\gamma$'s have an energy lower than $m_\chi$ (for trivial kinematical reasons), and do not contribute to the line background.

To summarize, we take Equ. 5 as representing the background, but we must keep in mind that it could be an order of magnitude smaller or larger. Since the aim is to detect a narrow line, much narrower than the energy resolution of the detector, the interesting quantity is the number of photons received in one energy bin during the time of observation. For a $1\,m^2\,sr$ detector with a 1% energy resolution (bin width $\Delta E_\gamma = 0.01\,E_\gamma$), one year of observation will give :

$$N_{background} \sim 2500 \text{ photons} \left(\frac{1\,GeV}{E_\gamma}\right)^{1.7\pm0.3} \tag{6}$$

If one compares the expected signal $N_{line}$ (Equ. 4) to the background $N_{background}$ (Equ. 6), the situation does not seem very promising. But this comparison is actually meaningless. We should *not* compare the expected signal to the background but to the *noise*, i.e. the error in measuring the background. The statistical uncertainty is the square root of the number of photons received :

$$Noise \sim 50 \text{ photons} \left(\frac{1\,GeV}{E_\gamma}\right)^{0.85\pm0.15} \tag{7}$$

## 3 - The photino case.

The photino $\tilde{\gamma}$ is the neutral spin 1/2 supersymmetric partner of the photon, and one of the foremost candidates for dark matter because it naturally implies a near-critical density for the universe. Photino annihilation proceeds through the exchange of the so-called sfermions – the supersymmetric spin 0 partners of the conventional fermions such as the electron or the quarks – whose mass is generically denoted by $\tilde{M}$. The larger $\tilde{M}$, the lower the annihilation cross section and the larger the fossil density $\Omega_{\tilde{\gamma}}\,h^2$ [13]. The latter is actually related to the two-photon annihilation cross-section through :

$$\sigma_{2\gamma} v \sim 3.1 \times 10^{-31} cm^3\,s^{-1}\,\left(\Omega_{\tilde{\gamma}}\,h^2\right)^{-1} \quad , \tag{8}$$

so that an ASTROGAM caliber $\gamma$-ray telescope, aimed toward the galactic pole, should collect each year :

$$N_{line} \sim 34 \text{ photons} \left(\frac{1\,GeV}{E_\gamma}\right)^2 \left(\Omega_{\tilde{\gamma}}\,h^2\right)^{-1} \quad . \tag{9}$$

However, experiments at the Large Electron Positron storage ring, LEP, at CERN have recently set the constraint $\tilde{M} > 45$ GeV from their unavailing searches for supersymmetric fermions [14]. That lower bound on the generic sfermion mass $\tilde{M}$ translates into an upper bound on the annihilation cross-section $\sigma_{2\gamma}v$. For a 1 $m^2$ sr detector, the $\gamma$-ray line has signal to noise ratio constrained to be $< 3$. Even in the best case, *i.e.*, for $\Omega_{\tilde{\gamma}} h^2 = 1/40$, detection of photinos in the galactic halo would imply a significantly larger telescope area. In order to achieve such a detection at, say, the 5 $\sigma$ level, a 3 $m^2$ sr $\gamma$-ray detector should operate during an entire year.

## 4 - Heavy neutrinos, LEP and the $\gamma$-ray line signal.

Experiments at LEP have also measured the total decay rate of the $Z^0$ boson [15]. From its invisible width, the conventional assumption that there are only three light neutrino families turns out to be distressingly valid. The LEP determination of the number of invisible species ruins an appealing explanation of the missing mass conundrum in terms of a fourth generation heavy neutrino. The latter should be heavier than $\sim$ 45 GeV in order to escape detection at LEP. For such a large mass, neutrinos annihilate so efficiently in the early universe that their fossil density is too low to be cosmologically relevant [16].

There is however a possible way out. Note that the Dirac or Majorana neutrinos so far considered have always been assumed to be embedded inside a gauge *doublet* as the conventional electron neutrino $\nu_e$ and its associated electron are. Such an assumption may actually be relaxed. A heavy gauge *triplet* neutrino, N, has recently been suggested [17] as a plausible dark matter candidate. This species and its singly charged gauge partner E have gauge triplet structure : $(E^+, N, E^-)$. Since the neutral particle N does not couple to the $Z^0$, it cannot be produced at LEP and is therefore invisible, at least in the first stage of the LEP experiments. N however couples to E through W boson exchange so that the delicate interplay between both species in the early stages of the Big-Bang leads to a closure fossil density of neutrinos, provided the neutrino mass $m_N$ lies in the range 30–80 GeV. Note that if on the one hand N cannot be produced directly at accelerators, on the other hand its charged companion E is expected to be detected at LEP as soon as the beam energy is cranked up to $\sim$ 100 GeV.

Another signature of the triplet neutrino model is precisely the fairly strong $\gamma$-ray line signal from galactic halo particles. Gauge couplings are significantly larger for triplet than for doublet species, so that the cross-section for the annihilation process $NN \rightarrow \gamma\gamma$ is quite large :

$$\sigma_{2\gamma}v \simeq \frac{96}{\pi^3}\alpha^2 G_F{}^2 m_N^2 \ , \qquad (10)$$

where $\alpha = 1/137$ is the electromagnetic fine structure constant, $G_F$ is the Fermi constant and $m_N$ is the neutrino mass. Note that $m_N$ gracefully cancels out from expressions (3) and (10). The flux $F_N$ of monochromatic photons with energy $E_\gamma = m_N$ due to neutrino N annihilations in the galactic halo does *not* depend therefore on the mass of this species : $F_N \simeq 10^{-10}$ photons $cm^{-2}\, s^{-1}\, sr^{-1}$.

We infer a signal of order $\sim$ 30 monochromatic photons (see Fig. 1) detected each year at a satellite or space station borne $\gamma$-ray telescope with a 1 $m^2$ sr effective area, in the

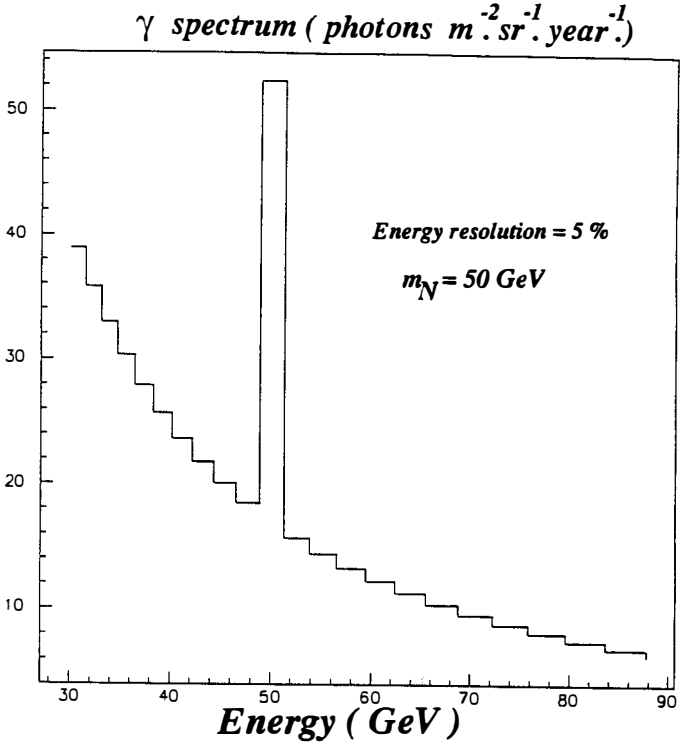


Figure 1

After an entire year of observation, a 1 $m^2$ sr $\gamma$-ray telescope, with a 5% energy resolution, would collect this photon spectrum in the case of a 50 GeV neutrino $N$ pervading the galactic halo. The annihilation line stands well above background. The galactocentric distance is set equal to $r_\odot = 8.5$ kpc whilst the dark matter halo has core radius $a = 7$ kpc and density $\rho_\odot = 0.45\,\mathrm{Gev\,cm^{-3}}$ in the solar neighbourhood.

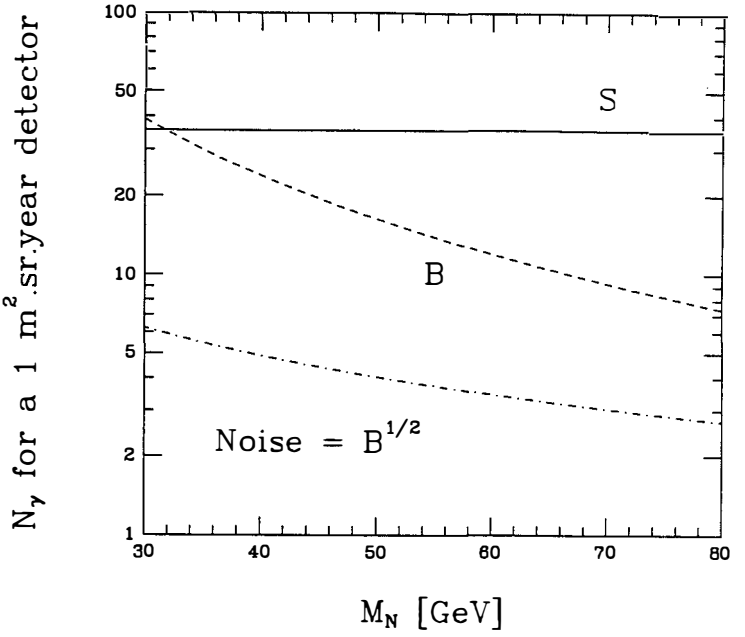


## Figure 2

Expected signal (S), background (B) and noise for monoenergetic $\gamma$-rays due to pair annihilation of triplet neutrinos N in the halo of our galaxy. The full line displays the total number of annihilation $\gamma$'s received for an entire year of exposure on a detector with a 1 $m^2$ sr detector surface and a 5% energy resolution. The short dashed line corresponds to the number of background photons collected in the same energy bin as the annihilation line, while the dotted - short dashed curve indicates the background noise. Note that if on the one hand the signal does not depend on the mass $m_N$ of the heavy triplet neutrino, on the other hand, background and noise do decrease with line energy $E_\gamma = m_N$. The heavier the neutrino, the easier the detection. Even for $m_N = 30$ GeV, detection will be achieved at the 5 $\sigma$ level wilst for $m_N = 80$ GeV, the signal to noise ratio may reach up to $\sim 10$.

energy range between 30 and 80 GeV. At these energies, the corresponding background is fairly small. If the latter is well modelled by expression (5), a 5% energy resolution corresponds to, at most, $\sim$ 40 background photons collected in the same energy bin as the annihilation line. Detection of the $\gamma$-ray line signature of galactic halo triplet neutrinos could therefore be achieved at least at the 5 $\sigma$ level, a fairly comfortable situation. We therefore urge high energy astrophysicists to explore the $\gamma$-ray sky and to hunt for such a signal. Should a narrow $\gamma$-ray line be discovered, the nature of the galactic halo would be unravelled.

## References


[1] J. Kormendy, and G.R. Knapp, *In* Dark matter in the Universe, IAU Symposium **117** (Reidel) (1987).

[2] J. Primack, D. Seckel, and B. Sadoulet, Ann. Rev. Nucl. Part. Phys. **38**, 751 (1988).

[3] P.F. Smith, and J.D. Lewin, Report Rutherford RAL-88-045 (1988).

[4] J. Silk, and M. Srednicki, Phys. Rev. Lett. **53**, 624 (1984).

[5] L. Bergström, and H. Snellman, Phys. Rev. **D37**, 3737 (1988).

[6] S. Rudaz, Phys. Rev. **D39**, 3549 (1989).

[7] A. Bouquet, P. Salati, and J. Silk, Phys. Rev. **D40**, 3168 (1989).

[8] M.S. Turner, Phys. Rev. **D34**, 1921 (1986).

[9] J.H. Adams *et al.*, Naval Research Laboratory proposal T-248-89 (1989); E.J. Fenyves, NASA Code E proposal UTD No. 890061 (1989).

[10] J.B.G.M. Bloemen, Astrophys. J. Lett. **317**, L15 (1987).

[11] F.W. Stecker, Astrophys. J. **223**, 1032 (1978).

[12] C.E. Fichtel and D.J. Thompson, Astron. Astrophys. **109**, 352 (1982).

[13] H. Goldberg, Phys. Rev. Lett. **50**, 1419 (1983).

[14] See for instance the DELPHI Collaboration, P. Abreu *et al.*, CERN-EP/90-79 preprint (1990).

[15] L3 Collaboration, B. Adeva *et al.*, Phys. Lett. **B231**, 509 (1989);
ALEPH Collaboration, D. Decamp *et al.*, Phys. Lett. **B231**, 519 (1989);
OPAL Collaboration, M.Z. Akrawy *et al.*, Phys. Lett. **B231**, 530 (1989);
DELPHI Collaboration, P. Aarnio *et al.*, Phys. Lett. **B231**, 539 (1989).

[16] K. Griest and J. Silk, Nature **343**, 26 (1990).

[17] P. Salati, preprint CERN-TH-5868/90 (1990); to be published in Phys. Lett. **B**.

## REMOTE CLUSTERS AND X-ray BACKGROUND

**Richard SCHAEFFER**
*Direction des Sciences de la Matière*
*Service de Physique Théorique Centre d'Etudes de Saclay*
*F—91191 Gif-sur-Yvette cedex*

**ABSTRACT**

We evaluate the cluster multiplicity function at the present epoch and in the recent past using a method based on the solution of the equations that describe non-linear hierarchical clustering. The cluster contribution to the $X$-ray background is deduced. They are found to produce a sizeable fraction of the observed background in the 0.1 – 1 keV band. We predict the presence of numerous small $X$-ray clusters at high redshift. These clusters also induce a measurable distortion of the microwave background though the Sunyaev-Zeldovich effect.

Rich clusters are powerful $X$-ray sources: a sizeable fraction of their mass is in the form of gaz, trapped by their gravitational potential and heated up to $10^8$ $K$. This gaz is quite likely to be primordial, although the observation of Iron lines shows it has been somewhat contaminated by galactic ejecta. It may represent the baryon fraction that has not yet turned into galaxies. This hot gaz radiates by thermal bremstrahlung an energy of the order of $L_x \sim 10^{44}$ erg s$^{-1}$, for a $\sim 10^{14}$ $M_\odot$ cluster. The corresponding cooling time $t_i \sim 10^{11}$y is much larger than the age of the universe. One therefore expects these clusters to have been $X$-ray emitters since their formation. The $X$-ray emission from the down ($z \leq 0.1$) rich, Abell clusters typically accounts (Schmidt and Green 1986) for 10% of the known background in the keV range.

No thorough investigation of the $X$-ray properties of the smaller clusters, or groups such as TG groups (Turner and Gott 1976), exists. Sarazin (1986) considers a few "poor" clusters, whereas Edge et al (1990) go down to luminosities of the order of $10^{43}$ erg s$^{-1}$ and temperatures of 0.3 keV. Numerous small clusters and groups are however expected to exist, and to have a gravitational potential in which hot gaz ($\sim 10^7$ $K$) may be trapped. With a large spread of radii and masses, centered respectively around 1 Mpc and $10^{13}$ $M_\odot$, they are expected to be $X$-ray emitters, with luminosities around $10^{42-43}$ erg s$^{-1}$, for about $10^{10}$ y.

Such a short cooling time raises the question wheter these smaller clusters are still ermitting at the present epoch. However, if ever no longer active now, these clusters must have been strong $X$-ray sources in a recent past.

Various estimates (Schaeffer and Silk 1985, 1988, Bernardeau and Schaeffer 1991) can be made for the cluster multiplicity function. They can be checked in the light of the observations at the present epoch, and then used to extrapolate the cluster distribution towards the past, and to estimate the cluster contribution to the $X$-ray background.

### Models for the cluster multiplicity function

The simplest estimate for the cluster luminosity function is to start from a fiven initial spectrum of fluctuations, to let it evolve according to linear theory and to count the number of non-linear fluctuations, the latter may be either defined as the number of peaks of the density fluctuations in the very early universe above a given threshold (Bardeen et al, 1986), or estimated from the number of random cells of a scale $R$, laid down in the early universe that contain enough matter so as to eventually become non-linear, whereas a slightly larger cell remains linear (Press and Schechter 1974, Schaeffer and Silk 1985, 198 a, Kaiser 1986—1991, Cole and Kaiser 1989). These two approaches lead to similar expressions. The one inspired from the pionneering work of Press and Schechter reads, at redshift $z$,

$$\eta(M)\mathrm{d}M \sim \frac{\rho}{M}\frac{1}{\sqrt{2\pi}}\frac{1+z}{\Sigma^2(M)}\left|\frac{\mathrm{d}\Sigma}{\mathrm{d}M}\right|\exp -\frac{1}{2}\frac{(1+z)^2}{\Sigma^2(M)}\mathrm{d}M \qquad (1)$$

where $\eta \mathrm{d}M$ is the number of objects of mass $M$ and $M + \mathrm{d}M$, and $\Sigma(M)$ the r.m.s. fluctuation of the matter distribution in a cell that on the average contains a mass $M$. This fluctuation $\Sigma(M)$ is calculated from linear theory, but its normalisation is estimated as what it would be at the present epoch in case the evolution of the density fluctuations would still be given by the linear approximation. It is adjusted to observations by imposing that it is unity in a sphere of radius $8h^{-1}$ Mpc, since the r.m.s. fluctuations of the galaxy distribution in the present (non-linear) universe are unity at his scale, which corresponds to a mass: $M_0 = 5.6\ 10^{14}\ \Omega h^2\ M_\odot$. The shape of $\Sigma(M)$ is usually taken from some hypothesis on the initial conditions. The standard choice is to use the so called "Cold Dark Matter" spectrum (Peebles 1982). The form (1) adjusted in this way reproduced reasonnably well (Schaeffer and Silk 1985) the present-day clustering which is observed. At the cluster scales we are interested in, it may be parametrized by

$$\Sigma(M) = (M/M_0)^{-\frac{n+3}{6}} \tag{2}$$

with $n \approx -1$. With this simplification, the multiplicity function is

$$\eta(M)\mathrm{d}M \sim \frac{\rho}{M_0}\frac{n+3}{6\sqrt{2\pi}}(1+z)(M/M_0)^{-\frac{9-n}{6}}\mathrm{e}^{-\frac{1}{2}(1+z)^2(M/M_0)^{\frac{n+3}{3}}} \tag{3}$$

The redshift dependence of (1) then provides for the needed extrapolation to high redshift. Due to the exponent which is proportional to $(1+z)^2$, the cluster counts diminish very rapidly with increasing redshift. Estimates of the cluster contribution to the $X$-ray background have been made along these lines (Schaeffer and Silk 1988b, Kaiser 1991, Blanchard, talk given at this conference). This approach leads to quite simple calculations, but relies on approximations whose accuracy is unknown.

Another approach that aims to estimate the redshift dependence of the cluster multiplicity function is to directly deduce the time-dependence from the efficiency of the clustering process in the non-linear regime. Under the assumption of hierarchical clustering, which implies that the $N$-body matter correlation functions behave as power-laws of scale ($\sim r^{-(N-1)\gamma}$, reminiscent of the observed galaxy two-and three-body correlation functions), it is possible to construct the galaxy and cluster multiplicity functions (Schaeffer 1987, Balian and Schaeffer 1988,1989). The same reason (Peebles 1980) that makes it believable that all correlation functions are power-laws (namely that such correlation functions are a solution of the equations of motion that describe their time evolution), also implies a well-defined redshift-dependence

$$\xi_N(r_{\mathrm{com}}, z) \propto \left[r_{\mathrm{com}}(1+z)^{1-\frac{3}{\gamma}}\right]^{-(N-1)\gamma}, \quad \gamma \approx 1.8 \tag{4}$$

The original argument for this was given by Peebles for $\Omega = 1$, but can be extended (BS88) to the case $\Omega \ll 1$. The multiplicity function in the non-linear regime can be

shown to reach (BS89, Bernardeau and Schaeffer 1991, see the talk given by Bernardeau).

$$\eta(M)\mathrm{d}M = \frac{\rho}{M} x H(x)\ \mathrm{d}x \tag{5}$$

$$x(M,Z) = M/\frac{4\pi}{3}\rho_0 R^3 (R/8h^{-1}Mpc)^{-\gamma}(1+z)^{-(3-\gamma)} \tag{6}$$

$$\text{with } R = 1.6(M/M_0)^{1/3}\ h^{-1}\ Mpc \tag{7}$$

being the final radius of the object after collappse and virialization. The scaling of (6) with $R$ and $1+z$ just reflects the scaling (4). The function $H(x)$ is a universal function that is independent of mass and redshift, all the latter dependence being carried by the parameter $x$. This function is defined once one knows the normalization coefficients that determine the strength of $\xi_N$ for each value of $N$. From very general theoretical grounds, it is expected behave as

$$\begin{array}{ll} H(x) & \underset{x\ll 1}{\sim} x^{\omega-2} \qquad 0 \le \omega \le 1 \\ H(x) & \underset{x\gg 1}{\sim} \mathrm{e}^{-x/x_*} \end{array} \tag{8}$$

As argued by BS89, one expect $\omega \approx 0.5 - 0.7$ and $x_* = 5 - 10$. Various determinations of these parameters using the CFA (Alimi et al 1990), the SSRS (Maurogordato et al 1991) lead to respectively $\omega = 0.5 \pm 1$ and $\omega = 0.7 \pm 1$, and a poor determination of $x_*$, whereas CDM simulations lead (Bouchet et al 1991) to $\omega = 0.4 \pm 0.1$ and $x_* = 10$. This behaviour is reminiscent of the behaviour of the Schechter form for the luminosity multiplicity function of galaxies. Note also that (6) implies

$$x = 7(M/M_0)^{\gamma}(1+z)^{3-\gamma} \tag{9}$$

and whence

$$\begin{array}{lll} \eta(M) & \propto (1+z)^{0.6}(M/M_0)^{-1-\gamma(1-\omega)} & M \ll M_0 \\ \eta(M) & \propto \mathrm{e}^{-0.7(1+z)^{3-\gamma}(M/M_0)^{\gamma/3}} & M \gg M_0 \end{array} \tag{10}$$

that for $\omega = 0.5$ and $\gamma = 1.8$ is **extremely close to the behaviour obtained from the previous approach** based on linear theory. This is why both forms can fit the present-day data with equal succes. There is however an **important difference:** the power of $1+z$ in the exponent of (10) is close to unity, whereas in (3) it was equal to 2. So, for a given number of clusters presently observed, it will predict **many more clusters in the past.** This approach is also quite different in spirit from the previous one, which assumes linear theory holds up to the formation of dense structure whose multiplicity thus depends directly on the initial spectrum of matter fluctuations $\Sigma(M)$. In the present approach, the matter fluctuations are assumed to be the result of the non-linear process, since the power-law form of the correlation is a solution of the non-linear equations of evolution (and not a solution of the linear equations). The non-linear approach is thus expected to describe more accurately the clustering process. It provides very specific predictions of the scaling of the **counts in cells,** namely that the

probability for a cell of radius $R$ to contain a mass between $M$ and $M+\mathrm{d}M$ should scale exactly in the same way as the multiplicity function (5) does whith a scaling function $h(x)$ that has the same properties (8) than $H(x)$ but is not necessarrly identical to the latter. This is seen to be the case (Alimi et al 1990) for the CfA (Huchra 1982) galaxy counts, as well as (Maurogodato et al 1991) for the SSRS (da Costa et al 1988) galaxies. Moreover, quite precise tests can be done (Bouchet et al 1991) using CDM numerical simulations of Davis and Efstathiou (1988). The scaling (5) is in the latter case seen to hold to a high degree of accuracy, allowing a quite precise determination of the scaling function $h(x)$. Finally, a detailed comparison (Bernardeau and Schaeffer 1991) of the galaxy and cluster multiplicity function also shows that the scaling (5) holds (see the talk given by Bernardeau) and allows the construction of $H(x)$. All these checks show that the multiplicity function obeys the scaling laws (5) to a high degree of accuracy. The same theory that leads to these scaling laws also implies a precise time, and thus redshift dependence. The scaling (6) of both $h(x)$, for the counts in cells, or $H(x)$, for the cluster multiplicity, as a function of redshift that we predict can be usefully checked again the results of numerical simulations. This remains to be done.

**X-ray emission from remote clusters**

The $X$-ray luminosity due to thermal bremstrahlung scales as

$$L_x \propto T^{1/2} M^2 R^{-3} \tag{11}$$

If we asume $M/L$ is a constant independent of the cluster that is considered, this luminosity can be directly deduced from the cluster parameter. It can be normalized to the Coma cluster, taken as a typical cluster of Abell richness II class. The cooling time can be estimated as

$$t_c \sim 510^{10} \left(\frac{n}{10^{-3}}\right)^{-1/2} \frac{R}{1\ \mathrm{Mpc}} \mathrm{y} \tag{12}$$

and for the rich clusters is much larger than to the age of the universe. The smaller clusters, however, have smaller radii and larger densities. They may no larger be $X$-ray ermitters since their cooling time $t_c \sim 10^{10}$y become dangerously close to the present age of the universe. $X$-ray emission, however, has been detected associated with poor clusters of galaxies (see discussion by Sarazin, 1986). It may, however, be due to primordial gaz trapped in their gravitational potential, or to gaz falling onto massive $cD$ galaxies. Objects of mass $\sim 10^{12}\ M_\odot$ cool so rapidly, however, that they become galaxies, and not clusters.

A calculation of the $X$-ray emission from remote clusters has been made (Schaeffer and Silk 1988b) using the multiplicity function deduced from the non-linear hierarchical clustering theory. This calculation is considerably more accurate than the one base on multiplicity functions such as (1) derived from linear theory. It shows that the contribution of remote clusters is much more important than thought previously.

This calculation predicts an $X$-ray multiplicity function that for large luminosities behaves as

$$\eta(L_x) \propto e^{-(L_x/L_{x*})^{0.45}} \tag{13}$$

the parameter $Lx_*$, that governs the rapidity of the fall-off behaves as a function of redshift like

$$L_{x*} \sim 1.5\ 10^{44}\ \mathrm{erg\ s^{-1}} (1+z)^{0.83}, \tag{14}$$

which **increases** with redshift. the same scaling (11), when applied to a Press-Schechter multiplicity function, equ.(1) leads (Kaiser 1986) to an exponential fall-off similar to (13), with $L_{x*} \propto (1+z)^{-0.5}$ that **decreases** with redshift.

The multiplicity function with the temperature as a variable gives a non-linear form similar to (13), with a fall-off given by $(T_x/T_{x*})^{0.9}$, where $T_{x*} = 2\ 10^7 (1+z)^{-0.33}\ K$, nearly **independent** of redshift. The estimate using linear theory would lead to $T_x \propto (1+z)^{-1}$, a much strong redshift dependence.

The contribution to the $X$-ray background is given in fig.1. With the assumption that the density of a cluster scales with its redshift of formation $z_F$ as $n \propto (1+z_F)^3$, the cooling time (5) can be rewritten as $t_c = t_H(z_F)\ R/R_{\mathrm{cool}}$ where $t_H(z_F)$ is the Hubble time at the cluster formation, and $R_{\mathrm{cool}} \sim 0.1$ Mpc is the parameter that describes the cooling efficiency. All objects that cool within a Hubble time of formation have radii smaller than $R_{\mathrm{cool}}$. These objects eventually become galaxies and contain too little energy to give a sizeable contribution to the background. Objects with $R > R_{\mathrm{cool}}$ end up as clusters of galaxies. They radiate their energy during a longer time, but get embedded into a larger cluster before their energy is exhausted. In this model, the cluster contribution to the $X$-ray background is made from all objects whose radius is larger than $R_{\mathrm{cool}}$. It can be seen in Fig.1, that for $R_{\mathrm{cool}} \sim 0.1$ Mpc, clusters make up a large fraction of the background below 1 keV, whereas for $R_{\mathrm{cool}} \sim 1$ Mpc their contribution would be only 10% of the observed flux. Similarly, the $N(>f)$ counts of clusters with flux larger than $f$ are quite sensitive to the choice of the cooling efficiency parameter $R_{\mathrm{cool}}$. This contribution comes from clusters at an average redshift of 2 and an average angular diameter of 2'. These objects shoud be detected by Rosat.

The cluster contribution to the $X$-ray background turns out to be quite sensitive to the choice of $R_{\mathrm{cool}}$. Rather than using an abrupt cut and retain all objects whose radius is larger than some threshold and reject the others, a more precise cooling history would be an useful improvement. Also, the calculations presented here use a model (Schaeffer 1987) for the non-linear luminosity function that has been considerably improved since (BS89, Bernardeau and Schaeffer, in preparation). Much more precise predictions are thus underway, in particular to assess how many small clusters should be $X$-ray emitters presently, and how their number evolved in the past.

An important consequence of the possible existence of these rather small clusters in the past is also the distortion of the microwave background they imply. There are a

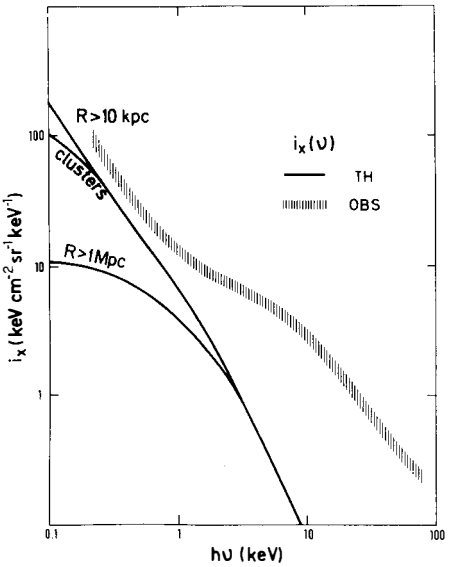


Diffuse X-ray background as a function of frequency $\nu$. Shaded area indicates the observations (Boldt 1986), and full lines represent the predicted contribution to the X-ray background from clusters (of radius $R \geq 0.1$ Mpc), as well as the effect of varying the minimum cluster radius. The cluster contribution represents a major component of the X-ray background between $h\nu = 0.1$ and 1 keV.

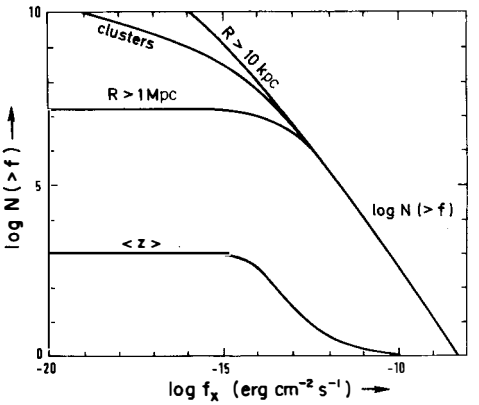


Integral counts of clusters $\log N(>f)$ in $4\pi$ sr with an X-ray flux larger than a given threshold $f$ (in units of ergs cm$^{-2}$ s$^{-1}$). The contribution of objects with a radius larger than 1 Mpc levels off beyond $f \sim 10^{-13}$ ergs cm$^{-2}$ s$^{-1}$, although for radii larger than 0.1 Mpc, there are clusters contributing down to much smaller fluxes. The average redshift of the clusters ($R > 0.1$ Mpc) is also plotted on a linear scale as a function of the limiting flux, and is seen to level off at $z \sim 3$

few (typically ~5 with our standard parameters) clusters along each lign of sight. the Sunyaev-Zeldovich distortion, as measured by the parameter $y$ may be as large as $y \sim 10^{-4}$ which is in the range of sensitivity of COBE. These clusters also induce fluctuations of the microwave background at the $10^{-5}$ level, which again will be measurable in the near future.

## Références


Alimi, J.M., Blanchard, A., Schaeffer, R.: 1990, *Ap. J.* **349**, L5.

Balian, R., Schaeffer, R.: 1988, *Ap. J.* **335,** L43. (BS88)

Balian, R., Schaeffer, R.: 1989, *A. A.* **220,** 1; *A. A.* **226**, 373. (BS89)

Bernardeau, F.: 1991, talk given at this conference.

Bernardeau, F., Schaeffer, R.: 1991, *A.A.* in press.

Blanchard, A.: 1991, talk given at this conference.

Cole, S., Kaiser, N.: 1989, *M. N.* **237**, 1127.

da Costa, L.N., Pellegrini, P.S., Sargent, W.L.W., Tonry, J., Davis, M., Meiskin, A., Latham, D.W., Menzies, J.W., Coulson, J.A.: 1988, *Ap. J.* **327,** 544.

Davis, M., Efstathiou, G.: 1988 unpublished.

Edge, A., Steward, S., Fabian, A., Arnaud, K.A.: 1990, *M.N.* **245,** 559.

Huchra, J.P., Davis M., Latham, D.W., Tonry, J.: 1982, *Ap. J. Supp.* **52,** 89.

Kaiser, N.: 1986, *M.N.* **219,** 785.

Kaiser, N.: 1991, to be published.

Maurogordato, S., Schaeffer, R., da Costa, L.N.: 1991, to be published.

Peebles, P.J.E.: 1980, "The Large Scale Structure of the Universe", Princeton University Press, Princeton N.J., USA.

Peebles, P.J.E.: 1982, *Ap. J.* **263,** L1.

Sarazin, C.L.: 1986, R.M.P. **58,** N°1, 1.

Schaeffer, R.: 1987, *A. A.* **180,** L5.

Schaeffer, R., Silk, J.: 1985, *Ap. J.* **292,** 319.

Schaeffer, R., Silk, J.: 1988 a, *Ap. J.* **323,** 1.

Schaeffer, R., Silk, J.: 1988 b, *Ap. J.* **333**, 509.

Schmidt, M., Green, R.: 1986, *Ap. J.* **305**, 68.

# Properties of x-Ray clusters

A.BLANCHARD

D.A.E.C., Observatoire de Meudon, 92195, Meudon, France.

JOSEPH SILK

Departments of Astronomy and Physics, University of California, Berkeley, CA , USA.

**Summary**: We investigate the properties of x-ray clusters in a simple sphericaly symmetric top-hat model for nonlinear structure formation. This allows us to study the luminosity and temperature distribution functions of clusters in galaxy formation theories. Comparison with observations allows us to set interesting constraints on different theories. The temperature distribution function is a powerful probe of the spectrum of the initial fluctuations. We find that the properties of observed x-ray clusters are in disagreement with the predictions of the standard CDM theory, unless there is a substantial incompleteness of low-temperature clusters.

# 1 Introduction

The present properties of observed x-ray clusters have been derived by several authors (Piccinotti et al. 1982, Edge et al. 1990 ). These properties could be in principle compared with predictions provided that we have a theoretical framework both for the x- ray properties and mass-function of virialised structures. The presently available sample of x-ray clusters already yields a useful constraint.

# 2 Properties of clusters in the top-hat model

The top-hat is a simple model for the formation of a virialised object that arises from the collapse of a initial small positive fluctuation. Let us assume that at some early epoch $z_i$, after recombination for instance, a fluctuation has a contrast density $\delta_i$, and that this fluctuation can be approximated by a spherical region with the same uniform contrast density. This fluctuation will reach a maximum expansion radius $R_m$ at a redshift :

$$1 + z_m \approx \frac{\delta_i (1 + z_i)}{1{\cdot}06} \tag{1}$$

at a cosmic time $t_m$. After the fluctuation collapses and virialises at a cosmic time $\approx 2t_m$ corresponding to the redshift $z_v$, its final radius is $R_m/2$ and the non-linear contrast density $\Delta \approx 170$. The gas content of the region is shocked-heated up to a temperature of

$$T_g \approx \frac{\mu m_p}{k} \frac{GM}{2R} \approx 5{\cdot}7 \times 10^5 (1 + z_v) M_{12}^{2/3} \quad \mathrm{K} \tag{2}$$

where $M_{12}$ is the mass of the fluctuation in unit of $10^{12}\mathrm{M}_\odot$, $\mu$ is the mean molecular weight. This very simple model is in good agreement with numerical simulations (Evrard 1990). It would be of great interest to derive similar scaling relations for the x-ray luminosity of clusters. Unfortunately the x-ray luminosity depends sensitively on the core radius $R_c$ of the gas density profil:

$$L_x \propto \int_0^{+\infty} \rho^2 (R) T^{1/2} R^2 dR \propto f^2 M^{2\beta} T^{1/2} R_c^{3(1-2\beta)} \tag{3}$$

where $f$ is the fraction of the baryonic content of the cluster that ends up in the intracluster medium. This fraction could depend on the mass of the cluster. Deriving a scaling law for the core radius with mass and redshift is highly uncertain. A common asumption is to assume that the core radius $R_c$ is prportionnal to the virial radius $R_v$. In such a case the scaling of $L_x$ is:

$$L_x \alpha (1 + z)^{3.5} M^{4/3}$$

However, given the uncertainty, we have assumed a parametric form $L_x \propto M^p$ . In principle, $p$ can be determined directly from the observations by the relation:

$$L_x \propto T_x^{3p/2} \tag{4}$$

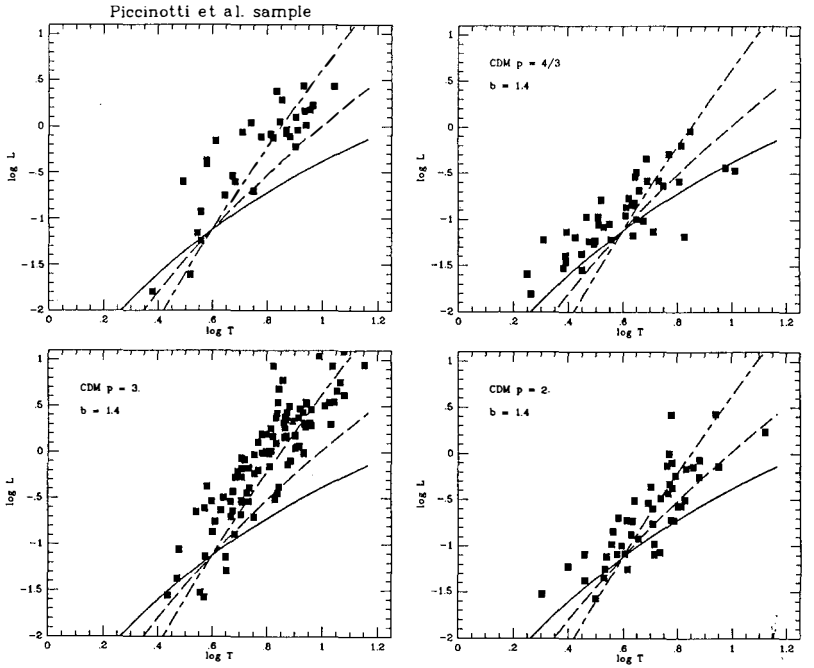


Figure 1: The theoretical $L_x - T_x$ relation for different values of $p$ (4/3, 2, 3) and a comparison with observations (left-top panel) and with Monte- Carlo simulated samples of clusters in CDM model.

In figure 1 we have plotted the expected $L_x - T_x$ relation for 3 different values of $p$. The left panel at the top holds for the clusters in the Piccinotti et al. (1982) sample. We have also presented similar diagramms for different values of $p$ using a Monte-Carlo set of clusters in the CDM picture (details are given in the next section). It is difficult to reach firm conclusions from this figure. Although, at low temperature the value $p = 3$ seems in good agreement with the data, a lower value seems to be preferred at high temperature. However, one should be extremely cautious before drawing firm conclusions: the absence of any clusters with temperature smaller than 2.5 keV in the presently available sample is very puzzling. If this is not due to a selection bias, this is a powerfull constraint on theoretical models of clusters. ROSAT should provide a much more reliable constraint in this temperature range. In any case the value $p = 4/3$, the standard scaling value (Kaiser 1986) seems to be ruled out on the basis of the data at least for the cold dark matter picture.

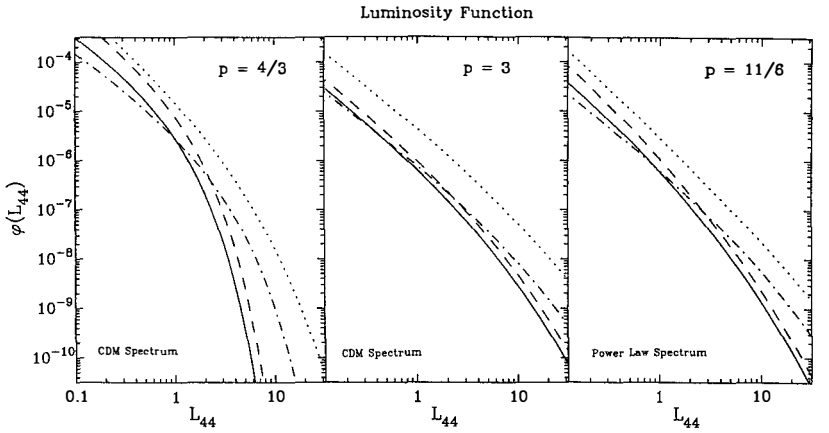


Figure 2: The theoretical luminosity function compared with the observations (Einstein band). The full line is the Einstein band (0.5-3.5 keV). The dashed line correspond to ROSAT (0.1-2.4 keV). The dashed-dotted line is for the HEAO-1 band (2-10 keV). The dotted line corresponds to the bolometric luminosity function. Case a) and b) corresponds to $p = 4/3$ and $p = 3$ for a CDM spectrum. Case c) corresponds to an initial power law spectrum for the fluctuations with $n = -2$.

# 3 Distribution function

Observations do provide the x-ray luminosity function as well as the temperature distribution function of clusters. This offers a potentially important tool to set constraints on galaxy formation theory. In order to set such constraints it is necessary to know the mass function. As is well known, Press and Schechter (1974) derive the mass function of objects, for any gaussian initial fluctuations power spectrum:

$$N(m) = \sqrt{\frac{2}{\pi}} \frac{\bar{\rho}}{m^2} \frac{f_c}{\sigma(m)} \frac{dln\sigma}{dlnm} exp\left(-\frac{1}{2}\left(\frac{f_c}{\sigma(m)}\right)^2\right) \quad (5)$$

Numerical simulations have shown that this formula is a good approximation for the mass function in the non-linear regime (Efstathiou et al., 1988). The applications of this formula to clusters is of great interest, because the above formula is of good accuracy close to the turnover of the mass function, precisely in the range where clusters lie. Therefore as soon as the relations between mass and temperature and mass and luminosity are specified, we can confidently estimate the luminosity function and the temperature distribution function.

In the top-hat model. Because of the uncertainties mentioned above in the $L_x - M$ relation, the constant in the relation 4was chosen in order to match the observed number of clusters with luminosity of the order of $3 - 4 \times 10^{44}$ erg/s/cm $^2$ . From figure 2, it

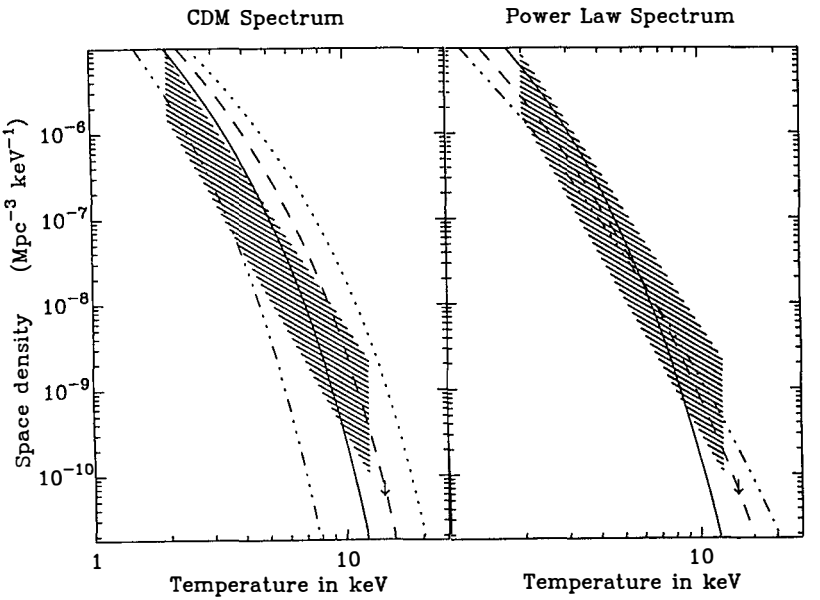


Figure 3: The theoretical distribution function of clusters compared with the observations (hashed area) by Edge et al (1990). The full line is the CDM model with the bias parameter $b = 1{\cdot}7$, the dashed line is for $b = 1{\cdot}4$, the dashed-dotted-dotted line is for $b = 2{\cdot}25$, the dotted line is for $b = 1{\cdot}2$. The second case is drawn for power law models with $b = 1{\cdot}7$, the full line is for an index $n = -1$ (this case in undistinguishable of the CDM model in that mass range), the dashed line for $n = -1.5$, the dotted-dotted-dashed line for $n = -2$.

appears that the shape of the luminosity function can be reproduced in CDM only with the extreme value $p = 3$. However we have performed a Monte-Carlo realization of CDM models to test whether this could be consistent with the data. The results are presented in figure 1. From this figure it appears that the temperature of the brightest clusters is a little too low compared with the observations i.e. the value $p = 3$ is only marginally consistent with the data. However the difference is small enough that such a possibility should not be ruled out on this issue. However, the temperature distribution function offers a complementary way to constraint the theory. The temperature distribution is a more interesting test because the $T_x - M$ relation 2 suffers less uncertainty. This is presented in figure 3.

The normalization of the mass function is uncertain (only the agreement on the shape has been unambigously established), and it is not therefore safe to ruled out a CDM model with $b = 2{\cdot}2$ on this basis. However it is rather clear that the x-ray temperature function is a sensitive test of the shape of the initial spectrum. This appears clearly in the case of power law models: the ratio of the number of clusters with temperature $T = 10$ keV to the number of clusters with $T = 2$keV changes by a factor 30 when the index changes from $n = -1$ to $n = -2$. On the basis of the observations the value $n = -1$ seems to be ruled out.

# 4 Conclusion

The properties of x-ray clusters offer a potentially interesting tool to constraint galaxy formation models. The luminosity function should be used with some cautioun because of the uncertainties in the theoretical relation between luminosity and mass. Actually we have shown that no conclusion can be drawn from this single constraint. On the other hand, the relation between temperature and mass suffers from less unceratinty. The presently available sample seems already to rule out a CDM model whatever the value of the bias parameter. One should however be aware of the possible incompleteness of low temperature clusters. The situation should be greatly clarified with ROSAT: the contribution of clusters to the total background in the soft energy band is far from being negligable (Silk and Schaeffer 1988; Blanchard et al., 1991) , and one can hope that ROSAT will provide a complete sample of low temperature clusters with considerabily less uncertainty.

**References**

Blanchard, A., Wachter, K., Evrard, A., Silk, J.: *Ap.J.*, submitted.
Edge, A.C., Steward, G.C., Fabian, A.C., Arnaud, K.A.: 1990, *Month. Notices Roy. astron. Soc.*, **245**, 559.
Evrard, A.E.: 1990, in *Clusters of Galaxies*, Ed Oegerle et al., Cambridge University Press.
Efstathiou, G., Frenk, C.S., White, S.D.M., Davis, M.: 1988, *Month. Notices Roy. astron. Soc.*, **235**, 715.
Kaiser, N.: 1986, *Month. Notices Roy. astron. Soc.*, **222**, 323.
Piccinotti, G., Mutshotsky, R.F., Boldt, E.A., Holt, S.S.,
Marshall, F.E., Serlemitsos, P.J., Shafer, A.: 1982, *Ap.J.* **253**, 485.
Press, W., Schechter, P.: 1974, *Ap.J.* **187**, 425.
Silk, J., Schaeffer, R.:1988, *Ap.J.*, **333**, 509.

# ULTRAVIOLET - VISIBLE - NEAR-INFRARED EXTRAGALACTIC BACKGROUND RADIATION

# EVIDENCE FOR EXTRAGALACTIC COMPONENTS IN THE DIFFUSE FAR ULTRAVIOLET BACKGROUND

Stuart Bowyer
Astronomy Department and Center for Extreme Ultraviolet Astrophysics,
University of California, Berkeley, California 94720 USA

## ABSTRACT

Ten years ago the intensity of the diffuse far ultraviolet background ($\lambda\lambda$ 1200–1800 Å) was virtually unknown; published data on this parameter varied by almost three orders of magnitude. It was generally reported that the flux was isotropic and hence was cosmological in origin. The spectrum of the flux was totally unknown. From work carried out in the last decade, we now know that the majority of this flux is correlated with neutral Galactic hydrogen, and hence most of this radiation is Galactic in origin. However, several lines of evidence indicate that a part of this flux with an intensity of 200 to (at most) 400 photons $cm^{-2}$ $s^{-1}$ $sr^{-1}$ $A^{-1}$ is isotropic and hence may in principle be extragalactic in origin. Two components of this isotropic component have been identified, one Galactic and one extragalactic. The observational evidence is critically reviewed and a number of theoretical suggestions are discussed.

## 1. INTRODUCTION

From the beginnings of space research, attempts were made to measure the cosmic far ultraviolet ($\lambda\lambda \sim 1000$–$2000$ Å) background. This work was strongly motivated by the hope that in this waveband a true extragalactic flux could be detected and characterized. Theoretical speculation as to possible sources for this radiation was unconstrained by the available data and included such diverse processes as emission from a lukewarm intergalactic medium, emission from hot gas produced in a protogalaxy collapse phase in the early universe, the summed emission from a star formation burst phase in young galaxies, and photons from the electromagnetic decay of real or hypothetical exotic particles that were produced, or may have been produced, in the early universe.

The first twenty years of measurements, carried out by a number of groups in at least five countries, covered the entire far ultraviolet band, but for a number of technical and astrophysical reasons, these efforts were concentrated on the wavelength band from 1300 to 2000 Å. The results obtained indicated that the flux was uniform across the celestial sphere and hence was cosmological in origin. Estimates of the intensity of this flux, however, varied by *three orders of magnitude*, with no clustering around a mean. For a review of this initial work and a discussion of the reasons for these discrepant results, the reader is referred to Davidsen, Bowyer, and Lampton[1] and Paresce and Jakobsen.[2] It is clear that a major problem with many of these measurements was the need for an uncertain correction for stellar signals. It is perhaps most useful to state that these initial results provided empirical evidence that measurements of the diffuse far ultraviolet background are intrinsically difficult.

A turning point in the study of this background occurred in 1980, when results were obtained from a far ultraviolet channel of a telescope flown as part of the *Apollo-Soyuz* mission. This instrument had a relatively large throughput and a sufficiently small field of view that a reasonable attempt could be made to exclude stars from the data set rather than to make a typi-

cally large and uncertain correction for their effects. The subset of highest quality data from this experiment exhibited a correlation between intensity and Galactic neutral hydrogen column as derived from 21 cm radio measurements, (see Paresce, McKee, and Bowyer[3]). Although these results were criticized on a variety of grounds, they were quickly confirmed by data from a large fraction of the sky that were obtained with an instrument on the *D2B* satellite. This telescope also had a small field of view and a large throughput (Maucherat-Joubert, Deharveng, and Cruvellier[4]). These results showed that the majority of the far ultraviolet flux was connected with processes in our Milky Way Galaxy and was not, in fact, extragalactic in origin.

Nonetheless, a fraction of the flux (ranging from 10 to 50% of the total signal, depending upon location) could be extragalactic in origin. Three lines of experimental evidence bear on this question. These are discussed in sections 2, 3, and 4. A number of theoretical considerations bearing on this issue are described in section 5.

## 2. THE POSITIVE ZERO-POINT INTERCEPT IN THE CORRELATION BETWEEN FAR ULTRAVIOLET BACKGROUND AND THE GALACTIC NEUTRAL HYDROGEN COLUMN

A number of experiments have been carried out to investigate the correlation between the intensity of the far ultraviolet background and parameters associated with the Milky Way Galaxy. The most common association investigated was that with Galactic neutral hydrogen column as derived from 21 cm radio studies. A key result obtained in almost all of these studies is that the far ultraviolet flux extrapolated to zero Galactic hydrogen column is always positive. An example of this effect is shown in Figure 1. These data were obtained by Hurwitz, Bowyer, and Martin with the Berkeley nebular spectrometer flown on the Space Shuttle as part of the NASA UVX payload[5]. A summary of the results obtained by all investigations is shown in Table 1.

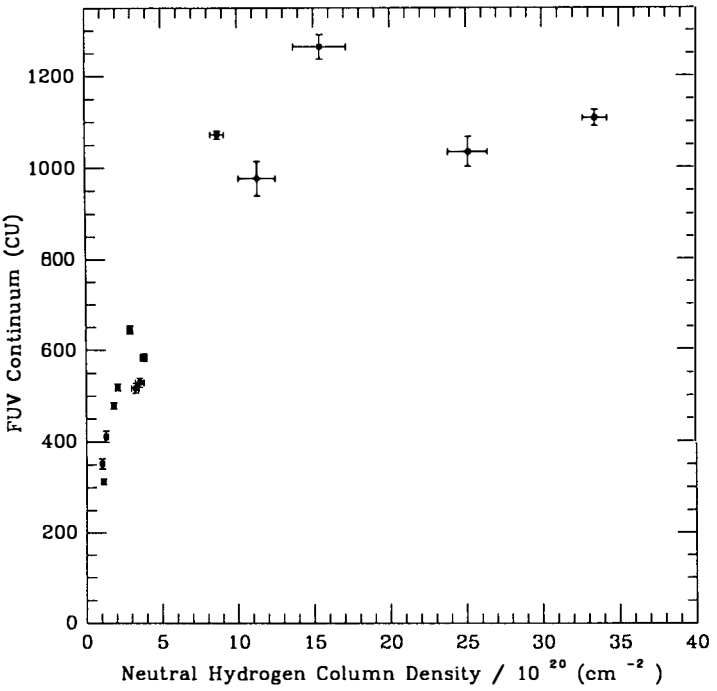


FIGURE 1.—The continuum far ultraviolet intensity as obtained with the UCB spectrograph on the UVX experiment versus neutral Galactic hydrogen column. The vertical error bars are statistical uncertainties only; the horizontal uncertainties indicate the range of hydrogen column covered in the observation. The intensity of the background is strongly correlated with hydrogen column at low hydrogen column densities; at higher column densities, the optical depth becomes greater than one and the background intensity remains constant with increasing hydrogen column.

The zero-point intercept flux ranges from 100 to 600 photons $cm^{-2}$ $s^{-1}$ $sr^{-1}$ $Å^{-1}$ (hereafter continuum units = CU). It is not clear that the dispersion in the results from various investigators is significant since this may simply be the result of experimental error. The important point to be emphasized here is that the minimum zero intercept flux may well be partially, or totally, an extragalactic flux.

TABLE 1—CORRELATION OF INTENSITY OF THE FAR ULTRAVIOLET BACKGROUND WITH GALACTIC NEUTRAL HYDROGEN COLUMN[a]

| Investigation | Slope of Correlation[b] | Intensity at $N_H = 0$ Intercept[c] | Comments |
|---|---|---|---|
| Paresce, McKee and Bowyer[3] | 90 ± 10 to 140 ± 20 | 106 ± 60 to 570 ± 80 | *Apollo-Soyuz* Mission: variation among four view directions |
| Maucherat-Joubert, Deharveng and Cruvellier[4] | 180 ± 80 | $600^{+0}_{-250}$ | *D2B* satellite $\|b\| > 40°$ |
| Zvereva *et al.*[6] | 150 | 470 | *Prognoz 6* satellite |
| Weller[7] | Not evaluated (Strong correlation with Galactic latitude) | Not evaluated 180 ± 75, 280 ± 88 at north and south Galactic poles | *Solrad 11* satellite |
| Joubert *et al.*[8] | 96 ± 6 | 677 ± 20 | Reanalysis of *D2B* satellite data; $\|b\| > 30°$ |
| Jakobsen *et al.*[9] | 100 ± 10 | 450 ± 30 | Aries rocket |
| Fix, Craven and Frank[10] | –60 | 530 ± 80 | *Dynamics Explorer 1* |
| Murthy *et al.*[11] | None found 100 to 300 at high Galactic latitudes | Not evaluated Shuttle experiment | Johns Hopkins UVX |
| Lequeux[12] | 96 | Not evaluated | Detailed reanalysis of *D2B* satellite data |
| Onaka[13] | (30) (see text) | 400 | Rocket flight scan of Virgo Cluster |
| Hurwitz, Bowyer, and Martin[5] | 102 ± 6 | 272 ± 13 | Berkeley UVX Shuttle experiment |

[a]Data reported since 1980. For earlier results, see Davidsen, Bowyer, and Lampton[1] and Paresce and Jakobsen.[2]
[b]Units of photons $(cm^2\ s\ sr\ Å)^{-1}/10^{20}$ H I $cm^{-2}$
[c]Units of photons $(cm^2\ s\ srÅ)^{-1}$

## 3. SPATIAL STRUCTURE IN THE FAR ULTRAVIOLET BACKGROUND

Spatial information on very weak far ultraviolet sources was obtained by Martin and Bowyer with an imaging detector sensitive over the band 1350 to 1900 Å[14]. This detector was flown at the focal plane of a 1 m extreme ultraviolet–far ultraviolet telescope developed as a collaborative effort between Berkeley and Tübingen (see Grewing *et al.*[15]). Data from this imager were subjected to a radial power spectrum analysis in a search for a component of the far ultraviolet background flux which was correlated with angular separation. This search was

motivated by the fact that field stars are essentially randomly distributed in angular separation on the sky, whereas galaxies are known to cluster, and the scale of this clustering is well characterized by a two-point correlation function derived from optical data by Peebles.[16] The results obtained by Martin and Bowyer[14] are shown in Figure 2. Here the observed radial

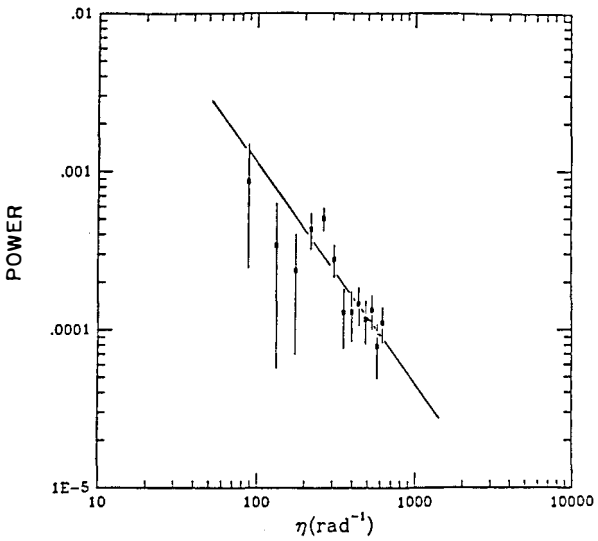


FIGURE 2.—Results obtained by Martin and Bowyer (1989) on the spatial distribution of weak far ultraviolet sources. Here the radial power spectrum of the sources is plotted against angular frequency. Stars contribute a noncorrelated, white-noise component to this data. The best-fit line is a power law with index −1.6, but, given the limited dynamic range of the measurement, this result is not well constrained. The solid line shows a power law with an index of −1.2, which is consistent with the data and is what is expected from the integrated light of galaxies.

power spectrum of the flux is plotted against angular frequency. The best-fit line to the data is a power law with index −1.6, but given the limited dynamic range of the measurement, this result is not well constrained. The solid line shows a power law with an index of −1.2, which is consistent with the data and is expected from the integrated light of galaxies. Any alternate processes producing this power would not only have to be the result of a spurious unknown effect, but would also have to produce, purely by chance, a power spectrum consistent with that

produced by galaxies. One may thus conclude that this component of the far ultraviolet background (~50 CU in intensity) is indeed the summed flux of galaxies. The far ultraviolet flux emitted by galaxies contributing to this component of the background is emitted by galaxies in the redshift range from 0.1 to 0.6. This flux is shifted out of the observed far ultraviolet band at distances corresponding to times earlier than the most recent one-third of a Hubble time.

## 4. MODELING OF THE LARGE-SCALE FAR ULTRAVIOLET BACKGROUND

Hurwitz, Bowyer, and Martin obtained indirect evidence for an extragalactic component of the far ultraviolet background from an analysis of the data obtained with the Berkeley UVX spectrometer.[5] In their analysis of the continuum emission, they folded a model of the Galactic stellar radiation field with the observational data and solved for four independent variables: (1) the albedo of the dust, (2) the scattering phase function of the dust, (3) residual dust at $N_{HI} = 0$, and (4) an "external" flux assumed to be independent of the Galactic radiation field and to be isotropic except for attenuation by foreground dust. The results of this analysis for the albedo and scattering phase function of the dust are discussed by Hurwitz, Bowyer, and Martin.[5] The "external" flux in this analysis has at least three components. One component is emission at 1550 and 1660 Å, with an intensity consistent with that reported by Martin and Bowyer for C IV and O III] produced in the Galactic halo.[14] Since the flux is produced well above the plane, this result provides a consistency check on the analysis. The second component of "external" flux is emission of ~120 CU over the entire wavelength band. Diffuse Hα emission line studies by Reynolds indicate that two-photon emission from a warm ionized medium with a large-scale height will contribute a continuum of about 50 CU in the far ultraviolet at high Galactic latitudes,[17] which will appear in this analysis as an "external" flux. The remaining flux is consistent with the value obtained directly by Martin and Bowyer as the summed flux of external galaxies.[14]

## 5. THEORETICAL CONSIDERATIONS

A number of suggestions for extragalactic components of the far ultraviolet background have long been the subject of substantial debate. I commment on two of these topics here: emission from active galactic nuclei (AGN) and emission from a possible intergalactic medium.

The integrated light from AGN, primarily quasi-stellar objects (QSOs), will contribute at some level to the diffuse far ultraviolet background. The intensity of this flux is of considerable interest because it is generally thought to be the factor that determines the ionization of intergalactic Lyman α clouds and it may photoionize the Galactic halo. A number of authors have estimated the intensity of this flux; the range of estimates is between 0.1 and 10 CU.[14,18–21]

It is clear that the far ultraviolet flux produced by AGN will be too small to be directly disentangled from existing measurements. Future specialized searches may be capable of providing information on this topic.

Early interest in the cosmic far ultraviolet background was motivated at least in part by its relevance to the existence of a cosmologically significant intergalactic medium (IGM). A high-temperature ($>10^6$ K) IGM would produce X-ray emission, and a lower-temperature ($<10^4$ K) medium would produce absorption effects in QSO spectra; observational constraints on these parameters were interpreted as ruling out these two scenarios, but the possibility of an intermediate-temperature IGM remained. An intermediate-temperature IGM would most likely be detected by its far ultraviolet emission; the most likely far ultraviolet radiation would be redshifted Lyman α transitions of H I 1216 Å and He II 304 Å from an ionized primordial gas, as indicated by the research of Field[22] and Kurt and Sunyaev.[23] In the early stages of galaxy formation, this gas might be reionized collisionally by the passage of shocks or by interactions with energetic particles,[24,25] or by photoionization.[26] The emission spectrum depends upon the details and time scales of the reionization; in particular, collisional ionization of the gas pro-

duces much more far ultraviolet radiation than photoionization. Motivated by these suggestions, a variety of data was searched for indications of radiation from an intermediate-temperature IGM.[18,27,28]

In the 1980s several groups developed more detailed models of far ultraviolet emission from a lukewarm IGM. Jakobsen showed that special conditions would be required if emission from this source were to contribute substantially (~300 CU) to the far ultraviolet background.[18] In particular, collisional ionization and substantial clumping of the IGM would be required, and the thermal input must be carefully proscribed, or direct observational constraints would be violated.

Paresce, McKee, and Bowyer suggested that fast shocks and photoionization would be the most likely ionization mechanisms and that these would produce prompt ionization with substantially less radiation.[3] They examined the case in which the gas is sufficiently highly ionized that the dominant emission lines are produced primarily by recombination. In this scenario, the far ultraviolet emission from the IGM is ~10 CU.

Martin, Hurwitz, and Bowyer[29] considered emission from an IGM for a variety of scenarios and compared their results with improved observational constraints provided by the X-ray background in work by Setti,[30] the lack of absorption troughs shortward of H Lyman $\alpha$ continuum in the spectra of QSOs (see Gunn and Peterson[31]), limits on emission in the far ultraviolet background as discussed in this article, and limits on spatial fluctuations in the far ultraviolet background in the work of Martin and Bowyer.[14] They found that even their most optimistic scenarios, including collisional ionization and clumping of the IGM, violated observational constraints for an IGM with even a relatively low density (15% of the critical density of the universe). This result is to some extent model-dependent, but the models employed were sufficiently broad that either very special and unexpected conditions occurred in the early universe, or the far ultraviolet background has at most a component <10 CU from the IGM. A component this small will be difficult to identify.

## 6. SUMMARY

Considerable progress has been made in our understanding of the far ultraviolet background. While it is now known that most of the flux is Galactic in origin, at least some of the flux has now been identified as being extragalactic in origin. In Table 2 I summarize my estimates of various components to the far ultraviolet background.

TABLE 2—COMPONENTS OF THE DIFFUSE COSMIC FAR ULTRAVIOLET BACKGROUND WITH APPROXIMATE INTENSITIES[a]

| | |
|---|---|
| Total intensity | 300--1500 |
| Galactic components | |
| Scattering by dust | 200--1500 |
| H II Two-photon emission | 50 |
| $H_2$ fluorescence | 100 (in molecular clouds) |
| Components of the "uniform" high-latitude background | |
| Dust (?) | 200 |
| Summed from all galaxies | 50 |
| HII two-photon emission | 50 |
| Hot gas line emission | 10 |
| QSOs/AGNs | < 10 |
| Intergalactic medium | <10 |
| Unexplained | none to <200 |

[a] Intensities dependent upon view direction. Intensities of processes producing discrete features are averaged over the 1400–1850 Å band. Units are photon $cm^{-2}$ $s^{-1}$ $sr^{-1}$ $Å^{-1}$.

**Acknowledgments**

I thank CNES for support during an extremely scientifically productive and personally rewarding year at the Laboratoire d'Astronomie Spatiale, where much of the material in this review was assembled and crystalized. I thank Jean-Michel Deharveng for his personal encouragement and scientific insights, and for his invitation to this delightful conference. This work was also supported by NASA Grant NRG05--003--450, which is administered by the Space Sciences Laboratory of the University of California.

**References**


1. Davidsen, A., Bowyer, S., and Lampton, M. 1974. *Nature*, 247:513
2. Paresce, F., and Jakobsen, P. 1980. *Nature*, 288:119
3. Paresce, F., McKee, C., and Bowyer, S. 1980. *Ap. J.*, 240:387
4. Maucherat-Joubert, M., Deharveng, J. M., and Cruvellier, P. 1980. *Astron. Astrophys.*, 88:323
5. Hurwitz, M., Bowyer, S., and Martin, C. 1991. *Ap. J.*, 372, in press
6. Zvereva, A. M., Severny, A. B., Granitsky, L. V., Hua, C. T., Cruvellier, P., and Courtés, G. 1982. *Astron. Astrophys.*, 116:312
7. Weller, C. 1983. *Ap. J.*, 268:899
8. Joubert, M., Masnon, J., Lequeux, J., Deharveng, J., and Cruvellier, P. 1983. *Astron. Astrophys.*, 128:114
9. Jakobsen, P., Bowyer, S., Kimble, R., Jelinsky, P., Grewing, M., Kramer, G., and Wulf-Mathies, C. 1984. *Astron. Astrophys.*, 139:481
10. Fix, J., Craven, J., and Frank, L. 1989. *Ap. J.*, 345:203
11. Murthy, J., Henry, R., Feldman, P., and Tennyson, P. 1989. *Ap. J.*, 336:954
12. Lequeux, J. 1990. In *Proc. IAU 139, The Galactic and Extragalactic Background Radiation,* ed. S. Bowyer and Ch. Leinert, Dordrecht: Kluwer Academic Publishers, p. 185
13. Onaka, T. 1990. In *Proc. IAU 139, The Galactic and Extragalactic Background Radiation,* ed. S. Bowyer and Ch. Leinert, Dordrecht: Kluwer Academic Publishers, p. 379
14. Martin, C., and Bowyer, S. 1989. *Ap. J.*, 338:677
15. Grewing, M., Kramer, G., Schultz-Luperty, E., Wulf-Mathies, C., Bowyer, S., Jakobsen, P., Jelinsky, P., and Kimble, R. 1983. *Adv. Space Explor.*, 2:153
16. Peebles, P. J. E. 1980. *The Large Scale Structure of the Universe*, Princeton: Princeton University Press
17. Reynolds, R. J. 1990. In *Proc. IAU 139, The Galactic and Extragalactic Background Radiation*, ed. S. Bowyer and Ch. Leinert, Dordrecht: Kluwer Academic Publishers, p. 157
18. Jakobsen, P. 1980. *Astron. Astrophys.*, 81:66
19. Sargent, W. L. W., Young, P. J., Boksenberg, A., and Tytler, D. 1980. *Ap. J.*, 42:41
20. Ikeuchi, S., and Ostriker, J. P. 1986. *Ap. J.*, 301:522
21. Bechtold, J., Weymann, R. J., Lin, Z., and Malkan, M. A. 1987. *Ap. J.*, 315:180
22. Field, G. B. 1959. *Ap. J.*, 129:536
23. Kurt, V. G., and Sunyaev, R. A. 1967. *J.E.T.P. Letters*, 5:246
24. Ginzberg, V. L., and Ozernoy, L. M. 1966. *Soviet Astr.-A.J.*, 9:726
25. Weymann, R. 1967. *Ap. J.*, 147:887
26. Arons, J., and McCray, R. 1970. *Ap. J. (Letters)*, 5:L123
27. Henry, R., Feldman, P., Weinstein, A., and Fastie, W. 1978. *Ap. J.*, 223:437
28. Anderson, R., Brune, W., Henry, R., Feldman, P., and Fastie, W. 1979. *Ap. J. (Letters)*, 233:L39
29. Martin, C., Hurwitz, M., and Bowyer, S. 1991. *Ap. J.*, in press
30. Setti, G. 1990. In *Proc. IAU 139, The Galactic and Extragalactic Background Radiation*, ed. S. Bowyer and Ch. Leinert, Dordrecht: Kluwer Academic Publishers, p. 345
31. Gunn, J. E., and Peterson, B. A. 1965. *Ap. J.*, 142:1633

# The Diffuse Ultraviolet Background and the Intergalactic Medium

Peter Jakobsen
Astrophysics Division, Space Science Department of ESA
ESTEC, NL-2200 AG Noordwijk, The Netherlands

## Abstract

The long-standing question of whether redshifted Ly$\alpha$ and HeII $\lambda$302Å line emission from the intergalactic medium can be detected in the diffuse far-UV ($\lambda\lambda$1300 – 2000 Å) background radiation is revisited in light of what has been learned about the IGM from the study of quasar absorption lines. The intensity of the metagalactic ionizing background at high redshifts derived by the so-called "proximity effect" displayed by the Lyman forest absorption lines suggests that the redshift-smeared backgrounds due to Ly$\alpha$ and HeII $\lambda$304Å recombination radiation from photoionized intergalactic gas are to be found at intensities far below current observational limits on the extragalactic background flux. The results of the Gunn-Peterson test at low redshifts derived from UV quasar spectra obtained with *IUE* constrain the intensity of redshifted collisionally excited Ly$\alpha$ emission from a shock-heated IGM component to an equally low intensity. The possibility that the IGM has gone through a phase of intense collisionally excited HeII $\lambda$304Å emission at $z \simeq 3-5$ cannot be completely ruled out until the HeII equivalent of the Gunn-Peterson test is carried out with *HST* or *Lyman/FUSE*. However, the statistics of quasar absorption lines imply that any far-UV background component stemming from $z \gtrsim 3$ will remain effectively hidden from view because of strong accumulated Lyman continuum absorption in the Lyman forest and Lyman limit types of quasar absorption systems. It is concluded that current observational limits on the extragalactic far-UV background intensity are at least an order of magnitude brighter than that expected from diffuse IGM emission.

## I. Introduction and Background

Historically, one of the driving motivations behind attempts to measure the diffuse background radiation at far-ultraviolet wavelengths has been the realization that such observations could potentially reveal the existence of a cosmologically significant ($\Omega_b \approx 1$), "lukewarm" ($10^3$ K$< T < 10^6$ K) intergalactic medium (IGM)[1,2,3].

If a baryonic intergalactic medium does exist, standard Big Bang nucleosynthesis calculations predict that it must consist primarily of a mixture of 90% hydrogen and 10% helium atoms. The dominant emission from such a mixture at temperatures between $T \simeq 10^3$ K and $T \simeq 10^6$ K is recombination and collisionally excited line radiation in the HI and HeII Ly$\alpha$ lines at $\lambda_l = 1216$Å and $\lambda_l = 304$Å, respectively. This line radiation, smeared by the redshift, will give rise to a diffuse background at wavelengths $\lambda \geq \lambda_l$ of intensity given by†

$$I_\lambda(\lambda_0) = \left[\frac{c}{H_0}\right] \frac{\epsilon_l(z)}{4\pi} \frac{1}{\lambda_l} (1+z)^{-5} (1+\Omega z)^{-\frac{1}{2}} \tag{1}$$

where $\lambda_0 \geq \lambda_l$ is the observed wavelength, $H_0$ is the Hubble constant and $\epsilon_l(z)$ is the line volume emissivity (in units of photons s$^{-1}$ cm$^{-3}$) evaluated at the appropriate redshift, $(1+z) = \lambda_0/\lambda_l$. In the case of a smooth IGM, the emissivity can be expressed as

$$\epsilon_l(z) = {n_H^0}^2 (1+z)^6 \gamma_l(T) \tag{2}$$

where $n_H^0 = 7.8\ 10^{-6} \Omega_b h^2$ cm$^{-3}$ is the IGM hydrogen density at $z = 0$, $\Omega_b$ is the baryonic IGM contribution to the cosmological density parameter, $H_0 = 100h$ km s$^{-1}$ Mpc$^{-1}$, and $\gamma_l(T)$ is a suitably normalized emission coefficient.

Figure 1 shows the run of $\gamma_l(T)$ as a function of temperature for a cosmological mixture of hydrogen and helium in collisional and thermal equilibrium. It is seen that collisionally excited emission in the HI and HeII Ly$\alpha$ lines is especially intense near the two "thermostat" temperatures $T \simeq 2\ 10^4$ K and $T \simeq 8\ 10^4$ K, *i.e.* at the temperatures at which the dominant ionization states change from HI to HII and HeII to HeIII, respectively. If, following recombination, the IGM was re-heated and re-ionized by dissipative processes, such as shock heating, the gas would have had to pass through these two temperatures. Depending on the redshift and duration of the re-heating process, the IGM emission could give rise to observable redshifted Ly$\alpha$ and HeII $\lambda$304Å spectral signatures in the ultraviolet background. Several detailed IGM models giving rise to such features can be found in the literature[4,5,6].

Of course, the intergalactic medium is not only constrained by limits on its possible *emission*, but also by its possible *absorption*. In particular, by far the most stringent constraint on the IGM comes from the classical Gunn-Peterson[7] test, which severely constrains the density of intergalactic neutral hydrogen at high redshift, $n_{HI}(z)$, from the observed lack of an intense redshift-smeared Ly$\alpha$ absorption trough seen just shortward of emitted Ly$\alpha$ in the spectra of high redshift quasars:

$$n_{HI}(z) = \frac{\tau(z)}{\sigma_l} \left[\frac{c}{H_0}\right]^{-1} (1+z) (1+\Omega z)^{\frac{1}{2}} \tag{3}$$

In this expression, $\tau(z)$ is the optical depth of the absorption and $\sigma_l = \lambda_l \frac{\pi e^2}{m_e c^2} f_{ij} = 4.5\ 10^{-18}$ cm$^2$ is the integrated Ly$\alpha$ absorption cross section. Both ground-based and *IUE* observations of the spectra of quasars[8,9] show little or no signs of absorption troughs over the redshift range $0 < z < 4$ at the $\tau(z) \lesssim 0.1$ level. The corresponding upper limit on the intergalactic neutral hydrogen density is of

†Throughout this paper $I_\lambda$ refers to the specific intensity of the background expressed in the units preferred by the observers; namely photons s$^{-1}$ cm$^{-2}$ sr$^{-1}$ Å$^{-1}$.

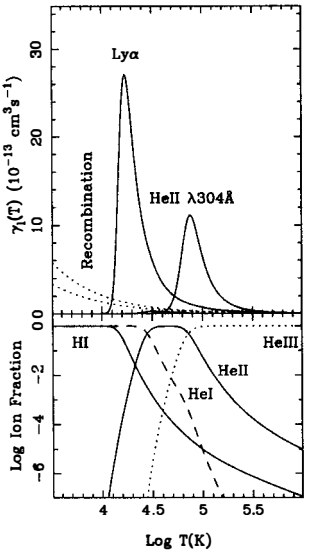


FIG. 1. — Lower frame: Ionization structure of a cosmological mixture of hydrogen and helium in collisional equilibrium as a function of temperature. Upper frame: Corresponding emissivity per hydrogen atom of collisionally excited HI and HeII Ly$\alpha$ emission. The dotted lines show the equivalent line emission due to recombination in a fully photoionized gas. Emission from HeI is negligible compared to that of HI and HeII.

order $n_{HI}(z) \lesssim 10^{-12}$ cm$^{-3}$. This stringent limit on the residual neutral hydrogen component of the IGM (and its HeI equivalent[10]) implies that the IGM – if it exists at all - must be highly ionized and have a temperature greater than $T \approx 10^5$ K (see lower frame of Figure 1).

Alternatively, if photoionization, due for example to the integrated ionizing flux of quasars, is the process responsible for re-ionizing the IGM, then the gas will still emit primarily in the HI and HeII Ly$\alpha$ lines, albeit somewhat less efficiently (see Figure 1). On the other hand, since the Gunn-Peterson test suggests that the IGM is transparent, the redshifted ionizing radiation source itself should be directly observable in the ultraviolet background. Hence absolute measurements of the ultraviolet background intensity can in principle be used to derive the maximum IGM density that can be photoionized by the observed flux to the level required by the Gunn-Peterson test. Unfortunately, the available observational limits on the extragalactic UV background intensity have generally been far brighter than anticipated for realistic intergalactic fluxes and the corresponding constraints placed on the IGM density from the UV background observations[2,3] have therefore not been particularly confining, *i.e.* typically $\Omega_b^2 h^3 \lesssim 10^2$.

Several recent developments call for this topic to be revisited. For one, not least thanks to the experimental efforts of the Berkeley group, the rather confusing observational situation concerning the origins of the far-ultraviolet background has gradually started to become much clearer. As reviewed by Bowyer at this conference (see also reference [11] – but also [12] for a dissenting voice), there is today good evidence that the diffuse ultraviolet background is dominated by emission due to interstellar processes occurring within the galaxy[13,14,15]. A conservative upper limit on the possible extragalactic

component to the background in the $\lambda 1300 - 2000$ Å range is[15] $I_\lambda \lesssim 100$ photons $s^{-1}$ $cm^{-2}$ $sr^{-1}$ $Å^{-1}$. Of this possible extragalactic flux, approximately half or more is expected to be due to the integrated light of galaxies[16]. This new observational constraint leaves somewhat less room for contributions from more exotic sources, such as IGM emission, than previously assumed.

The situation regarding the absorption studies of the IGM has changed even more radically over the last decade with the dramatic advances that have been made in the new field of quasar absorption lines – which can be considered to be the "high resolution" refinement of the classical Gunn-Peterson test. The discovery of the dense "Lyman forest" of weak Ly$\alpha$ absorption lines seen in the spectra of all quasars has revealed the existence of a highly clumped component of the IGM consisting of an abundant and evolving population of intergalactic clouds of possibly primordial gas. Surveys of the more massive metal-containing absorption systems associated with galaxies have also led to new understandings concerning the transparency of the universe in the ultraviolet out to large redshift. The remainder of this paper is concerned with re-assessing the possible contributions to the extragalactic far-ultraviolet background from the intergalactic medium in light of this new knowledge gained from quasar absorption line studies.

## II. Quasar Absorption Lines in Brief

In this section a few key results of quasar absorption line studies of particular relevance for the topic of the diffuse ultraviolet background are briefly highlighted. A series of excellent and more comprehensive reviews that do the far-reaching topic far better justice can be found in the compilation of Blades, Turnshek and Norman.[17,18,19,20]

If classified according to their HI column density, there are basically two classes of intervening quasar absorption line systems: the numerous "Lyman forest" systems, whose column densities fall in the range $N_{HI} \simeq 10^{13} - 10^{17}\mathrm{cm}^{-2}$ and the scarcer, but denser, "Lyman limit" systems having column densities $N_{HI} \simeq 10^{17} - 10^{22}\mathrm{cm}^{-2}$. Lyman limit systems nearly always show matching absorption from heavy elements, and are therefore thought to be associated with the gaseous halos of galaxies. The Lyman forest systems, on the other hand, show little or no evidence for heavy elements and are therefore believed to be due to intergalactic clouds of possibly primordial material.

The Lyman forest systems are extremely numerous and evolve rapidly with redshift. Their line-of-sight density evolution is usually parameterized in the form[21]

$$E[\frac{dn}{dz}] = N(z) = A(1+z)^\gamma \tag{4}$$

with $A \simeq 10$ and $\gamma \simeq 2 - 3$. Lyman limit absorbers are roughly ten times scarcer ($A \simeq 1$) and evolve less rapidly ($\gamma \simeq 1$) than Lyman forest systems[22]. The column density spectrum of both classes of absorber is approximately a power law, $dP/dN_{HI} \propto N_{HI}^{-s}$, with index $s \simeq 1.2 - 1.6$.[22,23] The fact that the detailed statistics of the various types of HI containing quasar absorption systems are now reasonably well known permits a re-assessment of the question of the overall transparency of the UV universe out to high redshift (Section V). These results have important implications for the interpretation of the UV background.

Particularly relevant for the topic at hand is the fact that the Lyman forest clouds are believed to be kept highly photoionized by a metagalactic flux of ionizing radiation. One key piece of evidence for this is found in the so-called "proximity effect"[21]. As the emission redshift is approached, the Lyman forest absorbers in a given quasar show a gradual under-density of absorbers with respect to the global density given by equation (4). This effect is interpreted as being caused by the radiation field of the background quasar enhancing the total ionizing flux above the metagalactic level. Since the quasar flux can be estimated from the magnitude and spectrum of the quasar, an estimate of the background metagalactic ionizing background intensity can be derived from the measured contrast of the proximity effect. Through this technique[23,24] one infers that the intergalactic ionizing background

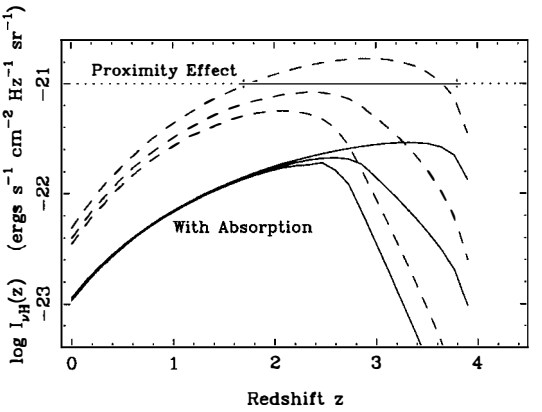


FIG. 2. — Predicted integrated ionizing background due to quasars for several quasar evolution models. The upper dashed curves show the integrated background intensity at the Lyman limit as a function of redshift according to the calculations of Bajtlik, Duncan and Ostriker[23]. The lower full curves show the same fluxes attenuated by the accumulated Lyman continuum absorption from the Lyman forest and Lyman limit classes of quasar absorption line systems (see Section V). The background level required to explain the proximity effect is also indicated.

at in the redshift range $1.7 \lesssim z \lesssim 3.8$ is consistent with an $I_\nu \propto \nu^{-\alpha}$, $\alpha \simeq 0.5$ power law with intensity at the Lyman limit of order $I_{\nu_H} \approx 10^{-21}$ ergs s$^{-1}$ cm$^{-2}$ sr$^{-1}$ Hz$^{-1}$.

The origin of this ionizing flux is a topic of debate. One obvious candidate is the integrated flux from quasars. However, only by pushing current uncertainties in our knowledge of the quasar luminosity function and evolution can the intensity required by the proximity effect barely be approached[23,25]. Moreover, taking into account absorption from the Lyman forest and Lyman limit systems themselves (Section V), worsens the discrepancy further by a factor of about 6 (Figure 2). Several authors[26,27,28] have suggested that an alternative candidate may be radiation from primordial galaxies. Regardless of its origin, this estimate of the ionizing flux at high redshift has important implications for the possible contributions to the extragalactic UV background from a photoionized IGM.

A final relevant result stemming indirectly from the quasar absorption line work concerns the information on the properties any pervasive IGM gas surrounding the Lyman forest clouds that result from considerations of Lyman forest cloud confinement and survival[29,30]. The classical Gunn-Peterson test limits, combined with constraints on cloud/IGM pressure and cloud lifetimes to evaporation, generally constrain the ambient IGM to have at density corresponding to $\Omega_b \approx 10^{-1}$ and a temperature $T \approx 10^5$ K. These constraints also translate into limits on possible IGM emission contributions to the background.

## III. Redshifted Lyman Alpha Emission from the IGM Revisited

Diffuse emission in Ly$\alpha$ $\lambda$1216Å from the IGM at redshifts $0 \lesssim z \lesssim 0.7$ will give rise to diffuse background radiation at far-UV wavelengths $\lambda\lambda$1200 – 2000 Å. Two processes are responsible for producing such diffuse Ly$\alpha$ radiation: radiative recombination in case of a photoionized IGM, and collisional excitation in the case of a shock-heated IGM.

As mentioned in Section II, the Lyman forest clouds and possibly any smooth ambient IGM are

believed to be held highly photoionized by a metagalactic ionizing radiation field, presumably due to the integrated light of quasars and primeval galaxies. What is the possible contribution to the UV background from redshifted Ly$\alpha$ recombination emission from this gas?

Consider first the case of recombination radiation from a smooth photoionized IGM. The line emissivity to be inserted into equation (1) is

$$\epsilon_l(z) = n_{HII}(z) n_e(z) \alpha_l(T) \tag{5}$$

where $\alpha_l \simeq 2\ 10^{-13}\mathrm{cm}^3\ \mathrm{s}^{-1}$ is the effective Ly$\alpha$ recombination coefficient, and $n_{HII}$ and $n_e$ are the proton and electron density in the gas. With an $I_\nu \propto \nu^{-\alpha}$ ionizing background of average intensity $I_{\nu_H}(z)$ at the Lyman limit, the equation for hydrogen photoionization equilibrium is

$$n_{HII}(z) n_e(z) \alpha_H = \frac{2}{\hbar} I_{\nu_H}(z) \sigma_H^0 \frac{1}{(\alpha+3)} n_{HI}(z) \tag{6}$$

where $\alpha_H \simeq 3\ 10^{-13}\mathrm{cm}^3\ \mathrm{s}^{-1}$ is the total recombination coefficient and $\sigma_H^0 = 6.3\ 10^{-18}\ \mathrm{cm}^2$ is the HI cross section at the Lyman limit. Combining equations (5) and (6) with the expression (3) for $n_{III}$ from the Gunn-Peterson test and inserting into equation (1) leads to the following expression for the intensity of the resulting redshift-smeared Ly$\alpha$ background due to recombination emission

$$I_\lambda(\lambda_0) = \left[\frac{\lambda_H}{\lambda_l}\right] \left[\frac{\alpha_l}{\alpha_H}\right] \left[\frac{\sigma_H^0}{\sigma_l}\right] \frac{\tau(z)}{(\alpha+3)} \left[\frac{I_{\nu_H}(z)}{2\pi\hbar\lambda_H (1+z)^4}\right] \tag{7}$$

In this expression, the last factor in brackets is simply the intensity of the ionizing flux, $I_{\nu_H}(z)$ converted to suitable units and redshifted to zero redshift; that is, the background intensity that would be seen today if the ionizing flux propagated freely from redshift $z$. Since the product of the remaining factors in equation (7) is of order unity or less, this equation is merely reminding us that since $\alpha_l/\alpha_H \simeq 0.7$ Ly$\alpha$ photons are emitted per photoionization event, the intensity of the resulting redshift-smeared Ly$\alpha$ recombination background can never be greater than that of the ionizing input flux itself. This principle of photon conservation, of course, applies equally well in the clumped case. The equivalent expression for the redshift-smeared recombination emission from the Ly$\alpha$ forest clouds can be obtained through the substitution

$$\tau(z) \rightarrow E[\frac{dn}{dz}(z)] \sigma_l \langle N_{HI} \rangle (1+z) \tag{8}$$

Note that since equation (6) implicitly assumes optically thin conditions, equations (7) and (8) are as they stand only valid in that limit. However, the fact that the redshifted recombination line emission is bounded by the intensity of the ionizing input flux is inherent to the nature of the recombination process and true *regardless* of the amount and detailed spatial distribution of the matter being photoionized and the recombination line in question. In other words, since the photoionized intergalactic gas is simply acting as a passive photon down-converter, the task of estimating the possible contribution to the UV background from line emission from photoionized intergalactic matter boils down to the task of estimating the intensity of the ionizing input flux at high redshift, $I_{\nu_H}(z)$.

As mentioned in Section II, the proximity effect displayed by the Ly$\alpha$ forest implies that $I_{\nu_H} \approx 10^{-21}$ ergs $\mathrm{s}^{-1}$ $\mathrm{cm}^{-2}$ $\mathrm{sr}^{-1}$ $\mathrm{Hz}^{-1}$ within the $1.7 \lesssim z \lesssim 3.8$ redshift range that can be probed with ground-based telescopes. Unfortunately, the proximity effect has not yet been detected within the $z \lesssim 1$ range of interest here due to the limited sensitivity and spectral resolution of *IUE* (although detailed observations of the Lyman forest at low redshift should be forth-coming with ***HST***). However, judging from Figure 2, one anticipates an even lower ionizing background of intensity $I_{\nu_H}(z) \simeq 10^{-22}$ ergs $\mathrm{s}^{-1}$ $\mathrm{cm}^{-2}$ $\mathrm{sr}^{-1}$ $\mathrm{Hz}^{-1}$ at $z \lesssim 1$. This expectation is confirmed observationally from limits on the local extragalactic ionizing flux derived from H$\alpha$ observations of high-latitude and extragalactic

HI clouds[31,32,33]. This ionizing flux, if redshifted from $z \simeq 0.5$, corresponds to an equivalent far-UV background of $I_\lambda \simeq 0.4$ photons s$^{-1}$ cm$^{-2}$ sr$^{-1}$ Å$^{-1}$ – an intensity about two orders of magnitude below the observational limits on a possible extragalactic contribution. It follows that redshifted Ly$\alpha$ recombination emission from neither the Lyman forest clouds nor a smooth photoionized IGM is likely to be a significant contributor to the far-UV background.

A similar conclusion can be reached in the alternative scenario of Ly$\alpha$ emission from a shock-heated IGM. In the case of collisionally excited emission from a smooth IGM component, the line emissivity can be written

$$\epsilon_l(z) = n_{HI}(z) n_e(z) \beta_l(T) \tag{9}$$

where $\beta_l(T)$ is the Ly$\alpha$ collisional excitation rate, and $n_{HI}$ and $n_e$ are the neutral hydrogen and electron densities in the IGM. The HI density is constrained observationally by the Gunn-Peterson limit, equation (3), while the electron density is constrained by the total baryonic density of the nearly fully ionized IGM. Combining, equations (1), (3) and (9), and introducing $n_e(z) = n_e^0(1+z)^3$ where $n_e^0 \simeq 1.2 n_H^0 = 9.3\ 10^{-6} \Omega_b h^2$ cm$^{-3}$ is the present epoch electron density, one obtains the following expression for the redshift-smeared Ly$\alpha$ background

$$I_\lambda(\lambda_0) = \frac{\tau(z)}{\sigma_l} \frac{n_e^0}{4\pi} \frac{\beta_l(T)}{\lambda_l} (1+z)^{-1} \tag{10}$$

For an ambient IGM temperature of $T \approx 10^5$ K as inferred from considerations of quasar absorption line cloud survival, the Ly$\alpha$ collisional excitation rate is $\beta_l \simeq 4\ 10^{-9}$cm$^3$ s$^{-1}$. This value, together with the Gunn-Peterson limit of $\tau(z) < 0.1$, yields a predicted smeared Ly$\alpha$ intensity of $I_\lambda \lesssim 4\ 10^{-2} \Omega_b h^2$ photons s$^{-1}$ cm$^{-2}$ sr$^{-1}$ Å$^{-1}$ in the far-UV. It follows that collisionally excited Ly$\alpha$ emission from a smooth IGM component at $0 \lesssim z \lesssim 0.7$ is a negligible contributor to the far-UV background for any reasonable value of $\Omega_b h^2$. The reason for this firm conclusion is simply that it takes intergalactic HI atoms to produce collisionally excited Ly$\alpha$ emission, and $n_{HI}(z)$ is severely constrained by the Gunn-Peterson test.

What about collisionally excited emission from the Lyman forest clouds? The equivalent expression to equation(10) for the redshift-smeared Ly$\alpha$ background in the clumped case can be obtained through the substitutions (8) and $n_e(z) \rightarrow n_e$. This leads to

$$I_\lambda(\lambda_0) = E[\frac{dn}{dz}(z)] \langle N_{HI} \rangle \frac{n_e}{4\pi} \frac{\beta_l(T)}{\lambda_l} (1+z)^{-3} \tag{11}$$

where $n_e$ is now the *in situ* electron density in the Lyman forest clouds. Based on studies of correlated Lyman forest absorption in quasar pairs combined with considerations of resonable ionization levels[17,19], $n_e$ is believed to be of order $\approx 10^{-3}$ cm$^{-3}$. The observed line widths of the Lyman forest systems[17] limit their temperatures to $T \lesssim 3\ 10^4$ K, in which case $\beta_l \lesssim 3\ 10^{-10}$ cm$^3$ s$^{-1}$. With these numbers and the values $E[dn/dz(z)] \simeq 34$ and $\langle N_{HI} \rangle \simeq 10^{15}$ cm$^{-2}$, appropriate to the Lyman forest at $z \simeq 0.3$, equation (11) yields $I_\lambda \lesssim 3\ 10^{-1}$ photons s$^{-1}$ cm$^{-2}$ sr$^{-1}$ Å$^{-1}$. Again, we conclude that collisionally excited Ly$\alpha$ emission from the Lyman forest is not a significant contributor to the far-UV background.

This leads to the final question of collisionally excited emission from the Lyman limit class of quasar absorbtion systems. For these systems $E[dn/dz(z)] \simeq 1.3$, but $\langle N_{HI} \rangle \simeq 10^{19}$ cm$^{-2}$, so the product of these parameters in equation (11) is $\approx 400$ times larger than for the forest systems, thereby raising the potential background limit to $I_\lambda \lesssim 1\ 10^2$ photons s$^{-1}$ cm$^{-2}$ sr$^{-1}$ Å$^{-1}$. Although this flux is indeed comparable to current observational limits on the extragalactic far-UV background, it has to be regarded as a strict upper limit since a significant fraction of the total HI column density contained in a typical Lyman limit absorber may arise in cool neutral gas as witnessed by the low ionization neutral species often seen in such systems. Moreover, since the Lyman limit systems contain heavy

elements, they presumably also contain interstellar dust at some level. This in turn leads to the classical problem of Ly$\alpha$ quenching due to dust absorption. In any event, since Lyman limit systems are believed to be associated with galaxy halos, one can argue that any possible Ly$\alpha$ background emission from such systems should not be be classified as bona fide IGM emission, but considered as an additional Ly$\alpha$ component to the integrated UV light of galaxies – which is indeed believed to be a significant contributor to the extragalactic far-UV background[16].

## IV. Redshifted HeII $\lambda$304Å Emission from the IGM Revisited

As mentioned in Section I, the second most important emission line from a luke warm photoionized or shock-heated intergalactic primordial plasma is HeII Ly$\alpha$ emission at $\lambda$304Å. The discussion of the possible far-UV background contribution due to this source from very high redshifts ($3 \lesssim z \lesssim 5$) is slightly more complicated with respect to that of HI Ly$\alpha$ for several reasons. For one, we presently know very little about the intergalactic abundance of the HeII ion, since the HeII $\lambda$304Å equivalent of the Gunn-Peterson test has yet to be carried out in the far-UV with *HST* or *Lyman/FUSE*. The expectation is that if the Lyman forest clouds and an ambient IGM are indeed photoionized by an $I_\nu \propto \nu^{-0.5}$ power law, then the HeII ion should be an order of magnitude more abundant than HI, in which case the HeII Gunn-Peterson effect should be extremely strong (and HeI absorption very weak). A second important difference with respect to HI Ly$\alpha$ is that HeII $\lambda$304Å emission falls below the photoionization edge of neutral hydrogen and is therefore subject to absorption by intergalactic HI in the Lyman forest and especially the Lyman limit classes of quasar absorption systems. This last topic is addressed in detail in the following section. In spite of these complications, it is nonetheless still possible to draw several reasonably firm conclusions concerning the possible contribution of HeII $\lambda$304Å emission to the far-UV background.

In the previous section, the intensity of redshifted far-UV Ly$\alpha$ recombination radiation from photoionized intergalactic gas was constrained on the basis of estimates on the metagalactic ionizing background derived from the proximity effect and more local observations of diffuse H$\alpha$ emission from high-latitude and extragalactic HI clouds. The fundamental constraint expressed by equation (7), namely that the redshifted line background from a photoionized IGM can never be greater than that of the input ionizing flux, obviously applies equally well in the case of redshifted recombination HeII $\lambda$304Å emission. In particular, with a flat $I_\nu \propto \nu^{-0.5}$ spectrum for the metagalactic ionizing background, the intensity of the ionizing flux at the HeII ionization edge at $\lambda$228Å is of the same order of magnitude as the flux at the Lyman limit at $\lambda$912Å of $I_{\nu_H}(z) \approx 10^{-21}$ ergs s$^{-1}$ cm$^{-2}$ sr$^{-1}$ Hz$^{-1}$ derived from the proximity effect at $1.7 \lesssim z \lesssim 3.8$. This intensity, if redshifted from $z \approx 4$ will give rise to a far-UV background of intensity $I_\lambda \lesssim 1$ photons s$^{-1}$ cm$^{-2}$ sr$^{-1}$ Å$^{-1}$. Since this background limit falls a factor $\approx 50$ below the observational limits – even without including the effects of absorption – redshifted recombination HeII $\lambda$304Å emission from photoionized intergalactic gas can also be ruled out as a significant source of far-UV background radiation.

Collisionally excited HeII $\lambda$304Å from a shock-heated IGM on the other hand is not quite as easily dismissed. Since, as mentioned above, the amount of HeII present in intergalactic space has not (yet) been measured by observations of the HeII version of the Gunn-Peterson test and the anticipated "helium forest" matching that seen in Ly$\alpha$, we cannot use the HeII equivalents of equations (10) and (11) to bracket the possible background contribution. Instead, we are forced back to the more theoretical predictions described by equation (2) and Figure 1. As shown in Figure 1, the net HeII $\lambda$304Å emissivity per HI atom peaks at $\gamma_l \simeq 1.2\ 10^{-12}$ cm$^3$ s$^{-1}$ at a temperature $T \simeq 8\ 10^4$ K. Inserting this maximum emissivity into equations (1) and (2) yields a predicted far-UV background intensity at $\lambda$1600Å of $I_\lambda \simeq 400\Omega_b^2 h^3$ photons s$^{-1}$ cm$^{-2}$ sr$^{-1}$ Å$^{-1}$. Hence depending on what one assumes for $\Omega_b$ and $H_0$, redshifted collisionally excited HeII $\lambda$304Å radiation from $z \simeq 3 - 5$ could in principle yield a significant far-UV background flux. On the other hand, considerations of the survival of quasar absorption line clouds and primordial nucleosynthesis both point toward $\Omega_b \lesssim 0.1$, in which case the HeII flux is insignificant. Moreover, as discussed in the following section, the census of absorbing

HI gas present in the Universe represented by the statistics of quasar absorption lines implies that the far-UV Universe is opaque in the Lyman continuum out to high redshift. This absorption will attenuate any diffuse HeII $\lambda 304$Å radiation emitted at $z \gtrsim 3$ by about two orders of magnitude, thereby reducing even the most optimistic HeII background flux to an unobservable level.

## V. Accumulated Lyman Continuum Opacity of the Universe

Any contribution to the far-UV background at observed wavelength $\lambda_0$ emitted originally at a wavelength below the Lyman limit, $\lambda_H = 912$Å, at a redshift $1+z_e > \lambda_0/\lambda_H$ will be subject to photoelectric absorption in any neutral hydrogen encountered along at least part of its path. Although it has been known for some time that the classical Gunn-Peterson test demonstrates that the Lyman continuum opacity of any *smoothly* distributed IGM is negligible, it has only recently been fully appreciated that the statistics of quasar absorption lines imply the that the accumulated absorption out to moderate and high redshift from the *clumped* component is quite substantial[26,34].

The character and magnitude of the accumulated Lyman continuum absorption from the Lyman forest and Lyman limit classes of quasar absorption lines has recently been discussed in detail in reference [34]. The general expression for the average transmission through a clumpy medium experienced by a photon emitted at wavelength, $z_e$, and received at wavelength, $\lambda_0$, is

$$E[q(\lambda_0, z_e)] = \exp(-\int_0^{z_e} N(z)(1 - \langle q_c(\lambda_0, z)\rangle)dz) \tag{12}$$

where $\langle q_c(\lambda_0, z)\rangle = \langle \exp(-N_H \sigma_H(\lambda_0/(1+z)))\rangle$ is the average individual cloud transmission and $\sigma_H(\lambda)$ is the HI photoelectric cross section given by

$$\sigma_H(\lambda) \simeq \begin{cases} \sigma_H^0 \left(\frac{\lambda}{\lambda_H}\right)^3 & \text{if } \lambda \leq \lambda_H \\ 0 & \text{if } \lambda > \lambda_H \end{cases} \tag{13}$$

where $\sigma_H^0 = 6.3\ 10^{-18}$ cm$^2$ is the photoionization cross section of neutral hydrogen at the Lyman limit.

As outlined in Section II, the statistics of quasar absorbers are today sufficiently well known to permit a reasonably accurate evaluation of equation (12). Figure 3 shows, as a a function of wavelength, the resulting accumulated average residual transmission out to various redshifts from the combined total absorption due to the Lyman forest and Lyman limit systems. The characteristic "Lyman valley" shape of the accumulated absorption spectrum is caused by the interplay between the $\sigma \propto \lambda^3$ dependence of the HI photoelectric cross section and redshift evolution and pathlength effects.

The main point to be read from Figure 3 is that the predicted net absorption out to high redshift in the ultraviolet is rather high. As an specific example, the lower panel of Figure 4 shows the average residual absorption at received wavelength $\lambda_0 \simeq 1600$Å as a function of emission redshift. From this figure it is seen that any HeII $\lambda 304$Å radiation emitted at $z_e \simeq 4.3$ will be attenuated by a factor of order $\approx 10^{-2}$. This high opacity effectively implies that even if the IGM did go through a phase of of intense HeII emission during re-heating, the resulting far-UV background radiation will in all likelihood remain forever hidden from our view.

It is important to stress that the accumulated intergalactic absorption given in Figures 3 and 4 refers to the *average* transmission. Since the dominant contributor to the opacity is the scarcer but optically thick Lyman limit systems, large fluctuations around this average are expected along any given line of sight (*i.e.* in any given quasar spectrum). The magnitude of the fluctuations can be calculated from the expression for the second moment of the accumulated transmission

$$E[q^2(\lambda_0, z_e)] = \exp(-\int_0^{z_e} N(z)(1 - \langle q_c^2(\lambda_0, z)\rangle)dz) \tag{14}$$

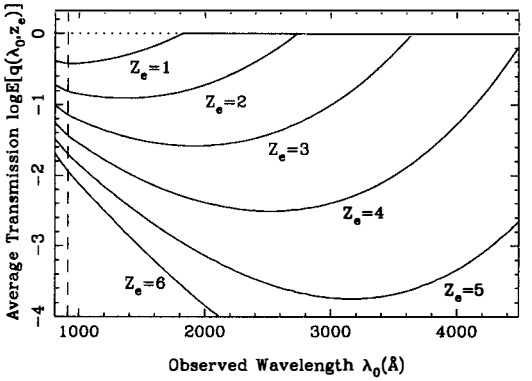


FIG. 3. — Average opacity of the UV universe out to high redshifts as a function of wavelength. The shown "Lyman valley" absorption spectra include the accumulated Lyman continuum opacity from both the Lyman forest and Lyman limit classes of quasar absorption systems. The same parameters as used in reference [34] are assumed.

The upper panel of Figure 4 shows the predicted relative transmission fluctuations, $(\delta q/q) = \left(E[q^2] - E[q]^2\right)^{\frac{1}{2}}/E[q]$, as a function of $z_e$, again for $\lambda_0 = 1600$Å. In the example of HeII Ly$\alpha$ emission from $z_e \simeq 4.3$ quoted above, the $1\sigma$ level fluctuations amount to a factor $\approx 5$. In other words, a characteristic signature of any contributor to the far-UV background originating at high redshift should be an extremely patchy background component.

This leads to the interesting prospect of detecting or constraining a high-$z$ component to the far-UV background – regardless of its origin – through measurements of background intensity fluctuations. In fact, from the measurements of Martin and Bowyer[16], it is known that the far-UV background at $\lambda_0 \simeq 1600$Å is very smooth on angular scales of $\theta = 8'$ and larger: $(\delta I/I)_\theta \simeq 6\%$. If it is assumed that the background consists of the sum of a smooth local component and an attenuated distant high redshift component of average intensity $E[q(z)]I_z$, the fractional contribution to the total average emission from the distant component, $\phi_z$, can be estimated from the observed dilution of the opacity fluctuations

$$\phi_z = \frac{E[q(z)]I_z}{I_{Total}} \simeq \left(\frac{\delta I}{I}\right)\left(\frac{\delta q}{q}\right)^{-1} \tag{15}$$

Taken at face value, the Martin and Bowyer fluctuation limit implies that less than $\phi_z \approx 6\%/5 \simeq 1\%$ of the far-UV background can originate from $z \simeq 4.3$. However, a slightly subtle point has been overlooked; namely that the $(\delta q/q)$ values in Figure 4 refer statistically to the absorption sampled along an infinitely narrow pencil beam (namely the line of sight to a quasar), whereas the UV background observations have been obtained with a finite $\theta = 8'$ beam size. Since the opacity is dominated by the Lyman limit absorbers, which are assumed to be associated with galaxy halos of, say, $D \approx 50$ kpc size, the absorption-generated background fluctuations on the sky are expected to be correlated only on very small scales of order $\theta_c \approx cD/H_0 \approx 10''$. Such small scale fluctuations would only appear in the finite beam measurements of Martin and Bowyer diluted by a factor of order $\theta/\theta_c \approx 50$. The upper limit on $\phi_z$ derived above therefore has to be relaxed by the same amount to $\phi_z \lesssim 50\%$. Given the severe practical problems of measuring UV background fluctuations on such small scales as $\theta \approx 10''$, it is unlikely that this constraint will be tightened much further in the forseeable future. On the other

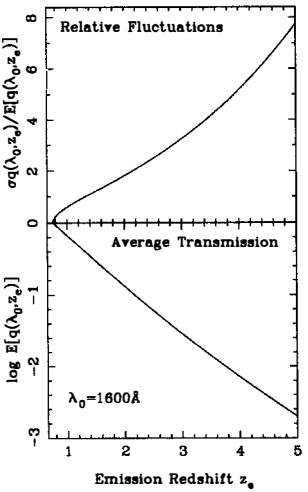


FIG. 4. — Lower frame: Average transmission of the Universe at received wavelength λ1600Å as a function of emission redshift. Upper frame: Predicted relative fluctuations around the average transmission for an infinitely narrow pencil beam due to fluctuations in the composition and location of the absorbing HI clouds along the line of sight.

hand, the above considerations do serve to demonstrate that, because of the very small size of the anticipated absorption coherence patch on the sky, use of the average attenuation given by equation (12) is well justified when dealing with the radiative transfer of diffuse background light.

## VI. Summary and Conclusions

A decade of study of quasar absorption lines has yielded unique new and unique information on both the gas content and ionizing radiation field present in intergalactic space over a large span in redshift. In summary, the quasar absorption line data suggest that there is not enough ionizing flux present in intergalactic space to produce diffuse recombination emission from photoionized gas at a level close to current observational limits on the extragalactic far-UV background flux; nor does there appear to be enough neutral gas present to produce collisionally excited Ly$\alpha$ emission from shock-heated intergalactic gas at a detectable level. On the other hand, there is more than enough neutral hydrogen contained in the more massive absorption systems associated with galaxies to produce a significant Lyman continuum opacity out to high redshift, thereby hiding from view any potential far-UV background contribution originating at $z \gtrsim 3$. In particular, any collisionally excited HeII λ304Å emission emitted during IGM re-heating will be attenuated by at least two orders of magnitude in intensity.

It is concluded that diffuse thermal line emission from the various components of the IGM is most likely not a significant contributor to the extragalactic diffuse far-UV background.

REFERENCES:

1. Kurt, V. G., Sunyaev, R. A.: 1967, *Cosmic Research*,**5**,496.
2. Davidsen, A., Bowyer, S., Lampton, M.: 1974, *Nature*,**247**,513.
3. Paresce, F., Jakobsen, P.: 1980, *Nature*,**288**,119.
4. Weymann, R.: 1967, *Astrophys. J.*,**147**,887.
5. Sherman, R. D.: 1979, *Astrophys. J.*, **232**,1.
6. Sherman, R. D.: 1982, *Astrophys. J.*, **256**,370.
7. Gunn, J. E., Peterson, B. A.: 1965, *Astrophys. J.*,**142**,1633.
8. Steidel, C. C., Sargent, W. L. W.: 1987, *Astrophys.J. (Letters)*, **318**,L11.
9. Kinney, A. L., Bohlin, R. C., Blades, J. C., York, D. G.: 1991, *Astrophys. J. Suppl.*, (in press).
10. Green, R. F., Pier, J. R., Schmidt, M, Estabrook, F. B., Lane, A. L., Wahlquist, H. D.: 1980, *Astrophys. J.*, **239**,483.
11. Bowyer, S.: 1991, *Ann. Rev. Astr. Ap.* (in press).
12. Henry, R. C.: 1991, *Ann. Rev. Astr. Ap.* (in press).
13. Martin, C., Bowyer, S.: 1990, *Astrophys. J.*,**350**,242.
14. Martin, C., Hurwitz, M., Bowyer, S.: 1990, *Astrophys. J.*,**345**,220.
15. Hurwitz, M., Bowyer, S., Martin, C.: 1991, *Astrophys. J.*,**372**,167 .
16. Martin, C., Bowyer, S.: 1989, *Astrophys. J.*,**338**,667.
17. Carswell, R. F.: 1988, in *QSO Absorption Lines: Probing the Universe* p. 91, eds. C. Blades, D. Turnshek, C. Norman, Cambridge University Press, Cambridge.
18. Hunstead, R. W.: 1988, in *QSO Absorption Lines: Probing the Universe*, p. 71, eds. C. Blades, D. Turnshek, C. Norman, Cambridge University Press, Cambridge.
19. Sargent, W. L. W.: 1988, in *QSO AbsorptionLines: Probing the Universe* p. 1, eds. C. Blades, D. Turnshek, C. Norman, Cambridge University Press, Cambridge.
20. Tytler, D.: 1988, in *QSO Absorption Lines: Probing the Universe* p. 179, eds. C. Blades, D. Turnshek, C. Norman, Cambridge University Press, Cambridge.
21. Murdoch, H. S., Hunstead, R. W., Pettini, M., Blades, J. C.: 1986, *Astrophys. J.*, **309**,19.
22. Sargent, W. L. W., Steidel, C. C., Boksenberg, A.: 1989, *Astrophys. J. Suppl.*, **69**,702.
23. Bajtlik, S., Duncun, R. C., Ostriker, J. P.: 1988, *Astrophys. J.*,**327**,570 .
24. Steidel, C. C., Sargent, W. L. W.: 1989, *Astrophys.J. (Letters)*, **343**,L33.
25. Lu, L., Wolfe, A. M., Turnshek, D. A.: 1991, *Astrophys. J.*,**367**,19 .
26. Bechtold, J., Weymann, R. J., Lin, Z., Malkan, M. A.: 1987, *Astrophys. J.*, **315**,180.
27. Miralda-Escudé, J., Ostriker, J. P.: 1990, *Astrophys. J.*, **350**,1.
28. Songaila, A., Cowie, L. L., Lilly, S. J.: 1990, *Astrophys. J.*,**348**,371 .
29. Ostriker, J. P., Ikeuchi, S.: 1983, *Astrophys. J.(Letters)*, **268**,L63.
30. Ikeuchi, S., Ostriker, J. P.: 1986, *Astrophys. J.*,**301**,522 .
31. Reynolds, R. J., Magee, K., Roesler, F. L., Scherb, F., Harlander, J.: 1986, *Astrophys. J. (Letters)*,**309**,L9.
32. Songaila, A., Bryant, W., Cowie, L. L.: 1989, *Astrophys. J. (Letters)*,**345**,L71 .
33. Kutyrev, A. S., Reynolds, R. J.: 1989, *Astrophys. J. (Letters)*,**344**,L9 .
34. Møller, P., Jakobsen, P.: 1990, *Astron. Astrophys.*,**228**,299.

# THE COSMOLOGICAL UV BACKGROUND FROM DECAYING NEUTRINOS

D.W. Sciama
International School for Advanced Studies, Trieste and
International Centre for Theoretical Physics, Trieste, Italy

ABSTRACT

The hypothesis that dark matter tau neutrinos decay into photons which ionise hydrogen throughout the universe leads to testable consequences for the cosmological UV background. Observations of the ionising component of this background are used to constrain the energy of the decay photons. The background of softer U-V decay photons can then be predicted, and is found to be close to the upper limit derived from observations made above the atmosphere.

1) Introduction

I have recently proposed[1,2,3] that dark matter tau neutrinos decay into photons with a lifetime $\tau \sim 1\text{-}3 \times 10^{23}$ seconds, and that these photons ionise hydrogen in galaxies, clusters of galaxies, Lyman $\alpha$ clouds and the intergalactic medium. This hypothesis solves several astronomical and cosmological puzzles, and seems to be in good agreement with a number of rather varied types of observation. In this talk I would like to discuss the contribution of the proposed decay photons to the cosmological u-v background. It is convenient to divide this discussion into two parts, one dealing with the background of Lyman continuum photons, and the other that of softer photons. The reason for this division is that these two backgrounds are detected in different ways. Before embarking on this discussion I shall describe recent negative attempts to detect the predicted emission line from dark matter neutrinos in clusters of galaxies, and explain why these negative results are not decisive.

2) Search for the Predicted Emission Line from Clusters of Galaxies

In the absence of absorption, one predicts an emission line of rest-energy in the range 14-15 eV from clusters of galaxies with an intensity I given by

$$I \sim \frac{4 \times 10^{-15}}{(1+z)^4} \left( \frac{\Sigma}{1 \text{gm.cm}^{-2}} \right) \text{ergcm}^{-2}\text{sec}^{-1}\text{arcsec}^{-2}$$

where $\Sigma$ is the surface density of dark matter in the detector aperture and z is the red shift of the cluster. Typical values of $\Sigma$ for clusters lie in the range 0.1-1 $\text{gm.cm}^{-2}$, on the basis of either an isothermal sphere model for the clusters, or of observations of gravitational arcs produced by the clusters[4,5].

In a first attempt, Fabian, Naylor and Sciama[6] used IUE data to study the spectrum of the moderately rich cluster surrounding the quasar 3C263. No unidentified line was detected. We concluded that

(i) $\Sigma < 0.34 \text{gm.cm}^{-2}$ in this cluster

or

(ii) $\tau > 2 \times 10^{23}$ secs

or

(iii) the line is absorbed by cold clouds in the cluster.

The first two possibilities are only marginally stringent. In my

opinion the most fruitful possibility is the third, that of absorption in the cluster. This possibility arises from the discovery by White et al.[7] of cold, X-ray absorbing clouds in the central regions of nearby clusters using X-ray spectra. The surface density of the HI clouds $\sim 10^{21} cm^{-2}$, which is very much greater than that required to absorb 14.5eV photons ($\sim 10^{17} cm^{-2}$). The existence of the cold clouds in the hot ($\sim 10^{7}$-$10^{8}$°K) intracluster gas demonstrates that cold and hot gas can co-exist without evaporation of the clouds taking place (magnetic fields presumably inhibit conduction). There is also observational evidence for significant quantities of dust in clusters[8]. Presumbably the dust is contained in the clouds, where it can be protected from rapid destruction by the hot intracluster electrons[9].

These ideas may be relevant for the reported[10] failure to detect an unidentified emission line in the cluster A665 by the Hopkins Ultra-Violet Telescope on the recently conducted ASTRO I mission. In a range of rest-energies of 14-16eV, if absorption in the cluster is neglected, a lower limit of $\tau \sim 10^{24}$-$10^{25}$ secs is obtained, the precise lower limit depending on the energy involved. The only exception to this lies in the narrow range 14.3±0.02eV, where the predicted line could be hiding under the strong geocoronal Lyman beta line which was observed. To exclude this unlikely coincidence one would need to observe a cluster with a different red shift from that of A665 (which has $z \sim 0.18$).

It is important therefore to make further studies of the possibility of substantial absorption of the line by HI and dust in the cluster. The predicted input energy flux would then be re-processed into various emission lines and into infra-red radiation emitted by the dust. Clearly this question gives rise to a number of new observational and theoretical problems which must be investigated (e.g. ref. 11). In particular, it is planned to use ISO to determine whether some clusters of galaxies are extended sources of infra-red radiation.

3) The Cosmological Background of Lyman Continuum Photons

We need to know this background in order to discuss the ionisation of the intergalactic medium and of Lyman $\alpha$ clouds. We must also ensure that the neutrino decay theory does not give rise to an excessive background. An observational upper limit at essentially zero red shift can be derived from H$\alpha$ data on HI clouds which are exposed to this background. There exists such data for high velocity clouds in or near our Galaxy, but in

these cases there may be significant absorption from nearby HI concentrations with a different velocity from that of the high velocity clouds. The most reliable value comes from Hα observations of Reynolds et al.[12] of an intergalactic HI cloud in Leo. Since some of the inferred Lyman continuum photons may be generated locally in the cloud, one actually obtains an upper limit on the extragalactic flux $F_1$ of Lyman continuum photons at z~0. Reynolds et al derived the limit

$$F_1 \leq 6\times10^5 \text{ cm}^{-2}\text{sec}^{-1}.$$

We now impose the requirement that the corresponding flux $F_2$ of decay photons should not exceed $F_1$. In calculating $F_2$ by integrating the flux from distant decaying neutrinos we must allow for the cosmological red shift acting on the initial energy $E_\gamma$ of the decay photons in the rest-frame of the parent neutrinos. Setting

$$E_\gamma = 13.6 + \epsilon \text{ eV},$$

we shall find that $\epsilon \ll 13.6$, so that the calculation of $F_2$ is elementary. We shall not need to take into account precise red shift dependent factors depending on an adopted model of the universe. In addition absorption effects from the accumulated influence of Lyman α clouds along the line of sight will be unimportant.

We then obtain

$$F_2 = \frac{n_\nu}{\tau} \frac{\epsilon}{13.6} R ,$$

where $n_\nu$ is the cosmological number density of decaying neutrinos and R is the radius of the universe ($=c/H_0$). The value of $n_\nu$ is standard, namely $\sim 100\text{cm}^{-3}$, and in our theory[2] $R\sim2\times10^{28}$cm. The condition $F_2 \leq F_1$ then implies that

$$\frac{\epsilon}{13.6} \leq 0.09 \left(\frac{\tau}{3\times10^{23}\text{sec}}\right) ,$$

so that

$$\epsilon \leq 1.2 \left(\frac{\tau}{3\times10^{23}\,\text{sec}}\right) \text{eV}$$

and

$$13.6 \leq E_\gamma \leq 14.8 \left(\frac{\tau}{3\times10^{23}\,\text{sec}}\right) \text{eV}.$$

The essential conclusion of this argument is that $E_\gamma$ is narrowly constrained. If our theory is correct this fact would lead to a number of important consequences for astronomy, cosmology and elementary particle physics which are discussed in refs. 1, 2 and 3. Further consequences arise from the red shift dependence of $F_2$. We have $n_\nu \alpha (1+z)^3$, and in our theory[2] $R\alpha(1+z)^{-3/2}$ (Einstein-de Sitter model), so that

$$F_2(z)\alpha(1+z)^{3/2} \ .$$

This relation enables one to explain[3] the otherwise puzzling high ionisation of Lyman $\alpha$ clouds and the intergalactic medium at large red shifts.

4) The Cosmological Background of Photons with $\lambda > 912$Å

Since the Galaxy is essentially transparent for photons softer than 13.6eV, this background is in principle detectable from observations made above the atmosphere, as discussed by Bowyer at this meeting. Again the red shifted flux $F_3(\lambda)$ of soft decay photons must not exceed the observed, or inferred, cosmological background. We can here make a genuine prediction, since $F_3$ is determined by $E_\gamma$ and $\tau$, both of which are now highly constrained. We predict that

$$F_3(\lambda) = \frac{n_\nu}{4\pi\tau} R \frac{\lambda_0^{1.5}}{\lambda^{2.5}} \qquad \lambda \geq \lambda_0$$

where $\lambda_0$ is $hc/E_\gamma$, the initial wavelength of the decay photon in the rest-frame of its parent neutrino.

At $\lambda$=1000Å, we obtain

$$F_3(1000\text{Å}) \sim 400 \text{ cm}^{-2}\text{sec}^{-1}\text{ster}^{-1}\text{Å}^{-1} \text{ (CU)}$$

If we make the usual allowance for absorption by dust in the Milky Way, we predict that at $b \sim 90^0$

$$F(1000\text{Å}) \sim 300 \text{ CU.}$$

Similarly, we derive

$$F(1400\text{Å}) \sim 200 \text{ CU}$$

and

$$F(2000\text{Å}) \sim 100 \text{ CU.}$$

These predictions are intriguingly close to the values discussed by Bowyer, after allowance for the integrated contribution from galaxies and from two-photon emission by the Reynolds layer of ionised gas in our Galaxy. Perhaps in the future it will be possible to test our theory in this way, and in particular to check the predicted $\lambda^{-2.5}$ spectrum.

REFERENCES


1) Sciama, D.W. 1990, Ap. J. 364, 549.
2) Sciama, D.W. 1990, Phys. Rev. Lett. 65, 2839.
3) Sciama, D.W. 1990, Comments Astrophys. 15, 71.
4) Soucail, G., Mellier Y., Fort, B., Mathez, G. and Cailloux, M. 1988 Astron. Astrophys. 191, L19.
5) Tyson, J.A., Valdes, F. and Wenk, R.A. 1990, Ap. J. 349, Ll.
6) Fabian, A.C., Naylor, T. and Sciama, D.W. 1991, Mon. Not. Roy. Astr. Soc., 249, 21P.
7) White, D.A., Fabian, A.C., Johnstone, R.M., Mushotzky, R.F. and Arnaud, K.A., Mon. Not. Roy. Astr. Soc., in press.
8) Boyle, B.J., Fong, R. and Shanks, T. 1988, Mon. Not. Roy. Astr. Soc., 231, 897.
9) Dwek, E., Rephaeli, Y. and Mather, J.C. 1990, Ap. J. 350, 104.
10) Davidsen, A.F. et al. 1991, preprint.
11) Soker, N., Bregman, J.N. and Sarazin, C.L. 1991, Ap. J. 368, 341.
12) Reynolds, R.J., Magee, K., Roesler, F.L., Scherb, F., and Harlander, J. 1986, Ap. J. 309, L9.

# THE EXTRAGALACTIC BACKGROUND LIGHT: OPTICAL AND NEAR-INFRARED OBSERVATIONS

K. Mattila[1], Ch. Leinert[2] and G. Schnur[3]

[1] Helsinki University Observatory
Tähtitorninmäki, SF-00130 Helsinki, Finland

[2] Max-Planck-Institut für Astronomie
Königstuhl, D-6900 Heidelberg, Germany

[3] Astronomisches Institut, Ruhr Universität Bochum
Postfach 102148, D-4630 Bochum 1, Germany

## ABSTRACT

We present a review of the presently available observations of the optical and near-IR extragalactic background light (EBL) obtained by means of night sky photometry. The EBL is a quantity of great cosmological importance; areas which are directly affected include galaxy formation and evolution, the appropriateness of different cosmological models, and the local luminosity density due to galaxies and other matter in intergalactic space. The basic problem in measuring the EBL is its separation from the other, much stronger components of the light of the night sky. We present first a review of the different methods utilized and the results obtained so far. Then we discuss in some more detail the dark cloud technique for EBL separation and describe our recent measurements carried out at ESO and at Calar Alto.

## 1. INTRODUCTION

The great cosmological importance of an isotropic background radiation component was already recognized in theoretical contemplations by Halley[1] (1721), Loys de Cheseaux[2] (1744) and Olbers[3] (1823) (For a review see Harrison[4,5]). The absence of a (very) bright background light, expected as the accumulation effect of more and more distant shells of stars in an infinite universe, is generally known as Olbers' Paradox. In spite of the long history of this problem in the optical, the background radiation was first detected in the microwave. The background radiation in the conventional optical and neighbouring infrared and ultraviolet wavebands have consistently defeated attempts to detect them.

The intensity of the background radiation due to galaxies (or other luminous matter) is given in the Friedmann models with a zero cosmological constant by the formula (see e.g. Partridge and Peebles[6])

$$I_0(\lambda_0,t_0) = \frac{c}{4\pi} L(\lambda_0,t_0) \times n(t_0) \int_{t_{min}}^{t_0} \frac{L(\lambda,t)}{L(\lambda_0,t_0)} \times \frac{n(t)}{n(t_0)} \times \frac{1}{[1+z(t)]^3}\, dt \qquad (1)$$

where $I_0(\lambda_0,t_0)$ is the background brightness and $L(\lambda_0,t_0)$ $n(t_0)$ the luminosity density at wavelength $\lambda_0$ at the present time $t_0$. There are $n(t_0)$ sources (galaxies) per unit volume, each of them emitting the flux $L(\lambda_0,t_0)$. The first factor under the integral describes the evolution of the energy output and spectral distribution of a galaxy. Here $L(\lambda,t)$ is the luminosity of the galaxy at the wavelength $\lambda=\lambda_0 . (1+z)^{-1}$ and at the time t. The second factor gives the evolution of the number of galaxies, while in the third factor the redshift z(t), being a function of the time, depends on the assumed cosmological model. The function z(t) also appears in the first factor because $\lambda=\lambda_0 . (1+z(t))^{-1}$. The lower limit of the integral, $t_{min}$, stands for the epoch when the oldest galaxies were formed. Thus, in Eq. (1) several quantities of great cosmological importance are included.

*1.1 Galaxy formation and evolution.* The principal interest for the extragalactic background light (EBL) during the past 20 years stems from the prospect of using it as a probe of galaxy formation and evolution. In a pioneering investigation Partridge and Peebles[6] pointed out that the redshifted radiation from very young galaxies could be observable as a background light component, especially if the forming galaxies went through a bright outburst phase during which some 20 % of primordial hydrogen was converted into helium. It is now generally believed that most of the helium was synthesized in the very early universe, before the galaxy formation. However, the concept of an initial starformation burst with accompanying strong UV radiation is nonetheless important for the EBL predictions and was analyzed by Tinsley[7] in extensive model calculations including realistic galaxy evolution assumptions. Her results indicated that for models including galaxy evolution the background is brighter by about a fctor of 3 to 10 as compared to the nonevolving models. Some of her models with recent galaxy formation (at z=3) produced a large optical background. Recently, Guiderdoni and Rocca-Volmerange[25] have presented results for the predicted EBL using

spectrophotometric modeling for the evolving galaxies, and a number of different cosmological models and galaxy formation epochs.

*1.2 Cosmological Models.* It has been often suggested that the integrated background light due to galaxies could be used as a test to discriminate between different cosmological models (see e.g. McVittie and Wyatt[8], 1959; Whitrow and Yallop[9]; Partridge and Peebles[6]). Calculations by Sandage and Tamman[10] for Friedmann world models with zero cosmological constant and no galaxy evolution show that for different values of the deceleration parameter $q_0$, the background at optical wavelengths is about 1 $10^{-9}$ erg $cm^{-2}$ $s^{-1}$ $sterad^{-1}$ $Å^{-1}$ and decreases only about 30 % when $q_0$ changes from -1 to +2.5 . Tinsley[7] found larger differences between the cosmological models with different $q_0$, especially when evolution was included. These differences are masked by the much larger uncertainties due to our incomplete knowledge of galaxy evolution. Yoshii and Takahara[11] have found similar effects of $q_0$ on the predicted EBL. The Hubble parameter $H_0$ does not influence the background when no galaxy evolution is assumed. But even with models with galaxy evolution Tinsley[7] found that the influence of $H_0$ is very small. Thus the selection of a specific cosmological model (i.e. $H_0$ and $q_0$) can cause only a minor variation in the value of the background light at optical wavelengths. It should be noted, however, that for the near-infrared background radiation the predicted differences between different cosmological models are much larger.

Stabell and Wesson[12] and Wesson et al.[13] have re-emphasized the fact, first pointed out by Harrison[14], that the specific cosmological model - even if expanding or nonexpanding - is of less importance as compared to the effect of the finite lifetime of galaxies.

*1.3 Local Luminosity Density.* The theoretical predictions which lead to the above mentioned value of ~$1 \cdot 10\text{-}9$ erg $cm^{-2}$ $s^{-1}$ $sterad^{-1}$ $Å^{-1}$ for the extragalactic light, are based on a local luminosity density of $3.6 \cdot 10^{-47}$ ( $H_0$/ 100 $kms^{-1}$ $Mpc^{-1}$) erg $cm^{-3}$ $s^{-1}$ $Hz^{-1}$ at 4300 Å.

This value has been derived by Shectman1[15] from the number of known galaxies (Kiang[16]); see also the discussion in Peebles[17]. Based on recent analyses of galaxy counts (e.g. Ellis[58]), Yoshii and Takahara[11]) have adopted a lower luminosity density of $2.3 \cdot 10^{-47}$ ( $H_0$/ 100 $kms^{-1}$ $Mpc^{-1}$) erg $cm^{-3}$ $s^{-1}$ $Hz^{-1}$ at 4600 Å.

Arp[18] pointed out that there may exist large numbers of hitherto unknown galaxies which, either because of their small angular extension or their low surface brightness, are not detectable with present observing techniques. Shectman[19], analyzing the small-scale anisotropy of the EBL has found, however, that, if the luminous matter is distributed in the same way as galaxies, the observed fluctuations are in accord with the conventional value of the local luminosity density. If the EBL is totally due to galaxies, then the galaxy clustering will produce an anisotropy to the spatial distribution of EBL which is of the order of ~20-30 % at scale lengths of a few arc minutes. This anisotropy may be the most efficient means of detecting the component due to galaxies of the EBL (see Shectman[15,19]; Martin and Bowyer[20]. However, there may be other components of the EBL which do not follow the galaxy clustering. Thus the detection of the isotropic EBL level is still of the greatest interest.

*1.4 Intergalactic Gas.* Besides galaxies, intergalactic clusters and stars also the intergalactic gas may contribute to the EBL. E.g. Weyman[21], Hogan and Rees[22], and Sherman and Silk [23] have discussed Ly-$\alpha$ emission by hot intergalactic ionized hydrogen, redshifted into the optical band. They suggest that this might constitute a measurable, even dominant, extragalactic background towards the red. A clumpy structure, varying both spatially and in frequency is expected if the HII gas is inhomogeneous.

## 2. BASIC OBSERVATIONAL CONSIDERATIONS: THE COMPONENTS OF THE LIGHT OF THE NIGHT SKY (LONS)

Observations of the EBL are hampered by the much stronger foreground components of the LONS. Typical minimum values of these components in the blue spectral region are given in Table 1. Unlike the other components the EBL is isotropic which, in combination with its weakness, complicates its separation. For ground based observations one has the additional problem of irregular and relatively rapid time variations due to the airglow.

The situation in the optical is very different from the microwave band, where the extragalactic component (2.7 K) is roughly equal to the atmospheric component (~2.3 K) (Penzias and Wilson[24]) and the solar system and the galactic component off the Milky Way are negligible.

The basic approach when trying to measure the EBL is to use either 1) the differences in the spatial distributions or 2) the differences in the spectra of the different LONS components. Since both these methods have difficulties one should 3) try to eliminate or minimize as many of the unwanted foreground components as possible by a suitable selection of the observing site and of the observing technique. If *only an upper limit* is measured for the EBL it is still possible to discuss the combined EBL and DGL. However, for a *measurement* of the EBL these two components must be also separated.

In the following sections we discuss the different methods developed for the separation of the EBL, and the results obtained so far. We do not discuss the galaxy count method for which other lectures are devoted (Rocca-Volmerange; Gardner; Franceschini, these Proceedings).

Table 1. Components of the Light of the Night Sky at $\lambda$ = 4000 Å. Unit is $1 \cdot 10^{-9}$ erg cm$^{-2}$ s$^{-1}$ sterad$^{-1}$ Å which at 4000 Å corresponds to ~0.5 $S_{10}$

| | |
|---|---|
| Extragalactic background light (EBL) | 1-10 |
| Integrated galactic starlight (ISL) (b=90°, m>8$^m$) | 30 |
| Diffuse galactic light (DGL) (b=90°) | 0-10 |
| Zodiacal light (ZL) ($\beta$=90°) | 60 |
| Airglow (zenith) | 60 |
| Atmospheric scattered light (zenith) | 20 |
| Total | 171-190 |

## 3. EBL SEPARATION USING ITS DEPENDENCE UPON GALACTIC LATITUDE

The first attempt to measure the EBL intensity photometrically was by Roach and Smith[26]. The separation of the EBL was based on the assumption that its observed intensity at galactic latitude b, $I'_{EBL}$, decreases towards the galactic plane in accordance to the cosecant-law:

$$I'_{EBL}(b) = I_{EBL}\, e^{-\tau_0 \mathrm{cosec} b} \qquad (2)$$

where $\tau_0$ is the optical half-thickness of the galactic dust layer. However, the two galactic components, the integrated starlight and the diffuse galactic light show a dependence on b and, being much stronger components, completely overwhelm the EBL.

Roach and Smith[26] derived from their analysis of a large data base of zenith sky observations an upper limit of 5 $S_{10}$ to the EBL at $\lambda$ = 5 300 Å. This upper limit is, however, too stringent since the analysis did not account for the indirect EBL component which is scattered by the galactic dust layer in analogy to the diffuse galactic light. The scattered EBL component is strongest towards the galactic dust layer and decreases towards the poles. The radiation transfer problem to be solved here is a plane parallel disk of dust embedded in an isotropic incident radiation field. For the observationally determined albedo values for dust, a≈0.60 (e.g. Mattila[27]) about half of the extinction according to Eq. (2) is compensated for. Thus the Roach and Smith[26] upper limit is transformed to $I_{EBL} \leq 10\, S_{10}$. It appears that this method does not have much promise for an actual measurement of the EBL.

## 4. THE METHOD OF DUBE ET AL.

Dube, Wickes and Wilkinson[28] carried out a very thorough ground-based photometry of the night sky where each of the individual foreground components is dealt with in a different way. The experiment used a relatively large field of view (diameter 16'), containing typically several hundred stars brighter than $20^m$. However, the stars were blocked with specific *star masks,* placed in the focal plane of the telescope and prefabricated with the help of the Palomar Sky Survey plates for each one of the 11 selected high latitude fields in the range b = 46°-89°.

The zodiacal light was separated on the basis of its solar like spectrum. The depth of the strong MgI double at 5175 Å was measured using a combination of a narrow and broad filter. Finally the airglow and the tropospheric scattered light were measured by assuming that they are proportional to sec z. The measuring fields were tracked accross the sky over a wide range of sec z-values, and the temporal variations of the airglow were modeled with a polynomial. The residuals in this fitting procedure contributed most of the error in the final result. After each of the foreground components had been eliminated with an accuracy approaching 1 % the remaining sky brightness contained only the EBL and DGL. These values with their error bars are plotted in Fig. 1 as a function of galactic latitude. As can be seen the individual values have typically errors of ±5 $S_{10}$. As a mean value of all

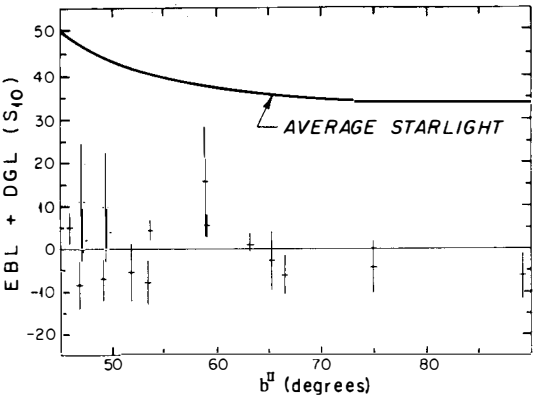


Fig. 1. Results of Dube et al.[28] for DGL+EBL versus galactic latitude. The continuous curve indicates the average starlight.

the data Dube et al. obtained 1.0±1.2 $S_{10}$. Because it was not possible to estimate the DGL contribution the result was interpreted as an upper limit on the EBL of 3.4 $S_{10}$ or $5.1 \cdot 10^{-9}$ erg cm$^{-2}$ s$^{-1}$ sterad$^{-1}$ Å$^{-1}$ at the 90 % confidence level.

A basic problem of this method is that it starts with the total brightness of the night-sky which is a factor of ~100 brighter than the EBL. Thus a very accurate elimination of the absolute amounts of the zodiacal light and airglow is required. Furthermore, the method does not differentiate between the EBL and DGL. The DGL which will also have a strong MgI absorption line in its spectrum is entangled in an unaccountable way with the zodiacal light.

The most critical point in the data analysis of Dube et al. was the way how they corrected for the airglow. After having subtracted zodiacal light and starlight, and having corrected for atmospheric extinction (in the same way as for stars), they found that the residual sky brightness was to a good approximation a linear function of sec z. Thus they assumed that a *linear* extrapolation to sec z=0 would give a value of the residual sky brightness, EBL + DGL, free of airglow. This assumption is, however, doubtful. We have reanalyzed the airglow problem as follows: (1) We have adopted an extraterrestrial airglow distribution as given by van Rhijn[59] for a height of 100 km. (2) We have made a correction for Rayleigh extinction, $e^{\tau_R}$, ($0^m.10$) and have added a term for Rayleigh scattering according to the tables of Ashburn[29]. This function is our prediction for the airglow intensity to be observed at the ground. (3) Following the recipe of Dube et al. we have then "corrected" these model airglow intensities for extinction by using the (full) atmospheric opacity (Rayleigh plus aerosol components). (4) The resulting function I(z) is in fact, to a good approximation, a linear function of sec z over the range from 1 to 2. (5) A linear extrapolation of this model airglow intensity does not, however, cross the sec z=0 axis at the zero point but at the negative side of it. (6) Using the values as given by Dube et al. for the average atmospheric extinction ($0^m.16$) and zenith airglow intensity (25 $S_{10}$) we find that the reduction method of Dube

et al. *overestimates* the airglow intensity by ~ 3 $S_{10}$. Thus their residual value for EBL + DGL should be increased by this amount, resulting in EBL + DGL = 4.2 ± 1.2 $S_{10}$, or an EBL upper limit of 6.4 $S_{10}$ at the 90 % confidence level.

## 5. MEASURING THE EBL BEYOND THE AIRGLOW AND THE ZODIACAL LIGHT

Observations from space platforms, which are imperative for UV and IR background radiation measurements, also have great advantages for measuring the optical background (Baum[30]). The ultimate method for EBL measurement would be provided by an experiment from beyond the zodiacal light cloud (Roach and Smith[26]).

An unprecedently favorable opportunity for the EBL measurement was offered by the Pioneer 10 spacecraft as it passed out of the asteroid belt, and the zodiacal light intensity dropped beyond 3 AU to vanishingly small values. The only remaining LONS components at this observing site were the integrated starlight (ISL), the DGL and the EBL. Because of the crude spatial resolution ($2^{o}$) of the Pioneer 10 photometer experiment, starlight unavoidably dominated the signal. Toller[31] analyzed the Pioneer 10 blue photometric data for 17 high galactic latitude areas using the Roach and Megill[32] and Sharov and Lipaeeva[33] star count data to subtract the ISL component. Toller estimated the DGL value in these high-latitude fields to 2.0±0.4 $S_{10}$ and derived an upper limit to the EBL of 3.9 $S_{10}(V)_{G2V}$ or 4.5 · $10^{-9}$ erg $cm^{-2}$ $s^{-1}$ $sterad^{-1}$ $Å^{-1}$ at the 2σ limit. Because of the relatively large uncertainties in both the Pioneer photometry (±4 $S_{10}$ or ±8%) and in the star count data (±15 %) an actual determination of the EBL appears not to be possible from these data. However, a larger optical telescope ($\phi \geq 50$ cm) sent above or beyond the zodiacal dust cloud has great promise for a clean measurement of the EBL and its spectrum. Equipped with an accurate photometer with ~2' field of view such a telescope could look *between* the stars down to ~$20^{m}$, rendering the starlight contribution negligible for the high galactic latitude areas. In fact, a photometer for zodiacal and other background light studies was included in the payload of the NASA spacecraft of the International Solar Polar Mission, which - like the recently launched Ulysses - was scheduled to fly outside the zodiacal dust layer. Unfortunately, this spacecraft was cancelled, however.

## 6. THE DARK CLOUD METHOD

*6.1 Description of the method.* We have been developing for several years a method for the measurement of the EBL which utilizes the screening effect of a dark nebula on the background light (Mattila[34,35]; Schnur[36]; Mattila and Schnur[37,38]). A differential measurement of the night-sky brightness in the direction of a high galactic latitude dark cloud and its surrounding area, which is (almost) free of obscuring dust, provides a signal which is due to two components only: (1) the extragalactic background light, and (2) the diffusely scattered starlight from interstellar dust.

All the large foreground components, i.e. the zodiacal light, the airglow, and the atmospheric

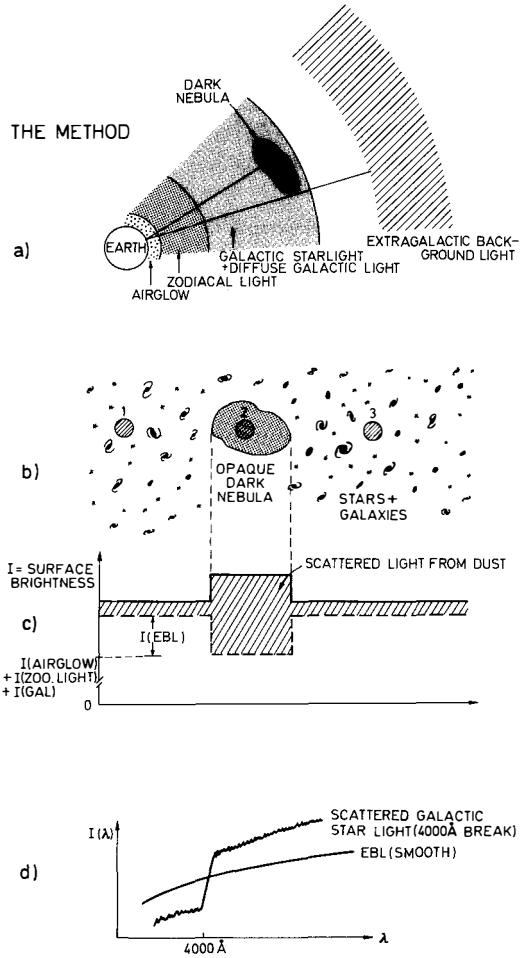


Fig. 2. (a) Principle of the dark cloud method for EBL measurement;
(b) Opaque dark nebula is shown in front of a high-galactic-latitude background of stars and galaxies. Measuring positions within the nebula (#2) and outside (# 1 and 3) are indicated;
(c) Schematic presentation of the surface brightness distribution across the dark nebula;
(d) the difference in spectral distributions of the galactic starlight and the EBL.

scattered light, are completely eliminated (see Fig. 2a). The direct starlight down to ~21st magnitude can be eliminated by selecting the measuring areas on a deep Schmidt plate. At high galactic latitudes ($|b| > 30^o$) the star density is sufficiently low to allow blank fields of ~2' diameter to be easily found. Galaxy models show that the contribution from unresolved stars beyond this limiting magnitude is of minor importance. If the scattered light from the interstellar dust were zero (i.e. the albedo of the interstellar grains a = 0), then the difference in surface brightness between a transparent comparison area and the dark nebula would be due to the EBL only, and an opaque nebula would be darker by the amount of the EBL intensity (dashed line in Fig. 2b-c).

Unfortunately, however, the scattered light is not zero. A dark nebula in the interstellar space is always exposed to the radiation field of the integrated galactic starlight, which gives rise to a diffuse scattered light (shaded area in Fig. 2c). Because the intensity of this scattered starlight in the dark nebula is expected to be equal or larger than the EBL, its separation will be the main problem in the present method.

The separation method utilizes the difference in the shape of the spectral energy distributions of the EBL and the galactic light around the wavelength $\lambda = 4000$ Å (see Fig. 2d). The spectrum of the integrated starlight can be synthesized by using the known spectra of stars representing the different spectral types, as well as data on the space density and distribution in the z-direction of stars and dust. Synthetic spectra of the integrated starlight have been calculated by Mattila[39,40]). The most remarkable feature in the spectrum is the abrupt drop of intensity shortward of $\lambda = 4000$ Å. The shape of the integrated starlight spectrum and especially the size of the 4000 Å discontinuity have been found to depend only weakly on the galactic latitude and the imagined z-distance of the observer, $z_o$.

It is possible to draw some conclusions about the spectrum of the EBL by using plausible theoretical arguments. Radiation from galaxies and other luminous matter over a vast range of distances, from $z = 0$ up to $z \approx 3$ at least, contribute to the EBL. Therefore, any sharp spectral features of the source spectrum, lines or discontinuities, are washed out. For the present study it is important to recognize that the discontinuity at 4000 Å, although present in all galaxy spectra, does not occur in the integrated background light.

Figure 3 illustrates how the spectral energy distribution of the observable surface brightness difference dark nebula minus surroundings changes for different assumed values of the EBL intensity.

*6.2 Results for different dark cloud areas.* The result of the first application of the above described method to the dark nebula L134 area ($l = 4^o$, $b = 36^o$) gave an unexpectedly high EBL intensity of $(23\pm8)\ 10^{-9}$ erg cm$^{-2}$ s$^{-1}$ sterad$^{-1}$ Å$^{-1}$ ($10\pm4\ S_{10}$) at 4000 Å (Mattila[34]). Later on, the same method was used again by Spinrad and Stone[47] at the same nebula; they obtained a 3 σ upper limit of $10\cdot10^{-9}$ erg cm$^{-2}$ s$^{-1}$ sterad$^{-1}$ Å$^{-1}$ (or 5 $S_{10}$). to the EBL at 4000 Å. Surprisingly, their measurements did not show any surface brightness excess in L134 although this excess is readily seen both on red and blue photographic plates obtained of the L134 area with the ESO 1-m Schmidt telescope. Boughn and Kuhn[44], again applying the dark cloud technique, observed a minimum excess surface brightness of 1.5 $10^{-9}$ erg cm$^{-2}$ sterad$^{-1}$ Å$^{-1}$ at 6500 Å in the L134 cloud centre.

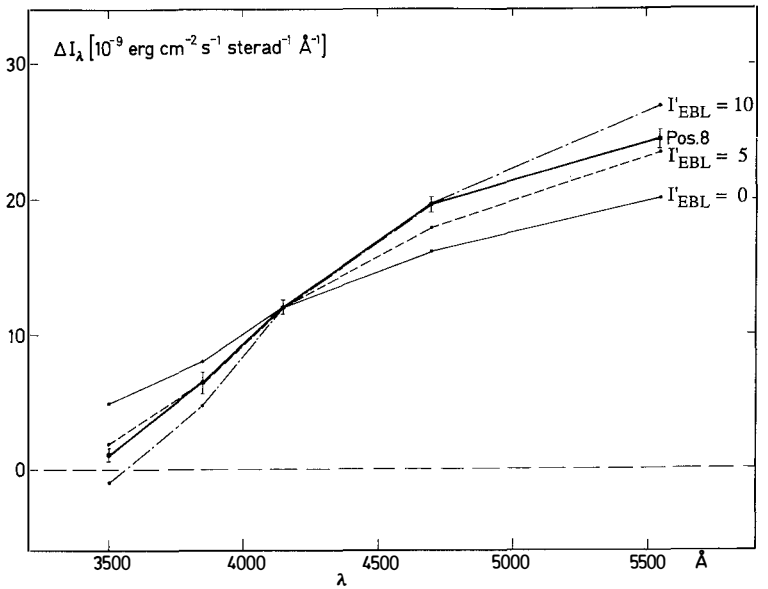


Fig. 3. The observed spectrum for Pos. 8 in L1642 (points with error bars) is compared with the pure scattered light spectrum ($I'_{EBL} = 0$) and two cases with corrections for an assumed EBL contribution, $I'_{EBL} = 5$ and $10 \times 10^{-9}$ erg cm$^{-2}$ s$^{-1}$ sterad$^{-1}$ Å$^{-1}$. The scattered light spectrum has been derived empirically from the observed L1642 spectra in the range $A_B = 1\text{-}2^m$. The spectra have been normalized to the observed value of Pos. 8 at 4150 Å. $I'_{EBL}$ is the fraction of EBL which the dark cloud is able to block along the line of sight. For Pos. 8 ($A_B \approx 4^m$) $I'_{EBL} \approx 0.9\, I_{EBL}$.

Their "clear" comparison areas were, however, quite close to the cloud and were probably contaminated by a considerable amount of dust. Thus a conclusive upper limit to the EBL was not obtained from this experiment.

We have continued the measurements of the EBL with the dark cloud technique in the area of the high-latitude dark nebula L1642 ($l = 210^o$, $b = -36^o.5$) in the galactic anticentre direction (Mattila and Schnur,see [35]). As compared to Mattila[34] the observing and data analysis methods have been considerably improved. The observations were carried out using the 1-m telescope of the European Southern Observatory. Five intermediate-band filters were used, centered at 3500 Å (u), 3850 Å, 4150 Å, 4700 Å (b) and 5550 Å (y). The field size was 88". Several positions were selected in transparent areas around the cloud for fixing the background level. Both starcount data and far infrared (IRAS) surface brightness maps of the L1642 area (see Laureijs, Mattila and Schnur[48]) were used to select transparent areas. In addition, uvbyβ-photometry of several A-F type stars in these areas has been performed by Franco[49], and his results prove that the extinction in our comparison areas is indeed very small, $A_V < 0^m.05$.

The photoelectric surface photometry of weak extended objects is hampered by the time

variability of the airglow. One has to repeat normally in single beam photometry the ON and OFF source measurements after each other. We have used in our observations a method in which the airglow fluctuations are eliminated by means of strictly simultaneous parallel observations with the ESO 50-cm telescope (see Schnur and Mattila[50]). The best chance of detecting the EBL is to look at the positions which have (a) the largest optical depth through the cloud and (b) the lowest surface brightness. In practice these two conditions are fullfilled for the same positions. In our observations of L1642 the Position No. 8 was identified to best fullfill these both conditions. An EBL contribution for Pos. No. 8 is suggested (see Fig. 3). At this position the surface brightness of the cloud at 3500 Å is only marginally higher than the clear background, i.e. $\Delta I = 1.1 \pm 0.5\ 10^{-9}$ erg $cm^{-2}\ s^{-1}$ $sterad^{-1}$ $Å^{-1}$, whereas the surface brightness of the cloud at the longer wavelengths, ( $\lambda$ = 3850, 4150, 4700 and 5550 Å) is clearly in excess above the background. This situation can arise only in one of the following two ways: (1) the albedo of the dust decreases strongly towards shorter wavelengths and drops to nearly zero at 3500 Å, or

(2) There is a background light component, emanating from behind the cloud, of the same order of magnitude as the scattered light surface brightness of the cloud. The first possibility is ruled out by the fact that at other, less opaque, positions in the same cloud the surface brightness at 3500 Å is significantly different from zero, and is about one half of the values obtained at $\lambda \geq 4000$ Å. It is not to be expected that the albedo specifically at 3500 Å would drop strongly towards opaque areas.

As shown by the model curves in Fig. 3, an EBL value of ~6 units can best fit the observations. A more quantitative analysis is presented in [35]. It gives

$I_{EBL} = 6.5 \pm 2.5\ 10^{-9}$ erg $cm^{-2}\ s^{-1}$ $sterad^{-1}$ $Å^{-1}$

as the result of the present observations. This value corresponds to $3 \pm 1\ S_{10}$(A0V) at 4000 Å. We would like to emphasize that this is still a preliminary value and refer to Mattila and Schnur (in preparation) for the final results.

## 7. THE EBL IN THE NEAR-INFRARED

Basically the same methods as discussed above for the optical band, can be used also in the near-infrared for the separation of the EBL. About 25 years ago, pioneering rocket experiments, carried out by the group at Cornell University, resulted in the first measurements of the extraterrestrial near-infrared surface brightness of the night sky and hence to upper limits for the near-infrared EBL. These limits of 5x10-6 $Wm^{-2}\ sr^{-1}\ \mu m^{-1}$ in the range 1-3 μm (Harwit et al.[51]) and 3x10-8 $Wm^{-2}\ sr^{-1}\ \mu m^{-1}$ at 5-6 μm (Soifer et al.[52]) were subsequently reduced by a balloon experiment to 5x10-7 $Wm^{-2}\ sr^{-1}\ \mu m^{-1}$ at 2.2 μm (Hofmann and Lemke[53]) and finally by the all-sky observations of the Cosmic Background Explorer COBE (Hauser et al.[54]) to the now best available limits of $7 \pm 3 \times 10^{-7}$ $Wm^{-2}\ sr^{-1}\ \mu m^{-1}$ at 1.2 μm, $1.5 \pm 0.6 \times 10^{-7}$ $Wm^{-2}\ sr^{-1}\ \mu m^{-1}$ at 2.3 μm, $4.4 \pm 1.8 \times 10^{-8}$ $Wm^{-2}\ sr^{-1}\ \mu m^{-1}$ at 3.4 μm and $7.6 \pm 3.1 \times 10^{-8}$ $Wm^{-2}\ sr^{-1}\ \mu m^{-1}$ at 4.9 μm.

Limits to the near-infrared EBL have also been derived from ground-based observations. Boughn and Kuhn[44], using the dark cloud method at 2.2 μm for the molecular cloud L134 derived an upper limit of $5 \times 10^{-8}$ $Wm^{-2}\ sr^{-1}\ \mu m^{-1}$. This, however, was not a strict upper limit but depended

on assumptions on the optical thickness of the cloud and the amount of galactic light scattered in it. On the other hand, Cowie et al.[55], from galaxy counts based on deep K imaging of selected fields, derived a lower limit to the near-infrared EBL of 1.7 x $10^{-9}$ $Wm^{-2}$ $sr^{-1}$ $\mu m^{-1}$. This leaves a range of roughly by factor of 50 between the lower and upper limit at 2.2 μm.

Experimentally, the main difficulty in measuring the near-infrared EBL consists in subracting the contribution of zodiacal light. Even around 3-4 μm, where the combined brightness of zodiacal light scattering and thermal emission is at its minimum, it still amounts to about $4x10^{-8}$ $Wm^{-2}sr^{-1}\mu m^{-1}$ (Hauser et al.[54]), which is about an order of magnitude higher than current model predictions for the EBL (Yoshii and Takahara[11], Franceschini et al.[56]).

Possible measurements of an isotropic extragalactic component in the near-infrared have been reported from a photometric rocket experiment at 2.2 μm and 3.5 μm (Matsumoto et al.[45]) and from 1-3 μm spectrophotometry, again during a rocket flight (Noda et al.[57]). However, the spatial and spectral coverage were not extended enough to allow an unambiguous determination of the contribution of zodiacal light. The reported measurements therefore should be considered as upper limits to the EBL brightness in the near-infrared; they are close, although somewhat lower, to the limits given by the sky brightness at the south ecliptic pole as observed by COBE[54].

Ideally, an experiment to measure the near-infrared EBL should have extended spatial coverage, covering the sky from the ecliptic to the ecliptic poles, at least one year of observing time to determine the efffects of the earth's orbital motion, a wide spectral range including the mid-infrared, where zodiacal light exclusively dominates the night sky emission, and measurements in the range around 1μm, where scattering of solar radiation is important - all this, in order to be able to derive a reliable model of the zodiacal light contribution. The COBE experiment so far has been the only one to fulfill these conditions and soon should be able to give a much improved upper limit or measurement of the near-infrared EBL. In addition, an ideal experiment should have a small ($< 0.10^{o}$) field of view in order to reduce the stellar contribution and the contribution by bright interstellar cirrus emission to insignificant amounts. These latter components may limit the accuracy achievable with the comparatively large field of view ($0.7^{o}x0.7^{o}$) of the COBE experiment. The photometric experiment on satellite ISO (see Leinert et al., this volume), with its much smaller field of view of $0.05^{o}$, should give an important improvement in this respect. The prospects that a real measurement of the near-infrared EBL will be obtained during the next few years are still difficult to appraise, but they are better than they have been ever before.

## 8. DISCUSSION

*8.1 Comparison of the EBL measurements.* A compilation of the different EBL determinations is presented in Table 2. The present result for the EBL intensity is significantly smaller than the previous value of Mattila[34], i.e. $I_{EBL} = 23\pm8$ $10^{-9}$ erg $cm^{-2}$ $s^{-1}$ $sterad^{-1}$ $Å^{-1}$, which was obtained for the direction of L134 ($l=4^{o}.0$, $b=35^{o}.9$). We think that most of the discrepancy is due to the much larger observational errors inherent in the 1976 values which were based on a single-telescope observing technique. A part of the discrepancy may be due to a real difference of the background light intensities in these two directions: any galactic contribution would be stronger in the center

direction (L134) as compared to the anticenter direction (L1642) because of the longer line of sight through the galactic halo. However, the galactic contamination of the present EBL results is expected to be minimal. In any case a repetition of the EBL measurement in the L134 area is of great interest and observations have already been started at La Silla (Mattila and Schnur) and at Calar Alto (Mattila and Leinert). Comparing the upper limits of Dube et al.[28] and Toller[31] with our present EBL measurement we conclude that there is no obvious discrepancy. Our measured value is close to these upper limits.

Recent galaxy counts by Tyson[41,42], extending to $m_J \approx 27^m$, have provided an estimate of the EBL due to galaxies: $I_{EBL} = 0.7\ 10^{-9}$ erg cm$^{-2}$ s$^{-1}$ sterad$^{-1}$ Å$^{-1}$. This value depends, however, crucially on the slope of the log N(m) curve which is used for extrapolation beyond the magnitude limit. According to Tyson, 75 % of this EBL value, i.e. $I_{EBL} = 0.5\ 10^{-9}$ erg cm$^{-2}$ s$^{-1}$ sterad$^{-1}$ Å$^{-1}$ is due to galaxies fainter than $m_J = 20^m$ (which is comparable to the magnitude limit in our measurement areas). Thus, according to Tyson's result only a small fraction of our present observed EBL intensity can be explained in terms of integrated light of galaxies.

Table 2. Compilation of results for the optical EBL intensity. The unit is $1{\cdot}10^{-9}$ erg cm$^{-2}$ s$^{-1}$ sterad$^{-1}$ Å$^{-1}$

| Authors | Year | $I_{EBL}$ | λ(Å) | Site | Method |
|---|---|---|---|---|---|
| Roach and Smith | 1968 | <6 | 5300 | ground | b-dependence |
| Lillie | 1968 | <5 | 4100 | rocket | subtraction of foreground components |
| Mattila | 1976 | 23±8 | 4000 | ground | dark cloud L134 |
| Spinrad and Stone | 1978 | <10 | 4000 | ground | dark cloud L134 |
| Dube et al. | 1977,1979 | <5.1 | 5115 | ground | subtraction of foreground components |
| Toller | 1983 | <4.5 | 4400 | R>3AU | subtraction of starlight |
| Boughn and Kuhn | 1986 | (<1.5)* | 6500 | ground | dark cloud L134 |
| Mattila and Schnur | 1989 | 6.5±2.5 | 3500<br>4000 | ground | dark cloud L1642 |
| Tyson | 1988 | 0.68+0.03<br>-0.01 | 4500 | ground | galaxy counts |

* Minimum surface brightness of the nebula (see text)

*8.2 Light from the galactic halo?* Part of the background light observed in any of the EBL experiments might actually originate within our Galaxy. Because of the differential observing method used in the dark cloud method, only light originating from behind the dark nebula, i.e. essentially in the galactic halo, can contribute to the measured EBL.

First, it is noted that if the unresolved starlight has the same spectral distribution around 4000 Å as the total starlight, it is eliminated when calculating the extragalactic light. For a much smaller discontinuity value, which is known to be valid for the metal-deficient halo stars, the unresolved starlight would not be eliminated. Using the galaxy model of Bahcall and Soneira[43] we find for l = 180°, b = 30° the ISL contribution $I_*(m_B \geq 20^m) = 0.16\ S_{10}$ corresponding to 0.4 $10^{-9}$ erg cm$^{-2}$ s$^{-1}$ sterad$^{-1}$ Å$^{-1}$. Only the small fraction of this total ISL which is due to metal-deficient stars having a flat spectrum in the 3500-4000 Å range is not eliminated by our separation technique. Thus the ISL

cannot be responsible for more than a negligible fraction of the observed EBL intensity.

As a crucial observational test to exclude the galactic contribution we emphasize the importance to observe the EBL in several directions with different path lengths through the galactic halo.

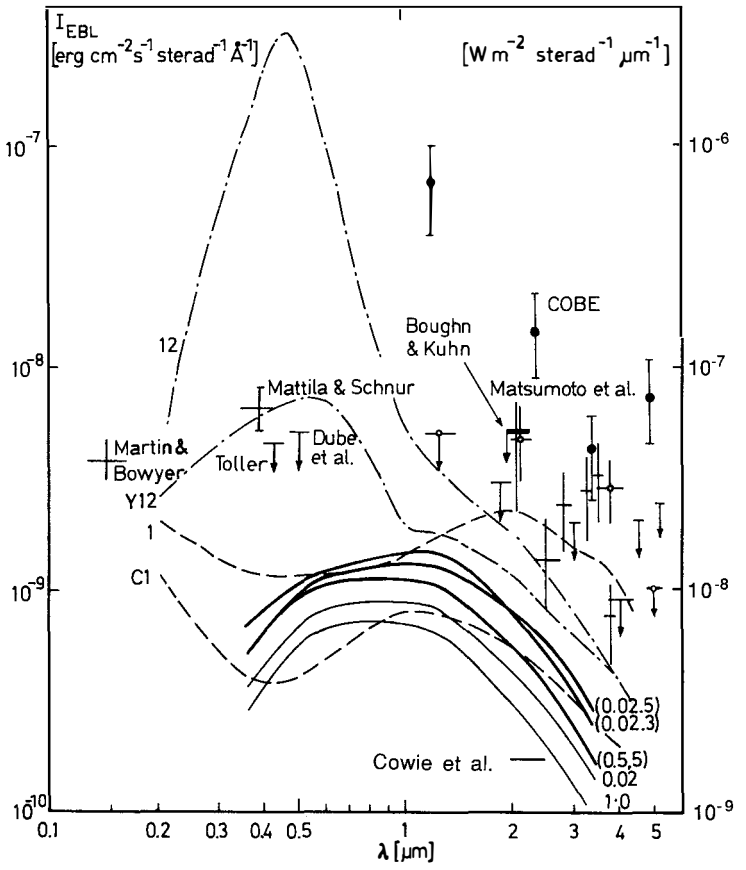


Fig. 4. Calculated spectral energy distributions of the integrated light of galaxies. The continuous curves are models from Yoshii and Takahara[11], the dashed curves are from Tinsley[7] (see text for details). Recent observational values and upper limits are indicated.

*8.3 Comparison with theoretical predictions.* We compare in Fig. 4 the observational EBL results with a number of theoretical predictions for the background light due to galaxies. The observational values are according to Table 2 with the addition of the near-IR results of Boughn and Kuhn[44] and Matsumoto et al.[45]. From the wealth of UV data points (see Bowyer[46]) we show only the recent result of Martin and Bowyer[20] at 1500 Å.

As an example of model predictions the continuous lines show the recent EBL calculations in the wavelength range 0.36-3.4 μm by Yoshii and Takahara[11]. The thick and thin lines represent the models with and without galaxy evolution, respectively. The curves are labeled by the value of the deceleration parameter $q_0$ (ranging from 0.02 to 1.0) and, for the evolutionary models, with $z_F$ (3 or 5), the redshift at which the galaxies formed. The total range of EBL intensities of Yoshii and Takahara is within a factor of ~2.

The dashed and dash-dotted lines in Fig. 4 show some of the cases previously calculated by Tinsley[7]. All four curves are for $q_0 = 0.02$. The curves labeled C1 and 1 assume distant galaxy formation epochs ($z_F = 35$ and 20 for ellipticals and spirals, respectively). Curve C1 is for no galaxy evolution whereas the other curves assume evolution. It is seen that curves C1 and 1 agree relatively well with the Yoshii and Takahara results. All these curves are an order of magnitude lower than the observational values or upper limits in the optical. Tinsley's models 12 and Y12 are for recent galaxy formation ($z_F = 3$) and they predict a much brighter EBL, with a maximum in the optical band. In these cases the strong UV radiation of young galaxies at $\lambda \approx 1000$ Å is shifted to $(1+z_F)\,\lambda \approx 4000$ Å. Case 12 which assumes a strong UV brightning in the past, can clearly be excluded. Case Y12 on the other hand is still compatible with the observational results. In this model the spectrum at $\lambda <$ 0.33 μm remains constant. In conclusion, nonevolving galaxy models cannot account for the observed level of EBL but models with evolution seem capable of producing enough background light if the circumstances are favorable for putting much of the radiated energy into the optical band at present.

## REFERENCES


[1] Halley,E.: 1721, Philosophical Transactions **31**, 22 and **31**, 24
[2] Loys de Chéseaux,J.-P.: 1744, Traité de la comète qui apparut en décembre 1743, Lausanne, p. 223
[3] Olbers,H.W.M.: 1823, Astronomisches Jahrbuch 1826 (hrsg. von J.E. Bode), p. 110
[4] Harrison,E.: 1987, Darkness at Night, (Cambridge and London: Harvard Univ. Press.)
[5] Harrison,E.: 1990, in IAU Symposium No. 139, eds. S. Bowyer and Ch. Leinert (Kluwer, Dordrecht), p. 3
[6] Partridge,R.B., Peebles,P.J.E.: 1967, Astrophys. J. **148**, 377
[7] Tinsley,B.M.: 1973, Astron. Astrophys. **24**, 89
[8] McVittie,G.C., Wyatt,S.P.: 1959, Astrophys. J. **130**, 1
[9] Whitrow,G.J., Yallop,B.D.: 1963, Monthly Notices Roy. Astron. Soc. **127**, 301
[10] Sandage,A., Tammann,G.A.: 1965, Ann. Rep. Mt. Wilson and Palomar Obs. 1964-1965, p. 35
[11] Yoshii,Y., Takahara,F.: 1988, Astrophys. J. **326**, 1
[12] Stabell,R., Wesson,P.S.: 1980, Astrophys. J. **242**, 443
[13] Wesson,P.S., Valle,K., Stabell,R.: 1987, Astrophys. J. **317**, 601

[14] Harrison,E.: 1964, Nature **204**, 271
[15] Shectman,S.A.: 1973, Astrophys. J. **179**, 681
[16] Kiang,T.: 1961, Monthly Notices Roy. Astron. Soc. **122**, 263
[17] Peebles,P.J.E.: 1971, Physical Cosmology, ( Princeton: Princeton Univ. Press.), pp. 59-63
[18] Arp,H.: 1965, Astrophys. J. **142**, 402
[19] Shectman,S.A.: 1974, Astrophys. J. **188**, 233
[20] Martin,C., Bowyer,S.: 1989, Astrophys. J. **338**, 677
[21] Weyman,R.: 1967, Astrophys. J. **147**, 887
[22] Hogan,C.J., Rees,M.J.: 1979, Mon. Not. R. Astr. Soc. **188**, 791
[23] Sherman,R.D., Silk,J.: 1979, Astrophys. J. **231**, L61
[24] Penzias,A., Wilson,R.: 1965, Astrophys. J. **142**, 419
[25] Guiderdoni,B., Rocca-Volmerange,B.: 1990, in IAU Symp. No. 139, eds. S. Bowyer and Ch. Leinert (Kluwer, Dordrecht), p. 365
[26] Roach,F.E., Smith,L.L.: 1968, Geophys. J. **15**, 227
[27] Mattila,K.: 1970, Astron. Astrophys. **9**, 53
[28] Dube,R.R., Wickes,W.C., Wilkinson,D.T.: 1977, Astrophys. J. **215**, L51; 1979, Astrophys. J. **232**, 333
[29] Ashburn,E.V.: 1954, J. Atmosph. Terr. Physics **5**, 83
[30] Baum,W.A.: 1956, Publ. Astron. Soc. Pacific **68**, 118
[31] Toller,G.N.: 1983, Astrophys. J. **266**, L79
[32] Roach,F.E., Megill,L.R.: 1961, Astrophys. J. **133**, 228
[33] Sharov,A.S., Lipaeva,N.A.: 1973, Soviet Astron. **17**, 69
[34] Mattila,K.: 1976, Astron. Astrophys. **47**, 77 (Paper I)
[35] Mattila,K.: 1990, in IAU Symp. No. 139, eds. S. Bowyer and Ch. Leinert, (Kluwer, Dordrecht), p. 257
[36] Schnur,G.F.O.: 1980, in ESO Workshop on Two Dimensional Photometry, Eds. P. Crane and K. Kjär, p. 365
[37] Mattila,K., Schnur,G.F.O.: 1983, Mitt. d. Astron. Gesellsch. **60**, 387
[38] Mattila,K., Schnur,G.F.O.: 1988, ESO Messenger No. 51, 34
[39] Mattila,K.: 1980a, Astron. Astrophys. Suppl. **39**, 53
[40] Mattila,K.: 1980b, Astron. Astrophys. **82**, 373
[41] Tyson,J.A.: 1988, Astron. J. **96**, 1
[42] Tyson,J.A.: 1990, in IAU Symposium No. 139 , eds. S. Bowyer and Ch. Leinert, (Kluwer, Dordrecht), p. 245
[43] Bahcall,J.N., Soneira,R.M.: 1980, Astrophys. J. Suppl. **44**, 73
[44] Boughn,S.P., Kuhn,J.R.: 1986, Astrophys. J. **309**, 33
[45] Matsumoto,T., Akiba,M., Murakami,H.: 1988, Astrophys. J. **332**, 575
[46] Bowyer,S.: 1990, in IAU Symposium No. 139 , eds. S. Bowyer and Ch. Leinert, (Kluwer, Dordrecht), p. 171
[47] Spinrad,H., Stone,R.P.S.: 1978, Astrophys. J. **226**, 609
[48] Laureijs,R., Mattila,K. Schnur,G.F.O.: 1987, Astron. Astrophys. **181**, 269
[49] Franco,G.: 1989, Astron. Astrophys. (in press)
[50] Schnur,G.F.O., Mattila,K.: 1989, in IAU Symposium No. 139 , eds. S. Bowyer and Ch. Leinert, (Kluwer, Dordrecht), p. 461
[51] Harwit,M., McNutt,D.P., Shivanandan,K., Zajac,B.I.: 1966, Astron. J. **71**, 1026
[52] Soifer,B.T., Houck,I.R., Harwit,M.: 1971, Astrophys. J. **168**, L73
[53] Hofmann,W., Lemke,D.: 1978, Astron. Astrophys. **68**, 389
[54] Hauser,M.G., Kelsall,T., Moseby,Jr.,S.H., Silverberg,R.F., Murdock,T., Toller,G.,Spiesman,W., Weilord,J.: 1991, to be published in the proceedings of "After the First Three Minutes" Workshop (College Park, Oct. 1990)
[55] Cowie,L.L., Gardner,I.P., Lilly,S.I., McLean,I.: 1990, Astrophys. J. **360**, L1
[56] Franceschini,A., Toffolaki,L., Mazzei,P., Danese,L., DeZotti,G.: 1991, Astron. Astrophys. (in press)
[57] Noda,M., Christov,V.V., Matsuhara,H., Matsumoto,T., Matsuara,S., Nogerchi,K., Sato,S., Musakami,H.: 1991, preprint
[58] Ellis,R.S.: 1983, in The Origin and Evolution of Galaxies, ed. B.J.T. Jones and J.E. Jones (Dordrecht: D. Reidel), p. 255
[59] Van Rhijn,P.J.: 1921, Publ. Astron. Lab. Groningen **31**, 1

# OBSERVATIONS OF THE INFRARED EXTRAGALACTIC BACKGROUND LIGHT WITH ISOPHOT

Ch. Leinert [1], K. Mattila [2], D. Lemke [1]

[1] Max-Planck-Institut für Astronomie, Heidelberg, F.R.G.
[2] Helsinki Observatory, Helsinki, Finland

**Extended abstract**

So far there exists no convincing measurement of the infrared extragalactic background light. In the near infrared, the results of Matsumoto et al.[3] and Noda et al.[5] suffer from the limited spatial and spectral coverage and the resulting uncertainty in the separation of the components. In the far infrared, the values obtained by the Nagoya-Berkeley experiment[4] are in doubt, because the sub-mm excess found by the same experiment was not confirmed by the COBE satellite. COBE[1] is expected soon to give more reliable results, but because of its comparatively large field of view (0.7° x 0.7°) the subtraction of the stellar component (in the near infrared) and the interstellar cirrus emission (in the far infrared) may limit the achievable accuracy.

Figure 1 stresses the importance of the separation of components for the measurement of the infrared extragalactic background light. The most important ones are zodiacal light

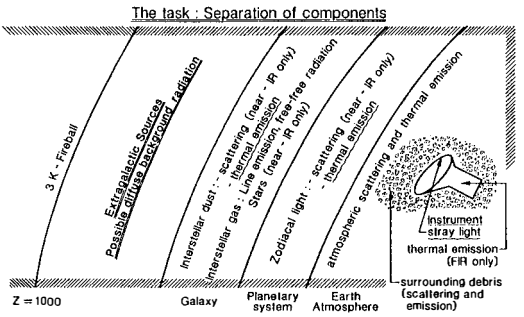


Fig. 1: Components contributing to a measurement of infrared sky brightness. Note that the extragalactic background light can only be evaluated after careful avoidance or subtraction of a number of contributing sources of brightness.

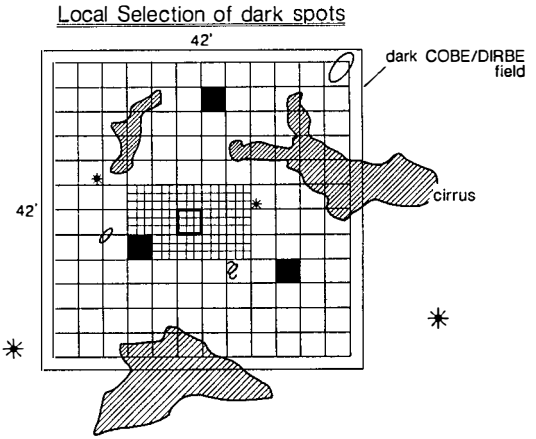


Fig. 2: Method envisaged to find the darkest spots on the sky for a measurement of the infrared extragalactic background light. Shown is a COBE field (42' x 42'), already selected for minimum sky brightness. This field will be mapped with a field-of-view of 3' x 3' (small squares) in a wavelength sensitive to "cirrus" emission of interstellar dust. Thus bright cirrus (shown as patches) can be avoided as well as bright stars or galaxies. The darkest ones (shown in black) will be selected for the attempted measurement of the infrared extragalactic background light. In addition, measurements of higher angular resolution (1' x 1', corresponding to the pixel size of the C100 camera) in the center of the field aim at detecting faint galaxies and fluctuations of the background radiation.

and stellar contribution in the near infrared, zodiacal light and thermal emission of interstellar dust ("cirrus") in the far infrared. The experiment to be performed with ISOPHOT has the following strong points:

- the field-of-view of 0.05° diameter together with the high sensitivity of a cooled telescope allows us to exclude all stars brighter than K = 15 and to avoid the contribution of bright cirrus, and thus it allows us to find the darkest points in the sky.
- the availability of 20 filter bands from 3-200 $\mu$m and the extended spatial coverage from the ecliptic to the ecliptic poles, and the availability of the COBE all-sky maps will help to create a trustworthy model of the zodiacal light and allow us to separate the zodiacal light contribution from the data with good accuracy.
- the extended spectral coverage allows us to estimate the contribution of interstellar cirrus emission to the zodiacal-light subtracted signal.

The residual - if significantly larger than zero - would be a measure of the infrared extragalactic background.

For a more detailed description of the ISOPHOT experiment and its capabilities to detect the infrared extragalactic background radiation see the report by Lemke et al.[2].

References

[1] M.G. Hauser, T. Kelsall, S.H. Moseley, Jr., R.F. Silverberg, T . Murdock, G. Toller, W. Spiesman, J. Weiland: The diffuse infrared background - COBE and other observations. COBE preprint No. 90-06. To be published in the proceedings of "After the First Three Minutes", in press 1991.

[2] D. Lemke, Ch. Leinert, K. Mattila: The capabilities of ISOPHOT to detect the infrared extragalactic background radiation. Adv. Space Res. Vol. 11, No. 2, p. 223, 1991

[3] T. Matsumoto, M. Akiba, H. Murakami: A search for the near-infrared background light. Astrophys. J. 332, 575, 1988.

[4] T. Matsumoto: Infrared extragalactic background light. In: The galactic and extragalactic background radiation, eds. St. Bowyer and Ch. Leinert, Kluwer 1990, p. 317

[5] M. Noda, V.V. Christov, H. Matsuhara, T. Matsumoto, S. Matsuura, K. Noguchi, S. Sato, H. Murakami: Rocket observation of the near-infrared spectrum of the sky. Preprint 1991.

# FAINT GALAXY COUNTS

# REDSHIFT CONSTRAINTS AND CLUSTERING OF FAINT GALAXIES

Puragra Guhathakurta
Institute for Advanced Study, Princeton, NJ 08540, USA.

ABSTRACT: Deep CCD images of the sky reveal a high surface density of faint, predominantly blue galaxies down to $B_J \sim 27$ that may be at high redshifts, $z \gtrsim 1$. Since our knowledge of these faint objects is quite limited, and not many of the ones fainter than $B_J = 23$ have known redshifts, their true nature has proved elusive. In this paper, we describe two model-independent redshift constraints on these faint galaxies. The first is an upper redshift limit $z < 3$ that is implied by the lack of any Lyman break candidates in our deep $UB_JR$ data. The second is a (rough) lower limit on the median redshift that follows from the fact that a large fraction of faint blue galaxies are gravitationally lensed by foreground galaxy clusters at $z \sim 0.5$. We have also examined the two-point angular correlation function of faint galaxies ($B_J = 24$-$26$), comparing it to that expected for progenitors of $L^*$ galaxies under various assumptions about redshift distribution, clustering evolution, and cosmology. The faint galaxies are found to be surprisingly weakly clustered. There are several possible explanations of this result: (a) the majority of the faint blue galaxies belong to a class of objects that is weakly clustered and intrinsically faint at the present epoch; (b) galaxy clustering evolves much more rapidly than expected in gravitational instability theories; or (c) the geometry of the Universe differs significantly from the Einstein-de Sitter model. If the first of the above explanations is correct (and this is the most likely one, in our opinion), it will be very difficult to learn about the geometry of spacetime from faint galaxy counts in the optical.

## I. Introduction

The nature of new-born galaxies and the epoch at which most galaxies were formed have been the focus of a lot of attention over the last few years[1]. Much effort has been invested in searches for high-redshift primaeval galaxies[2]. Although a few powerful radio galaxies have been found at redshifts $z \gtrsim 2$[3] and quasars are known to exist out to $z \lesssim 5$[4], their comoving space density is many orders of magnitude smaller than that of normal bright galaxies at the present day. QSOs and radio galaxies are thus very special objects and may bear little relation to the average galaxy at high redshift.

Since the discovery of faint field galaxies in optical photographic surveys about a decade ago[5], and with deep CCD imaging revealing fainter (and far more numerous) blue galaxies down to $B_J \sim 27$[6,7], the possibility that these objects may be ordinary galaxies at an early stage of evolution has excited much interest. For the bulk of the faint blue galaxies ($B_J$ = 24-27), the observed properties are limited to their projected number density, broad-band colours, and rough angular sizes and shapes. Galaxy evolution models are therefore underconstrained. It is possible that the faint population, instead of being related to today's typical $L^*$ galaxy (as is implicitly assumed in standard evolutionary models), represents an entirely new class of objects. A hint of the latter follows from the high space density implied by the faint counts which exceeds the space density expected of normal luminous galaxies[8,9].

Most of the discussion in this paper will be limited to faint galaxies in the range $24 \lesssim B_J \lesssim 27$, a range over which evolutionary effects are quite strong. No spectroscopic redshift data exist for galaxies this faint. In §II, we have tried to place broad redshift limits using indirect methods. Most of the galaxies must be between $0.7 \lesssim z < 3$, as implied by arguments about the Lyman break (upper limit) and gravitational lensing (lower limit). As a further test of the nature of the faint galaxies, their clustering properties have been studied[10]. The measurement of the angular correlation function is described in §III, while §IV calculates the clustering amplitude expected for normal luminous galaxies. The last section (§V) discusses the nature of faint blue galaxies, particularly the implications of their weak clustering amplitude.

## II. Redshift Constraints

Since all but the hottest O stars have a large drop in flux at 912 Å, and it takes only $10^{17}$ atoms $cm^{-2}$ of neutral gas to reach unit optical depth, galaxies are expected to have a Lyman break of at least a factor of 2-5[11]. At $z = 3$, the break would redshift past 3600 Å causing $U - B_J$ to go very red. Faint galaxies, on the other hand, typically have spectra that are almost flat across $UB_JR$. This implies that most, if not all, of them ($> 93\%$) are at $z < 3$[12]. Figure 1 shows no obvious Lyman break candidates (these would be to the upper left in the plot). The redshift limit cannot be circumvented even if the faint galaxies have small *intrinsic* Lyman breaks. Spectra of quasars at $z > 3$ show

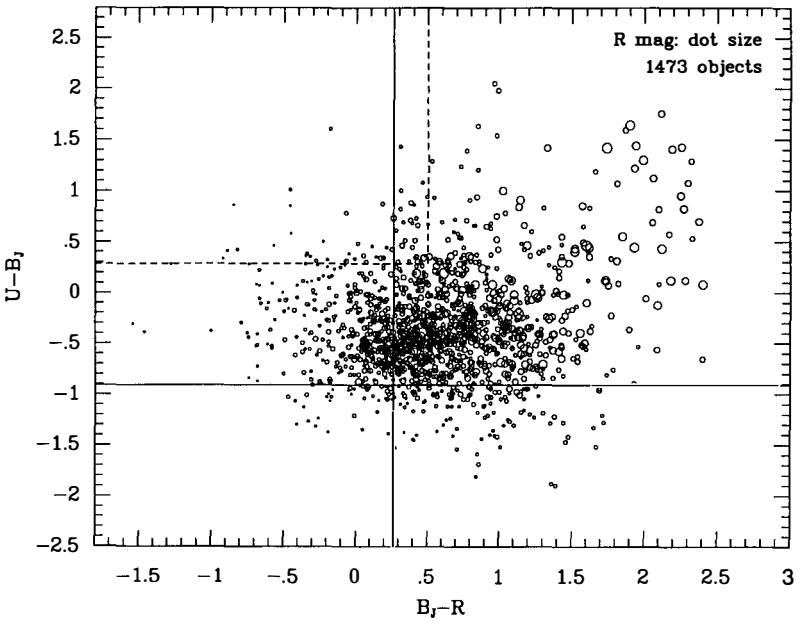


**Figure 1:** A $U - B_J$ vs. $B_J - R$ colour-colour plot for about 1500 galaxies with $B_J < 28$ in three fields covering 27 arcmin$^2$. Bigger dots represent brighter galaxies. The solid cross at $B_J - R = 0.26, U - B_J = -0.91$ represents flat spectrum colours. The absence of any significant population of galaxies with blue $B_J - R$ ($< 0.5$) *and* red $U - B_J$ (a Lyman break greater than a factor of 3) or of $U$ non-detections rules out any fraction $> 7\%$ of galaxies that could be at $z \gtrsim 3$. Such objects would occupy the top-left section of the plot enclosed by the dashed lines.

that there is a high probability of encountering an intervening Lyman-limit system at $z \sim 3$[13], and this would result in a non-detection in $U$.

A somewhat looser lower bound can be placed on the average redshift of faint galaxies from the fact that a large fraction appear distorted by the gravitational lensing effects of foreground galaxy clusters. The most extreme examples of these are the occasional giant luminous arcs seen in clusters[14]. A much more common phenomenon is to find background galaxies in the range $B_J = 24$-$27$ stretched by the shear of the lens into tiny arclets centered on the cluster[15]. For lensing to occur, the distorted faint galaxies have to be about twice as distant as the cluster (unless the cluster is unreasonably massive). The best lower limit on the median redshift of these faint galaxies comes from the 3C295 cluster (CL1409) at $z = 0.46$. An analysis of the distribution of shapes and orientations of the field galaxies seen in the direction of this cluster suggest that about half of them are at $z \gtrsim 0.7$[16]. Further, spectroscopy of five bright arcs in clusters yields redshifts between 0.72 and 2.2 and these have unmagnified magnitudes of $B_J \sim 25$[14,17].

### III. Observed Angular Correlation Amplitude

We estimate the angular two-point galaxy autocorrelation function, $w(\theta)$, using deep CCD images of high-latitude regions of the sky free of nearby galaxy clusters. The data used include: [1] 12 CCD fields surveyed in $B_J$, $R$, and $I$ by Tyson and Seitzer[18] (hereafter TS12), each field about 9 arcmin$^2$; [2] comparably deep $U$ data on three of the TS12 fields[12]; and [3] a deep (5100 s total exposure), large-format (49 arcmin$^2$), KPNO 4-metre CCD $B_J$ image of the SA68 field. The *FOCAS* software[19,20] is used to detect, photometer, and measure the positions of objects in each CCD image.

We use all galaxies with isophotal magnitude $24 < B_J < 26$ to compute $w(\theta)$. Within this range, the *FOCAS* detection list is reliable and is nearly complete for objects with surface brightnesses above our detection threshold of 29 $B_J$ mag arcsec$^{-2}$. The correlation functions derived for the TS12 fields are combined to compute a mean $w(\theta)$ and field-to-field rms deviation (Figure 2a). The correlation functions for SA68 are plotted in Figure 2b. For this field, the direct $w(\theta)$ estimates (filled circles) show a linear trend with $\theta$, going negative at $\theta \gtrsim 30''$. This behaviour suggests a weak, large-scale gradient

in the galaxy density across the field. The "ensemble-average" $w(\theta)$ estimates for this field (open circles) are close to zero at large scales and are likely to be more reliable.

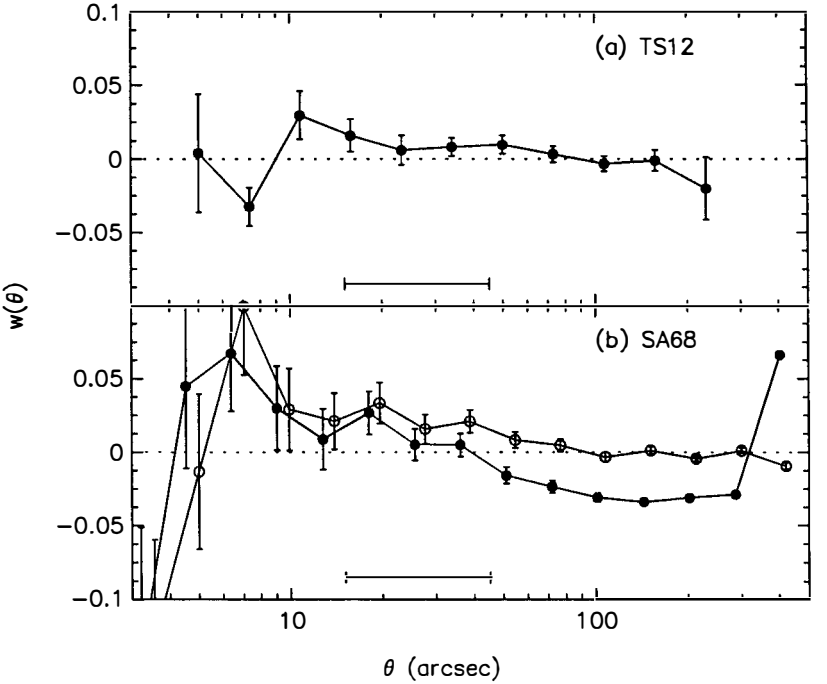


**Figure 2:** Angular correlation functions $w(\theta)$ for faint galaxies in the blue magnitude range $24 < B_J < 26$. Figure 2(a) shows the mean $w(\theta)$ for the TS12 fields and the $1\sigma$ error bars show field-to-field fluctuations. Figure 2(b) shows $w(\theta)$ for the SA68 field together with Poisson errors. The filled symbols in 2(b) show the direct estimate of $w(\theta)$ and the open symbols show the ensemble-average estimate that corrects for spurious large-scale gradients in the galaxy surface density. The horizontal lines show the range of angular scales used to compute the values of $w(30'')$ listed in Table 1.

We bin together all the data for $15'' \lesssim \theta \lesssim 45''$. These values of $\theta$ are large enough to avoid problems of undercounting caused by galaxy crowding [see $w(\theta)$ for $\theta \lesssim 10''$ in Fig 2], and yet are much smaller than the extent of the individual TS12 fields. The effective value of $\theta$ in this broad bin is $\sim 30''$. The correlation strengths, $w(30'')$, are listed in Table 1 for various samples. The correlation function has also been evaluated for objects in the ranges $23.5 < U < 25.5$ (three $U$ fields), $23 < R < 25$ (TS12), and

$22 < I < 24$ (TS12). The above ranges are chosen to be roughly centred on the mean $U$, $R$, and $I$ magnitudes of galaxies in the range $24 < B_J < 26$[6,12] There is about 50-75% overlap between the galaxies in the different ranges. In addition, the TS12 $B_J$ sample is divided into the "$B_J$ red" ($B_J - R > 0.6$) and "$B_J$ blue" ($B_J - R < 0.6$) samples.

**Table 1:** Observed Galaxy-Galaxy Angular Correlation (Uncorrected)

| | | | | TS12 | | | |
|---|---|---|---|---|---|---|---|
| | TS12 $B_J$ | SA68 $B_J$ | $U$ | $R$ | $I$ | $B_J$ red | $B_J$ blue |
| $w(30'')$ | 0.009 | 0.022 | −0.004 | 0.014 | 0.020 | 0.003 | 0.020 |
| $\sigma_w$ | 0.006 | 0.006 | 0.010 | 0.007 | 0.006 | 0.010 | 0.009 |
| $N_{\rm obj}$ | 3631 | 1570 | 639 | 2731 | 2560 | 1571 | 1538 |

The second line in Table 1 lists the $1\sigma$ error in the mean of $w(30'')$. For the TS12 samples, these errors are estimated from the field-to-field variance and are comparable to or slightly larger than (by up to 30%) the Poisson error. For SA68, we list the value of $w(30'')$ from the "ensemble-average" estimator. We quote Poisson errors for SA68 and for the three-field $U$ sample. The number of objects in each sample used to calculate $w(\theta)$ is given in the last row of Table 1.

In $B_J$, $w(30'')$ is clearly positive for SA68 and is higher than the TS12 estimate (see below). The $R$- and $I$-selected galaxies are clustered slightly more strongly than those in the TS12 $B_J$ and $U$ samples (no detectable correlation in $U$). The $B_J$ blue sample appears to have a larger $w(30'')$ than the red one but this effect is not statistically significant. These effects are currently being investigated using larger samples.

In estimating $w(\theta)$ for a field, we normalize by the *actual* object count $n_d$ in that field rather than by the mean $\langle n_d \rangle$ averaged over all fields. This avoids any spurious signals arising from field-to-field variations in seeing, noise level, extinction, and magnitude scale, but causes the angular correlation function to be underestimated by[21]

$$\sigma^2 = \frac{1}{\Omega^2} \int \int w(\theta) d\Omega_1 d\Omega_2, \qquad (1)$$

where $d\Omega_1$ and $d\Omega_2$ are solid angle elements separated by $\theta$ and the integrals are over the solid angle $\Omega$ of the field. Assuming a true correlation function $w^T(\theta) \propto \theta^{-0.8}$, we get $\sigma^2 = 0.53 w^T(30'')$ for the TS12 fields, while $\sigma^2 = 0.27 w^T(30'')$ for the larger SA68 field. The TS12 entries in Table 1 should therefore be divided by 0.47, and the SA68 entry by 0.73, to obtain corrected estimates of $w^T(30'')$. This explains why the TS12 $B_J$ estimate in Table 1 and Figure 1 is lower than that for the SA68 field. Combining the TS12 and SA68 corrected data, our best estimate of $w(30'')$ in the $B_J$ band is $0.024 \pm 0.004$.

Even in the absence of extinction variations, etc. (mentioned above), the field-to-field variance in counts $n_d$ is expected to *exceed* Poisson variance by the amount $\sigma^2$. The observed number count variance in the TS12 fields gives $\sigma^2 < 0.012 \pm 0.004$ for the $B_J$ sample. This is in excellent agreement with the expected excess variance (from eqn. 1) for a power-law correlation function with our 'best fit' amplitude of $w(30'') = 0.024$.

## IV. Expected Correlation

The two-point angular correlation function is related to its spatial counterpart $\xi(r)$ by an integral equation[22]. The spatial correlation function measured from nearby galaxy samples is well approximated by a power law $\xi(r) = (r_0/r)^\gamma$ at $r \lesssim 10h^{-1}$Mpc with $r_0 = 5.5h^{-1}$Mpc and $\gamma = 1.8$ (where $h$ is the Hubble constant $H_0$ in units of $100\,\mathrm{km\,s^{-1}Mpc^{-1}}$). For $\theta \ll 1$, the relation between $w(\theta)$ and a power-law $\xi(r)$ is

$$w(\theta) = \sqrt{\pi}\frac{\Gamma[(\gamma-1)/2]}{\Gamma(\gamma/2)}\frac{A}{\theta^{\gamma-1}}r_0^\gamma, \tag{2a}$$

$$A = \int_0^\infty g(z)(dN/dz)^2\,dz \Big/ \Big[\int_0^\infty (dN/dz)\,dz\Big]^2, \tag{2b}$$

$$g(z) = \Big(\frac{dz}{dx}\Big)x^{1-\gamma}F(x)(1+z)^{-(3+\epsilon-\gamma)}, \tag{2c}$$

where $x$ is the coordinate distance at redshift $z$, $dN/dz$ is the number of objects per unit redshift, and the metric is $ds^2 = c^2dt^2 - a^2[dx^2/F(x)^2 + x^2d\theta^2 + x^2\sin^2\theta d\phi^2]$, where $a$ is the cosmological scale factor[21]. In deriving equations (2), the spatial two-point correlation function is assumed to evolve as

$$\xi(r,z) = (r_0/r)^\gamma(1+z)^{-(3+\epsilon)}, \tag{3}$$

where $r$ is the proper separation between galaxies. If the clustering pattern were fixed in comoving coordinates, then $\epsilon = \gamma - 3 \approx -1.2$; this is expected in theories such as the biased cold dark matter model, where galaxies form at the matter density peaks and are strongly clustered *ab initio*[23,24]. However, if galaxy clustering is dynamically bound and stable at small scales (fixed in proper coordinates), then $\epsilon \approx 0$. We adopt $\epsilon = 0$ and $\epsilon = -1.2$, spanning the range expected in most models of galaxy formation/clustering.

The redshift distribution $dN/dz$ of faint galaxies appears in equation (2). At $B_J \sim$ 21-23, the median redshift of field galaxies is about 0.3-0.4[25,26,27], but little is known about $dN/dz$ for galaxies with $24 < B_J < 26$. Using the $z < 3$ limit imposed by Lyman break arguments[12], the angular correlation amplitude is minimized ($w_{\rm min}$) when

$$\left(\frac{dN}{dz}\right) = \left(\frac{dN}{dz}\right)_{\rm min} \propto \frac{1}{g(z)}, \qquad (z < 3). \tag{4}$$

The upper redshift limit is crucial; otherwise, one could dilute the angular correlation strength by setting $dN/dz \propto [g(z)]^{-1}$ out to some arbitrarily high redshift.

**Table 2:** Model Predictions for the Angular Correlation

| Model | $\Omega_0 = 0,\ \lambda = 0$ | | $\Omega_0 = 1,\ \lambda = 0$ | | $\Omega_0 = 0.1,\ \lambda = 0.9$ | |
|---|---|---|---|---|---|---|
| Parameters | $\epsilon = 0$ | $\epsilon = -1.2$ | $\epsilon = 0$ | $\epsilon = -1.2$ | $\epsilon = 0$ | $\epsilon = -1.2$ |
| $w_{\rm min}(30'')$ | 0.014 | 0.045 | 0.032 | 0.093 | 0.008 | 0.027 |
| $\bar{z}_{\rm min}$ | 2.05 | 1.66 | 1.78 | 1.33 | 2.01 | 1.67 |
| $w_{\rm A}(30'')$ | 0.014 | 0.056 | 0.037 | 0.17 | 0.008 | 0.033 |
| $w_{\rm B}(30'')$ | 0.025 | 0.070 | 0.050 | 0.16 | 0.014 | 0.039 |

Table 2 lists $w_{\rm min}(30'')$ for three cosmologies, an Einstein de Sitter model ($\Omega_0 = 1$), an open model with $\Omega_0 = 0$, and a spatially flat, low density model with $\Omega_0 = 0.1$ and a cosmological constant $\lambda = \Lambda_0/3H_0^2 = 0.9$. The second line in Table 2 gives the median redshift $\bar{z}_{\rm min}$ of the distribution $(dN/dz)_{\rm min}$ that minimises $w$. The correlation strength of the $B_J$-selected faint galaxies is inconsistent with their being the high-redshift counterparts of present day bright galaxies in an $\Omega_0 = 1$ universe if $\epsilon = -1.2$. Even if

$\epsilon \approx 0$ and $dN/dz = (dN/dz)_{\rm min}$, the predicted amplitude of the $\Omega_0 = 1$ models is only marginally consistent ($\sim$ 5% level) with our observations. Low density models with $\epsilon \approx 0$ are compatible with our $w(\theta)$ constraints. The shape of $(dN/dz)_{\rm min}$, with a sharp cutoff at $z = 3$, is quite unrealistic. We also use two somewhat more realistic models for $dN/dz$,

$$\frac{dN}{dz} \propto z^2 \exp\Big[ -(z/z_0)^\beta \Big]. \tag{5}$$

Model A ($z_0 = 3$, $\beta = 9$) just satisfies the constraint that $< 7\%$ of the faint galaxies are at $z > 3$ (§II), and has a median redshift $\overline{z} = 2.3$. For this distribution to be correct, there must be a rapid rise in the mean redshift of galaxies from $\overline{z} \sim 0.4$ at a magnitude limit of $B_J \lesssim 24$[26,27] to $\overline{z} \gtrsim 2$ for $24 < B_J < 26$. Model B ($z_0 = 1.8$, $\beta = 4$) with $\overline{z} = 1.5$ is perhaps a more feasible model for $dN/dz$[28,29]. Table 2 also lists the expected values of $w(30'')$ for these two models, which should be compared with the corrected estimate of $w(30'')$ given in §III. With the $dN/dz$ models A and B, the $\Omega_0 = 1$ predictions lie well above our measured amplitude for $w(\theta)$ (by at least $3\sigma$) while the low density cosmological models can produce an amplitude as low as that observed if $\epsilon \sim 0$.

## V. Implications

The results of the preceeding sections have the following possible interpretations:

[1] The geometry of the universe corresponds to an open Friedmann-Robertson-Walker model or a non-zero $\Lambda$ model *and* the clustering pattern evolves strongly ($\epsilon \approx 0$).

[2] The clustering evolves more rapidly than expected theoretically ($\epsilon > 0$).

[3] Most of the faint galaxies at $B_J \sim 26$ belong to a new population that is weakly clustered and intrinsically faint at the present epoch.

The last of these explanations appears to us to be the most plausible. All our model predictions assume a spatial correlation function with a correlation length $r_0 = 5.5h^{-1}$Mpc. The angular separation at which we measure the correlation amplitude, $30''$, corresponds to physical scales of 160-200$h^{-1}$kpc (130-110$h^{-1}$kpc) at $z$ = 1-3 in an $\Omega_0 = 0$ ($\Omega_0 = 1$) universe. The power law form of the spatial correlation function, with an index of $-1.8$, is observed to apply all the way down to separations of $\sim 10h^{-1}$kpc[22], so equation (3) should be valid over the relevant range of redshifts. However, $r_0$ has

been measured reliably in nearby samples only for luminous galaxies[30]. The clustering strength of intrinsically faint galaxies is poorly known and could possibly be weaker[31].

Several authors have argued that if $\Lambda = 0$, the high surface density of faint galaxies implies they have a space density much greater than that of local luminous galaxies[9,27]. This problem has led some authors to question whether galaxy numbers are conserved at high redshift[32,33,9]. The discrepancies between our models and the observed $w(\theta)$ cannot be explained if the objects at $B_J \sim 26$ are simply sub-galaxian clumps which will merge to form present-day luminous galaxies since in this case their clustering should be described by equation (3) with $r_0 \approx 5.5h^{-1}$Mpc on scales $\gtrsim 100h^{-1}$kpc. The high surface-density of galaxies could also arise from a new galaxy population that dominates over normal galaxies at magnitudes fainter than $B_J \sim 23$[33]. Our results would then suggest that this new population is more weakly clustered than present day luminous galaxies. Luminosity-dependent evolution models (*e.g.* models in which dwarf galaxies undergo frequent starbursts) may be successful at reconciling the count excess at $B_J \sim$ 21-23 with the shape of the observed redshift distributions which peak at $z \sim$ 0.2-0.4[25,34]. In this class of models, the excess faint galaxies are progenitors of present day dwarf galaxies. However, the local number density of low-luminosity galaxies rises relatively slowly at the faint end (at least for $M_{B_J} \lesssim -17 + 5\log_{10}h$[35]). It is therefore difficult to account for the high surface density of faint counts simply by invoking a bright phase in the early evolution of normal dwarf galaxies[33], unless these dwarfs somehow represent only a tiny visible fraction of a larger class of galaxies. The galaxies comprising the deep counts may thus belong to a genuine new population that has since faded to produce systems that are intrinsically faint, of low surface brightness, weakly clustered and more abundant than normal dwarf galaxies at the present day.

Some of the problems discussed above can be avoided in cosmological models with a non-zero cosmological constant. The faint blue counts can be explained with plausible assumptions about galaxy evolution in models with $\Omega_0 \sim 0.1$ and $\lambda \sim 0.9$[36]. As Table 2 shows, the angular correlation amplitude in such models is compatible with our observations of weak clustering, provided the faint galaxies are located at redshifts $z > 1$

and the clustering evolves with $\epsilon \sim 0$. Models with $\Omega_0 + \lambda = 1$ are compatible with the inflationary model of the early universe[37] and have many other attractive features[38,39]. However, a non-zero cosmological constant seems unnatural[40] and such models may be in conflict with the comparatively low galaxy counts in the near infrared $K$ band and with the observed frequency of gravitationally lensed quasars[41].

The best estimate of $w(30'')$ in our $24 < B_J < 26$ sample, after correcting for finite field-size effects and spurious large-scale gradients in galaxy density, is consistent with the amplitude found by Windhorst and Neuschaefer[42] at $g = 24.7$ ($B_J \sim 25$). They find that $w(\theta)$ obeys a power law, so that our evaluation of equation (1) is accurate. The authors point out that their sample is seriously incomplete beyond $g = 24.5$, so it is not clear whether the *rise* they see in the $w(\theta)$ amplitude at $g > 24.7$ is real.

Our data show a marginally significant trend from $U$ to $I$, in the sense of the correlations becoming stronger as we select galaxies at redder wavelengths. This may suggest that the dominance of the weakly clustered population over the progenitors of normal galaxies decreases as one goes to the $R$ and $I$ bands. A detailed investigation of the faint galaxy angular correlation function, using a variety of selection criteria, can prove useful in defining the distinguishing characteristics of the weakly clustered objects. This should allow us to identify the predecessors of normal, bright galaxies from the multitude of objects seen at faint magnitudes. After all, the ancestors of galaxies like our own must be present in these deep images of the sky.

**Acknowledgements:** I would like to thank my collaborators: G. Bernstein, G. Efstathiou, N. Katz, S. Majewski, and T. Tyson. This work has been supported in part by grants AST-8802533 (NSF) and NAS 5-29225 (NASA) to the IAS.

**References**

[1] Frenk, C.S., Ellis, R.S., Shanks, T., Heavens, A.F. & Peacock, J.A. (eds), 1989, *The Epoch of Galaxy Formation*, Dordrecht: Kluwer.
[2] Bergeron, J., Kunth, D., Rocca-Volmerange, B. & Thran-Thalın Van, J. (eds), 1987, *High Redshift & Primeval Galaxies*, Editiones Frontieres, Gif Sur Yvette Cedex, France.
[3] Chambers, K.C., Miley, G.K. & Joyce, R., 1988, *Ap. J.*, **329**, L75.
[4] Schneider, D.P., Schmidt, M. & Gunn, J.E., 1991, *Astr. J.*, in press.
[5] Kron, R.G., 1982, *Vistas in Astronomy*, **26**, 37.

[6] Tyson, J.A., 1988, *Astr. J.*, **96**, 1.
[7] Cowie, L.L., Lilly, S.J., Gardner, J. & McLean, I.S., 1988, *Ap. J.*, **332**, L29.
[8] Cowie, L.L., 1989, in reference [1], p. 31.
[9] Koo, D.C., 1991, in *The Evolution of the Universe of Galaxies: The Edwin Hubble Centenary Symposium*, ed. R.G. Kron (ASP Conf. Series), in press.
[10] Efstathiou, G., Bernstein, G., Katz, N., Tyson, J.A. & Guhathakurta, P., 1991, *Ap. J. (Letters)*, in press.
[11] Bruzual, G.A., 1983, *Ap. J. Suppl.*, **53**, 497.
[12] Guhathakurta, P., Tyson, J.A. & Majewski, S.R., 1990, *Ap. J.*, **357**, L9.
[13] Sargent, W.L.W., Steidel, C.C. & Boksenberg, A., 1989, *Ap. J. Suppl.*, **69**, 703.
[14] Soucail, G., Mellier, Y., Fort, B., Mathez, G. & Cailloux, M., 1990, in *Gravitational Lenses*, ed. Mellier, Y., Soucail, G. & Fort, B., Springer-Verlag, Heidelberg, p. 291.
[15] Tyson, J.A., Valdes, F. & Wenk, R.A., 1990, *Ap. J.*, **349**, L1.
[16] Tyson, J.A., 1991, in *Proceedings of the 1990 Texas/ESO-CERN Symposium on Relativistic Astrophysics*, New York Academy of Sciences, in press.
[17] Ellis, R.S., Allington-Smith, J. & Smail, I., 1991, *M.N.R.A.S.*, **249**, 184.
[18] Tyson, J.A. & Seitzer, P., 1988, *Ap. J.*, **335**, 552.
[19] Jarvis, J.F. & Tyson, J.A., 1981, *Astr. J.*, **86**, 476.
[20] Valdes, F., 1982, *Proc. SPIE*, **331**, 465.
[21] Groth, E.J. & Peebles, P.J.E., 1977, *Ap. J.*, **217**, 385.
[22] Peebles, P.J.E., 1980, *The Large-Scale Structure of the Universe* (Princeton University Press, Princeton).
[23] Davis, M., Efstathiou, G., Frenk, C.S. & White, S.D.M., 1985, *Ap. J.*, **292**, 371.
[24] Carlberg, R.G., 1991, *Ap. J.*, **367**, 385.
[25] Broadhurst, T.J., Ellis, R.S. & Shanks, T., 1988, *M.N.R.A.S.*, **235**, 827.
[26] Colless, M., Ellis, R.S., Taylor, K. & Hook, R.N., 1990, *M.N.R.A.S.*, **244**, 408.
[27] Lilly, S.J., Cowie, L.L. & Gardner, J.P., 1991, *Ap. J.*, **369**, 79.
[28] Guiderdoni, B. & Rocca-Volmerange, B., 1990, *Astr. Ap.*, **227**, 362.
[29] Koo, D.C., 1986, in *Spectral Evolution of Galaxies*, ed. C. Chiosi & A. Renzini (Dordrecht: Reidel), p. 419.
[30] Davis, M. & Peebles, P.J.E., 1983, *Ap. J.*, **267**, 465.
[31] Weinberg, D.H., Szomoru, A., Guhathakurta, P. & van Gorkom, J.H., 1991, *Ap. J.*, **372**, L13; also see references therein.
[32] White, S.D.M., 1989, in reference [1], p. 15.
[33] Cowie, L.L. & Lilly, S.J., 1991 in *The Evolution of the Universe of Galaxies: The Edwin Hubble Centenary Symposium*, ed. R.G. Kron (ASP Conf. Series), in press.
[34] Guhathakurta, P., 1989, Ph.D. thesis, Princeton University.
[35] Efstathiou, G., Ellis, R.S. & Peterson, B.A., 1988, *M.N.R.A.S.*, **232**, 431.
[36] Fukugita, M., Takahara, F., Yamashita, K. & Yoshii, Y., 1990, *Ap. J.*, **361**, L1.
[37] Peebles, P.J.E., 1984, *Ap. J.*, **284**, 439.
[38] Efstathiou, G., Sutherland, W.J. & Maddox, S.J., 1990, *Nature*, **348**, 705.
[39] Turner, M.S., 1991, *Physica Scripta*, **000**, in press.
[40] Weinberg, S., 1989, *Rev. Mod. Phys.*, **61**, 1.
[41] Turner, E.L., 1990, *Ap. J.*, **365**, L43.
[42] Windhorst, R.A. & Neuschaefer, L.W., 1991, in *After the First Three Minutes*, ed. S.S. Holt, C.L. Bennett & V. Trimble (AIP Conference Proceedings: New York), p. 322.

# VISIBLE AND NEAR-INFRARED GALAXY COUNTS AND THE IMPLICATIONS FOR THE COSMOLOGICAL GEOMETRY

Jonathan P. Gardner
Institute For Astronomy
University of Hawaii
2680 Woodlawn Drive
Honolulu HI 96822 USA

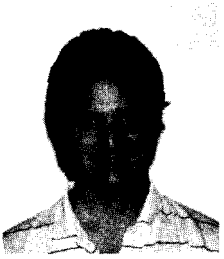

The Hawaii Deep Survey has obtained near-infrared faint galaxy counts to K=23. The low number of galaxies making up these counts favors a $q_0$=0.5, $\Lambda$=0 cosmological geometry. The B band number counts show a large excess of objects over this model. By combining spectroscopic redshift identifications with the K magnitudes, we show that this excess is caused by a population of faint blue dwarfs which is present at redshifts of $z \approx 0.4$, but is not counted in the local population. The dwarf galaxies contain as much K light as the normal galaxy population and may dominate the baryonic matter content of the universe.

**Introduction**

The cosmological deceleration parameter, $q_0$, can in principle be determined from galaxy number counts, but in practice luminosity and number evolution can easily dominate the geometrical effects. With samples selected in the radio and the optical evolution effects are strong because the nuclear activity producing the radio emission, and the massive stars producing the optical emission have short timescales relative to the age of the galaxy, and thus it is difficult to compare these samples to a present day population.

In the near-infrared, 2.2 microns or the K band, the light is from near solar mass stars whose lifetimes are similar to the age of the galaxy. The evolutionary corrections are much smoother as these stars do not change quickly. At high redshifts the K band samples the well understood rest frame optical part of the spectrum, which is much flatter than the rest frame ultraviolet. Thus the cosmological dimming due to the K correction is less, allowing us to sample to large redshifts at brighter magnitudes.

When we reach faint enough levels to break through and sample the whole of the galaxy occupied volume, the number counts contain information about the geometry and the redshift of galaxy formation in the same way that star counts give us the structure and limits of our own galaxy.

**Hawaii Deep Survey**

The Hawaii Deep Survey was designed to obtain deep K band galaxy samples with corresponding optical colors which can also be used as a basis for spectroscopic observations. We are using a Rockwell 256x256 HgCdTe array detector on the University of Hawaii's 2.2 meter telescope and on the Canada France Hawaii Telescope. We have K band galaxy counts to K=23, and spectroscopic identifications are nearly complete for the B<24 sample. We are just beginning

spectroscopic work on a K band selected sample. In addition, work has begun on a wide field sample which will provide good signal to noise on the number counts from K=14 to K=20. Results obtained to date are reported in Cowie *et al.*, 1990, Lilly, Cowie and Gardner, 1991, and Cowie *et al.*, 1991.

The B band galaxy number counts, normalized to a simple power law, are plotted in Figure 1 against galaxy evolution models adapted from Yoshii and Takahara (1988). The models have numerous assumptions about the present population mix, the galaxy luminosity function, and galaxy evolution (younger galaxies being bluer and more luminous,) however, there are several model-independent conclusions which can be drawn. Up to B=22, we can model the counts well. Beyond this the counts rise more rapidly than any of the models, even the extreme case with non-zero $\Lambda$. An open universe has more volume at high redshift than a closed universe, and a flat universe with $\Lambda$=0.9 and $\Omega$=0.1 has even more volume, giving higher number counts at the faint end. These models do not, however, predict enough galaxies to fit the data.

Luminosity evolution has a stronger effect than geometry for the B selected sample. Because younger galaxies are expected to be brighter in the blue, they are seen to greater distance, and therefore more galaxies are counted. These galaxies should be at high redshift. Spectroscopic work has shown that this is not the case. Until the K band counts existed, there were two proposed explanations for the excess B counts, one cosmological and one astrophysical. The cosmological hypothesis was that we live in a flat universe with $\Lambda$=0.9 and $\Omega$=0.1, and there is moderate galaxy evolution (see, e.g., Lilly, Cowie and Gardner, 1991). The B band number count data can be fit with this hypothesis, but they require a fairly low redshift of formation for the galaxies. The proposed astrophysical explanation is that there is a population of blue dwarf galaxies at redshifts of about 0.4 which is not included in the present day luminosity function (see e.g. Broadhurst *et al.*, 1988).

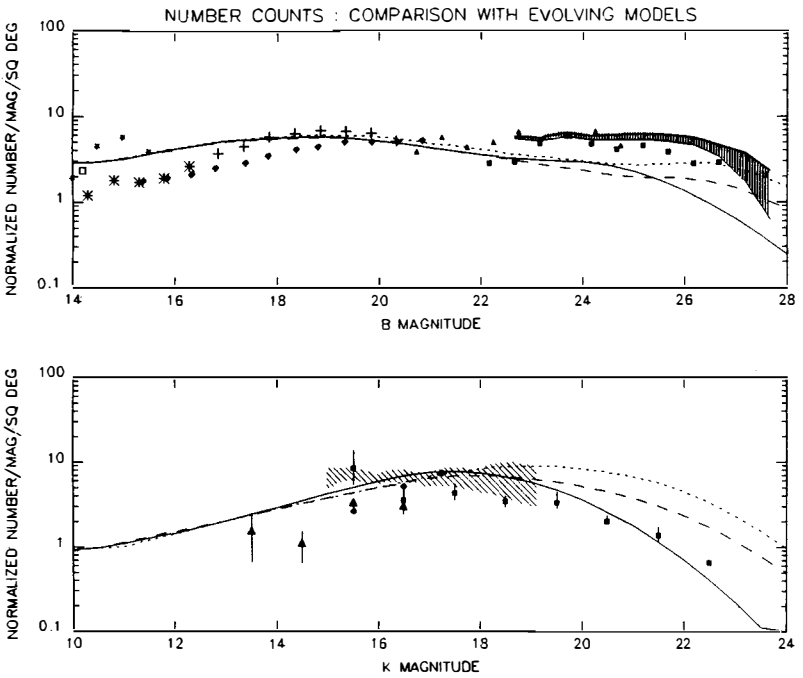


**Figure 1.** A comparison of blue and infrared galaxy counts with model predictions. The blue number counts are taken from the compilation of Metcalf *et al.* 1990, in addition to those of Tyson (1988; shaded region), Lilly *et al.* (1990; solid squares), and the APM survey (diamonds; Sutherland *et al.* 1990). The infrared counts are taken from Glazebrook *et al.* (1990; triangles), Jenkins and Reid (1990; shaded region), Gardner, in preparation (diamonds), and our data, reported in Cowie *et al.*, (1991; squares). The models follow those of Yoshii and Takahara, (1988), except that the luminosity function is extended to 10 magnitudes below $L_*$. The counts have been normalized to power laws of slope 0.45 normalized at B=16 and K=11 in order to show the full dynamic range of the data. The models correspond to three geometries, $q_0$=0.5 (solid line), $q_0$=0.2 (dashed line), and flat with $\Lambda$=0.9 and $\Omega$=0.1 (dotted line).

The K band counts are more sensitive to the cosmological geometry than the B band counts. At K=19, the counts stop rising rapidly and flatten out to a much shallower slope. At this point we are no longer sampling to greater distances, but are seeing through to the end of the galaxy occupied volume. The count's slope is the faint end shape of the luminosity function averaged through this volume.

Thus the counts at the faint end favor a $q_0$=0.5, $\Lambda$=0.0 geometry. This result is, of course, model dependent, but is more robust than it might seem at first. These curves represent models with redshift of galaxy formation of z=5. However, to fit the open universe model to the faint K band counts, we would need to make $z_{form}$ equal to 2, and for the more extreme non-zero $\Lambda$ model, $z_{form}$=1.5. In addition, this result is based upon a deficiency of galaxies, and this is much harder to explain away than the excess seen in B. Luminosity evolution makes galaxies bright in the past and would increase the number counts. The same holds true for merging models. The stars which give off the K band light have been there since the galaxy formed, so it is very difficult to dim the galaxy relative to its current luminosity. The model independent conclusion to draw from the number counts is that there is no way to fit both the B band and the K band number counts with the same population. The difference between the B and K counts is essentially a color problem.

Figure 2 is a plot of the median B-K color vs. K magnitude. At the bright end we have B-K of 5 to 6, which is typical of a nearby galaxy population. However, at the faint end B-K falls to 4, which is as blue as a local irregular. The surprise is that this happens in a K selected sample. The population must be dominated by starbursting galaxies. The blueness of the faint population is the cause of the discrepancy between the blue and the infrared number counts. What must be explained in any model is why there are so many faint blue galaxies.

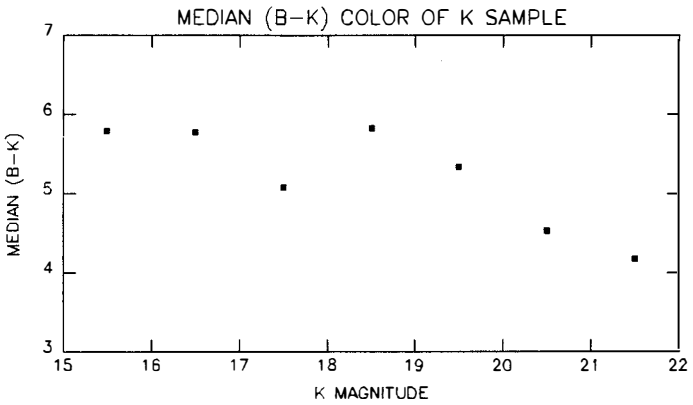


**Figure 2.** Median B-K vs. K magnitude for our K selected sample. While at bright magnitudes B-K is around 5 to 6, typical for a nearby galaxy population, at the faint end B-K has fallen to 4, which is as blue as a local irregular.

**The Spectroscopic Sample**

We have spectroscopic redshifts for 14 galaxies of the 18 galaxies in the B<24 sample. One galaxy remains unidentified, while three have not yet been attempted. Although our sample is small, we are complete at the 93% level. Figure 3 is our spectroscopic sample, with redshift plotted against B magnitude, along with the data from Broadhurst *et al.* (1988), and Colless *et al.* (1990). The data fits the no-evolution model, and the lack of high redshift objects rules out the strong evolution explanation for the excess B band number counts which are already a large effect at B=24.

We can combine the redshift data with the apparent K magnitude to determine what the population producing the B band excess actually is. That is, the absolute K magnitude, plotted in Figure 4 against apparent B magnitude, should give a good estimate of the galaxy mass, except for the most extreme starbursting case where it is an upper limit. At the brighter magnitudes the absolute K

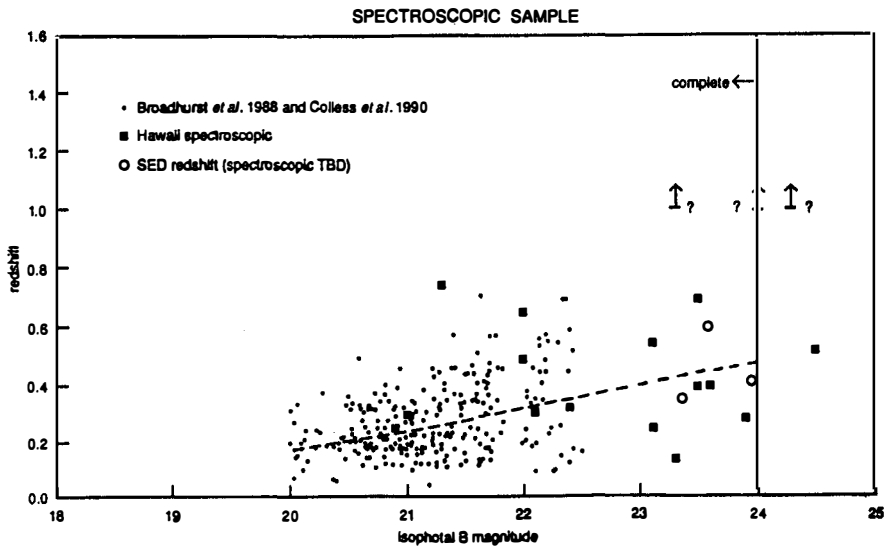


**Figure 3**. Spectroscopic samples for B magnitude selected samples. The dots show the B<21 and B<22.5 samples of Broadhurst *et al.*, (1988) and Colless *et al.* (1990). The latter is about 80% complete. The solid squares show our data (Lilly *et al.*, 1991) which is 93% complete to B=24. Open circles are objects for which we have not yet attempted spectroscopy and are plotted with redshifts estimated from their colors. One object at B<24 remains unidentified despite attempts and could be at high redshift (upward pointing arrow.) The dashed line shows a predicted mean redshift for a model with no galaxy evolution; it provides a remarkable good fit.

magnitudes center around $K_*$ for an elliptical galaxy. At the fainter end, however, which is where the excess B counts appear, we begin to see galaxies that are as much as 4 magnitudes fainter in K. This is unexpected in a magnitude-limited sample where we expect the counts to be dominated by the near-$L_*$ galaxies which can be seen to the limits of largest volumes. Roughly 2/3 of the faintest galaxies appear to be dwarfs of this type. If we try to turn this into a luminosity function we find that the total K luminosity density is $8.1x\,10^8\ L_\odot/Mpc^3$ with roughly half the light coming from the dwarfs and half from normal galaxies.

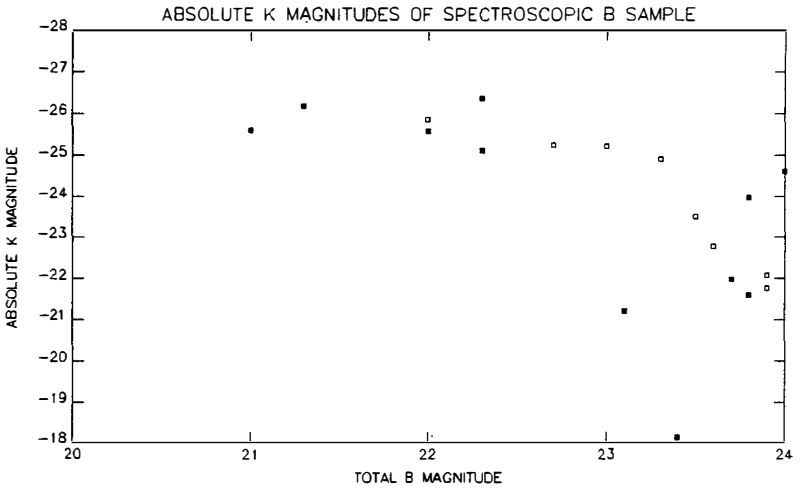


**Figure 4.** Absolute K magnitude vs apparent B magnitude. Solid symbols show objects with spectroscopic redshifts; open symbols those with estimated redshifts determined by SED fitting to the colors. This plot includes data from a field for which we have not yet begun spectroscopic identifications.

The blue dwarf population contains an equal amount of K band light as the normal population. Since they are likely to contain more gas than stars, this population could dominate the baryonic mass in the universe. In particular, if dwarfs contain four times as much mass in gas as in stars, then their baryonic density is $\rho_B = 1.4x\,10^{-31}\ gm\ cm^{-3}$. This is very approximate, but can be compared to the homogeneous Big Bang nucleosynthesis model of Yang *et al.* (1984.) which predicts $\rho = 2\text{–}9x\,10^{-31}\ gm\ cm^{-3}$

Looking back at the number counts in Figure 1 it is possible to see the impact of the blue dwarf galaxies. The population is very blue so it appears as an excess in the B counts, but does not appear in the K counts until we reach fainter levels. Thus these galaxies, instead of being an excess at the K = 18 to 22 level, does not appear until the K = 20 to 24 level, where they fit the models much better.

The observed $K_*$ of the dwarfs is similar to that of the local dwarf spheroid population, but the local density of such objects is far too low to be the same population. Even in the Virgo cluster the ratio of dwarfs to normal galaxies is too low. There are several explanations for where these blue dwarfs are at the present epoch which we must consider. The dwarfs detected in our survey are relatively compact objects, and it is unlikely that they have spread out to become too low surface brightness to be detected nearby.

The galaxies could have merged to form larger galaxies, and this would explain the baryonic density of the dwarfs. However, neither present day ellipticals, because of their colors, nor spiral, because of the fragility of their disks, are the likely result of merging at $z \approx 0.4$.

Two proposals which seem most likely are that the blue dwarfs are either biased away from the local population, or that they have disrupted themselves during the starbursting process. Both of these explanations imply that there is significant biasing of matter away from the light of normal galaxies.

**Conclusion**

All of our conclusions are model dependent and are yet to be confirmed by other groups. However, our K band number counts indicate that we are living in a $q_0=0.5$, $\Lambda=0$ universe. The B band counts indicate that there is a population of blue dwarfs which flourished at $z \approx 0.4$ but has now burnt out and destroyed itself, or in some other way is no longer counted in the present galaxy population.

If we accept the presence of the blue dwarf population then it contains at least as much baryonic mass as the present day normal galaxies and may account for the missing baryon problem which is suggested by primordial nucleosynthesis models.

**Acknowledgements**

I would like to thank my thesis advisor, Lennox L. Cowie, and our collaborators, Esther M. Hu, Richard J. Wainscoat, and Klaus W. Hodapp for allowing me to present the results of our work at this conference.

**References**

Broadhurst, T.J., Ellis, R.S., and Shanks, T. 1988, *M.N.R.A.S.*, **235**, 827.
Colless, M., Ellis, R.S., Taylor, K., and Hook, R.N., 1990, *M.N.R.A.S*, **244**, 408.
Cowie, L.L., Gardner, J.P., Lilly, S.J., McLean, I., 1990 *Ap. J. Lett.*, **360**, L1.
Cowie, L.L., Gardner, J.P., Hu, E.M., Wainscoat, R.J., and Hodapp, K., 1991, preprint.
Glazebrook, K., Peacock, J.A., Collins, C.A., and Miller, L., 1990, preprint.
Jenkins, C.R. and Reid, I.N., 1990, A.J., in press.
Lilly, S.J., Cowie, L.L., and Gardner, J.P., 1990, *Ap. J.*, **369**, 79.
Maddox, S.J., Sutherland, W.J., Efstathiou, G., Loveday, J., and Peterson, B.A., 1990, *M.N.R.A.S.*, **247**, 1P.
Metcalfe N., Shanks, T., and Fong, R., 1990, preprint.
Tyson, J.A., 1988, *A. J.*, **96**, 1.
Yang, J., Turner, M.S., Steigman, G., Shramm, D.N., and Olive, K.A., 1984, *Ap. J.*, **281**, 493.
Yoshii, Y., and Takahara, F., 1988, *Ap. J.*, **326**, 1.

# GALAXY COUNTS AT ULTRAVIOLET WAVELENGTHS (2000 Å)

Bruno MILLIARD, José DONAS, Michel LAGET, and Christiane ARMAND
Laboratoire d'Astronomie Spatiale
Trav. du Siphon, Les Trois Lucs
F–13012 Marseille, France

**Abstract**

Individual galaxy counts at 2000 Å derived from ultraviolet (UV) images obtained with a 40-cm balloon-borne telescope are presented and discussed. The galaxy number counts are high, with a steep differential log-counts slope. The detected galaxies show very blue $m_{2000} - b$ colours, typical of late type spirals. Galaxies brighter than $m_{2000} = 18.5$ contribute at the level of $20 - 30\ ph(cm^2 s Å sr)^{-1}$ to the extragalactic ultraviolet background in the far UV.

# 1. Introduction

Galaxies have been identified for a long time as a possible significant contributor to the ultraviolet (UV) Extragalactic Background Light (EBL). Nevertheless, the only published measurement of their integrated emission is the pioneering power spectrum analysis performed in [1]. They find 30 $ph(cm^2 s Å sr)^{-1}$ (thereafter PU) at 1500 Å, which is an appreciable fraction of the 250 or so extragalactic PU observed at high galactic latitude. Since non evolving discrete sources give half of their EBL contribution at redshifts below 0.3 (see *e.g.* [2]), UV galaxy counts should provide interesting lower limits to the fraction of the UV EBL due to galaxies, even from modest sensitivity data.

This paper presents galaxy counts derived from observations obtained at 2000 Å with a balloon-borne imaging telescope, and the resulting contribution to the ultraviolet EBL. The main characteristics of the instrument and of the observations will be given first, then the instrumental corrections performed and the galaxy numbers derivation, with some discussion of the results. This is the first direct measurement of field galaxy numbers at ultraviolet wavelengths below the atmospheric cutoff.

Before going further, it is worth noticing two specific aspects of our UV observations in the current state-of-the-art :

1. Below the sensitivity limit, the redshift of the bulk of the detected galaxies is in the range 0.1 – 0.2, and the corresponding look-back time is about 2 – 3 billion years. This leaves time enough for a significant evolution, since it is comparable with the gas depletion timescales of nearby late type galaxies, and since the lifetimes of the stars which dominate the UV emission are short. There is little dependence on the geometry of the universe. The exotic situation of a giant local hole in the density of galaxies (as discussed in [3]) is not taken into account here.

2. The in-flight angular resolution avoids crowding problems, but does not make possible a direct separation of stars and galaxies at the faint end of the UV observations. Nevertheless, at the depth level required ($B < 21.$), published catalogues like the ones of [4] and [5] allow identification of the detected objects by their positions on the sky in a limited area of the UV observations, with negligible chance coincidences.

## 2. Observations

The five high galactic latitude observations used here (Table 1.) have been obtained with a 40-cm entrance pupil telescope for imagery at 2000 Å, developed jointly by Laboratoire d'Astronomie Spatiale (scientific payload) and Observatoire de Genève (4 arcsec. r.m.s. stabilized gondola).

**Table 1: List of the observations.** The equatorial coordinates of the guide stars are taken from the *Centre de Données Stellaires de Strasbourg, France.* They lie within a few arcmin. from the actual centres of the observed fields. The last column gives the cumulative observing time in seconds.

| Name | Telescope | Alpha 1950 | Delta 1950 | Expos. |
|---|---|---|---|---|
| SA57 | F1500 | 13 03 47.14 | +29 17 48.3 | 1200 |
| M3 | F1500 | 13 39 52.94 | +28 37 37.9 | 3600 |
| A2111 | F1500 | 15 36 52.85 | +34 50 13.3 | 2700 |
| Coma | F1000 | 12 57 08.09 | +28 20 06.4 | 3000 |
| SA57 | F1000 | 13 03 47.14 | +29 17 48.3 | 3000 |

The two available focal lengths (referred to as F1500 and F1000) provide an angular resolution of 12 and 20 arcsec. (FWHI) on a 1.55 and 2.3 degree field of view respectively. Unresolved objects with flat energy spectra are detected in twenty minutes observing time with the F1500 instrument. The bandpass ($\lambda_0 \simeq 2000$ Å; $\Delta\lambda \simeq 150$ Å) is defined by the multilayer filters deposited on the primary and on the secondary mirrors, the CsTe photocathode and the in-flight residual absorption of ozone and molecular oxygen. At such a wavelength, the light of late type galaxies is dominated by stars of about five solar masses, with lifetimes of a few hundred million year. The measured fluxes then monitor the star formation activity (*e.g.* [6]). An important point to be noticed is that the very good blocking of visible light achieved, allows observation of cold objects down to $m_{2000} - B = 6$ (G0 type spectra) with a negligible contribution of light above 2200 Å. The ultraviolet magnitudes are derived from the digitized photographic frames translated into intensities, with a home made routine which integrates the surface brightness of the detected objects down to a certain criterion above the sky value. The difference with the total magnitude is estimated to less than 0.1 magnitude for normal galaxies. The linearity of the photometry has been checked on laboratory vacuum stars and should not be in error by more than .2 magnitude in the useful range. The zero point has

been established from several stars in common with observations performed with the previous experiment SCAP 2000 [7] and the evaluated uncertainty is $\simeq .25$ magnitude. In the high galactic latitude regions of interest here, the galactic extinction is low and has been neglected. We have excluded the regions near the M3 and Coma cluster centres, and the useful observed area is about 6 square degree.

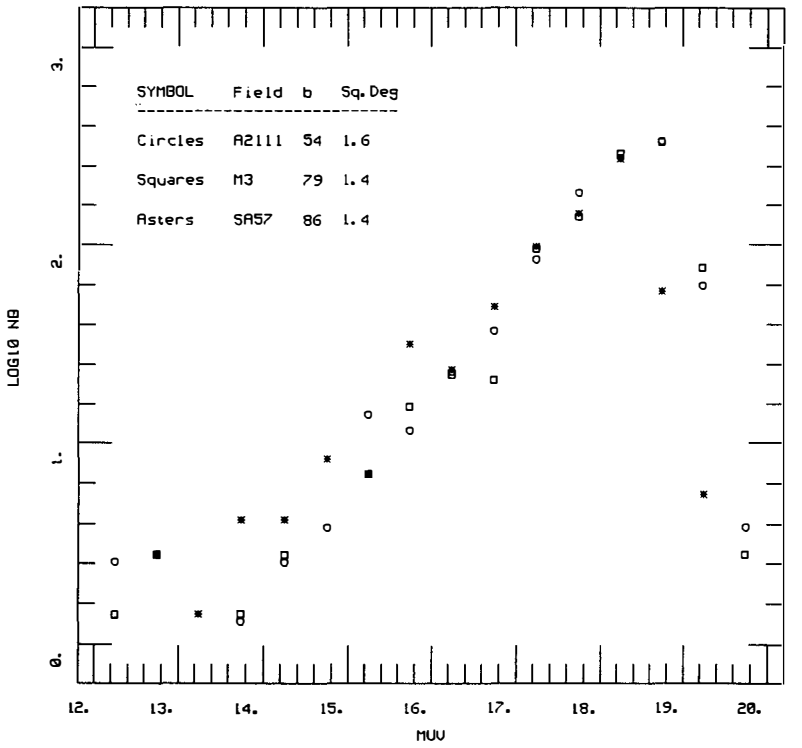


**Figure 1. Observed differential log-counts** in the three F1500 high galactic latitude fields as a function of UV magnitudes, with galactic latitudes in degree and useful areas in square degree. The values are given per square degree per magnitude.

## 3. Object counts and instrumental corrections.

The observed raw differential counts at 2000 Å, in number per square degree per magnitude, measured in 0.5 mag bins, show a rather good agreement of numbers and slopes in the three high galactic latitude fields M3, SA57 and A2111 (Fig. 1), all observed with the same instrument (F1500). In the following, we shall refer to the counts averaged over the three FOCA 1500 fields, excepted for the 18.25 magnitude bin where the SA57 F1500 observation which has a shorter observing time is discarded (Table 1, col. 5). The analysis which follows is restricted to UV magnitudes between 15.5 and 18.5 to avoid small numbers statistics and large instrumental corrections. The two F1000 observations are used to evaluate several corrections and the stellar contribution to the counts. To this purpose, we made a wide use of the galaxy catalogue of the Coma cluster region in [4] and of the star catalogue in the same region, kindly sent to us by Metcalfe [5]. In the following, both catalogues will be referred to as GMP catalogues.

**Table 2: Object counts:** *(1)* centres of the magnitude bins. *(2)* number of detections per magnitude per square degree. *(3)* fraction of spurious detections. *(4)* completeness fraction. *(5)* Malmquist bias. *(6)* corrected source counts, same units as col. 2. *(7)* galaxy counts, same units as col. 2.

| $m_{2000}$ (1) | Raw (2) | Spurious (3) | Complet. (4) | Malmquist (5) | Sources (6) | Galaxies (7) |
|---|---|---|---|---|---|---|
| 15.25 | 9.3 | 0.00 | 1.00 | 1.00 | 9.3 | 4.4 |
| 15.75 | 19.6 | 0.00 | 1.00 | 1.00 | 19.6 | 12.0 |
| 16.25 | 22.8 | 0.01 | 1.00 | 1.00 | 22.8 | 11.1 |
| 16.75 | 35. | 0.00 | 1.00 | 1.00 | 35. | 17. |
| 17.25 | 92. | 0.04 | 0.99 | 1.00 | 88. | 60. |
| 17.75 | 155. | 0.12 | 0.96 | 1.02 | 139. | 96. |
| 18.25 | 280. | 0.27 | 0.72 | 1.08 | 264. | 198. |

Corrections have been performed for spurious detections on the sky background and particle events in the detector, from the comparison with a laboratory uniformly illuminated frame, and from the visual inspection of the Palomar Observatory Sky Survey blue prints. The incompleteness has been evaluated essentially from the region in common to the two SA 57 observations, and

accounted for. Finally an *a priori* correction of the Malmquist bias has been performed. The counts obtained after these different steps are given Table 2, column 6, and are plotted Fig. 2. It is to be noticed that all the above corrections are small. A more detailed description of the instrumental corrections is given in [8].

## 4. Galaxy counts

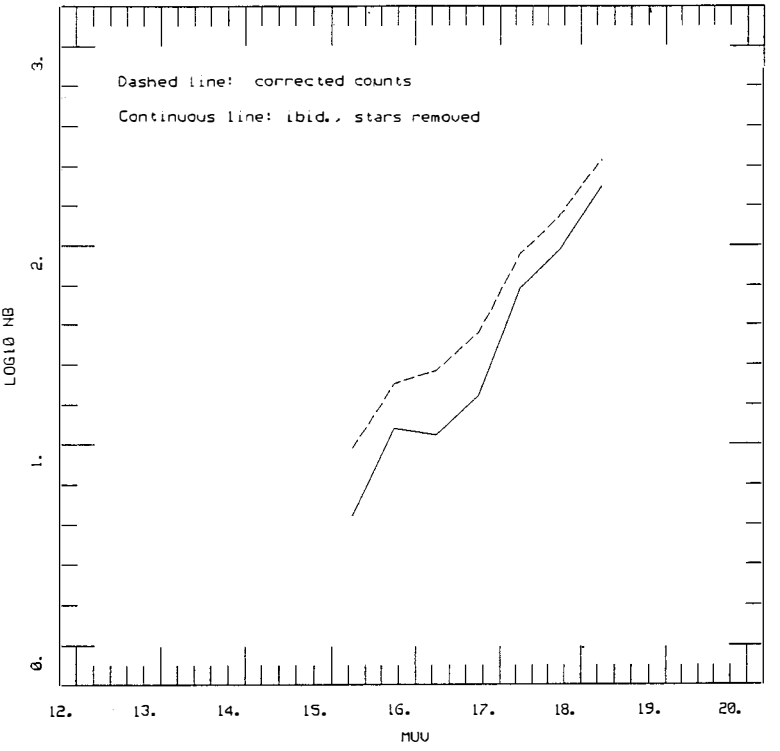


**Figure 2. Galaxy counts:** (same coordinates as in Fig. 1). The subtraction of the estimated stellar contribution to the corrected counts (dashed line), results in the estimated galaxy counts (solid line).

The galaxy counts have been deduced by subtracting to the corrected source counts, the observed star counts taken as the average of the identifications in the three observations overlapping the GMP star catalogue. The incompleteness of the UV data has been corrected for, and a correction has been made to take into account the difference between the galactic latitude of the GMP star catalogue and the average galactic latitude of the three UV observations used to derive the high latitude counts. The observed star numbers naturally include the possible red leak contribution of stars; it has been checked in the GMP galaxy catalogue that nearly all the detected galaxies show blue UV-to-visible colours, which excludes any significant contribution through the red leak for these objects. A fraction of the objects in the GMP star catalogue show colours typical of late type galaxies in $m_{2000} - b$ *vs* $b - r$ diagrams, and have been considered as QSO's or misclassified galaxies. The star catalogue is little affected by the Coma cluster, but the 1000 arcsec. radius region around the centre has been excluded in the star number estimates. The obtained galaxy numbers (Table 2, col. 7 and Fig. 2) are comparable to or higher than visible counts at the same flux level. The slope of a linear fit to the differential log-counts is a steep one, of 0.54 in the UV magnitude range $15.5 - 18.5$ and 0.67 in the UV magnitude range $16.5 - 18.5$ respectively. Due to the large error bars of the bright end counts, the latter estimate has more weight, and the real value of the slope is probably near euclidean or steeper.

## 5. Error estimate.

A rough error analysis taking into account essentially the uncertainties of the instrumental corrections and the large scale structure of the universe leads to a factor $\simeq 2$ uncertainty on the galaxy number counts. The Coma contamination cannot be calculated precisely, but must lie within ten percent at maximum since the agreement between the three F1500 counts is good, and since it is present in only one field whose centre is about 2 degree away from the cluster centre.

## 6. Discussion.

The galaxies which dominate the counts at 2000 Å show blue, mostly negative $m_{2000} - b$ colours, at least in the 0.4 square degree in common between the SA57 F1500 UV observation and the GMP catalogues. The galaxies differential counts per UV magnitude bin at high latitudes are high and the slope of the log-counts in the considered UV magnitude range is steep. The observed UV slope validates below the atmospheric cutoff the increase towards shorter wavelengths demonstrated in ground-based observations [9], [10] and [11], with

potential information on the recent evolution of field galaxies or of their luminosity function. It also implies an important contribution of field galaxies to the UV EBL: the contribution of galaxies brighter than $m_{2000} = 18.5$, evaluated from a linear least square fit to the log-counts in the UV magnitude range $15.5 - 18.5$ is found to be 32 $ph(cm^2 s\text{Å} sr)^{-1}$. This value is comparable to the 30 $ph(cm^2 s\text{Å} sr)^{-1}$ upper limit for the **total** galaxy contribution at 1500 Å to the EBL given in [1]. The difference in wavelength with the present results cannot explain this discrepancy, since the galaxy contribution to the EBL shows essentially a spectrum with a flat energy distribution [1]. It is worth noticing that the two linear least square fits to the log-counts in the UV magnitude ranges $15.5 - 18.5$ and $16.5 - 18.5$ produce the same contribution of $\simeq$ 65 PU to the EBL, in a crude log-linear extrapolation down to UV magnitude 20.5. The field galaxies then produce an important fraction of the Far UV extragalactic background light.

**Acknowledgements.** Thanks are due to the organizers for this stimulating meeting in a wonderful place. The experiment is supported by Centre National d'Etudes Spatiales and by Fonds National de la Recherche Scientifique for the Swiss part.

## References

1. Martin, C., Bowyer, S.: 1989, *ApJ*, **338**, 677
2. Longair, M.: 1990, in *Proc. I.A.U. 139, The Galactic and Extragalactic Background Radiation*, eds. S. Bowyer and Ch. Leinert (Kluwer Academic Publishers: Dordrecht), p.469
3. Maddox, S.J., Sutherland, W.J., Efstathiou, G., Loveday, J., Peterson, B.A.: 1990, MNRAS 247, 1p
4. Godwin, J.G., Metcalfe, N., Peach J.V.: 1983, MNRAS 202, 113
5. Metcalfe, N.: 1988, private communication.
6. Donas, J., Buat, V., Milliard, B., Laget, M.: 1990, A&A 235, 60
7. Donas, J., Deharveng, J.M., Laget, M., Milliard, B., Huguenin, D.: 1987, A&A 180, 12
8. Milliard B., Donas, J., Laget, M., Armand, Ch., Vuillemin, A.: 1991, submitted prep
9. Koo, D.C.: 1981, Ph.D. Thesis, University of California, Berkeley
10. Majewski, S.R.: 1989, in *The epoch of Galaxy Formation*, eds. C.S. Frenk, C.S., Richard, S.E., Shanks, T., Heavens, A.F., Peacock, J.A. (Kluwer Academic Publishers: Dordrecht), p. 85
11. Jones, L.R., Fong, R., Shanks T., Ellis, R.S., Peterson, B.A.: 1991, MNRAS 249, 481

# FAINT GALAXY COUNTS AND GLOBULAR CLUSTERS IN FORNAX ELLIPTICALS

Rainer Madejsky
Landessternwarte, 6900 Heidelberg, F.R. Germany
and
Monica Rabolli
Insituto de Astronomía y Física del Espacio, Buenos Aires, Argentina

**Abstract.** The luminosity function of globular clusters in elliptical galaxies belonging to the Fornax cluster of galaxies is investigated. In several fields near the elliptical galaxies NGC 1351, NGC 1379, NGC 1399 and NGC 1427 we obtained deep CCD-photometry in B, V and R. In addition, several comparison fields were observed, in order to determine the luminosity and spatial distribution of faint background galaxies. The precise determination of these faint galaxies is crucial, because they outnumber the globular clusters near the limiting magnitude and major variations from field to field of these faint galaxy counts are found. The faint galaxy counts are compared to those obtained by Tyson (1988).
Taking into account an averaged luminosity function of these faint galaxies, we find a clear turnover of the luminosity function of globular clusters in NGC 1399 at $m_B = 24.8$, $m_V = 24.0$ and $m_R = 23.4$mag. If a universal luminosity function of globular clusters is assumed, the distance to Fornax is m–M = 31.8, or d = 22.9 Mpc. Correcting for the peculiar motion of the Local Group we obtain $H_0 = 55 kms^{-1}Mpc^{-1}$. The luminosity functions of the much less numerous globular clusters associated with the other Fornax ellipticals needs further investigation to decide whether a universal luminosity function of globular clusters may exist.

**Observations and Reduction.** For the observational study of globular clusters in Fornax ellipticals we have chosen the two elliptical galaxies NGC 1379 and NGC 1399, which are both known to have abundant globular cluster systems (see e.g. Harris, 1988 for a list of galaxies where globular clusters have been detected), and two further elliptical galaxies, NGC 1351 and NGC 1427, which are located at larger distances from the core of the Fornax cluster.

For these 4 elliptical galaxies we obtained one near-central field and one comparison field, each. The near-central field always was chosen near the center of the galaxy, however, the very center of the galaxy was excluded. Detections of globular clusters are incomplete there because the diffuse background light of the galaxy cannot be subtracted accurately in the innermost 10 arcsec due to the steep gradient of the luminosity profile. The near-central ('target') fields are supposed to contain a large number of globular clusters. The comparison field always was chosen at a distance 20...60 arcmin from the center of the galaxy, so that it can be assumed not to contain anymore globular clusters belonging to the target galaxy. The comparison fields are used to determine the distribution and luminosity function of the background galaxies (see below).

We used the Eso Faint Object Spectrograph and Camera (EFOSC) attached to the ESO 3.6m telescope on La Silla, Chile. All fields were observed in three colours (standard Bessell B, V and R system). An RCA chip with 660×1030 pixels (15$\mu$m, 0.335 arcsec) was used, covering an area of $\approx$ 21arcmin$^2$. The seeing was only between 1.2 and 1.5arcsec, so that we could not fully exploit the scale. All fields were observed in a similar way: between 3 and 5 exposures were made in each colour, changing the telescope position by several arcsec between the individual exposures. Total integration time was 60 min per field and colour. Multiple exposures are extremely useful to eliminate cosmic events and to reduce defects of the chip and fringing which was substantial in V (see also Tyson, 1986; 1988). From the whole set of comparison images we were able to construct a master flatfield (in a similar way as described in Tyson, 1986). After subtracting a two-dimensional dark-frame

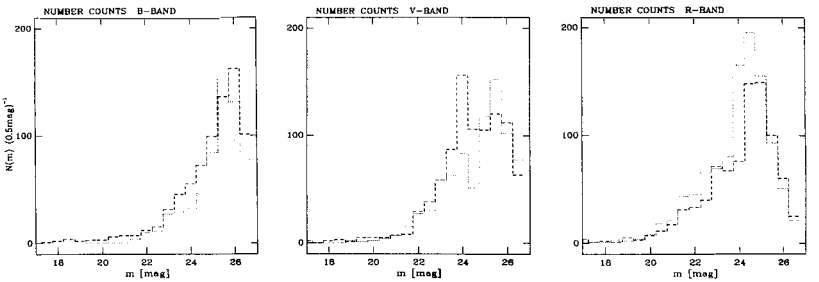


**Fig. 1a-c.** The differential number counts in B, V and R are shown for various comparison fields ($\approx$ 15arcmin$^2$). Significant variations from field to field are due to galaxy clusters at intermediate redshifts

and correcting for column offset, the images were divided by the master flatfield. Then the images were calibrated using a large set of photometric standard stars (Alcaino et al, 1988; Stobie et al, 1985a, 1985b) which were observed on all nights. Finally the individual images were summed up. These final images were then reduced with DAOPHOT (Stetson, 1987).

**Results.** The differential number counts of several comparison fields are shown in Figs. 1a-c. The total number of detected objects per half-magnitude bin and per field ($\approx$ 15arcmin$^2$) are displayed versus apparent magnitude. The number counts are deficient at the bright end because the fields were selected not to contain bright objects. Beyond 25mag, the number counts decrease due to detection incompleteness which needs correction (see below). The number counts of the comparison fields show large variations from field to field. Thus it seems difficult to define a reliable background.

The number count variations are due to clusters of galaxies at intermediate redshifts. In the target field of NGC 1399, e.g., is a cluster of galaxies with an estimated redshift $z\approx0.1$. The six brightest galaxies having apparent magnitudes $m\approx21$mag are clearly elongated. Many galaxies which are not seen at first inspection of the images may contribute to this cluster. After reduction with DAOPHOT, the luminosity function of the faint galaxies

shows an excess of objects which is due to this cluster (see Fig. 4b). Another rich cluster of galaxies at an estimated redshift $z \approx 0.5$ is seen on the images of a comparison field of NGC 1379. A large number of faint, mostly considerably elongated galaxies, belong to this cluster. The faintest galaxies which are still well resolved by eye have an apparent magnitude of $m \approx 24$mag.

In nearly half of the comparison fields, remote clusters of galaxies are seen by a first raw inspection of the CCD images, which contribute to the significant variations of the number counts from field to field. Already after raw inspection of the deep CCD-images by eye, we see that the distribution of faint galaxies is characterized by substantial variations from field to field. Since the globular clusters are outnumbered by the faint background galaxies, a mean background of faint galaxies must be defined if we want to determine reliable luminosity functions of globular clusters.

In order to compare the differential number counts with other published data, the logarithmic counts of these fields are displayed in Figs. 2a-c. The counts are scaled to an area of 1 degree$^2$ and are given in one-magnitude bin. Due to the detection incompleteness near the faint limiting magnitude, the counts decrease substantially beyond 25mag. It is shown that, except for the range of detection incompleteness, the differential number counts nearly follow an exponential law. The slope $\alpha$ of the (log N(m) – m) counts is well approximated by $\alpha_B = \mathbf{0.37}m_B$, $\alpha_V = \mathbf{0.34}m_V$ and $\alpha_R = \mathbf{0.32}m_R$. In all fields we obtain the same trend with colour: the bluer counts have the steeper slope. This trend with colour was already found in earlier investigations of faint galaxy counts (Tyson, 1988; Gardner, Guhathakurta, Milliard and others at this meeting). These counts are slightly less steep than Tyson's counts (see Fig. 2). Ferguson and Sandage (1988) obtained in their study of the central 2.4° radius core of the Fornax cluster a slope $\alpha_B = 0.16m_B$ at the faint end (the slope gets steeper towards the bright end). The quite different slopes are due to the different galaxy populations which are traced by the galaxy counts.

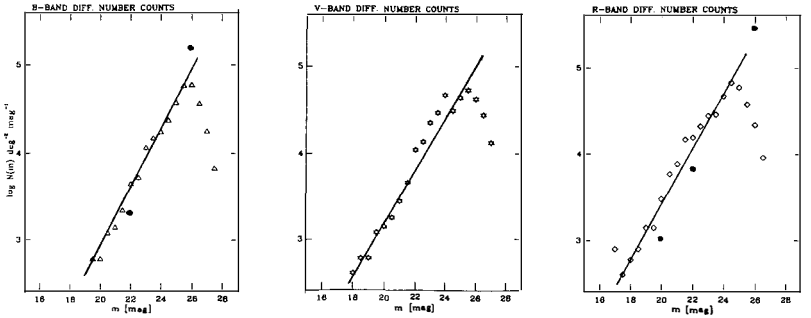


**Fig. 2a-c.** The (log N(m) – m) relation is displayed per magnitude-bin and per degree$^2$. The decrease beyond 25mag is due to detection incompleteness and needs correction. The straight line corresponds to a slope of 0.37 (2a), 0.34 (2b) and 0.32 (2c). For comparison Tyson's counts are drawn as dots at 22 and 26mag (2a and c)

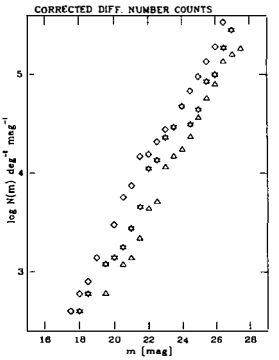


**Fig. 3.** The differential number counts after correction for incompleteness. The counts follow nearly an exponential law, except the faint blue counts, which seem to level off. Symbols correspond to colours as given in Fig. 2

After correction for detection incompleteness we obtain the differential number counts as displayed in Fig. 3. It is shown once more that the blue counts have a steeper slope than the red counts. More objects are found in the red than in the blue band. The red counts increase nearly with the same slope over the whole range of apparent magnitude. The blue counts seem to slightly level off beyond 26mag, however, the correction for incompleteness there is substantial (the correction factor near $m_B$ = 27mag is $\approx$ 10 !). Tyson already

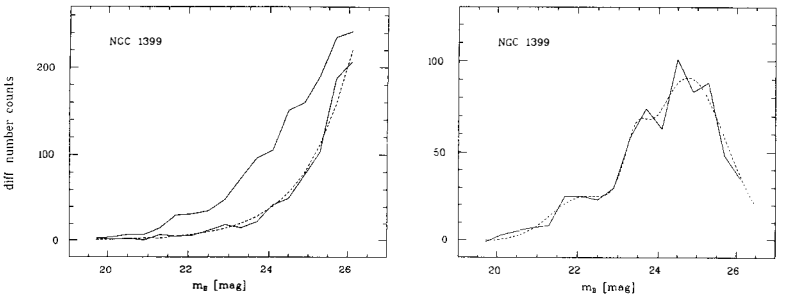


**Fig. 4a,b.** The differential number counts of the mean background (left, lower curve) and of the target field of NGC 1399 (left, upper curve), and the difference of both (right). The excess of objects in the target field of NGC 1399 is due to a galaxy cluster (brightest and intermediate peak) and most probably also due to an abundant globular cluster population (faintest peak)

noted a similar decrease of the differential number counts in the blue band (however, the limiting magnitude of his counts is more than 1mag fainter than our limit).

**Globular clusters associated with NGC 1399.** From the various comparison fields observed in this study, we determine a mean background of faint galaxies. Those fields where clusters of galaxies are clearly present, the differential number counts were corrected, i.e. the excess counts above a smooth increase of the differential number counts were not taken into account. As shown above, the differential number counts approximately follow an exponential law in the whole range of apparent magnitudes between 18 and 26mag. Therefore a reliable mean of the background can be obtained by averaging the corrected luminosity functions of the different fields. The finally obtained slopes of the (log N(m) – m) counts of faint background galaxies are $\alpha_B = \mathbf{0.36}m_B$, $\alpha_V = \mathbf{0.34}m_V$ and $\alpha_R = \mathbf{0.32}m_R$.

In Fig. 4a are shown the differential number counts of the mean background (lower curve) and of the target field of NGC 1399 (upper curve). The target field of NGC 1399 contains a large number of excess objects. Already the first inspection of the data has revealed the

presence of a cluster of galaxies at redshift $z \approx 0.1$ (see above) which contributes in part to this excess. The differential number counts of the excess objects are displayed in Fig. 4b. The two brightest peaks are probably due to the galaxy cluster. The faintest and richest population is assumed to be due to globular clusters belonging to NGC 1399. The peaks are present in all three bands. Taking the mean colours of these objects, we obtain B–V = 0.8mag, B–R = 1.4mag which are typical colours of globular clusters (Bridges et al, 1990; Geisler and Forte, 1990). Assuming a universal luminosity function of globular clusters, we determine a distance modulus m–M = 31.8mag for Fornax, based on the value for galactic globular clusters $M_B = -7.0$mag. Further correcting the radial velocity of NGC 1399 for Virgo infall (Yahil et al, 1977), we determine $H_0 = 55 \mathrm{kms}^{-1}\mathrm{Mpc}^{-1}$. Only a formal error accounting for the accuracy of the photometry and the determination of the peak can be given which is $\approx \pm$ 0.2mag, i.e. $H_0 = 55 \pm 5\ \mathrm{kms}^{-1}\mathrm{Mpc}^{-1}$. Much larger errors may be introduced by a systematically different luminosity function of globular clusters in Fornax ellipticals as compared to Local Group spirals.

The globular cluster systems associated with the other Fornax ellipticals are much less numerous. The peak luminosities are found at similar apparent magnitudes within $\pm$ 0.2mag, however, further reductions including a discrimination between extended faint background galaxies and unresolved globular clusters are necessary, before reliable luminosity functions for these globular clusters can be given.

**Conclusions.** Deep CCD-photometry was presented for several fields near 4 Fornax ellipticals to determine the luminosity functions of their associated globular clusters. The distribution of faint background galaxies which outnumber the globular clusters near their mean apparent magnitude, is determined with the aid of a number of comparison 'blank' fields. Large variations of the differential number counts of detected objects are found from field to field, which require determination of a 'mean background field'. All fields are well represented by a near exponential increase of the differential number counts. The comparison with Tyson's counts shows the same behaviour with colour, i.e. blue counts

are steeper than the red counts in all fields. However, all our fields are characterized by a less steep slope than those of Tyson. Similar number counts are found near 24mag, i.e. we observe more bright and less faint galaxies than Tyson. This result may be related to the different regions chosen in these works (Fornax vs. South Galactic Pole).

Taking into account a 'mean background field' constructed from the various comparison fields available, we determined an approximate luminosity function of globular clusters belonging to NGC 1399. Further assuming a universal luminosity function of globular clusters in galaxies, we determine the distance to the center of the Fornax cluster m–M = 31.8mag or 22.9 Mpc.

**References.**

Alcaino, G., Liller, W., Alvarado, F., 1988, Astron. J. **96**, 139
Bridges, T.J., Hanes, D.A., Harris, W.E., 1991, Astron. J. **101**, 496
Ferguson, H.C., Sandage, A., 1988, Astron. J. **96**, 1520
Geisler, D., Forte, J.C., 1990, Astrophys. J. Lett. **350**, L5
Harris, W.E., 1988, in 'Globular cluster systems in galaxies', IAU 126, eds. J. Grindlay, A. Philips, p. 237
Stetson, P.B., 1987, Dominion Astrophys. Observatory, Victoria, B.C.
Stobie, R.S., Gilmore, G., Reid, N., 1985a, Astron. Astrophys. Suppl. **60**, 495
Stobie, R.S., Sagar, R., Gilmore, G., 1985b, Astron. Astrophys. Suppl. **60**, 503
Tyson, J. A., 1986, J. Opt. Soc. Am. A **3**, 2131
Tyson, J. A., 1988, Astron. J. **96**, 1
Yahil, A., Tammann, G.A., Sandage, A., 1977, Ap.J. **217**, 903

# MODELS OF FAINT GALAXY COUNTS

Bruno GUIDERDONI
Institut d'Astrophysique de Paris
98bis Boulevard Arago, F–75014 Paris, France

**Abstract**

We review the present status of the models predicting faint galaxy counts, and redshift distributions, which are important steps on the way to estimate the contribution of high–$z$ and primeval galaxies to the extragalactic background light. We summarize the modelling of these data taking into account the evolution of galaxies, and we study the sensitivity of the predictions to the inputs: luminosity functions and scenarios of galaxy evolution. If the luminosity function and mix of spectral types are known, it is possible to get some information on the value of the density parameter $\Omega_0 = 2q_0$ (providing the cosmological constant $\lambda_0$ vanishes). The conservative interpretation of the data with simple scenarios of evolution gives $\Omega_0 \simeq 0.1$.

Such a result is inconsistent with the flat universe predicted by the inflationary paradigm. The data can be accomodated in this context with a non–zero cosmological constant. On the other hand, the high–$z$ objects do seem to be *smaller* than the nearby galaxies. It is possible to fit the counts with $\Omega_0 = 1$ and a dwarf–rich luminosity function at high $z$, although the non–detection of a large number of nearby dwarfs has to be explained in this latter case. Alternatively, one can relax the assumption of galaxy–number conservation and assume that the high–$z$ dwarfs have been accreted by giant galaxies. We give constraints on the amount of number evolution (and related mass evolution) which can fit all the data in an $\Omega_0 = 1$ universe.

## 1. Introduction

Faint galaxy counts can be used to constrain the value of the deceleration parameter $q_0$. In this test, galaxies are simply used as bench–marks tracing space. Providing the comoving number density is conserved, the number of galaxies in a shell at redshift $z$ is proportional to the volume of this shell and the faint counts are sensitive to space curvature through these volumes. It is difficult to get *redshifts* for a complete sample of galaxies which would be deep and large enough to extract cosmological information (this is known as the Loh–Spillar test[1]). So the most common test consists in counting galaxies against *apparent magnitudes*. The sensitivity of these latter counts to space curvature is maintained, even if galaxies are distributed in a wide luminosity function (LF). The status of the faint galaxy counts with respect to the series of classical cosmological tests designed to measure space curvature from observations of high–$z$ objects, is reviewed by Sandage[2] and Guiderdoni[3].

Moreover galaxies are not inert bench–marks. They evolve and it is necessary to understand this evolution before addressing cosmological problems. The evolution must be analysed by means of a model of spectrophotometric evolution which allows to compute evolving synthetic spectra of galaxies from a minimum set of assumptions about the star formation history. By coupling these results with Friedmann–Lemaître cosmological models, apparent magnitudes and colours can be derived, which take into account the entangling of the cosmological and evolutionary effects in a consistent way. The interpretation of galaxy counts must use these realistic magnitude and colour computations. It may be easier to understand the average evolution of the overall "field" population observed in the counts than that of the "standard candles" used in other tests, which are bright objects, and probably have peculiar histories. So it can be anticipated that the faint counts will in turn yield more informations on cosmology. Finally they allow to estimate the contribution of high–$z$ and primeval galaxies to the extragalactic background light (hereafter EBL; see Rocca–Volmerange, this conference).

## 2. Modelling faint galaxy counts

### *2.1 – Principles*

The predictions of faint galaxy counts are based on the assumption that the comoving number density of galaxies with spectral type $j$ is conserved once the galaxies formed at redshift $z_{for}$. The number of these galaxies at redshift $[z, z + dz[$ contributing to the counts per steradian and magnitude bin around apparent magnitude $m_\lambda$ (through the $\lambda$ filter) is:

$$d^2 A_j(m_\lambda, z) = \Phi_j(M_\lambda)(1+z)^3 \frac{dV}{dz} dm_\lambda \, dz \qquad (1)$$

$dV$ is the volume element per steradian of the shell $[z, z + dz[$ given in classical textbooks[4]. $\Phi_j(M_\lambda)$ is the comoving LF for type $j$ determined from the analysis of ***nearby*** galaxies. The

absolute magnitude $M_\lambda$ is computed from:

$$M_\lambda = m_\lambda - (m - M)_{bol}(z) - k_{j\lambda}(z) - e_{j\lambda}(z) \tag{2}$$

$(m - M)_{bol}(z)$ is the bolometric distance modulus[4]. The $k$–corrections account for the cosmological redshift of the spectra of distant galaxies. The $e$–corrections account for the intrinsic evolution of the rest–frame spectra with respect to nearby standards. The results are given for $H_0 = 50$ km sec$^{-1}$ Mpc$^{-1}$, with a weak dependence on $H_0$ through the $e_{j\lambda}(z)$.

The total counts per steradian in the magnitude bin $dm_\lambda$ are:

$$N(m_\lambda)dm_\lambda \equiv \sum_j \int_0^{z_{max,j}} d^2 A_j(m_\lambda, z) \tag{3}$$

$z_{max,j} = min(z_{for,j}, z_{lim})$ with $z_{lim}$ being the redshift above which the Lyman continuum break enters the $\lambda$ filter: $1 + z_{lim} \simeq \lambda/912$ Å.

The specific intensity per unit wavelength (EBL) in erg s$^{-1}$ cm$^{-2}$ Å$^{-1}$ sr$^{-1}$ is:

$$I_\lambda = I_{\lambda 0} \int 10^{-0.4 m_\lambda} N(m_\lambda) dm_\lambda \tag{4}$$

with $I_{\lambda 0}$ being the flux of an A0V star at apparent magnitude $m_\lambda = 0$ (in erg s$^{-1}$ cm$^{-2}$ Å$^{-1}$). The constraints given by the faint counts at magnitudes brighter than $m \simeq 27$ allow to extrapolate the total contribution of high–$z$ and primeval galaxies to the EBL.

### *2.2 - Spectrophotometric evolution*

Eq. (2) tells that all the spectrophotometric properties of galaxies which are relevant for the counts, are included in the $k$– and $e$–corrections. These quantities are computed from a model of spectrophotometric evolution. After Tinsley's pioneering works, the first model of this type was proposed by Bruzual[5,6]. This model is used by a number of other authors. We built a new model at the IAP, which is described in Rocca–Volmerange *et al.*[7] and in Guiderdoni & Rocca–Volmerange[8]. The latter reference gives the comparison with Bruzual's model. The computation of the $k$– and $e$–corrections is described in Rocca–Volmerange & Guiderdoni[9]. Yoshii & Takahara[10] gave predictions at high redshift, based on the photometric model of Arimoto & Yoshii[11,12].

In the last version of the IAP model, we use the new tracks of Maeder & Meynet[13] for stars with $1M_\odot < m_* < 120M_\odot$ and the tracks of VandenBerg[14] for stars with $m_* < 1M_\odot$. This distribution is combined with a library of stellar spectra in the UV, visible and near–IR, in order to estimate the synthetic spectrum of the stellar population. The internal extinction is estimated from the gas content and simple models of metal enrichment and transfer. The nebular emission is computed from the flux of ionizing photons. We keep a standard IMF

with a slope $x = 1.7$ for stars more massive than $2M_\odot$[15], $x = 1.35$ between 1 and $2M_\odot$, and $x = 0.25$ below. The synthetic spectra satisfactorily reproduce the colours of the Hubble sequence of spectral types, with a single parameter, namely the time scale for star formation[8]. The age of galaxies can be a secondary parameter. The $k$– and $e$– corrections at redshift $z$ are derived from these spectra after coupling with the standard cosmological models.

### *2.3 – Evolution of surface brightness*

The question is to know whether a low intrinsic surface brightness combined with the "cosmological fading" in $10\log(1+z)$ makes distant objects detectable at the level of the currently–available surveys. As in Guiderdoni & Rocca–Volmerange[16], we introduce the consistent estimate of surface brightness. We compute the current, rest–frame absolute magnitudes $M_B$ by correcting the absolute magnitudes at $z$ for cosmology and evolution, and we use standard observational relations of the luminosity profiles with $M_B$.

## 3. The faint galaxy counts in the case of pure luminosity evolution

The available data on the magnitude, and redshift distributions of faint galaxies, can be simply analysed under the assumption of conservation of the comoving number density (case of pure luminosity evolution). Tinsley[17], Bruzual & Kron[18], Shanks *et al.*[19], King & Ellis[20], Yoshii & Takahara[10], Koo[21], Guiderdoni & Rocca–Volmerange[22,23], Yoshii & Peterson[24], and Metcalfe *et al.*[25] proposed such analyses from their models of evolution of galaxies.

### *3.1 – Sensitivity to inputs*

The LF of galaxies is an important input of the models. We take type–dependent Schechter LF's. The standard magnitudes $M^*_{B_j}$ and standard fractions $f_j$ of each type in magnitude–limited samples, are drawn from observations collected in King & Ellis[20]. The slope of the LF's is $\alpha = -1.07$ in agreement with recent determinations[26]. It is interesting to investigate the sensitivity of the predictions to the input LF's. Figure 1a shows the influence of the slope $\alpha$ and of the faint–end cut–off, with the standard type mix. Clearly a steep slope of the LF can accomodate the data whith $\Omega_0 = 1$. As shown in section 4, it also works with $\Omega_0 = 0.1$.

Figure 1b shows the influence of the scenarios of star formation, with the standard LF. We test two extreme models in which all galaxies behave as ellipticals (here the 1 Gyr burst model[8]), or as late–type spirals (here with a constant SFR[8]). The change of the star formation history cannot reconcile $\Omega_0 = 1$ with the data. Figure 1c gives the sensitivity to the redshift of star–formation turn–on. Finally, figure 1d shows the sensitivity of the predictions to $\Omega_0 = 2q_0$ (with $\lambda_0 = 0$). With standard LF and type mix, high $z_{for}$ and low $\Omega_0$ are favoured.

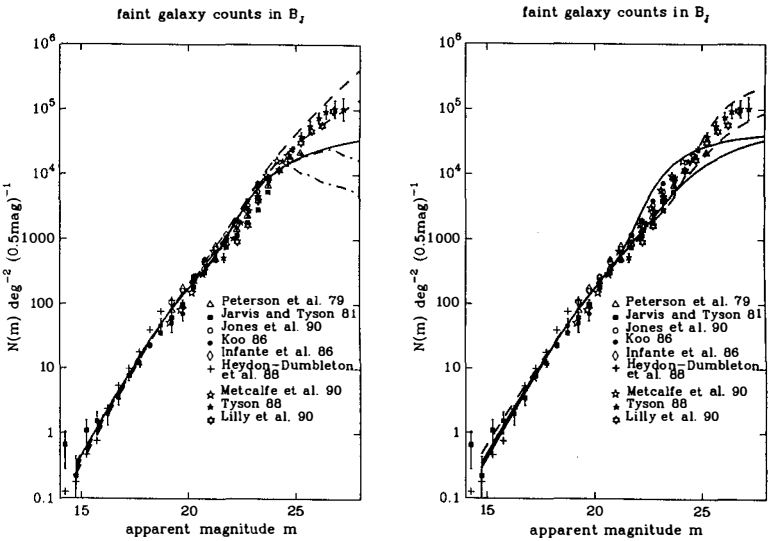


**Figure 1: Sensitivity of the predictions of faint galaxy counts to various inputs.** (a) Slope of the LF (with $\Omega_0 = 1$). *Solid line:* $\alpha = -1.07$; *dashes:* $\alpha = -1.5$ and $-1.8$; *dashes-and-dots:* faint-end cut-off 2 or 4 mag below the knee. (b) Scenarios of galaxy evolution: all ellipticals (*upper curves*) or all spirals (*lower curves*). *Solid lines:* $\Omega_0 = 1$; *dashes:* $\Omega_0 = 0.1$.

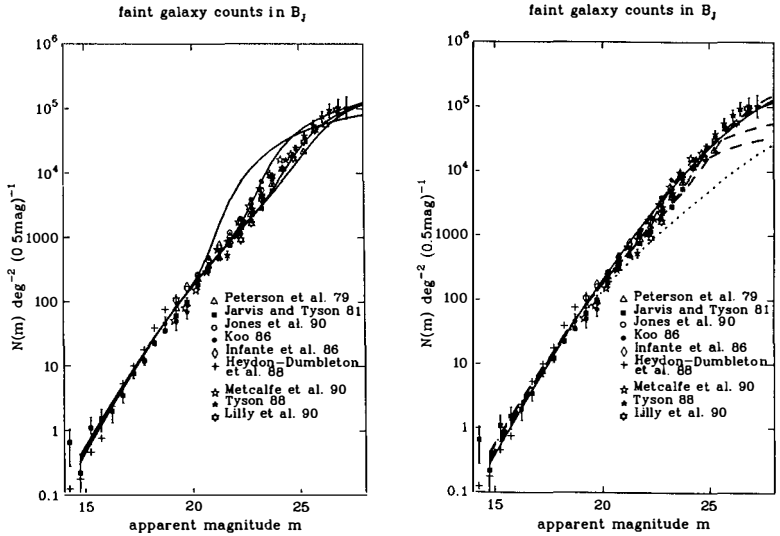


**Figure 1 (continued):** (c) Redshift of star-formation turn-on. From up to down: $z_{for} = 3$, 5, 10 or 30. (d) Cosmological parameters. *Dashes*, from up to down: $\Omega_0 = 0$, 0.1, 0.5, 1 (with

### *3.2 - Provisional conclusion*

The effects of evolution and cosmology are strongly entangled. If the properties of current galaxies are to be reproduced (shallow slope of the LF, and mix of spectral types describing the Hubble sequence), the evolution of galaxies is sufficiently constrained and we can get some information on the value of the density parameter. As a matter of fact, the fit of the number counts and redshift distribution requires a low $\Omega_0$ ($\sim 0.1$) and a high value of $z_{for}$ ($\sim 10$). None of the uncertainties due to the history of star formation (providing there is only luminosity and colour evolution), the IMF, the internal extinction or the nebular component can make the results consistent with the value $\Omega_0 = 2q_0 = 1$ required by the inflationary paradigm (if $\lambda_0 = 0$). This conclusion holds from the $U$-band counts to the red[8], and is very robust since it is due to the smaller volume elements at high redshifts for $\Omega_0 = 1$. On the contrary, Cowie *et al.*[27] suggest that the low-$\Omega_0$ open universes predict more galaxies than observed in the $K$-band counts. Nevertheless it may be easy to flatten the predicted counts in the open universes by hiding some of the high-$z$ galaxies (because of strong extinction, or low-surface brightness for instance). Moreover the $K$-band predictions are based on the nearby *blue* LF, corrected to near-IR by means of model-dependent colours. It would be necessary to check this conclusion with an observational near-IR LF.

In fact, a steep-slope LF can also accomodate the observed counts with $\Omega_0 = 1$. The degeneracy of the solutions in the $N(m)$ diagram can be removed by means of the redshift distribution $N(z)$. Figure 2 gives these predicted distributions compared with magnitude-limited samples[28,29,30]. Apparently the deepest sample cannot be fitted with the standard LF. In contrast, a dwarf-rich LF can accomodate the data, whatever value of $\Omega_0$ is taken. This suggests that high-$z$ galaxies are *smaller* on an average than those of the standard LF.

## 4. The bright galaxy counts

The bright end of the counts is not reproduced by standard models, which predict too shallow a slope. In fact, if the counts are normalised at magnitude 19 (that is, at an average redshift $z \simeq 0.1$), the *predicted* counts at magnitude 15 to 17 have twice the *observed* value. This discrepancy became obvious with the publication of the APM counts[31]. Of course, this can indicate that we are located in a hole and that the local number density is lower that the mean. Alternatively, the evolution of nearby galaxies may be stronger than derived from the classical scenarios. Large $e$-corrections steepen the slope of the counts. Figure 3 shows that steep-slope LF's ($-1.8 < \alpha < -1.5$) can accomodate the data with $\Omega_0 = 1$ as well as $\Omega_0 = 0.1$. Nevertheless the detection threshold of the APM is relatively bright. So it is not clear that most of the counted objects could be dwarfs.

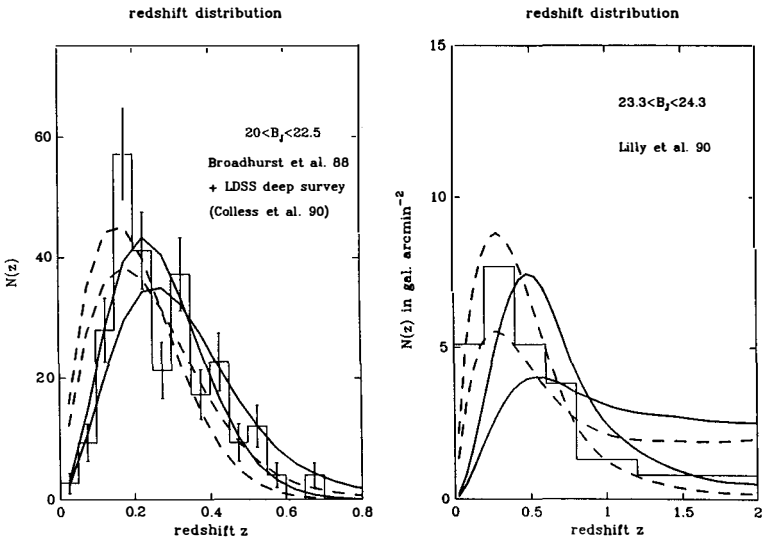


**Figure 2: Predicted redshift distributions.** *Solid lines:* $\alpha = -1.07$; *dashes:* $\alpha = -1.5$. *Upper curves:* $\Omega_0 = 0.1$; *lower curves:* $\Omega_0 = 1$. (a) $20 < B_J < 22.5$. Isophotal magnitudes at 26.55 mag arcsec$^{-2}$. (b) $23.3 < B_J < 24.3$. Isophotal magnitudes at 28.7 mag arcsec$^{-2}$.

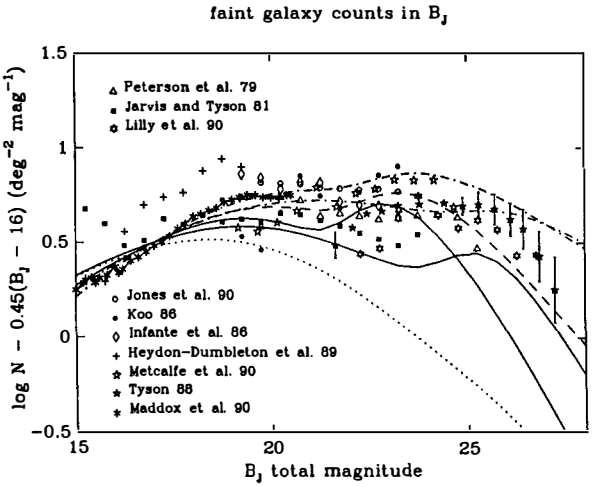


**Figure 3: Predictions for galaxy counts normalised at** $B_J = 17$. *Solid lines:* $\alpha = -1.07$ for $\Omega_0 = 0.1$ and 1; *dashes:* $\alpha = -1.5$ for $\Omega_0 = 1$; *dashes-and-dots:* $\alpha = -1.8$ for $\Omega_0 = 0.1$ and 1. At magnitude $\sim 24$, the $\Omega_0 = 1$ counts are over the $\Omega_0 = 0.1$ counts.

## 5. The faint galaxy counts revisited in the flat universe

In order to save inflation, Fukugita *et al.*[32] introduced a non–zero cosmological constant, which increases the observable volume of the universe, and consequently the observable number of galaxies. The authors reproduce the counts with $\Omega_0 = \Omega_b = 0.1$ (consistent with the constraints from primeval nucleosynthesis), and the suitable $\lambda_0 = 0.9$ for the flat universe. This case is shown in fig. 1d. In fact, a non–zero $\lambda_0$ can solve a number of observational puzzles[33]. Nevertheless, cosmologists are very reluctant to introduce a non–vanishing $\lambda_0$ since it would require the fine–tuning that the inflationary paradigm precisely tries to avoid.

Up to now, the general philosophy was to assume number conservation and to use the most plausible scenarios of evolution derived from previous studies in order to determine the values of $\Omega_0$ and $\lambda_0$. We shall hereafter assume that $\Omega_0 = 1$ and $\lambda_0 = 0$ (Einstein–de Sitter universe) and use the counts as constraints on the evolution of galaxies. For instance, a possible solution to reconcile the counts with the flat universe, is the introduction of a LF which differs from the one currently derived from nearby galaxy surveys. In order to reproduce the large number of faint objects, it is necessary to take a faint–end slope as steep as $\alpha = -1.5$. A large number of dwarfs is predicted by models of galaxy formation with the CDM power spectrum of fluctuations (see e.g. the most recent versions of these models in White & Frenk[34], and Lacey & Silk[35], and references therein). It is also suggested by the deep redshift surveys. Cowie *et al.*[27] reproduced the faint counts with such a population, although their fit is better in the near–IR than in the blue. The main problem is to assess the current fate of these objects. They might have so faint surface brightnesses by now that they are invisible in all surveys but the deepest ones. If we do not believe that most of the nearby galaxies are still undetected, we must conclude that these objects have disappeared. They might have been destroyed during an initial star burst, as preferred by Cowie *et al.*. Alternatively, a more plausible process is the accretion by bigger galaxies. In this latter case, there is no more number conservation, but there is still mass conservation.

## 6. The case of number evolution

### *6.1 – A scenario of merging–driven number evolution*

This assumption is a natural prediction of the CDM flat universe in which galaxies form from smaller units in a hierarchical scenario[36,37,38]. In Rocca–Volmerange & Guiderdoni[39], and Guiderdoni & Rocca–Volmerange[16], we presented a model in which evolution of galaxies is driven by merging. Giant galaxies result from the coalescence of a number of smaller objects. We model number–density evolution in a simple, phenomenological way by assuming two fundamental properties for the mass function (MF):

(1) *self–similarity.* We simply assume a Schechter comoving MF at redshift $z$:

$$\phi(M,z)dM = \phi^*(z)\left(\frac{M}{M^*(z)}\right)^{\alpha(z)} \exp -\frac{M}{M^*(z)} \frac{dM}{M^*(z)} \quad (5)$$

with $M^*(z)$ being the characteristic mass at the knee, $\phi^*(z)$ a characteristic density and $\alpha(z)$ the slope. These three parameters are allowed to vary with redshift. Such a formula can fit any evolving MF, at least approximately.

(2) *conservation of the total comoving mass density.* With eq. (5), this leads to:

$$M^*(z)\phi^*(z)\Gamma(\alpha(z)+2) = M^*(0)\phi^*(0)\Gamma(\alpha(0)+2) \quad (6)$$

The values $M^*(0)$, $\phi^*(0)$ and $\alpha(0)$ are fixed in order to fit the current LF of galaxies, with the consistent mass–to–light ratios computed in our model.

The actual number evolution probably acts on $M^*$, $\phi^*$ and $\alpha$. We introduce complementary attempts to approach this evolution, by assuming that only two of the three parameters change. We parametrize the evolution of one of the factors of eq. (6) as $(1+z)^\eta$, and we consistently compute the evolution of one of the other factors with keeping the last one as a constant. Thus, with the condition that galaxies are more numerous and less massive for increasing $z$, we get three series of models, namely the so–called $M^* - \phi^*$ model (with $\phi^*(z) = \phi^*(0)(1+z)^\eta$ and constant $M^*\phi^*$), $M^* - \alpha$ model (with $M^*(z) = M^*(0)(1+z)^{-\eta}$ and constant $M^*\Gamma(\alpha+2)$), and $\phi^* - \alpha$ model (with $\phi^*(z) = \phi^*(0)(1+z)^{-\eta}$ and constant $\phi^*\Gamma(\alpha+2)$). The actual evolution is probably a compromise between these three limiting cases. The parameter $\eta$ is free. Spiralling of companions down to galaxies due to dynamical friction could be the regulating process of merging and number evolution. Following Bahcall & Tremaine[40], we showed that it leads to values $\eta \simeq 1$ to 2[16].

Simulations suggested that in a forming galaxy, star formation triggered by cloud collisions exponentially decreases with time[41], as in our scenarios. So we keep our standard SFR histories. Of course, a more precise modelling of the merging–driven history of star formation would be needed. We only assume that it relatively acts more on colour distributions than on the number counts $N(m)$ that we consider as our primary constraint.

### *6.2 – Results*

Figure 4abc gives the results for the three limiting cases in visible and near–IR bands. Apparently all kinds of number evolution seem to conspire to reproduce the observational slope, whatever parameters of the LF are actually affected by evolution. Values $\eta = 1$ to 2 give comparable results[16]. The surface–brightness threshold in Tyson'counts[42] at $\mu_B = 28.7$ mag arcsec$^{-2}$ is so deep that the building blocks are visible in the survey. The second important point is that the condition of high $z_{for}$ is not necessary. The fit is here given for

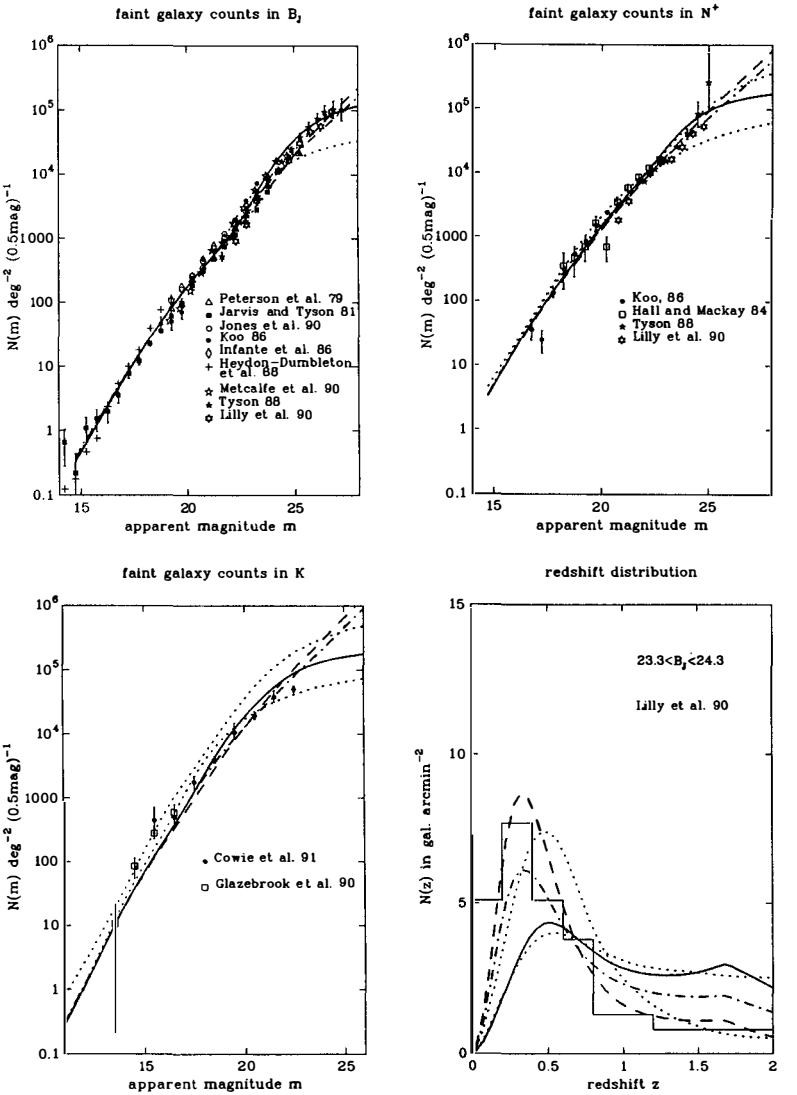


**Figure 4: Predictions with $(1+z)^\eta$ number evolution** in addition to the normal luminosity evolution, for three models (see text): *solid line:* $M^*$–$\phi^*$; *dashes:* $M^*$–$\alpha$; *dashes-and-dots:* $\phi^*$–$\alpha$. Here $\eta = 1.5$, $\Omega_0 = 2q_0 = 1$, and $\lambda_0 = 0$. The redshifts of galaxy formation are 5 for E's, 3 for Sa–Sb and 2 for later spirals. *Dotted lines:* predictions with the standard LF and $\Omega_0 = 0.1$ or 1. (a) Blue counts (4600 Å). (b) Red counts (7900 Å). (c) Near-IR counts (2.2 $\mu$m). (d) Redshift distribution at $23.3 < B_J < 24.3$.

$z_{for} = 2$ to 5, but the predictions are not very sensitive to the precise values. Figure 4d displays the redshift distributions. Apparently the best fit gives an increase of the slope $\alpha$ with redshift, suggesting that giant galaxies accrete dwarf objects. The colour distribution can also be accomodated with such a model[16], as well as other observational features[39].

The related mass evolution has to be as high as $\sim (1+z)^{-1.5}$. Such a large evolution is suggested by theoretical considerations on the accretion of companions by a giant galaxy after dynamical friction[16]. On an observational point of view, there is evidence for accretion of dwarfs in a lot of galaxies[43]. Nevertheless, strong number evolution is here needed, well above the current observational estimates based on *giant* galaxies. On the other hand, the thinness of galaxy disks put severe constraints on the amount of accretion[44]. In particular, the accreted objects must be diffuse enough in order not to heathen the disks.

## 7. Conclusions

(1) The increasing number of data on high–redshift galaxies now actually sets strong constraints on models of galaxy formation and evolution, and on the value of $\Omega_0$ (and $\lambda_0$).
(2) A conservative interpretation of the faint counts based on *standard* LF and type mix gives $\Omega_0 = 2q_0 \simeq 0.1$ and $z_{for} \geq 10$ (although the predicted near–IR counts seem to be too steep). Other cosmological tests using high–$z$ galaxies lead to this conservative conclusion[3].
(3) It is easy to save the flat universe by introducing a non–zero $\lambda_0$. It is also possible to accomodate the counts with $\Omega_0 = 1$ and $\lambda_0 = 0$, by introducing a dwarf–rich LF. In this latter solution, the current invisibility of the nearby dwarfs has to be explained.
(4) Alternatively one can relax the assumption of number conservation. We show that strong number evolution in the overall population of galaxies allows to fit the properties of high–redshift galaxies in an $\Omega_0 = 1$ universe with moderate redshifts of galaxy formation.

The deep redshift surveys do seem to suggest that the high–$z$ LF is dominated by dwarfs. This does not completely rule out the conservative $\Omega_0 \simeq 0.1$. Nevertheless it is more satisfactory to fit the counts in an Einstein–de Sitter universe with this dwarf–rich LF since it is a prediction of CDM models of galaxy formation. Either these objects are still present and we must explain why they are not detected in our environment, or they have been accreted by nearby galaxies. In this latter case, the evolution of galaxies is driven by merging. New studies of the properties of the blue, high–$z$ objects will help to confirm this interpretation.

**Acknowledgements.** I am grateful to Brigitte Rocca–Volmerange with whom most of this research has been done. I would like to thank the organizers for the stimulating ambiency of this Moriond meeting.

**References**

1. Loh, E.D., Spillar, E.J., 1986, *Astrophys. J.*, **307**, L1
2. Sandage, A., 1988, *Ann. Rev. Astron. Astrophys.*, **26**, 561
3. Guiderdoni, B., 1991, in *Observational tests of inflation*, T. Shanks et al. (eds.), Kluwer
4. Weinberg, S., 1972, *Gravitation and Cosmology*, Wiley, New York
5. Bruzual, G., 1981, Ph.D. dissertation, University of California Berkeley
6. Bruzual, G., 1983, *Astrophys. J.*, **273**, 105
7. Rocca–Volmerange, B., Lequeux, J., Maucherat–Joubert, M., 1981, *Astron. Astrophys.*, **104**, 177
8. Guiderdoni, B., Rocca–Volmerange, B., 1987, *Astron. Astrophys.*, **186**, 1
9. Rocca–Volmerange, B., Guiderdoni, B., 1988, *Astron. Astrophys. Suppl. Ser.*, **75**, 93
10. Yoshii, Y., Takahara, F., 1988, *Astrophys. J.*, **326**, 1
11. Arimoto, N., Yoshii, Y., 1986, *Astron. Astrophys.*, **164**, 260
12. Arimoto, N., Yoshii, Y., 1987, *Astron. Astrophys.*, **173**, 23
13. Maeder, A., Meynet, G., 1988, *Astron. Astrophys. Suppl. Ser.*, **76**, 411
14. VandenBerg, D.A., 1985, *Astrophys. J. Suppl. Ser.*, **58**, 711
15. Scalo, J.M., 1986, *Fundam. Cosmic Phys.*, **11**, 1
16. Guiderdoni, B., Rocca–Volmerange, B., 1991, *Astron. Astrophys.*, in press
17. Tinsley, B.M., 1980, *Astrophys. J.*, **241**, 41
18. Bruzual, G., Kron, R.G., 1980, *Astrophys. J.*, **241**, 25
19. Shanks, T., Stevenson, P.R., Fong, R., MacGillivray, H.T., 1984, *Month. Not. Roy. astron. Soc.*, **206**, 767
20. King, C.R., Ellis, R.S., 1985, *Astrophys. J.*, **288**, 456
21. Koo, D.C., 1989, in *The Epoch of Galaxy Formation*, C.S. Frenk, et al. (eds.), Kluwer
22. Guiderdoni, B., Rocca–Volmerange, B., 1989, in *The Epoch of Galaxy Formation*, C.S. Frenk et al. (eds.), Kluwer
23. Guiderdoni, B., Rocca–Volmerange, B., 1990, *Astron. Astrophys.*, **227**, 362
24. Yoshii, Y., Peterson, B.A., 1991, *preprint*
25. Metcalfe, N., Shanks, T., Fong, R., Jones, L.R., 1991, *preprint*
26. Efstathiou, G., Ellis, R.S., Peterson, B.A., 1988, *Month. Not. Roy. astron. Soc.*, **232**, 431
27. Cowie, L.L., Gardner, J.P., Wainscoat, R.J., Hodapp, K.W., 1991, *preprint*
28. Broadhurst, T.J., Ellis, R.S., Shanks, T., 1988, *Month. Not. Roy. astron. Soc.*, **235**, 827
29. Colless, M., Ellis, R.S., Taylor, K., Hook, R.N., 1990, *Month. Not. Roy. astron. Soc.*, **244**, 408
30. Lilly, S.J., Cowie, L.L., Gardner, J.P., 1990, *preprint*
31. Maddox, S.J., Sutherland, W.J., Efstathiou, G., Loveday, J., Peterson, B.A., 1990, *Month. Not. Roy. astron. Soc.*, **247**, 1P
32. Fukugita, M., Takahara, F., Yamashita, K., Yoshii, Y., 1990, *Astrophys. J.*, **361**, L1
33. Efstathiou, G., Sutherland, W.J., Maddox, S.J., 1990, *Nature*, **348**, 705
34. White, S.D.M., Frenk, C., 1991, *preprint*
35. Lacey, C., Silk, J., 1991, *preprint*
36. Frenk, C.S., White, S.D.M., Davis, M., Efstathiou, G., 1988, *Astrophys. J.*, **327**, 507
37. Carlberg, R.G., Couchman, H.M.P., 1989, *Astrophys. J.*, **340**, 47
38. Carlberg, R.G., 1990, *Astrophys. J.*, **350**, 505
39. Rocca–Volmerange, B., Guiderdoni, B., 1990, *Month. Not. Roy. astron. Soc.*, **247**, 166
40. Bahcall, S.R., Tremaine, S., 1988, *Astrophys. J.*, **326**, L4
41. Baron, E., White, S.D.M., 1987, *Astrophys. J.*, **322**, 585
42. Tyson, J.A., 1988, *Astron. J.*, **96**, 1
43. Larson, R.B., 1990, *Pub. Astron. Soc. of the Pac.*, **102**, 709
44. Ostriker, J., 1990, in *Evolution of the Universe of Galaxies*, R. Kron (ed.), Astr. Soc. Pac.

# MERGERS IN A CDM COSMOLOGY

R.G. CARLBERG
Department of Astronomy, University of Toronto,
60 St. George St., Toronto, Ontario, M5S 1A1, CANADA

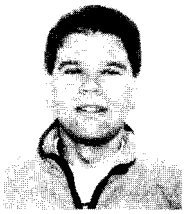

ABSTRACT Galaxy mergers are a consequence of gravitional forces in a clustered universe. Accounting for galaxy merging in a low bias CDM cosmology can reconcile the $\Omega = 1$, $\Lambda = 0$, CDM cosmology with recent measures of large scale clustering. At first sight a formal linear bias of $b_\ell \simeq 0.8$, which leads to the galaxies being anti-biased with respect to $\xi_{\rho\rho}$ on scales less than about $3h^{-1}$ Mpc, appears extreme, and might suggest very large $\Omega$ from dynamical estimators. However the galaxies in a cluster have velocities that are 0.69 of those in the dark matter, and as a result are more centrally concentrated, having a mean harmonic radius a factor of two less than the dark matter. Consequently the virial $\Omega$ measured in the cluster is 0.27. The pairwise peculiar velocities on small scales are 0.37 of those in the density field, where the single galaxy cooling is statistically augmented by the clustering anti-bias. The Cosmic Virial Theorem applied to the galaxy tracers yields $\Omega = 0.21$. A test of the importance of merging is the merger rate-redshift relation, which at low redshifts predicts that merging should increase approximately as $(1+z)^m$, with $m \simeq 4.5\Omega^{0.42}$. The current, scattered, data provides an indication that $m \simeq 5$. Although $z \lesssim 1$ merging does not significantly alter the mass function of galaxies, about 5%, it can cause significant perturbations to their luminosity function, which may account for the excess counts and weak correlations of faint galaxies.

## INTRODUCTION

Galaxies are a readily observed but nearly massless tracer of structure and dark matter in the universe. A basic understanding of galaxy formation, at least sufficient to identify their sites and kinematics of galaxies in relation to the dark matter is a crucial element for the interpretation of most cosmological observations. In any hierarchical theory for the formation of structure, such as CDM, merging is the fundamental process by which large objects are assembled from smaller units, and, as a gravitational process, is a relatively well defined problem accessible to current methods of quantitative study.

The significance of merging in the context of the standard $\Omega = 1$, $H_0 = 50\,\mathrm{km\,s^{-1}\,Mpc^{-1}}$, Cold Dark Matter (CDM) model for the formation of cosmic structure is considered here. The CDM model is characterised by one free parameter, the linear bias; $b_\ell = 1/\sigma_8$, where $\sigma_8$ is the *linear* extrapolation to $z = 0$ of the rms density fiuctuations in $8h^{-1}$ Mpc spheres. There are many apparent problems with standard CDM: the Hubble constant, $\Omega \sim 0.2$ for a galaxies trace mass interpretation of the data, and there are large "voids" and "walls" extending beyond 38 $h^{-1}$ Mpc where linear theory predicts *anti-correlation.*

Biasing the formation of galaxies to occur only at the high peaks of the density field results in a galaxy distribution which is more clustered than the overall density field (Kaiser 1984), which can correct the *biased* $\Omega \simeq 0.2$ from galaxies up to a *true* $\Omega = 1$ for the density field (Davis, *et al.* 1985, Bardeen *et al.* 1986). The value favoured in a landmark study was $b_\ell = 2.4$ (Davis *et al.* 1985). However observations of large-scale bulk velocities (Lynden-Bell *et al.* 1988) sets stringent upper limits on $b_\ell$: Kaiser and Lahav (1988) find $b_\ell \simeq 1.5$ for consistency with the CDM model, and the detailed velocity field reconstruction Bertschinger *et al.* (1990) indicates $b_\ell \simeq 0.74$. X-ray clusters are controversial and have been taken to indicate high (Evrard 1990) and low bias factors (Bond and Myers 1991). Moreover, the entire class of high-bias CDM models, in which large scale clustering is accurately predicted by linear theory, are excluded by the large scale structures found by de Lapparent, Geller and Huchra (1986) and the quantitative measures of the APM galaxy angular correlation function (Maddox *et al.* 1990a), the variance of counts in cells from the QDOT survey (Efstathiou *et al.* 1990, Saunders *et al.* 1991 ). On the other hand, fairly firm lower limits to the bias are provided by the upper limits to Microwave Background temperature fiuctuations, assuming standard recombination. Analysis of recent experiments at the Owens Valley radio observatory and the South Pole suggests $b_\ell \gtrsim 0.8$ (Bond *et al.* 1991 and Vittorio *et al.* 1991). The part of parameter space allowed in $\Omega = 1$ CDM models that remains relatively unexplored is thus less than a factor of two in linear amplitude.

A low bias, $b_\ell = 0.8$, CDM model is numerically constructed in Couchman and Carlberg (1991) to show that measurements of large-scale power and the existence of structure at high redshift can be accommodated within the CDM model. If galaxies accurately traced the clustering and kinematics of the dark matter this model would be stillborn, having an excessively steep correlation function, and absurdly large pairwise random velocities. A necessary and straightforward allowance for galaxy merging removes the first problem, and the previously recognized velocity bias removes the second. The degree of merging invoked can be tested for consistentency with observations thought to be directly related to interactions between galaxies, such as IRAS galaxies, quasars, and rather speculatively, the luminosity evolution of faint galaxies.

## LOW BIAS CDM

Evolving the CDM spectrum (e. g. Bond and Efstathiou 1984) to $b_\ell = 0.8$, approximately the limit allowed by the Microwave background measurements, is expected to enhance the structure on large scales, as indicated in the calculations of the correlation function with some low order nonlinearity (Bond and Couchman 1988, Coles 1990) which push the first zero of the correlation function to larger separations. The full nonlinear evolution still requires a large numerical simulation. A very large simulation is required,

since the large scale structure observations probe scales of $20\text{–}40h^{-1}$ Mpc, and simultaneously, individual galaxy size dark halos must be at least modestly resolved in the same simulation. Two dissipationless $\Omega = 1$ simulations were performed (Couchman and Carlberg 1991), each consisting of 2,097,152 particles in boxes with sides $100h^{-1}$ Mpc and $200h^{-1}$ Mpc. Individual particle masses then correspond to $2.65 \times 10^{11}\,M_\odot$ and $2.12 \times 10^{12}\,M_\odot$ in the small and large box respectively. Statistical quantities derived from these simulations were corrected by extrapolating the linear spectrum at the small wavenumbers beyond the size of the boxes to obtain the results for an effectively infinite universe. Running these large simulations to $b_\ell = 0.8$ presents a considerable technical challenge due to the high degree of clustering that develops. Couchman's (1991) hierarchical grid code, which is of order $10^2$ times faster than a standard $P^3M$ code for this problem, allowed a simulation to be done on a 4 Mflop machine in 2 cpu-months of time.

## GALAXY TRACER IDENTIFICATION

The statistical properties of the galaxies found in the "sticky particle" experiments of Carlberg & Couchman (1989) and the SPH experiments of Carlberg, Couchman and Thomas (1990) were approximately reproduced in the $b_\ell = 0.96$, small box, dissipationless, experiments of Carlberg (1991a) simply by identifying the particles in the dense central regions of galaxy mass dark halos at $z \simeq 2$ as galaxy tracers, and explicitly ignored any galaxy merging. That algorithm deliberately has no merging, to remove the statistical component of velocity bias (Berstchinger and Gelb 1991, and see below). Furthermore, conservation of galaxies from a high redshift in a $b_\ell = 0.8$ will give an unacceptably steep $\xi_{gg}$. Some modest allowance for galaxy merging, the information for which is already available in the dynamics of the experiment, is a necessary and desirable feature, and certainly is required for consistency with the results of the previous dissipative cosmological experiments.

The galaxy identification algorithm used is a "double filter" approach, motivated by the results of the dissipative experiments and the White and Rees (1978, and see White *et al.* 1987) scenario of galaxies forming at the bottom of dark halos with some subsequent merging. The algorithm proceeds as follows. First, identify "galaxy precursor" particles at $z \simeq 3$ (the precise results are not very sensitive to the selection parameter choices, see below) as those particles closer than 0.2 of the average interparticle separation, implying $\rho/\rho_0 > 125$; second, these particles are grouped into 'galaxies' at $z = 0$ at an overdensity of about 3000. This algorithm mimics the formation and merging of galaxies seen in the dissipative simulations, although the galaxies in the SPH simulations are considerably more cleanly defined and much less subject to tidal destruction. The standard results reported here used galaxy tracers having masses of 8-16 particles in the 100 $h^{-1}$ Mpc box, but the power spectrum is corrected using the long waves of the 200 $h^{-1}$ Mpc box, and the linear biased CDM spectrum beyond that box.

## CORRELATIONS AND ANTI-BIAS

The two-point spatial correlation function for both galaxies and density is shown in Figure 1 at an epoch corresponding to $b_\ell = 0.8$. The initial spectrum extrapolated to the same epoch is also shown. It is immediately apparent that non-linear effects are significant on large scales for this low value of $b_\ell$. Measured from the galaxy spectrum at the final epoch $J_3(10h^{-1}\,\text{Mpc}) = 0.83$ and the tophat variance $\sigma^2(8h^{-1}\,\text{Mpc}) = (0.95)^2$: extrapolation of the linear power spectrum would give values roughly 1.6 times larger.

The most striking feature of the galaxy correlation function is the presence of significant biases with respect to the density at both large and small scales. On separations exceeding 5 $h^{-1}$ Mpc the galaxy correlation is significantly enhanced near the scale of the downward break in the correlation function. This can be understood as the remnants of the high redshift statistical bias followed by strong dynamical clustering which draws galaxies into groups and

clusters whose correlation function and whose enhanced correlation is partially reflected in $\xi_{gg}$ at large separations.

The small-scale galaxy correlation is well fit by a power law of slope -1.7, which is measured to be relatively stable for quite wide variations in the parameters of the galaxy selection algorithm. For variations of the redshift of initial identification from 2 to 4.5, changes of the identification overdensities by an order of magnitude, varying the numbers of particles required in the galaxies by of a factor of 4 (which of course changes the numbers of galaxies) the correlation function for $\xi_{gg} > 0.1$ remains well approximated as $\xi_{gg} \sim (5.5 \pm 0.5/r)^{(-1.75 \pm 0.1)}$. It appears that in spite of the relatively simple nature of the galaxy algorithm, the basic features which it selects are generic to the dynamics of the simulations.

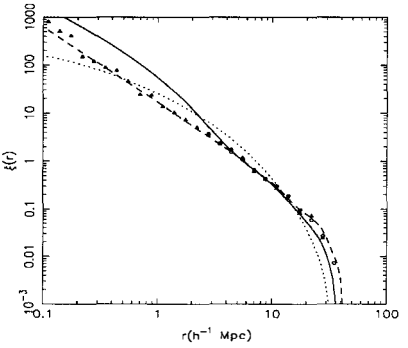


Figure 1: Correlations for the density (solid line) and galaxies (dashed line) at an epoch corresponding to $b_\ell = 0.8$. These correlations were obtained from the numerical simulations after correcting for the finite boxsize. The autocorrelation of the initial density field linearly extrapolated to $b_\ell = 0.8$ is shown by the dotted line. The filled symbols indicate the galaxy correlation measured directly from the $100h^{-1}$ Mpc box. Open symbols show the large-scale galaxy correlation measured from the $200h^{-1}$ Mpc box.

At separations of 0.1-3 $h^{-1}$ Mpc the galaxies are antibiased relative to the density by a factor of 2.5 to 3 in in correlation amplitude. An analysis of counts in cells shows that long tail to high densities that is present in the dark matter counts does not exist in the galaxy population. Hence, we conclude that the anti-bias arises because merging (and possibly tidal destruction) tends to reduce the numbers of galaxies in high density regions. The large antibias does raise a significant question about the $\Omega$ values that these simulations might give from virial theorem estimators, which is discussed in the next section.

The IRAS sparse sample (*c.f.* Saunders *et al.* 1990—the QDOT survey) has been used to estimate the variance of the galaxy distribution on large scales. Efstathiou *et al.* (1990) estimated the variance of counts in cubic cells and Saunders *et al.* (1991) estimated the variances when smoothed with Gaussian filters. The low bias simulation yields variances that are in accord with those observations with the exception of the 20 $h^{-1}$ Mpc Gaussian filter estimate, where there is some current controversy about the size of the error bar. There is no question that a high bias CDM cosmology would not have sufficient power to yield variances as large as those observed, as shown by Efstathiou *et al.* (1990). The enhanced clustering in the low bias CDM is a consequnce of considerable nonlinear evolution of the

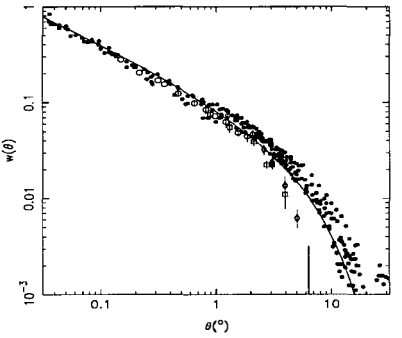


Figure 2: The angular correlation of galaxies. The symbols are as in Figure 3 of Maddox *et al.* (1990): filled circles indicate the new estimate of $w_{gg}(\theta)$, open symbols are from Groth & Peebles (1977). The solid line is the analytic projection of the galaxy correlation shown in Figure 1. The results have been scaled to the depth of the Lick survey as discussed in the text.

density field, a small positive clustering bias, $b_\xi \simeq 1.2$, at large separations, and including the long waves outside the box in the power spectrum.

The angular correlation function for galaxies measured from the APM galaxy survey provides a sensitive test of the galaxy two point correlation function at low amplitude on large scales due to the very large number of objects. Figure 2 shows the observed angular correlation as a function of angle after scaling to the depth of the Lick survey (see Maddox et al. 1990a for details). The symbols are the same as in Figure 3 of Maddox *et al.* (1990a). The luminosity function given by Maddox *et al.* (1990a) was used to calculate the effective selection function for galaxies as a function of coordinate distance assuming a catalogue magnitude limited at 18.4. At this limit the number density of galaxies is the same as in the Lick survey and assumes that the galaxy correlation function does not evolve significantly back to the effective depth of the Lick survey.

## COSMIC BIASES

The potential difficulty with low bias CDM is that the random peculiar velocities will be much larger those observed. This is certainly true in the dark matter where the 3D pairwise dispersion is $2300\,\mathrm{km\,s^{-1}}$ at $r = 0.5h^{-1}$ Mpc, whereas the observed values are in the range $400\text{-}1000\,\mathrm{km\,s^{-1}}$. The problems multiply in the presence of a small scale anti-bias, suggesting that the application of the virial theoreom would give $\Omega \simeq 3$.

The measured 1D pairwise velocities of the galaxy tracers in the simulation exhibit a large velocity bias, being 37% of that in the dark matter, amounting to $490\,\mathrm{km\,s^{-1}}$ at $r = 0.5h^{-1}\,\mathrm{Mpc}$. The origin of this velocity bias is briefly discussed in the next section. The observed value is somewhat unclear and subject to modelling uncertainties of projected data. Davis and Peebles (1983) give $\sim 350\,\mathrm{km\,s^{-1}}$, Bean *et al.* (1983) find $\sim 200\,\mathrm{km\,s^{-1}}$, but Hale-Sutton *et al.* (1989) find $\sim 600\,\mathrm{km\,s^{-1}}$. As the data of Carlberg, Couchman and Thomas (1990) show, there are large moment to moment fluctuations in this number, mainly depending on the state of large cluster mergers. Although the simulation velocities at this particular epoch are possibly somewhat high, the substantial uncertaintities of galaxy identification, and the current inability to perform simulations that resolve overdensities at which galaxies exist, $\gtrsim 10^6$, leads to sufficient uncertainties in the numerical value that it is premature to reject the low bias CDM on the basis of these slightly excessive velocities.

The Cosmic Virial Theorem estimate of the global $\Omega$, is given by $\sigma_{12}^2(r)/H_0^2 r^2 Q\xi(r)P_\gamma$ (Peebles 1980), where $\sigma_{12}$ is the pairwise peculiar velocity dispersion of galaxies, $P_\gamma$ is a constant fixed by the slope of the correlation function, and $Q$ is the amplitude in the standard model for the reduced three-point correlation function. The amplitude $Q$ was found to be roughly constant at $Q = 1.0 \pm 0.3$, within the errors, for a range of triangle shapes and sizes, interestingly smaller than the $Q = 1.5$ of the dark matter. The three point function measures the variance in numbers of galaxies around a galaxy, which merging would likely tend to reduce. The result is $\Omega \simeq 0.21$.

## RICH CLUSTER BIASES

The largest relatively quiet cluster has a total mass of $\simeq 4 \times 10^{15}\,M_\odot$ within an overdensity contour of 125 and contains 41 galaxies having 4 or more particles. The most massive, central galaxy of this cluster contains 67 particles. The chosen cluster has recently captured two small bound groups with which it is in the process of merging. The cluster had a line-of-sight dispersion in the dark matter of $\simeq 1480\,\mathrm{km\,s^{-1}}$. The dispersion in the galaxies was $\simeq 1020\,\mathrm{km\,s^{-1}}$ giving a bias in velocities 0.69. As a consequence of the cooler galaxies and equilibrium dynamics, the profile of the galaxy distribution is steeper than that of the dark matter (Carlberg and Dubinski 1991), a crucial feature if these model data are to be consistent with observed dynamical estimates of cluster mass-to-light ratios. The harmonic mean radius was $0.93h^{-1}$ Mpc; 53% that of the dark matter. The ratio of the estimated virial mass to the total mass, $\Omega = 0.27$. This estimate is mass-weighted except that the central group was assigned only average weight. Number weighting the estimate raises the implied $\Omega$ to 0.34.

## BIAS PHYSICS

The dominant biases in these simulations appear to have their primary origin in the dynamics of clustering. In the absence of merging the galaxy correlations would have a small positive bias with respect to the dark matter, a faint remnant of the original, large, statistical bias of galaxies, which is evident as the $b_\xi \simeq 1.1 - 1.2$ at separations beyond $10\ h^{-1}$ Mpc. Galaxy merging creates the anti-correlation on small scales. The fourteen most massive dark matter haloes contain 8% of the particles and contribute 66% of the total correlation. These haloes have 6% of the galaxies associated with them which contribute 38% of the galaxy correlation. This spatial segregation of pairs is roughly sufficient to account for the factor of 2.5 antibias for the galaxies.

Velocity bias is comprised of two nearly equal components. In the richest cluster, the individual galaxies are cooled to about 0.69 of the dark matter dispersion velocity, roughly in accord with with the biases found in a higher resolution experiment of a single cluster (Carlberg & Dubinski 1991). The value is a smoothly varying function of the overdensity of the initial selection of the galaxy tracers, and as a consequence of straightforward equilibrium stellar dynamics the radial density profile of the cool population is steeper and more centrally concentrated (West & Richstone 1988) than that of of the relatively hotter dark matter population. The reduction of pairs through merging in clusters (Bertschinger and Gelb 1991) accounts for about $1/\sqrt{2.5} \simeq 0.63$ of the bias, creating the total observed pairwise velocity bias 0.37. On scales $\gtrsim 10h^{-1}$ Mpc, the *pairwise* velocity bias, is consistent with the single galaxy bias found within clusters.

The origin of single galaxy velocity bias is controversial. The galaxies do not have the same velocity acceleration relation as test particles, roughly consistent with dynamical friction on the massive correlated halos as galaxies (and groups of galaxies) accrete onto a cluster. The massive dark halos are eroded by tidaly stripping as the galaxies fall in, ultimately leaving relatively light, low friction, galaxies to orbit in the cluster (Carlberg 1991a).

## THE MERGER RATE-REDSHIFT RELATION

Galaxy mergers are an important manifestation of the low redshift tail of galaxy formation activity and from the above discussion are quite important for the interpretation of cosmological measurements. The *approach* to a collision between two galaxies is completely dominated by well understood gravitational forces, although the eventual outcome of a merger may be dependent on such details as the relative masses, gas content, and star formation processes in the two galaxies. In any cosmology where galaxies grow from gravitational perturbations, the redshift dependence of the merger rate is relatively easily calculated, using no physics other than gravity, and with all free parameters normalized by well-determined dynamical properties of galaxies. The merger rate–redshift relation is important because it provides support for fundamental theory that describes the growth of structure from gravitational perturbations. The fact that the merger rate varies approximately as $(1+z)^m$, with $m \simeq 4.5\Omega^{0.4}$, permits a relatively sensitive low redshift cosmological test. It should be emphasized that as a *differential* measurement, normalized to galaxy data, the redshift variation is not strongly dependent on the particular value of the bias, $b_\ell$, that galaxies have.

The theoretical merger rate can be calculated as the merger rate of galaxy mass dark halos times the fraction of those mergers that occur at sufficiently low velocities that the visible galaxies will merge. The merger rate calculation is based on the Press-Schechter (1974) theory, which gives the number of dark halos as a function of mass and redshift, in terms of the variable $\nu$, the normalized Gaussian variable which gives the peak height of the perturbations which are just virializing, where $\nu = \delta_c/(\sigma_0(M)b(t))$, and $\delta_c$ is a constant close to unity that sets the overdensity required for turnaround and collapse ($\delta_c \simeq 1.4$ for a Gaussian filter) The fractional mass variance in a region containing mass $M$ at time $t$ is $b(t)\sigma_0(M)$. The fraction of galaxy encounters which lead to merging is taken to be the fraction of a Maxwellian velocity distribution which is at $v < v_{mg}$, the cutoff velocity for merging. The merger rates are not too sensitive to the precise value of $v_{mg}$, so, given a typical galaxy with a circular velocity of 200 km s$^{-1}$ , $v_{mg}$ is set at the escape velocity, 280 km s$^{-1}$ (Aarseth and Fall 1980). The galaxy merger rate is consequently (Carlberg 1991b),

$$\frac{d\,n_g}{dt}\Delta M = \frac{\rho_0}{\sqrt{8\pi}}\gamma\left(\frac{3}{2},\frac{1}{2}(\frac{v_{mg}}{v_p})^2\right)e^{(-\nu^2/2)}\nu\frac{d\ln b(t)}{dt}\Delta M, \tag{1}$$

for masses in the range $M$ to $M+\Delta M$. The three dimensional pairwise velocity dispersion for galaxy separation encounters at the current epoch is estimated to be 600 km s$^{-1}$ (Davis and Peebles 1983, Bean, *et al.* 1983). At earlier times the encounter velocity is,

$$v_p(t) = 600\,\mathrm{km\,s^{-1}}\left[\frac{b(t)}{b(t_0)}\right]^{\frac{1-n}{3+n}}\left[\frac{a(t)}{a(t_0)}\right]^{-1/2}, \tag{2}$$

where $n$ is the index that describes the slope of the density perturbation spectrum on the scale of galaxies, and $b(t)$ describes the growth of perturbations ($b(t) = (1+z)^{-1}$ for $\Omega = 1$). The observed correlation function and the rate of growth of velocities in simulations both indicate $n \simeq -1.5$.

A convenient parameterization of the merger rate dependence is, $\frac{dn}{dt} = \frac{dn}{dt_0}(1+z)^m$, where all the parameter dependence of the merger rate has been absorbed into the quantity $m$. As discussed in Carlberg (1991b) the dependence on the parameters in the vicinity of $\Omega = 1$, $\Lambda = 0$, is

$$m = 4.5\Omega^{0.42}(1-\frac{\Lambda}{3H_0^2})^{-0.11}M_{12}^{-0.04}\left(\frac{-n}{1.5}\right)^{0.81}\left(\frac{v_{mg}}{280\,\mathrm{km\,s^{-1}}}\right)^{-0.10}, \tag{3}$$

where $M_{12}$ is the mass of the galaxy and associated dark halo in units of $10^{12}M_\odot$. The equivalent power law index $n$ is constrained by the current epoch galaxy correlation function, and is directly observable as the pairwise velocity dispersion at small separations. The

adopted value, $n = -1.5$, predicts that at $z$=0.5 the pairwise dispersion has dropped to 0.71 of the $z$=0 value.

The best way to estimate the index $m$ of the merger rate-redshift relation is to ratio the merger rates at two relatively low redshifts. This differential measurement avoids the problem of having to determine the absolute merger frequency. Furthermore, low redshifts are relatively accessible to observation, and are farthest in time removed from the messy "epoch of formation" featuring multiple mergers, and a complex redshift dependence for the predicted merger rate.

A growing body of observational evidence suggests a rapid increase in the galaxy merger rate with increasing redshift. The evidence for a higher rate of dynamical interactions in the past (summarized in the Table below) is almost all indirect, and is necessarily limited to small samples of objects because of the faintness of galaxies at intermediate redshifts. The merger rate index $m$ is thought to lie in the range $3 \lesssim m \lesssim 7$. When averaged together, the current data on $m$ appear to marginally rule out $\Omega \lesssim 0.2$, for any $\Lambda$, and hence is not compatible with $H_0 t_0 \simeq 1.3$.

Table I

| *Objects* | $N(z > 0.1)$ | $m$ | *Comments* | *Ref* |
|---|---|---|---|---|
| Kepler Orbits | theory | 2.5 | scale free hierarchy | 1 |
| Peak Collapse | theory | $4.5\Omega^{0.42}$ | Press-Schechter | 2 |
| close pairs | $\simeq$10 | 4±2.5 | no redshifts | 3 |
| cluster blueing | $\simeq$300 | $\approx$5 | indirect merger estimator | 7, 12, 13 |
| faint galaxy $n(z)$ | $\simeq$100 | $\approx$5 | indirect | 4, 5 |
| IRAS counts | $\simeq 10^4$ | $\approx$3 | no redshifts, indirect | 8 |
| QSOs | $\simeq$300 | $\approx$6 | indirect, uncertain physics | 9,10 |
| IRAS z's | $\simeq$100 | 6.7±2.3 | indirect, wide $L$ sample | 11 |

References: *1.* Toomre 1977, *2.* Carlberg 1991b, *3.* Zepf and Koo 1989, *4.* Colless, *et al.* 1990, *5.* Broadhurst, *et al.* 1990, *7.* Butcher and Oemler 1984, *8.* Lonsdale *et al.* 1990, *9.* Schmidt and Green 1983, *10.* Boyle, Shanks and Peterson 1988, *11.* Saunders, *et al.* 1990, *12.* Dressler and Gunn 1983, *13.* Lavery and Henry 1988.

## FAINT GALAXIES

Faint galaxy counts, colours, redshift distribution, and correlations cannot be reproduced with the smooth reverse evolution of the stars in current epoch galaxies in an $\Omega = 1$ cosmology. Unfortunately, the inconsistencies can be removed by relaxing any of a number of assumptions. This section calculates the redshift evolution of the galaxy luminosity function as a result of the increasing rate of galaxy interactions which cause small changes in the numbers but large luminosity enhancements.

A long standing problem with faint galaxies is that their numbers exceed, by a factor of 4 or so, the prediction made using standard k correction (wavelength shifting of the spectrum) for non-evolving galaxies, and including e corrections (stellar evolution) still leaves a problem of about a factor of two (Tyson and Jarvis 1979, Peterson, *et al.* 1979, Kron 1980). It has long been realized that lowering $\Omega$ to values around 0.2, and optionally introducing a $\Lambda$ to retain a flat universe, can reconcile the counts with a standard evolution model Brown and Tinsley 1974, Bruzual and Kron 1980, Yoshii Takahara 1988, Guideroni and Rocca-Volmerange 1990, Fukujita, *et al.* 1990, Lilly 1991). There are several possible problems associated with lowering $\Omega$. Cowie, *et al.* (1991) find that the excess of faint galaxies in the K band over the standard evolution model requires a smaller reduction in $\Omega$ than the B band counts, suggesting that the effect may arise from galactic evolution rather than the geometry of the universe (Brown and Tinsley 1974).

Various forms of luminosity evolution, while conserving numbers, have been attempted to reconcile the number count problem. King and Ellis (1985) presented a model for the

evolution of the counts in which they considered the separate evolutionary corrections for bulges and disks, noting that the corrections are relatively larger for old spheroid populations. Broadhurst *et al.* (1988) proposed a qualitative model, in which lower luminosity dwarf spiral galaxies have increased brightnesses at $z \approx 0.5$, causing the effective luminosity function to have an increased density normalization, without an increase in the characteristic luminosity. The calculation presented here is in the spirit of the Broadhurst *et al.* (1988) model, but done with a detailed dynamical model for the evolution of merging interactions which predicts relatively little change in the underlying mass function at low redshifts. Rocca-Volmerange and Guideroni (1990) have presented a merger model for faint galaxies which requires that the mass of the average galaxy is about 5 times lower at a redshifts of 1.5, much larger than expected from the dynamical merger theory given above.

The overwhelming difficulty posed by faint galaxies is that the redshift distribution of faint galaxies was expected to contain objects with redshifts exceeing 1, particularly for the faint blue galaxies, none of which are found in the current surveys. In fact, the median redshift is so low as to be consistent with an unphysical model without any stellar luminosity evolution at all (Broadhurst, *et al.* 1988 Colless, *et al.* 1990, Lilly, Cowie and Gardner 1991). These spectroscopic data are of far smaller samples than the count distribution, and a significant fraction, about 20-30%, of the spectra have no identifiable redshift. The implications of the observed redshift distribution remains controversial, suggestions include a brightening of the numerous dwarf galaxies at modest redshifts (Broadhurst, *et al.* 1988) a rapid reduction in the numbers below $z \simeq 1$ through merging (Rocca-Volmerange and Guideroni 1990), a new population of objects for which there are no redshift zero counterparts (Efstathiou *et al.* 1991, Cowie *et al.* 1991). It is extremely important to determine the redshifts of *all* the galaxies at a given flux level, and to build up an empirical understanding of the k and evolution corrections for galaxy luminosities.

A number conserving, luminosity evolution model is advanced here as a necessary redshift correction above a smooth evolution model, although the particular form and parameters chosen are likely to be less universally accepted. At redshift zero the luminosity function contains a significant fraction, about 1%, of galaxies that have been increased in brightness through a merger or interaction (Larson and Tinsley 1978) which temporarily makes them bluer and increases their brightness. The fraction of such galaxies increases rapidly with redshift, and can be accurately calculated using the dynamical theory sketched above. Interactions cause a small, but temporarily very bright, burst of star formation, adding only a small amount to the stellar mass of the galaxies, about 4% over an entire Hubble time in the model advanced here, without significantly changing the number of galaxies, since the most common event is the interaction or infall of a relatively low mass galaxy, like the LMC, with one of the near $L_*$ galaxies that dominate the observed faint galaxy population. However, since the lumonsity function varies as $L^{-1}$, a factor of two brightness increase doubles the number of galaxies at a given luminosity, if the entire population is undergoing such bursts. Only the disk component of a galaxy is assumed to be capable of sustaining star formation, the large fractional mass in ellipticals and spheroids of disk galaxies does not participate in these bursts.

The change in the luminosity function at an observed redshift $z_o$ as a result of mergers and interactions is the number of galaxies brightened into the range $[L, L+dL]$ as a result of mergers occuring at any redshift greater than the redshift of observation, minus the number brightened out of that luminosity range,

$$\Delta\phi(L, z_o)dL = \int_{t(z_o)}^{z_m} R_{mg}(t)(\phi(L/B(t_o - t)) - \phi(L))\, dt\, dL \qquad (4)$$

where $t_o = \frac{2}{3}H_0^{-1}(1+z)^{-3/2}$, and the brightening factor for a merger at time $t_b$, observed at time $t_o$ is $B(t_o, t) = \frac{L_b}{M}/\frac{L_*}{M}$. The combination of k and e corrections in the specified observational band is encapsulated in the effective luminosity to light ratio $L_*/M$ and $L_b/M$, for the standard population and the standard plus burst population. A set of tables gives the $L/M$ ratios.

The basic luminosity function can be built from models having a high redshift for the beginning of star formation, $z_f = 30$ was used here, and with 5 different time scales for star formation, 1, 3, 5, 9, and 15 Gyr, in an exponential model, roughly corresponding to E/S0 galaxies, Sa, Sb, Sc, Sdm (Charlot and Bruzual 1991, Yoshii and Takahara 1988, Guideroni and Rocca-Volmerange 1990). The filter luminosities at an observed redshift $z_o$ of the galaxies that are underwent an induced burst of star formation at $z_b$ is $L_b(z_o) = L_s(z_o)(1+f_{gas}M/L_s(z_o)/L(z_o,z_b)/M)$ where $L(z_o,z_b)/M$ is computed under the assumption that the burst is very short, $5 \times 10^7$ years, although even 30 times longer timescale for star formation makes little difference to the results. The fraction of the galaxy's mass that can be converted into new stars is specified by $f_{gas}$ and is limited by the results to be no more than 3% of the galaxy's total stellar mass. The available gas contents of the [E, Sa, Sb, Sc, Sdm] galaxies are taken to be [0, 0.01, 0.02, 0.04, 0.20] (e. g. Mihalas and Binney 1981).

At redshift zero the luminosity function contains a small fraction of galaxies that have been brightened and blued by recent mergers. Therefore the luminosity function at an observed redshift $z_o$ is $\phi(L,z_o) = \phi_{ke}(L,z) - \Delta\phi_{ke}(L,z_o=0) + \Delta\phi_{ke}(L,z_o=0)$ where the burst component is the difference between the redshift zero rate and the $z_o$ rate of merging, with all luminosities k and e corrected.

The low redshift luminosity functions are critical input data, particularly for the gas rich lower luminosity galaxies. The general character of the results do not change, and with the exception of the redshift distributions quite a wide range of luminosity functions can fit the number counts, colour distributions, and correlations. For comparability we follow Yoshii and Takahara (1988) and Guideroni and Rocca-Volmerange (1990) and use Schechter fits to the various galaxy types. There is compelling evidence spirals have a steeper luminosity function, with $\alpha$ nearly 1.5, for spirals (Sandage, Binggelli and Tammann 1985, Efstathiou *et al.* 1988) accordingly the luminosity function parameters $(\phi_*, M_*, \alpha)$ for [E, Sa, Sb, Scd, Sdm] are chosen as [(0.35,-21.1,0.5), (0.07,-20.9,1.0), (0.18,-20.4,1.25), (0.17,-19.9,1.5), (0.23,-19.45,1.5)] with $\phi_*$ in units of $4.0 \times 10^{-3}\mathrm{Mpc}^{-3}$.

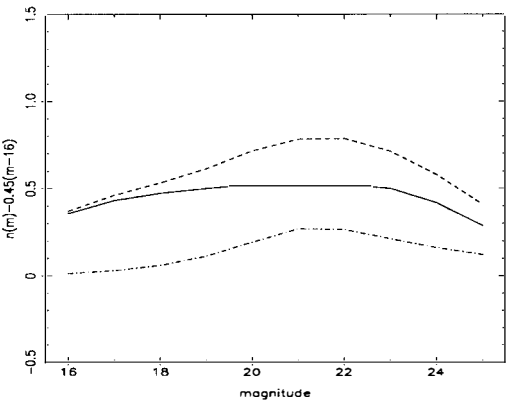


Figure 3: The predicted blue counts, normalized to a slope of 0.45. The solid line is the result standard evolution of the 5 galaxy types, the dashed line shows the effect of including the increase in galaxies whose luminosity has been enhanced through interaction induced star formation. The dot-dashed line gives the ratio of the two count predictions.

The addition of a brightened merging component increases the counts of faint galaxies, as shown in the $n(m_B)$ relation of Figure 3, address the difficulties raised in Maddox *et al.* (1990b) within an $\Omega = 1$, no merging model. To better constrain the models it would be extremely useful to have counts over larger, independent fields at $m_B > 24$.

The "extra" galaxies introduced by galaxy interactions peak at $z \simeq 1$ for the adopted parameter $\delta_c/\sigma = 1.2$. This appears to be the best compromise available, lower parameter values cause merging to peak at the present, higher ones create vast numbers of unobserved $z > 1$ galaxies. Even so, this model predicts 13% of the $m_B = 21$ galaxies are at $z \gtrsim 1$, which is apparently *not* observed. The statistical $\sim 20\%$ incompleteness of current redshift surveys (Broadhurst *et al.* 1988, Colless *et al.* 1990) gives a low statistical significance to the discrepancy. The median redshift at $m_B = 21.5$ is predicted to be 0.48, whereas 0.31 is observed by Colless *et al.* . On the other hand if the approximately 30% incompleteness is assigned to missing high redshift galaxies then the median redshift of the remaining objects is expected to be 0.35. The statistical difficulties are worsened by the clustering in redshift space.

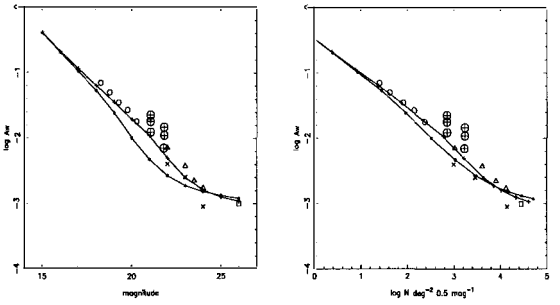


Figure 4: The predicted correlation amplitude as a function of blue magnitude, B for the theoretical estimates and $b_J$ for the data (about 0.25 magnitudes fainter typically). The circles are from the APM results of Maddox *et al.*, the x's from Infante and Pritchet (1991), the triangles from Koo and Szalay (1984), and the square from Efstathiou *et al.* 1991. The circled plus signs are calculated from the Broadhurst *et al.* (1988) and Colless *et al.* (1990) samples assuming $\epsilon = -1.2, 0, 2$, from top to bottom.

The amplitude of the expected and observed angular correlations are shown in Figure 4. These are $A_w$, the correlation amplitude at 1 degree, calculated under the assumption that the current correlation length is $5.4h^{-1}$ Mpc and the 3D correlation has a power law slope of $\gamma = 1.668$ (Maddox *et al.* 1990). The correlation evolves with redshift as $(1+z)^{-(3+\epsilon)}$, where $\epsilon$ is zero for a fixed cluster model, and $\epsilon = -1.2$ for clustering fixed in co-moving co-ordinates. Only the $\epsilon = 0$ model is acceptable, and there is n-body support for clustering evolution stronger than the $\epsilon = -1.2$ hypothesis (in which physical clustering decreases with time). At the faintest levels the correlation amplitudes are similar to those reported by Infante and Pritchet (1991) and is a little larger than the value of $9.8 \times 10^{-4}$ reported in Efstathiou *et al.* (1991) scaled from their 30″ measurement using their correlation slope of $\gamma = 1.668$. their measurement.

It is of interest to compute the predicted $A_w$ for the Broadhurst *et al.* (1988) and Colless *et al.* (1990) $n(z)$, shown in Figure 4 as circled plus signs. The highest correlation is produced by an $\epsilon = -1.2$ evolution, the lower two being $\epsilon = 0$ and 2, respecitively. It would appear that either the $m_B$ to B magnitude conversion requires about a shift of nearly an entire magnitude, or, that the sample is missing some galaxies at redshifts near 1 which would reduce the predicted correlation. Given that the counts are consistent with the models and

other datasets, it seems most likely that the inconsistency lies in the redshift distribution, possibly partly due to the $(1+z)^4$ surface brightness dimming and subsequent selection effects discussed in Guideroni and Rocca-Volemerange (1991).

At the very least, this model establishes that the lower limit to the merger time scale is 20 Gyr, and 40Gyr will fit most of the data. The total mass in stars formed over all redshifts in the "best fit" model is 4.1% of the pre-existing stellar population. The average number of interactions per galaxy from redshift 1 to the present is 0.5, most likely with a small companion rather than a rather improbable nearly equal mass merger.

This model can be conclusively ruled out with complete redshift samples, and certainly would call for a population of galaxies which are not numerous at redshift zero. Conventional cosmological dynamics argues against a large reduction due to merging between redshift 0 and 1/2. Similarly tidally destruction of galaxies should not be sensitively redshift dependent.

## SUMMARY

Understanding how galaxies reflect the large scale structure of the universe is a key problem. Accounting for the relatively modest amount of galaxy merging since the first appearance of galaxies can reconcile the current measures of large scale clustering in the universe with the CDM cosmology, although it requires a fairly drastic increase in the overall amplitude of the CDM spectrum, to $b_\ell = 0.8$. As a consequence of this hypothesis galaxies must be *anti-correlated* on separations of under 3 $h^{-1}$ Mpc. By itself such a large anti-bias would predict a huge $\Omega$ but the large cosmological velocity bias, 0.69 for individual galaxies in clusters, and 0.37 for the pairwise velocities produces reasonable virial theorem $\Omega$ values in clusters and in the field. The cooled galaxies must have a steeper density profile and be more concentrated in clusters than the dark matter, which represents a potential test of the idea. The particular value of $b_\ell = 0.8$ is an extreme limit. With slight modifications of the galaxy finding algorithm and simulations with increased resolution other values near $b_\ell \simeq 1$ should also be acceptable, although anything much exceeding 1 must fail due to the absence of any significant nonlinearity.

Galaxy merging continues to the present, which allows investigation of the evolution of merging in the universe. Aside from its importance to large scale clustering, various observations have emperically indicated a connection of merging and interactions to such diverse phenomena as IRAS galaxies, AGN activity, and blue galaxies in clusters, all of which indicate an interestingly rapid dependence of frequency of occurence on redshift. Since the merger rate measures the growth structure in the universe it is a constraint on the $\Omega - \Lambda$ pair. Current observations, when averaged together weakly exclude $\Omega \lesssim 0.2$, for any $\Lambda$.

The available data indicates a merger timescale considerable larger than a Hubble time, implying relatively little change in the galaxy mass function at $z \lesssim 1$. A somewhat speculative application of the merger and interaction rate-redshift relation to faint galaxies predicts increasing numbers ofluminosity enhanced galaxies, peaking around redshift 1, which is compatible with the counts, correlations, but is marginally inconsistent with the redshift distributions–however the current (somewhat incomplete) $n(z)$ distributions suffer the deffect that they are not compatible with the observed correlation estimates.

The general conclusion is that merging is a generic and important phenomenon which because of its gravitational nature is capable of a relatively clear theoretical understanding. Currently however, only a general sketch of the process is available requiring much improved n-body, theoretical and observational work for a complete and useful description of this low redshift tail of the epoch of galaxy formation.

## ACKNOWLEDGMENTS

The low bias CDM study was done in collaboration with Hugh Couchman. The Canadian NSERC provided financial support.

REFERENCES


Aarseth, S. J. and Fall, S. M. 1980, *Ap. J.*, **236**, 43
Bardeen, J. M., Bond, J. R., Kaiser, N. and Szalay, A. S. 1986, *Ap. J.*, **304**, 15
Bean, A. J., Efstathiou, G., Ellis, R. S., Peterson, B. A. and Shanks, T. 1983, *M.N.R.A.S.*, **205**, 605
Bond, J. R. and Couchman, H. M. P. 1987, in *Proc. Second Canadian Conference on General Relativity and Relativistic Astrophysics*, ed. Coley, A. and Dyer, C., World Scientific
Bond, J. R., and Efstathiou, G. E. 1984, *Ap. J. (Letters)*, **285**, L45
Bond, J. R., Efstathiou, G., Lubin, P. and Meinhold, A. 1991, Phys. Rev. Lett., **66**, 2179
Bond, J. R. and Myers, S. T. 1991, in *Trends in Astroparticle Physics*, ed D. Cline (World Scientific: Singapore)
Boyle, B. J., Shanks, T., Peterson, B. A. 1988, *M.N.R.A.S.*, **235**, 935
Broadhurst, T. J., Ellis, R. S. and Shanks, T. 1988, *M.N.R.A.S.*, , **235**, 827
Brown, G. S. and Tinsley, B. M. 1974, *Ap. J.*, **195**, 555
Bruzual, A. G. and Kron, R. G 1980, *Ap. J.*, **241**, 25
Butcher, H., and Oemler, A. 1984, *Ap. J.*, **285**, 426
Cowie, L. L., Garnder, J. P., Wainscoat, R., & Hodapp, K-W. 1991, preprint
Carlberg, R. G. 1990, **350**, 505
Carlberg, R. G. 1991a, *Ap. J.*, **367**, 385
Carlberg, R. G. 1991b, *Ap. J.*, **375**, 429
Carlberg, R. G. and Couchman, H. M. P. 1989, *Ap. J.*, **340**, 47
Carlberg, R. G., Couchman, H. M. P. and Thomas, P. A. 1990, *Ap. J. (Letters)*, **352**, L29
Carlberg, R. G. and Dubinski, J. 1991, *Ap. J.*, **369**, 13
Coles, P. 1990, *M.N.R.A.S.*, **243**, 171
Colless, M., Ellis, R. S., Taylor, K., and Hook, R. N. 1990, *M.N.R.A.S.*, **244**, 408
Couchman, H. M. P. 1991, *Ap. J. (Letters)*, **368**, L23
Couchman, H. M. P. and Carlberg, R. G. 1991, *Ap. J.*, submitted
Couchman, H. M. P. and Bond, J. R. 1987, in Large Scale Structure and Motions in the Universe, eds. Mezzetti, M., Giuricin, G., Mardirossian, F. and Ramella, M., Kluwer
Davis, M. and Peebles, P. J. E. 1983, *Ap. J.*, **267**, 465
Davis, M., Efstathiou, G., Frenk, C. S. and White, S. D. M. 1985, *Ap. J.*, **292**, 371
de Lapparent, V., Geller, M. J., and Huchra, J. P. 1986, *Ap. J. (Letters)*, **302**, L1
Dressler, A., and Gunn, J. E. 1983, *Ap. J.*, **270**, 1
Efstathiou, G., Ellis, R. S. and Peterson, B. A. 1988, *M.N.R.A.S.*, **232**, 431
Efstathiou, G., Kaiser, N., Saunders, W., Lawrence, A., Rowan-Robinson, M., Ellis, R. S. and Frenk, C. S. 1990, *M.N.R.A.S.*, **247**, 10P
Efstathiou, G., Bernstein, G., Katz, N., Tyson, J. A., and Guhathakurta, P. 1991, preprint
Evrard, G. 1990, *Ap. J.*, **363**, 349
Fukujita, M., Takahara, F., Yamashita, K, and Yoshii, Y. 1990, i *Ap. J. (Letters)*, **361**, L1
Groth, E. J. and Peebles, P. J. E. 1977, *Ap. J.*, **217**, 385
Guideroni, B. and Rocca-Volmerange, B. 1990, *Astr. Ap.*, **227**, 362
Guideroni, B. and Rocca-Volmerange, B. 1991, preprint
Hale-Sutton, D., Fong, R., Metcalfe, N. and Shanks, T. 1989, *M.N.R.A.S.*, **237**, 569
Kaiser, N. 1984, *Ap. J. (Letters)*, **284**, L9
Kaiser, N. and Lahav, O. 1988, in *Large-Scale Motions in the Universe*, ed. Rubin, V. C. and Coyne, G. V., Princeton University Press
King, C. R. and Ellis, R. S. 1985, *Ap. J.*, **288**, 456
Koo, D. C. and Szalay, A. S. 1984, *Ap. J.*, **282**, 390
Kron, R. G. 1980, *Ap. J. Suppl.*, 43, 305
Larson, R. B. and Tinsley, B. M. 1978, *Ap. J.*, **219**, 46
Lavery R. J. , and Henry, J. P. 1988, *Ap. J.*, **330**, 596
Lilly, S. J. 1991, preprint.
Lilly, S. J., Cowie, L. L., and Gardner, J. P. 1991, *Ap. J.*, **369**, 79
Lonsdale, C. J., Hacking, P. B., Conrow, T. P., and Rowan-Robinson, M. 1990, *Ap. J.*, **358**, 60

Lynden-Bell, D., Faber, S. M., Burstein, D., Davies, R. L., Dressler, A. Terlevich, R. J. and Wegner, G. 1988, *Ap. J.*, **326**, 19
Maddox, S. J., Efstathiou, G., Sutherland, W. J. and Loveday, J. 1990a, *M.N.R.A.S.*, **242**, 43P
Maddox, S. J., Sutherland, W. J. Loveday, J., Efstathiou, G., and Peterson, B. A. 1990b, *M.N.R.A.S.*, **247**, 1P
Mihalas, D. and Binney, J. 1981, *Galactic Astronomy*, (Freeman: San Fransisco)
Peebles, P. J. E. 1980, *The Large-Scale Structure of the Universe*, Princeton University Press
Peterson, B. A., Ellis, R. S., Kibblewhite, E. J., Bridgeland, M. T., Hooley, T., Horne, D. 1979 *Ap. J. (Letters)*, **233**, L109
Press, W. H. and Schechter, P. 1974, *Ap. J.*, **187**, 425
Rocca-Volmerange, B. and Guideroni, B. 1990, *M.N.R.A.S.*, **247**, 166
Saunders, *et al.* 1990, *M.N.R.A.S.*, **242**, 318
Saunders, W., Frenk, C. S., Rowan-Robinson, M., Efstathiou, G., Lawrence, A., Kaiser, N., Ellis, R., Crawford, J., Xia, X.-Y. and Parry, I. 1991, *Nature*, **349**, 32
Sandage, A., Binggelli, B., and Tammann, G. A. 1985, *A. J.*, **90**, 1759
Schmidt, M. and Green, R. F. 1983, *Ap. J.*, **269**, 357
Toomre, A. 1977, in *Evolution of Galaxies and Stellar Populations*, ed. B. M. Tinsley and R. B. Larson, (Yale Observatory: New Haven) p. 401
Tyson, J. A. and Jarvis, J. F. 1979, *Ap. J. (Letters)*, **230**, L153
Vittorio, N., Meinhold, P., Muciaccia, P. F., Lubin, P. and Silk, J. I. 1991, *Ap. J. (Letters)*, **372**, L1
West, M. J. and Richstone, D. O. 1988, *Ap. J.*, **335**, 532
White, S. D. M., Davis, M., Efstathiou, G. and Frenk, C. S. 1987, *Nature*, **330**, 451
White, S. D. M. and Rees, M. J. 1978, *M.N.R.A.S.*, **183**, 341
Yoshii, Y. and Takahara, F. 1988, *Ap. J.*, **326**, 1
Zepf. S. E., and Koo, D. C. 1989, *Ap. J.*, **337**, 34

# FAR-IR AND SUBMILLIMETER BACKGROUND RADIATION

# The Diffuse Background at Far-IR Wavelengths

M.H. Jones & M. Rowan-Robinson
Queen Mary and Westfield College, Mile End Road, London E1 4NS.

**Abstract**

The diffuse background at far-IR wavelengths (60-100$\mu$m) contains two sources of foreground emission; one arising from warm zodiacal dust and another from cool interstellar dust, as well as the contribution from any cosmological isotropic component. Using the IRAS survey data we describe a method of modelling the zodiacal emission based on a semi-empirical model for the interplanetary dust cloud. Subtraction of this model from the scan data yields maps of the large scale emission due to interstellar dust. Comparison with 21 cm data confirms that the known correlation between dust and gas distributions is valid over most of the sky and down to scales of a few arcminutes. We also review how an estimate to the upper limit to the isotropic background at 60$\mu$m has been obtained from the IRAS data. In conjunction with published COBE results, this allows estimates of the upper limits to the diffuse background at 100, 150 and 250 $\mu$m to be made. These limits may be used to constrain the evolution of spiral galaxies inferred from the QDOT redshift survey.

# 1 Introduction

There are two recognised components of foreground emission at far-IR wavelengths ($\lambda \sim 100\mu$m) which must be accounted for before any estimate may be made of the cosmological isotropic background in this band. These foreground components arise from emission from Zodiacal and interstellar dust. Although the emission from the Zodiacal dust is strongest at about 10-20$\mu$m, it still contributes significantly to the observed emission at 60 and 100$\mu$m. This dust cloud (in which the Earth is embedded) has a smooth density distribution which may be reasonably well described by an empirical model. Emission from cool dust in the galaxy is predominately at 100$\mu$m and reveals the complex structure of the interstellar medium. Although the distribution of interstellar dust can be approximately described by a cosecant law (Boulanger and Perault 1988) it cannot be predicted in detail using a simple model.

In this paper we shall describe, with reference to IRAS data, how the foreground and background components of diffuse emission have been separated. This allows an upper limit to the far-IR background to be estimated. Any isotropic far-IR background is likely to arise primarily from the summed contribution of unresolved sources. It is assumed here that these sources belong to the already known populations of far-IR emitting galaxies, these being predominately normal late spiral and starburst galaxies. The background limit is used to constrain the simple analytic models for the density or luminosity evolution that have been attributed to these populations.

# 2 Separation of the Components

Several approaches have been adopted to remove the smoothly varying Zodiacal component. Boulanger and Perault (1988) adopted a simple analytic form (a cosecant law) for the variation of Zodiacal emission with ecliptic latitude. In the study of narrow asteroidal band features near the ecliptic plane, Dermott *et al* (1986) used a Fourier decomposition to filter out the emission which varies with low spatial frequencies.

The approach used by Rowan-Robinson *et al* (1990) was to adopt a physical model for the zodiacal dust emission. This has an advantage over previously used techniques in that it gives allows the measurement of absolute fluxes from large scale emission. At present, theoretical models for the Zodiacal dust density distribution do not give a satisfactory fit to the observations. This is due to the considerable problem of calculation of dust particle trajectories which spiral in towards the Sun under the Poynting-Robertson effect but are perturbed by the planets (Misconi, 1980) and time variable Lorentz forces (Consolmagno, 1979). However, several analytic expressions for dust density distribution have been suggested as empirical models (see Giese *et al*, 1986, for a comparative study). The form adopted by Rowan-Robinson *et al* (1990) is the modified fan model, which had previously been found to be a good representation of 2-30$\mu$m sounding rocket data by Murdoch and Price (1985). This model is axially symmetric, but with a plane of symmetry which is tilted with respect to the ecliptic. It was assumed that the Sun lies at the centre of the plane of symmetry. The fan model has the form;

$$n(r) = n_0 r^{-\gamma} (\cos\beta_0)^Q \exp(-a \sin|\beta_0|) \quad (1)$$

Where $r$ is distance from the sun (in AU), $\beta_0$ is the angle between the line of sight and the symmetry plane of the dust cloud. The parameters of the model are; $n_0$, the dust density in the symmetry plane at 1 AU, and $Q$ and $a$ which essentially describe the scale height of dust above the plane. For the radial dependence it was assumed that $\gamma = 1.3$ as inferred from scattered Zodiacal light measured using Helios by Lienert *et al* (1981). As the dust emission is not obviously different from a blackbody (Hauser *et al*, 1984), grey-body emission was assumed. The temperature of grains was assumed to vary as $T(r) = T_0 r^{-1/2}$, where $T_0$ is the temperature at 1 AU.

The zero point for the calibration of the IRAS scan data was determined using a simple model for the the variation of the background diffuse emission at the ecliptic poles (see IRAS ***Explanatory Supplement***, section VI). With a more sophisticated model it is possible that the zero-point may change, but is still likely to lie

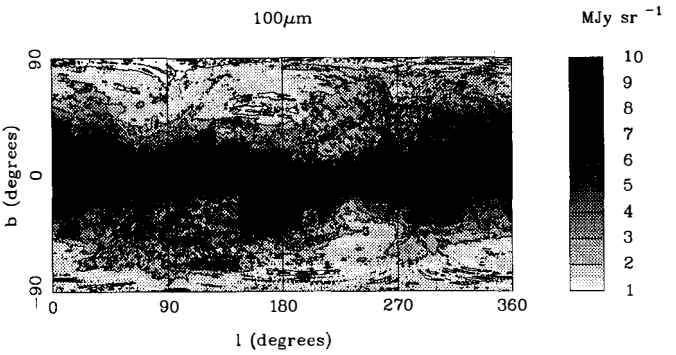


Figure 1: Grey-scale and contour map of 100$\mu$m emission, in galactic coordinates, after subtraction of the model of Rowan-Robinson *et al* (1990). The contours are from 1 to 10 MJy Sr$^{-1}$ in steps of 1 MJy Sr$^{-1}$.

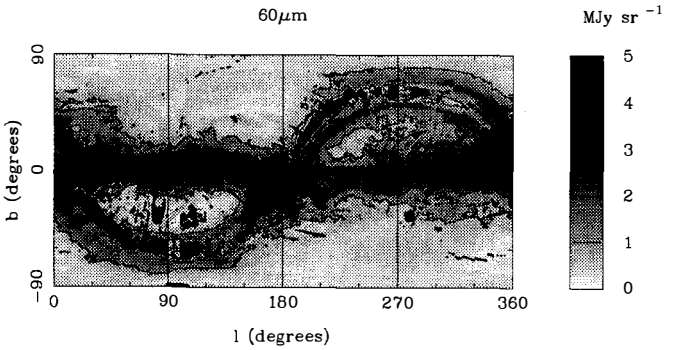


Figure 2: Grey-scale and contour map of 60$\mu$m emission, in galactic coordinates, after subtraction of the model of Rowan-Robinson *et al* (1990). The contours are from 0 to 5 MJy Sr$^{-1}$ in steps of 1 MJy Sr$^{-1}$.

Table 1: The Fitted Offset terms from the Zodiacal model fitting of Rowan-Robinson *et al* (1990), and the $1\sigma$ errors associated with the zero point of the IRAS calibration (from the IRAS *Explanatory Supplement*).

| $\lambda$ ($\mu$m) | 12 | 25 | 60 | 100 |
|---|---|---|---|---|
| Fitted Offset $D_\nu$ (MJy Sr$^{-1}$) | 1.3 | 1.7 | -1.2 | 2.2 |
| Zero point error (MJy Sr$^{-1}$) | 1.6 | 3.6 | 1.0 | 1.6 |

within the uncertainties quoted for the calibration value. To account for this, the fitted model also included a constant offset term ($D_\nu$) for each waveband. $D_\nu$ would also include any isotropic diffuse component.

The data set used to determine the parameters of the best fit model was version 3 of the Zodiacal Observation History File. This is a form of the IRAS scan data which has been rebinned to a resolution of $\approx 0.5°$. To remove biasing due to galactic emission and the asteroidal dust bands, the regions with $|b| < 30°$ and $|\beta| < 15°$ were excluded from the fitted data set.

The values of model parameters (including the angle between the symmetry plane and the ecliptic and longitude of the ascending node) obtained by fitting to this data set were found to be similar to those obtained in previous studies (e.g. Lienert *et al*, 1981). Of particular interest here are the values of $D_\nu$, which are summarised in table 1. In conjunction with the zero point errors, these values may be used to obtain upper limits to the diffuse background at these wavelengths.

## 3 Maps of Galactic Emission

By subtracting the best-fit Zodiacal model from the scan data, maps of emission due to interstellar dust may be formed. This has been done by Rowan-Robinson *et al*(1991) using the model described above to form 0.5° maps at 60 and 100$\mu$m. These maps may be of particular use at other wavelengths since the dust column density may be used to predict visual extinction and the magnitude of photoelectric absorption in a given direction.

These two maps are shown here in figures 1 and 2. In both maps the high column density of dust in the galactic plane is evident. Note that point sources have not been removed from the map, and some bright sources, such as the LMC at $l, b$=(280,-33) are clearly visible. The ecliptic plane is evident at 60$\mu$m due to the asteroidal dust bands. At 100$\mu$m it may be seen that the galactic poles are not dust free, but that there are several extended regions of low dust column density at high galactic latitude. These 'holes' are centered at $l, b = (160°, 55°)$ and $(85°, 75°)$. These correspond closely to the holes of 21 cm emission discovered by Lockman *et al* (1986) although their minima do not coincide exactly.

Boulanger and Perault (1988), in a detailed study of large scale emission from interstellar dust, note that the 100$\mu$m intensity ($I_\nu(100)$) follows the column density of HI ($N_{HI}$) as determined from 21 cm measurements, and found that;

$$I_\nu(100) = 0.085 \times 10^{19} N_{HI} \qquad (2)$$

(where $I_\nu$ is in MJy Sr$^{-1}$ and $N_{HI}$ is in atoms cm$^{-2}$). The validity of this relationship may be tested over a large region of the sky by forming a ratio map of $I_\nu(100)/N_{HI}$ (figure 3). This was done using the 100$\mu$m maps described above and the Bell Labs antenna 21 cm data of Stark *et al* (in preparation). Note that the resolution of the 21 cm data is $\approx 2.5°$. It was found that equation 2 is constant to within 30% over 90% of the sky. It is also evident from figure 3 that there is a decline in $I_\nu/N_{HI}$ towards the galactic anticentre due to the lower intensity of starlight in this direction. Towards the galactic centre $I_\nu/N_{HI}$ increases with the intensity of the interstellar radiation field.

A map which is sensitive to the temperature of dust may be formed by calculation of the quantity, $C = I_\nu(100) - 5 \times I_\nu(60)$ (as suggested by Wesselius, 1990, XXVIII COSPAR meeting). Cirrus at the mean observed temperature will have $C = 0$ and hot regions will have negative values. Figure 4 shows a map of $C$, and it

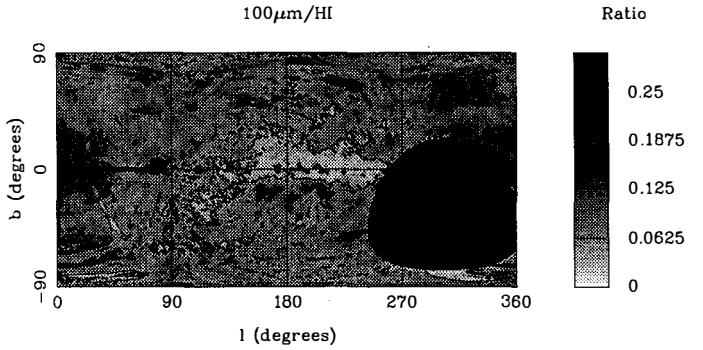


Figure 3: Grey-scale and contour map of the ratio $I_\nu(100)/N_{HI}$ in galactic coordinates. Contours from 0.0 to 0.3 in steps of 0.06, units are $10^{-19}$ MJy $Sr^{-1}$ $cm^2$.

may be seen that at high galactic latitudes the map is relatively bland, indicating a reasonably constant dust temperature. In the galactic plane, there are white (warm) regions which correspond to regions of active star formation. In many cases these are adjacent to black (cool) areas due to emission from dust in molecular clouds which is self-shielded from the interstellar radiation field. The association of these cool regions with molecular clouds is confirmed by the good correspondence with maps of CO emission.

## 4 Small Scale Correlation of Dust and Gas Distribution

Work is in progress to study the correlation of 100$\mu$m and 21 cm emission down to scales of a few arcminutes. High resolution maps may be formed by using the individual detector data to show small scale deviations from the large scale emission. Averaged over a few square degrees, the maps of Rowan-Robinson *et al* (1991) provide the best available estimate of diffuse emission at 100$\mu$m. It should be noted that in addition to the Zodiacal modelling described above, the coarse map data are subject to selection criteria and are smoothed - see Rowan-Robinson *et al* (1991) for details. In forming the high resolution maps scan data are normalised by demanding that the average brightness density over 5° x 0.5° strips equals that measured from the coarse map.

As yet the area covered by 21 cm data at a similar resolution is rather limited. It is found that for the 1° x 6° region for which we have detailed 21 cm mapping of a region of very low column density (courtesy of A. Pedlar, Jodrell Bank), that the correlation between 100$\mu$m emission and $N_{HI}$ is good. Figure 5 shows the 21cm and 100$\mu$m maps of the region at 3 arcmin resolution. There is good correspondence between the two maps, the area of very low column density between Dec = +52° and +53°, and the large triangular area of cirrus to the South of this area are clearly similar. The major difference between the two maps is the presence of point sources in the IRAS map. There is no evidence in these maps for any significant separation of the dust and gas on scales down to a few arcmin.

## 5 An Estimated Upper Limit to the Far-IR Background

While awaiting the results from COBE it is possible to use the IRAS data to estimate an upper limit to the diffuse background in the far-IR band. Oliver *et al* (1991) have shown that the strongest constraint is provided by the limit at 60$\mu$m. The fitted value of $D_\nu$ (table 1) is $(-1.2 \pm 1.0)$ MJy $sr^{-1}$, giving a $2\sigma$ limit

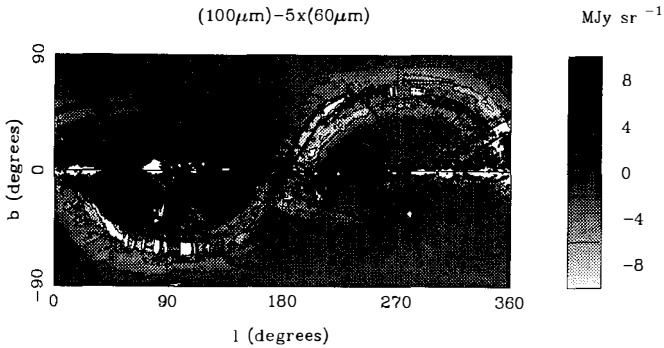


Figure 4: Grey-scale and contour map of the temperature sensitive quantity ($I_\nu(100) - 5 \times I_\nu(60)$) in galactic coordinates.

Table 2: The estimation of upper limits to the background at far-IR wavelengths, all brightness densities are given in MJy sr$^{-1}$. COBE data are from Mather *et al* (1990b).

| $\lambda$ ($\mu$m) | 60 | 100 | 150 | 250 |
|---|---|---|---|---|
| Measured Upper limit (IRAS) | $\leq 1.0$ | – | – | – |
| Total Observed (COBE) | 4.7 | 4.0 | 6.4 | 5.3 |
| Zodiacal Dust | 3.35 | 1.44 | 0.74 | 0.31 |
| Interstellar Dust | 0.33 | 1.71 | 3.64 | 3.23 |
| Total Foreground | $\geq 3.7$ | 3.1 | 4.4 | 3.5 |
| Inferred Upper limit | – | 0.9 | 2.0 | 1.8 |

of 2.0 MJy sr$^{-1}$. COBE was designed to make absolute flux measurements, and Mather *et al* (1990a) claim that there is a calibration error with the diffuse emission measured by IRAS. By comparison of the IRAS and COBE 60$\mu$m fluxes measured at the South ecliptic pole, it is found that the IRAS measurements are too large by a factor of 1.9. Thus the $2\sigma$ limit to the 60$\mu$m background is $\approx 1$ MJy sr$^{-1}$. The COBE flux measured at the SEP is 4.7 MJy sr$^{-1}$ (Mather *et al*, 1990b) and so the foreground emission at 60$\mu$m at the SEP must be at least 3.7 MJy sr$^{-1}$. The contribution to this from Zodiacal and interstellar dust is 3.35 MJy sr$^{-1}$ and 0.33 MJy sr$^{-1}$ respectively (see column 1 of table 2). The contribution to the foreground at longer wavelengths may be obtained using the spectral models for the foreground components. The models adopted by Oliver *et al* (1991) for this extrapolation are the Zodiacal model described above and the interstellar grain model compiled by Rowan-Robinson (1990) (see below). These foreground components at 100, 150 and 250$\mu$m are summarised in columns 2 to 4 of table 2. By subtraction of the predicted foreground from that observed using COBE, limits to the background are estimated to be 0.9, 2.0, and 1.8 MJy sr$^{-1}$ at 100, 150 and 250$\mu$m respectively.

## 6 Evolution of the Spiral Galaxy Population

Evidence for evolution of the population of IR emitting galaxies was given by Hacking *et al* (1987) following a deep IRAS survey near the South ecliptic pole (Hacking and Houck, 1987). It was found that the source counts at 60$\mu$m imply that there were either significantly more IR emitting galaxies at earlier epochs, or that they had

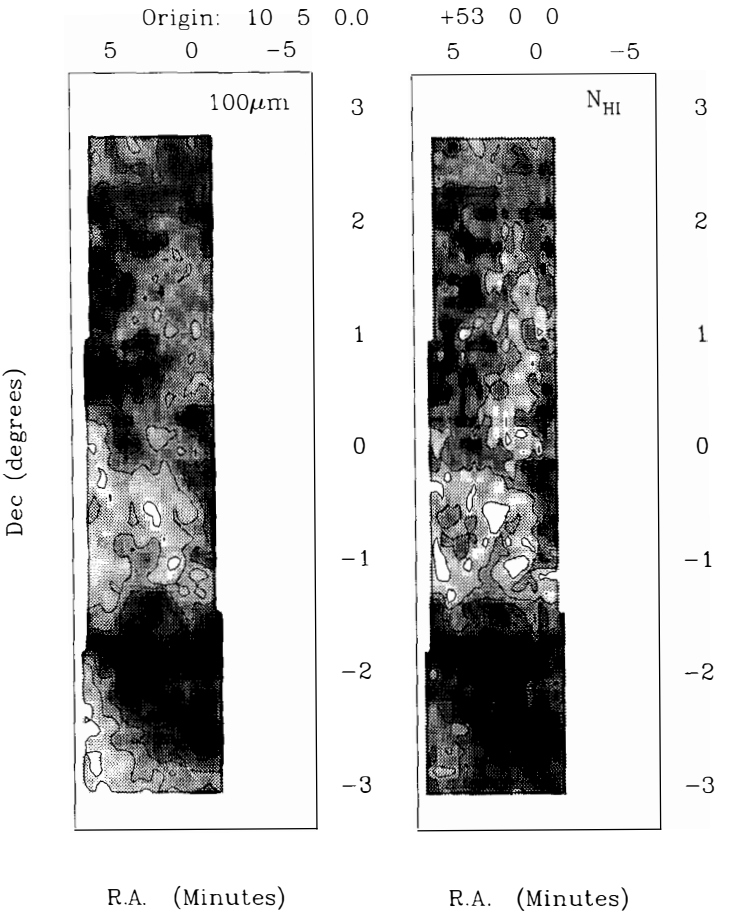


Figure 5: Grey-scale and contour maps of 100$\mu$m and 21 cm emission in a region of low column density. Both maps are at a resolution of 3 arcmin, 100$\mu$m data is contoured from 0.25 to 0.85 MJy $Sr^{-1}$, with a spacing of 0.12 MJy $Sr^{-1}$. The 21 cm data contours are from 0.6 to 1.1 x $10^{20}$ H atoms $cm^{-2}$. (21 cm data courtesy of A.Pedlar).

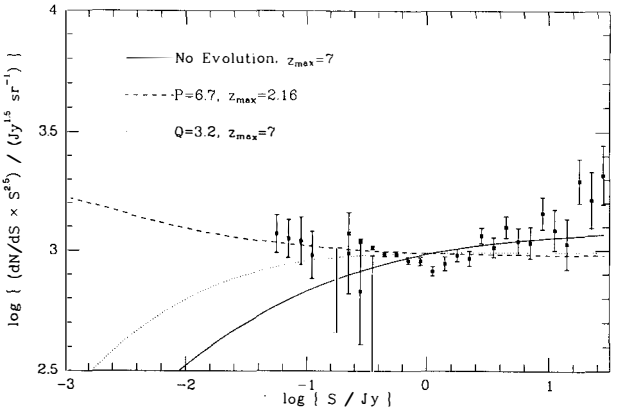


Figure 6: 60$\mu$m normalised differential source counts. Data from Lonsdale *et al* (1990, solid squares) and Hacking and Houck (1987, crosses). The theoretical curves are for no evolution (solid line), and density ($P = 6.7$, dashed line) and luminosity ($Q = 3.2$, dotted line). At these flux levels the counts are not sensitive to the redshift cut-off ($z_{\max}$) adopted.

higher luminosities in the past, or that there has been a combination of these two effects. Other surveys, such as presented by Danese *et al* (1987), Francheschini *et al*, (1988), and Lonsdale *et al* (1990), also support the view that there has been strong evolution of the population of IR emitting galaxies.

Simple analytic forms that are commonly used to describe this density or luminosity evolution are one parameter models. For density evolution, the comoving density of sources $\rho$ at a time $t$ (redshift $z$) is;

$$\rho(t) = \rho(t_0)(1+z)^P \tag{3}$$

Where $t_0$ is the current epoch. This form was suggested by Hacking *et al* (1987) on the basis that evolution is dominated by the collision rate between galaxies. If $\rho_p$ is the proper density of sources and $\bar{v}$ is the mean relative velocity, then $P = 6$ (rate $\propto \rho_p^2$) or P=7 (rate $\propto \bar{v}\rho_p^2$).

For luminosity evolution in a $\Omega_0 = 1$ universe, the model in which source luminosity decreases exponentially with time is;

$$L(t) = L(t_0)\exp\left(\frac{2Q(1-(1+z)^{-3/2})}{3}\right) \tag{4}$$

The physical motivation behind this model is that it should reflect the depletion of gas available for star formation with time.

Saunders *et al* (1990) has fitted both these forms of evolution to data from the QDOT (QMW, Durham, Oxford and Toronto) redshift survey of IRAS selected galaxies. The survey is a 1 in 6 selection of sources with $S_\nu \geq 0.6$ Jy, and contains 2163 galaxies at $|b| > 10°$. The evolution parameters obtained were $Q = 3.2 \pm 1.0$, $P = 6.7 \pm 2.3$. The 60$\mu$m differential source counts are shown in figure 6. Also shown are the predicted source counts for the best fit density and luminosity evolution models. It is not possible to discriminate between the two models with the QDOT data; source count studies are unlikely to resolve the question of which scenario is a better description of observed population evolution before the advent of ISO (which should be able to detect source fluxes down to the 10mJy level). However, these limits on the diffuse background do allow some constraints to be placed on these forms for the evolution.

There are three distinct emission components thought to be responsible for far-IR emission from galaxies, all of which seem to have reasonably well defined canonical spectra. These components are;

1. A 'cool' disc component. This arises from the heating of interstellar grains by the radiation field of the normal stellar population. The typical spectrum of this component is now reasonably well understood, having undergone refinement from the classical models of 0.1 $\mu$m radius silicate and graphite grains to the inclusion of short wavelength components ($3-60\mu m$) arising from a population of small (non-equilibrium) grains (see e.g. Puget and Leger, 1989). A spectrum compiled by Rowan-Robinson (1990) is shown in figure 7a.

2. A 'warm' Starburst component. Models of expected spectra have been developed by Crawford and Rowan-Robinson (1986) and Efstathiou and Rowan-Robinson (1991a) based on radiative transfer models in which hot stars are surrounded by optically thick (to UV) dust shells. See figure 7b.

3. A 'warm' Seyfert component. Dust in the narrow line region illuminated by a power law continuum can explain the characteristic spectrum, peaking at 25 $\mu$m see figure 7c. Models of this type, made under various assumptions of the geometry of the dust cloud have been investigated by Efstathiou and Rowan-Robinson (1991b).

Classification of observed IR galaxies on the basis of far infrared colour temperature was suggested by Rowan-Robinson and Crawford (1989) as a method of indication of the dominant component. Two classes were suggested; those with cool 25-60-100 $\mu$m colours primarily show emission from the disc component, whereas galaxies with warm 25-60-100 $\mu$m colours are dominated by Starburst or Seyfert emission.

Saunders *et al* (1990) used this classification and provided local densities of the two components, separating galaxies on the basis of whether the 60/100 micron colour temperature was less than or greater than 36 K. The space density of Seyferts is low enough that to a good approximation it may be assumed that the 'warm' component has a Starburst type spectrum. There is no evidence, as yet, that the cool and warm components evolve differently. The background spectra shown here (from Oliver *et al*, 1991) have calculated assuming the evolution described above applies to both components.

Figure 8a shows the results obtained from a luminosity evolution model which has been cut-off at a maximum redshift of $z_{max} = 10$ (the calculation for $z \gtrsim 10$ is unreliable because of the uncertainty of the spectrum at $\lambda \lesssim 2$ $\mu$m). The background lies well below the current upper limits. For the density evolution model however (figure 8b), the IRAS limits on the far-IR background are violated for modest cut-off redshifts, with a maximum allowable redshift of $z_{max} \approx 1.5$. Thus, if density evolution is occurring at the measured rate, then the background limit suggests a rather late epoch for Spiral galaxy formation. This would be expected in some scenarios of galaxy interaction, such as that suggested by Carlberg (this meeting) which would appear to be similar to density evolution with a cutoff at $z \sim 1$.

## 7 Summary and Future Prospects

The zodiacal modelling from the IRAS data now gives a reasonable description of the interplanetary dust cloud for $|\beta| \gtrsim 15°$. A full empirical description including the asteroidal dust bands which apparently originate from the Eos and Themis families (Dermott *et al*, 1984) is being developed. With a full zodiacal model it will be possible to make maps of interstellar dust emission at 60 and 100 $\mu$m which are reliable at all ecliptic latitudes. The present maps of interstellar dust emission show that there is no evidence for the separation of dust and gas on scales down to a few arcminutes. On large scales the most prominent change in the dust/gas ratio seems to arise from the variation in the interstellar radiation field throughout the galaxy.

The IRAS data provide an estimate to the upper limit to any isotropic diffuse background in the far-IR. Following foreground modelling similar to that described here, the COBE data should provide more precise limits than can be obtained from IRAS. This may, at last, provide a positive detection of the background in the far-IR. If this is near to the upper limit presented here, there is a possibility of measurement of fluctuation

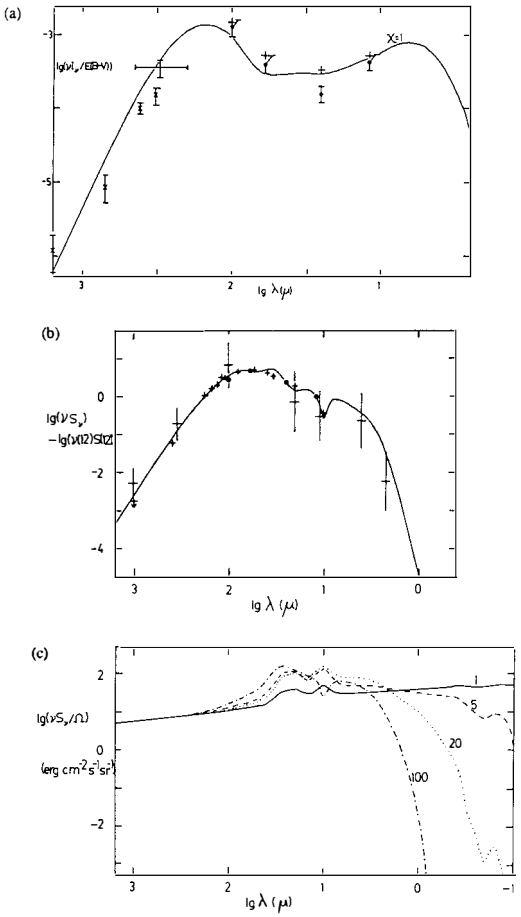


Figure 7: **(a)** Predicted emissivity (solid line) of interstellar grains in the solar neighbourhood, from Rowan-Robinson (1990). Observational data are from Boulanger & Perault (1988), Halpern *et al* (1988), Fabbri *et al* (1988). **(b)** The solid line shows a simple model for a star forming region of the type discussed by Crawford & Rowan-Robinson (1986); a spherically symmetric optically thick dust cloud ($\tau_{UV} = 100$) surrounding a star at $T = 40000$ K. The small crosses are the data of Telesco *et al* (1984) for the 3 kpc ring in NGC 1068, the large crosses are the average spectrum for regions of massive star formation in the Galaxy (Rowan-Robinson, 1979). **(c)** The 'Seyfert' component, modelled by Rowan-Robinson and Crawford (1989) by an $\alpha = 0.7$ power-law continuum source, illuminating a spherically symmetric dust cloud. The models shown here have optical depths of $\tau_{UV}$=1,5,20 and 100.

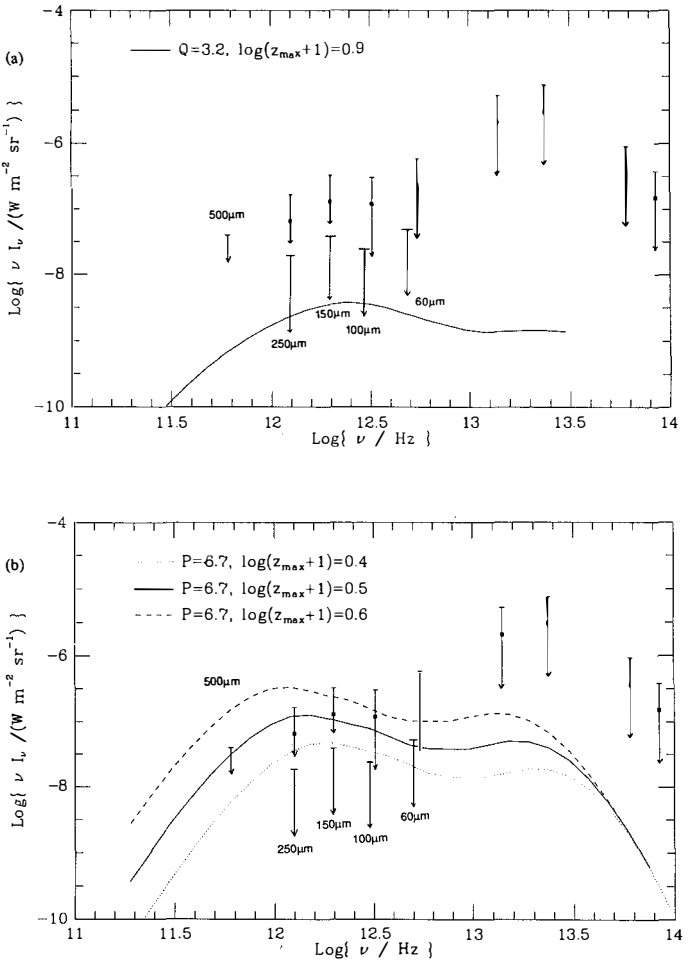


Figure 8: Upper limits to the far-IR background, from Mather *et al* (1990b, 500$\mu$m), Mather *et al* (1990a, solid squares). IRAS upper limits and predicted background spectra are from Oliver *et al* (1991). **(a)** The solid curve shows the predicted background in a luminosity evolution scenario. **(b)** Three predicted background spectra assuming pure density evolution. A cut-off at a redshift of $> 1.5$ is ruled out by the present limits.

of this background (provided that Galactic cirrus can be discriminated against, perhaps using 21 cm data), which would provide a useful diagnostic for the study of clustering on very large scales. If the background is much lower than the present upper limit, then models invoking substantial density evolution of far-IR emitting galaxies will probably have to be rejected.

## References


Boulanger, F. & Perault, M. 1988, *Astrophys. J.*, **330**, 964.
Consolmagno, G., 1979, *Icarus*, **38**, 398.
Crawford, J., & Rowan-Robinson, M., 1986, *Mon. Not. Roy. astr. Soc.*, **221**, 923.
Danese, L., de Zotti, G., Francheschini, A., & Toffolatti, L., 1987, *Astrophys. J.*, **318**, L15.
Dermott, S.F., Nicholson, P.D., Burns, J.A., & Houck, J.R., 1984, *Nature*, **312**, 505.
Dermott, S.F., Nicholson, P.D., & Wolven, B., 1986, in *'Asteroids, Comets, and Meteors, II,'*, ed. C.-I. Lagerkvist & H. Rickman. (Uppsala).
Efstathiou, A., & Rowan-Robinson, M., 1991a, in preparation.
Efstathiou, A., & Rowan-Robinson, M., 1991b, in preparation.
Fabbri, R., Guidi, I., Natale, V., & Ventura G., 1988, (preprint).
Francheschini, A., Danese, L., de Zotti, G., & Xu, C., 1988, *Mon. Not. Roy. astr. Soc.*, **233**, 175.
Giese, E., Kneißel, B., & Uttrich, H., 1986, *Icarus*, **68**, 395.
Hacking, P., Condon, J.J., & Houck, J.R., 1987, *Astrophys. J.*, **316**, L15.
Hacking, P., & Houck, J.R., 1987, *Astrophys. J. Suppl.*, **63**, 311.
Halpern, M., Benford, R., Meyer, S., Muehlner, D., & Weiss, R., 1988, *Astrophys. J.*, **332**, 596.
Hauser, M.G., *et al*, 1984, *Astrophys. J.*, **278**, L15.
IRAS *Explanatory Supplement*, 1985 ed. C.A. Beichman *et al*, (U.S. Government Printing Office, Washington D.C.)
Lienert, C., Richter, I., Pitz, E., & Plank, B., 1981, *Astron. Astrophys.*, **118**, 345.
Lockman, F.J., Jahoda, K., & McCammon, D., 1986, *Astrophys. J.*, **302**, 432.
Lonsdale, C.J., Hacking, P.B., Conrow, T.P., and Rowan-Robinson, M., 1990 *Astrophys. J.*, in press.
Low F.J., *et al.*, 1984, *Astrophys. J.*, **278**, L19.
Mather, J.C., *et al*, 1990a, (preprint).
Mather, J.C., *et al*, 1990b, *Astrophys. J.*, **354**, L37.
Misconi, N.Y., 1980, in *"Solid Particles in the Solar System"*, ed. I. Halliday and B.A. McIntosh, p49. (Reidel, Dordrecht).
Murdoch T.L., & Price, S.D., 1985 *Astr. J.*, **90**, 375.
Oliver, S.J., Rowan-Robinson, M., & Saunders, W., 1991, in preparation.
Puget, J.L., & Leger, A., 1989, *Ann. Rev. Astron. Astrophys.*, **27**, 161.
Rowan-Robinson, M., 1979, *Astrophys. J.*, **234**, 111.
Rowan-Robinson, M., 1990, in *"The Interstellar Medium in Galaxies"*, ed. J.M. Shull & H.A. Thronson, Jr., p121. (Kluwer).
Rowan-Robinson, M., & Crawford, J., 1989, *Mon. Not. Roy. astr. Soc.*, **238**, 523.
Rowan-Robinson, M, Hughes, J., Vedi, K., & Walker, D., 1990, *Mon. Not. Roy. astr. Soc.*, **246**, 273.
Rowan-Robinson, M, Hughes, J., Jones, M., Leech, K., Vedi, K., & Walker, D., 1991, *Mon. Not. Roy. astr. Soc.*, **249**, 729.
Saunders, W, *et al*, 1990, *Mon. Not. Roy. astr. Soc.*, **242**, 318.
Telesco, C.M, Becklin, E.E., & Wynn-Williams, G.G., 1984, *Astrophys. J.* **282**, 427.

Moriond

# COSMIC BACKGROUND EXPLORER (COBE) OBSERVATIONS: NEW SKY MAPS OF THE EARLY UNIVERSE

GEORGE. F. SMOOT
Lawrence Berkeley Laboratory and Space Sciences Laboratory,
Bldg 50-352 - 1 Cyclotron Road
University of California, Berkeley, 94720

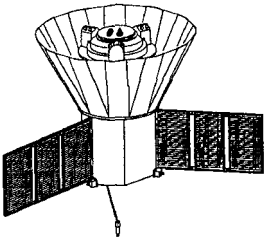

## ABSTRACT

This paper presents early results obtained from the first six months of measurements of the Cosmic Microwave Background (CMB) by instruments aboard NASA's Cosmic Background Explorer (*COBE*)* satellite and discusses the implications for cosmology. The three instruments: FIRAS, DMR, and DIRBE have operated well and produced significant new results. The FIRAS measurement of the CMB spectrum supports the standard Big Bang model. The maps made from the DMR instrument measurements show a spatially smooth early universe. The measurements are sufficiently precise that we must pay careful attention to potential systematic errors. The maps of galactic and local emission produced by the DIRBE instrument will be needed to identify foregrounds from extragalactic emission and thus to interpret the results in terms of events in the early universe.

* The National Aeronautics and Space Administration/Goddard Space Flight Center is responsible for the design, development, and operation of the Cosmic Background Explorer. GSFC is also responsible for the software development through to the final processing of the space data. The *COBE* program is supported by the Astrophysics division of NASA's Office of Space Science and Applications.

## 1. INTRODUCTION

The standard cosmological model was established in 1965 with the discovery of the cosmic microwave background (CMB) and the recognition of its implications. In the (Friedmann-Robertson-Walker) Big Bang model cosmologists had a theoretical framework for describing the development of the universe from a time of about one hundredth of a second through the present age of the universe. The most notable and precise successes of the Big Bang model were the calculation of the primordial nucleosynthesis of the light elements (notably $^4$He, $^3$He, D, T, and $^7$Li) and the existence of a thermal relic radiation (CMB) from this era."The First Three Minutes" by Steve Weinberg (1977) and "Physical Cosmology" by Jim Peebles (1971) provide an excellent account of this model.

With the development of the Standard Model of strong and electroweak interactions providing a theory of physics up to the weak scale (250 GeV) and ideas about grand unification, particle theory has provided a context and motivation for extending and expanding the original Big Bang model. That fundamental particles (quarks and leptons) are point like particles with asymptotic freedom from strong interactions at high energies provides a picture of the early universe as a dilute gas of weakly interacting quarks, leptons, and guage bosons. This picture is more readily understandable than the old view of the hadron era ($10^{-5}$ sec), when many particles were crowded together with separations and horizons less than a typical particle size (e.g. a proton). With this context it has been possible to develop a senario of the universe from very early times ($10^{-35}$ sec) including a phase transition induced period of inflation, a time of baryogenesis, and other events leading to the original Big Bang model including the fluctuations that lead to galaxy and other structure formation. In this standard model cosmology and particle physics come together for inspiration and consistency and the observations and experiments in each constrain and test each others models. "The Early Universe" by Rocky Kolb and Mike Turner is my recommended description of this extended standard model.

The light elements and the cosmic microwave background (CMB) are the most accessible relics from the eras during which the universe was a relatively structureless plasma prior to its evolving to the highly-ordered state observed today. In standard models of cosmology, CMB photons have travelled unhindered from the surface of last scattering in the early universe to the present era; as such, the CMB maps the large scale structure of space-time in the early universe. Despite a quarter-century of effort, no intrinsic anisotropy in the CMB has been detected. Likewise, there has been a fruitless search for distortions of the spectrum from a featureless blackbody. These measurements can constrain possible effects in the early universe and cosmology and particle physics theories.

The *COBE* (Cosmic Background Explorer satellite) experiments were designed and have turned out to be a precision test of the standard model of cosmology. *COBE* was launched on November 18, 1989 into a 900-km circular, near-polar orbit (inclination 99°). The Earth's gravitational quadrupole moment precesses the orbit to follow the terminator, allowing the instruments to point away from the Earth and perpendicular to the Sun to avoid both solar and terrestrial radiation. Throughout most of the year, the satellite orbit provides an exceptionally stable environment. During the two months surrounding summer solstice, the satellite is unable to shield the instruments and dewar from the Earth and Sun simultaneously, and the Earth limb becomes visible over the shielding surrounding the instrument aperture plane as the satellite passes over the North Pole. During the same period, the satellite enters the Earth's shadow as the orbit crosses over the South Pole. Prior to depletion of the liquid helium cryogen on September 20, 1990, the DIRBE and FIRAS instruments mapped the sky 1.6 times. As the dewar warms, the DIRBE instrument continues to take data in its four shortest wavelength bands. The DMR instrument does not require cryogenic cooling and continues to operate normally.

The *COBE* Science Working Group (SWG), consisting of C. L. Bennett, N. W. Boggess, E. S. Cheng, E. Dwek, S. Gulkis, M. G. Hauser, M. Janssen, T. Kelsall, P. Lubin, J. C. Mather, S. Meyer, S. H. Moseley, T. L. Murdock, R. A. Shafer, R. F. Silverberg, G. F. Smoot, R. Weiss, D. T. Wilkinson, and E. L.Wright, is responsible for the scientific oversight.

## 2. The DIRBE Instrument Description and Preliminary Results

The Diffuse Infrared Background Experiment (DIRBE) is designed to conduct a sensitive search for an isotropic cosmic infrared background (CIB) radiation over the spectral range from 1 to 300 microns. The cumulative emissions of pregalactic, protogalactic, and evolving galactic systems are expected to be recorded in this background. Since both the cosmic red-shift and reprocessing of short-wavelength radiation to longer wavelengths by dust act to shift the short-wavelength emissions of cosmic sources toward or into the infrared, the spectral range from 1 to 1000 microns is expected to contain much of the energy released since the formation of luminous objects, and could potentially contain a total radiant energy density comparable to that of the CMB. The discovery and measurement of the CIB would provide new insight into the cosmic 'dark ages' following the decoupling of matter and the CMB.

Observing the CIB is a formidable task. Bright foregrounds from the atmosphere of the Earth, from interplanetary dust scattering of sunlight and emission of absorbed sunlight, and from stellar and interstellar emissions of our own Galaxy dominate the diffuse sky brightness in the infrared. Even when measurements are made from space with cryogenically-cooled instruments, the local astrophysical foregrounds strongly constrain our ability to measure and discriminate an extragalactic infrared background. Furthermore, since the absolute brightness of the CIB is of paramount interest for cosmology, such measurements must be done relative to a well-established absolute flux reference, with instruments which strongly exclude or permit discrimination of all stray sources of radiation or offset signals which could mimic a cosmic signal.

The DIRBE approach is to obtain absolute brightness maps of the full sky in 10 photometric bands (J[1.2], K[2.3], L[3.4], and M[4.9]; the four *IRAS* bands at 12, 25, 60, and 100 micrometers; and 120-200 and 200-300 micrometer bands). To facilitate determination of the bright foreground contribution from interplanetary dust, linear polarization is also measured in the J, K, and L bands, and all celestial directions are observed hundreds of times at all accessible solar elongation angles (depending upon ecliptic latitude) in the range 64° to 124°. The instrument is designed to achieve a sensitivity for each field of view of $\mathrm{lI(l) = 10^{-13}\ W\ cm^{-2}\ sr^{-1}}$ (1 s, 1 year). This level is well below most estimated CIB contributions. Extensive modeling of the foregrounds, just beginning, will be required to isolate and identify any extragalactic component.

The DIRBE instrument is an absolute radiometer, utilizing an off-axis folded Gregorian telescope with a 19-cm diameter primary mirror. The optical configuration is carefully designed for strong rejection of stray light from the Sun, Earth limb, Moon or other off-axis celestial radiation, or parts of *COBE*. Stray light rejection features include both a secondary field stop and a Lyot stop, super-polished primary and secondary mirrors, a reflective forebaffle, extensive internal baffling, and a complete light-tight enclosure of the instrument within the *COBE* dewar. Additional protection is provided by the Sun and Earth shade surrounding the *COBE* dewar, which prevents direct illumination of the dewar aperture by these strong local sources. The DIRBE instrument, which is maintained at a temperature below 2 K within the dewar, measures absolute brightness by chopping between the sky signal and a zero-flux internal reference at 32 Hz using a tuning fork chopper. Instrumental offsets are measured by closing a cold shutter located at the prime focus. All spectral bands view the same instantaneous field-of-view, 0.7° x 0.7°, oriented at 30° from the spacecraft spin axis. This allows the DIRBE to modulate solar elongation angles by 60° during each rotation, and to sample fully 50% of the celestial sphere each day. Four highly-reproducible internal radiative reference sources can be used to stimulate all detectors when the shutter is closed to monitor the stability and linearity of the instrument response. The highly redundant sky sampling and frequent response checks provide precise photometric closure over the sky for the duration of the mission. Calibration of the photometric scale is obtained from observations of isolated bright celestial sources. Careful measurements of the beam shape in pre-flight system testing and during the mission using scans across bright point sources allow conversion of point-source calibrations to surface brightness calibrations.

Qualitatively, the initial DIRBE sky maps show the expected character of the infrared sky. For example, at 1.2 microns stellar emission from the galactic plane and from isolated high latitude stars is prominent. Zodiacal scattered light from interplanetary dust is also prominent. At fixed ecliptic latitude the zodiacal light decreases strongly with increasing solar elongation angle, and at fixed elongation angle it decreases with increasing ecliptic latitude. These two components continue to dominate out to 3.4 microns, though both become fainter as wavelength increases. The foreground emissions have relative minima at wavelengths of 3.4 microns and longward of 100 microns. A composite of the 1.2, 2.3, and 3.4 microns images is shown in Figure 1a. Because extinction at these wavelengths is far less than in visible light, the disk and bulge stellar populations of the Milky Way are dramatically apparent in this image. A composite of the 25, 60, and 100 micron images is shown in Figure 1b. At 12 and 25 microns, emission from the interplanetary dust dominates the sky brightness, again strongly dependent upon ecliptic latitude and elongation angle. At wavelengths of 60 microns and longer, emission from the interstellar medium dominates the galactic brightness, and the interplanetary dust emission becomes progressively less apparent. The patchy infrared cirrus noted in *IRAS* data is evident at all of these wavelengths. The DIRBE data will clearly be a valuable new resource for studies of the interplanetary medium and Galaxy as well as the search for the CIB.

*IRAS* measurements toward the south ecliptic pole have been compared with DIRBE results. The two experiments are seen to agree reasonably well at 12 and 25 microns, but the DIRBE results are substantially fainter at 60 and 100 microns, reaching a factor of 2.6 at 100 microns. We have made a more detailed comparison with *IRAS* data at several points on the sky. By choosing points of different brightness, we can distinguish zero-point offsets and gain differences. We find evidence for zero-point differences, evidently not constant in time, of a few MJy/sr at all *IRAS* wavelengths. These are most significant (as a fraction of total brightness) at the longest wavelengths. We also find that the *IRAS* dc gain at 60 and 100 microns is substantially too high, a result which can be understood in terms of the detector characteristics and the data reduction procedures used for *IRAS* image-format data (see the *IRAS* Explanatory Supplement (1988), pp. IV-9 and IV-10 for a discussion of the *IRAS* dc response). The combined effect of these discrepancies is particularly large at 100 microns toward faint sky regions. Since *IRAS* detector gain depends on source angular scale (a scan-modulated instrument) and source brightness, no simple conversion between the total brightness data from the two experiments is universally applicable. This discussion applies only to surface brightness measurements; point source flux calibration is not subject to similar problems.

The DIRBE flux limits (Hauser *et al.* 1991)[1] have the expected spectral shape. They can be compared in detail with other measurements, e.g. *IRAS*, ZIP, Matsumoto *et al.*, (1988A&B) and Noda *et al.* (1991). *IRAS* measurements toward the south ecliptic pole have been compared with DIRBE results. The two experiments are seen to agree reasonably well at 12 and 25 microns, but the DIRBE results are substantially fainter at 60 and 100 microns, reaching a factor of ~3 at 100 microns. The DIRBE and ZIP (Murdock & Price 1985) results at the north ecliptic pole agree to 10% at 10 and 20 microns. Comparison with Matsumoto *et al.* and Noda *et al.* shows fairly good agreement in the near infrared with a deeper minimum at 3.4 microns and reasonable agreement in the far infrared but not as sharp a bump at 160 microns. These results and interpretations are discussed in the lecture by Bernard Carr and, for example, a paper by Bond, Carr, & Hogan (1991). The DIRBE (and FIRAS) data already rule out significant early VMO's and explosions and constrain galactic evolution models. The DIRBE data will clearly be a valuable new resource for studies of the interplanetary medium and Galaxy as well as the search for the CIB.

The DIRBE team is headed by the Principal Investigator Micheal Hauser and Deputy Principal Investigator Tom Kelsall. In addition to the *COBE* SWG participation the following people are working on DIRBE: S. Burdick, G. N. Toller, G. Berriman, B. B. Franz, K. J. Mitchell, M. Mitra, N. P. Odegard, F. S. Patt, W. J. Speisman, S.W. Stemwedel, J. A. Skard, A. Aheam, W. Daffer, I. Freedman, S. Jong, A. Panitz, A. Ramsey, T. Roegner, V. Snowel, K. Tewari, H. T. Freudenreich, C. Lisse, J. Weiland.

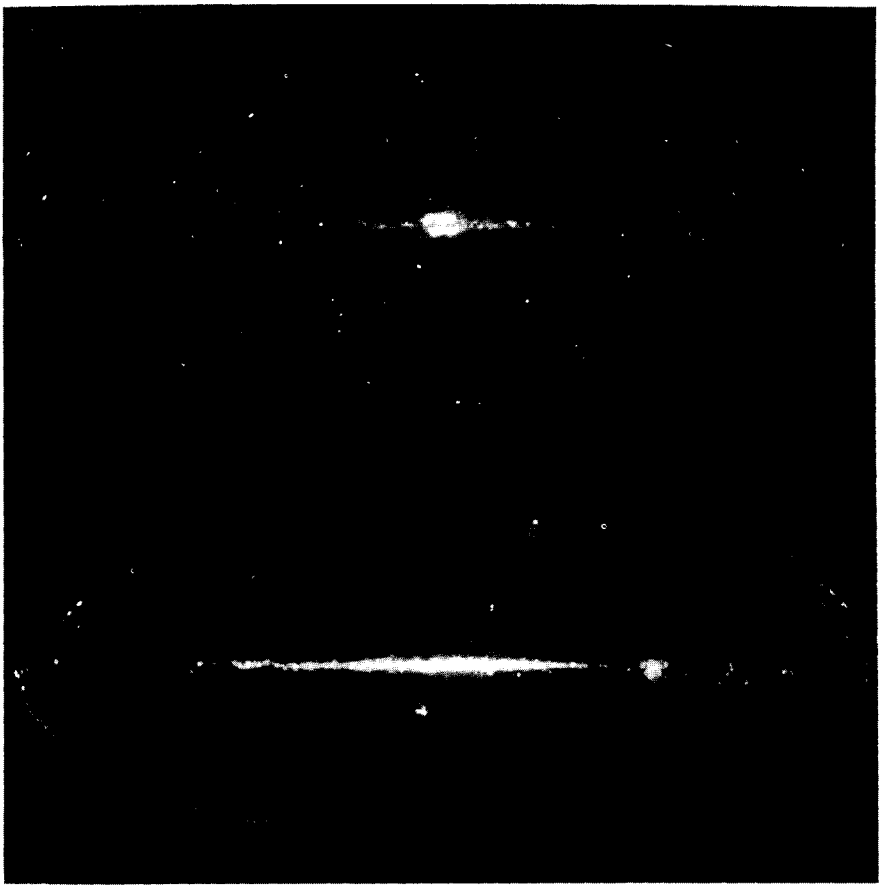

Figure 1. *COBE* DIRBE full sky maps in galactic coordinates. 1A. Combined 1.2, 2.2, and 3.4 micron map in respective blue, green, and red colors. The image shows both the thin disk and central bulge of the galaxy. 1B. Combined 25, 60, and 100 micron map in respective blue, green, and red colors. Both maps are preliminary results of a full sky scan by the DIRBE instrument. The discontinuities apparent are due primarily to the change in zodiacal light as the spacecraft and earth move around in the zodiacal dust but may in part be due to not having final instrument calibration.

**3. FIRAS** Instrument Description and CMB Spectrum Results

The FIRAS compares the spectrum of the CMB with that of a precise blackbody, enabling the measurement of very small deviations from a Planckian spectrum. The FIRAS instrument covers two frequency ranges, a low frequency channel from 1 to 20 $cm^{-1}$ and a high frequency channel from 20 to 100 $cm^{-1}$. It has a 7° diameter beam width, established by a non-imaging parabolic concentrator, which has a flared aperture to reduce diffractive sidelobe responses. The instrument is calibrated by a full beam, temperature-controlled external blackbody, which can be moved into the beam on command. The FIRAS is the first instrument to measure the background radiation and compare it with such an accurate external full-beam calibrator in flight. The spectral resolution is obtained with a polarizing Michelson interferometer, with separated input and output beams to permit fully symmetrical differential operation. One input beam views the sky or the full aperture calibrator, while the second input beam views an internal temperature controlled reference blackbody, with its own parabolic concentrator. Both input concentrators and both calibrators are temperature controlled and can be set by command to any temperature between 2 and 25 K. In standard operating condition the two concentrators and the internal reference body are commanded to match the sky temperature, thereby yielding a nearly nulled interferogram and reducing almost all instrumental gain errors to negligible values.

The external calibrator determines the accuracy of the instrument for broad band sources like the CMBR. It is a re-entrant cone shaped like a trumpet mute, made of Eccosorb CR-110 iron-loaded epoxy. The angles at the point and groove are 25°, so that a ray reaching the detector has undergone 7 specular reflections from the calibrator. The calculated reflectance for this design, including diffraction and surface imperfections, is less than $10^{-4}$ from 2 to 20 $cm^{-1}$. Measurements of the reflectance of an identical calibrator in an identical antenna using coherent radiation at 1 $cm^{-1}$ and 3 $cm^{-1}$ frequencies confirm this calculation. The instrument is calibrated by measuring spectra with the calibrator in the sky horn while operating all other controllable sources within the instrument at a sequence of different temperatures.

The first results of the FIRAS[2] may be summarized as follows: The intensity of the background sky radiation is consistent with a blackbody at 2.735 ± 0.06 K. Deviations from this blackbody at the spectral resolution of the instrument are less than 1% of the peak brightness. The quoted error is primarily due to an uncertainty in the thermometer calibration; we expect to reduce this uncertainty by additional tests. The measured spectrum is shown in Figure 2, and is converted to temperature units, where it is compared to previous measurements. The deviations can be fitted to the Sunyaev-Zel'dovich form for Comptonization[3], giving a limit of $|y| < 10^{-3}$ (3 σ). A fit to a Bose-Einstein distribution gives a limit on the dimensionless chemical potential of $|\mu| < 10^{-2}$ (3 σ). This places a strong limit on the existence of a smooth hot intergalactic medium: it can contribute less than 3% of the X-ray background radiation even at a reheating time as recent as $z$=2. There is no evidence of a spectral distortion, such as that reported by Matsumoto *et al.*[4], and the measured temperature is consistent with previous reports and the recent rocket result of Gush *et al.*[5].

The variation of the spectrum with sky position as measured by the FIRAS is dominated by the dipole anisotropy of the CMB, plus a variation in the interstellar dust emission. A preliminary dipole anisotropy spectrum was determined by calculating the average spectra in two large circular regions of the sky each of angular diameter 60°, one centered at (α, δ) = (11.1h, -6.3°) and the other at (23.1h, 6.3°), which lie along opposite ends of the dipole axis as determined by the DMR. The difference between these spectra is fit extremely well by the difference of two blackbodies, and is consistent with a peak dipole amplitude of 3.3 ± 0.3 mK and the assumed dipole direction.

These precise limits to potential distortions covering the major portion of the CMB photons provide support for a key element in the models of Big Bang nucleosynthesis - the baryon to photon ratio and the interpretation of that number relative to the critical density. The FIRAS measurement actually counts the vast majority of photons and the precision of the measurement gives us the density constraint

$$\rho_\gamma = 4.722\ (T/1K)^4 e^{4y}\ eV/cm^3 \sim 10^{-33}\ (To/2.7K)^4 e^{4y}\ gm/cm^3$$

$$n_\gamma = 20.286\ (T/1K)^3\ \text{photons/cm}^3 = 415\ (To/2.735K)^3\ \text{photons/cm}^3 \qquad (1)$$

The FIRAS measurements decrease the error on $n_g$ from greater than 20% to less than 5%. The limits on $|\mu|$ and $|y|$ in turn limit energy release in the early universe ($1+z < few\ 10^6$) to typically less than 1% of the energy in the CMB. This in turn provides limit on cosmologically significant events such as primordial particle decay, superconducting cosmic strings, and turbulence. A currently interesting restriction is on the parameters of neutrinoes that decay to photons. Examples at hand are a potential 17 keV neutrino and Sciama's 28 eV neutrino. The 17 keV neutrino lifetime cannot be between 1 year and about $10^{12}$ years because it would either distort the CMB spectrum or its decay photons must show up directly. Sciama's proposed 28 eV neutrino is similarly restricted but Sciama has cleverly proposed a sufficiently long lifetime and hidden the decay photons in the ultravoliet background.

The FIRAS instrument also measures the galactic emission and has made a survey of the dust and line emission in its bands. The dust emission is strong; the FIRAS provides good spectral information on that dust and has found some ten emission lines (Wright *et al.* 1991). In addition FIRAS has produced maps of the dust emission (205 μm for instance), the 205 μm NII line and 158 μm CII line.

The FIRAS team is headed by the Principal Investigator John Mather, Deputy Principal Investigator Rick Shafer and Deputy Project Scientist for Data Ed Cheng. In addition to the *COBE* SWG participation the following people are working on FIRAS: Dale Fixsen, Gene Eplee, Joel Gales, Rich Isaacman, Snehevadan Macwan, Derck Massa, Muriel Taylor, Alice Trenholme, Dave Wynne, Steve Alexander, Dave Bouler, Nilo Gonzalez, Ken Jensen, Shirley Read, Larry Rosen, Fred Shuman, Frank Varosi, Harte Wang, Will Daffer, Jim Krise, Nick Iascone, and Courtney Scott.

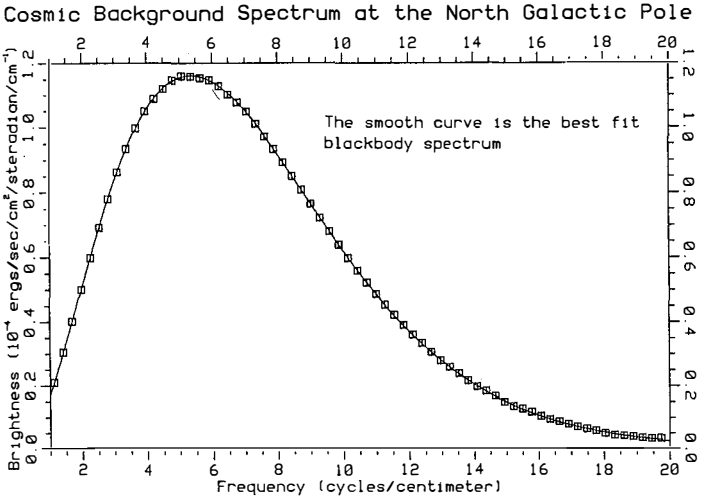


Figure 2. *COBE* FIRAS spectrum measurement. The boxes are the data points and the line the best fit Planckian (2.735 K). The data are taken near the north galactic pole.

## 4. DMR

### 4.1 DMR Instrument Description and Operation

The *COBE* Differential Microwave Radiometers (DMR) instrument is intended to provide precise maps of the microwave sky on large angular scales. It consists of six differential microwave radiometers, two independent radiometers at each of three frequencies: 31.5, 53, and 90 GHz (wavelengths 9.5, 5.7, and 3.3 mm). At these frequencies the CMB dominates foreground galactic emission by at least a factor of roughly 1000. The multiple frequencies allow subtraction of galactic emission using its spectral signature, yielding maps of the CMB and thus the distribution of matter and energy in the early universe. Each radiometer measures the difference in microwave power between two regions of the sky separated by 60°. The combined motions of spacecraft spin (75 s period), orbit (103 minute period), and orbital precession (~1 degree per day) allow each sky position to be compared to all others through a massively redundant set of all possible difference measurements spaced 60° apart.

Each radiometer consists of a superheterodyne receiver switched at 100 Hz between two identical corrugated-horn antennas. The compact low-sidelobe antennas' main beam profile is well described by a Gaussian of 7° FWHM and point 60° apart, 30° to either side of the spacecraft spin axis[6]. The two channels at 31.5 GHz share a single antenna pair with an orthomode transducer splitting the input into opposite circular polarizations. Both channels share a common enclosure and thermal regulation system. The 53 and 90 GHz radiometers are similar but have two antenna pairs at each frequency, each with identical linear polarization response. A detailed description of the DMR instrument may be found in Smoot *et al.*[7].

Three independent techniques are used to determine the radiometer calibration. Solid-state noise sources provide in-flight calibration by injecting broad-band microwave power into the front end of each radiometer at regular intervals (every two hours). Prior to launch the noise source signals were calibrated by comparing to the signal produced by targets of known, dissimilar temperatures (approximately 300 K and 77 K) covering the antenna apertures. The DMR observes the Moon for a fraction of an orbit during two weeks of every month providing an independent determination of the calibration factor. The Earth's ~30 km $s^{-1}$ motion about the solar system barycenter produces a Doppler-shift dipole of known magnitude (~0.3 mK) and direction. The modulation in amplitude and direction is apparent, but at low signal to noise. Given sufficient observing time (> one year), this method may produce the most accurate determination of the absolute calibration of the DMR instrument. A forthcoming paper[8] discusses the DMR calibration more fully.

The DMR has been operating well since about a week after the *COBE* launch (18 Nov 1989) and is approved for two years of operation. Two additional years of operation have been requested.

### 4.2 DMR Data Reduction and Analysis

A software analysis system receives data telemetered from the satellite, determines the instrument calibration, and inverts the difference measurements to map the microwave sky in each channel. Although the experiment has been designed to minimize or avoid sources of systematic uncertainty, both the instrument and the software can potentially introduce systematic effects correlated with antenna pointing, which would create or mask features in the final sky maps. Further details of the data processing algorithms may be found in Torres *et al.* [9]

The sky maps may in principle contain contamination from local sources or artifacts from the data reduction process itself. The data reduction process must distinguish cosmological signals from a variety of potential systematic effects. The most obvious source of non-cosmological signals is the presence in the sky of foreground microwave sources. These include thermal emission from the *COBE* spacecraft itself, from the Earth, Moon, and Sun, and from other celestial objects. Non-thermal radio-frequency interference (RFI) must also be considered, both from ground stations and from geosynchronous satellites. Although the DMR instrument is largely shielded from such sources, their residual or intermittent effect must be considered. A second class of potential systematics is the effect of the changing orbital environment on the instrument. Various instrument components have slightly different performance with changes in temperature, voltage, and local magnetic field, each of which can be modulated by the *COBE* orbit. Longer-term drifts can also affect the data. Finally, the data reduction process itself may introduce or mask features in

the data. The DMR data are differential; the sparse matrix algorithm is subject to concerns of both coverage (closure) and solution stability. Other features of the data reduction process, particularly the calibration and baseline subtraction, are also a source of potential artifacts. All potential sources of systematic error must be identified and their effects measured or limited before maps with reliable uncertainties can be produced.

The largest limit is the current 5% uncertainty in the absolute calibration of the instrument. The uncertainty in absolute calibration does not create artifacts in the maps but affects the calculated amplitude of existing features (e.g., the dipole anisotropy). We continue to acquire and analyze calibration information and we anticipate improved calibration in the future. The next largest effect is the modulation of the instrument output in the Earth's magnetic field; the primary effect is on the dipole term of a spherical harmonics expansion. The magnetic effects will be modelled and removed in future analysis. The 53A channel unambiguously shows a magnetic susceptibility; we do not include the 53A channel in the dipole results presented below. The largest potential effects upon the quadrupole and higher-order multipole coefficients are Earth emission and the possibility of undetected calibration drifts. The current 95% C.L. upper limits to combined systematic errors in the DMR maps are $\Delta T/T_0 < 8x10^{-5}$ for the dipole anisotropy and $\Delta T/T_0 < 3x10^{-5}$ for the quadrupole and higher-order terms.

As the DMR gathers redundant sky coverage and as analysis continues, we anticipate refined estimates of, or limits on, these effects. It is important to note, however, that the DMR is free from some of the systematics of previous large-scale sky surveys. The multiple differences generated by various chopping frequencies (spin, orbit, and precession periods) allow separation of instrumental from celestial signals. Two independent full-sky maps, produced with matched beams at each of three frequencies, provide a powerful tool for analysis and removal of possible systematic effects.

## 4.3 DMR Results

Figure 3 shows the microwave sky at 6 mm on a linear scale. The most noticeable effect is the extreme uniformity of the CMB. The preliminary maps of the microwave sky for each of the six DMR channels look very nearly the same in terms of the dipole while the galactic emission varies with frequency. The independent maps at each frequency enable celestial signals to be distinguished from noise or spurious features: a celestial source will appear at identical amplitude in both maps. The three frequencies allow separation of cosmological signals from galactic foregrounds based on spectral signatures. The maps are corrected to solar-system barycenter and do not include data with the Moon within 25° of an antenna; no other systematic corrections have been made. All six maps clearly show the dipole anisotropy and galactic emission. The dipole appears at similar amplitudes in all maps while galactic emission decreases sharply at higher frequencies, in accord with the expected spectral behavior.

An observer moving with velocity $\beta = v/c$ relative to an isotropic radiation field of temperature $T_0$ observes a Doppler-shifted temperature

$$T = T_0 \frac{(1 - \beta^2)^{1/2}}{1 - \beta\cos(\theta)} = T_0 [\, 1 + \beta\cos(\theta) + \frac{1}{2}\beta^2 \cos(2\theta) + O(\beta^3) \,] \qquad (2)$$

The first term is the monopole CMB temperature without a Doppler shift. The second term, proportional to b, is a dipole distribution, varying as the cosine of the angle between the velocity and the direction of observation. The term proportional to $b^2$ is a quadrupole with amplitude reduced by 1/2 b from the dipole amplitude. The DMR maps clearly show a dipole distribution consistent with a Doppler-shifted thermal spectrum, implying a velocity for the solar system barycenter of $\beta = 0.00123 \pm 0.00003$ (68% CL), or $v = 370 \pm 10$ km s$^{-1}$ toward $(l, b) = (264° \pm 2, 49° \pm 2°)$, where we assume a value $T_0 = 2.735$ K. The solar system velocity with respect to the local standard of rest is estimated at 20 km s$^{-1}$ toward (57°,23°), while galactic rotation moves the the local standard of rest at 220 km s$^{-1}$ toward (90°,0°)[10,11]. The DMR results thus imply a peculiar velocity for the Galaxy of $v_g = 550 \pm 10$ km s$^{-1}$ in the direction (266° ± 2°, 30° ± 2°). This is in rough agreement with independent determinations of the velocity of the local group, $v_{lg} = 507 \pm 10$ km s$^{-1}$ toward (264 °± 2°, 31° ± 2°)[12].

The angular distribution on the full sky maps is fully consistent with a dipole anisotropy. The spectrum of all published dipole parameters, including those from the *COBE* FIRAS experiment[2], is consistent with a Doppler-shifted blackbody origin. With high probability the dipole comes from peculiar motion and is not due to an intrinsic dipole either large scale gradient as suggested by Paczynski and Piran (1990) or net velocity of CMB relative to comoving frame[13]. The CMB dipole anisotropy is well established by the chi-squared of the dipole fit and the dipole amplitude spectrum. The dipole anisotropy is more than 30 times larger than any other large angular scale anisotropy. The dipole anisotropy is then either due to a Doppler shift or is intrinsic temperature anisotropy. It is very difficult to establish a universe with a large dipole anisotropy without comparable quadrupolar and higher order moment anisotropies We can compare the dipole anisotropy implied velocity with the velocity expected due to gravitational perturbations in the region 100 Mpc around our location. Our peculiar velocity can be estimated either by adding up observed sources (light⇒mass⇒potential), e.g. *IRAS* galaxies or by inferring potential from observing large scale velocity flows, e.g. the "Great Attractor", that one readily obtains 80% of the CMB dipole implied velocity. The errors in this calculation are on the order of 20% or greater so that the whole dipole anisotropy can easily be explained as due to the peculiar velocity of our galaxy. Thus we adopt the working hypothesis that the dipole is generated by the galactic peculiar velocity to the comoving frame and the resulting Doppler shift.

The DMR maps with this dipole removed from the data show the only large-scale feature remaining is galactic emission, primarily confined to the plane of the galaxy. This emission is present at roughly the level expected before flight and is consistent with emission from electrons (synchrotron and HII) and dust within the galaxy. The ratio of the dipole anisotropy (the largest cosmological feature in the maps) to the Galactic foreground reaches a maximum in the frequency range 60—90 GHz. There is no evidence of any other emission features.

We have made a series of spherical harmonic fits to the data, excluding data within several ranges of galactic latitude. The only large-scale anisotropy detected to date is the dipole. The quadrupole anisotropy is limited $\Delta T/T < 3 \times 10^{-5}$ and higher-order terms are limited to amplitude $\Delta T/T < 10^{-4}$. Similarly, a search for Gaussian or non-Gaussian fluctuations on the sky showed no features to limit $\Delta T/T < 10^{-4}$. The results are insensitive to the precise cut in galactic latitude and are consistent with the expected Gaussian instrument noise. The reported uncertainties are 95% confidence level unless otherwise stated, and include the effects of systematics as listed in Table 1.

These limits on the quadrupole are somewhat better than previous anisotropy studies, but are still limited by uncertainties in estimates of many systematic errors that may well be removed in further data processing. In an ideal case this might result in a 95% confidence level upper limit of < 5μK on the rms quadrupole. One important systematic error term that may well ultimately limit the detectable quadrupole and other large angular scale anisotropies is galactic emission. The rms quadrupole amplitude including galactic emission (DMR 31, 53, and 90 GHz data and the Relict 37 GHz data) decreases with increasing frequency. However, since the CMB amplitude begins to decrease with frequency, the DMR 53 and 90 GHz channels bracket the apparent best observing frequency range. Including the galactic plane produces a quadrupole amplitude at minimum of 50 μK. To obtain ultimate sensitivity we need a level 20 to 30 times lower. How much does simply cutting the galactic plane from the fitting achieve? Tests using the 408 MHz and *IRAS* 100 micron maps indicate that reasonable galactic latitude cuts gain roughly a factor of 5 to 10. We will have to obtain the remaining factor of 2 to 4 from careful modeling.

### 4.4 DMR Discussion

The DMR limits to CMB anisotropies provide significant new limits to the dynamics and physical processes in the early universe. The dipole anisotropy provides a precise measure of the Earth's peculiar velocity with respect to the co-moving frame. Limits to higher-order anisotropies limit global shear and vorticity in the early universe. If the universe were rotating (in violation of Mach's Principle), the resultant metric causes null geodesics to spiral; in a flat universe the resultant anisotropy is dominated by a quadrupole term[13,14]. The limit $\Delta T/T < 3 \times 10^{-5}$ for quadrupole and higher spherical harmonics limits the rotation rate of universe to $\Omega < 3 \times 10^{-24}$ s$^{-1}$, or less than one ten-thousandth of a turn in the last ten billion years.

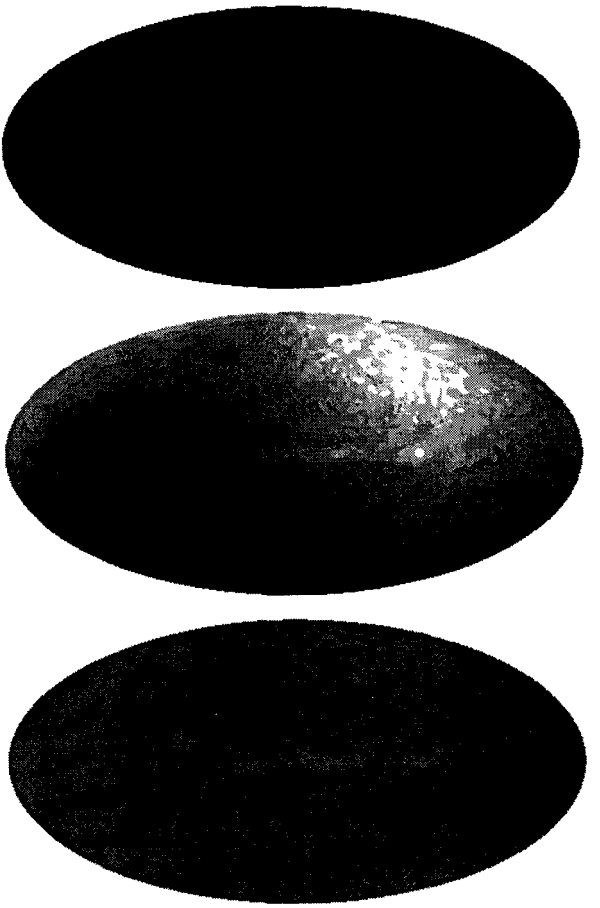

Figure 3 *COBE* DMR full sky maps of the temperature of the sky at 53 GHz (6 mm wavelength). The maps are in galactic coordinates and have been corrected to solar system barycenter.

3.A Absolute Sky Brightness on a scale from 0 to 3.6 K

3.B Relative sky brightness with mean removed and scale to about -4 to +4 mK. The dipole anisotropy (0.1%) and galactic plane are clearly visible.

3.C Relative sky brightness with monopole and dipole removed. The galactic plane is only significant visible signal. The other structure evident is consistent with instrument observing noise.

If the expansion of the universe were not uniform, the expansion anisotropy would lead to a temperature anisotropy in the CMB of similar magnitude. The large-scale isotropy of the DMR results indicate that the Hubble expansion is uniform to one part in $10^4$. This provides additional evidence for hot big bang models of cosmology, and indicates that the currently observed expansion of the universe can be traced back at least to the radiation-dominated era.

Inhomogeneities in the density in the early universe also lead to temperature anisotropies in the CMB as the CMB photons climb out of varying gravitational potential wells[15,16]

$$\Delta T/T \approx \frac{1}{2} \left(\frac{\delta\rho}{\rho}\right)_L \left(\frac{H_o L}{c}\right)^2 = \frac{1}{2} \left[\frac{L}{L_o}\right]^2 \left(\frac{\delta\rho}{\rho}\right)_L \qquad (3a)$$

The DMR results imply that the universe at the surface of last scattering was isotropic and homogeneous to the $10^{-4}$ level.

Inhomogeneities on scales outside the present horizon induce gradients and shear across the region within our horizon, and these cause anisotropy in the CMB. Grischuk and Zel'dovich[16] (1978) have shown that a very long wavelength density ripple in a spatially flat universe generates a quadrupole anisotropy in the CMB.

$$\left(\frac{\Delta T}{T}\right)_{quadrupole} \approx L_o^2 \nabla^2\delta\phi = (c/H_o)^2 \nabla^2\delta\phi \approx \frac{1}{2} \left[\frac{L_o}{L}\right]^2 \left(\frac{\delta\rho}{\rho}\right)_L \qquad (3b)$$

There is no dipole term because both the photons and the observer are in free fall. The effect that matters is the potential gradient associated with the inhomogeneities. If the universe is flat, the DMR limits on the quadrupole term constrain $(\delta\rho/\rho)_L < 10^{-4} (L/L_o)^2$. Inspite of what one might have thought, we can tell something about structure outside our present horizon up to of order 100 times the present horizon. The large scale geometry of the universe is thus well-described by a Robertson-Walker metric with only local perturbations.

One such potential local perturbation is gravitational radiation. Long-wavelength gravitational waves propagating though this region of the universe distort the metric and produce a quadrupole distortion in the CMB[17]. The limits $\Delta T/T < 3 \times 10^{-5}$ for quadrupole restricts the energy density of single plane waves or a chaotic superposition to

$$\Omega_{gw} < 3 \times 10^{-4} \left(\frac{\lambda_{gw}}{10\ Mpc}\right)^{-2} h^{-2} \qquad (4a)$$

where $\Omega_{gw}$ is the energy density of the gravity waves relative to the critical density, $\lambda_{gw}$ is the wavelength at the current epoch, and h is the Hubble constant in units 100 km $s^{-1}$ $Mpc^{-1}$.

Those gravity waves on the surface of last scattering will produce chaotic fluctuations. The DMR is sensitive primarily to gravitational waves with scale sizes > 7° at the surface of last scattering, or ~200 Mpc today. The temperature anisotropy observed is roughly half the strain that a freely falling observer at the surface of last scattering would observe. To determine the presnt energy density of the gravity waves present at the surface of last scattering one must propagate the waves to the present. A number of factors compensate and the limit is essentially independent of wavelength and is about

$$\Omega_{gw\text{-}lss} < 1/3 \left[\frac{\Delta T}{T}\right]^2 \approx 3 \times 10^{-10} \qquad (4b)$$

Cosmic strings provide another mechanism for local distortions in the metric. They are nearly one-dimensional topological defects predicted by many particle physics gauge theories and are characterized by a large mass per unit length, $\mu$[18]. The large mass and relativistic velocity produce CMB anisotropies through the relativistic boost and the Sachs-Wolfe effect (gravitational lensing alone does not produce anisotropy in an otherwise isotropic background). Many authors have calculated the anisotropy produced by various configurations of cosmic strings, with typical values[19,20]

$$\Delta T/T \sim 8\pi\beta\gamma \frac{G\mu}{c^2} \qquad (5)$$

The DMR experiment limits the existence of large-scale cosmic strings to $G\mu/c^2 < 10^{-5}$. There is no evidence for higher-order topological defects such as domain walls or textures. The large scale geometry of the universe appears to be uniform and without defects.

The observed isotropy of the universe on large angular scales presents a major problem for cosmology. At the time of primordial nucleosynthesis the presently observable universe was divided into about $10^{25}$ causally independent regions. The observed uniformity of light elements implies a baryon density uniformity of $\delta\rho/\rho < 3$ during synthesis[21]. At the surface of last scattering the horizon size subtends ~2° when viewed from here. Regions separated by more than 2° were not in causal contact; consequently, DMR measures some $10^4$ causally disconnected regions of the sky. Standard models of cosmology fail to explain why causally unconnected regions are the same to order unity, much less the $10^{-4}$ isotropy implied by the DMR observations. Inflationary scenarios provide one solution. In these models, the universe undergoes a spontaneous phase transition ~$10^{-32}$ seconds after the Big Bang, causing a period of exponential growth in which the scale size increases by 30 to 40 orders of magnitude. The entire observed universe would then originate from a small pre-inflationary volume in causal contact with itself, eliminating the problem. In the simplest inflationary models, the pre-inflationary matter and radiation fields are diluted to zero along with any pre-existing anisotropies. The process of inflation, however, generates scale-free anisotropies with a Harrison-Zel'dovich spectrum which result in small but detectable CMB anisotropies in the present universe[22,23]. During inflation zero point quantum fluctuations produce density fluctuations and gravitons (scalar and tensor fields) at levels comparable to the vacuum energy. Thus at the horizon wavelength scales they should produce comparable CMB anisotropies. The CMB anisotropy limits are now just pushing down to the level which is needed for observed velocities/gravitational potentials and begining to limit the energy scale of inflation at a natural level. If we were optimistic, we could hope to see anisotropies at the $10^{-5}$ level, giving us the density fluctuations we need and telling us the inflation energy scale.

Inflationary models predict quadrupole temperature fluctuations from gravitons or density fluctuations of order $\Delta T/T \sim H / M_{Planck}$, where H is the Hubble parameter during inflation (a period characterized by a constant Hubble parameter). As a result, the possible values of the Hubble parameter at the inflationary stage are significantly restricted by the anisotropy limits.

The relationship between the inflation vacuum Hubble parameter and the vacuum energy density is

$$H^2 = 8\pi/3\ G\ \rho_{vacuum} = 8\pi/3\ G\ M^4 = 8\pi/3\ M^4 / M_{Planck}^2 \quad (6)$$

where M is the energy scale of inflation and energy density of the vacuum, $\rho_{vacuum} = M^4$. The energy density of gravitons (see Figure 4) is

$$\Omega_{graviton} = 10^{-4}\ \rho_{vacuum} / M_{Planck}^4 = 10^{-4}\ (M/M_{Planck})^4 \quad (7)$$

for wavelengths significantly smaller than the horizon, rising to $\rho_{vacuum}/ M_{Planck}^4 = (M/ M_{Planck})^4$ at horizon size. The quadrupole CMB anisotropy and smaller angular scales limits imply $H_{inflation} < 3\ 10^{-5}\ M_{Planck}$, the inflation energy scale is far removed from the Planck scale ($M < 10^{17}$ GeV), and the energy density of the vacuum is $\rho_{vacuum} = M^4 < 10^{-9}\ M_{Planck}$. There is thus some reason to expect that the phase transition for grand unification (GUT) and the phase transition producing inflation are intimately related. The measurements are forcing the energy scale of each into the same region. After being separated for theoretical freedom and generalness, experiments may reunite them as in the original motivation. There would be a certain economy and beauty in having inflation and grand unification occur through the same mechanism and it would join together particle physics and cosmology at the birth of the universe.

A second major problem in cosmology is the growth of structure in the universe. The largest structures in the current universe (walls and voids) are observed to have density fluctuations $\delta\rho/\rho$ of order unity on scale sizes ~50 Mpc. Structures of this size are at the horizon scale at the surface of last scattering; consequently, the primordial density fluctuations are small and most of the

growth is in the linear regime. The assumption of linear growth requires peculiar velocities ~ 0.01c in order to move the matter the required $10^8$ light years of co-moving distance in the ~$10^{10}$ years estimated to have elapsed since the surface of last scattering, an order of magnitude greater than the peculiar velocity inferred from dipole anisotropy. To explain the observed structure without violating limits on CMB anisotropy, and to generate the critical density required by inflationary models, many astrophysicists have turned to cosmological models in which most of the matter in the universe (> 90%) is composed of weakly interacting massive particles (WIMPs). The dynamical properties of this "dark matter" allow it to clump faster than the baryonic matter, which later falls into the WIMP gravitational potential wells to form the structures observed today. The gravitational potential and motion of these particles produce CMB anisotropy whose amplitude depends on the angular scale size. For scale size ~ 10° most reasonable models predict $\Delta T/T \sim 1$—$3 \times 10^{-5}$, depending on the average density of the universe[24]. Although current observations do not provide significant limits to these models, we anticipate that the DMR will provide a stringent test of such models as it continues to accumulate data.

The DMR team is headed by the Principal Investigator George F. Smoot and Deputy Principal Investigator Charles Bennett. In addition to the *COBE* SWG participation the following people are working on DMR: Alan Kogut, Jon Aymon, Charles Backus, Giovanni De Amici, Kevin Galuk, Gary Hinshaw, Peter D. Jackson, Phil Keegstra, Robert Kummerer, Charles Lineweaver, Laurie Rokke, Luis Tenorio, Richard Mills, Jairo Santana, and Peter Young.

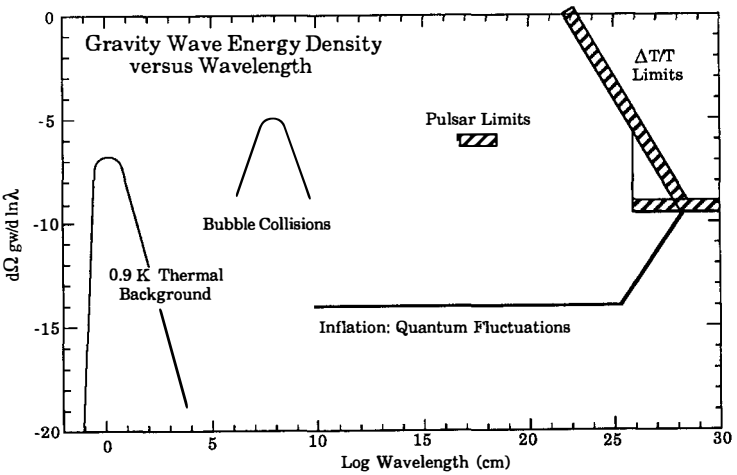


Figure 4. Limits on the energy density of long wavelength gravity waves. The DMR experiment sets two limits based upon the $\Delta T/T$ and strain to energy density relationships shown here and upon the formulas from Linder (1988): one is for the quadrupole and the other the surface of last scattering. The quantum fluctation curve is the predicted spectrum from inflation at maximum allowed normalization. This maximum curve corresponds to an energy scale of inflation slightly less than $10^{17}$ GeV. The potential inflation bubble collision spectrum is from Turner and Wilczek (1990). The normalization on the predictions depend upon the choice of elementary particle theory.

## 5. CONCLUSIONS

A year after launch, the *COBE* instruments are working well and continue to collect data. FIRAS has measured the CMB spectrum quite precisely and future improvements and maps are are expected. The FIRAS and DMR data show the expected dipole anisotropy, consistent with a Doppler-shifted thermal spectrum. Galactic emission is present at levels close to those expected prior to launch, and is largely confined to the plane of the galaxy. The results are currently limited by instrument noise and upper limits to potential sources of systematic error. There is no evidence for any other large-scale feature in the DMR maps. The DMR results limit CMB anisotropies on all angular scales >7° to $\Delta T/T < 10^{-4}$. The results are consistent with a universe described by a Robertson-Walker metric and show no evidence of anisotropic expansion, rotation, or defects (strings, walls, texture). As DMR sky coverage improves and the instrument noise per field of view decreases, we anticipate improved calibration, better estimates of potential systematics, and increasingly sensitive limits to potential CMB anisotropies. In principle, the DMR is capable of testing predictions of both inflationary and dark-matter cosmological models. DIRBE has produced exceptionally good and complete maps of the 1 to 300 micron sky.

## ACKNOWLEDGEMENTS

The *COBE* instruments and satellite have been working well and continue to collect data due to the excellent work by the staff and management of the *COBE* Project. It is a pleasure to thank and acknowledge their work and great success. The COBE research is a team effort including some 19 original Science Working Group members and other scientists (see for example, Smoot *et al.*). This work supported in part by the Director, Office of Energy Research, Office of High Energy and Nuclear Physics, Division of High Energy Physics of the U.S. Department of Energy under Contract No. DE-AC03-76SF00098. We express our appreciation of Tran Thanh van and the Moriond group for organizing this meeting.

## 6. REFERENCES

1. Hauser, M. G. *et al.* 1991, "After the First Three Minutes", AIP, Holt, Bennett, & Trimble
1a. Matsumoto, T., Akiba, M., & Murakami, H, 1988A, *Ap. J.*, **332**, 575.
1b. Murdock, T. L., & Price, S. D. 1985, *Astr. J.*, **90**, 375.
1c. Noda *et al.* (1991) preprint
2. Mather *et al.* 1990a, *Ap. J.*, **354**, L37-L41.,Cheng *et al.* 1990, *Bull. APS*, **35**, 937.
3. Zel'dovich Ya. B. and Sunyaev R. A. 1969, *Ap. Space Sciences*, **4**, 301.
4. Matsumoto *et al.* (1988B), *Ap. J.*, **329**, 567-571.
5. Gush, H.P., Halpern, M. & Wishnow, E. (1990) *Phys. Rev. Lett.*, **35**, 937.
6. Toral, M.A., *et al.*, *IEEE Transactions on Antennas and Propagation*, **37**, 171 (1989).
7. Smoot, G.F., *et al.*, *Ap. J.*, **360**, 685 (1990). also *Ap. J. Let.*, **371**,L1.
8. Bennett, C.L., *et al.*, in preparation.
9. Torres, S., *et al.*, *Data Analysis in Astronomy*, ed. Di Gesu *et al.*, Plenum Press (1990).
10. Kerr, F.J., and Lyndon-Bell, D., *MNRAS*, **221**, 1023 (1990).
11. Fich, M., Blitz, L., and Stark, A., *Ap. J.*, **342**, 272 (1989).
12. Yahil, A., Tamman, A., and Sandage, A., *Ap. J.*, **217**, 903 (1977).
13. Collins, C.B., and Hawking, S.W., *MNRAS*, **162**, 307 (1973).
14. Barrow, J.D., Juskiewicz, R., and Sonoda, D.H., *MNRAS*, **213**, 917 (1985).
15. Sachs, R.K., and Wolfe, A.M., *Ap. J.*, **147**, 73 (1967).
16. Grischuk, L.P., and Zel'dovich, Ya. B., *Sov. Astron.*, **22**, 125 (1978).
17. Burke, W.L., *Ap. J.*, **196**, 329 (1975).
18. Vilenkin, A., *Physics Reports*, **121**, 263 (1985).
19. Stebbins, A., *Ap. J.*, **327**, 584 (1988).
20. Stebbins, A., *et al.*, *Ap. J.*, **322**, 1 (1987).
21. Yang, J., *et al.*, *Ap. J.*, **281**, 493 (1984).
22. Gorski, K., *Ap. J. Lett.* **370**, L5. (1991).
23. Abbott, L.F., and Wise, M.B., *Ap. J. Lett.*, **282**, L47 (1984).
24. Bond, J.R. and Efstathiou, G, *Ap. J. Lett.*, **285**, L45 (1984).

# MODELLING THE EXTRAGALACTIC IR BACKGROUND LIGHT

*A. Franceschini* [1], *P. Mazzei* [2] and *G. De Zotti* [1]

[1] Osservatorio Astronomico, Padova, Italy
[2] Dipartimento di Astronomia, Padova, Italy

We discuss source counts and background radiation in the IR to mm wavelength domain. We address in particular the constraints on galaxy photometric evolution and light emission from primeval objects set by currently available data and by observations soon to be carried out with the forthcoming generation of both ground based and satellite-borne telescopes.

## 1. INTRODUCTION

Observations of the diffuse background radiation may provide relevant information on sources so faint that cannot be directly detected. As far as normal galaxies are concerned, measurements in the optical-UV band are hampered by strong local foreground emissions from the zodiacal light, star-light and reflection by high-latitude galactic dust (Mattila, 1990; Paresce, 1990; Bowyer, 1990), while the radio and X-ray backgrounds are dominated by nuclear activity (radio galaxies, QSO's, AGN's).

On the other hand, at least two prominent spectral windows are available in the wavelength domain from the near-IR to the millimeter, where the local backgrounds are at the minimum (see Puget, these Proceedings): one at $\lambda \sim 3$ to 4 $\mu m$ is bounded by the Zodical light and the Interplanetary dust (IPD) emissions; the other at $\lambda \sim 300$ to 500 $\mu m$ in the prominent hole between the galactic cold dust emission and the Cosmic Microwave Background (CMB). It is a remarkable and happy coincidence that these two wavelength ranges lie just where one would like to observe the redshifted photons from the two most prominent broad emission features in the galaxy spectra: the emission peak at $1 \sim \mu m$ and at 100 $\mu m$ due to stellar photospheric emission and dust re-radiation, respectively.

A third cosmological window, but much less prominent, opens around 60 $\mu m$ within the tight boundaries set by the IPD and galactic *cirrus* emissions. Note a further curious coincidence: even in the most favourable cases (i.e. in the near-IR and sub-mm windows), the expected level of the integrated emission of distant galaxies turns out to be roughly comparable to that of the Galaxy (Franceschini *et al.*, 1991). In any case, a delicate subtraction of the foreground components is mandatory to explore the extragalactic domain.

Several attempts have been carried out in the last few decades to measure extragalactic background in these IR windows. Unfortunately, poor sensitivity and shallow sky coverage have so far prevented to get definite results. Now, the implementation of high-sensitivity detectors at the focal plane of large ground-based telescopes and extensive explorations by low background noise space equipments are quickly changing the state-of-the-art.

After a brief overview on the observational status (Section 2), we expand to discuss in Section 3 predictions of galaxy counts and their contribution to the spectral intensity and anisotropies of the background light: such predictions relate the observed properties of "local" populations to those of the possible distant contributors to the background. Then we summarize some predictions implied by models of primeval objects concerning the IR background light (Section 4). Exciting prospects of future observations are addressed in the last Section.

## 2. OBSERVATIONAL STATUS

We report here on some of the observations on background light, source counts and galaxy luminosity functions in the IR. It is only an incomplete list of what we consider the most relevant results.

### *2.1 Background observations*

*The cosmological window in the near-IR* has been the target of extensive observational efforts, starting from the first exploratory rocket experiment by Harwit *et al.* (1966). Measurements on the diffuse emission obtained by Matsumoto *et al.* (1988a) with broad-band photometers has been confirmed by a recent experiment, with improved spectral and spatial

resolution, of the same group at the Nagoya University (Noda *et al.*, 1991). These results are also roughly consistent with the total sky brightness observed by DIRBE on COBE in the direction of the South Ecliptic Pole (SEP).

However, if rough agreement exists on the total sky emission, the deconvolution of the local foregrounds, needed to infer the intensity of any extragalactic component, which is currently beeing performed by the various groups, is much more uncertain and controversial. Noda *et al.*, for example, with their small field-of-view of 0.2x0.2 degrees, claim to be essentially unaffected by star-light. After a suitable modelling of the zodiacal component, they infer the possible existence of an extragalactic component at the level observed by Matsumoto *et al.* ($\nu I_\nu \sim 10^{-4}\ erg/cm^2\ s\ sr$). Their improved spectral resolution ($\lambda/\Delta\lambda \sim 10$ in the range from 1.4 to 2.5 $\mu m$) has allowed them to conclude that such a background is smooth, without any signs of spectral features. Hauser *et al.* (1991), using the preliminary results by DIRBE, which are based on a quite reliable band-to-band calibration, find a steeper 1 $\mu m$ to 4 $\mu m$ energy distribution and suggest it is more probably consistent with the expected contributions from star- and zodiacal- lights. We defer to Sect. 3 a discussion of this point.

*Longward of 4 $\mu m$ up to 60 $\mu m$* the sky brightness is by far dominated, even outside the ecliptic plane, by IPD emission. Measurements of its peak intensity at 10 and 20 $\mu m$ by COBE, IRAS and other rocket experiments (Murdock & Price, 1985) are in very good agreement. Much is still to be done, however, to accurately define the temperature and spatial distribution of the IPD, which are essential to estimate the extragalactic component. For example, current uncertainties in the temperature distribution of the IPD imply order-of-magnitude errors in its estimated contribution at $\lambda = 4\mu m$. The all-sky surveys by DIRBE, in particular, are expected to allow investigation down to $\sim 0.1\%$ of the IPD emission intensity.

Preliminary estimates of the extragalactic sky background at 100 $\mu m$ has been attempted by various groups using the all-sky surveys of IRAS. However, a comparison with COBE data for several points in the sky (Hauser *et al.*, 1991) has shown that the IRAS data are subject to zero-point and responsivity errors. The COBE estimate of the sky brightness at 100$\mu m$ in the direction of the SEP is $\nu I_\nu \sim 10^{-4}\ erg/cm^2\ s\ sr$, a factor of 3 below the level observed by IRAS. A rocket experiment by Matsumoto *et al.* (1988b; see also Matsumoto, 1990, and Hauser *et al.*, 1991) allowed to set an upper limit to any extragalactic component of less than 1 MJy/sr, after subtraction of the interstellar dust emission, as traced by the n(HI) column density. Matsumoto (1990) reports indications that the observed *isotropic* component at 100 $\mu m$ is due to IPD, so that the truly extragalactic background may be well below the quoted limit.

*The cosmological window at 200 $< \lambda <$ 500 $\mu m$*, where the galactic cold dust, IPD and CMB are at the minimum, has been explored by Matsumoto *et al.* (1988b), Matsumoto (1990), Gush *et al.* (1990). The most impressive limit is reported by the latter, corresponding to a BB temperature of the total sky emission $T < 3°$ (or $\nu I_\nu < 2\ 10^{-6}\ erg/cm^2\ s\ sr$ at 300 $\mu m$). A more conservative limit ($\nu I_\nu \sim 2\ 10^{-5}\ erg/cm^2\ s\ sr$ is reported by Matsumoto (1990) at 262 $\mu m$, based, however, on a rather low signal-to-noise ratio. Also the DIRBE preliminary calibration is quite uncertain here, but results seem to be consistent with those by Matsumoto. The final expected sensitivity of FIRAS (COBE) in this wavelength range is expected to be better than $10^{-6}\ erg/cm^2\ s\ sr$.

*At still longer wavelengths ($\lambda >$ 500 $\mu m$)*, the background radiation starts to be dominated by the CMB (whose spectrum does not seems to deviated by more than 1% from a BB with $T = 2.735\ K$, according to Mather *et al.*, 1990). This obviously sets up a natural boundary to the measurement of the spectral intensity of any other background

components. In spite of that, due to the well proved smoothness of the spatial distribution of the CMB, we can still hope to infer interesting information from analyses of the sky cell-to-cell fluctuations. Preliminary results have already been reported by Kreysa & Chini (1989) at $\lambda = 1.3\ mm$: the 95% upper limit to the rms sky *graininess* for an 11 arcsec beam turns out to be $\sigma < 0.8\ mJy$.

### *2.2 Source counts and luminosity functions*

In a few selected spectral regions of the IR domain, source counting has been performed down to faint flux levels, sometimes also followed by spectroscopic observations. These data are essential for the interpretation of the background radiation, since they allow to define the properties of the local source populations responsible of at least a fraction of the observed background.

*In the near-IR*, thanks to new high-sensitivity detector arrays and to suitable observational techniques (e.g. *micro-scanning*, that allows to reduce the effects of a very high sky noise), imaging observations are becoming competitive with those in the optical. In particular, very deep counts in the K band have been reported by Cowie *et al.* (1990) and Cowie (1991) down to $K \simeq 23$, with an areal density of already 50 $objects/arcmin^2$ (see Figure 4). Counts at brighter magnitudes over more extended sky areas are given by Glazebrook *et al.* (1990). At variance with results obtained in the optical band, where the source counts are seen to steeply increase down to very faint magnitudes (B=26-27), the counts in K quickly flatten already at K=20. At the faintest magnitudes the optical counts show 3 times more sources than those in K. Models predicting no- or a weak luminosity evolution of galaxies easily explain the K-band counts (see Sect. 3.3), but keep significantly below the optical ones. The latter may be interpreted as an evidence for an additional population of low luminosity blue galaxies undergoing an active phase of star formation at moderate z (Cowie, 1991), that should have disappeared by the present time. The relationship of such a faint source population to the local galaxies is quite unclear as yet.

*In the far-IR*, the IRAS survey at 60 $\mu m$, although limited in sensitivity, has been able to detect galaxies up to moderate distances, due to their prominence at these wavelengths. Source counts have been reported down to $S_{60} = 70\ mJy$ (Hacking, Condon & Houck, 1987), which already corresponds for a spiral galaxy to a flux density in the centimetric bands of less than 1 mJy. Redshift distributions and luminosity functions from bright samples have been estimated by various authors (Lawrence *et al.*, 1988; Smith *et al.*, 1987; Soifer *et al.*, 1987; Lonsdale & Hacking, 1989).

Galaxy selection at far-IR wavelengths, as well as those in the radio and in the optical-UV, tend to preferentially detect objects characterized by an enhanced star-formation activity. This activity is generally limited to short-lived bursts during which a small fraction of a galactic mass is turned into massive stars. On the other hand, the near-IR emission is dominated by much older stellar populations, with lifetimes more comparable to the age of the universe.

Therefore, these two IR wavebands provide rather complementary information: the one in the near-IR is very promising about the definition of the geometry of the Universe (Cowie, 1991), the other may soon provide relevant information on the properties of galaxy evolution with cosmic time.

## 3. MODELLING THE IR BACKGROUNDS: KNOWN SOURCE CONTRIBUTION

The first logical step in the interpretation of a diffuse background is to subtract, from the observed values of the intensity and sky fluctuations, the contributions of sources whose statistical properties are already known well enough to allow a virtually model independent operation. We discuss in this Section problems related to the estimate of the contributions of stars and galaxies to the IR backgrounds.

### *3.1 The IR star-light*

To predict star counts we have used the *Galaxy* model by Bahcall (1986), suitably extrapolated from the optical band, where it is defined, to the IR. The extrapolation to the J and K bands has been performed following Mamon & Soneira (1982), who have tentatively transformed, using the IR colors of the different luminosity classes (supergiants through white dwarfs), the various stellar luminosity functions from the V band to the IR. However, predictions based on these luminosity functions fall short of the star counts in the K-band at bright magnitudes by Elias (1978). The reason is that very red late-type stars are obviously under-represented in the optical model. To correct for this, we have increased the cutoff absolute magnitude $M_K^*$ of the disk luminosity function from the proposed value of 2 to 1 and also increased by 50 pc the scale height of main sequence stars. This empirical procedure produced the star counts represented by the thick-line in Figure 1, quite in agreement with the Elias's (1978) counts, as well as with those at very faint magnitudes estimated by Cowie *et al.* (1990). The same figure shows star counts in K for a range of values of the galactic latitude and longitude.

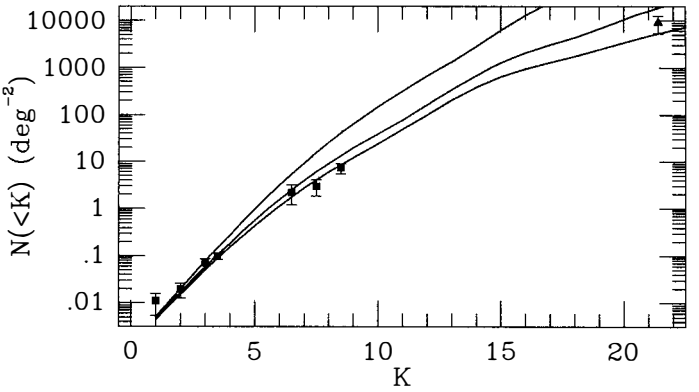


**Figure 1.** Star counts in the K band. Full squares are counts at the galactic pole by Elias (1978), the triangle is the estimated count by Cowie *et al.* (1990). The lower curve is the model prediction for the same galactic direction. The other curves refer to galactic latitudes of 20° and 50°, top to bottom.

The average K-L colours for main sequence stars are typically $\simeq$ 0.2 for V-K< 5 (i.e. B-V< 1.6) and become larger than 0.2 only for stars redder than B-V=1.6. The latter, however, can be neglected for our purposes. Similar results hold for giant stars too. Then

we have estimated star counts at 3.6 $\mu m$ by transforming the total counts in the K band to the L band with an average colour correction K-L=0.2.

Star counts in the 12 $\mu m$ IRAS band have been computed using the procedure described in Hacking (1987). In this case too, modifications to the Bahcall's *Galaxy* model are required by a comparison with data from the IRAS 12 $\mu m$ survey. Predictions of integral counts at 3.6 and 12 $\mu m$ for various galactic coordinates can be found in Franceschini *et al.* (1991).

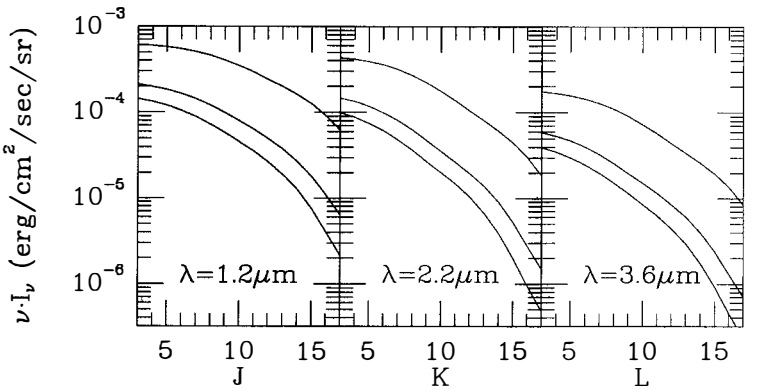


**Figure 2.** Residual contributions to the near-IR background radiation of stars fainter than a given apparent magnitudes, for galactic latitudes of 20°, 50° and 90° (from top to bottom, respectively).

Figure 2 shows, for different values of the galactic latitude, the contributions of stars to the background in various near-IR bands. We see that, due to the flatness of the counts, an important contribution to the starlight comes from bright sources, and this allows a relatively easier subtraction of this component even in surveys with poor angular resolutions.

The confusion limit due to stars in the K band, computed following the procedure described in Franceschini *et al.* (1989), is reported in Figure 3.

### *3.2 Interpretation of near-IR background observations*

As an useful illustration of how delicate is the procedure of deconvolving foreground emissions from observations of the IR background, let us go back to the recent impressive result reported by Noda *et al.* (1991) (see Sect. 2.1). Their claim of the existence of a significant extragalactic component (at a level of $\nu I_\nu = 10^{-4}$ $erg/cm^2$ $s$ $sr$) relies on two basic assumptions on the star-light and Zodiacal contributions. According to Fig. 3, in the sky directions surveyed by the experiment, their 0.2° × 0.2° beam turns out to be limited by confusion already at K=6: then it seems likely that only stars down to this flux limit, rather than to K=8 as they assume, have been excluded by the survey. As shown by Fig. 2, this implies a non negligible difference in the estimated residual star-light at $\lambda = 2.2$ $\mu m$: we find $\nu I_\nu \simeq$ 3.4 $10^{-5}$ and 5.8 $10^{-5}$ $erg/cm^2$ $s$ $sr$ for K=8 and K=6, respectively. A second difference is related to the adopted Galaxy model: for K> 8 Noda *et al.* find a residual star-light of $\sim$ 2 $10^{-5}$ $erg/cm^2$ $s$ $sr$, which is some 50% below that predicted by our model.

All the above translates into significant differences in the estimate of the residual extragalactic component. With reference to the averages in the λ=2.15 and 2.28 $\mu m$ channels

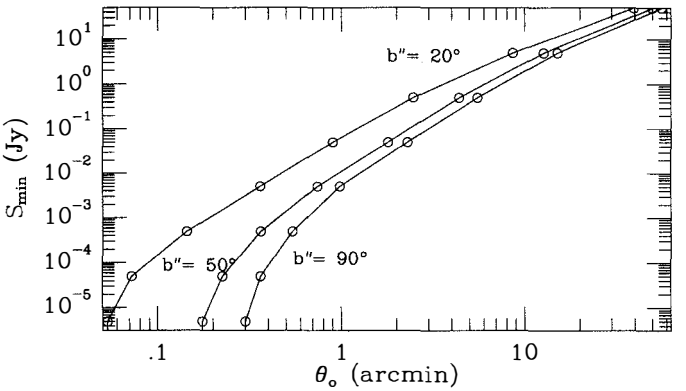


**Figure 3.** Estimates of the confusion limit due to stars for a survey in the K band as a function of the FWHM size of the beam (assumed gaussian). The three curves correspond to galactic latitudes of $|b''| = 20°$, 50° and 90° (from top to bottom, respectively). The limit is set to 5 times the confusion noise.

at the acquisition point B (for which the Zodiacal contamination is less uncertain), the subtraction from the total observed level of $\nu I_\nu \simeq 1.9\ 10^{-4}\ erg/cm^2\ s\ sr$ of a value $\simeq 10^{-4}\ erg/cm^2\ s\ sr$ due to Zodiacal scattering (following Noda *et al.*) results in a residual, possibly extragalactic, component of

$$\nu I_\nu \simeq 3.2\ 10^{-5}\ \ or\ \ 5.6\ 10^{-5}\ erg/cm^2\ s\ sr, \tag{1}$$

if we assume star-light subtraction to K=6 or K=8, respectively. Since the Zodiacal component may easily be somewhat higher than the value assumed above (as suggested by Noda *et al.*), then the estimates in eq. (1) are to be taken as upper limits only. We see that uncertainties by factors of at least 2 or 3 in the estimate of the 2.2 $\mu m$ cosmic background are still present. Note that a dedicated survey in K to better define the star-light contamination would not allow to entirely solve the problem, the estimate of the Zodiacal light's contamination providing still the major uncertainty. All-sky surveys (such as those of COBE) are needed to significantly reduce it.

### *3.3 Galaxy IR counts and cosmological evolution*

Two well distinct approaches can be followed to model the extragalactic background light. One is to start from suitable initial conditions for the spectrum of initial perturbations, develop a model for the formation of the structures, and then predict the background. We will briefly touch on this in Sect. 4, while a more detailed discussion can be found in Carr (these Proceedings). The alternative is to start from the properties of the local source populations (normal and active galaxies, AGN's, etc.) and extrapolate them to the past. This approach has been followed, among others, by Franceschini *et al.* (1991), as briefly summarized hereafter.

The galaxy local luminosity function (LLF) exhaustively describes the statistical properties of local galaxies, under the assumption of homogeneity of the universe on large scales. We have estimated K-band LLF's for various classes of galaxies (E/S0, early- and

late-type spirals, Actively Star Forming and Seyferts) using complete samples selected in the optical. Transformations to the K-band have been performed using average B-K colors, as derived from IR observations of representative galaxy samples. Eventually, reliable LLF's should be obtained from all-sky surveys in K, such as that one planned at ESO for the southern sky.

Photometric models for the various classes are needed to fit the sparse existing data on galaxy IR colors and to transform the K LLF's to the other IR wavebands. Finally, an evolution model, able to consistently reproduce the existing data on galaxy photometry and possibly also chemistry, is needed to derive broad-band spectra of galaxies at moderate redshifts ($z \sim 1$) from those of the local ones: as well known, a dominant contribution to the background radiation is expected from sources at $z \sim 1$, unless dramatic effects of evolution are at work.

We have adopted the model by Mazzei *et al.* (1991), taking into account the effects of evolution with cosmic time of the gas fraction and of the metal abundance. Standard expressions for the IMF and the SFR have been adopted, as well as stellar isochrones based on up-to-date models of stellar evolution (Bertelli *et al.*, 1990). The contribution, mostly relevant in the mid-IR, of hot circumstellar dust shells around AGB stars has been estimated. The evolution of internal extinction in the discs has been taken into account following Guiderdoni & Rocca-Volmerange (1987). Dust re-radiation has been modelled in terms of two components: *warm* dust (typically within HII regions), whose emission has been assumed to evolve proportionally to the SFR; and *cold* dust, heated by the interstellar radiation field and assumed to radiate proportionally to the overall luminosity of the galaxy.

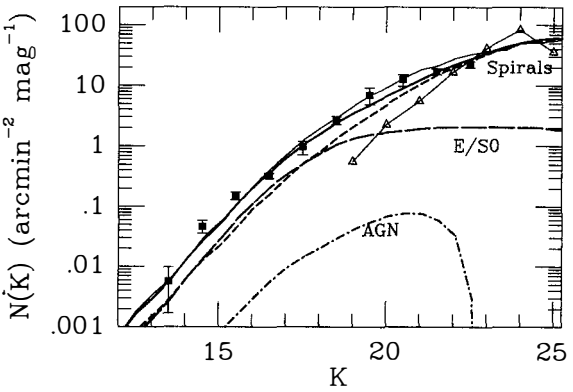


**Figure 4.** Differential counts of galaxies in the K band. The data are from deep surveys by Glazebrook *et al.* (1990), Cowie *et al.* (1990) and Cowie (1991). The heavy solid line shows the global counts predicted assuming a $q_0 = 0.5$ universe, a galaxy formation epoch of 1 Gyr after the Big-Bang, pure luminosity evolution for galaxies and a LLF (in $M_K^{-1}$) keeping constant at $M_K > -20$. Partial contributions of various sub-classes are also indicated. The line marked with open triangles is an estimate of the counts in K of faint blue galaxies and was obtained by transforming B band counts by Tyson (1988) with B-K=3.

The main result of the model is that in the case of disc galaxies the evolution of the bolometric luminosity from the UV to the far-IR is very weak for galactic ages in the range from 2 to 15 Gyr, and weak also are the spectral variations. For early-type galaxies,

the combined effects of spectral evolution and K-correction may provide sensible effects in the near- and mid-IR. Predictions of galaxy counts in the K-band based on this model are compared in Figure 4 to the observed counts. Our results are in good agreement with those by Cowie (1991): if we assume that the LLF of galaxies (in units of $Mpc^{-3} M_K^{-1}$) keeps constant from $M_K = -20$ (where it can be reliably estimated) down to very faint magnitudes, then an Einstein-deSitter world model is indicated by the data. It is interesting that a similarly good fit to the data could in principle be obtained with an open $q_0 = 0.05$ model and a LLF cut-off at $M_K > -20$. To infer any conclusion about the geometry of the universe, a precise definition of the galaxy LLF at such faint absolute magnitudes is clearly mandatory. LLF's derived from galaxy samples at bright magnitudes (e.g. de Lapparent *et al.*, 1989) are affected in this luminosity regime by the uncertainties due to local inhomogeneities: exploitation of redshift surveys at fainter magnitudes (e.g. Broadhurst *et al.*, 1988) could eventually help to solve the problem.

### *3.4 IR background due to galaxies*

The contribution to the diffuse background at $\lambda = 2.2\ \mu m$ from galaxies already detected in deep K band surveys (K< 21.4) amounts already to $\nu I_\nu \simeq 5\ 10^{-6}\ erg/cm^2\ s\ sr$ (Cowie *et al.*, 1990). Extrapolation to fainter magnitudes performed with our model provide a galaxy contribution of

$$\nu I_\nu \simeq 0.75\ 10^{-5}\ \ or\ \ 0.90\ 10^{-5}\ erg/cm^2\ s\ sr \qquad (2)$$

for the two models with $q_0 = 0.5$ and 0.05, respectively. We see that the uncertainties in the contribution of "normal" galaxies to the 2.2 $\mu m$ background are already small, as it should be expected: both models are bound to comply with the very deep counts in K. Use of galaxy evolution models by Yoshii & Takahara (1988) would not significantly change this conclusion. The estimate in eq. (2) may be taken as a lower limit to any extragalactic contribution to the IR background light.

A further significant contribution might be expected from the other numerous component of the extragalactic sky: the faint blue galaxies responsible for the excess counts observed in the optical (Sect. 2.2). A crude estimate of their maximum contribution to the 2.2 $\mu m$ background radiation allowed by the existing data has been obtained in the following way. We have assumed that all sources counted in the B band at $B > 23$ belong to this new population and that their K-band source counts are as steep as in the optical (a clearly extreme case, since the evolution in the near-IR is in any case expected to be less than in the B). The B-K color correction to be applied to these sources was defined by the condition that they should make up the observed counts in K at the faintest limit (see Fig. 4): this is again an extreme case, as the normal galaxies discussed in Sect. 3.3 already saturate these counts. The contribution of this source population to the 2.2 $\mu m$ background would only be $\nu I_\nu \simeq 0.15\ 10^{-5}\ erg/cm^2\ s\ sr$, a small fraction of that of normal galaxies. This illustrates that the result expressed in eq. (2) is fairly robust and that it is quite difficult to significantly increase it with known source populations.

Figure 5 is a summary of background observations in the IR, compared to model predictions. We see, in particular, that the galaxy contribution in the far-IR (curves G1 and G2) is only weakly dependent on the assumption of evolution or no-evolution, adopting the luminosity evolution model described in Sect. 3.3. Both this and the galaxy background in the near-IR cosmological window are still a factor 3 or more lower than best current upper limits. Note that the limit set by Gush *et al.* at 300-500 $\mu m$ (Sect. 2.1) would have already reached the level expected from distant galaxies, but this is to be confirmed by space

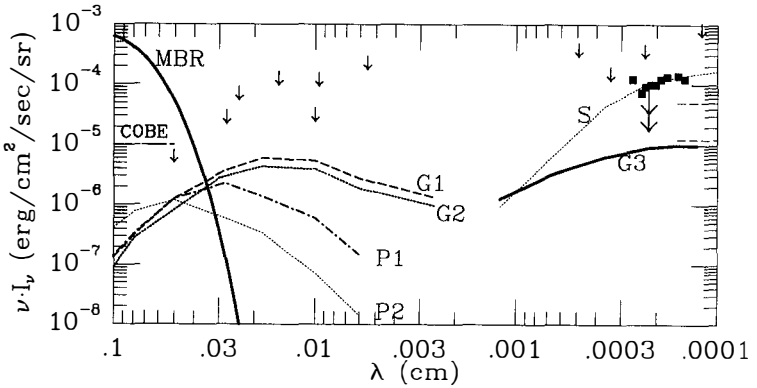


**Figure 5.** Background radiation in the IR. G1 and G2: contribution of dust emission from distant galaxies assuming evolution or no-evolution of the various classes. G3: near-IR background due to photospheric emission of galaxies. The evolution model is described in Sect. 2.2. P1 and P2: primeval dusty galaxies (Sect. 4). S: starlight emission towards the galactic poles, including the very brightest stars. Small downward pointing arrows are upper limits to the extragalactic background set by COBE (cfr. Hauser *et al.*, 1990) and Matsumoto (1990), as discussed in Sect. 2.1. Filled squares are an estimate of a possible extragalactic component by Noda *et al.* (1991). The two long arrows show the reassessment of limits to such a component discussed in Sect. 3.2.

observations.

## 4. CONSTRAINTS ON ENERGY RELEASE BY PRIMEVAL OBJECTS

We do now a step forward and briefly discuss where, in the background spectrum, radiation processes occurring in the primeval universe could have let significant imprints. Due to the effects of the cosmological redshift and of dust re-radiation, most of the energy released by stars and galaxies since their formation is expected to fall in the IR to mm spectral domain. The amount of energy released, however, is severely constrained by the background observations discussed in the previous Sections: upper limits of $\nu I_\nu \sim 3\ 10^{-5}\ erg/cm^2/s/sr$ to any residual extragalactic component in the near- and far-IR, after subtraction of IPD, starlight, galactic dust and normal galaxy contributions, have been obtained.

A number of different pre- and proto-galactic sources have been discussed by various authors. Among others, primeval galaxies, that is galaxies in a very early stage of their evolution. A long-standing discussion has developed on how should they have appeared, as for their size, compactness, spectra, etc. The guiding lines have been inferred from observations of the oldest stellar populations in the Galaxy: the oldest stars already contain some heavy elements ($Z \simeq 1/10$ solar), and the production of all metals in the Galaxy should have quickly occurred in the early phase of its evolution. A rather general, model independent argument has been developed by Lilly & Cowie (1987): the background level expected from a dust-free population of primeval galaxies releasing the energy associated to the production of a solar abundance of heavy elements is simply related to the redshift of formation $z_F$ and to the mean cosmic density of the material processed $\rho$. The two rightmost curves in Fig. 5

correspond to the rather extreme cases of $z_F = 2$ and $\rho = 10\%$ of the critical density (the upper), and to $z_F = 5$ and $\rho = 5\%$ (the lower one). We see that current limits are already constraining the less conservative one.

A more conservative estimate of the diffuse ratiation possibly produced by primeval *dusty* galaxies (PG's) is also shown in Fig. 5. It is based on the following assumptions: 1) PG's emit the bulk of the energy released for the synthesis of a solar metal abundance during a flash lasting 2 $10^8$ $yr$, when galaxy luminosities were a factor 100 larger than today; 2) all optical radiation is absorbed and re-emitted in the far-IR with the typical spectrum of a starburst galaxy; 3) the galaxy formation redshift is $z_F = 2$ (curve P1) or $z_F = 5$ (curve P2). The mean cosmic density of the material processed in this case is significantly less (by roughly a factor 10) than those assumed in the previous paragraph.

If dust is present in massive amounts at high redshifts, either uniformly spread or confined within galaxies, then the peak wavelength $\lambda_{peak}$ of the radiation increases, while $\nu I_\nu$ keeps roughly constant. Imposing thermal balance between dust and radiation and assuming that the radiation density is high enough ($\nu I_\nu > 10^{-6}$ $erg/cm^2/s/sr$), Bond *et al.* (1991) find that $\lambda_{peak} \sim 700$ $\mu m$. In such a case, three backgrounds from primeval objects would be expected: the cosmic MBR, the sub-mm and the residual near-IR backgrounds. Fluctuations in the sub-mm and near-IR sky brightness are expected to be anti-correlated, due to the effects of dust emissions and absorption. Suitable observational strategies of imaging and positional anti-correlation at these two wavebands could be devised to take proper advantage of this effect.

Current observational limits already constrain or rule out some scenarios for the formation of cosmic structures; among others, the "mock" gravity instability (Bond *et al.*, 1991) and the pregalactic explosion scenarios. As for the latter, for example, the current limits imply that the radiation energy density generated by each seed star should not have been larger than the mechanical energy density, which is quite unphysical. Emission processes by pre-galactic stars and very massive objects, black-hole accretion, decaying particles are also under severe strain. Finally, redshifted $Ly\alpha$ emission from high-z ($z > 10$) objects and Pop.III stars should be well below the limits set by the spectroscopic survey of Noda *et al.* (1991).

## 5. CONCLUSIONS

Hard observational challenges, due to the very high noise level, and delicate subtractions of foreground local emissions hinder the full exploitation of the rich information content hidden in the IR background. To give an example, in the near-IR both an high spatial resolution (to subtract stars) and full sky coverage (to deal with the Zodiacal light) are needed. In spite of that, significant progresses have been done in the past few years and are expected from the next ones.

Background observations in the most favourable windows of the IR sky show brightness levels already approaching the values expected by normal weakly evolving or non-evolving galaxies. As a consequence, background observations not only will soon provide information on the cosmological evolution of stellar populations and dust content of galaxies, but are also already setting significant constraints on processes occurring in the dark ages of the universe.

## REFERENCES


Bahcall, J., 1986, *A.R.A.A.*, **24**, 577.

Bertelli, G., Betto, R., Bressan, A., Chiosi, C., Nasi, E., and Vallenari, A., 1990, *Astr. Ap. Suppl.*, **85**, 845.

Bond, J.R., Carr, B.J., and Hogan, C.J., 1991, *Ap. J.*, **367**, 420.

Bowyer, S., 1990, in *The Galactic and Extragalactic Background Radiation*, I.A.U. Symp. **139**, p. 171.

Broadhurst, T.J., Ellis R.S., and Shanks, T., 1988, *M.N.R.A.S.*, **235**, 827.

Cowie, L.L., Gardner, J.P., Lilly, S.J., and McLean, I., 1990, *Ap. J. Lett.*, **360**, L1.

Cowie, L.L., 1991, in *Physical Cosmology*, 79*h* Nobel Symp., Sweden, in press.

Elias, J.H., 1978, *A. J.* **83**, 791.

Franceschini, A., Toffolatti, L., Danese, L., and De Zotti, G., 1989, *Ap. J.*, **344**, 35.

Franceschini, A., Toffolatti, Mazzei, P., L., Danese, L., and De Zotti, G., 1991, *Astr. Ap. Suppl. Ser.*, July issue.

Glazebrook, K., Peacock, J.A., Miller, L., and Collins, C.A., 1990, preprint.

Guiderdoni, B., and Rocca-Volmerange, B., 1987, *Astr. Ap.* **186**, 1.

Gush H.P., Halpern M., and Wishnow E.H., 1990, *Physical Rewv. Lett.*, **65**, 537.

Hacking, P.B., 1987, Ph. D. Thesis, Cornell University.

Hacking, P.B., Condon, J.J., and Houck, J.R., 1987, *Ap. J. Lett.* **316**, L15.

Harwit M., D.P. McNutt, K. Shivanandan, and B.J. Zajac, 1966, *A. J.*, **71**, 1026.

Hauser M., *et al.*, 1991, Proceedings of the *After the First*

Kreysa, E., and Chini, R., 1989, in *"Astronomy, Cosmology and Fundamental Physics"*, M. Caffo *et al.* eds., Kluwer, p. 433.

Lawrence, A., Walker, D., Rowan-Robinson, M., Leech, K.J., and Penston, M.V., 1986, *M.N.R.A.S.* **219**, 687.

de Lapparent, V., Geller, M.J., and Huchra, J.P., 1989, *Ap. J.*, **343**, 1.

Lilly, S.J., and Cowie, L.L., 1987, *"Infrared Arrays and Instrumentation"*, Wynn–Williams C.G. and Becklin E.E. eds., University of Hawaii, p.473.

Lonsdale, C.J., and Hacking, P.H., 1989, *Ap. J.* **339**, 712.

Mamon G., and Soneira R., (1982), *Ap. J.* **255**, 181.

Mather, J.C., *et al.*, 1990, *Ap.J. Lett.* **354**, L37.

Matsumoto, T., Akiba, M., and Murakami, H., 1988a, *Ap.J.* **332**, 575.

Matsumoto, T., Hayakawa, S., Matsuo, H., Murakami, H., Lange, A.E., and Richards, P.L., 1988b, *Ap.J.*, **329**, 567.

Matsumoto, T., 1990, in *The Galactic and Extragalactic Background Radiation*, I.A.U. Symp. **139**, p. 317.

Mattila, K., 1990, in *The Galactic and Extragalactic Background Radiation*, I.A.U. Symp. **139**, p. 257.

Mazzei, P., Xu, C., and De Zotti, G., 1991, submitted to *Astron. Astroph.*

Murdock, T.L., and Price, S.D., 1985, *A.J.* **90**, 375.

Noda M., *et al.*, 1991, Preprint.

Paresce, F., 1990, in *The Galactic and Extragalactic Background Radiation*, I.A.U. Symp. **139**, p. 307.

Smith, B.J., Kleinmann, S.G., Huchra, J.P., and Low, F.J., 1987, *Ap.J.*, **318**, 161.

Soifer, B.T., Sanders, D.B., Madore, B.F., Neugebauer, G., Danielson, G.E., Elias, J.H., Persson, C.J., and Rice, W.L., 1987, *Ap.J.*, **320**, 238.

Tyson, A., 1988, *A. J.* **96**, 1.

Yoshii, Y., and Takahara, F., 1988, *Ap. J.*, **326**, 1.

# COBE AND THE POST-RECOMBINATION ERA

B.J.Carr
Astronomy Unit, Queen Mary & Westfield College, London E1 4NS

J.R.Bond
CITA, University of Toronto, Ontario M5S 1A1

C.J.Hogan
Astronomy Department, University of Washington, Seattle, WA 98195

ABSTRACT

We examine the upper limits placed by COBE and other experiments on the extragalactic background radiation density in the infrared and submillimetre bands. We infer constraints on scenarios involving radiation production in the period between recombination and galaxy formation. Various sources could have produced photons in this period. If affected only by redshift, the photons would generally reside in the near-IR today. However, in some circumstances, they would have been reprocessed into the far-IR or submillimetre bands by cosmological dust. In this case, a crucial signature of such scenarios will be the anisotropies arising from the dust clumpiness and temperature variations. One interesting source of pregalactic radiation would be the VMOs whose black hole remnants are sometimes invoked to explain the dark mass in galactic halos. The VMO-plus-dust scenario is still consistent with FIRAS data but it may soon be excluded, in which case the radiation would need to be in the near-IR.

## 1. INTRODUCTION

FIRAS shows[1] that the cosmic background radiation (CBR) is well fit by a perfect black-body spectrum of temperature 2.735±0.06 K over the waveband 500$\mu$ to 5000$\mu$. In particular, the chemical potential $\mu$ is below $10^{-2}$, the Compton parameter y is below $10^{-3}$, and any excess flux $\Delta I(\lambda)$ must be less than 1% of the CBR peak flux $I(\lambda_{peak})$ over the relevant waveband. These results place general constraints on processes in the early Universe and we start off by summarizing these.

$\mu<10^{-2}$ places constraints[2] on any energy released in the redshift range $10^6>z>10^4$. In this period the Compton interactions of energetic electrons with the CBR photons produce a Bose-Einstein spectrum with a chemical potential $\mu$ which is measure of the energy imput relative to the CBR density. However, there is no time for Bremmstrahlung processes to produce the extra photons necessary to produce a black-body spectrum except at very low frequencies. Only for $z>10^6$ would any heat input be completely thermalized. The limit on $\mu$ places interesting constraints, for example, on superconducting cosmic strings[3,4], evaporating primordial black holes[5] , and the dissipation of primordial density perturbations[6,7].

$y<10^{-3}$ places constraints on energy released in the redshift range $z<10^4$. In this period complete relaxation to a Bose-Einstein distribution is not possible but Compton effects still remove photons from the Rayleigh-Jeans region of the CBR and redeposit them in the Wien region. This process is important both before and after decoupling, the y parameter being a measure of the integral of the electron pressure over redshift[8]. The limit on y may already exclude the explosion[9] and mock-gravity[10] scenarios for large-scale structure formation, and it constrains dark matter scenarios involving decaying elementary particles[11,12]. It also restricts the thermal history and present density and temperature of any hot intergalactic medium[13], implying in particular that a smooth IGM could not produce the observed X-ray background[14,15].

$\Delta I(\lambda)<10^{-2}I(\lambda_{peak})$ places a direct constraint on any submillimetre photons produced in the period after decoupling, as distinct from the indirect constraints (discussed above) associated with interactions with pre-existing photons. The DIRBE results extend these constraints to the the IR bands[16]. One important source of photons in these bands is dust[17-23] and this will be a particular focus of attention in this paper.

The DMR measurements also have important cosmological implications[24]. Besides confirming the dipole anisotropy due to our peculiar motion, they constrain the quadrupole anisotropy to be less than $3\times10^{-5}$ and this places limits on the shear and rotation of the Universe. The anisotropies on smaller scales must be less than $5\times10^{-5}$ above $7^{o}$ and this constrains, for example, the form of the density fluctuations at decoupling[25], various features of large-scale structure[26], the spectrum of primordial gravity waves[27], and the existence of cosmic strings[28]. It also constrains models for spectral distortions produced by dust[10,23], as discussed later.

## 2. BACKGROUND LIGHT LIMITS

Despite various claims in the past, there is currently no positive evidence for an extragalactic background in the IR to submillimetre bands, mainly because of the problem of subtracting foregrounds associated with interstellar dust (ISD), interplanetary dust (IPD) and scattered zodiacal light (ZL). All one claim is upper limits on the background light density and we start by summarizing these. They are conveniently expressed in critical density units by defining a quantity

$$\Omega_R(\lambda) \equiv \frac{4\pi\nu I(\nu)}{c^3\rho_{crit}} = 7\times10^{-7}h^{-2}\left[\frac{\lambda}{100\mu}\right]^{-1}\left[\frac{I(\nu)}{MJy/sr}\right] \qquad (1)$$

where h is the Hubble parameter in units of 100 km/s/Mpc. For comparison, the CBR peaks at $\lambda_{peak}=1400\mu$ with a density $\Omega_R(\lambda_{peak})=1.8\times10^{-5}h^{-2}$. The limits are summarized in Figure (1), along with the local foregrounds.

We have seen that the current FIRAS results[1] imply that any excess background must have an intensity less than 1% of the peak CBR intensity over the range 500-5000$\mu$. This implies

$$\Omega_R(\lambda) < 2\times10^{-7}h^{-2}(\lambda/\lambda_{peak})^{-1} \qquad (2)$$

although the limit could soon be strengthened by a factor of 10. In particular, this disproves the Nagoya-Berkeley claim[29] of an excess at 700$\mu$. The DIRBE results at the south ecliptic pole[16] give upper limits in the J, K, L, M, 12$\mu$, 25$\mu$, 60$\mu$, 100$\mu$, 120-200$\mu$ and 200-300$\mu$ bands. However, the limits indicated in Figure (1) are very conservative since they do not include any subtraction for foreground emission. Stronger but less definite constraints in the far-IR band come from the most recent analysis[30] of the

Nagoya-Berkeley data: careful modelling of the interstellar and interplanetary dust contributions gives $\Omega_R(275\mu)<7\times10^{-7}h^{-2}$, $\Omega_R(135\mu)=(1.4\pm0.4)\times10^{-6}h^{-2}$ and $\Omega_R(100\mu)<8\times10^{-7}h^{-2}$. The 135$\mu$ result may contain an isotropic component, although it would not necessarily be extragalactic.

Some of the IRAS limits are also shown in Figure (1). At one stage it was claimed[31] that IRAS data indicated a 100$\mu$ background with $\Omega_R(100\mu)=3\times10^{-6}h^{-2}$. However, this is inconsistent with both the Nagoya-Berkeley and DIRBE results. A combination of the DIRBE and IRAS data may allow better 60$\mu$ and 100$\mu$ limits[32] but these are not shown in Figure (1). Both the DIRBE and IRAS limits are of order $10^{-4}h^{-2}$ at 12$\mu$ and 25$\mu$. They are very weak there because the interplanetary dust emission is so large. Indeed it may never be possible to get good cosmological light limits in this waveband. In the near-IR, a Japanese rocket experiment[33] gave a limit $\Omega_R(1\text{-}5\mu)<3\times10^{-5}h^{-2}$, with a possible detection of a "line" at 2.2$\mu$ with $\Omega_R(2.2\mu)=3\times10^{-6}h^{-2}$. However, this claim was always controversial and it seems to be disproved by the recent limits of Noda et al.[34].

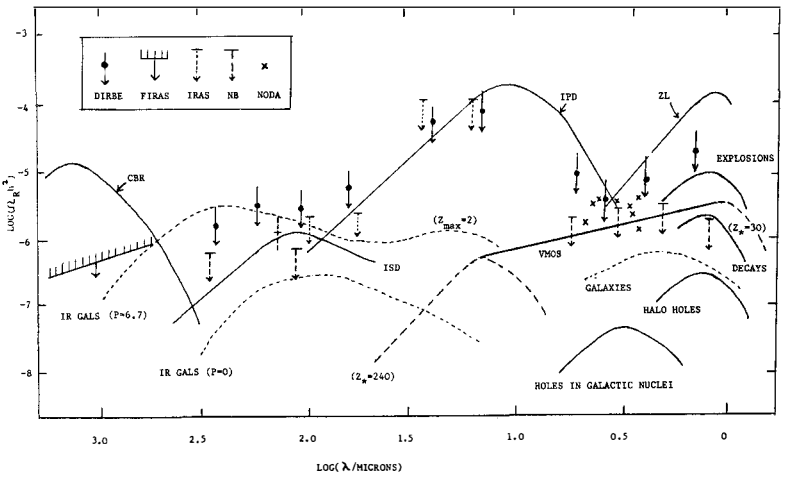


FIGURE (1). This compares the observational constraints on the background radiation density from DIRBE, FIRAS, IRAS, Nagoya-Berkeley and Noda with the local foregrounds and the backgrounds expected in various scenarios.

## 3. SOURCES OF RADIATION IN THE POST-RECOMBINATION ERA

There must be some background radiation in the near-IR due to galaxies[35]. As shown by the dotted curve in Figure 1, the theoretical prediction is only slightly below the upper limits of Noda et al. Dusty galaxies must also produce a far-IR background, although the associated density is very uncertain because of unknown evolutionary factors. If the evolutionary effects are as large as inferred by Saunders *et al.* from the IRAS redshift surveys[36], and if this is due to the source density evolving as $(1+z)^P$ with P=6.7, then the DIRBE results would already constrain[32] the redshift of galaxy formation $z_{max}$ to be less than 2, as indicated by the upper dotted curve in Figure (1). On the other hand, with more modest evolution the background could be several orders of magnitude smaller, as shown by the lower dotted curve (with P=0) of Franceschini[37].

These galactic sources of an IR background are discussed in more detail elsewhere in this volume[32,35,37]. Here we focus on more speculative pregalactic sources. These are discussed in detail in Bond, Carr & Hogan[18] [BCH1], so we only summarize them briefly here. The total density $\Omega_R$ associated with various scenarios is indicated in Table (1). In most cases it is expected to be of order 1% to 10% of the CBR density. While some of the sources are rather exotic, three of them should certainly exist at some level. Most of the backgrounds would currently be in the optical to near-IR if the radiation was affected only by redshift effects,

In the "pregalactic stars" scenario, the stars are assumed to have a density parameter $\Omega_*$ (normalized to the density associated with visible material) and to burn at a redshift $z_*$ (normalized to a value somewhat larger than that associated with galaxy formation). They are also assumed to produce radiation with an efficiency $\epsilon$ (normalized to the value associated with very massive stars). In the "black holes in galactic nuclei" scenario, the holes are supposed to accrete a gas density $\Omega_{acc}$ at a redshift $z_*$ and to produce radiation from accreted material with an efficiency $\epsilon$ (normalized to an optimal value of 0.1); the normalization of $10^{-4}$ for $\Omega_{acc}$ corresponds to a scenario in which one has a $10^8 M_\odot$ black hole at the centre of every galaxy which doubles its mass through accretion. In the "halo black holes" scenario, holes of mass M (normalized to the maximum value consistent with dynamical constraints) are assumed to accrete pregalactic gas with density $\Omega_g$ and temperature $T_g$ at the Bondi rate in some period before galaxy formation.

TABLE (1): background radiation density $\Omega_R$ generated by various pregalactic sources, expressed in units of $10^{-6}$ and compared to the CBR density

| | |
|---|---|
| CBR | $26h^{-2}$ |
| Pregalactic stars | $4\left(\frac{\Omega_*}{0.01}\right)\left(\frac{1+z_*}{10}\right)^{-1}\left(\frac{\epsilon}{0.004}\right)$ |
| Black holes in galactic nuclei | $\left(\frac{\Omega_{acc}}{10^{-4}}\right)\left(\frac{1+z_*}{10}\right)^{-1}\left(\frac{\epsilon}{0.1}\right)$ |
| Halo black holes | $0.6\left(\frac{M}{10^6 M_\odot}\right)\left(\frac{\epsilon}{0.1}\right)\left(\frac{\Omega_g}{0.1}\right)\left(\frac{T_g}{10^4 K}\right)^{-3/2}$ |
| Bound structures | $0.01\left(\frac{\Omega_c}{0.1}\right)\left(\frac{V}{300 km/s}\right)^2\left(\frac{1+z_c}{5}\right)^{-1}$ |
| Explosion scenario | $30\left(\frac{\Omega_g}{0.1}\right)\left(\frac{d}{10 Mpc}\right)^2$ |
| Decaying particles | $5B_X\Omega_{Xi}\left(\frac{1+z_d}{10^5}\right)^{-1}$ |
| Sciama's scenario | $\Omega_{Xi}\left(\frac{\tau_d}{10^{23} s}\right)^{-1}$ |

The background produced in the "bound structures" scenario is associated with the cooling of gravitationally bound objects, the radiation density depending on the density of the cooling gas $\Omega_c$, the redshift of cooling $z_c$, and the velocity dispersion V in the final bound structure (the parameters being normalized to the values appropriate for galaxies). In the "explosion scenario", we assume that stellar explosions produce shells of radius d. In the "decaying particles" scenario, the particles are assumed to have an initial density $\Omega_{Xi}$ and to decay at a redshift $z_d$, with a fraction $B_X$ of their rest mass going into photons. The "Sciama scenario" is the special case in which the particles decay on the timescale $\tau_d$ required to ionize the interstellar and intergalactic medium[38].

We now focus in more detail on the "pregalactic stars" scenario. One reason for invoking this is that the most recent cosmological nucleosynthesis arguments[39] indicate that the baryonic density parameter must lie in the range 0.04 to 0.06 for a Hubble parameter of 50, whereas the density associated with visible galaxies is only 0.01. This indicates that a large fraction of the baryons must be dark. It is possible that the dark baryons are in a hot intergalactic medium[13] but, more likely, they have

been processed into dark remnants through a first generation of "Population III" stars. In this case, their density could at least suffice to explain the dark matter in galactic halos, although one would still need non-baryonic dark matter to explain the critical density required by the inflationary picture. A variety of arguments[40] show that the Population III objects must be either the black hole remnants of "Very Massive Objects" (VMOs) larger than 100 $M_\odot$ which collapse during their oxygen-burning phase or "brown dwarfs" which are too small to burn hydrogen at all.

The most striking signature of the VMO scenario would be the background radiation generated during the stars' hydrogen burning phase. This can be predicted rather precisely since all VMOs have a surface temperature $T_S$ of about $10^5$K and generate radiation with efficiency $\epsilon \approx 0.004$. (Both quantities are almost independent of the VMO mass[41].) We assume that the VMOs have a density parameter $\Omega_* = 0.02h^{-2} = 0.1h_{50}^{-2}$, corresponding to the sort of density required to explain the dark mass in galactic halos, and that they produce black-body radiation with temperature $T_S$. If the radiation is affected only by cosmological redshift, it should then have a peak wavelength and density

$$\lambda_{peak} = 4\left[\frac{1+z_*}{100}\right]\mu, \qquad \Omega_R(\lambda_{peak}) = 10^{-6}h^{-2}\left[\frac{1+z_*}{100}\right]^{-1}\left[\frac{\Omega_* h_{50}^2}{0.1}\right] \qquad (3)$$

at the present epoch, where $z_*$ is the redshift at which the VMOs burn their nuclear fuel. We can place an upper limit on $z_*$ by noting that the main-sequence time of a VMO is $t_{MS} = 2\times10^6$y (independent of mass), so that $z_*$ cannot exceed the redshift when the age of the Universe is $t_{MS}$. This implies $z_* < 240h^{-2/3}$ and hence $\lambda_{peak} < 15\mu$ and $\Omega_R > 5\times10^{-7}h^{-2}$. We can place a lower limit on $z_*$ from UV-IR background light limits. As discussed by McDowell[19], these imply a constraint on the density of VMOs burning at any redshift $z_*$. If one requires $\Omega_* = 0.1h_{50}^{-2}$, this places a lower limit on $z_*$, mainly because one needs the radiation density to be redshifted into the near-IR band, where the background light limits are weaker. In the absence of neutral hydrogen absorption, one requires $z_* > 30$ and this implies $\lambda_{peak} > 1\mu$ and $\Omega_R < 3\times10^{-6}h^{-2}$. The peak of the VMO background must then lie somewhere on the heavy line in Figure (1) and the spectrum must lie within the region to the right of the broken line. This could soon be detectable unless $z_*$ is so large ($\gtrsim 100$) that the VMO light is pushed to $10\mu$, where it would be hidden by interplanetary dust emission.

## 4. REPROCESSING OF PREGALACTIC RADIATION BY COSMIC DUST

If the pregalactic radiation is absorbed by dust, the energy densities indicated in Table (1) still apply but it will be shifted into the far-IR or submillimetre bands. In BCH1 we adopted a rather simplistic analysis, in which the dust cross-section for photons of wavelength $\lambda$ is assumed to be

$$\sigma_d = \frac{\pi r_d^2}{1+(\lambda/r_d)^\alpha} \qquad (4)$$

where $r_d$ is the grain radius. Thus one has a geometric cross-section for $\lambda \ll r_d$ but $\sigma_d$ falls as $\lambda^{-\alpha}$ for $\lambda \gg r_d$. This implies that pregalactic grains with density parameter $\Omega_d$ would absorb photons with $\lambda < r_d$ for

$$1+z_d > 10\left[\frac{\Omega_d}{10^{-5}}\right]^{-2/3}\left[\frac{r_d}{0.1\mu}\right]^{2/3}\left[\frac{\rho_{id}}{3g/cm^3}\right]^{2/3} h^{-2/3}\Omega^{1/3} \qquad (5)$$

where $\Omega$ is the total density parameter and $\rho_{id}$ is the internal grain density. Here we have normalized $\Omega_d$ to the sort of value appropriate for galaxies; the pregalactic value is presumably less than this. Even if there is no pregalactic dust, the dust within galaxies themselves could still reprocess any pregalactic radiation providing eqn (5) with $\Omega_d = 10^{-5}$ is satisfied and providing galaxies cover the sky. The latter condition requires that the redshift of galaxy formation $z_G$ satisfy

$$1+z_G > 11\left[\frac{R_G}{10kpc}\right]^{2/3}\left[\frac{\Omega_{GB}}{0.01}\right]^{-2/3} \Omega^{1/3}h^{-1/3} \qquad (6)$$

where $R_G$ is a typical galactic radius and $\Omega_{GB}$ is the density parameter associated with the baryons in galaxies. We have normalized $R_G$ and $\Omega_{GB}$ to the sort of values appropriate for galaxies like our own, although dwarf galaxies might have a somewhat larger covering factor.

If either pregalactic or galactic dust does reprocess the pregalactic radiation, then the BCH1 analysis implies that it should currently peak at

$$\lambda_{peak} = 700\mu\left[\frac{\Omega_R h^2}{10^{-5}}\right]^{-1/5}\left[\frac{r_d}{0.1\mu}\right]^{1/5}\left[\frac{1+z_d}{10}\right]^{1/5} \quad (\alpha=1) \qquad (7)$$

where we have normalized the radiation density $\Omega_R$ to the sort of value anticipated in Table (1). The crucial point is that the wavelength is very

insensitive to the various parameters appearing in eqn (7) because the exponents are so small. (The exponents would be even smaller for $\alpha$=2.) The fact the Nagoya-Berkeley experiment[29] appeared to find a submillimetre excess peaking at almost exactly the wavelength predicted was, of course, very exciting and prompted us to embark on a much more detailed attempt to fit the data. The Nagoya-Berkeley excess has now been disproved but the need for a more careful analysis remains since there must be reprocessed pregalactic light at some level.

In the more sophisticated analysis of Bond et al.[23] (BCH2), we characterize the dust by a function $A_d(\lambda)$, related to the grain radius $r_d$ and grain absorption cross-section $\sigma_d$ by

$$A_d(\lambda) = \left[\frac{\sigma_d}{\pi r_d^2}\right]\left[\frac{3\lambda}{8\pi r_d}\right] \quad , \tag{8}$$

and allow for the fact that the exponent $\alpha$ in eqn (4) could itself be wavelength-dependent. $A_d$ is a useful parameter because it is constant over the wavelength domain in which $\alpha$=1. The grain model is then specified by three parameters rather than two: an "effective" grain radius $r_s$ for the source radiation ($r_s$=$r_d$ for a geometrical cross-section), the value of $A_d$ at 100$\mu$ (denoted as $A_{d100}$), and the value of $\alpha$ in the far-IR. We also introduce a more realistic model for the source luminosity history $L_s(z)$, allowing for both "burst" and "continuous" models. In the latter, $L_s(z)$ is assumed to evolve as $(1+z)^P$ between a turn-on redshift $z_1$ and a turn-off redshift $z_o$. We assume that the dust density $\Omega_d(z)$ is created at some redshift $z_d$ and remains constant thereafter.

With these assumptions, the dust temperature evolves according to

$$\frac{T_d(z)}{T_c(z)} = \left[1+\left[\frac{10}{1+z}\right]^{\alpha}\left[\frac{r_s A_{d100}}{100\mu}\right]^{-1}\left[\frac{\Omega_{RS}(z)}{\Omega_c(z)}\right]\right]^{1/(4+\alpha)} \tag{9}$$

where $\Omega_{RS}$ and $\Omega_c$ are the source radiation and CBR density at redshift z. For $r_s$=$r_d$ and $\alpha$=1, this would correspond to the $\lambda_{peak}$ of eqn (7) but the parameter $\Omega_{RS}$ must be interpreted carefully. If the UV opacity up to the epoch corresponding to redshift z is small, $\tau_{uv}(z)<1$, then $\Omega_{RS}$ is just associated with the integral of $L_s$ over time until then. (This was essentially the case considered in BCH1.) However, if $\tau_{uv}(z)>>1$ and P<4, then the energy density at any point comes only from the region within one UV optical depth of that point. In this case, $\Omega_{RS}$ is roughly the

radiation density generated over a cosmological time at redshift z divided by $\tau_{uv}(z)$. In particular, this includes the case in which the sources are completely shrouded in local dust clouds (cf. IRAS galaxies). If $\tau_{uv}>>1$ and P>4, then the emission from the turn-on redshift $z_1$ dominates and one effectively has a "burst" with $\Omega_{RS}(z)$ being the radiation density at $z_1$ divided by $\tau_{uv}(z_1)$ and multiplied by $\exp[\tau_{uv}(z)-\tau_{uv}(z_1)]$.

In BCH2 we consider 14 different models (corresponding to different values of $\alpha$, $\Omega_d$, $\Omega_R$, $z_1$, $z_o$ and P) and the resulting spectra are shown in Figure (2). Also shown are the current and ultimate FIRAS limits, the 275$\mu$ Nagoya-Berkeley limit, and the limit of Gush et al. (GHW). We can apply the BCH2 analysis to the VMO scenario in particular by noting that eqn (3) implies that each value of $\Omega_R$ corresponds to a specific value of $z_*$. Figure (2) then shows that the VMO-plus-dust scenario is viable in all models except 1, 5 and 6. For example, if $r_d=0.01\mu$, $z_*=100$ and $z_1=9$, then one is below the constraints for $\Omega_d=10^{-6}$ but above them for $\Omega_d=10^{-5}$. If the COBE results do eventually eliminate the VMO-plus-dust scenario, it should be stressed that one would not necessarily expect dust reprocessing anyway. There may no pregalactic dust at all and protogalactic dust would only suffice if the conditions specified by eqns (5) and (6) were satisfied. Although galaxies might be expected to cover the sky at redshifts exceeding 4 in the CDM picture[42], the analysis of Fall et al.[43] indicates that the dust-to-gas ratio in primordial galaxies may only be in the range 1/20 to 1/4 that of the Milky Way for $2<z<3$, which makes condition (5) difficult to satisfy. Therefore, if COBE does eliminate the far-IR backround predicted, the VMO light could still reside in the near-IR.

## 6. ANISOTROPIES

One of the important implications of the above discussion is that the mere detection of a far-IR or submillimetre background will not identify its astrophysical source, since the expected spectrum depends only weakly on the epoch and mode of radiation production. However, crucial information about the source could come from the detection of any anisotropies in the background. Indeed, since the peak of dust background is so close to that of the CBR, interesting constraints on dust models can already be inferred from CBR anisotropy limits.

In BCH1 we argued that the dust emission can be regarded as coming from a "shell" of thickness $\sim 1h^{-1}$Gpc at a distance $6h^{-1}$Gpc. We then

FIGURE (2a). All these models have the same energy release ($\Omega_R h^2=10^{-6}$) but the quantity and character of dust varies. $\alpha$=1 in 1 and 2; $\alpha$=2 in 3 and 4; $\Omega_d=10^{-5}$ in 1 and 3; $\Omega_d=10^{-6}$ in 2 and 4. All the models have $z_1$=9 and $z_o$=0 and the energy is released in a burst.

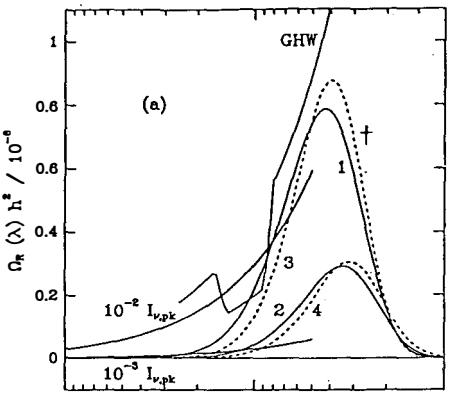


FIGURE (2b). In these models the dust properties are fixed ($\alpha$=1.5) but the amount and characteristic redshifts are varied. $\Omega_d=10^{-5}$ in 5 and 7; $\Omega_d=10^{-6}$ in 6 and 8; $z_1$=50 and $z_o$=25 in 5 and 6; $z_1$=5 and $z_o$=0 in 7 and 8. All the models have $\Omega_R h^2=10^{-6}$. The energy is released in a burst in 7 and 8.

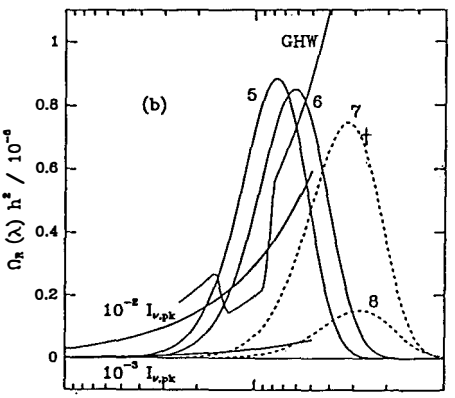


FIGURE (2c). All these models have $\alpha$=1.5 and $\Omega_R h^2=10^{-7}$ but the other dust characteristics vary. $\Omega_d=10^{-5}$ in 9, 11 and 14; $\Omega_d=10^{-6}$ in 10 and 13; $z_1$=50 and $z_o$=25 in 9 and 10; $z_1$=9 and $z_o$=0 in 11 and 13; $z_1$=5 and $z_o$=0 in 14. The energy is released in a burst in 11 and 14.

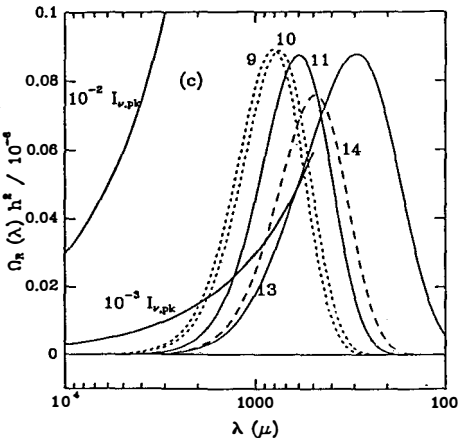

calculated the anisotropies on the assumption that the dust clumps in the same way as galaxies, with a statistical fluctuation in the number of galaxies within each beam. If the galaxy correlation function[44] has the form $\xi_g(x)=(x/x_0)^{-\gamma}$ with $\gamma\simeq1.8$ for $x<x_0$, then one just has Poisson fluctuations for beam sizes $\sigma$ exceeding the angular scale $\theta_0$ associated with the correlation scale $x_0$ but the fluctuations are enhanced for $\sigma<\theta_0$. One can infer that the rms intensity fluctuations have the form[18]

$$\left\langle\left[\frac{\Delta I}{I}\right]^2\right\rangle^{1/2} = \begin{cases} \left[\frac{x_0}{ct}\right]^{1/2}\left[\frac{\sigma}{\theta_0}\right]^{-1} & (\sigma>\theta_0) \\ \left[\frac{x_0}{ct}\right]^{1/2}\left[\frac{\sigma}{\theta_0}\right]^{(1-\gamma)/2} & (\sigma<\theta_0) \end{cases} \qquad (10)$$

Here ct is the horizon size and $x_0$ is the correlation length at the epoch of dominant emission. This would be about $5h^{-1}(1+z)^{-1}$Mpc if there were no evolution of the clustering pattern, corresponding to $\theta_0\simeq1'$, so eqn (10) gives fluctuations of a few percent on arcmin scales. The distinctive feature of the dust anisotropies is that they are wavelength-dependent and much larger than the primary anisotropies at small angular scales (where the latter are expected to be erased).

In BCH2, we confirm that the concept of an emission shell is a good one but we have refined the anisotropy estimates by allowing for fluctuations in the temperature of the emission shell as well its optical depth. (The temperature fluctuations are just associated with spatial fluctuations in the luminosity of the sources.) We have also extended the analysis to the high optical depth case, so as to include, for example, the situation with IRAS galaxies where the dust and sources are highly clumped. Our analysis includes both the linear regime, appropriate when the density fluctuations are small, and the "shot noise" regime, appropriate after galaxies form.

Some of the results of our analysis are summarized in Figure (3), where we compare the predicted anisotropies at 1300$\mu$ with the current limits from the IRAM experiment of Kreysa & Chini[45], the OVRO experiment of Readhead et al.[46] and the VLA experiment of Hogan & Partridge[47]. Figure (3) represents the ability of each experiment to probe the submillimetre anisotropy as a filter in multipole space. (Note that the $l$-pole probes an angular scale of $3438/l$ arcmin.) When one multiplies this by the angular power spectrum $C_l(\lambda)$ of the background and integrates over $d\ln l$, one obtains the rms anisotropy for the experiment. The overall normalization is the rms energy density fluctuation $\sigma_I = \langle(\Delta I/I)^2\rangle^{1/2}$, which is straightforwardly related to the rms temperature fluctuation $(\Delta T/T)_{rms}$.

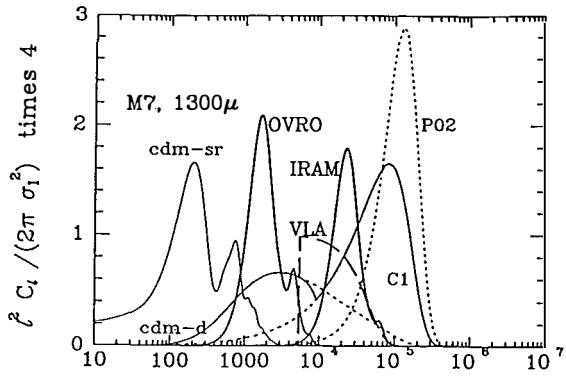


FIGURE (3). This shows the ability of various experiments to probe the anisotropies predicted in some of the dust scenarios discussed in the text.

The figure shows the fluctuations associated with model 7 and also the primary fluctuations in the CDM scenario (cdm-sr indicates the "standard recombination" case). "PO2" is the Poisson fluctuation model in which the galaxies are placed randomly; "C1" is the $\xi \sim r^{-1.8}$ continuous clustering model, with the amplitude appropriate for observed galaxies; "cdm-d" assumes the usual CDM linear fluctuation spectrum with biasing and linear growth. One can also consider a hybrid of the last two cases in which one has both Poisson and continuous clustering contributions. The figure confirms that the dust fluctuations peak on a smaller scale ($\ell=10^3$ to $10^6$) than the primordial density fluctuations. The optimal filter scale would be around 1" but the resolution achievable with submillimetre telescopes is generally above 10". One can also infer from the figure which experiments place the most interesting constraints on each dust scenario.

As a specific example, consider a CDM-like scenario with galaxies and $\alpha=1.5$ dust forming at $z_G=5$ and the burst of radiation having energy $\Omega_R h^2=10^{-6}$. The Kreysa & Chini experiment[45] at 1300$\mu$ uses a beam with $\theta_{fwhm}=11"$ and $\theta_{throw}=30"$ and gives a constraint $(\Delta T/T)_{rms}<2.6\times10^{-4}$. This implies that the number density of the sources must satisfy $n_G^*>0.06(h^{-1}\text{Mpc})^{-3}$ and their correlation length must be $x_o<4h^{-1}$Mpc. If one took the background at 1300$\mu$ to have the maximum density compatible with the COBE constraints, then one would need $n_G^*>1(h^{-1}\text{Mpc})^{-3}$ and $r_o<0.7h^{-1}$Mpc. Future anisotropy experiments will be able to strengthen these limit on $n_G^*$ and $r_o$, thus providing a very promising probe of the formation of protogalaxies at high redshift.

REFERENCES


1. Mather, J.C. et al., 1990, Ap.J.Lett., 354, L37.
2. Danese, L. & De Zotti, G., 1980, Astr.Astrophys., 84, 364.
3. Ostriker, J.P. & Thompson, C., 1987, Ap.J.Lett., 323, L97.
4. Sanchez, N. & Signore, M., 1990, Phys.Lett.B., 241, 332.
5. MacGibbon, J. & Carr, B.J., 1991, Ap.J., 371, 447.
6. Daly, R.A., 1991, Ap.J., 371, 14.
7. Barrow, J.D. & Coles, P., 1991, Mon.Not.R.Astr.Soc., 248, 52.
8. Zeldovich, Ya.B. & Sunyaev, R.A., 1969, Astrophys.Space Sci., 4, 301.
9. Levin, J.L., Freese, K. & Spergel, D.N., 1991, Ap.J., in press.
10. Hogan, C.J., 1989, Ap.J., 340, 1.
11. Field, G.B. & Walker, T.P., 1989, Phys.Rev.Lett., 63, 117.
12. Fukugita, M. & Kawasaki, M., 1990, Ap.J., 353, 384.
13. Bartlett, J.G. & Stebbins, A., 1991, Ap.J.Lett., in press.
14. Lahav, O., Loeb, A. & McKee, C.F., 1990, Ap.J.Let., 349, L9.
15. Taylor, G.B. & Wright, E.L., 1989, Ap.J., 339, 619.
16. Mather, J.C. et al., 1991, Ap.J., in press.
17. Rowan-Robinson, M., Negroponte, J. & Silk, J.,1979, Nature, 281, 635.
18. Bond, J.R., Carr, B.J. & Hogan, C.J., 1986, Ap.J., 306, 428 [BCH1].
19. McDowell, J.C., 1986, Mon.Not.R.Astr.Soc., 223, 763.
20. Negroponte, J., 1986. Mon.Not.R.Astr.Soc., 222, 19.
21. Hayakawa, S. et al., 1987, Pub.Astr.Soc.Japan, 39, 941.
22. Adams, F.C., Freese, K., Lenon, J. & McDowell, J.C.,1989,Ap.J.,344, 24.
23. Bond, J.R., Carr, B.J. & Hogan, C.J., 1991, Ap.J., 367, 420 [BCH2].
24. Smoot, G.F. et al., 1991, Ap.J., in press; also this volume.
25. Bond, J.R. & Efstathiou, G., 1984, Ap.J.Lett., 285, L45.
26. Bertschinger, E., Gorski, K.M. & Dekel, A., 1990, Nature, 345, 507.
27. Burke, W.L., 1975, Ap.J., 196, 329.
28. Stebbins, A., 1988, Ap.J., 327, 584.
29. Matsumoto, T. et al., 1988, Ap.J., 329, 567.
30. Lange, A.E. et al., 1990, Ap.J., in press.
31. Rowan-Robinson, M., 1986., Mon.Not.R.Astr.Soc., 219, 737.
32. Jones, M.H. & Rowan-Robinson, 1991, this volume.
33. Matsumoto, T, Akiba, M. & Murakami, H., 1988, Ap.J., 332, 575.
34. Noda, M. et al., 1991, Nagoya University Preprint DPNU-91-02.
35. Leinert, C. & Mattila, K., 1991, this volume.
36. Saunders, W. et al., 1991, Mon.Not.Roy.Astron.Soc., 242, 318.
37. Franceschini, A., 1991, this volume.
38. Sciama, D.W., 1990, Comm. Astrophys., 15, 71.
39. Olive, K.A., Schramm, D.N., Steigman, G. & Walker, T., 1990, Phys.Lett.B., 236, 454.
40. Carr, B.J., 1990, Comm.Astrophys., 14, 257.
41. Bond, J.R., Arnett, W.D. & Carr, B.J., 1984, Ap. J., 280, 825.
42. Najita, J., Silk, J. & Wachter, K.W., 1990, Ap.J., 348, 383.
43. Fall, S.M., Pei, Y.C. & McMahon, R.G., 1989, Ap.J.Lett., 341, L5.
44. Peebles, P.J.E., 1980, "The Large-Scale Structure of the Universe", Princeton University Press.
45. Kreysa, E. & Chini, A., 1989, Particle Astrophysics Workshop, Berkeley, Dec.1988.
46. Readhead, A.C.S. et al., 1989, Ap.J., 346, 566.
47. Hogan, C.J. & Partridge, R.B., 1989, Ap.J.Lett., 341, L29.

# THE ROTATIONAL EXCITATION TEMPERATURE OF CN

Philippe Crane
European Southern Observatory
Munich, Germany

E. Palazzi, and N. Mandolesi
Istituto TE.S.R.E.
Bologna, Italy

**Abstract**

A difference between the excitation temperature of CN and the temperature of the Cosmic Background Radiation as determined by recent space interferometers is established. Several possible origins for this difference are explored, none of which seem to explain the difference.

# 1 Introduction

The CN molecule has provided one of the most accurate measures of the temperature of the the Cosmic Background Radiation to date(Crane *et al.*[1]; Kaiser and Wright[2]). However, two recent measurements both using Michelson interferometers in space( Mather *et al.*[3]; Gush *et al.*[4]), have determined an accurate temperature for the CBR which is about 85 mK below the temperature determined from CN. At first sight, this difference might be expected if there were other processes beside the CBR which are exciting the CN rotational levels used to determine the CBR temperature. We show here that the available evidence does not support this contention and suggest further observations of translucent clouds which might shed new light on this subject.

The following discussion is a summary of results which are being prepared for publication(Palazzi, Mandolesi, and Crane[5]) and the interested reader is referred to this paper for a more detailed discussion.

# 2 Data

We have used the ESO CAT and associated Coudé spectrometer to observe 10 new sight lines in order to determine the CN excitation temperature, and have collected data from the literature to compile a total of 27 sight lines with measured $T_{exc}$(CN) of reasonable precision. This data set is drawn from sight lines with enough variety of conditions so that we may hope to understand all the various parameters which might effect $T_{exc}$(CN). For as many as possible of these sight lines, we have collected data on the $H_2$ and HI column densities, the CaI and CaII column densities, as well as other related data. These data are collected in the tables where Table 1 presents the data for the new sight lines, Table 2 presents the data from the literature, and Table 3 presents the ancilliary data relevant to the discussion.

Figure 1 shows the excitation temperature of CN for the stars listed in Tables 1 and 2. Most remarkable about this is the fact that all but one of these values lie above the space interferometer value of 2.735±0.030 K. In assigning the error to the space interferometer result, we have tried to represent the statistical uncertainty in the results and not the residual systematic errors. The weighted average of the excitation temperatures given in Figure 1 is 2.820±0.020 K. This does not include the value for $\zeta$ Oph since this value being considerable more accurate than the others would unduly weight the average. Including $\zeta$ Oph gives $T_{exc}$(CN)= 2.805±0.020 K.

The result that the weighted average of $T_{exc}$(CN) is close to the value for $\zeta$ Oph is to be expected since the few sight lines that have been well studied have been chosen to have relatively small column densities and hence small local excitation of CN.

Thus it is pretty clearly established that the excitation temperature of CN is about 85±30 mK above the space interferometer value for the CBR temperature.

Table 1: Data From New Sight Lines

| Star | $W_\lambda$ R(0) (mÅ) | $W_\lambda$ R(1) (mÅ) | $W_\lambda$ P(1) (mÅ) | b (Km $s^{-1}$) | $T_{exc}$ (K) |
|---|---|---|---|---|---|
| HD73882 | 34.83 ± 1.93 | 17.31 ± 0.55 | 10.23 ± 0.42 | 1.06 ± 0.09 | 2.75 ± 0.23 |
| HD147933 | 6.11 ± 0.48 | 2.08 ± 0.67 | 1.05 ± 0.59 | 0.84 ± 0.22 | 2.94 ± 0.48 |
| HD147933a | 6.85 ± 0.43 | 2.12 ± 0.67 | 1.38 ± 0.66 | 0.84 ± 0.22 | 2.86 ± 0.43 |
| HD148184 | 3.45 ± 0.31 | 1.03 ± 0.47 | 0.46 ± 0.47 | 1.24 ± 0.42 | 2.78 ± 0.61 |
| HD148379 | 1.83 ± 0.47 | 0.61 ± 0.67 | 0.46 ± 0.66 | 1.48 ± 0.45 | 3.17 ± 1.73 |
| HD149404 | 7.73 ± 0.43 | 2.48 ± 0.60 | 1.34 ± 0.59 | 0.67 ± 0.30 | 2.77 ± 0.33 |
| HD150136 | 1.93 ± 0.54 | 0.92 ± 0.59 | 0.15 ± 0.54 | 1.16 ± 1.00 | 3.29 ± 1.58 |
| HD152236 | 6.09 ± 0.32 | 2.09 ± 0.60 | 0.74 ± 0.59 | 0.65 ± 0.40 | 2.80 ± 0.43 |
| HD169454 | 25.10 ± 0.70 | 15.50 ± 0.88 | 10.85 ± 0.83 | 0.64 ± 0.17 | 2.84 ± 0.18 |
| HD170740 | 13.60 ± 0.43 | 6.68 ± 0.61 | 3.82 ± 0.60 | 0.84 ± 0.20 | 3.49 ± 0.22 |

# 3 Discussion

There are several possible mechanisms which might cause the CN excitation temperature to be above the CBR temperature. We discuss these below. It is important to note that for most of these mechanisms, CN emission at 2.64mm is predicted and observations of this emission can be used to verify that indeed the CN is out of thermal equilibrium with the ambient radiation field.

The most effective mechanism for excitation of the CN rotational levels is electron collisions. If this were the case, then any excess excitation might be expected to correlate with the electron density in the individual clouds. However, the electron density is a difficult parameter to determine. We have used the CaI/CaII ratio to determine $n_e$, and then attempted to correlate this value with the observed CN excitation temperature. We find no correlation. We conclude that the determinations of $n_e$ are too uncertain to provide a key to any possible excess CN excitation.

We have also looked at the effect of collisions with HI and $H_2$. We again find no effect. In fact, we are not able to find a correlation of the the CN excitation temperature with any of the parameters givens in Table 3. In particular, we do not find a correlation of $T_{exc}$(CN) with the linewidth parameter, b, used to determine the saturation correction to the observed equivalent widths. This is important since it one major source of possible systematic error in the optical observations.

We note that for the sight lines toward $\zeta$ Oph(Crane *et al.*[1]), and HD154368(Palazzi *et al.*[13]), there are sensitive observations at 2.64 mm which can be used to determine the extent to which the CN molecules are excited above the ambient radiation field. For the case of HD154368, where $T_{exc}$(CN) = 2.87 ± 0.08 K. and we predict a millimeter line of 75mK if $T_{CBR}$ = 2.735 K, we find a millimeter line of only 35mK. This is a particular convincing case since it clearly indicates that either there is something amiss with the CN observations or that $T_{CBR}$ is different from 2.735K.

Table 2: Data taken from the literature

| Star | $W_\lambda$ R(0) (m$\AA$) | $W_\lambda$ R(1) (m$\AA$) | $W_\lambda$ P(1) (m$\AA$) | b (Km $s^{-1}$) | $T_{exc}$ (K) | Ref |
|---|---|---|---|---|---|---|
| HD21483 | 44.05 ± 0.28 | 23.04 ± 0.20 | 13.79 ± 0.17 | 1.29 ± 0.03 | 2.81 ± 0.03 | 6,7 |
| HD23180 | 4.69 ± 0.10 | 1.39 ± 0.06 | 0.69 ± 0.06 | 1.30 ± 0.4 | 2.78 ± 0.07 | 8 |
| HD24398 | 8.99 ± 0.02 | 2.89 ± 0.02 | 1.30 ± 0.02 | 1.25 ± 0.02 | 2.79 ± 0.03 | 2 |
| HD26571 | 21 ± 3 | 11 ± 4 | 8 ± 3 | 0.70 | 3.22 ± 0.96 | 9 |
| HD29647 | 62 ± 3 | 46 ± 3 | 31 ± 3 | 1.40 ± 0.2 | 2.90 ± 0.08 | 10 |
| HD62542 | 26.45 ± 0.50 | 18.35 ± 0.40 | 11.60 ± 0.40 | 0.79 ± 0.1 | 3.30 ± 0.20 | 11 |
| HD80077 | ... | ... | ... | ... | 2.90 ± 0.20 | 7 |
| HD147343 | 18.2 ± 3.4 | 9.7 ± 2.7 | ≤ 6.0 ± 2.3 | 0.80 ± 0.2 | ≤ 3.52 ± 0.91 | 12 |
| HD147701 | 24.3 ± 2.1 | 14.1 ± 1.8 | 7.5 ± 1.5 | 0.80 ± 0.2 | 3.13 ± 0.42 | 12 |
| HD147889 | 36.7 ± 1.5 | 20.0 ± 1.4 | 10.2 ± 1.0 | 1.40 ± 0.3 | 3.19 ± 0.18 | 12 |
| HD149757 | 7.75 ± 0.04 | 2.45 ± 0.02 | 1.25 ± 0.02 | 0.88 ± 0.2 | 2.796 ± 0.013 | 1 |
| HD154368 | 24.62 ± 0.13 | 15.12 ± 0.11 | 9.74 ± 0.09 | 0.65 ± 0.01 | 2.87 ± 0.08 | 13 |
| HD206267 | 22: | 8: | ... | ... | 3.19: | 11 |
| HD207198 | 15: | 4: | ... | ... | 2.70: | 11 |
| HD210121 | ... | ... | ... | 1.0 | 2.80 ± 0.20 | 7 |
| HD210839 | 7: | 3: | ... | ... | 3.54: | 11 |
| TY CrA | 21.00 ± 2.75 | 13.00 ± 2.75 | 8.0 ± 4.5 | 0.60 ± 0.3 | 3.10 ± 1.05 | 14 |

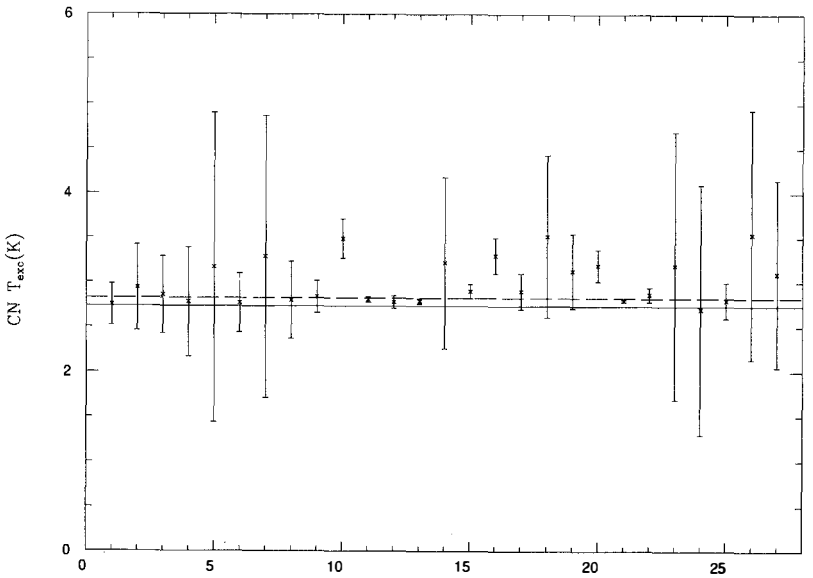


Figure 1: Plot of the CN temperatures from Tables 1 and 2. The full line indicates the space interferometer results. The dashed line is the weighted average mentioned in the text.

There is one possible mechanism that could account for the difference between the CN excitation temperature and the space interferometer results for $T_{CBR}$, and not produce a visible emission at 2.64 mm. This is cool dust in the clouds being observed. This would act like a uniform local gray body radiation field and would essentially be an addition to the CBR radiation field in the clouds being observed. If we model the dust radiation as a black body at temperature $T_{dust}$ with a dilution factor $\eta$ and try to match the excess CN excitation temperature at both 1.32 and 2.64 mm, we do not find a dilution factor that matches at both wavelengths for any reasonable value of $T_{dust}$. Thus we can rule out this mechanism for the sight lines where we have observations at both 2.64 and 1.32 mm.

Future observations which might clarify the difference between the space interferometer results and the CN result would include optical spectra of increased precision along selected sight lines, and millimeter observations of emission at 2.64 mm.

## References


1. Crane, P., Kutner, M.L., Hegyi, D.J., and Mandolesi, N., 1989, *Ap.J.*, **346**, 146.
2. Kaiser, M.E., and Wright, E.L., 1990, *Ap.J.* Lett., **356**, L1.
3. Mather, J.C., *et al*, 1990, *Ap.J. Lett.*, **354**, L37.
4. Gush, H.P., Halpher, M., and Wishnow, E.H., 1990, *Phys.Rev.Lett.*, **65** 537.
5. Palazzi, E., Mandolesi, N., and Crane P., 1991, *Ap. J.*,to be submitted.
6. Meyer, D.M., Roth, K.C., and Hawkins, I., 1989, *Ap.J.* Lett., **343**, L1.
7. Black, J.H., and van Dishoeck, E.F., 1991, *Ap.J.* Lett., **369**,L9.
8. Meyer, D.M., and Jura, M., 1985, *Ap. J.*, **297**, 119.
9. Crawford, J.A., Barlow, M.J., and Blades, J.C., 1989, *Ap.J.*, **336**, 212.
10. Crutcher, R.M., 1985, *Ap.J.*, **288**, 604.
11. Chaffee, F.H. Jr., and Dunham, T. Jr., 1979, *Ap.J.* , **233**, 568.
12. Cardelli, J.A., and Wallerstain, G., 1986, *Ap.J.* , **302**, 492.
13. Palazzi, E., Mandolesi, N., Crane, P., Kutner, M.L., Blades, J.C., and Hegyi, D.J., 1990, *Ap.J.*, **357**, 14.
14. Cardelli, J.A., and Wallerstain, G., 1989, *Astron.J.* , **97**, 1099.

Table III
Ancilliary data

| Star | E(B - V) | Dist (pc) | $W_\lambda$ CaI (mÅ) | $W_\lambda$ CaII H (mÅ) | $W_\lambda$ CaII K (mÅ) | $b_{CaII}$ (Km $s^{-1}$) | $T_{Kin}$ (K) | log N(HI) ($cm^{-2}$) | $logN(H_2)$ ($cm^{-2}$) | $n_e$ ($cm^{-3}$) |
|---|---|---|---|---|---|---|---|---|---|---|
| HD21483 | 0.58 | ... | ... | 145.0 | 90.0 | ... | 25 | ... | 20.81* | ... |
| HD23180 | 0.30 | 239 | 1.46 ± 0.46 | 82.0 | 58.0 | 2.63 | 25 | 20.90 | 20.61 | 0.03 |
| HD24398 | 0.32 | 394 | 0.86 ± 0.29 | 55.0 | 36.0 | 2.14 | 30 | 20.81 | 20.67 | 0.04 |
| HD26571 | 0.77 | 140 | ≤ 3 | 90.0 | ... | 3.0 | 25 | 19.65 | 20.81* | 0.098 |
| HD29647 | 1.04 | 140 | ≤ 5 | 280.0 | 150.0 | 15.0 | 10 | 20.16 | 21.54 | 0.002 |
| HD62542 | 0.33 | 400 | ≤ 0.6 | 43.2 | 23.5 | 5.2 | 55 | ... | 20.98* | 0.074 |
| HD80077 | 1.52 | 3000 | ... | ... | ... | ... | 25 | ... | 21.40* | ... |
| HD147343 | 0.64 | 167 | 8.4 ± 2.3 | 97.8 | ≤ 55 | 4.5 | 40 | 21.43 | 20.78 | 0.14 |
| HD147701 | 0.73 | 220 | ≤ 4.0 ± 1.7 | ≤ 44.0 | ≤ 35.0 | 4.5 | 40 | 21.50 | 20.90 | 0.14 |
| HD147889 | 1.09 | 206 | 5.8 ± 1.5 | 46.0 | 36.0 | 4.5 | 40 | 21.46 | 21.37 | 0.075 |
| HD149757 | 0.33 | 138 | 1.6 ± 0.4 | 35.0 | 21.0 | 7.03 | 30 | 20.72 | 20.64 | 0.17 |
| HD154368 | 0.82 | 800 | ... | ... | ... | ... | 25 | ... | 21.28* | ... |
| HD206267 | 0.51 | 800 | ≤ 3 | 236.0 | 159.0 | 8.4 | 40 | 21.15 | 20.91 | 0.02 |
| HD207198 | 0.61 | 1017 | 15 | 277.0 | 186.0 | 10.0 | 40 | 21.15 | 21.01 | 0.09 |
| HD210121 | 0.32 | 210 | 2.0 ± 1.0 | ... | ... | ... | 20 | ... | 20.98* | ... |
| HD210839 | 0.56 | 800 | 9.2 | 215 | 149 | 7.2 | 40 | 21.11 | 20.78 | 0.065 |
| TY CrA | 0.48 | ... | ≤ 6 | 27.0 | ... | ≥ 5 | 25 | ... | 21.10* | 0.026 |
| HD73882 | 0.66 | 398 | ... | ... | ... | ... | 25 | ... | 20.94* | ... |
| HD147933,a | 0.46 | 170 | 4.5 ± 0.6 | 46 | 39 | 1.6 | 45 | 21.54 | 20.57 | 0.19 |
| HD148184 | 0.44 | 134 | 4.0 ± 4.0 | 51 | 27 | ... | 45 | 21.15 | 20.63 | 0.77 |
| HD148379 | 0.74 | 1400 | ... | 470 | 280 | ... | 25 | ... | 20.41* | ... |
| HD149404 | 0.68 | 1400 | 8.45 | ... | ... | ... | 25 | 21.40 | 20.89* | ... |
| HD150136 | 0.49 | ... | ... | 300 | 220 | ... | 25 | ... | ... | ... |
| HD152236 | 0.68 | 1900 | 0.2: | 370 | 230 | ... | 25 | 21.74 | 20.67* | ... |
| HD169454 | 1.14 | 1700 | 0.8: | 690 | 360 | ... | 15 | ≥ 19.95 | 21.16* | ... |
| HD170740 | 0.46 | ... | ... | 75 | 41 | ... | 25 | ... | 20.81* | ... |

# THE SPECTRUM DISTORTION OF RELIC RADIATION IN THE MOMENT OF UNIVERSE RECOMBINATION

V. V. Burdyuzha [1], A. N. Chekmezov [2], V. N. Lukash [1]

[1] Astro Space Center Lebedev Physical Institute
Profsoyuznaya 84/32, Moscow, USSR

[2] Institute of General Physics,
Leninskii 53, Moscow, USSR

The calculation of spectrum distortions of the CMB in the $L_{\alpha}$ line is discussed.

At present, the cosmic microwave background radiation (CMB) is our only direct probe of physics between redshift of about $z \sim 5\text{-}10^3$. Observations of the CMB by COBE have confirmed its Planck spectrum with the temperature 2.735±0.02 (Mather et al, 1990). The CMB spectrum in the homogeneous and isotropic Universe does not change during expansion. The distortion of the CMB from the Planck spectrum may necessarily arise because of the production of energetic quanta in the process of recombination, which leads to its retarding and the distortions both in the Wein and Rayleigh-Jeans regions.
We reanalysed the recombinational dynamics from point of view of the nonequilibrium kinetics after the papers of Peebles (1968), Zeldovich, Kurt and Sunyaev (1969), Jones and Wyse (1985) and Krolik (1989,1990). The result of Matsumoto et al. (1988) stimulated of us to do it. Earlier, Burdyuzha et al. (1991) have shown that the radiation in lines of Balmer series does not lead to distortion of the relic radiation in the submillimeter region within $\sim 10^{-2}$. Here, we argue that the CMB distortion in $L_\alpha$ line takes place in the region $\lambda \sim$ 100-150 $\mu$. This is caused by the deviation of a population of the ground state of H from a the equilibrium population which can be calculated due to the Saha formula. Below, we outline briefly our calculations (see the original paper for detail).

The kinetic equation for the degree of ionization $\alpha = \alpha(t)$ is as follows:

$$\frac{d\alpha(t)}{dt} = (1 - \alpha(t) - \beta(t)\,\alpha^2(t)) \times \left[F_1(t) + \sum_{m=2}^{M} \gamma_m(t)\,(F_m(t) - F_1(t))\right] \quad (1)$$

For $\gamma_m$ $(M \geq m \geq 2)$, we have:

$$\sum_{m'=2}^{M} (K_{m1}(t) - K_{mm'}(t))\,\gamma_{m'}(t) + F_m(t)\gamma_m(t) = K_{m1}(t) \quad (2)$$

$$F_m(t) = \frac{\epsilon_m}{\hbar}\left(\frac{\epsilon_m}{\pi c \hbar}\right)^2 \sigma_m \left[\sum_{n=1}^{\infty} \int_{\epsilon_m/T(t)}^{\infty} \frac{dx}{x}\, e^{-nx}\right] \quad (3)$$

Here, $\epsilon_m$ is the ionization energy of the $m$ level:

$$\beta(t) = \sum_{m=1}^{M} \beta_m(t)$$

$$\beta_m(t) = \frac{3{,}31\ 10^{-22} N(t)}{(T(t))^{3/2}}\, m^2\, e^{\epsilon_m/T(t)} \quad (4)$$

Here $N(t)$ is the density of number of particles:

$$K_{m'm}(t) = -\sum_{m'=1}^{m-1} K_{m'm}(t) - \sum_{m'=m+1}^{M} K_{m'm}(t) \quad (5)$$

$K_{m',m}(t)$ is the relaxational matrix.

$$K_{m',m}(t) = \begin{cases} m' \neq 1,2 & m \neq 1,\ 2 \\ m' < m & K_{m',m}(t) = A_{m',m}\,\Theta_{m',m}(t) \\ m' > m & K_{m',m}(t) = (g_{m'}/g_m)A_{mm'}\Theta_{mm'}(t)e^{-\frac{\hbar\omega_{mm'}}{T(t)}} \end{cases} \tag{6}$$

$$K_{12}(t) = A_{12}\Theta_{12}(t) + \frac{g_1}{g_2}A^*_{12}$$

$$K_{21}(t) = \left[\frac{g_2}{g_1}\,A_{12}\,\Theta_{12}(t) + A^*_{12}\right] e^{-\frac{\hbar\omega_{12}}{T(t)}}$$

$A^*_{12}$ is the probability of the two-quantum decay of the second level

$$\Theta_{mm'}(t) = \left[1 - \exp(-\tau_{mm'}(t))\right] / \tau_{mm'}(t) \tag{7}$$

$\Theta_{mm'}$ is the coefficient of escape.

The optical depth $\tau_{mm'}$ is determined by the following formula

$$\tau_{mm'}(t) = \frac{A_{mm'}}{\omega_{mm'}}\left(\frac{\pi c}{\omega_{mm'}}\right)^2 \frac{c\,N(t)}{H(t)}\left[\frac{g_{m'}}{g_m}\alpha_m(t) - \alpha_{m'}(t)\right] \tag{8}$$

Here $g_m$ is the statistical weight of m - level

$$\alpha_m(t) = \beta_m(t)\alpha^2(t) + \gamma_m(t)\left[1 - \alpha(t) - \beta(t)\,\alpha^2(t)\right]$$

$$\alpha_1(t) = \beta_1(t)\alpha^2(t) + \left[1 - \sum_{m=2}^{M}\gamma_m(t)\right]\left[1 - \alpha(t) - \beta(t)\alpha^2(t)\right]$$

$\alpha_m$ is the degree of population of m-level of H,

$$N(t) = N_o(1 + Z)^3$$
$$T(t) = T_o(1 + Z)$$
$$H(t) = H_o(1 + Z)^{3/2}$$
$$Z = Z(t) = \left[\frac{3}{2} H_o t\right]^{-2/3} - 1$$

Here $N_o$, $T_o$ and $H_o$ = h 100 km/sec Mpc are the H-number density, temperature and Hubble parameter today. The initial condition on the degree of ionization is

$$\alpha(t_o) = \alpha_{eq}(t_o)$$
$$1 - \alpha_{eq}(t) - \beta(t)\alpha_{eq}^2(t) = 0$$
$$\alpha_{eq}(t) = 1/2\beta(t)\left[\sqrt{4\beta(t)+1} - 1\right] \qquad (9)$$
$$t_o = \frac{2}{3H_o}(1 + Z_o)^{-3/2}$$
$$N_o = \rho_{cr}\frac{\Omega_b}{m_H}$$
$$\rho_{cr} = \frac{3H_o^2}{8\pi G}$$

Here $\Omega_b$ is the density of baryons, $m_H$ is the H-mass , G is the gravitational constant.

We took into account only 5 lower levels (M = 5). The calculations show the degree of populations $\alpha_m$ for $m \geq 2$ coincides up to accuracy of $\sim 10^{-2}$ with equilibrium populations

$$\alpha_m^{eq} = \beta_m \alpha^2$$

However, for the ground state the degree of population is distinguished from the equilibrium one. The optical depth of the Universe in all H-lines besides the $L_\alpha$ is small in the process of recombination (for instance, $\tau_{H_\alpha} < 10^2$ ) and, therefore, the radiation in these lines is also small in comparison with the Planck radiation. The optical depth in the $L_\alpha$ line is very large $10^7 < \tau_{L_\alpha} < 10^9$ (but in other lines of L-series it is still small). Therefore only the radiation in $L_\alpha$ line can be compared with the Planck spectrum

$$\frac{\alpha_1^{eq}}{\alpha_1} \approx \left( \frac{\alpha}{\alpha_{eq}} \right)^2 \frac{1-\alpha_{eq}}{1-\alpha}$$

At early stage of recombination the degree of ionization is practically equal to the equilibrium degree of ionization (Saha-Boltzman):

$$\frac{\alpha_1^{eq}}{\alpha_1} \approx 1$$

Thus,the radiation from early stage of recombination comes to us with the Planck spectrum. During the recombination, since $\alpha$ deviates from $\alpha^{eq}$ we have

$$\frac{\alpha_1^{eq}}{\alpha_1} \neq 1$$

and the Planck spectrum is distorted in the submillimetre region. Fig. 1 shows the dependence of the degree of ionization on the redshift. Fig. 2 demonstrates the calculated distortion of temperature of the CMB.

## REFERENCES

Burdyuzha V.V., Chekmezov A.N., Lukash V.N., Yakovlenko S.I. 1991, in Proceedings 1990 COSPAR, Ed. P.R.Wesselius (in press).
Zeldovich Ya.B., Kurt V.G., Sunyaev R.A. 1969, Soviet Phys. JETP 28, 146.
Jones B.J.T., Wyse R.F.G. 1985 Astron. Astrophys. 149, 144.
Krolik J.H., 1989. Astrophys. J. 338, 594.
Lumbarskii Y., Sunyaev R.A., 1983. Astron. Astrophys. 123, 171.
Mather J.I.et al. , 1990. Astrophys. J. 354, L37.
Matsumoto T., Hayakawa S., Matsuo H., Murakami H., Sato S., Lange A.E., Richards P.L. , 1988. Astrophys. J. 329,567.
Peebles P.J.E., 1968. Astrophys. J. 153, 1.

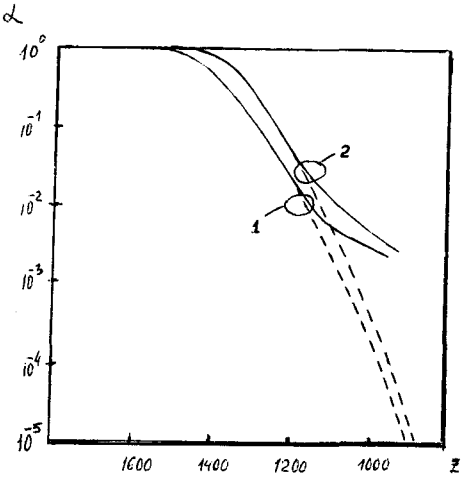


**Fig. 1.** The dependence of the degree of ionization on red shift. The dasshed lines correspond to equilibrium recombination. 1 is the model with parameters h=1, q=0.5, $\Omega_b$ =0.1 $\Omega_R$=4.3 $10^{-5}$; 2 is the model with Krolik's parameters h = 0.5, q= 0.5, $\Omega_b$ = 0.09, $\Omega_R$ = 0

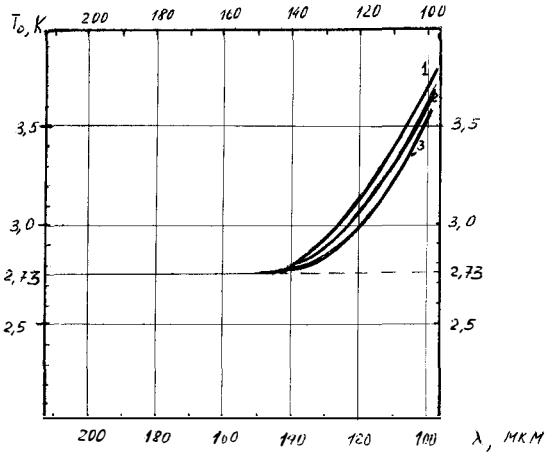


**Fig. 2.** The distortion of temperature of the CMB from equilibrium temperature for $\Omega_b$=0.03 (1), $\Omega_b$=0.1 (2), $\Omega_b$=0.3 (3) if h=0.75, q=0.5

# INTERGALACTIC MEDIUM, GALAXY EVOLUTION, GALAXY FORMATION MODELS

# GALAXY EVOLUTION MODELS AND THE EXTRAGALACTIC BACKGROUND LIGHT

Brigitte ROCCA-VOLMERANGE
*Institut d'Astrophysique*
*98 bis Bd Arago*
*F-75014 PARIS*

**Abstract**

Theoretical prediction for the background light due to galaxies is estimated with spectrophotometric evolutionary models on the basis of evolution scenarios and a cosmogony. Recent improvements of such models are described. New stellar libraries in the near-infrared (JHK) allow extension of the synthetic spectral Atlas of galaxies down to 10$\mu$m. From analyses in the far-UV and visible, observed colors and counts of faint galaxies are fitted by modelling a standard luminosity evolution and a low value of $\Omega_0(\simeq 0.1)$ while, in a $\Omega_0$=1 Universe, models only fit data with a standard luminosity evolution and a number density evolution $\simeq (1+z)^{1.8}$: such a modelling is simulating a merging process. Another solution would be a tidally triggered star formation rate in a model in which galaxies form by hierarchical clustering of a dominant dark matter component. From evolution of M/L ratio, these models allow to link observed luminosity functions with mass distributions predicted from galaxy formation models and then to significantly connect evolution to formation models. Nevertheless these two models are not sufficient to fit some observational data such as the Hubble diagrams and faint galaxy counts in the near-infrared, the bright galaxy counts in visible and the Extragalactic Background Light (EBL). So new evolution scenarios are needed implying other constraints for cosmological parameters.

## 1. Introduction

The large samples of high-redshift galaxies and the deepest surveys give more and more constraints on galaxy evolution. The unresolved galaxy contribution to the diffuse light, predicted by models, can be significantly compared to the EBL observations. The stake is important: early evolution of galaxies makes up the keystone of cosmology : a link between the observable Universe and predictions from initial fluctuations. For the first time, a large variety of distant galaxies marks out with light or matter the way to the primeval phases. Individual sources or galaxy populations discovered through narrow pencil beams at distances up to now never reached, explore deep into the structures and likely test evolution. Distant galaxies turn up as stellar populations with typical spectral, dynamical and chemical signatures. However their appearance is depending on the geometry of the Universe and a model of galaxy evolution is needed to deconvolve the respective effects of evolution and cosmology. Such a model based on the physical processes driving birth and evolution of stars or triggering emission of gaseous components, has to simultaneously interpret signatures of intervening, absorbing and diffusing matter.

Significant results are essentially depending on three conditions : i) input data have to be mostly observational, ii) evolution scenarios fit various observational samples at z=0 on a large wavelength range (far-UV to IR) iii) when it is possible, details of data processing are taken into account in modelling. Several models have been built. Mostly they have similar basic principles and essentially differ from their input data. We shortly review some of them and their recent improvements. Then we show that at the present time the most convincing interpretation of the large redshift samples corresponds to luminosity and number density evolution which could be a phenomenological simulation of the merging process. An excellent compilation of the present status of EBL measurements is given by Mattila, this conference. These observational results are compared to theoretical predictions for the background light due to galaxies. We propose some empirical fit with a spectral distribution of bursts; so our conclusion is a perspective of a better understanding of galaxy evolution with new scenarios simultaneously fitting observations from the far-UV to the infrared.

## 2. Standard Scenarios and Improvements

Historically these models were built in two phases. The first models of evolving stellar populations were simultaneously proposed by [1] and [2]. Respectively based on isomass tracks and isochrones following evolution of stars in the Hertzsprung–Russell diagram, they interpreted blue galaxies with bursts of massive stars. These photometric models were improved with nebular emission lines [3] and with far–UV colors and metallicity effects [4]. Some recent models are still photometric, most of them take into account a simplified chemical evolution [5] and [6].

A second generation of models appeared when atlases of spectra replaced stellar colors as input data [7] and[8], down to the far–UV from the IUE atlases [9] and [10]. From then, several improvements were taken into account:

i) Standard scenarios of evolution have been proposed. Table 1 gathers star formation laws and time scales for eigth spectral types from bursts and elliptical galaxies to spirals and irregulars. The initial mass function $m^x$ has a slope $x$=0.25 for stars less massive than $1M_\odot$, 1.35 between $1M_\odot$ and $2M_\odot$, and 1.7 for $m \geq 2\ M_\odot$. ii) Recent improved stellar tracks have been published by [11]. Time duration phases may increase by a factor 3 compared to the Yale tracks, due to the overshooting of convective cores. Mass loss rates and opacities given by the most recent determinations [12]. Maeder's models essentially fit massive stars, typically M≥1.5 M⊙ (Maeder, private communication). Low mass stars are from [13]. These new tracks were introduced in our models by 1988 and the integration time step was refined down to $10^5$ yr for calculating burst models. Most of recent results on ages of radiogalaxies [14] and faint counts [15] are based on these new input data. Tracks from [11] were recently introduced in Bruzual's model [16] and a more refined integration is carried out from a large ($\simeq$ 150) number of interpolated isochrones as used by [2]. Another model [17] based its calculations in the far–UV from "so–called template" galaxies, observed with the ANS or IUE satellites. So their calculations of evolution in the far-UV are not explicit. This could explain why this model needs the help of a cosmological constant to fit faint count observations [18] in a low density universe [19]. Detailed models with recent data of massive stars were proposed by [20] and [21]. Some models are extended in the near-infrared by using stellar photometry or consistent black-body emission of stellar effective temperatures [6] and [22].

iii) An extinction correction is proposed assuming stellar emitters mixed with gas. The optical depth through a spiral disk depends on inclination, gas content and metallicity (GRV).
iv) A nebular component (continuum plus lines) is calculated by estimating the number of Lyman continuum photons from stellar models [23] and[24] and the current radiation field.
v) The metallicity effect can be taken into account in stellar evolutionary tracks. It corresponds to an increase of age with metallicity due to an increase of opacities. As a consequence, at a given age, the giant/dwarf number ratio is lower in metal-rich galaxies since giants take more time to reach the giant branch phase [25]. For other effects of increasing metallicity (lowering effective temperature and blanketing effect), [5] gave rough estimates. Most uncertain are the evolutionary parameters of the Asymptotic Giant Branch (AGB) and post-AGB phases. If luminosities and effective temperatures can be derived from observations [26] , the phase duration can vary from $10^6$ to $10^8$ yrs according to models (see e.g. [27]).

### 3. Extension to the near-infrared

To extend spectrophotometric models to the near-infrared, two complementary libraries of stellar spectra have been observed and compiled:
i) Our far-UV and visible stellar library has been linked to the near-IR with observational infrared colors in the JHK bands. The caracteristics of this library are a wavelength range from 200Å to 10$\mu$m and a resolution $\Delta\lambda$ =10Å below 1$\mu$m. An extension of our Atlas of synthetic spectra of galaxies [28], based on scenarios of evolution for 8 morphological types (table 1), intends to reproduce colors of the Hubble Sequence: an example is shown on Figure 1. These spectra are used to calculate cosmological and evolutionary corrections (respectively k- and e- corrections) needed to predict apparent magnitudes and colors of distant galaxies according to:

$$m_\lambda(z) = M_\lambda(0) + (m - M)_{bol}(z) + k_\lambda(z) + e_\lambda(z)$$
$$C_\lambda(z) = C_\lambda(0) + k_{\lambda,c}(z) + e_{\lambda,c}(z)$$

with $M_\lambda(0)$ and $C_\lambda(0)$ respectively intrinsic magnitude and color at the present epoch. The important point is that colors and Hubble diagrams at high $z$ are not well fitted by models [22], whatever the cosmological parameters of a Friedman-Lemaître model. All the spectral UV to IR stellar data are observational, they cannot be the origin of the discrepancy between observations and model predictions in the near-infrared and so evolution scenarios for the Hubble sequence or basic cosmological models have to be revised.
ii) To study in more details the stellar populations of nearby and distant galaxies, Rocca -Volmerange and Maillard observed a new library of high resolution stellar spectra (≃40 dwarfs, giants and supergiants) with the Fourier Transform Spectrograph (FTS) at C.F.H.T. by 1989, 1990 through a large filter covering the H and K bands and with a high spectral resolution (2-3 Å) showing typical signatures of CO and $H_2O$ bands, Brackett lines and many others. Data have been processed; an example of such spectra is given on figure 2 [29].

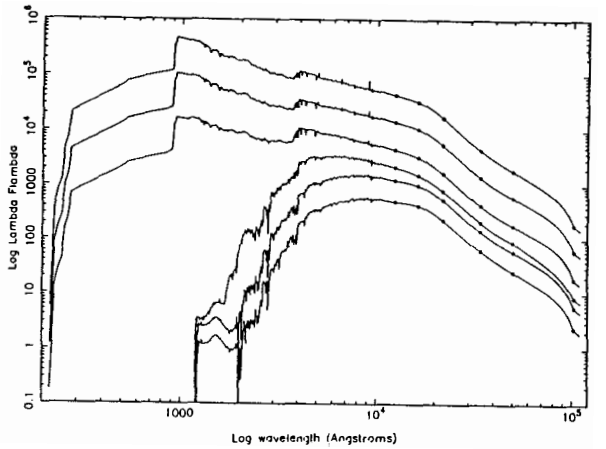


Fig. 1: Examples of synthetic spectra of galaxies extended from the far-UV (200Å) to the IR ($\simeq 10\mu$m) calculated with an updated version of our model (Rocca-Volmerange and Gros, 1991).

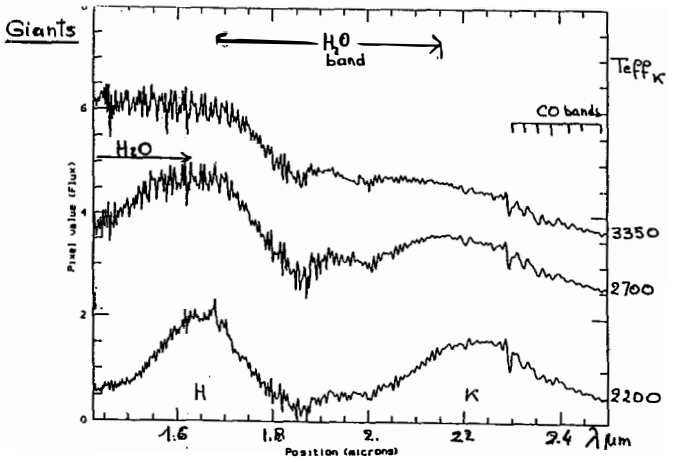


Fig. 2: High resolution spectra of the stellar library observed with the FTS instrument at C.F.H.T. through an H+K filter. Signatures of CO bands and $H_2O$ bands are strongly varying with temperatures (Lançon et al, 1991).

## 4. Evidences of galaxy evolution

From the pionneer works of [30], these last ten years confirmed a star formation evolution for distant galaxies providing vital clues to the process of luminosity evolution. Related to a starburst phenomenon, it has been firstly analysed in the optical from extremely blue colors [2] and recently in the far-IR from the IRAS satellite [31]. In these last cases, an extreme evolution of the ultraluminous starbursts is associated to a dynamical interaction [32]. At a lower level, the star formation activity in cluster galaxies has been related to dynamical processes to explain the morphological segregation [33] and the discovery of A stars in elliptical galaxies [34].

The recent deepest surveys of faint counts of galaxies [18] and [35] strongly constrain scenarios of galaxy evolution and/or cosmological parameters. Evolution models fit number counts, redshift or color distributions on a large dynamic range down to $B \simeq 27$ [15]. As number counts are strongly depending on the size of the covolume element, they give constraints on cosmological parameters: standard evolution models reproduce the data in a low density Universe while, by adding a number density evolution, data are compatible with models in a $\Omega_0 = 1$ Universe [14] and [36]. However a large-scale structure survey of bright galaxies (the APM survey by [37]) gives results in number counts, correlation functions, and other large scale properties in disagreement with the current models of galaxies. In particular, the evolution of galaxy number density between $m = 14$ and 19 is higher than predicted by models. Similar conclusions were given by [38] followed by [39] who suggested a new population of blue galaxies vanished at the present time; we prefer another solution which would be new evolution scenarios, relaxing our initial hypotheses [22].

Other signatures of galaxy evolution are given from the optical and infrared counterparts of powerful radiosources. The two most distant radiogalaxies: 0902+34 at $z = 3.395$ [40] and 4C41.17 at $z = 3.8$ [41] show signatures of stellar populations. Their typical features are: i) a large gap ( up to a factor 10) of the observed fiux from the far-UV plateau to the visible (rest frame) ii) the alignement of the radio and far-UV axes in most cases iii) an enormous Lyman-$\alpha$ (1215Å) line with an equivalent width of roughly 1000Å, implying a considerable star formation rate, about 1% of the total mass [14] iv) different morphologies according to the wavelength range v) a narrow relation in the K-$z$ Hubble diagram.

According to different authors, estimated ages spread from $\simeq$ 0.3Gyr to about 1.5 Gyr [40], [42] and [43]. In fact, arguments leading to a unique solution are not sound [14] first because stellar evolutionary data of respectively supergiants, asymptotic giant branch stars and giants are not well established. Second, present status of observational data show that current star formation erases most of spectral features which could give a significant age (figure 3). Third, the infra-red emission associated to the radio jet [44] and possibly a dust contribution of these distant radiogalaxies could partly mask the stellar emission to be dated. Relative to the number density evolution, there is some evidence that radiogalaxies with $1 < z < 3.8$ are objects undergoing a rapid merging of the available clumps, as suggested by [45]. The 16 3C radiogalaxies carefully imaged with sub–arcsecond seeing at the Canada–France–Hawaii Telescope all show a number of clumps, from 2 to 5, [46]. [47] used a deep survey of distant galaxies to estimate the relative frequency of close pairs at faint magnitudes ($B \leq 22$) relative to that for nearby bright galaxies. A statistically significant excess of faint pairs is consistent with an increase in the frequency of interactions $f = (1+z)^{4.0 \pm 2.5}$.

### 5. Star Formation in merging-driven evolution models

Among models of galaxy formation, more or less dissipative collapses [48] of clumpy turbulent protogalaxies with anisotropic stellar velocity [49] reproduce disks and spheroïds. On the other hand, dynamical friction acting on two or more building blocks could result in a merging process forming a condensed galaxy [50]. Many observations favor, with a more or less high degree, a merging scenario. Fundamentally, a merging process is dynamical depending on the mass distribution of intervening blocks. For high masses of interacting components, a starburst strongly emits in the far-IR and/or in the far-UV. However such extreme cases are rare and the essential question is: what star formation rate (SFR) is induced by the bulk of interactions predicted by galaxy formation models? Likely it depends on intrisic and relative dynamical properties of components (mass, velocity,..) but we ignore on what way. Moreover the classical modelling $(1+z)^n$ increases the confusion because it is not clear if luminosity or number density are in fact multiplied by this factor.

According to the simultaneous approach of distant radiogalaxies and faint galaxy counts, [14] and [36] proposed an unifying model in which all galaxies form from the merging of building blocks for which the spectral evolution is computed. The following scenario is suggested: the collapse and cooling of gas in the potential wells of dark-matter haloes lead to fragmentation into a number of clumps, say $N \simeq 10$ with a characteristic mass of an order of magnitude below the total baryonic mass. These clumps are the gas reservoir for star formation. The general rule for field galaxies would be that star formation begins at relatively high redshift in these clumps ($z_{for}$=10 to 5, derived from the colour distribution of faint galaxies as well as from the radiogalaxies). The clumps also "slowly" merge according to an 'average' $(1+z)^n$ law. Star formation continues in the merged objects from the residual gas. These objects would essentially be those observed in faint galaxy counts. Dynamical friction could be the process regulating merging and number evolution. In a small fraction of the massive, high–redshift objects, the merging of the available clumps could be more rapid, simply as a Poisson fluctuation. Since the clumps would then still be gas–rich, the star formation would be stronger, and the large amount of gas could also feed some central compact object and initiate the radiogalaxy phenomenon. The small number of high–redshift, active objects could be found from a search of radio sources, but would have no significant effect on faint galaxy counts. Finally, the subsequent growth of these objects is impeded by the large cooling time of very massive haloes (see e.g. [51]). This scenario is compatible with most observations of radiogalaxies and faint galaxy counts and it has the essential property to save $\Omega_0$=1 because the pure luminosity evolution models only fits the data in a low $\Omega_0$ Universe incompatible with inflation. The number density evolution varies as $(1+z)^{1.8}$ and the luminosity evolution roughly follows our standard scenarios.

Another solution is a model in which galaxies form by hierarchical clustering of a dynamically dominant dark matter component and in which the rate of star formation is controlled by the frequency of tidal interactions with neighbouring galaxies. This has been proposed by [52]. Owe to the mass-luminosity ratio M/L as a fruitful output of evolution models, luminosities, colours, surface brightnesses and circular velocities of nearby bright galaxies as well as distributions of redshifts, colours and numbers of distant faint galaxies are analysed with our spectrophotometric model [53]. Several constraints for the scenarios of galaxy evolution result from this complete study which will be extended to other galaxy formation models. Figure 4 shows the relation of mass-luminosity used in this model by

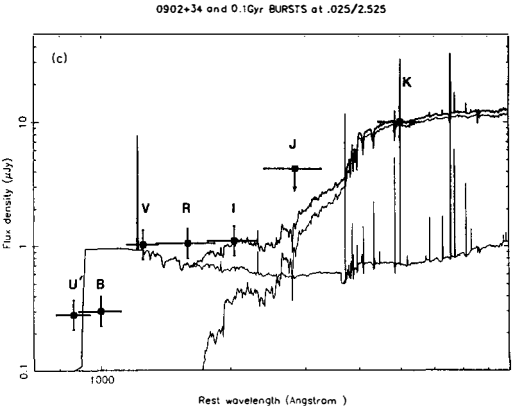


**Fig. 3**:Fit of the spectral energy distribution of 0902+34 in the U'BVRIJK bands at $z$=3.395. The spectra of two 0.1 Gyr and 2.5 Gyr are superimposed. Most of the evolution signs in the old burst are cancelled by the current ones.

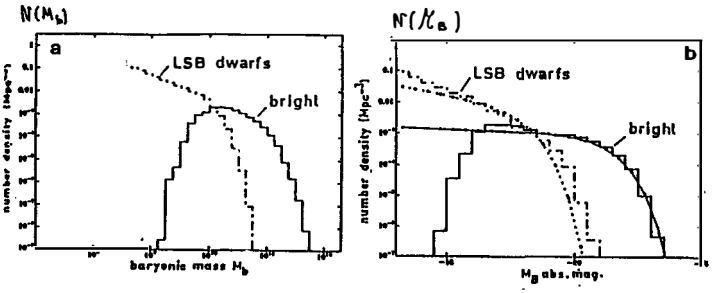


**Fig. 4**: Distribution of baryonic masses (a) compared to the corresponding luminosity functions (b) computed for bright galaxies and low-surface-brightness dwarf galaxies. The galaxy formation model and refinements of our evolution model are described in Lacey et al, 1991.

adding a dwarf population. Early winds induced by supernovae explain their low surface brightnesses and the reason why this population is not detected at the present time (Silk, this conference).

These last solutions are compatible with the recent observations of bright galaxies [37] only at a low level. Moreover, the blue (B) and red (K) number distributions are not fitted with the same models [35]. As a confirmation, we show in [22], that the JHK Hubble diagrams are not so well fitted that the corresponding blue diagrams. At evidence, new populations or new basic hypotheses of evolution scenarios have to be proposed. And only a significant confrontation of the blue and red will be avalaible to find the solution.

## 6. Extragalactic Background Light

Several authors proposed predictions of the EBL due to the galaxy contribution [7] and [17]. In fact they are only avalaible if models are in good agreement with observational galaxy counts, evaluated by the surface density of galaxies per magnitude bin and steradian $N(m_\lambda)$. We proposed interpretations of these counts in [15] and [36]. Then the EBL is calculated by:

$$I_\lambda / I_{\lambda 0} = \int 10^{0.4 m_\lambda} N(m_\lambda) dm_\lambda$$

where the fluxes are normalised to a reference flux of an A0 star. Evolution of galaxies follows a standard luminosity evolution in various cosmologies ($\Omega_0$=0.1 and 1) and various redshifts of formation ($z_{for}$=2 or 30). All these curves are an order of magnitude lower than the observational values or upper limits in the UV, optical and IR (Figure 5). Similar conclusions were derived from Bruzual models and Yoshii and Takahara results. The important point is that merging models with number density evolution *gives roughly similar fits* since we assume that the total comoving mass density is conserved. Moreover Figure 5 presents a strong near-IR emission due to a current starburst extincted with various $E_{B-V}$=0., 0.1 and 0.5, added to the global galaxy emission. the SED of the burst corresponds to a $(1+z)\lambda$ shift with 1+z=10 and fits satisfyingly the observations [54] and [55]. This population could be a solution for the EBL to be included in the new scenarios of galaxy evolution.

To summarize, spectrophotometric models are the tools needed to constrain scenarios of galaxy evolution. Fitted on nearby galaxies, they are used to separate the respective contribution of evolution and cosmology in the various samples of distant galaxies. Their avalaibility are however depending on significant stellar input data (tracks, effective temperatures,..). Since the stellar energy distribution is produced by different stars in the red and in the blue, a simultaneous analysis in the two wavelength ranges is needed: one way is to extend the synthetic spectra of galaxies to the infrared. Two stellar libraries were built in this intention and a comparison with observational data is at present in progress on the basis of new scenarios, more specifically by relaxing some basic assumptions of calculations of faint galaxy counts.

TABLE I

| (1) | (2) | (3) | (4) | (5) |
|---|---|---|---|---|
| $\tau_*(t)$ $M_\odot \mathrm{Gyr}^{-1}\ M_\odot^{-1}$ | $t_*$ Gyr | age Gyr | $B-V$ | "average" type |
| 1 Gyr burst | 0.63 | 17.4 | 0.88 | red envelope |
| $\exp -t$ | 1.0 | 13.2 | 0.97 | UV-cold E/SO |
| $1g(t)$ | 0.9 | 13.2 | 0.92 | UV-hot E/SO |
| $0.4g(t)$ | 2.2 | 12.5 | 0.74 | Sa |
| $0.3g(t)$ | 3.0 | 12.5 | 0.66 | Sb |
| $0.1g(t)$ | 9.0 | 12.5 | 0.51 | Sc |
| 0.060 | 10.5 | 12.5 | 0.45 | Sd |
| $7.7\ 10^{-4}t_*^2$ | 13.5 | 12.5 | 0.35 | Im |

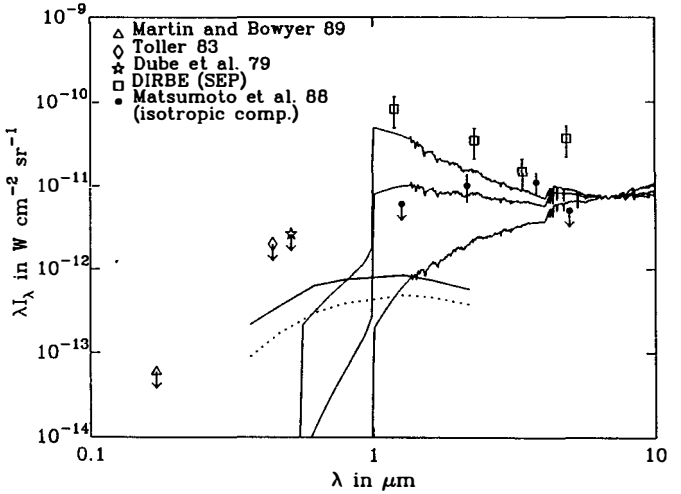


Fig. 5: Predictions of the global emission of galaxies with evolution (full line) and without evolution (dotted line) are far below observations. The contribution of a synthetic burst formed at $z$=9 with various extinction factor would fit the near- infrared recent data from DIRBE or Matsumoto et al, 1988.

**References**


(1. Tinsley, B.M., 1972, *Astron. Astrophys.*, **20**, 383
(2. Searle, L., Sargent, W.L.W., Bagnuolo, W., 1973, Astrophys. J., **179**, 427
(3. Huchra, J.P., 1977, Astrophys. J., **217**, 928
(4. Rocca–Volmerange, B., Lequeux, J., Maucherat, M., 1981, *Astron. Astrophys.* **104**, 177
(5. Arimoto, N., Yoshii, Y., 1986, *Astron. Astrophys.*, **164**, 260
(6. Franceschini, A., Toffolati, L., Mazzei, P., Danese, L., de Zotti, G., 1991, preprint
(7. Bruzual, G., 1983. *Astrophys. J.* **273**, 105
(8. Guiderdoni, B. & Rocca–Volmerange, B., 1987. *Astron. Astrophys.* **186**, 1
(9. IUE Ultraviolet Spectral Atlas, 1983, Wu *et al.*, NASA N$^0$22
(10. Heck, A., Egret, D., Jaschek, C., 1984, Battrick., B., ESA SP-1052.
(11. Maeder, A. & Meynet, G., 1988. *Astron. Astrophys. Suppl. Ser.* **76**, 411
(12. de Jager, C., Nieuwenhuijzen, H., van der Hucht, K.A., 1988, *Astron. Astrophys.*, **164**, 260
(13. VandenBergh, D., Bell, R.A., 1985, *Astrophys. Supp. Series*, **58**, 561
(14. Rocca–Volmerange, B., Guiderdoni, B., 1990, *Month. Not. Roy. Astron. Soc.*,, **247**, 166
(15. Guiderdoni, B. & Rocca–Volmerange, B., 1990. *Astron. Astrophys.* **227**, 362
(16. Charlot, S., Bruzual, G., 1991, preprint
(17. Yoshii, Y., Takahara, F., 1988, Astrophys. J., 326, 1
(18. Tyson, A., 1988. *Astron. J.* **96**, 1
(19. Fukujita, F., Takahara, F., Yamashita, K., Yoshii, Y., 1990, *Astrophys. J.*, **361**, L1
(20. Olofsson, K., 1989, *Astron. Astrophys. Supp. Ser.*, **76**, 317
(21. Leitherer, C., 1989, *Astrophys. J. Supp. Ser.*, **73**, 1
(22. Rocca–Volmerange, B. & Gros, L., 1991, in preparation
(23. Clegg, R.E.S., Middlemass, D., 1987, *Mon. N. Roy. astr. Soc.*, **244**, 408
(24. Kudritski, R.P., in *Massive stars in starbursts*, C. Leitherer (ed), Baltimore, in press
(25. Guiderdoni, B. & Rocca–Volmerange, B., 1984. *Astron. Astrophys.* **109**, 355
(26. Mould, J., 1991, in *Stellar Populations of Galaxies*, B. Barbuy ed, Brazil, in press
(27. Renzini, A., 1991, in *Stellar Populations of Galaxies*, B. Barbuy ed, Brazil, in press
(28. Rocca–Volmerange, B. & Guiderdoni, B., 1988. *Astron. Astrophys. Suppl. Ser.* **75**, 93
(29. Lançon, A., Rocca-Volmerange, B., Maillard, J.P., 1991, submitted
(30. Butcher, H.R., Oemler, A., 1978, *Astrophys. J.*, **219**, 18
(31. Sanders D.B., Soifer, B.T., Elias, J.H., Madore, B.F., Matthews, K., Neugebauer, G., Scoville, N.Z., 1988, *Astrophys. J.*, **325**, 74
(32. Mirabel, I. F., Sanders, D.B., 1988, *Astrophys. J.*, **340**, L53
(33. Dressler, A., 1980, *Astrophys. J.*, **236**, 351
(34. Dressler, A., Gunn, J.E., 1983, *Astrophys.J.*, 270,7
(35. Cowie, L., Lilly, S., Gardner, J., 1991, preprint
(36. Guiderdoni, B., Rocca–Volmerange, B., 1991, in press
(37. Maddox, S.J., Efstathiou, G. & Sutherland, W.J., 1990, *Mon. Not. R. astr. Soc.* **211**, 833
(38. Broadhurst, T.J., Ellis, R.S. & Shanks, T., 1988. *Mon. Not. R. astr. Soc.* **235**, 827
(39. Colless, M., Ellis, R.S., Taylor, K., Hook, R.N., 1990, *Mon. N. Roy. astr. Soc.*, **244**, 408

(40. Lilly, S., 1988. *Astrophys. J.* **333**, 161
(41. Chambers, K.C., Miley, G.K. & van Breugel, R.R., 1988. *Astrophys. J.* **329**, L75
(42. Rocca–Volmerange, B., 1988. *The Messenger* **53**, 26
(43. Chambers, K.C. & Charlot, S, 1990. *Astrophys. J.* **348**, L1
(44. Joy, M., Harvey, P.M., Tollestrup, E.P., Sellgren, K., Mc Gregor, P.J., Hyland, A.R., 1991, *Astrophys. J.*, **366**, 82
(45. Djorgovski, S., Spinrad, H., McCarthy, P., Dickinson, M., Van Breugel, W. & Strom, R.G., 1988. *Astron. J.* **96**, 836
(46. Le Fèvre, O., Hammer, F. & Jones, J., 1988. *Astrophys. J.* **331**, L73
(47. Zepf, S.E., Koo, D.C., 1989, Astrophys. J., 337, 34
(48. Larson, R., 1975, *Mon. Not. R. astr. Soc.* **173**, 671
(49. Carlberg, R.G., 1985, in *the Milky way Galazy*, H. van Woerden, R.J. Allen, W.B. Burton (ed), Dordrecht, Reidel, p.165
(50. Toomre, A., Toomre, J., 1972, *Astrophys. J.*, **178**, 623
(51. Evrard, A.E, 1989. *Astrophys. J.* **341**, 26 **366**, 7
(52. Lacey, C., Silk, J., 1991, in press
(53. Lacey, C., Guiderdoni, B., Rocca-Volmerange, B., Silk, J., submitted
(54. Hauser, M.G., Kelsall, T., Moseby, Jr., S.H., Silverberg, R.F., Murdock, T., Toller, G., Spiesman, W., Weilord, J., 1991, in *After the First Three Minutes* Workshop, College Park.
(55. Matsumoto, T., Akiba, M., Murakami, H., 1988, *Astrophys. J.*, **332**,

# SOME COMMENTS ON GALAXY FORMATION

Simon D.M. White
Institute of Astronomy, Cambridge

ABSTRACT

Hierarchical clustering is the only paradigm for the growth of structure in the Universe that has so far offered any clear explanation for the characteristic sizes, masses, and angular momenta of galaxies. After a brief review, I describe why predictions of the galaxy luminosity function from this theory tend to produce too many faint objects. I then discuss possible origins for the dichotomy between spheroidal and disk components in galaxies, and I argue that the existence of large, centrifugally supported disks requires isolated spiral galaxies to be surrounded by extended, massive dark halos. Simple models for the formation of such disks are severely constrained by a variety of observational data.

## 1 Introduction

There is still relatively little understanding of the origin and evolution of structure in the Universe, and a number of quite different possibilities have been proposed. In these comments I will focus on the recent development of structure and in particular on the processes which gave rise to the observed population of galaxies. In the 1970's there were two widely accepted schools of thought about galaxy formation. One held that damping processes just before recombination eliminated all small scale structure in the primordial plasma; the first structures to form were then the size of clusters or superclusters of galaxies, and galaxies themselves were the result of the fragmentation of sheet-like shocks, or "pancakes", formed as these larger structures collapsed. The second school held that small scale fluctuations were able to survive until late times, when they gave rise to the first nonlinear objects to form in the Universe; these small lumps then clustered hierarchically and merged, first to form galaxies, then to form clusters.

In the 1980's the neutrino-dominated (or Hot Dark Matter) universe was an example of the first type of model, while the Cold Dark Matter universe developed from the second train of thought. The strong point of the pancake theory was its natural explanation for the growing impression that galaxies are distributed along coherent sheets and filaments surrounding apparently empty voids. It was less successful as a theory of galaxy formation because the characteristic fragmentation scale of the cold gas layer in a pancake is too small for the fragments to be identified with galaxies (Sunyaev and Zel'dovich 1972). For hierarchical clustering theories the problem is the opposite. The scale of galaxies can be identified as the largest on which the gaseous component of a protogalactic cloud can cool (Rees and Ostriker 1977; Silk 1977). As larger objects build up, stars form with ever increasing efficiency until this cooling barrier is reached. Thus most stars are formed in galaxies near the limiting luminosity. However, the large scale coherence of the galaxy distribution is much harder to understand, since there is no obvious organising process on such scales. The Cold Dark Matter model attempts to avoid this problem by compressing the hierarchy so that objects on a wide range of scales form simultaneously. Opinion is divided on how well it succeeds.

Several other hypotheses for the formation of galaxies and larger structures have been proposed since 1980. The explosion model suggests that galaxies might form within shocks caused by the injection of large amounts of energy into the intergalactic medium,

either by supernovae in young galaxies, or by superconducting cosmic strings (Ostriker and Cowie 1981; Ostriker, Thompson, and Witten 1986). The strong upper limit on Compton distortions of the microwave background provided by COBE, makes it very unlikely that processes of this kind could be responsible for the large scale coherent features seen in the galaxy distribution (Levin, Freese and Spergel 1991). As in the pancake model, it is also difficult to understand why shock fragmentation would give rise to objects with the characteristic mass of galaxies. Cosmic strings offer an alternative to hierarchical clustering. In the original model individual string loops acted as seeds onto which galaxies could accrete (Vilenkin 1981). However, detailed numerical simulations have shown that the evolution of a string network produces too few massive loops for this to work (Bennett and Bouchet 1988). More recent attempts to generate structure from cosmic strings focus on the wakes created by long strings, and do not yet address galaxy formation in any detail. Another possibility for seeding galaxy formation is cosmic texture (Turok 1989); this relic of an early phase transition may escape many of the difficulties associated with strings and lead to a galaxy formation picture which is rather similar to hierarchical clustering. In a CDM-dominated universe textures generate present-day structure similar to that in a standard CDM model; however, the first objects form much earlier (Gooding *et al.* 1991).

In the rest of this article I address several questions related to galaxy formation in a hierarchical clustering model. I begin by giving an argument, originally due to White and Rees (1978), which shows how a galaxy luminosity function can be estimated for such a model. The result has the right characteristic luminosity but predicts more faint galaxies than are seen. This problem carries over into most more modern attempts to calculate luminosity functions directly. I then discuss how the disk/halo dichotomy can be understood in the context of hierarchical clustering, and I show that observed galaxy disks must be embedded in massive halos if their angular momentum is to be attributed to tidal effects during galaxy formation (Fall and Efstathiou 1980). Finally, I review a simple theory for the formation of disks, and I stress possible tests based on the properties of the gaseous halos it predicts around spiral galaxies.

## 2 Luminosity Functions

The simplest hierarchical clustering theories suppose that structure grew from initial conditions with no characteristic scale. The density fluctuation field at early times, $\delta(\mathbf{x}) = \rho(\mathbf{x})/\langle\rho\rangle - 1$, must then be scale-free, and its Fourier power spectrum must be

a power law, $|\delta_{\mathbf{k}}|^2 \propto |\mathbf{k}|^n$. As clustering proceeds, structures of larger and larger mass collapse. In a flat universe this nonlinear evolution should be self-similar as long as all dissipative effects are neglected; the characteristic mass, density, velocity dispersion, and temperature of nonlinear lumps then scale with redshift as:

$$m_c \propto (1+z)^{-6/(n+3)}; \quad \rho_c \propto (1+z)^3; \quad V_c^2 \propto T_c \propto (1+z)^{(n-1)/(n+3)}. \tag{1}$$

Thus for $1 > n > -3$, the range of relevance, typical objects were lower mass, denser, and cooler at earlier times. Note that these scalings apply to the *typical* objects present at *different* times, not to the different objects present at any given time. At any given time objects of differing mass are expected to have similar mean densities. Their velocity dispersions are then related to their mass through the virial theorem, giving $T \propto m^{2/3}$ independent of $n$. These points are discussed by Press and Schechter (1974) and White and Rees (1978). The first paper also derives a simple formula for the mass distribution at any given time, which turns out to give quite a good fit to the results of numerical simulations (Efstathiou *et al.* 1988).

The simple scaling of equation (1) breaks down as soon as dissipative effects are included. Most of the gas in present day groups and clusters of galaxies is unable to cool in a Hubble time. However, because the radiative cooling time of a gas decreases with density and increases with temperature, equations (1) imply that before some modest redshift, $z_{cr}$, all the gas in typical objects was able to cool rapidly, and thus was available to make stars. The gas mass of a typical object at the critical redshift, $Fm_c(z_{cr})$, can then be identified with the characteristic stellar mass of a bright galaxy ($F$ here is the fraction of the mass in the form of gas; $F \sim 0.1$ in present day clusters). Few objects of higher mass will be able to make stars, because at $z > z_{cr}$ such objects did not exist, while at $z < z_{cr}$ their gas is unable to cool. For reasonable parameters, this argument does indeed imply a characteristic mass similar to that of observed bright galaxies (White and Rees 1978).

In this model all the mass at early times is expected to be in small objects with high density and low temperature. Thus, if short cooling and dynamical times were all that was required to turn gas into stars, no gas would survive the first stages of the hierarchy, all stars would be born in small "galaxies", and the argument of the last paragraph would have no bearing on the galaxy luminosity function. To avoid this situation one must

suppose that star formation is inefficient at early times, a natural "explanation" being energy injection from supernovae which can eject the rest of the gas from a protogalaxy once a small fraction, $\epsilon$, has turned into stars (Larson 1974). Energetic considerations suggest $\epsilon \propto V^2$ as a natural scaling for this efficiency, an assumption which allows the faint-end slope of the galaxy luminosity function to be calculated as follows. At redshift $z > z_{cr}$ most of the material in the universe is in objects of mass $m \sim m_c(z)$, which therefore have abundance (*i.e.* number per comoving volume per unit mass interval),

$$n(m)\, dm \sim \langle\rho\rangle/m\, dm/m, \tag{2}$$

where $\langle\rho\rangle$ is the present mean density. The stellar mass formed in these objects is $\epsilon F m \propto V^2 m \propto m^{(7-n)/6}$, where I have used the scaling of equation (1). If the galaxies so formed survive without merging to the present day, they will have a luminosity approximately proportional to this stellar mass. One can thus use $L \propto m^{(7-n)/6}$ to convert equation (2) to a "no merger" luminosity function,

$$n(L)dL \sim L^{(13-n)/(7-n)}dL, \tag{3}$$

which will cut off exponentially above the luminosity, $L_* = \epsilon(V_c(z_{cr})^2)\ F\ m_c(z_{cr})/(\mathrm{M/L})$. The power law index here varies between $-2$ for $n = 1$ and $-1.6$ for $n = -3$ and so is substantially more negative than the values $-1$ to $-1.3$ usually quoted for the observed galaxy luminosity function (*e.g.* Efstathiou, Ellis and Peterson 1988; but compare Bothun, Impey and Malin 1991).

The problem here is that it seems very easy *a priori* for small objects to cool and make stars at early times in a hierarchically clustering universe; thus it is unclear why only a rather small fraction of stars are in such objects today. There are a variety of ways to embellish the above "no merging" model in order to reduce the predicted number of faint galaxies. The most obvious is to allow galaxy merging which will clearly reduce the number of objects surviving from early times. However, detailed modelling suggests that the effect is not strong enough to eliminate the difficulty (White and Frenk 1991). Another possibility is to argue that most of the small objects have large (M/L), and correspond to a population not usually included in determinations of the galaxy luminosity function (Lacey and Silk 1991). Alternatively one might imagine that early radiative input might heat the pregalactic gas sufficiently that it would be unable to clump into the small halos

expected at early times (Kaiser, in preparation). Yet another escape might be to argue that although gas cools effectively at early times, little star formation occurs because there is not enough available time; the gas might be then be reheated at a later stage of the hierarchy without making stars. All these possibilities need more detailed investigation before they can be accepted or refuted.

## 3 Disks and bulges

One of the most striking properties of galaxies is the coexistence of disk and spheroidal components with quite different morphology, kinematics, and stellar and gas content. This dichotomy suggests very different formation paths for the two kinds of structure. In normal galaxies we observe ongoing star formation only in disks, and so, following Toomre (1976), one might suppose that star formation only ever occurs in disks. Bulges and ellipticals would then need to be made from progenitor disks. This idea is controversial because observed bulges have older stellar populations and shorter dynamical times than observed disks, so it seems more natural to assume bulges form first. However, many investigators have shown that mergers of stellar disks, and indeed the violent collapse and eqilibration of almost any irregular distribution of *stars*, leads to objects with structure very like that of elliptical galaxies. Furthermore, many kinematic and photometric irregularities have been found in ellipticals, and seem to indicate recent merger activity. Much debate on this topic can be found in Wielen (1990) and I will not address it further here, except to note that the central objects in some cluster cooling flows (*e.g.* NGC 1275 in Perseus) do seem to offer a counterexample where significant star formation is observed without a disk (Fabian, Nulsen and Canizares 1991).

One clear conclusion from N-body simulations of galaxy formation is that bulge-like systems are formed whenever star formation is complete before an object reaches dynamical equilibrium. Mergers of pre-existing galaxies provide one example of this, but so, plausibly, might the early stages of hierarchical clustering, for densities are then sufficiently high that cooling times for protogalaxies are much shorter than their collapse times. This idea accords well with the observed high densities of bulges and ellipticals. Disks, in contrast, must come to dynamical equilibrium *before* they turn into stars, because their thinness and their highly ordered kinematics require dissipative processes during formation which are not available to a stellar system. Furthermore, their dynamical context cannot have been violently disturbed by further accretion after their stars formed, for they would not

then have been able to remain thin. Thus in hierarchical clustering, the most plausible situation would seem to be for bulges and ellipticals to form early when cooling and star formation times were short, and for disks to form late from lower density gas that had to settle into centrifugal equilibrium before it could make stars. Late formation of stars in disks is suggested by the star formation history of the Solar Neighbourhood, and by observed star formation rates in spirals. As I now discuss, late formation of the disks themselves may be required by their large angular momentum.

## 4 Disk angular momentum

Within hierarchical clustering models, galactic angular momentum can be explained by Hoyle's (1949) tidal torque mechanism; gravitational forces from neighbouring lumps act on the quadrupole moment of an irregular protogalaxy and spin it up. N-body simulations demonstrate that this mechanisms works, and induces a spin which has little systematic dependence either on clump mass or on power spectrum index, $n$. If spin is characterised by the dimensionless parameter,

$$\lambda = J\,|E|^{1/2}/(G\,M^{5/2}), \tag{4}$$

where $J$, $E$, and $M$ are the angular momentum, binding energy, and mass of a virialised clump (defined as a centrally concentrated region with mean overdensity $\langle\delta\rangle \sim 200$), then the median value of $\lambda$ is about 0.05 and the 10% and 90% points of the distribution are about a factor of two larger and smaller (*e.g* Efstathiou *et al.* 1988).

If we model a galactic disk by an exponential disk of mass, $M_d$, scale length, $r_0$, and constant rotation velocity, $V_{rot}$, then its angular momentum is $J = 2M_d r_0 V_{rot}$. Let us assume that the disk material was part of a protogalactic perturbation with mass, $kM_d$, and angular momentum, $kJ$. We can then use equation (4) to express the binding energy of the protogalaxy in terms of the properties of the disk, of $\lambda$, and of $k$. This leads to an estimate for the collapse time of the protogalaxy, derived as the value for a uniform sphere of the same mass and binding energy:

$$t_c = 2.92\,G\,M^{5/2}|E|^{-3/2} = 23.4\,(r_0/V_{rot})\,(r_0 V_{rot}^2/GM_d)^2\,k^{-2}\,\lambda^{-3}. \tag{5}$$

This is likely to be an underestimate of the value for a nonuniform protogalaxy. For large, late-type, spirals, $r_0 \sim 3h^{-1}$kpc, $V_{rot} \sim 200$ km/s, and the second factor in equation (5) must exceed 0.18 (so that the mass density of the nondisk component is everywhere

positive). In a flat universe, the redshift of protogalactic collapse must therefore be bounded above by

$$1 + z_c < 22\left(\frac{r_0}{3h^{-1}\mathrm{kpc}}\right)^{-2/3}\left(\frac{V_{rot}}{200\mathrm{km/s}}\right)^{2/3} k^{4/3}\lambda^2. \qquad (5)$$

For $\lambda = 0.05$, we require $k > 9$ to get collapse by the present, and $k > 15$ to get collapse by $z = 1$. These factors are the amount by which the total mass of the initial protogalaxy must exceed the *maximum* disk mass allowed by the observed rotation velocity. Thus the origin of the angular momenta of spirals can only be explained by Hoyle's mechanism if protogalaxies, at collapse, contained at least an order of magnitude more mass than is currently found in the visible region of galaxies. Note that if the protodisk lost any of its angular momentum to halo material while settling into centrifugal equilibrium, then the above reasoning yields an underestimate of $k$. This argument in favour of extended massive dark halos was first clearly presented by Fall and Efstathiou (1980).

## 5 Model for disk formation

If disks indeed form slowly by dissipative settling within a quasi-equilibrium dark halo, it is natural to try and model the process as the cooling of a hot atmosphere within a steady potential well, a situation closely analogous to standard models for cooling flows in galaxy clusters. In the hierarchical models of section 2, this corresponds to epochs when the cooling times of protogalaxies are longer than their collapse times, but are not much longer than the age of the universe. As noted above, it is important to include feedback effects in such models in order to inhibit the efficiency of cooling and star formation at early times. A detailed discussion of such galaxy formation models in a CDM universe can be found in White and Frenk (1991), and I give a simplified version, requiring no assumptions about the nature of the dark matter and applied specifically to disks, in White (1991). These models assume that infalling material is a mixture of gas and dark matter, and that the gaseous component is shocked to the virial temperature. For small galaxies or for large gas fractions the shocked material cools again immediately, and disk formation is a competition between cosmological infall and feedback from massive stars. For large galaxies or for small gas fraction, only the central regions of the shocked gas atmosphere can cool; disk mass is then controlled by the competition between cooling and feedback. For gas fractions of about 10% (similar to those seen in rich clusters), such models can

reproduce the observed relation between disk mass and circular velocity, as well as giving angular momenta of approximately the correct size.

If cooling regulates disk growth these models suggest $M_d \propto t^{1/2}$, whereas infall regulated growth would give $M_d \propto t$. These dependences agree well with the observation that star formation rates in our own and in other spirals seem to be at most weakly declining functions of time (*e.g.* Kennicutt 1990) but they sit less comfortably with the observed infall rate into our own disk which appears to be an order of magnitude less than $H_0 M_d$ (van Woerden *et al.* 1983). Continuing accretion models also suggest that large galaxies like the Milky Way should have hot gaseous halos containing a similar gas fraction to that seen in galaxy clusters. There is little evidence for such a halo and it is difficult to see how it can be reconciled with the relatively small observed diffuse background in soft X-rays, or with the observed pressure of the local interstellar medium. Standard numbers for both these quantities imply that gas at the expected temperature of 0.15 keV cannot have a local density exceeding about 1% of that inferred for halo dark matter. This may not eliminate the possibility that 10% of the mass within the cooling radius ($\sim$ 150 kpc) is gaseous, since feedback effects, which the model requires anyway, may well rearrange material throughout the halo. They will certainly produce a complex, multiphase structure in the gas. Nevertheless, such complications weaken the model because they make its predictions much harder to calculate. It is perhaps worth noting that gaseous halos, in the form of MgII absorbing clouds, *are* observed around star-forming galaxies at modest redshift, and that in these cases, at least, material seems to have been mixed to radii well outside the star-forming regions (Bergeron 1987).

A cooling flow model seems a direct generalisation from the observed situation in galaxy clusters, but it is by no means required within the overall framework of hierarchical clustering. The simulations of Katz and Gunn (1991) show that gas can settle into a disk during, or immediately after, protogalactic collapse, provided that evolution is well synchronised throughout the system and is not too irregular. The major requirement for obtaining a realistic result is that star formation be delayed until after equilibration. In the contrary case when a galaxy forms by infall over an extended period, the infalling material may be sufficiently lumpy that it is never shocked to the virial temperature of the halo. Galaxy halos would then appear empty because all their associated gas had remained cold. In a flat universe this requires the gas fraction in protogalaxies (*i.e.* the ratio of observed

stars and gas to total halo mass) to be much less than in galaxy clusters. Lumpy infall is also constrained by the requirement that stellar disks should not be unduly thickened by gravitational jostling. This may be a serious problem for any hierarchical clustering model, and a sufficient suppression of merging may require an open universe (Tóth and Ostriker 1991). The problem could perhaps be circumvented if it could be shown that most accreted lumps are disrupted before they can shake up the disk. An open universe may also required by the most obvious explanation for empty halos: that residual gas was blown away by a wind during an initial bright formation phase. In a flat universe most of the mass of a galaxy/halo system has been added since $z = 1$. However, at such epochs events sufficiently spectacular to blow away $\sim 10\%$ of the halo mass can be observationally excluded. Thus for $\Omega = 1$, the contrast between gas rich cluster halos and apparently "empty" galaxy halos remains puzzling. This is an area where ROSAT may make a major contribution to our understanding of galaxy formation.

**Acknowledgement** Some of the original research reported above was supported by NSF grant AST-8822297 to the University of Arizona.

## References

Bennett, D., and Bouchet, F. 1988, *Phys.Rev.Lett.*, **60**, 257.

Bergeron. J. 1987,in *High Redshift and Primeval Galaxies*, eds Bergeron, J. *et al.* , Editions Frontiéres, p. 371.

Bothun, G.D., Impey, C.D. and Malin, D.F. 1991, *Ap.J.*, **376**, 404.

Efstathiou, G., Frenk, C.S, White, S.D.M. and Davis, M. 1988, *Mon.Not.R.astr.Soc*, **235**, 715.

Efstathiou, G., Ellis, R.S. and Peterson, B.A. 1988, *Mon.Not.R.astr.Soc.*, **232**, 431.

Fabian, A.C., Nulsen, P.E.J. and Canizares, C. 1991, *Astr.Ap.Rev.*, **2**, 191.

Fall, S.M. and Efstathiou, G. 1980, *Mon.Not.R.astr.Soc.*, **193**, 189.

Gooding, A.K., Park, C., Spergel, D., Turok, N. and Gott, J.R., 1991 Princeton Observatory Preprint 416.

Hoyle, F., 1949, in *Problems of Cosmical Aerodynamics*, eds Burgers, J.M. and van de Hulst, H.C., Ohio, p. 195.

Katz, N. and Gunn, J.E. 1991, *Ap.J.*, , in press.

Kennicutt, R.C. 1990, in *Evolution of the Universe of Galaxies*, ed. Kron, R.G., A.S.P.Conf. **10**, 141.

Lacey, C. and Silk, J.I. 1991, *Ap.J.*, , in press.

Larson, R.B. 1974, *Mon.Not.R.astr.Soc.*, **169**, 229.

Levin, J.J., Freese, K., and Spergel, D.N. 1991, in *After the First Three Minutes*, ed. Holt, S.S., Bennett, C.L., and Trimble, V., AIP Cof. Proc. **222**, p. 73.

Ostriker, J.P., and Cowie, L.L. 1981, *Ap.J.Lett.*, **243**, 127.

Ostriker, J.P., Thompson, C., and Witten, E., 1986, *Phys.Lett.*, **180**, 231.

Press, W.H. and Schechter, P.L. 1974, *Ap.J.*, **187**, 425.

Rees, M.J., and Ostriker, J.P. 1977, *Mon.Not.R.astr.Soc*, **179**, 541.

Silk, J.I. 1977, *Ap.J.*, **211**, 638.

Sunyaev, R.A., and Zel'dovich, Ya.B. 1972, *Astron. Ap.*, **20**, 189.

Tóth, G. and Ostriker, J.P. 1991, *Ap.J.*, , in press.

Toomre, A. 1977, in *Evolution of Galaxies and Stellar Populations*, eds Tinsley, B.M. and Larson, R.B., Yale Univ.Obs., p. 401.

Turok, N., 1989, *Phys.Rev.Lett.*, **63**, 2625.

van Woerden, H., Schwarz, U.J., and Hulsbosch, A.N.M., 1983 in *The Milky Way Galaxy*, eds van Woerden, H., Allen, R.J. and Burton, W.B., Reidel, p. 387.

Vilenkin, A., 1981, *Phys.Rev.Lett.*, **46**, 1169.

White, S.D.M. 1991, in *Dynamics of Galaxies and their Molecular Cloud Distributions*, eds Combes, F. and Casoli, F., Reidel, p. 383.

White, S.D.M. and Frenk, C.S. 1991, *Ap.J.*, **379**, in press.

White, S.D.M., and Rees, M.J. 1978, *Mon.Not.R.Astr.Soc.*, **183**, 341.

Wielen, R. (editor) 1990, *Dynamics and Interactions of Galaxies*, Springer, Berlin.

# STAR FORMATION DRIVEN BY GALAXY INTERACTIONS: A MODEL FOR THE EVOLUTION OF THE GALAXY LUMINOSITY FUNCTION AND NUMBER COUNTS

Cedric G. Lacey
Department of Physics, Oxford University, Keble Road, Oxford, UK

ABSTRACT. A model is presented for the evolution of the galaxy luminosity function, based on the CDM model for galaxy formation, together with the assumption that the star formation rate in galaxies is controlled by the frequency of interactions with other galaxies. The model also includes the effects of gas cooling, and star formation feedback driving mass loss from galaxies. The predictions of the model are compared with observational data on the present galaxy luminosity function, number counts, colour distributions and redshift distributions. The agreement is generally good, but problems remain in matching the colour distributions and the faint-end slope of the present luminosity function.

## 1. Introduction

In current models for galaxy formation, most of the mass in the universe is assumed to be in some collisionless dark form, typically some type of weakly interacting elementary particle, while baryons are just a trace component. Given the initial spectrum of density fluctuations, the evolution of the dark matter component can be calculated using only gravitational physics, which is in principle straightforward using N-body techniques. Thus one can predict the distribution and dynamics of halos of dark matter. However, most of our information about the universe comes from studying the properties of that fraction of the baryons which have become luminous by forming stars. Predicting the properties of this luminous component is more complicated. (1) It involves the dissipative dynamics of gaseous baryons, including shock heating, radiative cooling, and energy injection from stars. (2) It involves star formation, for which no predictive theory currently exists. In fact, it is not even clear whether the rate of conversion of gas into stars is controlled mainly by dynamical processes causing compression of the gas, or whether some sort of balance between energy injection by young stars and radiative cooling of the gas is more important. One can directly estimate the effects of dissipation in the gas under various assumptions, but to compute star formation rates, it is necessary to take a more phenomenological approach, and try various models. I will describe here an example of such a model for the evolution of the luminous components of galaxies, based on work done in collaboration with Joe Silk, Bruno Guiderdoni, and Brigitte Rocca-Volmerange (Lacey & Silk 1991, Lacey *et al.* 1991). While our aim is to describe the evolution of the galaxy luminosity function, such models also have implications for studies of large-scale structure, since the comparison of theory and observations in this area depends on the relation assumed between the distributions of mass and of light on large scales, which are controlled by the efficiency of star formation in various galactic environments.

## 2. Formulation of the Model

We assume that $\Omega = 1$, $H_0 = 50 \mathrm{km\,s^{-1}\,Mpc^{-1}}$, and that the initial spectrum of density fluctuations has the form predicted by the Cold Dark Matter (CDM) model, normalized so that the r.m.s. density fluctuation in a 16 Mpc sphere is 0.5. Starting from this, one could compute the distribution of dark matter halos in mass and formation redshift using N-body simulations, but to make the model more tractable, we instead use an approximate analytical method, based on studying peaks in the initial density fluctuation field $\delta \equiv \delta\rho/\rho$. Adapting the results of Bardeen *et al.* (1986), we obtain an approximate expression for the comoving number density of peaks as a function both of the peak mass $M_g$ and overdensity $\delta_g$, and of the overdensity $\delta_{gr}$ of the surroundings on a mass scale $M_{gr} > M_g$, where $M_{gr}/M_g$ is taken to be constant:

$$\frac{\mathrm{d}^3 n_{pk}}{\mathrm{d}M_g \mathrm{d}\delta_g \mathrm{d}\delta_{gr}} = \frac{\mathrm{d}n_{pk}}{\mathrm{d}M_g} P(\delta_g, \delta_{gr}; M_g, M_{gr}/M_g)$$

In this equation, $dn_{pk}/dM_g$ and $P(\delta_g, \delta_{gr})$ can be calculated in terms of the CDM power spectrum. We identify $M_g$ with the mass of a galaxy halo, and $M_{gr}$ with that of the sur-

rounding galaxy group. Each overdense peak i s assumed to collapse dissipationlessly to form a dark halo, with the collapse redshift and final density of the halo after virialization being calculated assuming a spherical "top hat" collapse:

$$1 + z_{f,g} = \delta_g / \delta_{cr}$$

$$\rho_{f,g} = \left(10\delta_g/3\right)^3 \overline{\rho}_0$$

where $\delta_{cr} = 1.69$, and $\delta$ is the linear theory extrapolation of the overdensity to the present day. Similar expressions apply for the collapse of the group. We will assume throughout that $M_{gr}/M_g = 8$.

When the galaxy halo collapses, the gas in it is assumed to be shock heated to the virial temperature of the halo. If the gas can radiatively cool before the surrounding group collapses, *i.e.* if

$$t_{cool} < t_{f,gr} - t_{f,g}$$

where $t_{f,g}$ and $t_{f,gr}$ are the collapse times of the galaxy halo and group, and $t_{cool}$ is the cooling time calculated assuming a primordial composition, then the gas is assumed to condense into a dense baryonic core at the centre of the halo. Otherwise, the gas is assumed be reheated and dispersed by the collapse of the group. Once a baryonic core has formed in this way, it is assumed to survive any subsequent merging of the surrounding halos. Thus, we have no merging of the luminous parts of galaxies. The half-mass radius of the baryonic core is assumed to be a constant fraction $f_{diss}$ of the virialized "top hat" radius of the halo in which it forms. If the baryons contract in radius until they are centrifugally supported, then one expects a dissipative collapse factor $f_{diss} \sim \lambda_{spin} \sim 0.1$, where $\lambda_{spin}$ is the dimensionless spin parameter, whose value is estimated assuming that the angular momentum of galaxies results from tidal torques (Fall 1983).

The most distinctive feature of our model is our assumption that the star formation rate in the baryonic cores is controlled by the frequency of interactions with neighbouring galaxies. The main motivation for considering such a model is the observational evidence that star formation rates are enhanced in interacting galaxies, as indicated by $UBV$ colours (Larson & Tinsley 1978) and by ratios of far infrared and $H\alpha$ luminosities to optical luminosities (Lonsdale *et al.* 1984, Kennicutt *et al.* 1987). The star formation presently occuring in these strongly interacting systems is only $\sim$ 10% of the total, but we will assume in our model that *all* star formation is associated with galaxy interactions in some way. The physical mechanism driving the star formation would be tidal interactions, either acting directly to cause compression of the interstellar medium in galaxies, or indirectly, by inducing spiral density waves in galactic disks, which then continue to induce star formation even after the immediate effects of a tidal encounter are over. Secondary motivations for this picture are: (1) The observed morphology-density relation for galaxies (Dressler 1980, Postman & Geller 1984), showing that the fraction of elliptical and S0 galaxies relative to spirals increases with the density of the local environment. This could be explained if more frequent galaxy

encounters promoted more rapid conversion of gas into stars. (2) The problem of *biasing*: the amount of mass which is associated with luminous galaxies (where this includes the dark halos of these galaxies) is inferred observationally to be $\Omega \approx 0.1 - 0.2$. To reconcile this with having $\Omega = 1$ globally, it is necessary for the luminous galaxies to have a distribution which is biased relative to the mass.

Since the details of the tidal forcing of star formation are undoubtedly quite complicated, we use a very simple parametrization which we hope captures the main effects. We assume that the timescale for star formation $\tau_*$ is simply proportional to the encounter time within the galaxy group, which is calculated assuming that the group contains $N_{gr}$ identical galaxies of mass $M_g$, and that each galaxy interacts with the geometrical cross-section of the halo:

$$\begin{aligned}\tau_* &= \frac{1}{A_*}\frac{t_{d,gr}}{N_{gr}}\left(\frac{r_{gr}}{r_g}\right)^2 \\ &= \left(\frac{\pi}{2}\right)\left(\frac{3}{5}\right)^{3/2}\frac{1}{H_0 A_*}\left(\frac{M_g}{M_{gr}}\right)^{1/3}\left(\frac{\delta_g}{\delta_{gr}}\right)^2\frac{1}{\delta_{gr}^{3/2}}\end{aligned}$$

where $r_g$, $r_{gr}$ and $t_{d,gr}$ are the radii and dynamical times for the galaxy and group halos, calculated using the spherical collapse model. The proportionality coefficient $A_*$ is treated as an adjustable parameter. The star formation rate in a galaxy is then assumed to be given by

$$\Psi(t) = M_{g,gas}(t)/\tau_*$$

where the gas mass $M_{g,gas}$ evolves due to star formation and the recycling of gas by dying stars, giving a roughly exponential decay of the star formation rate with time. The initial gas mass is simply $M_b = f_b M_g$, where the baryon fraction $f_b \sim 0.03 - 0.1$ according to primordial nucleosynthesis (Kawano *et al.* 1988). Since we are assuming that all star formation is induced by galaxy interactions within the group, star formation begins only when the group containing the galaxy has collapsed, which happens at redshift

$$1 + z_* = \delta_{gr}/\delta_{cr}$$

This condition results in a form of *natural biasing*, since only some fraction of galaxy halos will have begun star formation by the present day, and these will preferentially be in regions which are overdense on larger scales, where the group collapse condition is statistically more likely to be satisfied. We emphasize that, although star formation is assumed to be driven by interactions, the model assumes no merging of the luminous components of galaxies.

The final effect we include is feedback from star formation: energy injection by supernovae will heat the gas, and if the escape velocity from the galaxy is low enough, can drive a galactic wind which removes much of the gas from the galaxy, as suggested by Larson (1974) and Dekel & Silk (1986). Since the escape velocity is proportional to the velocity dispersion $v_g$ of the halo, we parametrize the mass loss by assuming that the fraction $f_*$ of the baryons converted into stars before mass loss occurs varies as

$$\begin{aligned} f_* &= f_{*cr}(v_g/v_{crit})^\gamma \qquad (v_g < v_{crit}) \\ &= 1 \qquad\qquad\qquad\quad (v_g > v_{crit}) \end{aligned}$$

Star formation is assumed to proceed normally until the fraction $f_*$ is reached, after which the remaining gas is lost essentially instantaneously. Following Dekel & Silk, we assume $v_{crit} = 100\,\mathrm{km\,s^{-1}}$. The parameters $f_{*crit}$ and $\gamma$ are treated as adjustable.

The star formation rate in a galaxy is thus described by four parameters ($M_b$, $z_*$, $\tau_*$, $f_*$), which can be related to the three parameters ($M_g, \delta_g, \delta_{gr}$) describing peaks in the initial linear fluctuation field, for which one can compute the differential number density. We compute the luminosity and spectral evolution of each galaxy using the stellar population synthesis program of Guiderdoni & Rocca-Volmerange (1987), which allows us to calculate galaxy magnitudes and colours for various passbands, including the effects of evolution and k-corrections. We assume throughout that the initial mass function of the stars has the same form as inferred for the solar neighbourhood by Scalo (1986). Guiderdoni & Rocca-Volmerange's models include a "standard" amount of internal extinction, uniformly distributed over the galaxy, and amounting to $A_V \sim 0.3\,\mathrm{mag}$ for typical spirals. As discussed below, we found it necessary to include an additional extinction of $A_V = 1\,\mathrm{mag}$ for O and B stars only, in order to match observed galaxy colours. We justify this on the basis that young stars are more likely to be found in regions of dense gas, where the extinction is larger.

### 3. Results of the Models

After comparing the predictions of our models with the observational data, we have chosen the following set of parameters for our standard model: $f_b = 0.06$, $A_* = 8$, $f_{diss} = 0.05$, $\gamma = 1$, $f_{*,cr} = 1$. There follow the results of this comparison.

Figure 1 shows the prediction for the present day luminosity function (LF) of galaxies, together with the Schechter function fit to the observed field galaxy LF obtained by Efstathiou *et al.* (1988) by fitting to data over the absolute magnitude range $-18 \lesssim \mathcal{M}_B \lesssim -23$. The model is seen to give a good fit for bright galaxies ($\mathcal{M}_B \lesssim -19$): the natural bias inherent in our star formation model produces the correct number density at the "knee" of the LF ($\mathcal{M}_B \approx \mathcal{M}_{B*} \approx -21$), while the cooling condition produces the cutoff at the bright end. For fainter galaxies ($\mathcal{M}_B \gtrsim -19$), the situation is less clear. The models predict that the LF increases towards fainter magnitudes as $dn/dL_B \propto L_B^{-1.6}$. This is less steep than the halo mass function in this range, for which $dn/dM \propto M^{-2}$, because of mass loss, which sets in at $M_b \lesssim 10^{10}\,\mathrm{M_\odot}$, corresponding to $\mathcal{M}_B \gtrsim -18$. The field galaxy LF in this range is not well determined observationally, mainly because of the low surface brightness of most faint galaxies. The predicted faint-end LF agrees roughly *in shape* with that found for dwarf galaxies in the Virgo Cluster by Sandage *et al.* (1985), but Binggeli *et al.* (1990) find that the observed LF for dwarf galaxies in the field is flatter than this, closer to the extrapolation of Efstathiou *et al.* 's Schechter function fit. This would be in conflict with the models. It is possible that the number of dwarf galaxies is still being under-estimated, because of the difficulty of detecting low surface brightness objects. We could make the model LF flatter at the faint end, by increasing the amount of mass loss assumed, but this would then make the predicted number counts at $B \gtrsim 24$ too low.

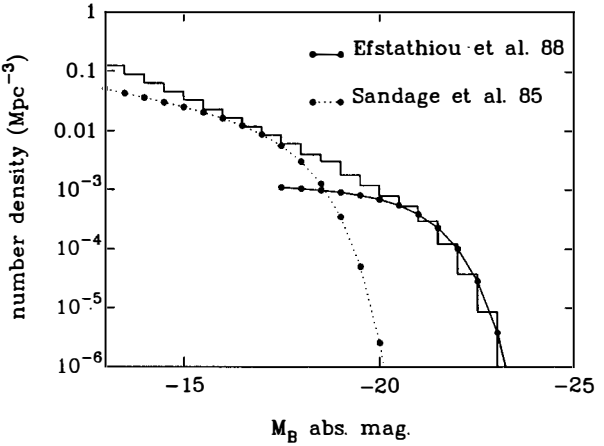


**Figure 1.** Present luminosity function. Solid histogram shows the predicted number density of galaxies per unit absolute magnitude. Solid curve shows the Schechter function fit to the observed field galaxy LF from Efstathiou *et al.* (1988). Dotted curve shows the Virgo Cluster dwarf galaxy LF from Sandage *et al.* (1985), normalized to fit the model at $\mathcal{M}_B = -17$.

Figure 2 shows the predicted relation between mean surface brightness within the half-light radius and absolute magnitude, for present-day galaxies, compared to the observed relation for Virgo Cluster ellipticals. It is seen that the fit is fairly good for $\mathcal{M}_B \gtrsim -21$, but breaks down for the brightest galaxies, where the model predictions are too high. It is possible that this could be explained by the formation of bright ellipticals by mergers, an effect not included in our models, but which might tend to make galaxies more distended.

Figure 3 shows the predicted colour distribution in an apparent magnitude limited sample at $19 < B < 21$, both with and without the extra extinction on OB stars, compared to photographic data from Jones *et al.* (1990). The galaxies in this sample are mostly at fairly modest redshift ($z \sim 0.2$). We see that the model with no extra extinction predicts far too many blue galaxies, which results from the large number of galaxies which turn on star formation at low redshifts, $z_* \lesssim 1$, due to our assumption that star formation begins only after group collapse. On the other hand, the model with the extra extinction provides a reasonable fit to the colour distribution, and continues to do so to somewhat fainter magnitudes, $B \lesssim 23$. There remains the problem that reddest galaxies nearby are all ellipticals, which are red because their stellar populations are old, while in our model, many bright galaxies are red because of extinction. The extra extinction has been included in all the plots shown here, but only has a large effect on the colour distributions.

Figure 4 shows the prediction for the galaxy number counts in the B-band, compared to

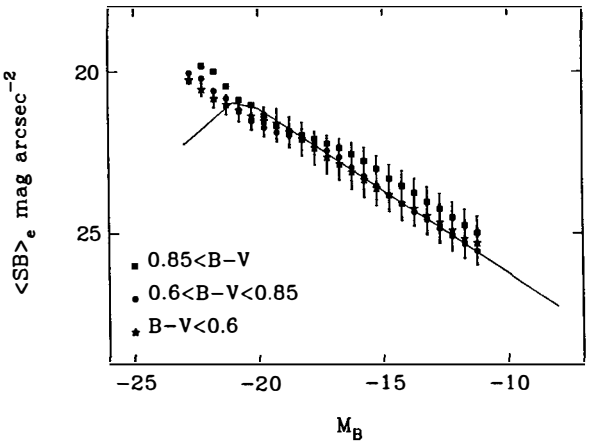


**Figure 2.** Mean surface brightness within half-light radius versus absolute magnitude. Symbols show predicted relations for three different colour ranges. Solid curve shows observed relation for Virgo Cluster ellipticals from Binggeli *et al.* (1984).

the observational data. The model is seen to give a good fit over the whole range $15 \lesssim B \lesssim 27$. At $B \lesssim 24$, the counts are dominated by the galaxies with $v_g > v_{crit}$, which do not lose any mass. At $B \gtrsim 24$, the counts are dominated by the mass-losing dwarf galaxies with $v_g < v_{crit}$, which begin forming stars at $z_* \sim 1-2$, form stars on a timescale $\tau_* \sim 0.1-1$ Gyr, and then have their star formation terminated by mass loss, after which they rapidly fade.

Figure 5 shows the predicted redshift distributions compared with observations for galaxies in apparent magnitude ranges (a) $20 < B < 22.5$, with data from Broadhurst *et al.* (1988) and Colless *et al.* (1990), and (b) $23 < B < 24$, with data from Cowie *et al.* (1991). In (a), the observational magnitudes used were isophotal, and it is necessary to allow for this in comparing with the models. We computed isophotal corrections in the models using the predicted half-light radii of the galaxies, together with either exponential or $r^{1/4}$-law surface brightness profiles, depending on whether $\tau_* > 1$ Gyr or $\tau_* < 1$ Gyr. The isophotal corrections suppress the high redshift tail in $N(z)$ which is predicted otherwise. The agreement is then fairly good, except for an excess in the model distribution at $z \sim 0.1$ compared to the data. This excess is due to the population of dwarf galaxies with $v_g < v_{crit}$, most of which formed their stars at $z \sim 1$, and have since faded after losing their remaining gas. However, the observational sample is $\sim 30\%$ incomplete, and would be biased against galaxies lacking strong emission lines associated with active star formation, because of the way redshifts were estimated. Thus, the galaxies in this excess might have been missed. In (b), the observational sample is very small, only 21 galaxies. The agreement with the models here is reasonable.

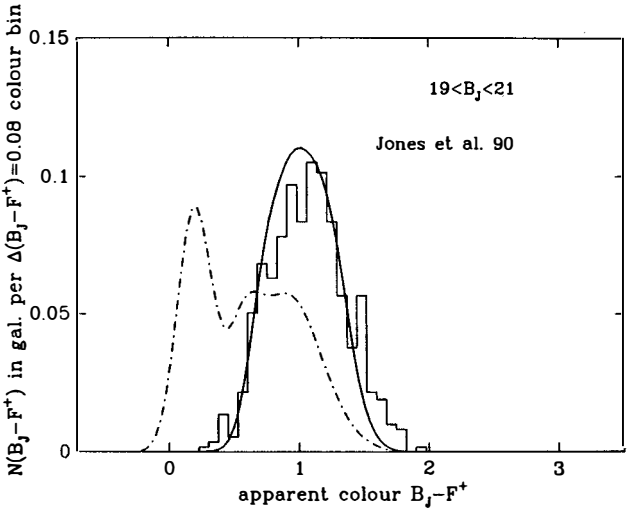


**Figure 3.** Colour distribution in apparent magnitude limited sample with $19 < B_J < 21$. Solid curve: prediction with extra extinction on OB stars. Dot-dash curve: prediction without extra extinction. Histogram: observational data from Jones *et al.* (1990).

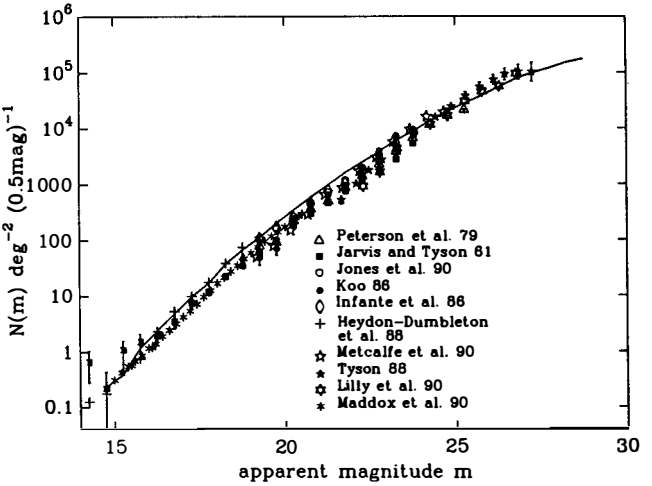


**Figure 4.** Number counts in $B_J$-band. Solid curve shows model prediction. Symbols show various observational determinations.

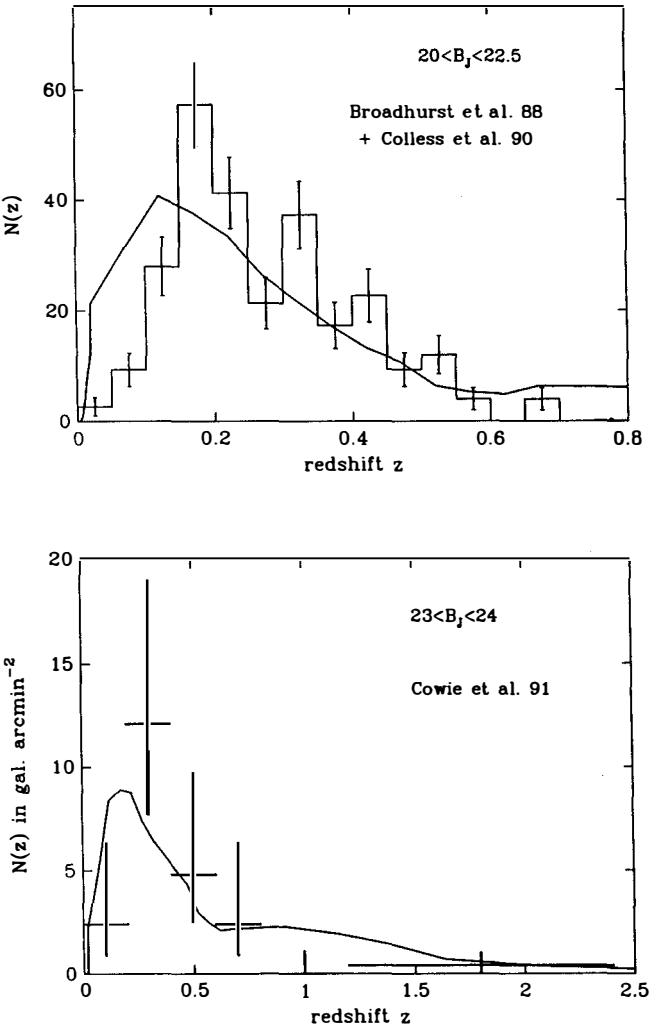


**Figure 5.** Redshift distributions in apparent magnitude-limited samples. (a) $20 < B_J < 22.5$. Solid curve: model. Histogram: observational data. (b) $23 < B_J < 24$. Solid curve: model. Points with error bars: observational data.

**4. Conclusions**

(1) Our model for the evolution of the galaxy luminosity function based on star formation induced by galaxy interactions gives good agreement with the present-day luminosity function for bright galaxies, but may have a problem in predicting too many faint galaxies. The model provides a natural biasing mechanism: most dark halos have not yet formed luminous galaxies because the surrounding group has not yet collapsed.
(2) The model gives reasonable agreement with the observed number counts. The faint ($B \gtrsim 24$) counts are predicted to be dominated by dwarf galaxies ($M_b \sim 10^9 - 10^{10}\,\mathrm{M}_\odot$, $v_g \sim 50 - 100\,\mathrm{km\,s^{-1}}$), undergoing their initial burst of star formation at $z \sim 1$.
(3) Our model can fit the observed colour distributions at bright magnitudes ($B \lesssim 23$), but only if we include extra extinction for young (OB) stars.
(4) The model fits the observed redshift distributions at $B \lesssim 24$, with the possible exception of an excess in the predicted distribution at $z \sim 0.1$.

**Acknowledgements** I thank my collaborators in all of this work, Joe Silk, Brigitte Rocca-Volmerange and Bruno Guiderdoni.

**References**

Bardeen, J.M., Bond, J.R., Kaiser, N. & Szalay, A.S. 1986. *Astrophys. J.*, **304**, 15.

Binggeli, B., Sandage, A., & Tarenghi, M. 1984. *Astron. J.*, **89**, 64.

Binggeli, B., Tarenghi, M., & Sandage, A. 1990. *Astron. Astrophys.*, **228**, 42.

Broadhurst, T.J., Ellis, R.S., & Shanks, T. 1988. *Mon. Not. Roy. Astron. Soc.*, **235**, 827.

Colless, M., Ellis, R. S., Taylor, K., Hook, R.N. 1990. *Mon. Not. Roy. Astron. Soc.*, **244**, 408.

Cowie, L.L., Gardner, J. P., Wainscoat, R. J., and Hodapp, K. W. 1991. Preprint

Dekel, A., & Silk, J. 1986. *Astrophys. J.*, **303**, 39.

Dressler, A. 1980. *Astrophys. J.*, **236**, 351.

Efstathiou, G., Ellis, R.S., & Peterson, B.A. 1988. *Mon. Not. Roy. Astron. Soc.*, **232**, 431.

Fall, S.M. 1983. In *IAU Symposium 100: Internal Kinematics and Dynamics of Galaxies*, ed. E. Athanassoula, p.391 (Dordrecht: Reidel).

Guiderdoni, B., & Rocca-Volmerange, B. 1987. *Astron. Astrophys.*, **186**, 1.

Jones, L.R., Fong, R., Shanks, T., Ellis, R.S., & Peterson, B.A. 1991. *Mon. Not. Roy. Astron. Soc.*, , .

Kawano, L., Schramm, D., & Steigman, G. 1988. *Astrophys. J.*, **330**, L1.

Kennicutt, R.C., Keel, W.C., van der Hulst, J.M., Hummel, E., & Roettiger, K.A. 1987. *Astron. J.*, **93**, 1011.

Lacey, C.G., & Silk, J. 1991. *Astrophys. J.*, **381**, .

Lacey, C.G., Guiderdoni, B, Rocca-Volmerange, B., & Silk, J. 1991. In preparation.

Larson, R.B. 1974. *Mon. Not. Roy. Astron. Soc.*, **169**, 229.

Larson, R.B., & Tinsley, B.M. 1978. *Astrophys. J.*, **219**, 46.

Lonsdale, C.J., Persson, S.E., & Matthews, K. 1984. *Astrophys. J.*, **287**, 95.

Postman, M., & Geller, M.J. 1984. *Astrophys. J.*, **281**, 95.

Sandage, A., Binggeli, B., & Tamman, G.A. 1985. *Astron. J.*, **90**, 1759.

Scalo, J.M. 1986. *Fundamentals of Cosmic Physics*, **11**, 1.

# GALAXY COUNTS AND CORRELATION FUNCTIONS ON LARGE-SCALES

Stephen Maddox
Oxford Astrophysics,
Keble Road, Oxford OX1 3RH,
England.

**Abstract.**

The number of galaxies counted in the APM survey as a function of magnitude suggests that there has been extremely strong evolution in the galaxy luminosity function since $z \sim 0.1$. The slope of the number counts between magnitudes $b_J = 16$ and $b_J = 20$ is close to Euclidean so there are at least 50% more galaxies at $b_J \sim 20$ than predicted by simple models of galaxy evolution.

The angular autocorrelation function of galaxies, $w_{gg}(\theta)$, shows more large-scale clustering than expected from the standard CDM model. The differences between $w_{gg}(\theta)$ measured for galaxies in different magnitude ranges are consistent with the predictions from Limbers equation. Several tests show that these $w_{gg}(\theta)$ measurements are not significantly affected by systematic errors in the galaxy selection for the survey.

Catalogues of rich galaxy clusters selected from the survey show that the amplitude of the cluster autocorrelation function, $w_{cc}(\theta)$, depends strongly on the algorithm used to identify the clusters. Using a careful choice of selection algorithm an unbiased catalogue can be obtained, for which $w_{cc}(\theta)$ is relatively stable. A redshift survey of the richest 200 clusters in this catalogue shows that the amplitude of the three dimensional clustering corresponds to $r_0 \sim 13 h^{-1}$ Mpc, consistent with the amplitude of $w_{cc}(\theta)$.

## 1. THE APM GALAXY SURVEY

The construction of the APM Galaxy Survey is described in detail by Maddox *et al.* [1,2], and only a brief summary is given here. The original survey is based on 185 UKST J survey plates centred with declination $\delta < -20°$ and galactic latitude $b \lesssim -40°$. We have recently extended the survey to include 84 extra plates near the celestial equator, covering the south galactic cap up to $\delta = +2.5°$. The Automatic Plate Measuring (APM) system in Cambridge [3] was used to digitise and measure the magnitude, position and shape for typically 200,000 images on each plate. The complete survey contains about $5 \times 10^7$ images with $b_J \lesssim 22$.

To ensure a uniform magnitude limit across each field, the magnitudes were corrected for the effects of vignetting and differential desensitisation on each plate. Then the magnitude zero point for each plate was adjusted to match the neighbouring plates and so make the magnitudes uniform across the whole survey area. Finally the overall magnitude zero point and linearity were determined from CCD photometry of 339 calibrating galaxies, observed at the South African Astronomical Observatory, and the Mt. Stromlo Observatory. After applying these corrections, the survey contains $2 \times 10^7$ images to a uniform magnitude limit of $b_J = 21.5$.

The surface brightness profiles and shape parameters of the images were used to automatically distinguish between galaxies, stars and overlapping images. Visual inspection of over 4000 images on the Schmidt plates and 4-meter plates has shown that, over the magnitude range $16 \lesssim b_J \lesssim 20$, the galaxy catalogue is $\sim 95\%$ complete with $\sim 5\%$ contaminating non-galaxy images. For images fainter than $b_J \sim 20.5$, the classification reliability decreases rapidly, so to ensure an acceptably uniform galaxy sample, we use only galaxies brighter than $b_J = 20.5$. This leads to a catalogue of about $3 \times 10^6$ galaxies with $b_J \leq 20.5$, as shown in Fig. 1a.

The galaxies brighter than $b_J = 16.5$ have all been visually inspected on the plates and analysed separately to form the APM Bright Galaxy Survey [4]. This catalogue is the basis of the Stromlo/APM redshift survey [5], and also the APM Compact Group survey [6]. Detailed results from these surveys will be discussed elsewhere.

The distribution of galactic dust in the area of the APM survey can be deduced from the $100\mu m$ thermal emission measured by IRAS satellite [7]. A greyscale map of the inferred extinction in the area of the APM survey is shown in Fig. 1b. At low galactic latitude, towards the edges of our survey, there is a clear anticorrelation between dust emission and galaxy density. Several large patches of dust lead to regions where we detect a low density of galaxies. At high galactic latitudes, $b \lesssim -50°$, and $\delta \lesssim -15°$ there is very little dust emission, and the variations in extinction are less than 0.05 magnitudes. In this area we can be confident that the apparent structure accurately reflects the true galaxy distribution.

## 2. NUMBER COUNTS AND EVOLUTION AT LOW REDSHIFT

### *2.1 Measurements*

The number of galaxies as a function of magnitude has been the primary observational test for galaxy evolution since deep 4-metre plates showed that the number of galaxies at $B \gtrsim 22$ is larger than predicted by non-evolving models [8,9]. However the measurement

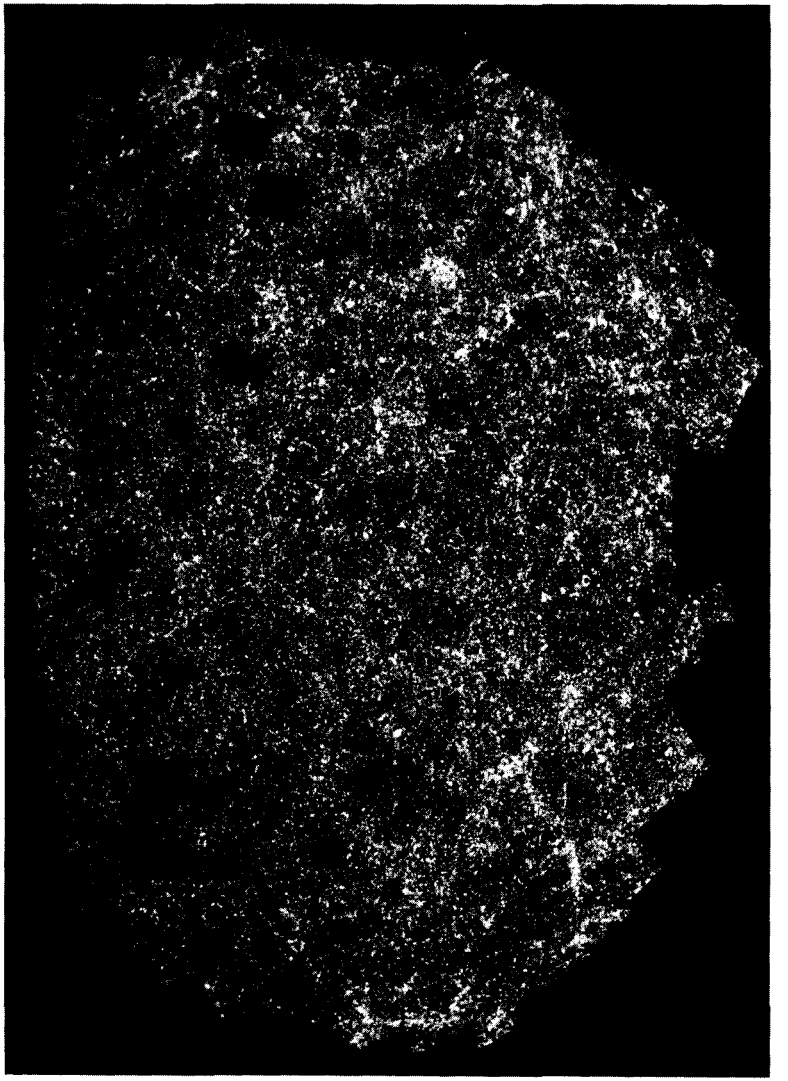

Figure 1. (a) The distribution of galaxy density in the APM survey shown in an equal area projection centred on the south galactic pole. The map shows $\sim 3 \times 10^6$ galaxies with the greyscale proportional to the galaxy density.

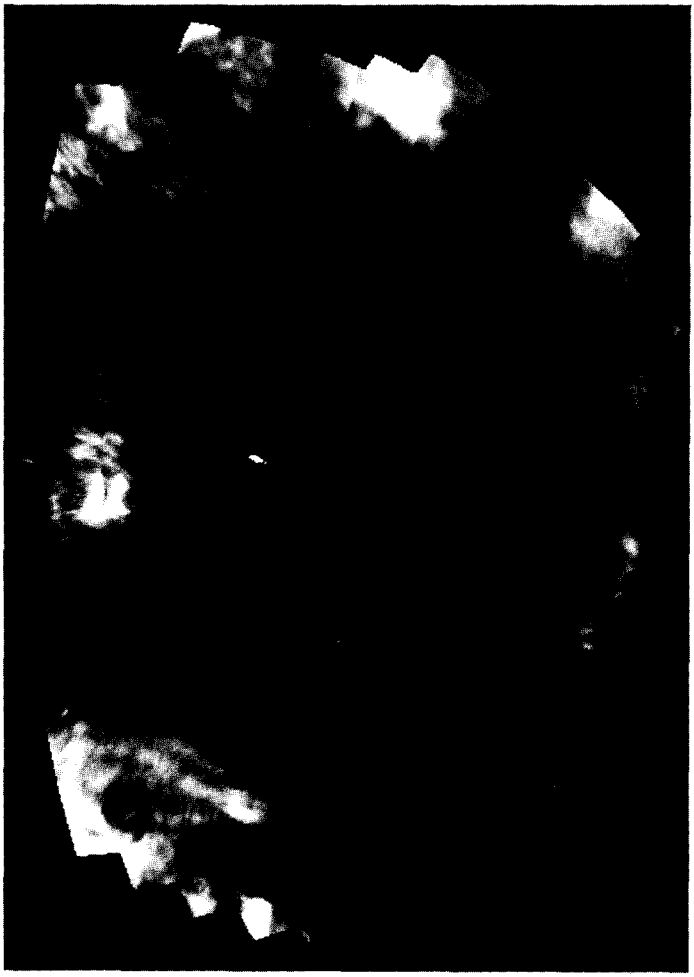

Figure 1. (b) A map of the galactic extinction inferred from the 100$\mu$m emission measured by the IRAS satellite [7]. The extinction at the pole is 0.05 magnitudes (corresponding to black in the map) and at the edge of the survey it is 0.2 magnitudes (corresponding to white). Over the area used for our clustering measurements, the variations in extinction are $\lesssim 0.05$ magnitudes.

of galaxy counts, especially at bright magnitudes, has been plagued by large uncertainties from the effects of galaxy clustering in the small area of the surveys, and also from limited photometric calibration. Given these difficulties, most work has concentrated on the slope of the counts, which is independent of the normalisation. However the slope is not a sensitive test of evolution; in fact, by normalising to the highest values of the counts at $\sim$ 18th magnitude it is possible to argue [10] that evolution is not significant until $b_J \sim 23$.

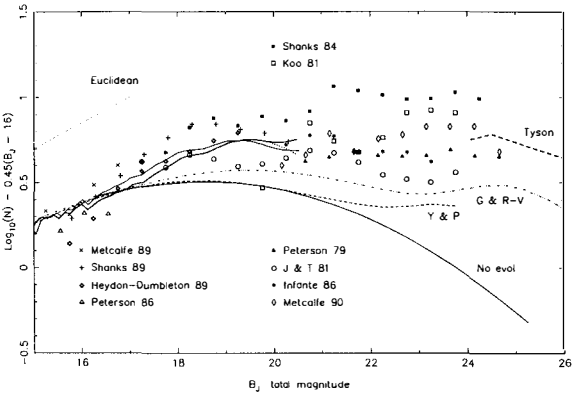


**Figure 2.** Differential galaxy counts per square degree per magnitude (i.e. count in 0.1 mag bins $\times 10$, or count in 0.5 mag bins $\times 1.98$). All counts have been multiplied by $\mathrm{dex}[-0.45(b_J - 16)]$ to provide an expanded ordinate. The thin and thick solid lines show our results with linear and quadratic calibrations, with correction for incompleteness. The thick dotted line shows our results with quadratic calibration *before* correction for incompleteness. The thick dashed line shows the Tyson [12] faint CCD counts. The various data points are as indicated on the figure [8,9,10,12,13,14,15,16,17,18,19]. The thin smooth line shows the no-evolution model of Ellis [20], normalised to our counts at $b_J \approx 17$, and we also plot two evolution models [24,25].

The large solid angle and good calibration of the APM survey provides a reliable fair sample of galaxies even as bright as $b_J = 16$, so we do not have to rely on the count slope to see galaxy evolution. We counted the average galaxy surface density in the APM survey in 0.1 magnitude bins [11] as shown in Fig. 2. Note that we have plotted $\log N - 0.45(b_J - 16)$, so that the faint counts appear approximately flat. This plot is clearly preferable to a simple plot showing $\log N$, since this would span some 6 orders of magnitude, and make 50% discrepancies difficult to see. These counts indicate evolution that is *much* more dramatic than previously thought; at $b_J \sim 19$ we observe 60% more galaxies than predicted by normal galaxy evolution models.

In Fig. 2 we have also shown the counts from several other studies [8–19]. At bright magnitudes, $16 < b_J < 17$, we see that our counts are close to the mean of the other results. In contrast to the large scatter seen in other surveys, the uncertainty in the APM count is small enough that the normalisation is well determined at this bright magnitude. Between $17 < b_J < 19$ our counts are slightly lower than the mean of the other results. The best independent measurement at magnitudes $17 < b_J < 20$ is that from the 100 square degree

region of Heydon-Dumbleton *et al.* [14]; this is $\sim 15\%$ higher than our result. Their area is part of our survey, and our counts for this region agree very well with their results. Fainter than $b_J = 19$ our counts are also consistent with the mean of other work. The differences between our measurements and earlier work are consistent with sampling fluctuations and small zero-point uncertainties.

*2.2 Evolution at low redshift*

The no-evolution model of Ellis [20], renormalised to match our count at $b_J \approx 17$ is also plotted on Fig. 2. The observed number counts show a remarkably steep slope, leading to an excess of 60% over the model at $b_J = 19$. At this magnitude, galaxies have a mean redshift of only $z \approx 0.1$ corresponding to a look-back time of only 1.8 Gyr (assuming $h = 0.5, \Omega = 1$). The observed excess galaxy count rises to 100% at $b_J = 20.5$.

Though our counts agree with the mean of previous work, the excess of 0.3dex in the number of galaxies at $b_J = 20.5$ has not been clearly detected before. This surprising fact is due to several factors which have contributed to obscuring the count excess. The models were previously normalised at $b_J \sim 18$, which accounts for 0.12dex of the excess; the lower counts of Jarvis & Tyson [17] and Peterson *et al.* [8] were preferentially used, rather than the mean of all measurements at $b_J = 20.5$, accounting for another 0.1dex. Thus it has been generally argued that the count excess at 20.5 is $< 0.1$dex, consistent with mild-evolution models. The remaining discrepancies have been further obscured by plotting the counts with a highly compressed ordinate.

It is apparent from our counts that dramatic galaxy evolution is occurring at low redshift. However, the faint galaxy redshift surveys of Broadhurst *et al.* [21], Koo [22] and Colless *et al.* [23] show that the redshift distribution to 22nd magnitude is the same as for a no-evolution model, despite the number count excess. Broadhurst *et al.* showed that simple models of luminosity evolution made to match the number counts at $b_J \sim 21$ predict a substantial number of galaxies with $z > 0.5$. This is inconsistent with their observed redshift distribution, and they suggest that the overall evolution of the galaxy luminosity function must look more like pure density evolution than pure luminosity evolution.

In Fig. 2 we plot two theoretical models [24,25] which match the observed redshift distribution and, if normalised at $b_J \approx 18$, also match the faint galaxy counts. When normalised to match our counts at $b_J \approx 17$ both fail to match the counts at $b_J \gtrsim 19$ by a wide margin.

*2.3 Discussion*

Given the dramatic evolution required to explain our counts at face value, we have investigated possible errors which might eliminate the need for such a radical suggestion. We consider errors in the completeness and linearity of our counts and in the local normalisation of the models.

We estimated the incompleteness of our counts as a function of magnitude using visual checks and fits to the classifier histograms as described by Maddox *et al.* [1]. The resulting incompleteness estimates are $\sim 5\%$ at $b_J \lesssim 20.0$, 10% at $b_J = 20.0$ and 58% at $b_J = 20.9$. The thin dotted line in Fig. 2 shows our measured number counts, with no corrections for incompleteness. The uncertainties in this correction brighter than $b_J = 20.5$ are *much*

smaller than the count excess, so the correction does not weaken the evidence for rapid evolution.

Our CCD photometry provides an estimate of the mean calibration curve needed to correct for small non-linearities in the raw APM magnitudes and give standard $b_J$. Possible errors in this calibration curve can change the form of the galaxy counts by at most 5-10%, which is much too small to explain the count excess. To be consistent with no evolution at $b_J = 20$, our calibration at bright magnitudes would need to be wrong by $\sim 0.5$ magnitudes which is clearly inconsistent with our CCD data [11] and would have been obvious in our comparisons with other photometry.

The last possibility is that our local neighbourhood is underdense by about 50% out to $\gtrsim 150h^{-1}$Mpc, which would mean that we have underestimated the local normalisation. The galaxy distribution in the sparse-sampled redshift survey of APM galaxies [5] with $b_J \lesssim 17$ shows that a local underdensity can account for at most a 10% reduction in the number counts at $b_J \approx 17$. Also the angular correlation function measured from the whole APM survey [26] implies that the *rms* variation in galaxy density in a $150h^{-1}$Mpc cube is only $\approx 7\%$. Both arguments suggest that it is very unlikely that the local normalisation is more than 10% underdense.

Thus we believe that our number counts are correct and that our survey constitutes a fair sample of the Universe. In the most conservative interpretation of our data, we could argue that our bright counts are low by 10% due to a local underdensity, and by a further 10% due to non-linearities in the photometric calibration. Even then our counts at $b_J = 20$ would show an excess of $\approx 60\%$ over non-evolving models, and $\approx 30\%$ over the best evolutionary models. This indicates that current models of galaxy evolution require fundamental revision.

## 3. THE TWO-POINT GALAXY CORRELATION FUNCTION

### *3.1 Measurements and error estimates*

The projected galaxy two-point correlation function, $w_{gg}(\theta)$, is a convenient statistic to quantify clustering in a galaxy survey. For the APM survey, we restricted our analysis to the central area where galactic obscuration is negligible, and so the measurements should represent the true galaxy clustering. We selected galaxies in six disjoint half magnitude slices and used the counts in cells to estimate the correlation function, $w_{gg}(\theta) = \frac{\langle N_i N_j \rangle}{\langle N_i \rangle \langle N_j \rangle} - 1$, where $N_i$ is the count of galaxies in cell $i$ and the angle brackets denote averages over pairs of cells at separation $\theta$. We chose this estimate after testing the ability of several estimators to reproduce $w_{gg}(\theta)$ from Soneira-Peebles simulations [27]. The simulations showed that our chosen estimator and the Fourier transform of the power spectrum give similar results, reproducing the input correlation function with a relatively small variance. In contrast, normalising $\langle N_i N_j \rangle$ by the global mean $\bar{N}^2$, rather than $\langle N_i \rangle \langle N_j \rangle$ leads to rather unstable estimates with a large variance.

The resulting measurements for the six slices are shown in Fig. 3a. Each slice has the same general shape: on small scales $w_{gg}(\theta)$ is well represented by a power law; at intermediate scales the measurements drop smoothly towards zero, falling well below the extrapolation of the power law; the measurements are consistent with zero on larger scales.

For brighter galaxies $w_{gg}(\theta)$ has a higher amplitude, and does not fall below the power law until larger separations, as expected from Limbers equation.

For $1° \lesssim \theta \lesssim 7°$ the faintest two slices show small distortions at low amplitudes; these are due to the small residual errors in the plate matching and field correction. We have analysed a detailed model for the propagation of errors in the construction of the survey [2], and calculated the expected effect on $w_{gg}(\theta)$. We estimated that the $w_{gg}(\theta)$ measurements would be affected at the $\sim 2 \times 10^{-3}$ level, consistent with the effects seen. We have approximately corrected these small errors by subtracting the estimated error correlation function from each slice. The resulting estimates with a further small correction to allow for the integral contraints are shown in Fig. 3b.

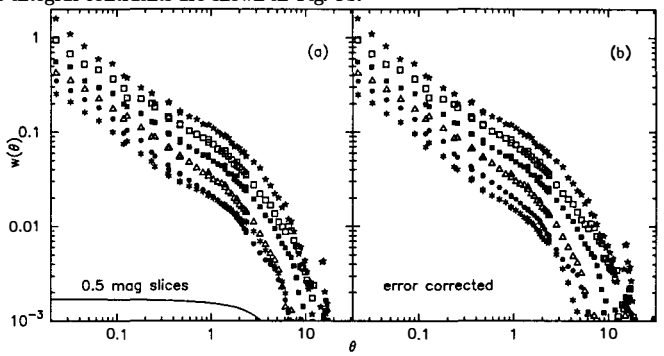


**Figure 3.** (a) The raw $w_{gg}(\theta)$ measurements for 6 magnitude slices of the APM Survey. The solid line shows the error correlation function normalised to $1.7 \times 10^{-3}$ at $\theta = 0$. (b) The 6 measurements after subtracting the expected contribution from residual errors, and approximately correcting for integral contraints.

Our error analyses are based mainly on internal consistency checks, so we used our CCD photometry as an external check to test for errors on large-scales. We found no evidence for significant gradients, but the error limit from this test is less stringent than from our internal error estimates, even though we have photometry for over 300 galaxies. More recently we have made a preliminary comparison between our data and CCD photometry of $\sim$ 16000 galaxies from the KOSST survey [28]. We find no evidence for large-scale gradients between the surveys.

*3.2 Scaling and comparison to other work.*

To quantitatively test Limbers equation we calculated the angle and amplitude scale factors which should scale $w_{gg}(\theta)$ for each slice to the depth of the Lick catalogue [29]. After applying these scale factors there is good agreement between the different measurements, as shown in Fig. 4a. The mean of these scaled measurement is plotted in Fig. 4b, which also shows the Groth and Peebles [30] measurements from the Lick map. It can be seen that the two estimates are consistent for scales $\theta_{Lick} \lesssim 2°$. For larger angles, the Lick measurement is slightly lower than ours. Although highly significant compared to the uncertainty in our measurements, the discrepancy is only $\sim 2\sigma$ in terms of the Lick error estimates. The

difference is probably caused by the difficulty in distinguishing between true large-scale structure and artificial gradients in the Lick map.

Recently two other measurements of $w_{gg}(\theta)$ from relatively large area surveys have been published: first from the EDSGC [31] and second from the new Palomar sky survey [32]. Preliminary $w(\theta)$ measurements from a 500 square degree area of the EDSGC showed a break at rather a small angle, but a more recent analysis of 1500 square degrees shows large-scale clustering consistent with our measurements. The difference between their results and our measurement is consistent with the effects of sampling fluctuations in the smaller area. The Picard results are based on two disjoint areas each covering about 200 square degrees of sky. The northern area is consistent with our measurements, but the southern area shows a much higher amplitude between 0.7° and 10°. The IRAS 100$\mu m$ sky map shows that the southern area is partially obscured by a patch of galactic dust, which produces a significant gradient across the area and leads to an artificially high $w_{gg}(\theta)$ at large angles. Therefore we believe that these new measurements are consistent with our estimates.

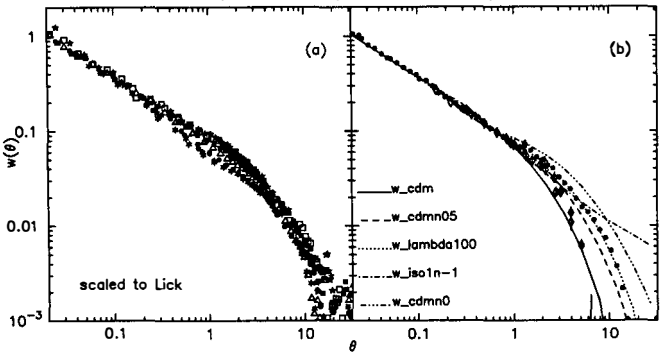


**Figure 4.** (a) Our 6 measurements of $w_{gg}(\theta)$ after scaling to the Lick depth. (b) The solid points show the mean of the 6 scaled measurements. The diamonds show the GP77 measurements from the Lick map. The various lines show linear predictions for models as labeled in the figure.

Linear theory predictions [33] for a selection of cosmological models are plotted in Fig. 4b. It can be seen that the standard $\Omega = 1, h = 0.5, b = 2$ CDM model [34] predicts too little large-scale clustering. The CDM model with an initial power spectrum of slope $n = 0$, and the isocurvature baryon model with initial slope $n = -1$ both predict too much large-scale clustering. Models which are consistent with our measured $w_{gg}(\theta)$ include: the low density CDM model with $\Omega h = 0.2$, $n = 1$ and a non-zero cosmological constant to give a flat geometry; the CDM model with $\Omega = 1$ and $n = 0.5$. Also models with a biassing factor that varies as a function of scale can be made to fit the data.

## 4. GALAXY CLUSTER CATALOGUES

We have selected many catalogues of galaxy clusters from the basic galaxy survey. Our cluster selection procedures involve two steps: first the identification of potential cluster sites; and second, the estimation of the cluster parameters for each position. We tried three methods for finding the candidate cluster sites: selecting percolated groups of galaxies;

selecting peaks in the smoothed galaxy density map; and stepping over a rectangular grid of positions. To ensure that the final cluster catalogues are complete, we selected many more candidate cluster sites than the final number of clusters: typically $\sim 10000$ sites were tested to produce a catalogue of $\sim 500$ clusters. In practice, there is little difference between the large-scale structure in the catalogues based different candidate lists. We decided to use the centres from the percolation method because it does not bias against the selection of close pairs of clusters. The initial groups were selected to have at least 20 galaxies linked with a percolation radius of 0.7 times the mean galaxy separation. Although large-scale structure in the catalogues is not strongly dependent on this first step in the selection, the next step of selecting clusters by richness and distance, can lead to very different catalogues.

To estimate each cluster distance and richness we used an iterative routine which essentially mimics Abell's procedure [35]. A first estimate of the cluster distance is used to define a circle with metric radius $r_A$, and all galaxies within this circle are sorted on magnitude. Then we count down the list of galaxies until there are 10 galaxies more than the expected field galaxy count. The magnitude of this galaxy is used to give a new estimate of the distance to the cluster, and hence a new counting radius. These steps are repeated until the distance estimate is consistent with the radius used; typically 4-6 iterations are required for this to converge. If the candidate centre does not correspond to a rich cluster, the iterations do not converge; the radius tends to decrease until there are less than ten galaxies within the circle. At each iteration we estimate the richness, $\mathcal{R}$, by counting the number of galaxies with magnitudes in the range $[m_3, m_3 + 2]$ and subtracting the expected field galaxy count within the circle. The value at the final iteration is taken as the best richness estimate.

Several modifications can be made to the algorithm described above and we made catalogues using combinations of the following options: fixing the centre to the initial estimate, or allowing it to be updated after each iteration; estimating the distance using $m_{10}$, or $m_{20}$, or $m_x$, where $x = \mathcal{R}/4$; estimating the richness by counting galaxies in $[m_3, m_3 + 2]$ or $[m_{10} - 0.5, m_{10} + 1.5]$ or $[m_x - 0.5, m_x + 1.5]$ or $[m_x - 0.5, m_x + 1.]$; using various radii and radial weighting schemes in counting the galaxies; for close pairs of clusters either assigning galaxies to only one cluster, or to both; using a fixed global normalisation to estimate the background field counts or using a normalisation defined locally for each cluster.

We found that the large-scale distribution of clusters in all the catalogues follows the same general features seen in the galaxy map (Fig. 1), but that the relative contrast of the features is different in different catalogues. The differences are shown quantitatively by the amplitude of the cluster-cluster correlation function, $w_{cc}(\theta)$, as plotted in Fig. 5a. The catalogues with multi-counted galaxies and a global background estimate have an amplitude about four times higher than the single-counted local background catalogues.

The large differences in clustering amplitude arise because some selection procedures give catalogues which contain spurious angular clustering not related to the true spatial clustering [36]. The apparent richness of a cluster can be enhanced by the galaxies from another cluster that is nearby on the sky, even if the pair of clusters are not spatially

correlated. Such richness enhancements can bias a catalogue to include more apparently close pairs of clusters than would be seen in a catalogue with a truly uniform richness selection. These spurious close pairs increase the amplitude of $w_{cc}(\theta)$, giving a biased estimate of the clustering. Since the number of clusters in a catalogue increases very rapidly towards poorer clusters, even relatively small projection biases can produce a large effect on the apparent clustering in a catalogue.

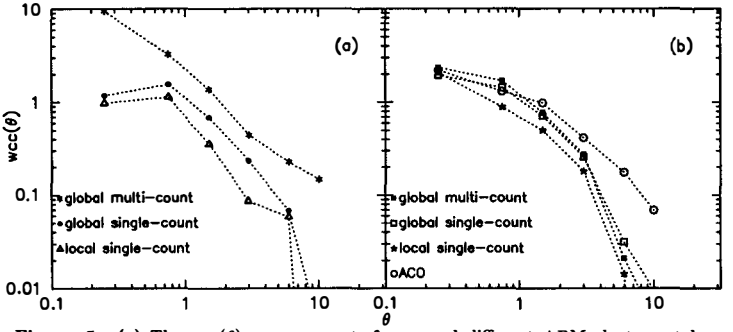


**Figure 5.** (a) The $w_{cc}(\theta)$ measurements for several different APM cluster catalogues as labelled. (b) $w_{cc}(\theta)$ for the more stable, less biased APM cluster catalogues. Also plotted is $w_{cc}(\theta)$ for the relevant area of the Southern Abell catalogue [37].

In order to reduce such biases, we gave more weight to galaxies near the centre of each cluster, where the contrast relative to the background is highest. We weighted the counts according to $W \propto r_A/(2r + r_A)$ for galaxies with $r < r_A$ and $W = 0$ for $r > r_A$, and used $r_A = 0.75h^{-1}$Mpc, half the standard Abell radius. With this scheme, the changes in $w_{cc}(\theta)$ caused by multi-counting or single counting galaxies, or using a globally or locally defined background estimate, are much reduced, as shown in Fig. 5b. Of these catalogues the single counted, local background catalogue is least biased by projection effects, and so has one of the lowest amplitudes for $w_{cc}(\theta)$.

Also plotted in Fig 5b is $w_{cc}(\theta)$ for the Abell clusters in our area [37]. The higher amplitude at large angles suggests that the Aell catalogue may be biassed by projection effects, and this interpretation is confirmed by the highly anisotropic clustering in redshift space [36]. The projection bias introduces spurious cluster pairs with very large redshift separation but small angular separation, thus distorting the apparent clustering in redshift space. With no corrections this bias leads to a high amplitude, $r_0 = 25h^{-1}$Mpc and very anisotropic clustering [38]. However applying a correction [36] makes the clustering more isotropic, and leads to a smaller amplitude $r_0 = 14h^{-1}$Mpc.

We have recently completed a redshift survey of the richest 243 clusters from our best catalogue. The spatial correlation function is nearly isotropic in redshift space, with a slight distortion along the redshift direction consistent with the redshift error estimates. We conclude that the clustering we measure in our catalogue represents the true spatial clustering of clusters. The measured amplitude corresponds to $r_0 = 13h^{-1}$Mpc, roughly in

line with the prediction of the standard CDM model [39].

**Acknowledgements:** All of the projects described here have been collaborative efforts involving major contributions from G. Efstathiou, W.J. Sutherland, J. Loveday, G.B. Dalton, S.V. Vassar and the APM group in Cambridge.

**References**

1. Maddox, S.J., Sutherland, W.J., Efstathiou, G. & Loveday, J. 1990a *M.N.R.A.S.*, 243, 692.
2. Maddox, S.J., Efstathiou, G. & Sutherland, W.J., 1990b. *M.N.R.A.S.*, **246**, 433.
3. Kibblewhite, E.J., Bridgeland, M.T., Bunclark, P., and Irwin, M.J., 1984, *Astronomical Microdensitometry Conference*, NASA Conf. Pub., **2317**, p277.
4. Loveday, J., 1989. *Ph.D. thesis*, University of Cambridge.
5. Loveday, J., Efstathiou, G. & Peterson, B.A., 1991. *Ap. J.*, submitted.
6. Vassar, S.V., 1991 in preparation.
7. Rowan-Robinson, M., Hughes, J., Jones, M., Leech, K., Vedi, K., & Wallke, K., 1991, *M.N.R.A.S.*, **249**, 729.
8. Peterson, B.A., Ellis, R.S., Kibblewhite, E.J., Bridgeland, M.T., Hooley, T. & Horne, D., 1979. *Ap. J. Lett.*, **233**, L109.
9. Koo, D.C., 1981, *PhD thesis*, University of California, Berkeley.
10. Shanks, T., 1990. In *Proceedings of IAU Symposium 139*, ed. S. Bowyer, & C. Leinhart, Reidel.
11. Maddox, S.J., Sutherland, W.J., Efstathiou, G., Loveday, J. and Peterson, B.A., 1990d, *M.N.R.A.S.*, **247**, 1P.
12. Tyson, J.A., 1988. *A. J.*, **96**, 1.
13. Metcalfe, N., Fong, R., Shanks, T. & Kilkenny, D., 1989. *M.N.R.A.S.*, **236**, 207.
14. Heydon-Dumbleton, N., Collins, C.A. & MacGillivray, H., 1989. *M.N.R.A.S.*, **238**, 379.
15. Peterson, B.A., Ellis, R.S., Efstathiou, G., Shanks, T., Bean, A.J., Fong, R. & Zen-Long, Z., 1986. *M.N.R.A.S.*, **221**, 233.
16. Shanks, T., Stevenson, P.R.F., Fong, R. & MacGillivray, H.T., 1984. *M.N.R.A.S.*, **206**, 767.
17. Jarvis, J.F. & Tyson, J.A., 1981. *A. J.*, **83**, 1549.
18. Infante, L., Pritchet, C. & Quintana H., 1986, *A. J.*, **91**, 217.
19. Metcalfe, N., Shanks, T., Fong, R. & Jones, L.R., 1991, *M.N.R.A.S.*, **249**, **498**.
20. Ellis, R.S., 1987. In *"Observational Cosmology"*, Proceedings of IAU Symposium 124, eds. Hewitt *et al.*, Reidel.
21. Broadhurst, T.J., Ellis, R.S. & Shanks, T., 1988. *M.N.R.A.S.*, **235**, 827.
22. Koo, D.C., 1990. In *The Evolution of the Universe of Galaxies*, ed. R. Kron, ASP Conference Series, Vol. 10.
23. Colless, M.M., Ellis, R.S., Taylor, K. & Hook, R.N., 1990. *M.N.R.A.S.*, **244**, 408.
24. Yoshii, Y., & Peterson, B.A., 1991, *Ap. J.*, **372**, 8.
25. Guiderdoni, B. & Rocca-Volmerange, B., 1990, *A. & A., Astrophys.*, **227**, 362.
26. Maddox, S.J., Efstathiou, G., Sutherland, W.J. & Loveday, J. 1990c. *M.N.R.A.S.*, **242**, 43P.
27. Soneira, R.M. and Peebles, P.J.E., 1978, *A. J.*, **83**, 845.
28. Tucker, D., Kirshner, R.P., Oemler, A., Schechter, P.L., and Schechtman, S.A., private communication.
29. Shane, C.D. and Wirtanen, C.A., 1967, . *Pub. Lick Obs.*, **22**, Part 1.
30. Groth, E.J. and Peebles, P.J.E., 1977, *Ap. J.*, **217**, 385 (GP77).
31. Collins, C.A., Heydon-Dumbleton, N.H. & MacGillivray, H.T., 1989, *M.N.R.A.S.*, 236, 7P.
32. Picard, A., 1991. *Ap. J. Lett.*, **368**, L7.
33. Sutherland, W.J., 1991, in "Observational Tests of Inflation", NATO ASI proceedings, eds. Shanks *et al.*.
34. Davis, M., Efstathiou, G., Frenk, C.S. and White, S.D.M., 1985, *Ap. J.*, **292**, 371.
35. Abell, G.O., 1958, *Ap. J. Suppl.*, **3**, 211.
36. Sutherland, W.J., 1988, *M.N.R.A.S.*, **234**, 159.
37. Abell, G.O., Corwin, H.C. and Olowin, R.P., 1989, *Ap. J. Suppl.*, **70**, 1.
38. Bahcall, N.A. and Soniera, R.M., 1983, *Ap. J.*, **270**, 20.
39. White, S.D.M., Frenk, C.S., Davis, M. and Efstathiou, G., 1987, *Ap. J*, **313**, 505.

# Is Standard CDM Compatible With All Available Data?

MARC DAVIS

*IAP, Paris, FRANCE, & University of California, Berkeley USA*

**Abstract**

I summarize briefly some current problems in the confrontation of the Cold Dark Matter theory with observations. A more detailed discussion was presented by Frenk[1].

## 1. The Standard Model

The Cold Dark Matter (CDM) model of the evolution of structure in the Universe has had considerable success in the last decade, but has had its share of controversy as well. New challenges to this "standard model" seem to arise every year, and in the newspapers one frequently reads announcements of the "death of CDM". But the theory has more than once arisen from the grave as observations contradicting its predictions have been shown to

be incorrect. Is the present situation any different?

Let us define *simple* CDM as the basic model resulting from an inflationary early Universe, i.e. scale invariant initial fluctuations, zero curvature k=0, and $\Omega = 1$. In this case the coherence length scale of structure is proportional to $H_0^{-2}$. CDM pundits have always used $h = .5$, (or less) because larger values lead to hopelessly inadequate large scale structure. From the earliest prehistory[2], it was recognized that a model in which galaxies traced the mass distribution was incompatible with $\Omega = 1$, and the concept of bias with its infamous parameter $b$ was introduced[3] as a fudge to reconcile the low $\Omega$ inferred from the dynamics of groups and clusters with the mandates of inflation. Much of our ignorance of the details of galaxy formation is thus absorbed within $b$. In the simplest case, known as the linear bias model, one imagines that $b$ is constant with scale, in which case it is convenient to define $b$ in terms of the ratio of the *rms* galaxy and matter fluctuations on a scale of $8h^{-1}$ Mpc, $b = \sigma_{gal}(8)/\sigma_{\rho}(8)$.

The dynamics of small systems works best for relatively large $b = 2.5$, but such a low amplitude of matter fluctuations leads to large scale velocity fields that seem far too small to match observations[4]. The velocity field observations suggest $b < 1.6$, which would be more compatible with the abundance of large clusters, as well as the relatively weak segregation of galaxies as a function of luminosity or depth of potential well.

It is important to recall why the $b = 1$, mass traces light model is incompatible with the observations[2]. First, in such a model, the pair velocity dispersion would be 1000 km/s, compared to an observed pair dispersion of 300 km/s. This gross discrepancy could be somewhat reduced by velocity bias (i.e. the galaxies move more slowly than the dark matter because of the effects of dynamical friction and dissipation[5]), but recent tests do not show the effects of velocity bias in clusters to be extraordinarily large. A second point is that the evolution of the CDM spectrum is not self-similar; the slope of the matter correlations steepens with time. In fact, if galaxies trace the mass, then a simultaneous match of the observed amplitude and slope of $\xi(r)$ occurs for $\Omega h = .25$, or $H_0 = 25$ km/s/Mpc in an $\Omega = 1$ Universe[2]. In the extreme velocity bias model[5], the galaxies are taken to be slightly antibiased, $b = .8$. But for

$h = .5$, the slope of the matter correlations is $\gamma = 2.2$, considerably above the value observed for galaxies $\gamma = 1.8$. For this to be true, the efficiency of galaxy formation must decrease substantially in dense regions, which is the opposite of the expectation of the high peaks model. Since we do not understand galaxy formation in any detail, we cannot immediately reject such a model, but it is pushing credibility. Low $b$ models predict large amplitude CMB fluctuations, so a definitive test should be possible very soon.

On larger scales, the cluster-cluster correlation function as reported by Bahcall and Soneira[6] is completely incompatible with CDM models for any bias value. In the past several years, the Abell cluster list used for this analysis has come under increasing attack, primarily for excessive projection contamination. Now a new catalog of clusters extracted from the APM catalog in a fashion that greatly reduces projection contamination has resulted in a cluster correlation function fully consistent with the CDM predictions[7]. Another example of CDM being resurrected from the grave.

The only serious (in my opinion) challenge to the simple CDM model comes from the large scale clustering of galaxies, and the reports of excess power on large scales. There are several anecdotal discussions of great walls, periodic structure, etc, but the only quantitative and significant discrepancies are based on the angular correlation functions derived from the APM catalog[8]. All the other pieces of evidence, such as 100 Mpc walls and seemingly periodic structure are perhaps telling us the same story: the CDM spectrum does not seem to have sufficient large scale power.

Although the additional power needed on scales on large scales is not large, it is not easy to modify the standard CDM theory because it is so constrained. The simplest mechanism for generating the needed large scale power is to set the Hubble constant $H_0 < 30$ km/s/Mpc. Barring this, one needs an extreme astrophysical biasing such as a modulation of the efficiency of galaxy formation on scales of 50 Mpc (via changes in the IGM caused by QSO'?) Alternatively, perhaps we need additional physics, such as a deviation from scale invariant initial conditions, or nonzero vacuum energy density ( $\Lambda \neq 0$), or a feature in the initial power spectrum generated by some physical process such as a decaying 17 keV neutrino[9].

In summary, the past decade has witnessed amazing progress in our understanding of large scale structure in the Universe. The simplest model consistent with inflation has led to the development of a standard model of structure, simple CDM. This theory qualitatively explains virtually all aspects of the observed large scale Universe, but detailed quantitative tests are hampered by our poor understanding of galaxy formation and the degree to which galaxies should trace the underlying mass distribution. Simple, constant amplitude bias models are apparently too simple. Can more sophisticated, but plausible, models of bias explain the excess power on large scales, or is it time to insist on new physics? To break the present impasse, a new type of observational constraint in needed. Perhaps this will come from positive detection of the small scale microwave background fluctuations. Low $b$ models are just barely consistent with current limits, so further improvements in the experiments should finally detect the long sought imprints of the nascent cosmic structures.

## References


1. Frenk, C. F., 1990, Nobel Symposium 79, to appear in *Physica Scripta.*
2. Davis, M., Efstathiou, G. P., Frenk, C. F., & White, S. D. M., 1985, *Ap. J.*, **292**, 371.
3. Kaiser, N., 1984, *Astrophysical J. Lett.*, **284**, L49.
4. Gorski, K., Davis, M., Strauss, M. A., White, S. D. M., & Yahil, A., 1989, *Ap. J.*, **344**, 1.
5. Carlberg, R. & Couchman, H., 1991, *Ap. J.*, in press.
6. Bahcall, N., & Soneira, R. M., 1983, *Ap. J.*, **270**, 20.
7. Dalton, G. B., Efstathiou, G. P., Maddxo, S. J., & Sutherland, W. J., 1991, *Astrophysical J. Lett.*, in press.
8. Maddox, S. J., Efstathiou, G. P., Sutherland, W. J., & Loveday, J., 1990, *MNRAS*, **242**, 43p.
9. Bond, J. R., & Efstathiou, G. P., 1991, *Phys. Lett. B*, in press.

# DARK MATTER AND LIGHT DISTRIBUTION

F. BERNARDEAU

Service de Physique Théorique de Saclay†, F-91191 Gif-sur-Yvette Cedex France.

**Abstract.** Hierarchical matter correlation functions can be used to calculate the global clustering properties in a non-linear universe. Thus, the mass distribution function of astrophysical objects of any kind can be derived from a unique universal function. The comparison with the observed luminosity functions provides some information about the behaviour of the ratio $(M/L)$ for the galaxies as well as for the groups or the clusters. Tree-Hierarchical Models for the matter correlation functions also permit to calculate the "light" two and three-body correlation functions. The galaxy, group and cluster correlation luminosity dependences are presented. The resulting bias for the bright galaxies is found to be about 2.7. The three-point correlation function is found to have the observed tree-shape with a normalization parameter $Q \approx 1$.

† Laboratoire de la direction des Sciences de la Matière du Commissariat à l'Energie Atomique.

## 1. THE EXPECTED MATTER CORRELATION FUNCTIONS.

The matter distribution in the present universe can be assumed to be essentially determined by the gravitational dynamics in an expanding universe. The distribution is then governed by

- the initial conditions, that reduce to a power spectrum in case of purely Gaussian fluctuations;

- the dynamics, for which the equations are known.

The resolution of this problem gives in principle the complete hierarchy of the matter correlations. The comparison with the observations, however, remains complicated due to the biases that inevitably spoil the galaxy distributions: Galaxies exist where large amount of matter have been gathered, and so mark a very particular subset of the matter points.

Attempts have been made to determine the kind of biases that can be reasonnably expected, assuming only that galaxies (or clusters ...) trace the large matter condensations in the present non-linear universe (Bernardeau and Schaeffer 1991b).

Unfortunately, no complete solution for the dynamics are known, and only global scaling properties can be derived both by observations and theory. Peebles (1980) proposed a self-similar solution, for which the time dependence is known and which implies some particular scaling rules between the correlation functions:

$$\overline{\xi}_N(V) = S_N \left[\overline{\xi}_2(V)\right]^{N-1} \tag{1}$$

where $\overline{\xi}_N(V)$ is the mean value of the $N$-point correlation functions in a volume $(V)$, the coefficients $S_N$ being independent of the size of the volume. Such a self similar behaviour can be seen as a possible late-time asymptotic solution for the dynamics, *whether the initial conditions are self-similar or not.*

The relations (1) then imply some scaling, actually observed, in the galaxy distribution and particularly for the void probability function. More precisely, the measurements of the three-point galaxy correlation functions give

$$\xi_3(r_1, r_2, r_3) \approx Q[\xi_2(r_1, r_2)\xi_2(r_2, r_3) + sym.] \tag{2}$$

with $Q \simeq 1$ and with a two point galaxy correlation function given by

$$\xi_2(r) \simeq \left(\frac{r}{r_0}\right)^{-\gamma}, \ \gamma = 1.8, \ r_0 \simeq 5h^{-1} \text{ Mpc}, \tag{3}$$

the Hubble constant being $H_0 = 100h$ km/s/Mpc.

Similar scaling properties, as (3) for the power law behaviour of the two-point correlation function and (1) for the scaling relations between the higher orders, will naturaly be assumed for the matter correlations.

## 2. WHERE IS THE DARK MATTER ?

The only hypothesis (1) for the matter correlations implies the existence of a *universal* mass multiplicity function (Balian and Schaeffer 1989, Bernardeau and Schaeffer 1991a) $H(X)$: Whatever the kind of objects you consider, as soon as their size is smaller than the correlation length, you have

$$M(L)\phi(L)dL = XH(X)dX \tag{4}$$

with

$$X = \frac{M(L)}{\rho_0 V \overline{\xi}_2(V)} \tag{5}$$

where $\phi(L)dL$ is their luminosity function, $M(L)$ their *total* mass, $\rho_0$ the mass density of the universe and $\overline{\xi}_2(V)$ the mean value of the matter two-body correlation function in the volume $V$ of the object. The scaling parameter $X$ measures the overclustering inside an object of size $R$, and is close to its velocity dispersion $\sigma$:

$$X = 1.6 \frac{b^2}{\Omega} \left( \frac{\sigma}{250\ \mathrm{km/s}} \right)^2 \left( \frac{R}{10\, h^{-1}\mathrm{kpc}} \right)^{\gamma-2}$$

So, once a scale has been specified, $X$ is proportional to the mass and $H(X)$ turns out to be a mass multiplicity function.

Numerical simulations suggest that $H(X)$ has a Schechter like form (fig. 1) with a power law behaviour at the faint end characterized by a parameter $\omega \simeq 0.4$ (Bouchet et al. 1991)

$$H(X)dX \propto X^{\omega-2}dX\,. \tag{7}$$

The comparison with known astrophysical objects involves the knowledge of their total extension and their total mass. For galaxies, it means that their dark haloes must explicitely be taken into account. A very useful and reasonnable assumption is to suppose that $X$ is independent of the radius at which it is determined, which occurs when the density of the object varies as $r^{-\gamma}$ from its center. *The relation $X(L)$ is then directly given by the observations.* Thus, for the faint galaxies we obtain,

$$X(L) \sim L^{\mu}, \quad \mu \simeq 0.25, \tag{8}$$

from velocity dispersion measurements.

The fulfilement of the relation (4) then involves the determination of the total mass of the objects or equivalently their total extension. One obtains,

$$\left( \frac{M}{L} \right) \sim L^{-\epsilon} \tag{9.a}$$

with

$$\epsilon = \alpha + 2 - \mu\omega\,, \tag{9.b}$$

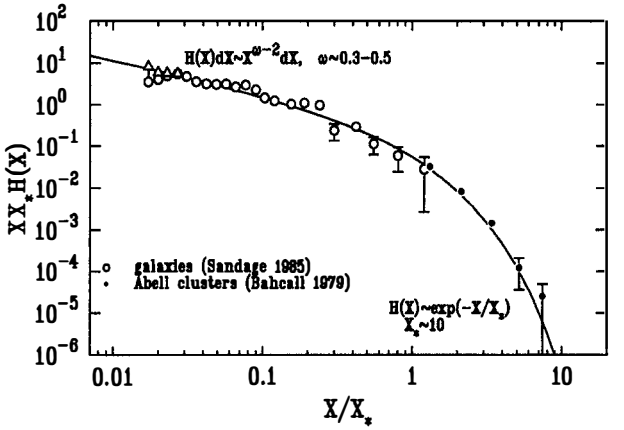


Figure 1. The universal mass multiplicity function $H(X)$. $X$ measures the overclustering inside an object, $X \propto M/R^{3-\gamma}$, and is propotionnal to the mass of the object once the scale has been fixed. The comparison with observed luminosity functions, according to (4), leads to the determination of the total $(M/L)$ ratio.

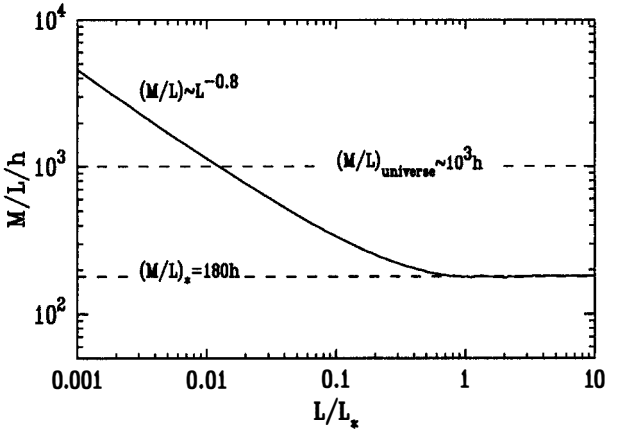


Figure 2. The $(M/L)$ ratio for the galaxies. It has been normalized so that $\int M(L)\phi(L)dL / \int L\phi(L)dL = (M/L)_{\text{universe}}$. It appears to be a decreasing function of $L$ and its value for the bright galaxies is found to be $(M/L)_* \simeq \frac{1}{6}(M/L)_{\text{universe}}$.

where $\alpha$ is the index of a Schechter like luminosity function. $\alpha \simeq 1.1$, $\omega \simeq 0.4$ implies

$$\epsilon \simeq 0.8\,, \tag{9.c}$$

*with a weak $\omega$ dependence.*

As a result $\left(\frac{M}{L}\right)$ is a decreasing function of the luminosity (fig. 2). Moreover, assuming that the total mass of the universe is concentrated in the galaxies and in their dark haloes one obtains,

$$\left(\frac{M}{L}\right)_* \simeq \frac{1}{5}\left(\frac{M}{L}\right)_{universe}\,, \tag{10}$$

where $\left(\frac{M}{L}\right)_*$ is the ratio for the bright galaxies: *The major part of the mass of the universe is in the faint galaxies.*

Similar results can be obtained for clusters and groups:

$$\left(\frac{M}{L}\right)_{\text{Abell clusters}} \simeq 200 - 300\Omega h, \tag{11.a}$$

and

$$\left(\frac{M}{L}\right)_{\text{T.G. groups}} \simeq 300 - 400\Omega h\,. \tag{11.b}$$

## 3. THE "LIGHT" CORRELATIONS.

$H(X)$ gives the expected mass fluctuations within a unique given volume. Similar calculations can be made with two volumes at a given distance $r$ away (Bernardeau and Schaeffer 1991) assuming a Tree-Hierarchical model for the matter distribution: The N-point matter correlation functions $\xi_N(r_1, ..., r_N)$ are then given by the product of $N-1$ two-body correlation functions, times a normalization parameter,

$$\xi_N(r_1, ..., r_N) = \sum_{(\alpha)} Q_N^{(\alpha)} \sum_{t_\alpha} \prod_{N-1} \xi_2(r_i, r_j)\,, \tag{12}$$

where $(\alpha)$ is a particular tree topology connecting the N-1 points without making any loop (to be in accordance with the scaling properties of $\xi_N$); $Q_N^{(\alpha)}$ is a parameter associated with the order of the correlation and the topology involved; $t_\alpha$ is a particular labelling of the given topology $(\alpha)$ and the last product is made over the $N-1$ links between the $N$ points with two-body correlation functions. The form (12) for the matter correlations is inspired by the known behaviour of the three-body galaxy correlation function (2). The resulting joint mass distribution function takes the form

$$H(X_1, r_1; X_2, r_2) dX_1 dX_2 = H(X_1) H(X_2) \left[1 + b(X_1) \xi_2(r_1, r_2) b(X_2)\right] dX_1 dX_2\,. \tag{13}$$

Applied to the galaxy distribution it means that

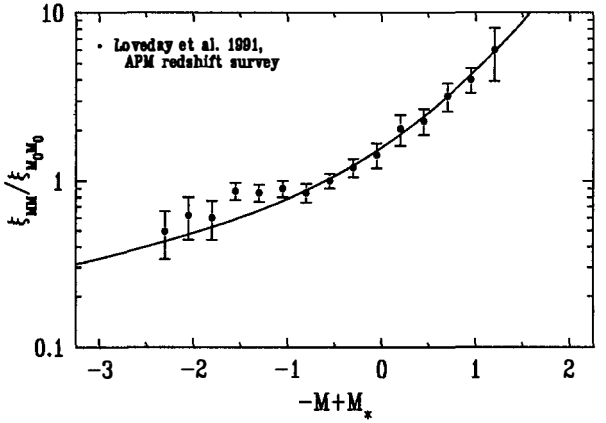


Figure 3a. The clustering strength of the galaxies. The full line is the model prediction. The data are the preliminary results obtained from the APM redshift survey.

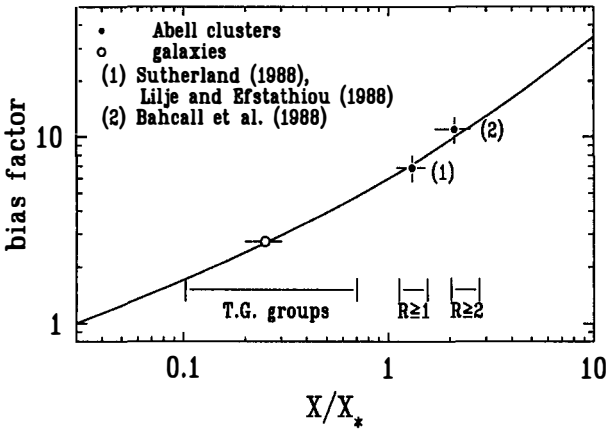


Figure 3b. The bias parameter $b(X)$ (eq. 12) as a function of the overclustering $X$ inside the object. The full line is the model prediction. The representing point of the galaxies corresponds to the observed mean value of $b(X(L))$ according to the Limber equation, whereas the Abell cluster representing points have been placed according to the measurement of their scaling parameter $X$ and to the measure of the enhancement factor between galaxy and cluster correlations. The group bias factor is expected to be comparable to the one of the galaxies.

-The galaxy-galaxy two-body correlation is proportional to the matter two-body correlation function with the same distance dependence.

- The correlation is completely factorized as a function of the distance and two biasing functions $b(X)$.

- The bias is an intrinsic property depending only on the internal overclustering of the object: Luminosity segregation (fig. 3) and comparison of galaxies with clusters (fig. 4) can be derived.

- The asymptotic behaviours of the bias as a function of the luminosity are then $b(L) \propto L$ for $L \gg L_*$ and $b(L) \propto L^{\sim 0.1}$ for $L \ll L_*$.

The resulting observable bias, $b$, calculated as the mean value of $b(X(L))$ obtained when one mimics the measurement of the real space galaxy correlation length in 2-D catalogues with the Limber equation, is $b \simeq 2.7$.

We have also calculated the shape of the three-point correlation function as a check to the credibility of such calculations. We find that the three-point galaxy correlation function take the desired form (2) with a normalization parameter $Q$ close to 1, whatever the nature of the object (galaxies or clusters) or the detailed parameters involved for the matter distribution. This result is at variance with what is obtained in a gaussian field in the frame of the peak formalism, for which the three-point galaxy correlation function also contains an unobserved loop of three two-body correlation functions as stressed by Bonometto (1988).

## 4. THE REDSHIFT DEPENDENCE

All the universal functions that have been calculated, $H(X)$ and $b(X)$ are independent of time. The only dependence is in the strength of the two-body correlation function. This dependence is in principle known from the self similar behaviour of the correlation length,

$$r_0(z) = r_0 * (1+z)^{-\frac{3-\gamma}{\gamma}}$$

where $r_0(z)$ is the comoving correlation length.

Thus such calculations allow to explore recent evolution in the clustering properties of the universe. Number densities of specified objects, such as X-ray emitting clusters, can be predicted (Scheaffer's contributed paper). The evolution of the galaxy correlation strength could in principle be calculated.

## CONCLUSION

Such models provide a consistent description of the highly non-linear clustering properties of the universe. The theoretical major results obtained are the following

- the dark matter is mainly in the faint galaxies;

- the expected bias is about 2.7;

- the three-point parameter $Q$ is close to 1 for galaxies but is not necessarily equal to the corresponding value of $Q$ for the matter distribution.

- the redshift evolution is known.

## REFERENCES

Bahcall, N.A.: 1979 *Astrophys. J.*, **232**, 689.

Bahcall, N.A., Batuski, D.J., Olowin, R.P.: 1988, *Astrophys. J. (Letters)*, **333**, L13.

Balian, R., Schaeffer, R.: 1989, *Astron. Astrophys.*, **220**,1.

Bouchet, F., Schaeffer, R. Davis, M.: 1991, to be published.

Bernardeau, F., Schaeffer, R.: 1991a *Scale invariant models of the Galazy and Cluster Luminosity Functions,* to be published.

Bernardeau, F., Schaeffer, R.: 1991b *Galazy correlations, matter correlations and biasing,* to be published.

Bonometto, S.: 1988, *Morphological Cosmology,* Cracow Lecture notes in Physics, Flin P. and Duerbeck H.W. (Springer-Verlag, Heidelberg).

Lilje, B., Efstathiou, G.:1989, *M.N.R.A.S.*, **236**, 851.

Loveday, J., Peterson, B.A., Eftathiou, G., Maddox, S.J.:1991, to be published.

Peebles, P.J.E.: 1980, *The Large Scale Structure of the Universe,* Princeton University Press, Princeton, N.J., USA.

Sandage, A., Bingelli, B., Tamman, G.A.: 1985 *Astron. J.*, **90**, 1759.

Sutherland, W.: 1988, *M.N.R.A.S.*, **234**, 159.

# GREAT ATTRACTOR MODELLING AND GALAXY FORMATION

V. N. Lukash

Astro Space Centre, Academy of Sciences

Profsouznaya 84/32, 117810 Moscow, USSR

The Great Attractor (GA) is analysed and modelled for Gaussian perturbation theories of the structure formation. We argue that the cold dark matter (CDM) standard model cannot provide for GA phenomenon if the latter is a statistically representative feature in the Universe. The hybrid dark matter models and anisotropy of the relic background radiation are discussed

**CONFRONTATION**

The largest ratings among the up-to-date cosmological observations are those due to the relic background anisotropies and GA phenomenon. The reason is that both experiments provide the direct probes of the primordial (postrecombination) cosmological perturbations which brought about the large scale structure appearance we observe today in the form of distribution of galaxies and their velocities. More of this, these two experiments confront each other. If $\Delta T/T$ ($\theta > 1^{o}$) upper limits we have now force us to lower down the perturbation amplitudes then GA existence evidences for sufficiently high power of the perturbations on scales, $l \geq 40\ h^{-1}$Mpc. The first topic ($\Delta T/T$) is happily promoted by COBE, RELIC and other experiments. The second one (GA) needs modelling to be statistically meaningful.

For the Gaussian perturbation theories the gap between these confronting requirements is less than a factor of two. However since we deal with a single GA object, not to speak that half of its volume is not yet measured, a lot depends on the interpretation of observational data. One needs modelling today to relate GA with the statistically standard objects arising in given theory. We understand that being more than observations, our models can be corrected in future with new data coming.

The GA definition introduced below leaves practically no room for any theoretical speculations on the possibility to change the postrecombination primordial spectrum, and gives a great optimism for its detection and testing by $\Delta T/T$ observations.

**REASONS**

The conservative approach is mainly based on two points[1]:

(i) Let us measure bulk velocity of the matter within some sphere around, say, $V\,(R_{TH} = 60\ h^{-1}\mathrm{Mpc}) \simeq 330$ km/s, and compare it with the r.m.s. velocity for a given model, say for CDM $V\,(R_{TH} = 60\ h^{-1}\mathrm{Mpc}) = 220\ b^{-1}$km/s. Then the comparison will be O.K. for CDM: only $\sim 1.5\ b$ standard deviations. (Here $h$ and $b$ are the Hubble and biasing parameters).

(ii) Let us compare the overdensity in the GA centre smoothed by a Gaussian filter, say, $\delta\,(R_f = 14\ h^{-1}\mathrm{Mpc}) \simeq 1.2$ which corresponds to $\delta \equiv \delta\rho/\rho \simeq 0.7$ extrapolated to $z = 0$ according to the linear theory, with the r.m.s. perturbations (e.g., for CDM $\sigma_o\,(R_f = 14\ h^{-1}\mathrm{Mpc}) \simeq 0.34\ b^{-1}$ ). Then it is O.K. for CDM again: $\nu = \delta/\sigma_o \sim 2b$ .

However, both points are confused by the contrarguments.

(i) *Position effect.* The Local Group (LG) is as far from GA as the GA-size. So, if we center the top-hat (TH) sphere on LG, we underestimate the effect.

(ii) *Scale effect.* If we center TH-sphere on GA then the parameter $\nu$ (versus to $R_{TH}$) will be negligible for both, small and large $R_{TH}$ . So, it is the position of the $\nu$-maximum that indicates the GA peak scale, while any calculations of $\nu$ for smaller or larger scales underestimate the effect, as well. (According to Fig.3, the GA scale is found as 25 to 35 $h^{-1}$Mpc)

Thus, the quantitative description requires modelling. We will assume the following basics for it.

(*) *GA definition*: GA is a large scale coherent flow field of galaxies with the characteristic correlation length larger than the averaging filter scale to be used for getting such potential velocity field ($l_c \geq 40\ h^{-1}$Mpc $> R_f \sim 10\ h^{-1}$Mpc).

(**) *Statistical hypothesis*: The real density peak to be developed to the GA is close to the mean density peak that can be derived in the theory. As we know, in case of high peak ($\nu_{max} >> 1$) the latter has a spherically symmetric profile $\delta(r)$ proportional to the dynamical correlation function.

Under these hypotheses the GA formation was modelled in [2] for the two-component postrecombination medium – dark WIMPs (Weak Interacting Massive Particles) and primordial baryonic matter – with different primordial spectra and $\Omega_{tot} = 1$.

Below, we analyse the results.

**RESULTS**

They are rendered in three groups

(i) Some basic parameters of the linear initial peaks required to form GA, are practically independent of the model. Best fits to the observational data [3] are profiled between two limit curves on Fig.1,2. The corresponding $\nu$-functions for these limits are given on Fig.3. Note, that the central overdensity in the linear peaks is $\delta(0) = (1-2)(1+z)^{-1}$ while the non-linear evolution results in $\delta_{nl}(0) > 3$. If we average the actual overdensities $\delta_{nl}(0)$ with the filter $R_f = 14\ h^{-1}$Mpc, they will come to $1\text{-}1.6\ h^{-1}$Mpc, in accordance with the POTENT.

(ii) The realization probability for the GA peaks is dratically different in different models. This depends on many parameters the most important of which is the GA symmetry. Say as a single positive peak GA can form in CDM, HDM and hybrid models on the levels $\delta(0) \sim (4\text{-}5)\sigma_0$ , $(1\text{-}2)\sigma_0$ and $(2\text{-}4)\sigma_0$ repectively, depending on h, b and other parameters. Note,that middle and low peaks can significantly deviate from sphericity.

(iii) Central region of peaks with $\delta(0) > 1.5\ (1+z)^{-1}$ collapses before z = 0, resulting in the galactic contraflows, shock waves and other observable phenomena.

Summarizing, we see that the standard CDM model is now found in a similar position which the HDM model had some years ago : CDM (HDM) is good to form galaxies (GAs) while it is helpless for GAs (galaxies) origin. The way out is to have the spectrum with high enough power on both, GA and galaxy scales.

## HYBRIDS

One of the possibilities to design the postrecombination spectrum leaving the fundamental Harrison-Zeldovich spectrum at postinflation, is granted by hybrid (hot+cold) dark matter models. The calculations show that about 30% of the total density in the form of neutrino-type particles adding to CDM , can ensure the necessary power enhancement on GA scales (see Fig.4 )[4]. There are some other possibilities open.

## CONCLUSIONS

The main assumption necessary to relate the GA phenomenon

with $\Delta T/T$ predictions is that there exist many GAs within the contemporary horizon. Here, the symmetry of the local GA is an important test in itself: if it deviates from sphericity, then we deal with a typical object in the Universe. For the latter case, one can easily derive the model independent prediction $\Delta T/T\ (\theta \geq 1^{o}) \sim 10^{-5}$ which, in case of the Harrison-Zeldovich postinflationary spectrum, scales up to quadrupole ($\theta \sim 90^{o}$). Note, that our number ($\Delta T/T \sim 10^{-5}$ for $h = 0.5$) is a factor of two higher than that given by other authors because the modelling we briefed gives a sertain advantage for the gain factor.

The absence of galactic contraflows and of X-ray gas in the GA central region evidences for the small initial overdensities, $\delta(o) < 1.5\ (1+z)^{-1}$, and thus, for the broad distribution of the GA mass.

The confrontation of the GA with $\Delta T/T$ may result in the direct detection of the postrecombination primordial density spectrum

**REFERENCES**

1. Bertschinger,E., Dekel,A., Faber,S.M., Dressler,A. and Burstein,D., Ap.J.**364**, 370 (1990)

2. Hnatyk,B.I., Lukash,V.N. and Novosyadly,B.S., Astron. Zh. Lett. **17**, 3991 (1991)

3. Faber,S.M. and Burstein,D., Large Scale Motion in the Universe, Proc. Pontific. Acad. Study Week 27 (1988)

4. Lukash,V.N., Great Attractor – a Challenge to Theory, Proc. TEXAS-ESO-CERN Conference, 16-25 December (1990)

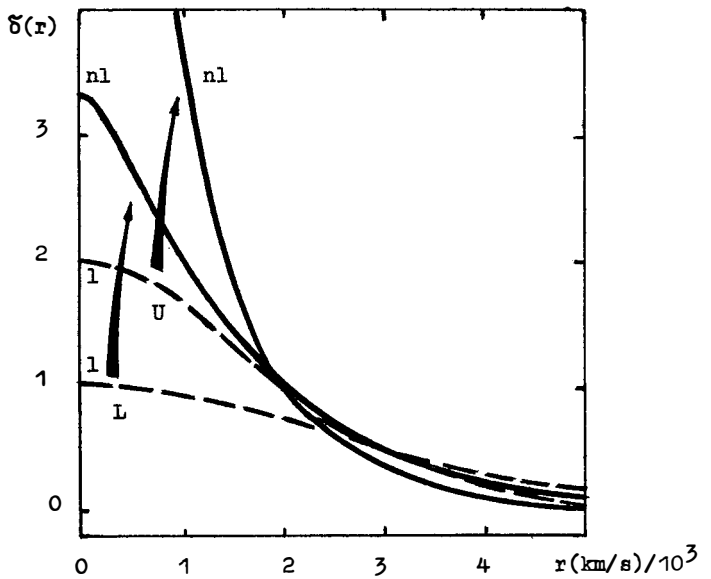


Fig.1 Low (L) and upper (U) limit profiles $\delta(r)$ of linear (l) and non-linear (nl) GA density peaks best fit to observations

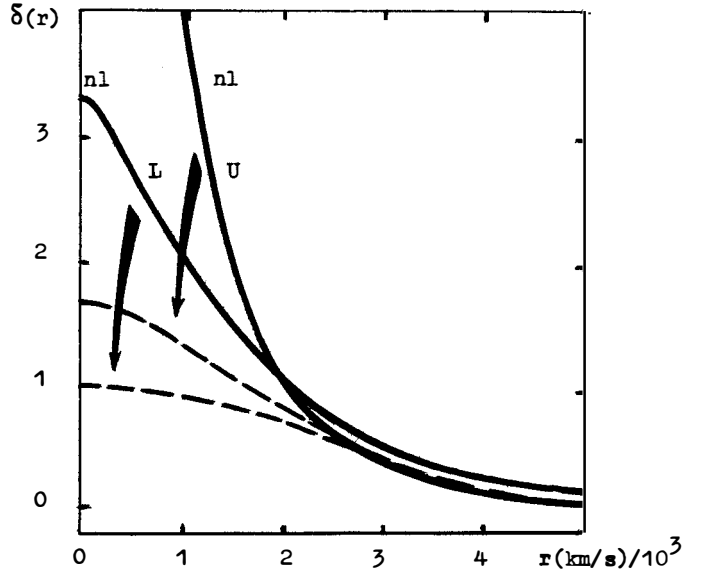


Fig.2 The limit non-linear profiles $\delta(r)$ (see Fig.1) reduced after smoothing by the Gaussian filter $R_f = 14\ h^{-1}$Mpc

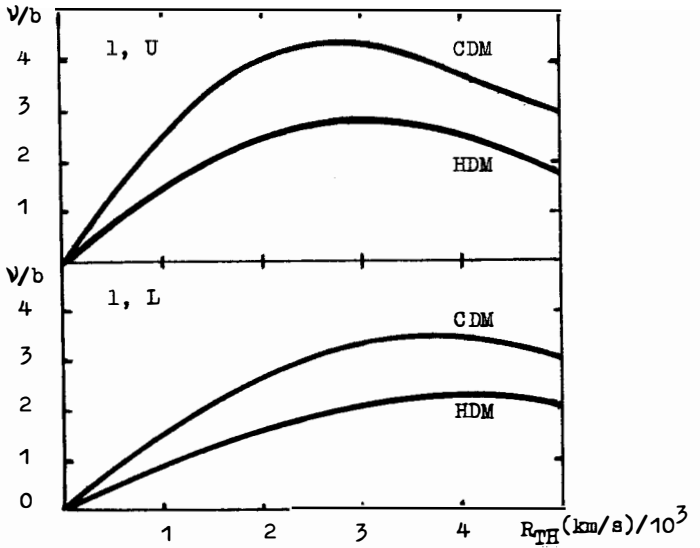


Fig.3 Parameter $\nu = \delta/\sigma_0$ averaged over the top hat sphere with radius $R_{TH}$, for the limit linear profiles (see Fig.1)

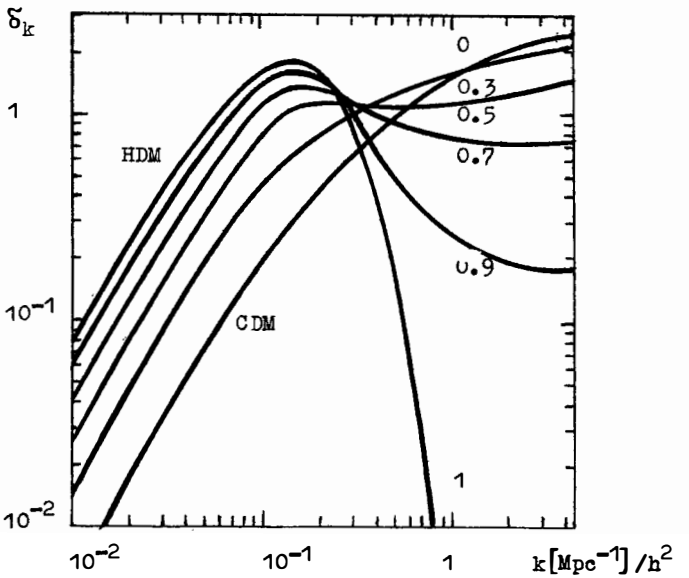


Fig.4 Primordial perturbation spectra $\delta_k = (k^3P(k)/2\pi^2)^{1/2}$ in hybrid models with the hot particle density parameter $\Omega_h$ ( P(k) is the power spectrum $\sigma_8$ (R = 0.26 $h^{-1}$Mpc) = 1 ) $h$

# NONLINEAR COMPARISON OF LARGE-SCALE DENSITIES AND VELOCITIES

**Amos Yahil**

DAEC, Observatoire de Paris
F–92195 Meudon, FRANCE
and
Astronomy Program, State University of New York
Stony Brook, NY 11794–2100, U. S. A.

ABSTRACT

The large-scale distribution of the *IRAS* galaxies is compared with the mass density computed by the *POTENT* technique from the collected data on peculiar velocities. Special care is taken properly to calibrate the considerable sampling bias remaining in the *POTENT* analysis due to the uneven sky and depth coverage of the velocity data. In the linear approximation it is possible to determine the combination $f(\Omega)/b = 1.2 \pm 0.4$ of the cosmological density parameter, $\Omega$, and the galaxy biasing parameter $b$, but not any one of them separately. This degeneracy is broken in a nonlinear comparison of the density and velocity fields, which yields an initial lower bound $\Omega \gtrsim 0.4$ on the density parameter.

## 1. Introduction

One of the most important goals of observational cosmology is to measure the deceleration of the universe, and to determine whether or not it is bound. In the past fifteen years or so, attention has shifted from the original program, to measure the deceleration directly over cosmological distances (Sandage 1961), to *local* determinations of the cosmological density parameter, $\Omega$. In these local investigations it is assumed that the presently observed structure grew by gravitational instability from an initially smooth universe. The dynamics of this growth, and in particular the mean density of the universe, can be determined by comparing the deviations of the expansion of the universe from a pure Hubble law—the so-called peculiar velocities—with the density inhomogeneities which have given rise to them.[1]

In this paper we avoid the study of dynamics on a small scale, where intensive dynamics has resulted in "virialization". Detailed modeling, beyond the scope of this paper, is required in order to understand the complex processes of galaxy formation, as well as the interaction between galaxies on scales commensurate with the sizes of their halos. We concentrate instead on the large-scale structures, which preserve a memory of their initial conditions, and which are more directly amenable to an interpretation of the observational data.

The analysis of the data, however, is by no means simple, and this paper addresses its many facets. §2 describes the density and velocity data, showing the basic agreement between these independent datasets. The theory is briefly summarized in §3, with special emphasis on the need for nonlinear dynamics, and recent developments in that area. The comparison of the density and velocity fields is presented in §4, giving first separate estimates of $\Omega$ and the biasing parameter, $b$. A discussion follows in §5.

## 2. Data

An impetus for significant improvement in the measurement of density on large scales came with the discovery of about 20,000 galaxies in the Point Source Catalogue (PSC) of the Infrared Astronomical Satellite (*IRAS*). From the observational point of view, the *IRAS* galaxies are ideal tracers, since they are homogeneously detected over most of the sky, and their fluxes are unaffected by galactic extinction. A U. S. redshift survey has measured the *IRAS* density field over the last few years (Strauss *et al.* 1990; Yahil *et al.* 1991; Davis *et al.* 1991; Strauss *et al.* 1991; Fisher *et al.* 1991). A parallel effort has been underway by a British–Canadian team (Efstathiou *et al.* 1990; Saunders

[1] In order to avoid confusion we will use the term "velocity" only for peculiar velocities, and will always refer to the total velocity of a galaxy as "redshift".

*et al.* 1990; Rowan-Robinson *et al.* 1990; Kaiser *et al.* 1991; Rowan-Robinson *et al.* 1991; Saunders *et al.* 1991).

The best measured velocity is the motion of the Local Group with respect to the cosmic microwave background. Unfortunately, the *IRAS* prediction of this velocity suffers both from the lack of information about structures at large distances (Vittorio & Juszkiewicz 1987; Juszkiewicz, Vittorio & Wyse 1990; Lahav, Kaiser, & Hoffmann 1990), as well as from the need to smooth over small distances (Strauss *et al.* 1991). In order to avoid these difficulties, we consider only velocities of nearby galaxies relative to the Local Group, which are obtained by comparing their observed redshifts with independent distance estimators (Aaronson *et al.* 1982, 1986, 1989; Lynden-Bell *et al.* 1988; Dressler & Faber 1990; Willick 1991; only data included in the compilation by Burstein 1989 are used in this investigation). These relative velocities can be compared more reliably with the accelerations relative to the Local Group, as measured by *IRAS*, since neither are sensitive to the dipole moment of the unobserved structures at large distances, which is the latter's most important contribution.

The disadvantage of the velocities of nearby galaxies is the large uncertainty in each one, which becomes progressively worse with distance. It is therefore necessary to average over many galaxies in order to determine a reliable velocity field. This smoothing is now performed using a powerful new technique, called *POTENT*, which takes advantage of the irrotational nature of the velocity field (Bertschinger & Dekel 1989; Dekel, Bertschinger & Faber 1990; Bertschinger, Dekel, Faber, Dressler & Burstein 1990). Monte Carlo simulations have been used by these authors to assess the errors in the deduced density field. They remain typically twice as large as the *IRAS* errors. Since the two errors are independent and add in quadrature, the *POTENT* errors dominate 80–90% of the total error.

In spite of these large errors, there is striking similarity between the *IRAS* and *POTENT* estimates of density. Fig. 1 shows a comparison of the two density fields in the Supergalactic plane relative to their respective means, smoothed with a Gaussian of 1200 km $s^{-1}$($\Omega = 1$ is assumed for *POTENT*). The black boundary marks a *POTENT* confidence limit, such that the error in each *POTENT* density is estimated to be $\sigma_\delta < 0.2$, and the distance of the fourth nearest galaxy is $R_4 < 1500$ km $s^{-1}$. It is impressive how similar the density structures in the two panels in Fig. 1 are, within the *POTENT* confidence limit, and this is a good first indication that the gravitational instability picture is basically correct.

Fig. 2 shows the *POTENT* densities (again assuming $\Omega = 1$) versus the *IRAS* densities. The comparison is made at the points of a cubic grid of spacing 500 km $s^{-1}$, which are within the above *POTENT* reliability boundary. As can already be seen in Fig. 1, the two densities are clearly correlated, so the slope of the regression line can be

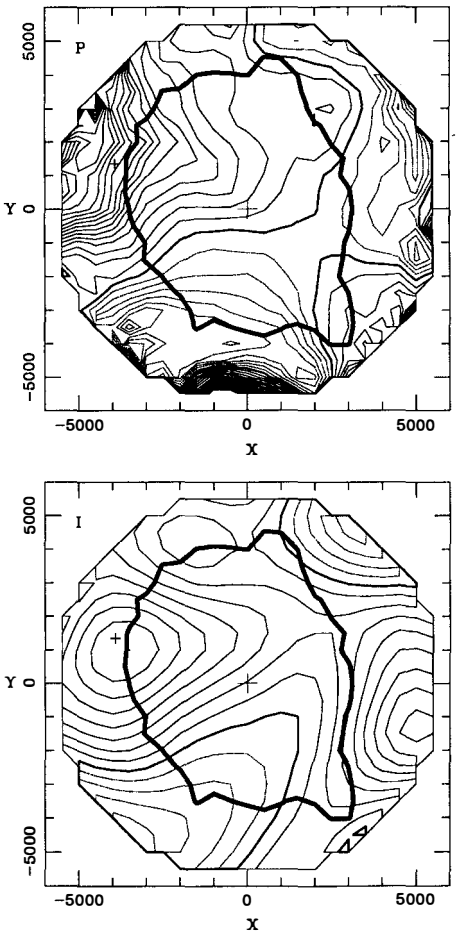


**Figure 1:** Comparison of the mapped density fields in the Supergalactic plane: *POTENT* for $\Omega = 1$ (top) and *IRAS* (bottom). Contours are separated by intervals of 0.1 in $\delta$, with positive contours marked by solid lines and negative contours by dotted lines. The thick line marks a *POTENT* confidence limit (see text), within which the two data sets may be compared. (The *IRAS* data are trustworthy in most of the plane.)

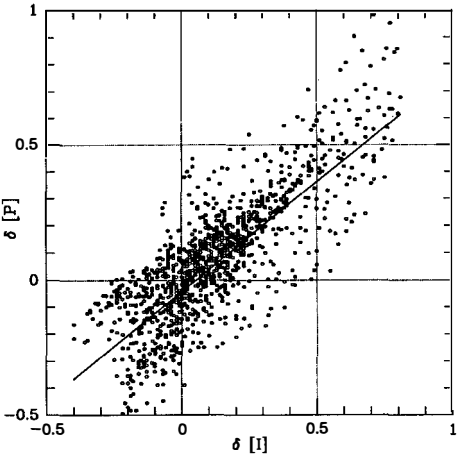


**Figure 2:** Direct comparison of *POTENT vs. IRAS* at the points of a cubic grid of spacing 500 km $s^{-1}$ inside the same *POTENT* confidence limit shown in Fig. 1. The slope of the regression line, which is used to determine $\Omega$, is affected by biases in *POTENT*.

used to estimate $\Omega$ (§3). However, the regression is also seriously affected by the uneven sampling of the velocity data, and it is essential to calibrate it (§4).

## 3. Theory

The dynamics of gravitational instability is most easily studied in the linear domain, in which the density perturbations are still small compared with the mean density of the universe. In this regime, the velocity field, $\mathbf{v}$, and relative density perturbation, $\delta$, are related by a Poisson-like equation

$$\nabla \cdot \mathbf{v} = -f(\Omega)\delta \quad , \tag{1}$$

where $f(\Omega) \approx \Omega^{0.6}$ is the logarithmic derivative of $\delta$ with respect to the scale factor of the universe.[2]

The mass density perturbation, $\delta$, can not be measured directly, and must be estimated from the density of observed tracers, such as the *IRAS* galaxies, $\delta_I$. If the galaxy density is proportional to the mass density, at least when smoothed over sufficiently

[2] Our investigation is independent of the extragalactic distance scale. We set $H_o = 1$ and express all distances in km $s^{-1}$.

large scales, then the two $\delta$'s are equal. In general, galaxy formation may depend on local conditions and the observed density of galaxies may be a biased estimator of the underlying mass density. The physics of such a possible bias is not known, and it has been customary to assume that the bias takes the relatively simple linear form

$$\delta_I = b\delta \quad , \tag{2}$$

where the biasing parameter, $b$, is an unknown constant. In this case, the relation between the observed velocity and density fields becomes

$$\nabla \cdot \mathbf{v} = -\frac{f(\Omega)}{b}\delta_I \quad . \tag{3}$$

It is seen at once from Eq. (3) that in the linear approximation a regression of $\nabla \cdot \mathbf{v}$ on $\delta_I$, as in Fig. 2, only yields an estimate of the combination $f(\Omega)/b$. In order to obtain separate estimates of $\Omega$ and $b$, it is necessary to study perturbations which have become nonlinear. Fortunately, the density perturbations are of order unity, even when smoothed considerably as in Fig. 1, so nonlinear deviations from Eq. (3) are measurable.

It is not simple to compute the nonlinear growth of gravitational instabilities of arbitrary geometry, and the problem is further complicated by the multivalued nature of the solutions. N-body codes are not useful, because they solve only initial-value problems. The computation needed here involves mixed boundary conditions in which positions or velocities are given at the present epoch, and the other boundary conditions follow from the requirement that the universe is smooth in the limit of high redshift.

Nevertheless, well-defined nonlinear procedures have now been developed. In the linear regime the displacement of a particle from its original position is well represented as a separable product of a particle-dependent coefficient and the universal density growth function. Zel'dovich (1970) argued that this representation continued to be a good approximation well into the nonlinear domain.

An application of the Zel'dovich approximation, tested and calibrated using N-body simulations, has recently been proposed by Nusser *et al.* (1991). They suggested to replace Eq. (1) by

$$\delta = \left\| I - f(\Omega)^{-1} \frac{\partial \mathbf{v}}{\partial \mathbf{r}} \right\| - 1 \quad , \tag{4}$$

where $I$ is the unit matrix, $\partial \mathbf{v}/\partial \mathbf{r}$ is the Jacobian matrix of $\mathbf{v}$ with respect to the *current* position $\mathbf{r}$, and the double vertical lines denote the determinant. Eq. (4) is easily used to predict the mass density from the velocity field, and Eq. (1) is recovered in the limit in which the elements of the Jacobian matrix are much smaller than unity. But it is much more difficult to invert Eq. (4), so a velocity field can be computed from a density field. Instead, Nusser *et al.* proposed to solve a Poisson-like equation with a local correction to the density

$$\nabla \cdot \mathbf{v} = -\frac{f(\Omega)\,\delta}{1 + 0.18\delta} \quad . \tag{5}$$

Here we use the method of Nusser *et al.* For each $\Omega$, the *POTENT* densities are derived from the smoothed velocity field using Eq. (4), and velocities are predicted from the *IRAS* densities by solving Eq. (5). Actually, it is necessary to modify the linear biasing model in voids, at least to avoid negative mass densities if $b < 1$. To overcome this difficulty we replace Eq. (2) for $\delta < 0$ by

$$1 + \delta_I = (1 + \delta)^b \qquad (\delta < 0) \quad , \tag{6}$$

which reduces to Eq. (2) in the limit $\delta \to 0$, but has the correct behavior as $\delta \to -1$.

## 4. Results

In spite of the smoothing used by *POTENT*, uneven sky and depth coverage continue to be problems and result in significant sampling bias (cf., Dekel *et al.* 1990). Consequently, the slope measured by a regression, such as in Fig. 2, may not give the correct value of $f(\Omega)/b$. We demonstrate this statistical bias, not to be confused with the dynamical bias in galaxy formation, by providing *POTENT* with a known velocity field—the velocities predicted by *IRAS*—but only at the positions for which there exist real data, and asking it to reproduce the density field from which they were derived. The velocities inputted into *POTENT* are the *exact* ones, so we are only measuring errors due to the uneven sampling, and not those due to the considerable additional errors resulting from the imperfect distance estimators used for the real data in Fig. 2.

Fig. 3 shows the large scatter between the input *IRAS* density and the one estimated by *POTENT*. More importantly, a regression of the *POTENT* density on that of *IRAS* gives a slope which is significantly different from the input $f(\Omega)/b = 1$. In other words, even without any velocity noise, a naive interpretation of this slope, which fails to take into account the sampling bias, results in a wrong answer. The situation is, of course, worse when the velocity noise is included.

To overcome this bias, we seek a quantitative measure of the values of $\Omega$ and $b$ which would best reproduce the observed, albeit biased, regression of the *POTENT* density on that of *IRAS* seen in Fig. 2. To this end, we characterize such a regression by two numbers: its slope, here called $\lambda$, and the rms vertical (*POTENT*) scatter, $S$. Then, for each value of $\Omega$ and $b$, we compare the observed values of $\lambda$ and $S$ with the expected distribution, just as in a standard maximum-likelihood fit.

The only difference is that the complexity of the *POTENT* analysis does not allow an analytical computation of the distribution function used in the maximum-likelihood fit. Instead, we evaluate it using Monte Carlo simulations. For each trial value of $\Omega$ and $b$ we generate 100 simulations of the *IRAS* density field, using bootstrapping to simulate the *IRAS* noise. From each *IRAS* density field we predict velocities at the position of each *POTENT* galaxy, using Eqs. (2), (5) and (6). These velocities are further perturbed

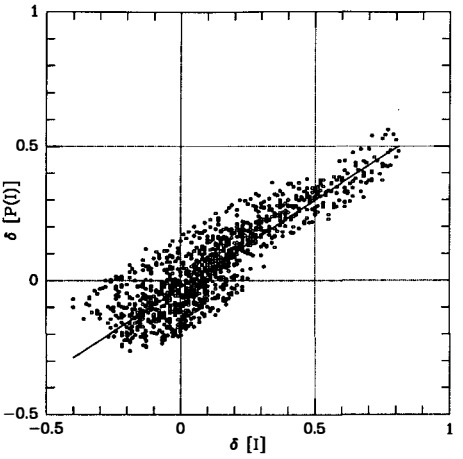


**Figure 3:** Scatter and bias in the density computed by *POTENT* due to uneven sky and depth coverage. *POTENT* is provided with the velocities predicted by *IRAS*, but only at the positions for which there exist real data, and is asked to reproduce the input *IRAS* densities. Even though no observational errors in the velocities are included, the slope in this figure deviates significantly from unity, showing the statistical bias in the determination of $f(\Omega)/b$.

by the error resulting from the uncertainty in the observed distance estimators, and the perturbed velocities are then inputted into *POTENT* which smoothes the velocity field, and uses Eq. (4) to predict a *POTENT* density, $\delta$.

Finally, we perform a linear regression of $f(\Omega)\delta$ on $\delta_I$ to obtain estimates of $\lambda$ and $S$. The dependent variable in the regression is chosen to be the product $f(\Omega)\delta$, instead of $\delta$ itself, so as to minimize the dependence of the *POTENT* value on $\Omega$. Strictly speaking, a maximum-likelihood fit requires that the data not depend on the parameters at all, and in the linear limit $f(\Omega)\delta$ is indeed independent of $\Omega$. In the nonlinear regime we are unable to provide a completely parameter-independent *POTENT* density, so we choose this product as the quantity least dependent on $\Omega$. The resulting frequency distribution of $\lambda$ and $S$ is well fit by a bi-variate Gaussian in $\lambda$ and $\log S$, and this Gaussian is used in the maximum-likelihood estimate of the $\Omega - b$ parameter space.

Fig. 4 shows such distributions for four pairs of values of $\Omega$ and $b$. The Monte Carlo points are shown by crosses, the smooth bi-variate Gaussian fit to them by the contours, and the observed point by a filled circle. In the bottom two panels, the observed point

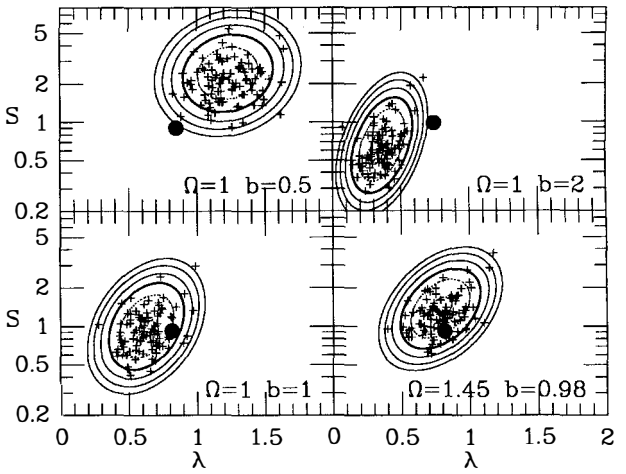


**Figure 4:** Likelihood in the $\lambda - S$ plane for four different choices of $\Omega$ and $b$. The crosses correspond to 100 Monte Carlo noise simulations. The contours describe the resulting Likelihood function, determined by fitting a bi-variate Gaussian to the 100 points in $\lambda - \log S$. The heavy contour is likelihood unity and the contours are spaced by a factor $e$. The solid circles mark the observed point from Fig. 2.

falls reasonably within the Monte Carlo simulation, while in the top two panels it is well outside them.

Fig. 5 is a plot of the likelihood values of $\Omega$ and $f(\Omega)/b$. The points show the trial values used in the Monte Carlo simulations. The equi-likelihood contours, obtained by interpolation, mark the 50%, 75%, and 90% confidence limits of these parameters. (The maximum likelihood point is marked by a cross, but its exact value is not so important in view of the large area of parameter space covered by the confidence limits.) It is seen that the confidence limits are more tightly spaced in the vertical direction, so the degenerate combination $f(\Omega)/b = 1.2 \pm 0.4$ is the better determined quantity. Along the horizontal direction, the right side of Fig. 5 corresponds to larger values of $b$. The nonlinear effects are therefore smaller there, since a given *IRAS* density $\delta_I$ corresponds to a smaller mass density $\delta$, and it is more difficult to obtain separate estimates of $\Omega$ and $b$. On the left side of the figure, on the other hand, the nonlinear effects become more significant, and we are able to place an initial lower limit $\Omega \gtrsim 0.4$ on the density parameter. (The contours at the very top left part of the figure should be ignored because our nonlinear approximation breaks down there.)

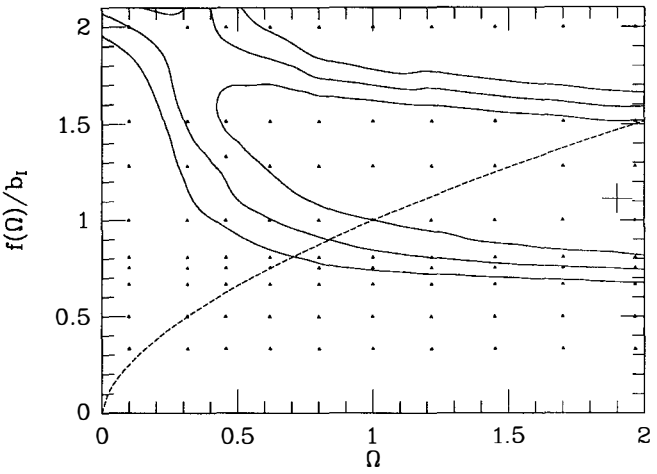


**Figure 5:** Limits on $\Omega$ and $f(\Omega)/b$, at the 50%, 75% and 90% confidence levels, obtained from a nonlinear comparison of the *IRAS* density structure and large-scale motions. The dashed line is the relation between the two parameters for $b = 1$. Low values of $\Omega$ are excluded by this fit. The contours at the top left part of the figure should be ignored, because our nonlinear scheme breaks down there.

## 5. Discussion

The independently derived *IRAS* and *POTENT* density fields show remarkable similarity. We are thus encouraged to correlate them in detail in order to determine $\Omega$. From linear theory it is possible to determine the combination $f(\Omega)/b = 1.2 \pm 0.4$, and this is the more secure parameter. A nonlinear analysis, however, has provided an initial separate bound $\Omega \gtrsim 0.4$ on the cosmological density parameter.

The main limitation of the current data is the accuracy of the observed peculiar velocities. Great improvement in the velocity data is expected over the next few years, however, both from a significant increase in the number of galaxies observed, and from better distance indicators (e.g., Tonry, Ajhar & Luppino 1989). These will, of course, have to be matched by better density measurements, both by obtaining redshifts for the remaining *IRAS* galaxies, and from other all-sky galaxy surveys, such as the $2\mu$m surveys now proposed in the U. S. and in Europe.

The new velocity data should be able to test the basic underlying hypothesis of the gravitational origin of the large-scale velocities. A devil's advocate might argue

that Eq. (1) can be mimicked by the continuity equation, $\nabla \cdot \mathbf{v} = -\dot{\delta}$, as long as $\delta$ varies on a timescale comparable to the age of the universe, even if due to causes other than gravity. There is no complete answer to this criticism, but it may be expected that such other sources of peculiar velocity will, in general, vary from one location to another, so the constant of proportionality "$f(\Omega)$" in the fake Eq. (1) will be different for different perturbations, while the gravitational $f(\Omega)$ is universal. In order to test for this universality, it is necessary to measure densities and velocities separately around several perturbations. We are not at that stage yet, as can be seen in Fig. 1, which shows that most of the comparison between the density and velocity fields is currently carried out around the single large-scale density enhancement known as the "Great Attractor" on the left sides of the maps. Velocity data are beginning to come in around the Perseus-Pisces region on the other side of the sky, however, and it should soon be possible to extend the *POTENT* confidence limit and begin to answer this objection.

More accurate nonlinear dynamics is also needed in order to secure the separate estimates of $\Omega$ and $b$. In this respect mention should be made of the generalizations to the Zel'dovich (1970) approximation recently proposed by Giavalisco *et al.* (1991) and Yahil (1991b), based on a variation of the action, as initially suggested by Peebles (1989, 1990). The new variational techniques promise to be the ultimate nonlinear computations, because they can be carried out to arbitrary accuracy in the nonlinear regime.

I thank my collaborators, E. Bertschinger, M. Davis, A. Dekel, J. Huchra, and M. Strauss, for many useful discussions. This research was supported in part by NASA grant NAG 51228.

## References

Aaronson, *et al.* 1982, *Astrophys. J. Suppl.*, **50**, 241.

_____.1986, *Astrophys. J.*, **302**, 536.

_____.1989, *Astrophys. J.*, **338**, 654.

Bertschinger, E., Dekel, A., Faber, S. M., Dressler. A., & Burstein, D. 1990, *Astrophys. J.*, **364**, 370.

Bertschinger, E., & Dekel, A. 1989, *Astrophys. J. (Letters)*, **336**, L5.

Burstein, D. 1989, private communication.

Davis, M., Strauss, M. A., & Yahil, A. 1991, *Astrophys. J.*, **372**, 394.

Dekel, A., Bertschinger, E., & Faber, S. M. 1990, *Astrophys. J.*, **364**, 349.

Dressler, A., & Faber, S. M. 1990, *Astrophys. J.*, **354**, 13.

Efstathiou, G., Kaiser, N., Saunders, W., Lawrence, A., Rowan-Robinson, M., Ellis, R., & Frenk, C. 1990, *Mon. Not. Roy. Astr. Soc.*, **247**, 10p.

Fisher, K. B., Strauss, M. A., Davis, M., Yahil A., & Huchra, J. P. 1991, *Astrophys. J.*, in press.

Giavalisco, M., Mancinelli, B., Mancinelli, P., & Yahil, A. 1991, *Astrophys. J. (Letters)*, to be revised.

Juszkiewicz, R., Vittorio, N., & Wyse, R. 1990, *Astrophys. J.*, **349**, 408.

Kaiser, N., Efstathiou, G., Ellis, R., Frenk, C., Lawrence, A., Rowan-Robinson, M., & Saunders, W. 1991, *Mon. Not. Roy. Astr. Soc.*, **252**, 1.

Kaiser, N., Lahav, O., & Hoffman, Y. 1990, *Astrophys. J.*, **352**, 448.

Lynden-Bell, D., Faber, S. M., Burstein, D., Davies, R. L., Dressler, A., Terlevich, R. J., & Wegner, G. W. 1988, *Astrophys. J.*, **326**, 19.

Nusser, A., Dekel, A., Bertschinger, E., & Blumenthal, G. R. 1991, *Astrophys. J.*, in press.

Peebles, P. J. E. 1989, *Astrophys. J. (Letters)*, **344**, L53.

_____.1990, *Astrophys. J.*, **362**, 1.

Rowan-Robinson *et al.* 1991, *Mon. Not. Roy. Astr. Soc.*, in press.

Sandage, A. 1961, *Astrophys. J. (Letters)*, **133**, 355.

Saunders *et al.* 1991, *Nature*, **349**, 32.

Saunders, W., Rowan-Robinson, M., Lawrence, A., Efstathiou, G., Kaiser, N., Ellis, R. S., & Frenk, C. S. 1990, *Mon. Not. Roy. Astr. Soc.*, **242**, 318.

Strauss, M. A., Davis, M., Yahil, A., & Huchra, J. P. 1990, *Astrophys. J.*, **361**, 49.

_____.1991, *Astrophys. J.*, in press.

Strauss, M. A., Yahil, A., Davis, M., Fisher, K. B., & Huchra, J. P. 1991, in preparation.

Tonry, J., Ajhar, E. A., & Luppino, G. A. 1989, *Astrophys. J. (Letters)*, **346**, L57.

Vittorio, N., & Juszkiewicz, R. 1987, in *Nearly Normal Galaxies*, ed. S. M. Faber, (Berlin: Springer), pp. 451–454.

Willick, J. 1991, *Ph. D. Thesis*, U. C. Berkeley.

Yahil, A. 1991a, in *The Early Universe and Cosmic Structures*, eds. J.-M. Alimi *et al.* (Gif-sur-Yvette: Editions Frontières), pp. 483–500.

Yahil, A. 1991b, *Astrophys. J. (Letters)*, to be revised.

Yahil, A., Strauss, M. A., Davis, M., & Huchra, J. 1991, *Astrophys. J.*, **372**, 380.

Zel'dovich, Ya. B., 1970, *Astrofizika*, **6**, 319; *Astr. Astrophys.*, **5**, 84.

# PROSPECTS

# THE DIFFUSE SKY EMISSION AT X AND GAMMA RAY ENERGIES AND THE FUTURE SPACE MISSIONS

**Giovanni F. Bignami**
Dipartimento di Ingegneria Industriale
Universita' di Cassino
and
Istituto di Fisica Cosmica del CNR
Milano, ITALY

"We are only going up to the Sinai to get the tablets. We have no right to write the Commandements."

Carlo Rubbia, 1985

## 1- Introduction

The region of the electromagnetic spectrum which includes X and Gamma rays is exceedingly wide, over seven decades in photon energy from about a tenth of a KeV to tens of GeV. The lower limit is arbitrarly set by the interface with the EUV/XUV range, and the upper simply by the decrease in the number of photons meaningfully measurable in space platforms. This is roughly comparable to the energy gap between the optical region and the radio millimetric. As is well known, inside such a vast range photons have a different interaction physics, not only with the large scale matter and fields but also within the detectors, thus requiring basically different astronomical techniques. In this sense, surely the most important energy boundary is that between photons which can realistically be focussed and those which cannot and never will. Where the wavelenghts become smaller than the surface irregularities or, in the limiting case, smaller than the interatomic distances in solids, each photon must be detected singularly in the presence of its full background, without the possibility of increasing the signal against the noise, as with focussing.

Operationally, for the purposes of the present work, we shall call X-rays "anything which can be focussed", i.e. photons with $h\upsilon \leq 10$ KeV. The rest can be treated as "gamma-rays", albeit with different intrinsic detection techniques.

On the subject of the diffuse sky emission at X-ray wavelengths, one can refer to the nice paper by De Zotti for a description of the observational and theoretical current wisdom(s), as well as for some future prospects. On the other hand, the work now in progress on this topic is mostly coming from the ongoing ROSAT mission, and what is so far available is very well presented somewhere else in this volume.

As for the "near future" X-ray astronomy missions, i.e. those the launch date of which will not approach the end of millennium, it is not obvious to see which one potentially has the combination of throughput, angular resolution and low-background to seriously compete with ROSAT, if this mission performs as planned. The list includes the Japanese ASTRO D, surely the first, to be launched in mid '93, then, nominally, the Italian-Dutch SAX (December '93, but very likely to slip further), the Soviet Spectrum X-$\gamma$ (nominally 31

December, 1994), and, sometime later, NASA'S XTE, of the "new" Explorer series. These are all missions dedicated to the strong sources, in some cases with emphasis on the spectral properties or on studing the time variability of the brighter ones. The important exception may be JetX, a collaboration European, English-led instrument on board Spectrum-X. Featuring a good-throughput optics with CCD focal plane detectors can probably go a significant step further in the studies of the intrinsic structure, and thus nature, of the CDXB.
Further downstream, approaching the end of the millennium, NASA'S Advanced X-ray Astrophysics Facilities (AXAF) will be the third (after the Hubble Space Telescope and the Gamma-Ray Observatory, both currently in orbit) of the Great Observatories series.
The capabilities of that mission towards the resolution (if any) of the CDXB problem will be considerable.
In what follows, after an impromptu selenic aside, owing to obvious personal biases a brief description will be given of Europe's best chances for advanced X-ray observations of the CDXB: the EPIC instrument aboard XMM, ESA's science programme second "cornerstone". Moving then to ground so far not covered in this volume, we shall give more room to $\gamma$ – rays, if anything for three main reasons: the existing wisdom on CDGB (from hundreds of keV to hundreds of MeV) is based on old data which need a hard, reassessing look; GRO has just gone in orbit and may give important answers, especially at the high-energy end; one of the few missions currently pipelined in ESA also has excellent potentials, at least at the low energy end.

## 2- Selenic Aside

Beauty being hard to resist, we can but refer the reader to the cover of Nature, 6310, 14 Feb.1991, for a splendid ROSAT image of the Moon in X-rays. As in the idea behind the original 1962 rocket flight which started X-ray astronomy, the moon is seen to shine bright at $\geq$ 1 keV in its sunlit crescent. The terminator, as expected, is well defined, but not knife-edge sharp: could one speculate about the tips of the moon mountains, as in the 1610 optical observations "permultae apparent lucidae cuspides intra tenebrosam Lunam partem"( Galilei, 1610).

The dark part of the lunar disc is in itself not totally dark, but, above the (very low) instrument background, it appears to possess a faint emission which can probably be linked to the cosmic ray/lunar surface interactions. What matters most here, however, is that the lunar disc is clearly seen as an absorber of the CXDB, so that one is indeed sure, for example, that it originates beyond the moon.... The ROSAT picture, of course, has also a significant scientific value: among else, a clear measurement of the low level of the lunar surface emission renders meaningful the calculation performed recently by Mereghetti et al (1990) on the possibility of astronomical measurements by lunar occultation.

Already used in the past for bright sources, lunar occultation is essentially a timing technique, which can work for weak sources as well, given a high enough instrumental throughput. In the presence of reasonable background, for example, it can be shown that sources of ~ 1 count/sec can be positioned at the arcsecond level, provided, of course, that they be conveniently located in the sky. For a good throughput, yielding e.g. ~ 50 μCrab per count, there are ~ 5,000 one count sources in the sky, which is swept by the moon at a rate of ~ 550 $deg^2$ /year. Thus, in ~ 5 years, 250 sources could be positioned at the arcsec level, and basically for free: 20 minutes of observation per source is all that is needed (and possible).

However, what really deserves more attention, and, possibly, detailed calculations, is the chance of using the lunar occultation technique for refinements of the CDXB measurements. What kind of angular structure, if any, could be investigated? Would it improve the existing data on the absolute flux level? These are the kinds of questions, and no doubt many others, one may want to spend sometime on in optimizing the big X-ray astronomy missions of the future.

## 3- X-Ray Astronomy in Europe: an EPIC future

As is well known by now, EPIC stands for European Photon Imaging Camera, an instrument approved for XMM, the second cornerstone of ESA's science program, dedicated to X-ray astronomy. The mission, described in Peacock and Ellwood (1988), is still going through a definition phase for what concerns especially the delicate problem of the X-ray optics, the difficulty basically being that of combining

throughput with lightness. In any case, three separate mirror modules are present, for each of which one focal plane instrument is foreseen. EPIC represents the sum of such three focal instruments, for a total effective surface of about 3000 $cm^2$, the detectors being mosaic of CCD chips. The development of the X-ray CCD chips, currently in progress, is aimed at maximising the mission science return: this mean both an extended energy range response and good energy resolution throughout such range. With the work currently in progress in England (University of Leicester/EEV), France (CEN Saclay/Thomson) and Germany (MPI Garching- Munich/MBB) there are good hopes of achieving high sensitivity in the interval 0.1 to ~10 keV (also the optics limit) with a spectral resolving power from about 10 to about 50 over the same range. The high sensitivity of EPIC will allow detection of sources at $\sim 10^{-15}$ erg/$cm^2$ sec (0.5-5 keV interval, for comparison with Einstein) in a $<10^5$ sec (deep) exposure. This will allow, of course, a direct measure of the faint end of the Log N-Log S for the extragalactic sources, deemed to be important contributors to the CDXB and now seen by ROSAT to flatten very significantly below a flux of ~ 5 $10^{-14}$. One can go through the standard sensitivity/source confusion calculation: if there are e.g. 10 to 20 sources/square deg at the Einstein limit , if the Log N-Log S extrapolates reasonably, and the beam size of XMM+EPIC will be e.g. 30"x30", then the canonical confusion limit of ~40 "beams"/source will be just reached by EPIC in the deep exposures mentioned above or for appropriately longer exposures for a flatter Log N Log S. In this case, something like 100 faint sources will be detected over the full experiment field of view, and about half of the CDXB will be directly imaged. However, the above conclusions not only are reached on the basis of assumptions on the Log N-Log S slope etc., but also do not take into consideration possible spectral differences between the various detectable source classes as well as with the CDXB. This is now also suggested by ROSAT, showing a steepening of the CDXB below 3 keV. However, the evidence suggesting this is limited by source statistics, energy resolution and energy bandpass. Addressing specifically the optimization of such parameters, EPIC should be the ideal tool for finally solving with observational data the CXDB. Finally it may be of general interest to publicize some of the characteristics of EPIC as an observatory. The data will be gathered in a central location (the Observatory) for analysis by the Guest

Observers, supported by the P.I. team. Clearly, for the CDXB problem, it would be impractical to have many different GO's: probably a crucial role will be played by the Survey Scientist Team. It is a team, yet to be selected by ESA, wich will have the duties of ensuring the completion of large scale science projects, in full interaction with the community at large. It seams important that such team plan ahead to devote a solid effort to the CDXB problem, and that ESA follow closely this aspect in selecting and setting up the Survey Scientist group.

## 4- High-Energy γ-Rays: the Need for New Data

At the start of the GRO mission, it may be of interest to review, somewhat critically, the conventional wisdom on the CDGB for cosmic diffuse γ-ray background, firstly in the energy range >100 MeV.

Apart from the historic (~1968) OSO III data, numbering a grand total of 631 photons, of which a small fraction was attributed to an extragalactic component, the burden of the proof rests with the equally historic SAS-2 mission (1972-73). It was the first satellite to use a digitized wire spark chamber, as yet the instrument of choise for high energy γ-ray astronomy, to wit EGRET now working on GRO. With an effective area of a few tens of $cm^2$ over the range 30-300 MeV, it managed to collect a total of ~8,000 photons during its 8 month mission, prematurely terminated (see Fichtel et al.1975, for a completed description). In hindsight, one can say that it was an excellent mission, typical of the pioneering spirit of the early '70s, perhaps not by chance coming right after Uhuru. With a very well designed payload, and a low background orbit, it did achieve results which were not to be possible for its much lukier European follower, COS-B.

Most importantly, the low background allowed the galactic emission to be smoothly followed from the bright equator to the high latitudes, where few hundred photons were collected over about 50% of the sky. As expected, such emission followed the cosec b law, which characterizes the emission from the disk as seen from the equator. The possibility of detecting an "extra-disk" component was then tied to the analysis of such cosec b curves, which have to be averaged over different longitudes.

Such work, carefully performed by Fichtel et al. (1978) indeed yielded a small flux component above that of the disk. This was basically assimilated to an isotropic, extragalactic flux, measured above 35 MeV and up to 100 MeV or so. Hopefully, GRO's EGRET will show that such conclusion, from the scanty SAS-2 data, was correct. However, a number of facts should be taken into account before rushing to conclusions:

- even at high latitude, a significant galactic disk diffuse component is present from the 2 $10^{20}$ or more H atom along the line of sight. This fact was considered by the SAS-2 team, who noted, however, that the disk spectral shape is very different and that a window for extragalactic observations is open above 35 MeV, but closes for good around 120 MeV. Considering the very limited energy measurement capabilities of SAS-2, based exclusively on the observations on multiple electron scattering in the spark chamber, this fact certainly requires great caution.
- at high latitudes, like everywhere else, the local, instrumental background is present and obviously appears as diffuse. This effect was very macroscopic in the case of COS-B, actually drawing a line at b~45° for the latitude value up to which one could follow the cosec low. As is known, COS-B was in a high background orbit and was, in general, less carefully designed than SAS-2 from the point of view of backgroud rejection. However, the amount of diffuse flux seen by SAS-2 is so minute (compared to the galactic flux) that one can only be worried of the accuracy with which the SAS-2 backgroud correction needs to be applied
- the isotropic nature of a diffuse flux is certainly a suggestion of its extragalactic nature. However, diffuse halo emission can also, to some extent, mimic an isotropic distribution. Significant diffuse emission from a galactic halo has been recently reproposed by Dogiel and Ginzburg (1989), both with a spectrum and an isotropy level similar to the rather coarse SAS-2 measurements. The problem is then shifted to the content and to the dimensions of the halo, which the SAS-2 data, taken at face value, would require as unrealistically large.

In summary, while it is appropriate to commend here once again the painstaking accuracy of the SAS-2 data analysis, as well as the care and skill in the design of the instrument, one cannot exclude that one

or more of the effects mentioned above could have combined with the limited statistics to mask, at least in part, an extragalactic flux of cosmologic significance. What is rock solid, however, is that any truly CDGB cannot exceed the SAS-2 data points, and this, in itself, is a major result.

As for the rest of the γ-ray range, the existing diffuse results suffer from similar, if more severe, drawbacks. In the MeV range (actually from 100 keV to 10 MeV), the lack of an imaging detector so far as been very detrimental, both towards background rejection and isotropy measurements. Background is particularly critical in this range where all the nuclear lines are to be found.

Altogether, before any profound cosmological significance is attached to the existing 100 keV-100 MeV data (a range as wide as that separating the optical from x-rays) it would be perhaps prudent to wait for GRO and in particular for its first year survey results. It is also appropriate to remember that the presence of the galactic disk component probably renders impossible any extragalactic diffuse maesurements above 100-150 MeV.

## 5- High-Energy : the Chances of GRO

Is is certainly ackward to speak about the capabilities of a mission just off the launching pad: one can at least make sure that the audience is aware of the global GRO mission characteristics and then possibly try some predictions relative to the extragalactic work, mostly on the high energy side.

The Gamma Ray Observatory was finally launched on April 5 ,1991 after many years of delay due to difficulties both in NASA's science program and in the Shuttle Transportation System, including the Challanger tragedy. Thus the payload suffers from a somewhat outdated conception, as unavoidable for all great missions. Very few years before launch NASA management decided, quite correctly, that this was a mission of observatory caliber, not just a collection of P.I.-driven instrumentation: with its 17 ton, bay-filling mass, GRO is the heaviest civilian satellite ever flown.

Table 1 shows the main capabilities of the GRO experiments, all now performing nominally, after the successful injection in the Shuttle type orbit .

As far as the problem of the CDGB is concerned , it is not easy to predict the possible impact of the GRO instruments as a whole, spanning, as they do, about 6 decades in γ-ray energies and using widely different techniques and physical principles. A priori, one would expect the best results to come from the two imaging instruments, EGRET and COMPTEL. Quantitative predictions on the capabilities of the two instruments, covering the range above 1 MeV, have been made, for example, by Bignami and Mereghetti (1989) on the basis of an extragalactic source Log N- Log S relation at X-ray energies, and of a statistical tranfer function from X-rays to γ-rays. Briefly, this means that if EGRET and COMPTEL behave as planned, including the instrumental background, and, at the same time, the sources (mostly AGNs) also behave, GRO could yield a significant γ-ray Log N-Log S for extragalactic sources. This means at least a few tens of objects, so as to be able to extract some global meaning from the measurements.

Potentially more interesting is the chance for a direct measure of the CDGB fluctuations, at least theoretically possible with EGRET. If the instrument has indeed the advertized 1500 $cm^2$ at 20 MeV (where the CDGB flux should be 1.5 $10^{-4}$ photon/$cm^2$ sec sr), for an observation (or the sum of different observations) of $10^6$ secs, about 2,000 bona fide CDGB photons should be collected in $10^{-2}$ sr (6°x6°) of the sky. Following the definition of detectable fluctuation, figure 7 of Bignami and Mereghetti (1989) gives the maximum detectable 5 σ fluctuations vs the recorded instrumental background. In the above example, for a S/N=1 (number of background photons = 2,000) fluctuations should be measurable at the 10-15% level. A difficult but very important potential GRO result.

## 6- A Difficult Energy Range: the Chances of INTEGRAL

The γ-ray energy range below 1 MeV is well known to be an especially difficult one for doing astronomy. It is the range in which no imaging instrument is available on GRO, and yet imaging is obviously needed for any CDGB reliable measurement. It is also the range where background produced by local nuclear processes is maximum, and masks any potentially important signature of nuclear processes of astrophysical origin. The available data on the CDGB around 1 MeV are

quite old (more than 20 years), and are, in all cases, severely limited by the local background in spite of the care with which the original measurements (to wit the Apollo program data) were taken.

Unfortunately the currently active French SIGMA telescope (Paul et al. 1990) on board the Soviet Granat mission, albeit possessing imaging, is not well suited for CDGB measurements. While providing excellent new results on galactic sources, the sensitivity of SIGMA appears limited for extragalactic work. There are two fundamental lessons to be learned from SIGMA for the design of a new generation experiment :

- the particle-induced background must always be much less than the sky photon background. This imposes strong requirements on the design of the experiment, the type of orbit etc., etc.
- the point source sensitivity must be significantly better than $10^{-6}$ photons /cm$^2$ sec keV at 1 MeV or roughly 1 mcrab. Only with such a sensitivity can one hope to approach the sort of quantitative Log N-Log S work now possibly just within reach of EGRET above 100 MeV.

One of the candidate new "medium sized" missions of ESA does just all of the above. It is called INTEGRAL (for INTErnational Gamma Ray Astrophysics Laboratory) and has recently been awarded a Phase A study by the Agency. It is a mission which couples fine imaging, with arcminute sorce location accuracy, to fine spectroscopy with a resolving power between several hundreds and 1,000. It is currently being studied in collaboration with NASA, for a prospective launch in the year 2,000.

The mission is well described in the Assessment Study Report (Courvoisier et al 1991), where it can be seen that great care has been placed in background suppression and maximum source sensitivity. A careful, MonteCarlo-backed, analysis shows that by far the main cause of "background" will be precisely the CDGB entering through the telescope aperture. This will be the limiting factor to the point source sensitivity, predicted to be about 100 times better than that of SIGMA. This should yield an extragalactic source number in the hundreds, if, indeed, AGN as a population continue to exist at 1 MeV. The low energy sky could thus be well matched to the higher energy GRO one, giving a good spectral leverage arm for a comparison between sources and actual CDGB spectra, which INTEGRAL could also take directly.

References

-Bignami,G.F. and Mereghetti S. 1989 "Gamma-Ray Observatory Science Workshop" GSFC April
-Courvoisier,T.J.L.: et al:1991 ESA SCI 91,1
-Dogiel,V.A., Ginzburg, V.L.:1989 Space Science Reviews **49**,311
-Fichtel,C.E. et al: 1975 Ap.J.**198**,163
Fichtel,C.E., Simpson,G.A., Thompson D.J.:1978 Ap.J. **222**,833
-Galilei,G.:1610 Sidereus Nuncius, Venezia, apud Tommaso Baglioni
-Mereghetti,S. Bignami G.F., Zaidins,C.: 1990 Experimental Astronomy **1**,165
-Paul J.A. et al.: 1990: Advances in Space Research, Cospar Symposium on "Imaging and Spectroscopy for Gamma Ray Space Missions"
-Peacock,A. adn Ellwood,J.:1988Space Science Reviews **48**,343

## Table 1: SUMMARY OF GRO DETECTOR CHARACTERISTICS

| | OSSE | COMPTEL | EGRET | BATSE | |
|---|---|---|---|---|---|
| | | | | LARGE AREA | SPECTROSCOPY |
| **ENERGY RANGE (MeV)** | 0.10 to 10.0 | 1.0 to 30.0 | 20 to $3 \times 10^4$ | 0.03 to 1.9 | 0.015 - 110 |
| **ENERGY RESOLUTION (FWHM)** | 12.5% at 0.2 MeV<br>8.6 " 1.0 "<br>4.0 " 5.0 " | 8.8% at 1.27 MeV<br>6.5 " 2.75 "<br>8.3 " 4.43 " | ~ 20%<br>100 to 2000 MeV | 32% at 0.06 MeV<br>27 " 0.09 "<br>20 " 0.66 " | 8.2% at 0.09 MeV<br>7.2 " 0.66 "<br>5.6 " 1.17 " |
| **EFFECTIVE AREA ($cm^2$)** | 2013 at 0.2 MeV<br>1480 " 1.0 "<br>569 " 5.0 " | 25.6 at 1.27 MeV<br>29.3 " 2.75 "<br>29.4 " 4.43 " | 1200 at 100 MeV<br>1600 " 500 "<br>1400 " 3000 " | 1000 ea. at 0.03 MeV<br>1800 " 0.1 "<br>550 " 0.66 " | 100 ea. at 0.3 MeV<br>127 " 0.2 "<br>52 " 3 " |
| **POSITION LOCALIZATION (STRONG SOURCE)** | 10 arc min square error box (special mode; 0.1 x Crab spectrum) | 8.5 arc min (90% confidence at 2.75 MeV - 20σ source) | 5 to 10 arc min (1σ radius; 0.2 x Crab spectrum) | 1° (strong burst) | — |
| **FIELD OF VIEW** | 3.8° x 11.4° | ~ 64° | ~ 0.6 sr | 4 π sr | 4 π sr |
| **MAXIMUM EFFECTIVE GEOMETRIC FACTOR ($cm^2$ sr)** | 13 | 30 | 1050 ( ~ 500 MeV) | 15000 | 5000 |
| **ESTIMATED SOURCE SENSITIVITY** ($10^6$ sec; off Galactic plane) — LINE | (2-5) x $10^{-5}$ $cm^{-2} s^{-1}$ | 3 x $10^{-5}$ to 3 x $10^{-6}$ $cm^{-2} s^{-1}$ | | | 0.4% equivalent width (5 sec integration) |
| CONTINUUM | 2 X $10^{-7}$ $cm^{-2} s^{-1}$ keV $^{-1}$ (@ 1 MeV) | 5 x $10^{-5}$ $cm^{-2} s^{-1}$ | 5 x $10^{-8}$ $cm^{-2} s^{-1}$ (> 100 MeV)<br>1.5 x $10^{-8}$ $cm^{-2} s^{-1}$ (> 1000 MeV) | 6 x $10^{-8}$ erg $cm^{-2}$ (10 sec - burst) | |

# FUTURE OBSERVATIONS OF THE FAR ULTRAVIOLET BACKGROUND

Jean-Michel Deharveng
Laboratoire d'Astronomie Spatiale du CNRS
Traverse du Siphon, Les Trois Lucs
F–13012 Marseille, France

**Abstract**

Past experiments have revealed the existence of a component of extragalactic origin in the far ultraviolet background. This component is difficult to disentangle from contributions of galactic origin. It conveys information on the evolution of galaxies at small look-back time and perhaps more if contributions other than the integrated light of galaxies are identified. Future approaches with dedicated and low angular resolution instruments are reviewed. The possibility of direct galaxy counts with high angular resolution instruments is discussed.

## 1. Introduction

In the 80s, a number of experiments have shown the complexity and the richness of the far ultraviolet (900-2000 Å) background radiation[1]. They revealed a significant contribution arising from processes in the Galaxy and a residual likely to be of extragalactic origin. The most recent interpretation[2] favour the view that the extragalactic component should be as low as 50 $photons\ cm^{-2}s^{-1}Å^{-1}ster^{-1}$ (hereafter CU) in the wavelength range 1400-1700 Å. It would be entirely explained by the contribution of galaxies as indicated by a study of the small scale fluctuations of the background[3]. The difference between this value and the 250 CU found by extrapolation of the total signal to zero neutral galactic hydrogen column should then be accounted for by two-photon emission from galactic ionized gas and light scattered by dust without HI gas.

In addition to providing the opportunity of a thorough study of the interstellar processes which are responsible for the emission of galactic origin, a further investigation of the far ultraviolet background is clearly needed to better understand the nature of the extragalactic component. Implications concern the evolution of galaxies at small look-back time and the possible existence of exotic sources[4], since there are solid reasons to think that the contribution from quasars and intergalactic medium is marginal[5].

Up to now, most of the measurements of the diffuse far ultraviolet background radiation have been obtained by dedicated instrumentation with low angular resolution; all ultraviolet sources in the field of view of photometers or not resolved by imaging detectors contribute to the background. I will first discuss further possible approaches with this category of instruments. On the other hand, space telescopes are now becoming available which have good angular resolution and are able to detect faint point sources. In addition to broad scientific objectives they offer the possibilities of ultraviolet source counts with subsequent evaluation of the background due to discrete sources. I will discuss this second approach which is something new for the ultraviolet spectral range.

## 2. General features of dedicated instrumentation

Because of the low surface brightness of the diffuse background in the ultraviolet, it is necessary to collect as many photons as possible. As the collecting area and the solid angle cannot be increased independently, this is obtained by keeping the f-number of the optical system as small as possible. Values as small as $\sim$ 1 have been reached in the instruments *FUVIS* and *FAUST* which will be described later on. The grasp of photon requires also to minimize the number of optical surfaces and to use a detector with the

best quantum efficiency. With the f-number (and not the focal length or the aperture size) as the driver of the optical design, this category of instrument can be kept reasonably small with moderate requirements in terms of pointing and guidance. These characteristics explain the development of this category of experiments in the early ages of space astronomy[6,7]. A practical limit to the desire of a small instrument is set by the need to have a field of view sufficiently small to avoid bright stars.

The requirement to avoid bright stars is not too difficult to satisfy in the far ultraviolet since the stellar radiation field arises from a small number of very luminous, galactic plane concentrated, early-type stars. This may be quantified by using the results of the *TD-1* all sky survey[8] or models of star counts which have been transported into the ultraviolet by Brosch[9]. Anyway, because of the accuracy presently needed ( of the order of 10 CU to place interesting constraints on galaxy evolution) the possibility to eventually resolve a few residual stars is a significant advantage offered by imaging and long-slit spectroscopy over simple photometry.

The far ultraviolet wavelength range is a remarkable window for studying diffuse background radiation because of the relative absence of contamination due to airglow and zodiacal light. A notable exception is the presence of the bright Lyman $\alpha$ 1216 Å geocoronal emission which can be efficiently rejected (calcium fluoride window) for observations at longer wavelengths but makes the observations at shorter wavelengths a real pain. As mentioned above, a significant galactic contribution has however to be subtracted before reaching the extragalactic component. This situation calls for observing many directions in order to retrieve the extragalactic background offset from the variation pattern of the total signal by means of extrapolation or modelling. This is not a trivial task since the extragalactic background may not appear perfectly isotropic because of extinction in the Galaxy and a fraction of the galactic background may look nearly isotropic. Additional information such as characteristic spectral signatures or characteristic power spectrum of fluctuations are therefore of prime importance.

## 3. An imaging experiment:FAUST

The *FAUST* instrument has been described in its most recent version by Lampton, Deharveng and Bowyer[10] and is shown in Figure 1. It is part of the *ATLAS-1* Shuttle mission, presently scheduled for flight in 1992. It gives an angular resolution of $\sim$ 2 arcmin over a field of view of 8° (diameter). The photon grasp is optimized by the following features: a f-number as low as 1.12 (there is however a 25 percent central obscuration) with only two mirrors as permit-

ted by the unconventional Wynne configuration, an electronic pulse counting image detector[11,12] consisting of a sealed tube with a cesium iodide photocathode deposited upon a microchannel plate and a wedge-and-strip charge collecting anode. The photon grasp is however lower than potentially possible because a filter was deposited onto the entrance calcium fluoride window for rejecting the geophysical OI 1356Å emision line which is feared to be present under some cicumstances at Shuttle altitude flight. The net result is that a surface brightness of $\sim$ 300 CU should be detectable in 20 minutes at a signal to noise ratio of 7 and at a 2 arcmin scale ( or much fainter at larger angular scale).

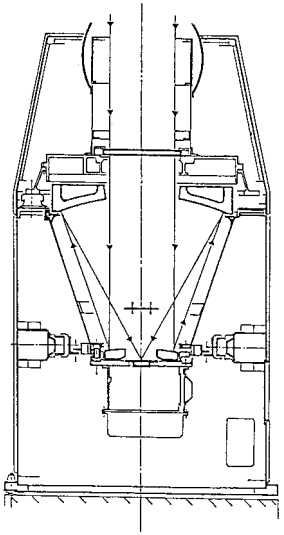

Figure 1: Optical layout of the *FAUST* camera
(overall height is 120 cm; overall diameter is 60 cm)

In addition to obvious capabilities for mapping the structure of the galactic background component at medium and large scale, this instrument is expected to measure the extragalactic background by two methods. The first is the dark cloud method of Mattila[13] consisting in a differential measurement of the background in the direction of a high latitude dark cloud and its surrounding area. The second is the analysis of the small scale fluctuations in search of the signature of an integrated contribution from normal galaxies. A first measurement was performed by Martin and Bowyer[3]; a higher signal to noise ratio is now expected from much longer exposures and in-flight flat field determinations.

## 4. Spectroscopic projects

A spectroscopic instrument has obvious advantages both to improve the separation of various components and to provide spectral information on the extragalactic residual itself. It is also motivated by physical study of hot gas emission and molecular hydrogen fluorescence which contribute to the galactic component of the background. The interest of spectroscopic investigation is exemplified by the results obtained with the *UVX* experiment flown on the Space Shuttle[2,14,15]. In the following we will describe briefly three projects which aim at obtaining better spectral resolution than the *UVX* experiment (spectral resolution of 15 Å).

### 4.1 FUVIS (Far Ultraviolet Imaging Spectrograph)

This project, planned for flight on the Space Shuttle as part of the Spartan-281 mission, was described by Carruthers *et al.*[16]. One mode provides 5 Å resolution with a slit of 1.5' by 2.7°. In the present version, the detector is a microchannel-intensified electrographic camera and does not provide remote electronic readout capability.

### 4.2 HUBE (Hopkins Ultraviolet Background Experiment)

This project was described in detail by Kimble,Henry and Paresce[17]. A spectral resolution of 5 Å from 1230 to 1800 Å is obtained by a spectrograph of the same type as the Berkeley *UVX* spectrograph (a Rowland spectrograph fed by an off-axis parabolic primary). With an f-number of 2 and an aperture of 20 cm, the entrance slit defines a solid angle of 2.1' by 2.5°.

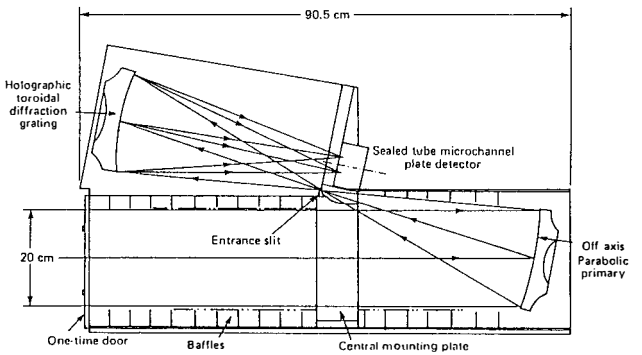


Figure 2: Optical layout of the *HUBE* spectrograph (from Kimble, Henry and Paresce[17])

An interesting feature of this project is to complement the spectrograph with an imaging capability, providing an angular resolution of $\sim$ 2' over a field of view of 2°.5 and a broad bandpass from 1350 to 2000 Å. Both the spectrograph and camera employ the same type of detectors, identical to that used in the *FAUST* instrument. This project has been proposed as a Scout-class free-flyer in the Small Explorer program and as an attached payload on the Space Station.

### 4.3 CUBE (Cosmic Ultraviolet Background Experiment)

This is a joint project from Space Sciences Laboratory, Berkeley and Laboratoire Astronomie Spatiale, Marseille. Since it has not yet been described, we provide more details than for the previous instruments. This project has the two basic options of a high spectral resolution (1-2 Å) and an exploration down to 900 Å.

The rationale for the high spectral resolution is twofold: (i) Simulations[18] have shown that a complex spectrum with a large number of emission features is expected from hot gas emission, molecular hydrogen fluorescence and possible residual airglow. Following the detection of the brightest of these features[14,15], a correct separation of the components and an understanding of the relevant physical conditions require an improvement of the spectral resolution. (ii) The detection of an emission line over the continuum due to dust scattered light is not optimal when the spectral resolution is larger than the line width; with a resolution of 1-2 Å, we approach the optimal conditions for the relevant galactic processes.

The rationale for pushing the investigation down to 900 Å is first to access important emission line such as OVI 1032,1037Å which is known to trace high temperature regime. The interest, as far as the extragalactic component is concerned, is obvious: if consisting of the integrated light of relatively nearby galaxies, the extragalactic component should decrease when approaching the Lyman break at 912 Å; the opposite would be expected from an exotic contribution such as discussed by Sciama [4].

With the implementation of these two options we run immediately into a series of difficulties. The photon grasp is decreased for two reasons: the solid angle is first decreased because it is necessary to reduce the entrance slit size in order to accomodate more spectral elements in the same detector size (assuming the same total wavelength range). This situation which is typical of nebular spectroscopy should not be mistaken for the reduction in energy per spectral element affecting continuum sources in proportion of the gain in resolution. Second, the f-number has to be increased in order to keep the geometrical aberrations much smaller than the entrance slit image. In the wavelength range

shortward of 1150 Å, this decrease of photon grasp which is of geometrical origin is further aggravated by the lower reflectivity of mirror or grating coatings. Another serious difficulty arises from the intense geocoronal Lyman $\alpha$ emission line (a few kiloRayleighs) which is scattered by the diffraction grating. As mentioned above, it can be rejected effectively only in the case of observations longward of Lyman $\alpha$.

Trade-off design studies show that the extent of the spectral domain is a critical parameter; Lyman $\alpha$ appears also as a breaking point in the spectrum for technical reasons as well as for the scattered light problem. Attempts to use an echelle spectrometer[18] have been shown unable to adequately solve this latter problem. A split into two parallel but distinct channels, one for the domain 1300-1900 Å, one for the domain 900-1200 Å emerges as the only reasonable approach.

For the channel (1300-1900 Å) the current Rowland spectrograph design can provide a resolution of 1.5 Å with the f-number only increased to f/4 and a special holographic grating. Off the plane of symetry in a direction perpendicular to the dispersion, the aberrations increase severely and limit the useful height of the slit. This leaves room for two wider slits at the edge of the main slit, providing a low resolution spectroscopy mode. At the entrance slit level, a calcium fluoride window rejects Lyman $\alpha$ and shorter wavelengths. The spectral range allows to use a sealed detector identical (but with 70 mm diameter) to that installed on the *FAUST* instrument. The high resolution entrance slit defines a solid angle of 1.3' by 50', which is 20 times less than the Berkeley *UVX* spectrograph and 5 times less than the *HUBE* spectrograph. Nevertheless, an emission line of 500 $photons\ cm^{-2}s^{-1}ster^{-1}$ should be detected over a continuum of 200 CU in 1 hour at a signal to noise ratio of 4.

The Lyman $\alpha$ scattered light is the crucial problem for the second channel. There are no known transmission filters over the 900-1200 Å bandpass capable of rejecting the Lyman $\alpha$ line. The possibility of coatings for selectively reducing the reflectivity at Lyman $\alpha$ has been explored by Edelstein[19]. However, as a Lyman $\alpha$ rejection of $\sim 10^6$ is required, only double dispersion spectrometer can provide viable solution. Edelstein and Bowyer[20] have investigated various configurations in the context of a rocket experiment. Their selected design consists of a Wadsworth grating fed by a grid collimator and followed by a Rowland spectrograph. It employs a detector of the same type as above but in a windowless version. Such a design which provides a 2.5 Å resolution and fits well along the long wavelength channel can be adopted as the short wavelength channel. The short wavelength limit of this mode has been set to 900 Å because it is the current limit of the Extreme Ultraviolet domain and it

is understood that other instruments are being developed specifically for this entire wavelength range[21]. If none of such instruments are available, nothing prevents the present short wavelength channel to be extended shortward by a few 100 Å, especially for testing the signature of radiative neutrino decay[4].

## 5. What high angular resolution instruments can do

### 5.1 Galaxy counts

We have seen that galaxy counts down to a magnitude of 18.5, obtained recently with the *FOCA* experiment at 2000 Å[22], make a contribution of $\sim$ 25 CU to the ultraviolet background. Extrapolation (with arguments based on the redshift) indicate that these results may be challenging the contribution of $\sim$ 50 CU presently assigned to the integrated light of all galaxies[2,3].

Counts at fainter magnitudes are expected to bring direct and therefore more solid constraints. They are first expected from the observations with the *UIT (Ultraviolet Imaging Telescope)* which was part of the *ASTRO* mission and was advertised[23] with limiting magnitude deeper than the *FOCA* experiment (essentially because of a broader bandpass). A number of projects under study for deep survey at ultraviolet wavelengths[24,25] would have capabilities in this domain, either directly (source counts) or indirectly (improvement in the determination of the ultraviolet colors of galaxies). It is finally interesting to note that constraints may come from parallel or archive observations with the *Hubble Space Telescope* despite the very small field of view. In order to illustrate this statement, we have calculated the total number of galaxies per *Wide Field Camera* frame as a function of ultraviolet magnitude which would result from an extrapolation of the trend observed on bright objects. A conservative extrapolation compatible with the total contribution of 50 CU would produce 2 galaxies per frame brighter than $m_{uv} = 20$ and 4 brighter than $m_{uv} = 21.7$. Constraints on the background due to galaxies should be obtainable with a reasonable number of frames; elaboration on several feasibility aspects (filter red leak,etc) and on whether it would be better to use the *Faint Object Camera* in spite of much smaller field of view is outside the scope of this paper.

### 5.2 Long-term aspects

A more speculative aspect may conclude this review. We have moved between two extremes: on the one hand dedicated instrumentation is able to detect the background and faint extended sources larger than a few arcmin, on the other hand the *HST* has faint limiting magnitude but is not limited by the sky background (in the ultraviolet) because of the very small solid angle. Between, there is nothing to fully exploit the fact that the sky is a factor of

40 darker in the ultraviolet than at any wavelength on the ground[26]. An instrument with a resolution of a few arcsec and a reasonably small f-number (not that far from *UIT* but with an image photon counting detector) would fill this gap and would offer the capability of detecting a large variety of very low-surface-brightness objects at smaller scale (sub-arcmin) than possible with the current background experiments.

In our context of the background study, such an instrument would perhaps give the opportunity to see the HI (1216 Å) or HeII (304 Å) Lyman $\alpha$ emission expected from few bright clumps[27,28] in the intergalactic medium, even though the emission averaged over large field of view is marginal in the ultraviolet background radiation[5].

## References


1. Bowyer, S. 1991, this volume
2. Hurwitz, M., Bowyer, S., & Martin, C. 1991,ApJ,372,167
3. Martin, C., & Bowyer, S. 1989,ApJ,338,677
4. Sciama, D. 1991, this volume
5. Jakobsen, P. 1991, this volume
6. Davidsen, A., Bowyer, S., & Lampton, M. 1974,Nature,247,513
7. Paresce, F., & Jakobsen, P. 1980,Nature,288,119
8. Gondhalekar, P.M., Phillips, A.P., & Wilson, R. 1980,A&A,85,272
9. Brosch, N. 1991,MNRAS,250,780
10. Lampton, M., Deharveng, J.M., & Bowyer, S. 1990,in IAU Symposium 139, The Galactic and Extragalactic Background Radiation, ed. S.Bowyer &Ch.Leinert (Dordrecht:Kluwer),449
11. Lampton, M., Siegmund, O.H.W., Bixler, J., & Bowyer, S. 1986, Proc. SPIE, vol627,383
12. Siegmund, O.H.W., Lampton, M., Bixler, J., Chakrabarti, S., Vallerga, J., Bowyer, S. & Malina, R.F. 1986,JOSA,3,2139
13. Mattila, K. 1990,in IAU Symposium 139, The Galactic and Extragalactic Background Radiation, ed. S.Bowyer & Ch.Leinert (Dordrecht:Kluwer),257
14. Martin, C., & Bowyer, S. 1990,ApJ,350,242
15. Martin, C., Hurwitz, M. & Bowyer, S. 1990,ApJ,354,220
16. Carruthers, G.R., Heckathorn, H.M., Witt, A.N., Raymond, J.C., Opal, C.B., & Dufour, R.J. 1990, in IAU Symposium 139, The Galactic and Extragalactic Background Radiation, ed.S.Bowyer&Ch.Leinert (Dordrecht:Kluwer),459
17. Kimble, R.A., Henry, R.C., & Paresce, F. 1990,in IAU Symposium 139, The Galactic and Extragalactic Background Radiation, ed. S.Bowyer &Ch.Leinert (Dordrecht:Kluwer),441
18. Martin, C. 1986, Proc.SPIE, vol627,387
19. Edelstein, J. 1989, Proc.SPIE, vol1160,19
20. Edelstein, J. & Bowyer, S. 1990, 28th COSPAR meeting, The Hague

21. Bowyer, S. 1991, this volume
22. Milliard, B. 1991, this volume
23. O'Connell, R.W. 1987, in Starbursts and Galaxy Evolution, ed. T.X. Thuan, T.Montmerle &J.Tran Thanh Van (Gif:Editions Frontieres),569
24. Martin, C. & Steiner, J. 1990, in IAU Symposium 139, The Galactic and Extragalactic Background Radiation, ed.S.Bowyer&Ch.Leinert (Dordrecht:Kluwer),456
25. Brosch, N. 1990, in IAU Symposium 139, The Galactic and Extragalactic Background Radiation, ed. S.Bowyer &Ch.Leinert (Dordrecht:Kluwer),453
26. O'Connell, R.W. 1987,AJ,94,876
27. Hogan, C.J., & Weymann, R.J. 1987,MNRAS,225,1p
28. Deharveng, J.M., & Buat, V. 1987, in High Redshift and Primeval Galaxies, ed.J.Bergeron et al. (Gif:Editions Frontieres),441

# HIGH SPECTRAL RESOLUTION SURVEYS OF THE X-RAY BACKGROUND

W. T. Sanders
R. J. Edgar, M. Juda, D. McCammon, P. Plucinsky, C. Snedeker, J. Zhang
Department of Physics
University of Wisconsin - Madison
Madison, WI 53706
USA

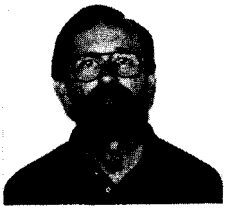

ABSTRACT

Following an overview of the observations of the 0.1 - 10 keV x-ray diffuse background and their current interpretation, future experiments to observe the x-ray background with high spectral resolution are discussed. In the 1990s, we plan to survey the x-ray diffuse background using detectors with much higher spectral resolution (≈ 5 eV) than previously obtainable. The Diffuse X-ray Spectrometer (DXS) experiment uses a Bragg crystal spectrometer to obtain spectra over the 0.1 - 0.3 keV range on a Space Shuttle flight and the X-ray Background Survey Spectrometer (XBSS), an attached payload on the Space Station, uses similar detectors over the 0.1 - 1.1 keV range. Another kind of detector is an x-ray quantum calorimeter that will observe the diffuse background in the 0.1 - 2 keV range on a sounding rocket flight next year (1992). The latter detector is also a candidate for a small Explorer satellite later in the 1990s.

1. Introduction

Figure 1, from the recent review article by McCammon and Sanders [1], summarizes the observations of the x-ray background in the 0.1-10 keV range. At energies greater than 3 keV, the x-ray background is isotropic and generally believed to be of extragalactic origin, although the source is not certain. The integrated emission from active galactic nuclei probably contributes significantly to it and perhaps accounts for all of it. A 40 keV thermal bremsstrahlung spectrum provides an excellent fit to the observed data from 3 to 50 keV [2]. At energies less than 0.3 keV, the x-ray background is quite anisotropic and generally anticorrelated (but not in detail) with the ga-

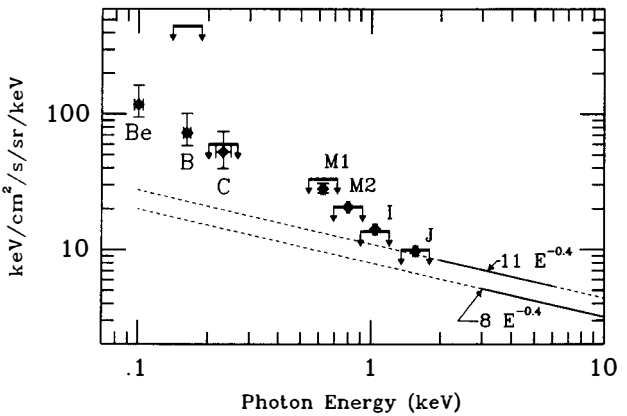


Figure 1. Average observed diffuse background intensity vs. energy. The plotted points are the all-sky averages (with certain non-typical regions excluded). The upper "error bar" is the average for $|b| > 60°$, while the lower "error bar" is for $|b| < 20°$. Be-band points assume that the unobserved part of the sky also tracks the B band. The intensities are plotted for an assumed $E^{-1}$ power-law spectrum. The correct effective energy for each point is sensitive to the assumed spectral index: The horizontal error bars show the effect of a ±0.5 change. The heavy bars represent the best upper limits that can be placed at each energy for the flux incident on the Galaxy from an extragalactic or halo source.

lactic neutral hydrogen. The spectrum is consistent with that calculated by Raymond [3] for a million degree thermal plasma. It is generally thought to arise from a high temperature component of the interstellar gas in our Galaxy, and most of it originates within a few hundred parsecs of the Sun.[1] Any halo or extragalactic x-rays in this energy range to reach the earth must survive absorption by several optical depths of interstellar matter (unit optical depth for 0.2 keV x-rays corresponds to $N_H \approx 10^{20}$ cm$^{-2}$). At intermediate energies, 0.5 - 3 keV, it is not yet clear just how much of the x-ray background is galactic or extragalactic. There are background features that are identified with galactic objects (such as the North Polar Spur or Eridanus fossil supernova remnants), but at high galactic latitudes the majority of the intermediate energy background is probably extragalactic.[1]

At energies less than 0.3 keV, it now seems likely that very little of the observed x-ray background originates outside the Galaxy. But in determining the upper limit on the extragalactic component, corrections must be made for the opacity of the interstellar gas along a line of sight out of the Galaxy. In addition to the opacity correction inferred from the neutral galactic hydrogen, account must also be taken of the opacity associated with the ionized galactic hydrogen component, which has a scale height of ~ 1 kpc and a total column density averaging ~ 1 x $10^{20}$ csc($b$) cm$^{-2}$.[4] Even toward the galactic poles the opacity correction is large. The resulting extragalactic upper limits are comparable to the maximum observed intensity, about four times more than a power-law extrapolation of the extragalactic spectrum [1] (see Figure 1), but after galactic

absorption, the detected flux of x-rays with an extragalactic origin is at most 13% of the total observed flux (in the direction of the SMC) with a best fit value of 5%. It should be possible to improve this limit by about a factor of 7 using the ROSAT x-ray telescope to look for shadows of the extragalactic flux cast by galactic clouds.

In the 0.5 - 1 keV range, the present best upper limits to the extragalactic flux are 2-3 times more than the power-law extrapolation of the extragalactic spectrum. It should also be possible to improve these limits with high-resolution observations of dense clouds. If the galactic emission is thermal, 99% of the photons will be in lines and it may be possible to to look between the lines for an excess continuum due to an extragalactic component if sufficiently high spectral resolution can be used. From 1 to 3 keV, the observed diffuse flux is probably mostly extragalactic, but it may be 25-30% higher than an extrapolation of the 3-10 keV spectrum. This excess could have implications for models of AGN contributions to the diffuse background if it is extragalactic.[1)]

The remainder of this talk describes several experiments that our research group at Wisconsin plans to fly in the next few years to observe the x-ray background with high spectral resolution. These involve two fundamentally different types of detectors: Bragg crystal spectrometers and x-ray quantum calorimeters, but with either detector we obtain much higher spectral resolution (< 10 eV) than was previously obtainable for the diffuse background.

## 2. Bragg Crystal Spectrometers

Bragg crystal spectrometers are used to obtain spectra

of the diffuse x-ray background by the Diffuse X-ray Spectrometer (DXS) experiment on a one-week Space Shuttle flight and by the X-ray Background Survey Spectrometer (XBSS) on a year-long Space Station mission. Each spectrometer (see Figure 2) has a large-area cylindrically-curved Bragg crystal panel that reflects the entering x-rays into the detector, a position-

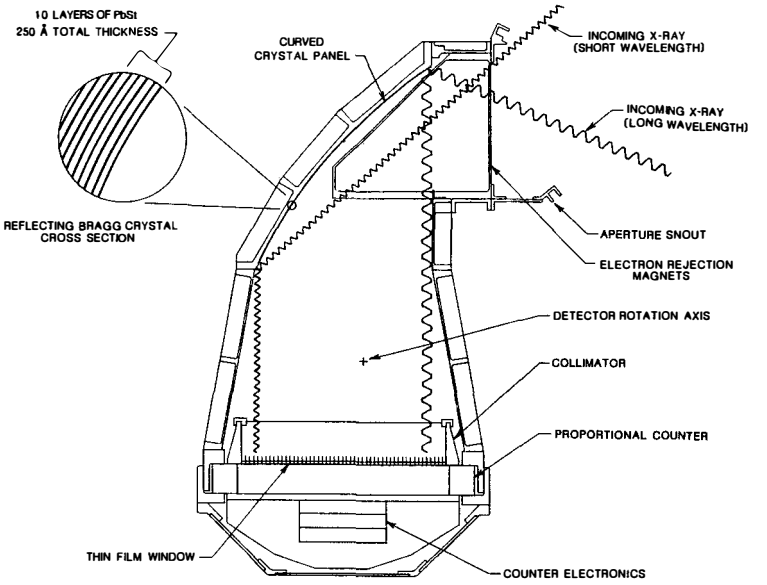


Figure 2. X-rays enter the DXS (or XBSS) detector through an entrance aperture at the upper right and are Bragg-reflected by the curved "crystal". The proportional counter is position sensitive (resolution ≈ 0.5 mm) in one dimension - the dispersion direction of the crystal panel. Because the proportional counter has a collimator before it, each positional element of the counter "sees" a different limited segment of the crystal panel. Due to the panel curvature, different counter elements "see" the crystal at different angles of incidence. By the nature of Bragg reflection, $n\lambda=2d\sin\Theta$, different counter elements thus "see" different wavelength x-rays that originated from different directions on the sky. Rotation of the spectrometer is necessary to obtain a complete spectrum from one direction.

sensitive collimated proportional counter. The proportional counters use 15° x 15° collimators, 90 μg $cm^{-2}$ Formvar windows and P-10 gas (90% argon, 10% methane) at one atmosphere.

The DXS has two such spectrometers; each uses lead stearate "crystals" to provide sensitivity (≈ 0.02 $cm^2$ sr) over the 0.148-0.295 keV (42-84 Å) range. During four days of data collection, DXS obtains spectra from each of ten 15° x 15° sky elements with resolution $\Delta E \approx 5$-10 eV. The DXS is built and tested, and currently undergoing safety-mandated modifications. The launch data is currently in early 1992.

The XBSS has four spectrometers, two identical to those of DXS and two additional ones with TAP (thallium acid phthalate) crystals to provide sensitivity (≈ 0.005 $cm^2$ sr) over the 0.52-1.1 keV (11-24 Å) range. During nine months of data collection, XBSS obtains spectra from the whole sky in 15° x 15° resolution elements. The spectral resolution of the TAP detectors is limited by the collimators to $\Delta E \approx 40$ eV. XBSS is currently in a Phase A/B study. Its mission start date is currently "in the late 1990s or early 21st century."

3. X-ray Quantum Calorimeters

The x-ray quantum calorimeter is a device that measures the energy of a single x-ray by measuring the temperature rise of a silicon slab attached to an x-ray absorber. In principle, the measurement uncertainty can be made very small, making the devices potentially useful for high resolution non-dispersive x-ray spectroscopy.[5] If there were no noise in the thermalization of the x-ray, resolution better than 1 eV would be possible for detectors operating at 0.1 K. Thus a thermal detector operating at cryogenic temperatures can offer the high effi-

ciency of a solid state detector and resolution comparable to that of dispersive spectrometers.[5]

Our research group has been working with the x-ray group at the NASA/Goddard Space Flight Center to develop x-ray quantum calorimeters (XQC) for space flight applications. We are currently constructing a sounding rocket payload that is designed to obtain high resolution spectra of the x-ray diffuse background over the energy range 0.06-2.0 keV. We have recently obtained in the laboratory a resolution of 7.1 eV for 5.9 keV x-rays. In order to obtain a reasonable number of counts from the diffuse background during a 200 s sounding rocket flight, we need an area-solid angle product of at least 1 $cm^2$ sr. We obtain this using a 1 sr field of view and a detector with an area of 1 $cm^2$. But to keep the energy uncertainty small, the heat capacity of the detectors must be kept low and instead of one large calorimeter, we are using an array of 25 calorimeters each 2 mm on a side. The detectors will be cooled during the flight by an on-board adiabatic demagnitization refrigerator to an operating temperature of 0.07 K. The XQC payload is currently being assembled and a flight is planned for the spring of 1992. Figure 3 is a Monte Carlo simulation of the results we expect with a 200 s sounding rocket flight.

The XQC is also an obvious candidate for a small Explorer satellite, if such an opportunity is available later this decade. A 1 $cm^2$ detector array as described above, with a $10^\circ$ field of view, could obtain a 500 s exposure of each of the 100 square degree resolution elements on the entire sky in six months. Such a mission would replace the XBSS mission, because it could return better quality data sooner and cheaper.

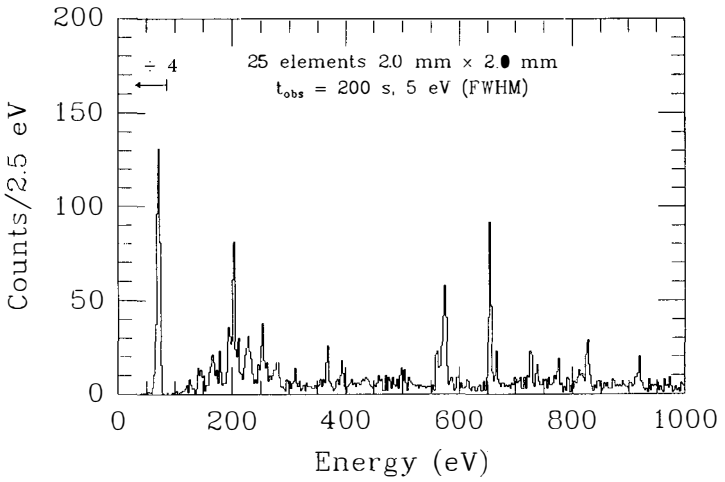


Figure 3. Monte Carlo simulation of the spectrum expected from a 200 s sounding rocket flight.

Acknowledgements

This work was partially supported by NASA contracts NAS8-39664 and NAS5-26078.

References

1) McCammon, D. and Sanders, W. T. 1990, *Annu. Rev. Astron. Astrophys.*, **28**, 657.

2) Marshall, F. E., Boldt, E. A., Holt, S. S., Miller, R. B., Mushotzky, R. F., et al. 1980, *Ap. J.*, **235**, 4.

3) Raymond, J. C. 1980, in *Hot Thin Plasmas in Astrophysics*, ed. R. Pallavicini (Dordrecht: Kluwer), 3.

4) Reynolds, R. J. 1989, *Ap. J. Lett.*, **339**, L29.

5) Moseley, S. H., Mather, J. C., and McCammon, D. 1984, *J. Appl. Phys.*, **56**, 1257.

# THE DIFFUSE EXTREME ULTRAVIOLET BACKGROUND

Stuart Bowyer and Jerry Edelstein
Astronomy Department and Center for Extreme Ultraviolet Astrophysics,
University of California, Berkeley, California 94720 USA

## ABSTRACT

Observations of the diffuse extreme ultraviolet (EUV; λλ 100–912 Å) background are reviewed. This background is the most poorly known of any of the diffuse astronomical backgrounds. Only upper limits to this flux exist. The best limits have been obtained with spectrometers with very crude resolution (~30 Å), and these limits are one to three orders of magnitude larger than expected sources of cosmic flux. A variety of source mechanisms that will radiate in this bandpass have been postulated, and these are briefly discussed. One source which is certainly producing flux in this band is the hot phase of the interstellar medium. The detection of just a few lines from this source will add tremendously to our knowledge about this poorly understood material. A second mechanism which is known to emit radiation in this band is the inflowing interstellar medium which is resonantly excited by solar radiation. A third source of EUV line emission is atmospheric airglow emission, and the study of this emission will elucidate processes occurring in the upper atmosphere. Finally, a variety of more exotic processes have been suggested which may be producing emission in this band; a speculative but highly exciting possibility is that dark matter associated with our Galaxy is producing radiation in this band.

## THE OBSERVATIONAL SITUATION

The majority of the data on the diffuse background in the EUV has been obtained with broadband detectors. The diffuse EUV background was first detected in a Berkeley sounding rocket experiment (Cash, Malina, and Stern 1976). These measurements covering the 115–155 Å band were later confirmed by the data obtained with the *Apollo-Soyuz* EUV telescope, which performed longer observations on many different regions of the sky in the same band (Stern and Bowyer 1979). Bloch et al. (1986) used a sounding rocket experiment to scan a portion of the sky in the 115–155 Å band, and this instrument has been flown on a subsequent rocket flight (Juda 1988). These experiments are the only ones to have *detected* diffuse EUV background radiation; all other observations have only provided upper limits to this background.

In addition to the 115–155 Å band measurements obtained with the *Apollo-Soyuz* EUV telescope, data were also obtained with this instrument on the diffuse background in bands covering 170–600 Å and 500–800 Å. Unfortunately, the intensity measured in these bands is dominated by the bright, resonantly scattered solar lines of He II at 304 Å and He I at 584 Å, making direct observations of interstellar lines impossible. Stern and Bowyer (1979) analyzed the *Apollo-Soyuz* observations in the antisolar direction, where the scattered 304 Å geocoronal line intensity is greatly reduced, to obtain upper limits on the background in the 170–600 Å band. Paresce and Stern (1981) argued that the signal detected in this band is consistent with emission from a single line at 584 Å. They employed a differencing technique to obtain a more stringent upper limit on this intensity.

Holberg (1986) obtained data with 30 Å resolution on the cosmic EUV and far UV background from 1,508,198 s of observations at high galactic latitude with the *Voyager 2* ultraviolet spectrometer. The EUV part of this observation was dominated by the solar He I 584 Å line that is resonantly scattered by neutral helium flowing through the solar system. Holberg removed this bright He I line from his spectra along with other sources of background to derive upper limits to interstellar emission between 520 and 1100 Å.

Labov and Bowyer (1991) flew a grazing incidence spectrometer, sensitive from 80 to 650 Å with a resolution of 10 to 20 Å, on a sounding rocket. The instrument may have detected emission from a $10^{5.6}$ K interstellar medium (ISM), but the feature observed was close to the limiting sensitivity of the measurement and may be spurious. A conservative view would be to consider these results as upper limits to a true background at these wavelengths.

A summary of the observational situation is provided in Figure 1.

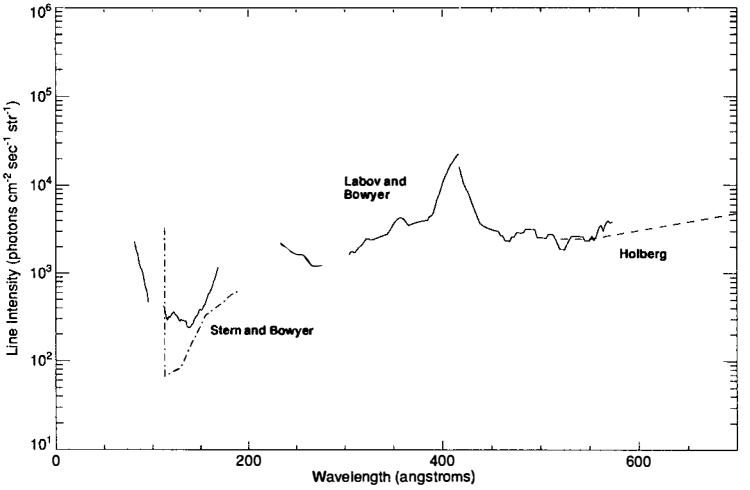


Figure 1 – Existing limits on the cosmic diffuse EUV background.

## POTENTIAL SOURCES OF DIFFUSE EUV EMISSION

We first briefly address the question of whether diffuse EUV emission will be observable even in principle because of the problem of absorption by the ISM. This is a potential concern since the Sun is commonly believed to be imbedded in a local cloud of ~1–5 pc diameter with a density of $N_H$~0.1 atoms cm$^{-3}$. Using the effective cross-section for absorption at EUV wavelengths (Cruddace et al., 1974), one finds that one optical depth is reached at a wavelength of ~450 Å. A closer study reveals that in a number of view directions hot white dwarfs at distances >50 pc have been spectroscopically observed almost to the Lyman limit at 912 Å (Holberg, et al 1980; Green, Jelinsky, and Bowyer 1990). These objects are in directions toward the pole (HZ 43) and the plane (G191–B2B) of the Galaxy. Hence the local cloud will not prevent observations of astronomical phenomena in at least some view directions. The extent of these "open" regions is not known, but the limited information available suggests they may include substantial portions of the celestial sphere (see, for example, Frisch and York 1991).

In the following we discuss a number of phenomena which are expected to produce diffuse EUV emission.

## 1. Emission from the Hot Phase of the Interstellar Medium

It has been more than thirty years since it was first suggested that hot, million-degree gas exists within our Galaxy (Spitzer 1956), and more than twenty years since the soft X-ray background was first detected (Bowyer, Field, and Mack 1968). It is now generally believed that this diffuse soft X-ray background is produced by a high-temperature component of the ISM. However, evidence of the thermal nature of this emission is based not on observations of line emission, but in the indirect evidence that no plausible nonthermal mechanism has been suggested which does not conflict with some component of the observational evidence. If the diffuse soft X-ray background is the product of emission from a hot gas, much of the radiated power will be in emission lines from highly ionized atoms radiating at EUV wavelengths (Kato 1976; Shapiro and Moore 1976; Raymond and Smith 1977; Stem, Wang, and Bowyer 1978; Mewe, Gronenschild, and van den Oord 1985).

The line emission from the hot ISM is strongly dependent upon the temperature and emission measure of this material. Indeed, one of the strengths of these measurements is that they will provide crucial information on these parameters. Several temperatures have been suggested for the hot phase of the ISM. Soft X-ray data suggest $10^6$ K gas (McCammon et al 1983). Absorption line data showing O VI (Jenkins 1978a; Jenkins 1978b) is often cited in combination with the soft X-ray data as further evidence for a $10^6$ K gas, but the peak of the emission curve for O VI is at the substantially lower temperature of $\sim 10^{5.5}$ K. It should be noted, however, that substantial O VI is present over the temperature range $10^5$–$10^6$ K. High ionization absorption lines observed in stellar spectra taken with *IUE* indicate a temperature of $10^{5.5}$ K (Savage 1987) as does the observation of emission lines at these wavelengths (Martin and Bowyer, 1989). There is also limited data suggesting gas at $10^5$ K (Labov and Bowyer 1991).

## 2. Emission from the Local Cloud and the Local Cloud Interface

It is generally believed from a variety of data that the Sun is surrounded by a low density cloud that extends ~1–5 pc around the Sun with $N_{HI} \sim 0.1$ cm$^{-3}$ and a temperature of $\sim 10^4$ K (Frisch and York 1982; Bruhweiler and Kondo 1982; Lallement, Vidal-Madjar, and Ferlet 1986). This "local fluff" is in tum surrounded by a hot ($10^6$ K) plasma "bubble" extending from 50 to 200 pc from the Sun (Cox and Reynolds, 1987). In the following, we estimate the emission both from the $10^4$ K gas comprising the local fluff and from the interface material between this local fluff and the hot ISM.

### *A. Emission from the $10^4$ K Local Cloud*

From the results of Shapiro and Moore (1976), we find the strongest lines from a cosmic plasma at a temperature of $10^4$ K are S II 877 Å and C II 904 Å. Folding the emission

parameters provided by Shapiro and Moore with a cloud of the size described above, we find the emitted flux from each of these lines is ~1 photon $cm^{-2}s^{-1}ster^{-1}$.

*B. Emission from the Local Cloud Interface*

The local fluff is subject to heating by the local EUV radiation field of stars and by thermal conduction and EUV radiation from the surrounding hot ISM. This heating will create an ionization zone at the cloud's surface. Cheng and Bruhweiler (1990) derive an ionization model of the local cloud skin structure. They model the effects of an incident field from discrete stellar sources and from thermal bremsstrahlung-radiative recombination produced by the hot ISM. The flux is assumed to be constant and uniform over half of the sky. Using boundary conditions of N(H I) = $10^{18}cm^{-2}$ for the local fluff and N(H I) = 0.06 $cm^{-3}$ for the particle density at the Sun, they predict the ionic column densities through the local cloud skin. They note that the population of highly charged species is formed predominantly by collisional ionization.

We fold the thin plasma emission line power predictions of Raymond and Smith (1977) together with the ion column estimates of Cheng and Bruhweiler to predict the intensity of the most powerful EUV cooling lines from the local cloud skin. The Raymond and Smith code was used to determine the primary cooling line species from a thin plasma at about $10^5$ K. Of these lines, only C III was predicted directly by Cheng and Bruhweiler. To estimate the column of other strongly emitting cloud skin species, we scale the predicted column of their species that would co-exist in thermal equilibria. The average ionic concentration of each species about its temperature of highest abundance (Shapiro and Moore, 1976) and the relative cosmic abundance of atoms were used for this scaling.

The resulting emission line intensities for the local cloud skin appear in Table 1. Each intensity is shown unabsorbed, and with an absorption corresponding to a neutral column of N (H I) = $4.0 \times 10^{17}$. The ability to observe the cloud skin emission will depend critically

**TABLE 1**

| Species | Å | Intensity[a] | Absorbed Intensity[a] |
|---|---|---|---|
| N IV | 765 | 122 | 28 |
| O IV | 789 | 55 | 11 |
| N III | 686 | 52 | 18 |
| O III | 834 | 50 | 7 |
| O IV | 554 | 31 | 18 |
| N III | 764 | 31 | 7 |
| O III | 703 | 29 | 9 |

[a] Intensity in photons $cm^{-2}s^{-1}ster^{-1}$

upon the neutral hydrogen column along the specific line of sight. A low column direction could allow EUV observations through the local cloud and the optically thin hot bubble to the next cloud in the line of sight. In this case, two cloud skins would be visible, and the predicted line intensity could increase by as much as a factor of 2.

### 3. Upper Atmospheric Airglow

Limited data exist in this bandpass; the only available data were obtained with a spectrometer flown on the *P-78* spacecraft (Bowyer et al. 1981). The only line detected in an upward direction at night was the O II 834 Å line, which was observed at an intensity of ~$10^5$ photons $cm^{-1}sec^{-1}ster^{-2}$ (Chakrabarti, Kimble and Bowyer, 1984). Nonetheless, it is certain that a number of faint airglow lines will be present at some level at satellite altitudes.

### 4. Diffuse Emission Producing Ionization Throughout the Galaxy

There is now extensive evidence for a source of ionization in the Galaxy which is both widespread and has a very large (~ 1 Kpc) scale height (see Reynolds, 1990 for a review). The primary evidence for this source of ionization is the detection of Hα emission (a product of the subsequent recombination) in every view direction searched. Additional support for this source of ionizing radiation and an estimate of the scale height of the source are provided by pulsar dispersion measures to pulsars at known distances. This scale height is much larger than that of early-type stars and supernovas, yet the energy input is roughly the same as that produced by these two classes of objects. It is generally agreed that no known sources of ionization can supply this energy with the smoothness and scale height observed.

These results have led to some provocative suggestions for the source of this ionization (see the following section). Whatever one thinks of any of the particular suggestions for the source of this flux, a major point is that the flux is indeed present, and by necessity it falls at a wavelength below 912 Å. Its intensity cannot be estimated without knowing whether the flux is continuous or is line emission. However, it is hard to conceive of a potential source mechanism that does not result in a substantial flux at Earth.

### 5. Emission from Dark Matter in and Around Our Galaxy

A speculative, but extraordinarily exciting, possible contributor to the cosmic EUV background is emission from the radiative decay of dark matter. The possibility that dark matter is undergoing radiative decay and is emitting in the EUV has been explored in substantial detail in a series of papers by Professor Denis Sciama, of the Internazionale Superiore Di Studi Avenzate in Trieste, and his co-workers. Sciama assumes, for the sake of concreteness, that this matter is neutrinos; however, all that is required is that the dark matter be a weakly interacting particle which decays electromagnetically with the proper energy. Sciama has explained a complex set of diverse astronomical observations with the single hypothesis that this dark

matter decays with a lifetime of ~$10^{23}$ seconds (Salucci and Sciama, 1990; Sciama 1990a, 1990b). The intensity of the line predicted by Sciama is ~150 photons $cm^{-2}sec^{-1}ster^{-1}$ at Earth. The predicted photon energy is ~14 eV (Sciama, 1991).

Evidence for this type of line has been searched for in other galaxies in *IUE* data taken on a quasi-stellar object which lies in a cluster of galaxies (Fabian, Naylor, and Sciama, preprint, 1991), and with the Hopkins Ultraviolet Telescope (HUT), which observed a cluster of galaxies on the flight of *ASTRO I* (Davidsen et al., 1991). In both of these cases the line would have been sufficiently redshifted to move it into the bandpass observed. Neither data set showed evidence for this line. The HUT result was especially stringent and ruled out the existence of the line at the 99.9% confidence level. Sciama (private communication) points out, however, that a new result by Fabian et al (preprint, 1991) provides strong evidence for large amounts of H I in clusters of galaxies. This gas would have sufficient opacity to absorb the line and render it unobservable in these measurements. Hydrogen Lyman $\alpha$ emission would be a strong byproduct of this interaction, and this might be observable. However, this emission is strongly absorbed by dust, and there is, in fact, some evidence for dust in clusters of galaxies.

## 6. Radiation Scattered by Interstellar Dust

Radiation scattered by interstellar dust may be present at some level, but it is impossible to make any qualitative predictions because both the radiation field that will be scattered and the scattering properties of dust at EUV wavelengths are unknown. It can be said with some certainty that emission from this process will be very low in intensity and will be highly localized spatially. The primary contributors to the radiation field shortward of 912 Å are O and B stars which are confined to the plane. Given the column densities in the direction of even the closest of these objects, there is no hope that this radiation will reach the Earth. It may be that, in special cases, chimneys will have been formed in the disc gas by supernovas. In these chimneys radiation from early stars could illuminate clouds high above the plane. After scattering, this radiation could be observed at Earth, in principle, but this radiation would have had to penetrate any neutral gas in our line of sight to these clouds. We believe this scenario to be unlikely.

## 7. Solar Radiation Resonantly Scattered from the Inflowing Interstellar Medium

The strongest line which will be observed in the EUV background is the He I 584 Å line which is produced by solar radiation resonantly scattering from neutral helium in the ISM flowing through the solar system. This effect, first predicted by Blum and Fahr (1970), has been utilized by many workers to characterize the very local interstellar medium (Grzedzielski and Page, ed., 1990).

## SUMMARY

In Figure 2 we show the expected night sky diffuse line emission for the mechanisms discussed. Emission lines marked A are airglow and resonantly scattered solar radiation (Chakrabarti et al 1984). Those lines marked C show the expected emission from evaporation of cool interstellar cloud material at the boundary with hotter gas. The feature at 900 Å marked D is emission from decaying dark matter predicted by Sciama (1990a/b). Unmarked lines represent emission from hot interstellar gas at $10^6$ K (Snowden et al. 1990). The upper limits obtained by Holberg (1986), and Labov and Bowyer (1991) are shown by curves marked H, and LB.

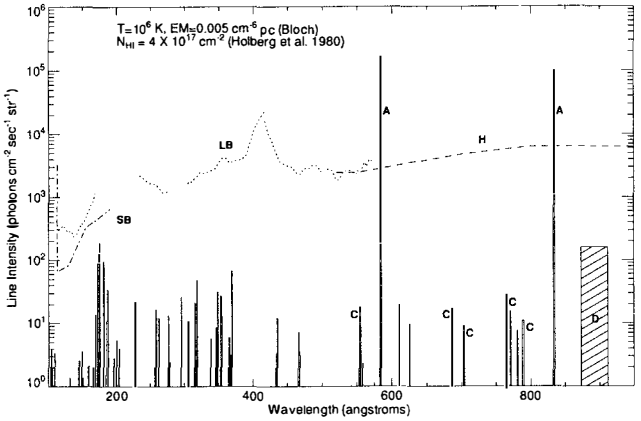


Figure 2 – Comparison of expected night sky diffuse line emission and existing upper limits. Emission lines marked A are airglow and resonantly scattered radiation (Chakrabarti et al. 1984). Those marked C represent expected emission from evaporation from the local cloud boundary. The cross-hatched area marked D represents the possible location and intensity of a line due to the emission from decaying dark matter, as predicted by Sciama (1990a,b). Unmarked lines represent emission from hot interstellar gas, as modeled by Bloch (1988). Sensitivity measurements by Stern and Bowyer (1979), Holberg (1986), and Labov and Bowyer (1991) are shown by the curves marked SB, H, and LB.

### Acknowledgments

We thank Eric Korpela for useful discussions. We thank Jean-Michel Deharveng for his invitation to this delightful conference. This work was supported by NASA Grant NRG05-003-450, which is administered by the Space Sciences Laboratory of the University of California, Berkeley.

**References**


Bowyer, S., Field, G., and Mack, J. 1968, Nature, 217, 32.
Bowyer, S., Kimble, R., Paresce, F., Lampton, M., and Penegor, G., 1981, *Appl. Opt.*, 20, 477.
Bloch, J. J. 1988, PhD thesis, University of Wisconsin, Madison.
Bloch, J.J., Jahoda, K., Juda, M., McCammon, D., Sanders, W.T., and Snowden, S.L. 1986, Ap. J. (Letters), 308, L59.
Blum, P.W. and Fahr, H.J. 1970, Ap. J. Letters, 6, 127.
Bruhweiler, F.C., Kondo, Y. 1982, Astrophys. J., 259, 232.
Cash, W., Malina, R., and Stern, R. 1976, Ap. J. (Letters), 204, L7.
Chakrabarti, S., Kimble, R., and Bowyer, S. 1984, J. Geophy. Res., 89, 5660.
Cheng, K.P. and Bruhweiler, F.C. 1990, Ap. J., 364, 573.
Cox, D.P. and Reynolds, R.J., 1987, Ann. Rev. Astron. & Astrophys., 25, 303.
Cruddace, R., Paresce, F., Bowyer, S., and Lampton, M. 1974, Ap. J., 189, 497.
Davidsen, A., et al., 1991, to be published in Nature.
Fabian, Naylor, and Sciama. 1991, preprint.
Frisch, P.C. and York, D.G. 1991, in *Extreme Ultraviolet Astronomy*, ed. R.F. Malina and S. Bowyer (New York: Pergamon), p. 302.
Frisch, P. and York, D.G. 1982, Astrophys. J. Letters, 271, L59.
Green, J., Jelinsky, P., and Bowyer, S. 1990, Ap. J., 359, 499.
Grzedzielski, S. and Page, D. E., eds. 1990, *Physics of the Outer Heliosphere*, Oxford: Pergamon.
Holberg, J.B. 1986, Ap. J., 311, 969.
Holberg, J.B., Sandel, B.R., Forerester, W.T., Broadfoot, A.L., Shipman, H. and Barry, D. 1980, Ap. J. (Letters), 242, L119.
Jenkins, E.B. 1978a, Ap. J., 219, 845.
Jenkins, E.B. 1978b, Ap. J., 220, 107.
Juda, M. 1988, PhD thesis, University of Wisconsin, Madison.
Kato, T. 1976, Ap. J. Suppl., 30, 397.
Labov, S. E. and Bowyer, S. 1991, *Ap. J.*, **371**, 810.
Lallement, R., Vidal-Madjar, A., and Ferlet, R. 1986, Astron. Astrophys., 168, 225.
Martin, C. and Bowyer, S. 1989, Ap. J., 338, 677.
McCammon, D., Burrows, D.N., Sanders, W.T., and Kraushaar, W.L. 1983, Ap. J., 269, 107.
Mewe, R., Gronenschild, E.H.B.M., and van den Oord, G.H.J. 1985, Astr. Ap. Suppl., 62, 197.
Paresce, F. and Stern, R. 1981, Ap. J., 247, 89.
Raymond, J.C. and Smith, B.W. 1977, Ap. J. Suppl., 35, 419.
Reynolds, R.J. 1990, in *The Galactic and Extragalactic Background Radiation*, ed. S. Bowyer and C. Leinert, Kluwer Academic Publishers, Dordrecht, Netherlands, p. 171.
Salucci, P. and Sciama, D.W. 1990, accepted by Mon. Not. R. Astr. Soc., 244, 9P.
Savage, B.D. 1987, in *Interstellar Processes*, ed. Hollenbach and Thronson, D. Reidel Publishing, Dordrecht, Netherlands.
Sciama, D.W. 1990a, Mon. Not. R. Astr. Soc., 244, 1P.
Sciama, D.W. 1990b, Mon. Not. R. Astr. Soc., 246.
Sciama, D. W. 1991, accepted for publication in Astron. & Astrophys.
Shapiro, P.R. and Moore, R.T. 1976, Ap. J., 207, 460.
Snowden, S.L., Cox, D.P., McCammon, D., and Sanders, W.T. 1990, Astrophys. J., 354.
Spitzer, L., Jr. 1956, Ap. J., 124, 20.
Stern, R. and Bowyer, S. 1979, Ap. J., 230, 755.
Stern, R., Wang, E., and Bowyer, S. 1978, Ap. J. Suppl., 37, 195.

# SUBMILLIMETER PROJECTS

F. Pajot
Institut d'Astrophysique Spatiale, Bat. 120, Université Paris XI
F-91405 Orsay Cedex, France

ABSTRACT

The development of ground based and space submillimeter astronomy opens the way to new galactic, extragalactic and cosmological observations. Spectrophotometric instruments based on direct detection -together with heterodyne spectrometry- will play a key role in this exploration. The instrumental program for the CalTech Submillimeter Observatory includes a Fabry-Pérot spectrophotometer : high sensitivity measurements using this large antenna will help to understand the physics of the extreme IRAS galaxies and their links with quasars. As a first step towards submillimeter space telescopes, the PRONAOS balloon program with the SPM instrument will make the first measurement of the positive part of the Sunyaev-Zel'dovich effect by clusters of galaxies. With additional observations of the negative part of the effect, the peculiar velocities of these clusters will become available, giving a first view of the large scale velocity field of the universe. This type of programs are essential to the success of the submillimeter space instruments such as SMMM (NASA-CNES) and FIRST (ESA).

## INTRODUCTION

Submillimeter astronomy is the field of many new instrumental programs : after a decade of ground based instruments, limited in their goals by the opacity of the atmosphere, space projects will allow the first complete coverage of the submillimeter range. Preparing these projects implies instrumental progress in the domains of focal instruments and light antennas. Balloon and airborne programs, or specific ground programs are the keys to these developments. However it should be noted that when high spatial resolution, or high sensitivity on unresolved sources, is needed, submillimeter ground based observations with large antennas or interferometers have better performances than will have the first space programs. Space projects are under preliminary studies : only one satellite with sharp scientific goals, COBE (the COsmic Background Explorer[1]), is in operation. The new projects will benefit from the experience learned with infrared satellites (IRAS[2], and ISO).

This paper deals with a set of representative submillimeter programs and their cosmological applications. The submillimeter Fabry-Pérot spectrophotometer for the 10 m CalTech Submillimeter Observatory (CSO) is a typical example of a focal instrument development. The PRONAOS balloon program (PRogramme National d'AstrOnomie Submillimetrique[3], CNES and CNRS, France) is the next step before space programs among which are the intermediate satellite SMMM (SubMilliMeter Mission, NASA/CNES[4]), the ESA cornerstone project FIRST (Far InfraRed Space Telescope[5]) and the long-term program LDR (Large Deployable Reflector[6], NASA).

## 1. SUBMILLIMETER SPECTROPHOTOMETRY

Spectrophotometric instruments are based on direct detection (bolometers, photoconductors) and their spectral resolving power covers from 3 to 10 (filters) up to $10^5$ (interferometers). At low resolving power (wide band observations), the high sensitivity gives access to very weak continuum sources :

- the interstellar dust (thermal emission) in molecular clouds, in galactic cirrus and in external galaxies. The distribution and the physical properties of the dust are thus investigated.
- the Sunyaev-Zel'dovich effect towards the clusters of galaxies, the Cosmic Background Radiation (CMB, 2.73 K cosmological blackbody) spatial fluctuations are typical observations of prime interest for cosmology .

At higher resolving power (for instance using a Fabry-Pérot interferometer), a huge number of lines lying in the submillimeter range can be studied :

- fine structure transitions of interstellar atoms and ions (CII at 157 μm is one of the most efficient lines in the cooling of the neutral or low excitation hydrogen regions of the interstellar medium)
- rotational transitions of interstellar molecules (CH, OH, $H_2O$, CO, $O_2$...)
- PAH bands (Polycyclic Aromatic Hydrocarbonates)

In this domain, the spectrophotometry is complementary to the heterodyne spectrometry, the later reaching higher sensitivities for narrower lines (corresponding to resolving powers higher than $10^4$) at long wavelength (typically 500 μm and up).

## 2. HIGH REDSHIFT IR GALAXIES : SUBMILLIMETER SPECTROMETER FOR THE CSO

The objectives of ground based submillimeter instrumental programs are :

- to obtain scientific data when the space projects are not yet in operation. The specificity of large antennas is used.
- to develop the techniques needed by these space projects. When possible, a 3 steps approach (ground - balloon/plane - space) is followed.

IRAS discovered a new class of galaxies which radiates more than 95% of their energy in the infrared. Most of them are starburst galaxies and the most luminous ($>10^{12}$ $L_\odot$) are interacting systems. The intensity of the CII line is predicted to be 10% to 20% of the Ly α intensity and is one of the best tools to discover the still mostly unknown physics of these galaxies : this study will help in the determination of their possible relations with quasars. The submillimeter

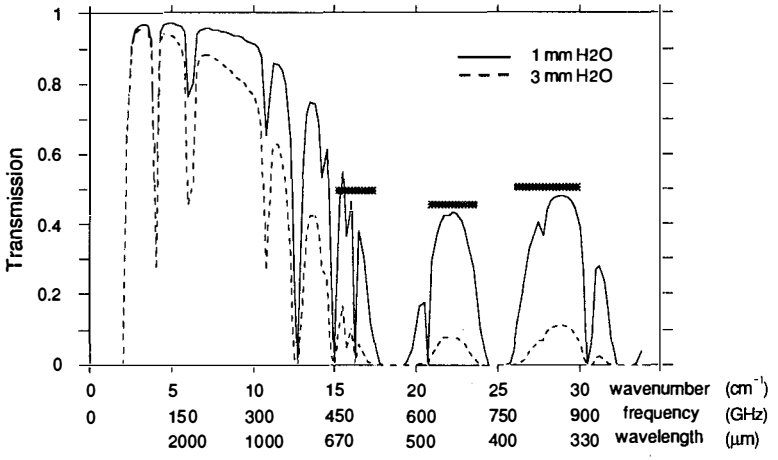


Figure 1 : Atmospheric transmission from a ground based site (4.2 km elevation)

Fabry-Pérot spectrophotometer for the CSO is designed to attempt the first detection of the 157 μm line of CII in these extreme galaxies. This line will be observed for object with appropriate redshifts through the atmospheric windows (z=1.21 for 340 μm, z=1.8 for 440 μm, z=2.8 for 600 μm - figure 1).

This program is a collaboration between French (Institut d'Astrophysique Spatiale, Commissariat à l'Energie Atomique, Institut d'Astrophysique de Paris, Centre d'Etude Spatiale des Rayonnements, Laboratoire d'Astronomie Spatiale) and US laboratories (CalTech, NASA-Goddard). This instrument is a precursor of similar instruments planned for the future submillimeter space observatories. We aim at a medium resolution (1500) spectrophotometer well suited to the expected width of the CII line in these objects (more than 300 $kms^{-1}$). A Fabry-Pérot and a grating (to sort the modes of the Fabry-Pérot) is placed in front of a 100 mK bolometer array (figure 2). The expected sensitivity is about $4 \times 10^{-19}$ $Wm^{-2}$ ($1\sigma$, 1000 s integration time) and the beam is 10 to 15 arcsec (depending on the wavelength) using the 10 m CSO antenna in Hawaii. This to be compared to the expected fluxes comprised between

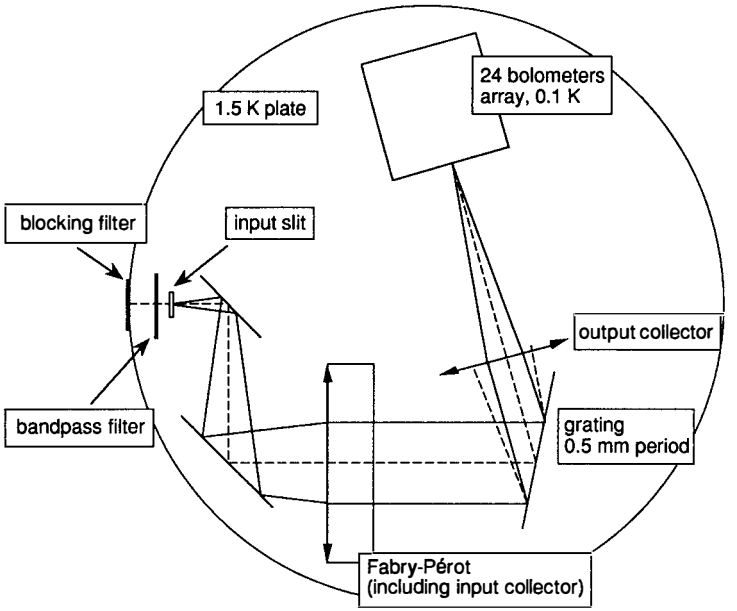


Figure 2 : Optical principles of the Fabry-Pérot spectrophotometer for the CSO

2.5 x $10^{-19}$ $Wm^{-2}$ (at 600 μm) and 30 x $10^{-19}$ $Wm^{-2}$ (at 340 μm). First observations are planned during the 1982-1983 winter.

## 3. THE SUNYAEV-ZEL'DOVICH EFFECT BY CLUSTERS OF GALAXIES : PRONAOS-SPM

The CMB is distorted when passing through a cluster of galaxies : the hot electrons of the cluster interact with the CMB photon via Thomson scattering[7]. The negative part of the Sunyaev-Zeldovich effect has already been detected at 20 GHz[8]. PRONAOS-SPM will attempt to measure the positive part of the effect (at short wavelength). A complementary program, DiaBolo will attempt to measure the negative part of the effect (λ=2 mm) from the ground using the IRAM 30 m telescope. These observations will allow to determine the

peculiar velocity of the clusters. Figure 3 shows the cluster velocity effect on the Sunyaev-Zeldovich effect. The knowledge of the large scale velocities of the galaxies is a key to fundamental parameters of cosmology ($\Omega$, q). In addition, this measurement will set limits on the small scale (8 arcmin) CMB anisotropy which are powerful constraints to the models of the early universe.

PRONAOS consists in a 2 meter carbon fiber telescope (segmented, active control) carried on a gondola pointing with a 5 arcsec rms accuracy. At the flight altitude (38 km), the residual pressure is only 3 mb. Two focal instruments will operate in turn : a multiband spectrophotometer (SPM) and a heterodyne spectrometer (SMH). With SPM, the beam ranges from 2 to 3.5 arcmin corresponding to wavelengths from 240 $\mu$m to 1200 $\mu$m in 4 bands. The first flight is scheduled in 1993 with SPM, optimized for the detection of the positive part of the Sunyaev-Zel'dovich effect (700-1200 $\mu$m band). The expected sensitivity is 1.6 $JyHz^{-1/2}$ or 410 $\mu KHz^{-1/2}$ for this band, which turns for the best candidates (clusters

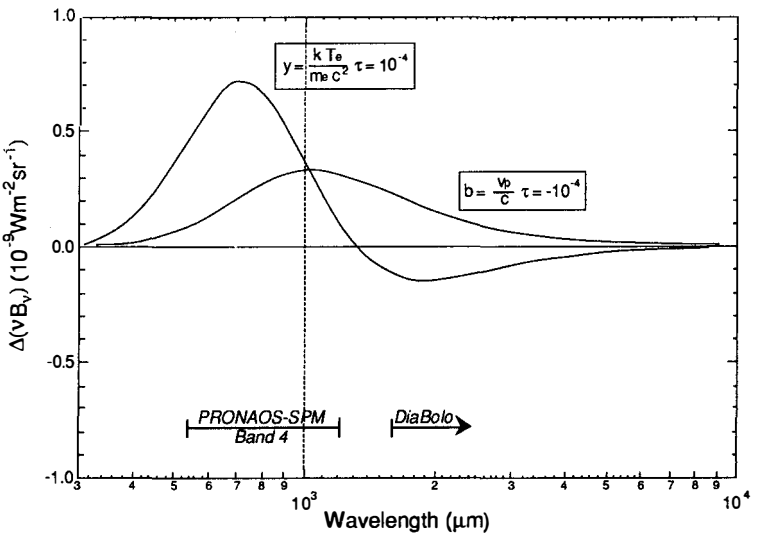


Figure 3 : The 2 Sunyaev-Zel'dovich effects. $T_e$ is the electron temperature in the cluster, $\tau$ the Thomson optical depth and $v_p$ the peculiar velocity of the cluster.

Abell85, A1795, A2029, A2218, A2319, 0016+16...) into a typical $5\sigma$ detection time of 3 to 4 hr.

## 4. SUBMILLIMETER SPACE PROJECTS

Space telescopes will give access for the first time to the full submillimeter spectral range. Systematic spectral exploration as well as mapping in lines hidden to observers on the ground by the atmosphere will bring exciting and original results : new molecules, physical characteristics of the interstellar medium, physics of extragalactic objects such as the galaxies studied with the CSO submillimeter spectrophotometer. In the far infrared range, spectrophotometers are considered to be the most sensitive instruments, but at longer wavelength (excluding the case of wideband photometry whose main goals are related to cosmology - see SPM-PRONAOS objectives) heterodyne spectrometry is the most promising. Sensitivity to point sources of a 4 m passively cooled telescope using 100 mK bolometers is at least an order of magnitude better than ISO in the far infrared range (200 $\mu$m), mainly limited by confusion due to galactic and extragalactic sources.

SMMM is a 2.4 m or 3.7 m (depending on launcher) class telescope with passive cooling. In addition to a heterodyne spectrometer, it includes a Fabry-Perot spectrophotometer (FIRS) in a configuration equivalent to the CSO instrument. This instrument will cover two bands (100-185 $\mu$m and 170-310 $\mu$m) on adjacent fields with a mid range resolving power (10 000). Sensitivities with 100 mK bolometers are given in table 1. Priority is thus given to systematic spectral exploration. The time scale of the project is compatible with an launch date in the late nineties.

FIRST features a 4.5 m class telescope with passive cooling carrying heterodyne instrumentation, a submillimeter spectrophotometer and a submillimeter photometer. The direct detection instruments of the model payload consist in a double Fabry-Perot spectrophotometer (high and low resolution) with a bidimentionnal detectors array giving access to high resolution spectro-imaging in a given line (85-125 $\mu$m and 130-180 $\mu$m bands) with a high resolving

power (100 000), and a wide band photometer for the 100-1800 μm range dedicated to cosmology (photometer sensitivity about 10 mJy $Hz^{-1/2}$). FISRT schedule is directly dependant on its selection as 3rd or 4th cornerstone of the ESA Horizon 2000 program.

Table 1 : Sensitivities for point sources of the FIRS spectrophotometer on SMMM

| λ (μm) | SMME (4.5 $m^2$) NEFD (Jy $Hz^{-1/2}$) | SMILS (10 $m^2$) NEFD (Jy $Hz^{-1/2}$) |
|---|---|---|
| 100 | 92 | 42 |
| 150 | 138 | 62 |
| 180 | 166 | 75 |
| 300 | 276 | 125 |

REFERENCES


1) Mather, J.C., 1982, *Opt. Eng.* **21**(4), 769
2) Neugebauer, G., Habing, H.J., van Duinen, R., Aumann, H.H., Baud, B., Beichman, C.A., Beintema, D.A., Boggess, N., Clegg, P.E., de Jong, T., Emerson, J.P., Gautier, T.N., Gillett, F.C., Harris, S., Hauser, M.G., Houck, J.R., Jennings, R.E., Low, F.J., Marsden, P.L., Miley, G., Olnon, F.M., Pottasch, S.R., Raimond, E., Rowan-Robinson, M., Soifer, B.T., Walker, R.G., Wesselius, P.R., Young, E., 1984, *Astrophys. J.* **278**, L1
3) Lamarre, J.M., Encrenaz, P., Serra, G., Pajot, F., Bellaiche, G., 1990, *Journal of Optics* **21**, 141
4) Phillips, T., 1990, *Proceedings of the 29th Liège International Astrophysical Colloquium*, ESA SP-314, 221
5) Frisk, U., 1990, *Proceedings of the 29th Liège International Astrophysical Colloquium*, ESA SP-314, 37
6) Wilson, R., 1990, *Proceedings of the 29th Liège International Astrophysical Colloquium*, ESA SP-314, 215
7) Sunyaev, R.A., Zel'dovich, Y.B., 1980, *Ann. Rev. Astron. Astrophys.* **18**, 537
8) Birkinshaw, 1990, *IInd Rencontres de Blois "Physical Cosmology"*, Blois, August 28th - September 1st 1990, A. Blanchard Eds, Frontières Editions, in press

# THE ITALIAN OASI OBSERVATORY

G. Dall'Oglio[1], P. Ade [2], P. Calisse[1], A. Iacoangeli[1]
L. Martinis [3], L. Piccirillo [4,5], L. Pizzo[1], L. Rossi[6]

(1) Physics Department - University "La Sapienza" - Rome (I)
(2) Queen Mary College - London (UK)
(3) ENEA - T.I.B. Dept. - Frascati (I)
(4) Istituto Superiore PT - Rome (I)
(5) ESA - ESTEC Astrophysics Division - Noordwijk (NL)
(6) CNR - Istituto di Astrofisica Spaziale - Frascati (I)

**Abstract**

OASI - Infrared and Sub-mm Antarctic Observatory- is the first large telescope permanently installed in Antarctica. It is located near the Italian Antarctica Base (Terra Nova Bay) at a latitude of 74.39 S and a longitude of 164.09 E. The OASI first light was received on December 1990 when the wobbling secondary mirror was mounted. The telescope can operate in the wavelengths range between 3 mm and 350 $\mu$m covering the Southern Hemisphere from the Celestial Pole to a declination of about $-20$ degrees.

## 1. Introduction

The OASI is composed mainly by two telescopes. The main instrument (2.6 m diameter) is devoted to investigate the Cosmic Background Radiation (CBR) small scale anisotropy while the secondary instrument (1.5 m diameter off-axis) is devoted to the CBR intermediate scale anisotropy. The main instrument has been installed during the 1989/90 Italian Antarctica expedition and became operative during the 1990/91 expedition. With the same instruments the galactic (for ex. $\eta$ Car, Centaurus A etc.) and extragalactic (LMC, SMC etc.) diffuse cold dust emission can be investigated.

## 2. The OASI telescope

The main characteristics of the OASI telescope are given in tab. I. The OASI reflector is a Cassegrain telescope whose primary mirror is made of Aluminum alloy. The secondary mirror is mounted on a wobbling system in order to perform the beam switching in the sky. A relevant reduction in the induced vibrations on the structure is obtained by wobbling, in counter-phase, a second equal mass. The net sky modulation of the system is sinusoidal and the amplitude can be selected between few arcsecs and one degree. The tracking and pointing systems have an accuracy of about 10arcsec.

## 3. The detectors

The focal plane is equipped with Si-composite bolometric detectors. The operating temperature (0.35 K) is achieved by means of a $^3He/^4He$ refrigerator [1]. The available optical bands are 850 $\mu$m, 1250 $\mu$m and 2070 $\mu$m with a bandwiths of respectively 80 $\mu$m, 350 $\mu$m and 400 $\mu$m. All the bands are well matched to the standard atmospheric windows.

The 2 mm channel has been calibrated by observing the Moon, Venus and Saturn. We obtain the following optical parameters:

$S_{2mm} = (0.86 \pm 0.08) \times 10^{-6}$ V/K

$R_{2mm} = (1.2 \pm 0.1) \times 10^{6}$ V/W

NET = 23 mK/$\sqrt{Hz}$

NEP = $1.7 \times 10^{-14}$ W/$\sqrt{Hz}$

The previous values were obtained by using an uncorrect optical match between the telescope and the cold optics. The final configuration of the photometer will enable us to improve the previous figure by more than a factor 3.
In fig. 1 a tipical calibration scan of Venus is shown.

**Tab. I**

| | |
|---|---|
| Primary mirror diameter | D=2600 mm |
| Focal length | f=1300 mm |
| Focal ratio | f/D=0.5 |
| Secondary mirror diameter | d=410 mm |
| Equivalent focal length | F=10400 mm |
| Equivalent focal ratio | F/D=4 |
| Cassegrain magnification | 8 |
| Distance between mirrors | H=1018.7 mm |
| Secondary mirror - focal plane distance | h=1597.1 mm |
| Primary mirror - focal plane distance | L=578.4 mm |
| Angular resolution | 6.4 arcmin ($\lambda$ = 2 mm) |
| Angular resolution | 3.2 arcmin ($\lambda$ = 1.25 mm) |
| First Airy disc diameter | 19.5mm ($\lambda$ = 2 mm) |
| First Airy disc diameter | 9.7 mm ($\lambda$ = 1.25 mm) |
| Surface r.m.s. roughness | $\leq 0.3\mu$m |
| Pointing accuracy | 1 arcmin |

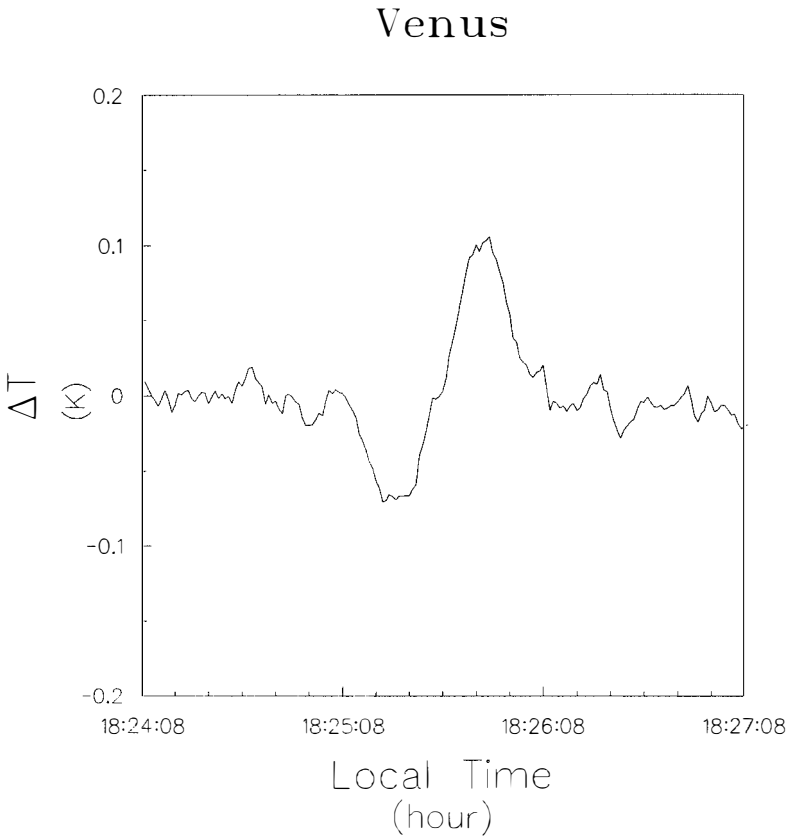


This work was supported by ENEA - PROGRAMMA NAZIONALE DI RICERCHE IN ANTARTIDE.

**References**

[1] Dall'Oglio G. et al., Cryogenics, 31, 61, 1991

# Search for macroscopic dark matter in the galactic halo through microlensing

Eric Aubourg
Institut d'Astrophysique de Paris
98$^{b}$ Bd Arago
75014 Paris
bitnet: AUBOURG@FRCPN11

**Abstract**

We present a status report of our project to search for dark objects in the Galactic Halo via gravitational microlensing of stars in the Large Magellanic Cloud. The search uses a combination of Schmidt photographic plates and CCD images and is sensitive to lensing by objects in the range $10^{-7}$ $M_{\odot}$ to $10^{-1}$ $M_{\odot}$ . An automated analysis software has been succesfully tested on CCD test images taken last year. Using these preliminary results, we calculate the number of microlensing events expected on plate and CCD programs.

## Introduction

It is widely believed that the flat rotation curves observed for spiral galaxies like our own indicate that such galaxies are surronded by a "halo" of dark matter[1]. While the mass of the dark haloes should be as much as ten times that of the visible parts of galaxies, the composition of the haloes is not known. Candidates range from new weakly interacting elementary particles to dark astronomical objects like brown dwarfs or black holes. The elucidation of the nature of the halo inhabitants would have profound implications for cosmology and theories of galaxy formation.

The mass of hydrogeneous compact halo objects could range from $10^{-7}$ to $10^{-1}$ solar masses[2]. As Pasczynski pointed out[3], objects in this range of mass could be detected by monitoring the brightness of individual stars in the Large Magellanic Cloud. An massive object $D$ passing close enough to the line of sight to the observed star $S$ induces a relativistic light deflection and magnification (fig. 1). Only the magnification is measurable, and its amplitude is more than 0.3 magnitude if the impact parameter is less than the Einstein radius of the deflector,

$$R_E^2 = \frac{4GMD}{c^2}, \qquad D = \frac{OD.DS}{OS}$$

Due to the perfect alignment required for a sizeable magnification, the microlensing phenomenon is sensitive to the relative motion of the observer, star and deflector. The result is an achromatic and symmetric light curve. For stars in the LMC, a deflector of mass $M$ and relative speeds of order 200 km/s, the mean time $\tau$ during which the magnification is greater than 0.3 magnitude is given by

$$\tau = (70 \text{ days}) \sqrt{\frac{M}{M_\odot}}$$

Since $R_E^2$ is proportional to the deflector mass and the number of deflectors, for a given halo total mass, is inversely proportional to their mass, the probability that a given star is amplified by a given amount at any moment is independent of the deflector mass. For stars in the LMC, a halo with total mass $4\ 10^{11}\ M_\odot$ and a microlensing threshold of 0.3 magnitude this probability is about $0.5\ 10^{-6}$. And if one assumes that all deflectors have mass $M$, since $\tau$ is proportional to $\sqrt{M}$, the number of microlensing events expected is a fixed observation time is inversely proportional to $\sqrt{M}$.

The selection criteria for microlensing events are light curve achromaticity and symmetry, and uniqueness of the event.

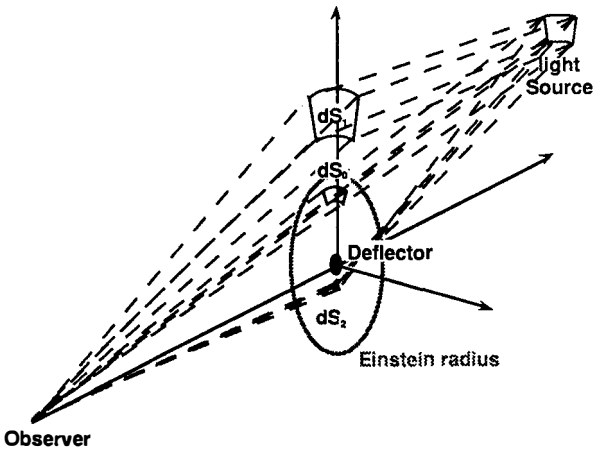


figure 1: A microlensing event.

Undeflected light coming from light source crosses deflector plane on $dS_0$. The deflected light gives two images, $dS_1$ and $dS_2$ in deflector plane. The surface brightness is the same for all dS, the apparent amplification is then $\frac{dS_1+dS_2}{dS_0}$.

## Two experiments

Our group[a] [4] has two experiments under way: the first, using photographic plates taken at ESO Schmidt telescope, will monitor more than one million stars with a time scale of the order of the day, and then will be sensitive to mean lensing durations between 1 and 30 days corresponding to deflector masses between $10^{-4}$ and $10^{-1}$ $M_\odot$. Plates are taken in two colours, B and R, with one hour exposure time, and then digitized at the MAMA (Machine Automatique à Mesurer pour l'Astronomie, Observatoire de Paris). Each plate requires 8 hours and generates 2 gigabytes of information.

The second, using a large CCD mosaic, will monitor more than 30,000 stars with a time scale of half an hour, and then will probe lensing durations between 1 hour and 3 days, corresponding to deflector masses between $10^{-7}$ and $10^{-3}$ $M_\odot$. The CCD camera is under construction in Saclay, and will have a total area of 76mm x 29mm consisting in an array of 2x8 Thomson CCD. Images are taken in two colours with 10 mn exposure time, assuming a 40-cm telescope with wide filters.

## Data analysis

The analysis has to be completely automated, given the huge quantity of data to process. An analysis software has then been developed. It works according to the following steps:

---

[a] Institut d'Astrophysique de Paris, Observatoires de Paris et Marseille, Laboratoire d'Astronomie Spatiale de Marseille, Département d'Astrophysique et de Physique des Particules Élémentaires du CEN Saclay, Laboratoire de l'Accélérateur Linéaire.

• A reference file is created either from the "best" couple of image, or from a composite image. All stars found on other images will be mapped to the stars found on it, so it has to be of very good quality.

• For each image, a pattern recognition algorithm finds a first order fit to the reference image, in a completely automatic way. This algorithm was succesfully used to map images from different telescopes.

• A least squares fit is made on isolated stars to fit more accurately the two images.

• For each star, the algorithm searches for a star at an equivalent position on the reference image.

• A relative calibration then maps all brightnesses to the brightnesses measured on the reference image. The algorithm used is a generalization of the classical method for variable stars observation consisting in the observation of a stable neighbouring star. We make the assumption that the mean brightness of a large sample of neighbouring stars in a given range of brightness is constant. In a small area of an image, we then choose different subranges of brightness, and measure the mean brightness of these samples of stars on this image and on the reference image. We can interpolate the relative calibration curve from these points[1]. If we have an absolute calibration on the reference image, the result is an absolute calibration.

• The final output is a light curve (luminosity vs time) per star and per colour.

• The resolution in relative photometry is measured by the r.m.s. dispersion of the light curves, assuming that most stars are of constant brightness.

Careful optimization allowed an execution time between O(n) and O(n Log n), where n is the number of stars. Most of the time is spent in the photometry routine, on which a lot of work is under way. The results shown below have been obtained using a very primary algorithm, which provides a relative precision good enough for our minimal needs. The whole set of data has been processed in 6 minutes CPU time[2], extrapolating to 3 hours for a photographic plate.

## December, 1990 CCD test run

To test the deasibility of the CCD program, our group observed the LMC with the 40-cm GPO refracting telescope at La Silla. A single 576 pixel x 405 pixel Thomson CCD chip was mouted on the telescope giving a field of 11' x 8'. The essential part of the observations consisted of 63 exposures in the middle of the bar of the LMC. The high chromatic aberration of the GPO forced us to use narrow filters ($\lambda$ = 4520 Å, $\Delta\lambda$ = 340 Å, and $\lambda$ = 6480Å, $\Delta\lambda$ = 110Å) and then long exposure time (30 mn) to reach $m_B$ = 19.

We found a relative precision shown in fig. 2 as a function of magnitude, ranging from 4 to 13%.

A casual inspection of stars with large fluctuation in magnitude resulted is the discovery of three candidate cepheid variables, an eclipsing binary and some long-

---

[1] In fact, to take into account the non-linearity of photographic plates, the algorithms maps both sky background and measured brightness, with a multi-dimensional interpolation.

[2] The computer used was an IBM 3090/600 VF.

period variable stars (fig. 3 sqq). We note, however, that we found no light curves that resemble that expected for a microlensing event.

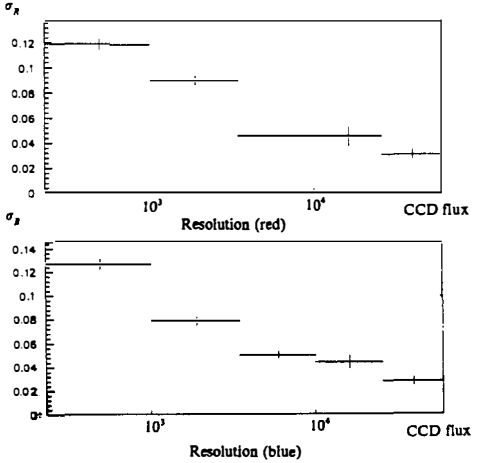


figure 2: Magnitude resolution for CCD images using the red and blue filters versus the CCD flux. A flux of $10^3$ corresponds to about $17^{th}$ magnitude.

We have investigated several possible algorithms for identifying microlensing events from the characteristics of observed light curves. In order to be sensitive to microlensing by objects in our halo, an algorithm should have an inefficiency for the rejection of random fluctuations of the light curves of less than $10^{-6}$. The inefficiency for rejection of variable stars will depend on their type and number. For cepheids, our measurement of their rate indicates that a rejection inefficiency of $10^{-3}$ is necessary. On the other hand, an algorithm should have a good efficiency for accepting real microlensing events. The efficiency must be estimated via a Monte Carlo simulation of the observation sequence and detector resolution. The efficiency will depend on the distribution of deflector masses and, to a lesser extent, on the halo model.

In our present algorithm, we search for stars whose light curves exhibit, within any time window, a sufficiently large deviation from the mean of the measurements outside the window. The threshold for accepting a deviation is chosen so as to eliminate random fluctuations of light curves due to the system resolution. Each light curve is tested with window widths and positions varying over the total duration of the observing period. Each time a sufficiently large deviation is found, the light curve is fitted with Paczynski's theoretical light curve separately in the two colours. The event is accepted as a candidate microlensing event if the fit gives compatible amplifications and times (of maximum light) for the two colours.

For our observing sequence of December, 1990, we have used the Monte Carlo to study the algorithm's efficiency to accept events of peak amplification of at least 0.3 magnitude. The efficiency is zero for masses below $M = 10^{-8}\ M_\odot$ where the mean lensing time is shorter than the exposure time. It increases with mass above this value reaching a value of 20% for deflector masses of $M = 10^{-5}\ M_\odot$ It falls to zero for $M = 10^{-1}\ M_\odot$ where the mean lensing time is of order the total observation time (1

month). The number of events expected for the 1990 sequence is about 0.01 for deflector masses in the range $10^{-7}$ — $10^{-3}$ $M_{\odot}$. The number of events is nearly indepedent of deflector mass in this range because the rising efficiency is compensated by the falling total number of microlensing events.

For the next observing season, we plan to use the CCD camera now under construction, multiplying by 16 the number of monitored stars. We also hope to increase the number of observing nights to 100. The number of microlensing events that can be expected with this program as a function of the assumed deflector mass is shown in Table 1. Since the number of expected events is of order one, we will be able to definitively test the hypothesis that the Halo is made of dark astronomical objects only is the star-finding and photometric algorithms are improved so as to increase the efficiency for observing microlensing events.

It is hoped to replace the GPO with a 40-cm reflector, allowing wider band filters and shorter exposure times. The number of microlensing events expected is shown in Table 1.

## The near future

During the winter of 1990-1991, 28 pairs of Schmidt plates were taken at La Silla. Their digitization is under way at the MAMA. As a preliminary step, we have digitized two entire plates and five 4-cm$^2$ zones on 10 pairs of plates. The first measurements give a precision of 0.14 magnitude for relative photometry on the 1000 brightest stars per cm$^2$. Using this result, we can compute the expected number of events for the plate program. The figures are shown in table 1 for 1990-91 observations and for a proposed 1991-92 program.

## Acknowledgements

We have benefitted greatly from discussions with C. Alcock, A. Baranne, D. Benett, A. Bijaoui, A. de Rújula, P. Felenbok, B. Fort, K. Greist, Y. Mellier, C. Pennypacker, B. Sadoulet, C. Stubbs and A. Terzan. We thank J.-P. Berger, R. Burnage and Ph. Veron of the Observatoire de Haute Provence for the help with the GPO telescope and CCD tests. We thank S. D'Odorico and H. Van der Laan of ESO for encouragement and help with the CCD camera. finally, we thank the ESO staff at La Silla, especially O. & G. Pizarro, D. Hoffstadt and H.E. Schuster, for the observations with the Schmidt telescope and for help with the CCD observations.

## References

1) General reviews of dark matter by Virginia Trimble, Ann. Rev. Astron. Astrophys. 1987; J.R. Primack, D. Seckel and B. Sadoulet, Ann. Rev. Nucl. Sci. 1988.

2) A. De Rújula, Ph. Jetzer, and E. Massó, CERN preprint CERN-TH 5787/91.

3) B. Paczynski, Ap. J. 304, 1-5 (1986).

4) A. Milsztajn, 10th Moriond Workshop on new and exotic phenomena, Les Arcs, January, 1990; M. Moniez, 10th Moriond Astrophysics Meeting, Les Arcs, January, 1990 (both Éditions Frontières, 1991).

**Table 1.**

The expected number of observed microlensing events as a function of assumed deflector mass, $M$, for the Schmidt program (1990-91 alone and combined with proposed 1991-92 observations), for the proposed 1991-92 CCD program, on GPO and on 40-cm reflector. The estimates are based on an isothermal halo model with a total mass of 4.0 $10^{11}$ $M_\odot$ between the galactic core and the LMC. For the 1991-92 Schmidt program we assume 100 pairs of plates spread over 5 months, $10^6$ stars per plate with a mean relative photometric resolution of 0.14 magnitude in red and blue. For the CCD program we assume 150 consecutive nights from which we substract the weeks centered on the full moon and 20% randomly selected unusable nights. We assume 30,000 monitored stars with a mean resolution of 0.1 magnitude.

| $M(M_\odot)$ | Schmidt 1990-91 | Schmidt 1990-92 | GPO 1991-92 | 40 cm 1991-92 |
|---|---|---|---|---|
| $10^{-0}$ | 0.3 | 2.6 | | |
| $10^{-1}$ | 1.0 | 4.8 | | |
| $10^{-2}$ | 1.9 | 8.2 | | |
| $10^{-3}$ | 2.2 | 10. | 1.2 | 3.0 |
| $10^{-4}$ | 1.5 | 7.5 | 2.2 | 5.7 |
| $10^{-5}$ | | | 2.8 | 10. |
| $10^{-6}$ | | | 2.3 | 11. |
| $10^{-7}$ | | | 1.3 | 6.6 |

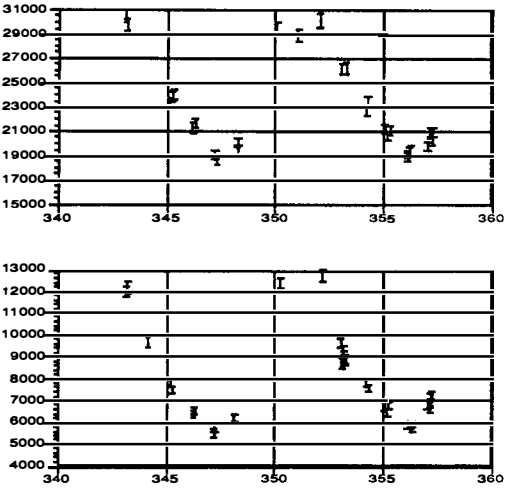


figure 3: A candidate Cepheid variable (top: blue filter, bottom: red filter). The abscissa is the day of the year 1990, the ordinate the measured CCD flux.

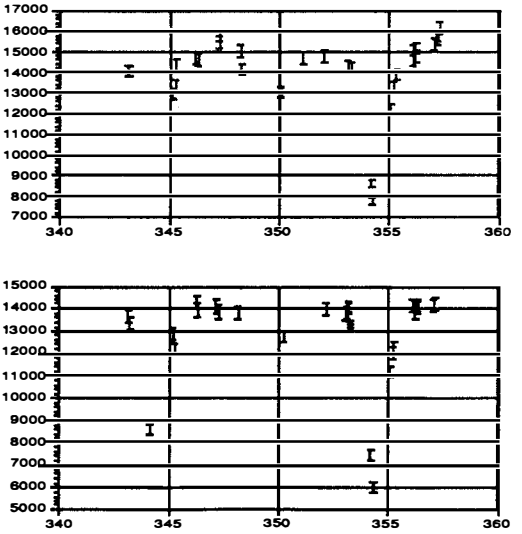


figure 4: A candidate eclipsing binary.

# LISTE DES PARTICIPANTS


**ARMAND Christiane**
CNRS
Lab. d'Astronomie Spatiale
Traverse du Siphon
**F- 13012 MARSEILLE**
**FRANCE**

**AUBOURG Eric**
Institut d'Astrophysique
98 Bd Arago

**F- 75014 PARIS**
**FRANCE**

**AUDOUZE Jean**
Institut d'Astrophysique
98 Bd Arago

**F- 75014 PARIS**
**FRANCE**

**BABUL Arif**
University of Cambridge
The Observatories - Inst of Astrophysics
Mandigley Road
**CB3 OHA CAMBRIDGE**
**UNITED KINGDOM**

**BALLET Jean**
C E N Saclay
DPhG/SAp

**F- 91191 GIF sur YVETTE Cedex**
**FRANCE**

**BERNARDEAU Francis**
CEN Saclay
SPThP

**F- 91191 GIF sur YVETTE Cedex**
**FRANCE**

**BIGNAMI Giovanni**
IFC

Via Bassini 15
**I- 20133 MILANO**
**ITALY**

**BLANCHARD Alain**
Observatoire de Paris Meudon
DAEC

**F- 92195 MEUDON PRINCIPAL Cedex**
**FRANCE**

**BOUQUET Alain**
Université Paris VII
LPNHE - Tour 24 - 5ème Etage
2, Place Jussieu
**F- 75251 PARIS**
**FRANCE**

**BOWYER Stuart**
Center for EUV Astrophysics
University of California

**CA 94720 BERKELEY**
**USA**

**BURDYUZHA Vladimir**
Lebedev Physical Institute
Astro Space Center
Profsoyusnaya 84/32
**117810 MOSCOW**
**U S S R**

**CARAVEO Patricia**
IFC

Via Bassini 15
**I- 20133 MILANO**
**ITALY**

**CARLBERG Ray**
Dept of Astronomy
University of Toronto

**M5S IA1 TORONTO**
**CANADA**

**CARR Bernard**
University of London
Queen Mary College - Applied Math. Dept.
Mile End Road
**E1 4NS LONDON**
**UNITED KINGDOM**

**CASSE Michel**
C E N Saclay
DPhG/SAp

**F- 91191 GIF sur YVETTE Cedex**
**FRANCE**

**CESARSKY Catherine**
C E N Saclay
DPhG/SAp

**F- 91191 GIF sur YVETTE Cedex**
**FRANCE**

**CHARDONNET Pascal**
LAPP
Lab. de Physique des Particules
B. P. 110
**F- 74941 ANNECY LE VIEUX Cedex**
**FRANCE**

**COLLIN Susy**
Institut d'Astrophysique
98 Bd Arago

**F- 75014 PARIS**
**FRANCE**

**CRANE Philippe**
ESO
European Space Telescope
Karl Schwarzschild Str 2
**D- 8046 GARCHING BEI MUNCHEN**
**FEDERAL REP. OF GERMANY**

**DAVIS Adam**
Institut d'Astrophysique
98 Bd Arago

**F- 75014 PARIS**
**FRANCE**

**DE ZOTTI Gianfranco**
Universita di Padova
Istituto di Astronomia
Vic. dell'Osservatorio 5
**I- 35100 PADOVA**
**ITALY**

**DEHARVENG Jean-Michel**
CNRS
Lab. d'Astronomie Spatiale
Traverse du Siphon
**F- 13012 MARSEILLE**
**FRANCE**

**EBELING Harald**
Max Planck Institut
für Extraterrestrische Physik
Karl-Schwarzschild Str.
**D- 8000 MUNCHEN 40**
**FEDERAL REP. OF GERMANY**

**FRANCESCHINI Alberto**
Universita di Padova
Istituto di Astronomia
Vic. dell'Osservatorio 5
**I- 35100 PADOVA**
**ITALY**

**GARDNER J. P.**
University of Hawaii
Dept of Physics and Astronomy
2505 Correa Road
**HI 96822 HONOLULU**
**USA**

**GUHATHAKURTA Puragra**
Princeton University Observatory
Peyton Hall

**NJ 08540 PRINCETON**
**USA**

**GUIDERDONI Bruno**
Institut d'Astrophysique
98 Bd Arago

**F- 75014 PARIS**
**FRANCE**

**JAKOBSEN Peter**
ESTEC
Space Science Division
Zwarteweg 62
**NL- 2200 ZH NOORDWIJK**
**NETHERLANDS**

**JONES Mark**
Queen Mary College
Dept of Physics
Mile End Road
**E1 4NS LONDON**
**UNITED KINGDOM**

**LACEY Cedric**
University of Oxford
Dept of Astrophysics
South Parks Road
**OX1 3RQ OXFORD**
**UNITED KINGDOM**

**LEINERT Christoph**
Max Planck Institut
für Astronomie
Koenigstuhl
**D- 6900 HEIDELBERG 1**
**FEDERAL REP. OF GERMANY**

**LUKASH V.**
Lebedev Physical Institute
Astro Space Center
Profsoyusnaya 84/32
**117810 MOSCOW**
**U S S R**

**MADDOX Steve**
University of Oxford
Dept of Astrophysics
South Parks Road
**OX1 3RQ OXFORD**
**UNITED KINGDOM**

**MADEJSKY Rainer**
Institut für Astronomie
Landessternwarte Heidelberg
Konigsthuhl
**D- 6900 HEIDELBERG**
**FEDERAL REP. OF GERMANY**

**MATTILA Kalevi**
University of Helsinki

Tahtitorninmaki
**SF- 003130 HELSINKI 3**
**FINLAND**

**MILLARD Bruno**
CNRS
Lab. d'Astronomie Spatiale
Traverse du Siphon
**F- 13012 MARSEILLE**
**FRANCE**

**MORRISON Douglas**
CERN
European Organization for Nuclear Res.

**CH- 1211 GENEVE 23**
**SWITZERLAND**

**PAJOT François**
L. P. S. P.

B. P. 10
**F- 91371 VERRIERES BUISSON Cedex**
**FRANCE**

**PICCIRILLO Lucio**
ESTEC
Space Science Division
Zwarteweg 62
**NL- 2200 ZH NOORDWIJK**
**NETHERLANDS**

**PUGET Jean-Loup**
Université Paris Sud
IAS - Bât. 105

**F- 91405 ORSAY Cedex**
**FRANCE**

**ROCCA-VOLMERANGE Brigitte**
Institut d'Astrophysique
98 Bd Arago

**F- 75014 PARIS**
**FRANCE**

**SALATI Pierre**
CERN
TH Division

**CH- 1211 GENEVE 23**
**SWITZERLAND**

**SANDERS Wilton**
University of Wisconsin
Dept of Physics
1150 University Ave
**WI 53706 MADISON**
**USA**

**SCHAEFFER Richard**
CEN Saclay
DPhT
Orme des Merisiers
**F- 91191 GIF sur YVETTE Cedex**
**FRANCE**

**SCHMIDT Maarten**
Max-Planck Institute
für Extraterrestrische Physik
Karl-Schwarzschild-Str. 1
**D- 8046 GARCHING bei MUNCHEN**
**FEDERAL REP. OF GERMANY**

**SCIAMA Dennis**
Scuola Internazionale Superiore
di Studi Avanzati (SISSA)

**I- 34100 TRIESTE**
**ITALY**

**SHAPIRO Paul**
University of Texas
Dept Astronomy

**TX 78712-10 AUSTIN**
**USA**

**SIRONI Giorgio**
Universita di Milano
Istituto di Fisica
Via Celoria 16
**I- 20133 MILANO**
**ITALY**

**SMOOT George**
Lawrence Berkeley Laboratory
Dept of Physics
1 Cyclotron Road
**CA 94720 BERKELEY**
**USA**

**WHITE Simon**
Cavendish Laboratory
Mullard Radio Astronomy Obsservatory
Mandigley Road
**CB2 ITA CAMBRIDGE**
**UNITED KINGDOM**

**YAHIL Amons**
SUNY - STONY BROOK
Astronomy Group

**NY 11794-2100 STONY BROOK**
**USA**